

David Jorge Rocheta Cassiano

# POST SEISMIC STRUCTURAL ROBUSTNESS IN MOMENT RESISTING FRAME STEEL BUILDINGS

Tese de doutoramento em Construção Metálica e Mista,  
orientada pelo Professor Doutor Carlos Alberto da Silva Rebelo  
e co-orientada pelo Professor Doutor Mario D'Aniello e  
pelo Professor Doutor Raffaele Landolfo, apresentada ao  
Departamento de Engenharia Civil da Faculdade de Ciências  
e Tecnologia da Universidade de Coimbra

Fevereiro de 2017



UNIVERSIDADE DE COIMBRA





**FCTUC** DEPARTAMENTO DE ENGENHARIA CIVIL  
FACULDADE DE CIÊNCIAS E TECNOLOGIA  
UNIVERSIDADE DE COIMBRA



Institute for Sustainability and  
Innovation in Structural Engineering

# **Post seismic structural robustness in moment resisting frame steel buildings**

**Tese apresentada para obtenção do grau de Doutor em  
Construção Metálica e Mista**

***Thesis presented in fulfilment of the requirements for the degree of  
Doctor of Philosophy in Steel and Composite Construction***

**Autor**

**David Jorge Rocheta Cassiano**

**Orientador**

**Professor Doutor Carlos Alberto da Silva Rebelo**

**Co-Orientadores**

**Professor Doutor Mario D'Aniello**

**Professor Doutor Raffaele Landolfo**

**ISISE, Departamento de Engenharia Civil – Universidade de Coimbra**

***ISISE, Department of Civil Engineering – University of Coimbra***

**Coimbra, 2017**



À memória do meu avô,

Casimiro Jorge



## RESUMO

A robustez de estruturas porticadas em aço é geralmente avaliada considerando que o colapso progressivo se inicia com o edifício em condição não danificada. No entanto, no caso da existência prévia de um dano inicial, tal como o causado pela ação sísmica, as estruturas podem revelar-se mais sensíveis ao colapso progressivo. Esta consideração motivou a presente tese de doutoramento, a qual é dedicada ao estudo da robustez estrutural pós-sísmica de estruturas de aço porticadas.

De forma a atingir este objetivo, é realizado um estudo numérico paramétrico, para o qual as configurações de pórticos estudadas foram selecionadas de forma a serem representativas de um largo espectro de estruturas existentes. Foi analisada a influência dos seguintes parâmetros: número de pisos, altura entre pisos, comprimento do vão e configuração do edifício em planta.

A robustez é avaliada considerando as contribuições da estrutura secundária e dos painéis não-estruturais de revestimento de fachada, que são tipicamente desprezadas, mas que estudos recentes indicam que possam apresentar uma contribuição significativa para parar o colapso progressivo. Em particular, a resposta dos painéis de fachada é modelada numericamente e calibrada com base em resultados de literatura. O comportamento dos nós da estrutura secundária é modelado de acordo com resultados de um estudo numérico paramétrico relativo ao comportamento à perda de coluna de nós viga-coluna com placa de extremidade. Neste estudo foram usados modelos de parafusos calibrados com base em resultados de ensaios experimentais conduzidos e descritos na presente tese.

Os resultados do estudo paramétrico dos nós viga-coluna permitiram identificar dois mecanismos de resistência à ação de perda de coluna, nomeadamente por arco em compressão e por ação de catenária. Conclui-se que a espessura da placa de extremidade tem um papel fundamental na resposta dos nós, sendo proposto um critério de dimensionamento para a espessura da placa que permite maximizar a resistência e capacidade de rotação dos nós. São ainda propostas recomendações adicionais referentes ao tipo de soldadura, número de linhas de parafusos internos e diâmetro dos parafusos para aumentar a resistência dos nós.

No que diz respeito aos resultados do estudo da robustez das estruturas porticadas, conclui-se que, para as estruturas analisadas, a configuração estrutural

influencia significativamente a robustez, tendo-se verificado que estruturas com poucos pisos e grandes vãos são altamente propensas ao colapso progressivo. Verifica-se igualmente que estruturas com maior número de pisos são menos propensas ao colapso pós perda de coluna, dado que a maior capacidade de redistribuição interna compensa o aumento de carga na coluna. A caracterização em termos de acelerações, velocidades e deslocamentos da zona diretamente afetada permite verificar que os fatores de reserva de ductilidade pós perda de coluna são muito baixos em estruturas de grande vão em comparação com estruturas de médio vão, evidenciando assim diferenças significativas na robustez estrutural.

Através da análise da capacidade dos diversos elementos estruturais, conclui-se que os nós viga-coluna dos pórticos resistentes são os elementos mais solicitados e que determinam o colapso. Conclui-se ainda que a adoção de regras de pormenorização para o colapso progressivo nestes elementos pode potencialmente melhorar significativamente a robustez estrutural. Verifica-se também que a presença de painéis de fachada não-estruturais pode prevenir o colapso progressivo em alguns casos de estruturas com baixa robustez, nomeadamente em estruturas baixas com grandes vãos.

No que se refere à avaliação da robustez pós-sísmica, constata-se que a ação sísmica moderada em estruturas porticadas de classe DCH dimensionadas segundo a EN 1998-1, ao contrário de ações sísmicas elevadas, não introduz dano suficientemente significativo a ponto de reduzir de forma relevante a robustez estrutural. Neste caso o dimensionamento ao colapso progressivo em cenário pós-sísmico pode assim ser realizado analogamente ao dimensionamento para a estrutura sem dano inicial. Neste sentido, é proposta uma metodologia para o dimensionamento, bem como regras de pormenorização baseadas na propensão ao colapso progressivo, que poderão constituir uma contribuição para uma futura revisão da EN 1991-1-7. Adicionalmente e com base nos resultados referentes ao grau de plasticidade da zona diretamente afetada, é proposto um procedimento de intervenção para os Serviços de Proteção Civil em estruturas danificadas que sofreram perda de coluna.

**Palavras-Chave:**

Robustez | Colapso progressivo | Estruturas porticadas | Ligações com placa de extremidade | Painéis não estruturais



## ABSTRACT

The robustness of steel frames is generally evaluated considering that the initiation of progressive collapse occurs in buildings in the undamaged condition. However, in case of an existing initial damage, as that potentially caused by seismic action, structures may be more prone to progressive collapse. This consideration motivated this doctoral thesis, which is aimed at studying the post seismic structural robustness of moment resisting frame steel structures.

To achieve this purpose, a numerical parametric study is carried out, for which the examined frame configurations have been selected in order to be representative of a large set of realistic frames. The influence of the following parameters is analysed: number of storeys, interstorey height, span length and building plan layout.

The robustness is evaluated considering the contributions of the secondary frame and of the façade claddings, which are typically disregarded, but which recent studies indicate to potentially provide a significant contribution to progressive collapse arrest. In particular, the response of the façade claddings is numerically modelled and calibrated to experimental results from literature. The contribution of the secondary frame joints is modelled according to results from a numerical parametric study on the column loss response of flush end-plate beam-to-column joints. In this study, bolt assembly models calibrated to experimental test results conducted and described in this thesis, were adopted.

The results from the beam-to-column joint parametric study enabled to identify two resistance mechanisms to column loss action, namely compressive arching and catenary action. It is concluded that the end-plate thickness plays a key role in joint response and an end-plate thickness design criterion to maximise joint strength and rotational capacity is proposed. Additional recommendations are made regarding the type of welding, number of internal bolt rows and bolt diameter in order to enhance joint capacity.

For what concerns the robustness study of the moment frames, it is concluded that, for the analysed structures, structural configuration significantly influences robustness, with low-rise long-span structures displaying high propensity to progressive collapse. It is also verified that structures with a higher number of storeys are less prone to collapse following column loss, given that the higher internal

redistribution capacity compensates for the load increase in the column. The characterisation in terms of acceleration, velocity and displacement of the directly affected zone has enabled to verify that the ductility factors post column loss are very low for long span structures in comparison to medium span structures, highlighting the significant differences in structural robustness.

From the analysis of the capacity of the different structural elements it is concluded that the moment resisting frame beam-to-column joints are the most strained elements and determine the collapse. It is further concluded that the adoption of detailing rules for progressive collapse in these elements can potentially significantly improve structural robustness. Furthermore it is also verified that the use of non-structural claddings can prevent progressive collapse in some cases for structures with low robustness, namely for low-rise long-span structures.

For what concerns the evaluation of the post seismic robustness, it is verified that moderate seismic action in moment resisting frames in DCH class designed in accordance with EN 1998-1, unlike for strong seismic action, does not introduce a sufficient damage to the point of reducing structural robustness significantly. In this case the design for progressive collapse in the post-seismic scenario may therefore be conducted analogously to the design of an initially undamaged structure. In this sense, a design methodology, as well as detailing rules based on the propensity to progressive collapse are proposed, which may constitute a contribution to the future revision of the EN 1991-1-7. Additionally and on the basis of the degree of plasticity results of the directly affected zone, a Civil Protection Services intervention procedure is proposed for the case of structures damaged by column loss.

**Keywords:**

Robustness | Progressive collapse | Moment resisting frame | Flush endplate joints | Claddings

## ACKNOWLEDGEMENTS

I would like to express my gratitude and appreciation to Professor Carlos Rebelo for his supervision, support and availability to solve all the scientific, technical and institutional issues throughout the duration of the doctoral program. I am also thankful to Professor Raffaele Landolfo for his supervision and for having accepted my stay at the Department of Structures for Engineering and Architecture of the University of Naples “Federico II”.

I would like to express my personal gratitude to Dr. Mario D’Aniello, for his excellent guidance, supervision, availability, dedication and support throughout the years I spent working with him. His contributions of time, knowledge, advices, innovative ideas and motivation helped me greatly during difficult times in the pursuit of the Ph.D. and were an invaluable help to the successful completion of this work.

I also want to thank the many Ph.D. and M.Sc. colleagues, friends and flatmates from around the world that I have had the pleasure of getting to know. The contact I have had with them rendered my Ph.D. experience much richer and contributed to make my stays at both the University of Coimbra and at the University of Naples even more memorable.

A great word of appreciation goes to Eng. Joaquim Pereirinha Rodrigues, with whom I had the privilege of working as a structural engineer, prior to enrolling in this doctoral program. Still today I consider him as my mentor and as the person who, by far, taught me the most about structural engineering. I would like to thank him for his generosity in teaching and in passing on his knowledge of steel structures. It was throughout the many inspirational, enlightening and funny discussions we had that I developed my passion for steel structures. A proper thank you was long overdue.

Last but not least, I would like to thank my family. Words cannot express how grateful I am to my parents and grandparents for all the help and sacrifices you have made on my behalf during this Ph.D. and throughout my life. You have always been and continue to be my daily source of inspiration and strength and my role models in

## ACKNOWLEDGEMENTS

life. Thank you for all your patience, for having agreed to let me live far from Portugal, for enduring my absences, for your never-ending support and encouragement in good and bad moments and for always believing in me. This work was possible, first and foremost, because of you. Thank you!

A very special thank you goes to my girlfriend Vittoria, for having always been by my side throughout this Ph.D., for always believing in me, for having helped me in good and bad times and for all the funny and great moments we shared. Finally, I hold an enormous debt of gratitude to the Galli family for having welcomed me in their home, for always being so kind to me, for their support, for being my friends and for all they have done for me. Thank you for all the good moments we shared.

# TABLE OF CONTENTS

RESUMO.....	i
ABSTRACT.....	iii
ACKNOWLEDGEMENTS .....	v
TABLE OF CONTENTS .....	vii
NOTATIONS .....	xiii
<b>Chapter 1 Introduction .....</b>	<b>1</b>
1.1 <i>Relevance and scope</i> .....	1
1.2 <i>Objectives</i> .....	5
1.3 <i>Structure of the thesis</i> .....	7
<b>Chapter 2 Literature review .....</b>	<b>9</b>
2.1 <i>Introduction</i> .....	9
2.2 <i>Robustness codes and design approaches</i> .....	10
2.2.1 <i>Comparative analysis of design approaches and detailing requirements for structural robustness</i> .....	11
2.3 <i>Discussion on design concepts</i> .....	17
2.3.1 <i>Building risk classification</i> .....	17
2.3.2 <i>Tie force method</i> .....	20
2.3.3 <i>Tolerable area at risk of collapse</i> .....	23
2.3.4 <i>Key element design</i> .....	29
2.3.5 <i>Alternative Loadpath Method</i> .....	34
2.3.6 <i>Scenario dependency modelling</i> .....	35
2.4 <i>Probability of a progressive collapse</i> .....	36
2.5 <i>Risk assessment</i> .....	36

## TABLE OF CONTENTS

2.6 Robustness indexes.....	38
2.6.1 Risk based robustness index .....	38
2.6.2 Probabilistic robustness index .....	39
2.6.3 Deterministic robustness index .....	40
2.7 Robustness studies .....	43
2.7.1 Experimental robustness studies.....	43
2.7.2 Analytical robustness studies .....	46
2.7.3 Numerical robustness studies.....	51
2.8 Flush end-plate joint behaviour.....	57
2.8.1 Components method modelling.....	58
2.8.2 Experimental studies.....	66
2.8.3 Numerical studies.....	70
2.9 Claddings.....	72
<b>Chapter 3 Definition of parametric study and design of frames .....</b>	<b>75</b>
3.1 Introduction .....	75
3.2 Parametric variables and analysis cases.....	75
3.2.1 Parametric variables.....	75
3.2.2 Analysis cases.....	76
3.3 Design assumptions .....	77
3.3.1 Structural solution.....	77
3.3.2 Materials .....	80
3.3.3 Actions .....	81
3.3.4 Imperfections and 2 <sup>nd</sup> order effects.....	83
3.3.5 Modelling.....	84
3.4 Conclusive remarks .....	85

<b>Chapter 4 Preliminary robustness assessment.....</b>	<b>87</b>
4.1 <i>Introduction</i> .....	87
4.2 <i>Background</i> .....	88
4.3 <i>Framework of the study</i> .....	89
4.3.1 Investigated parameters .....	89
4.3.2 Design assumptions .....	90
4.3.3 Monitored parameters .....	92
4.3.4 Analysis methodology .....	94
4.3.5 Modelling assumptions .....	97
4.4 <i>Results</i> .....	101
4.4.1 Pushdown analysis results.....	101
4.4.2 Nonlinear dynamic analysis results.....	109
4.5 <i>Simplified prediction model for DFL</i> .....	118
4.6 <i>Conclusive remarks</i> .....	120
<b>Chapter 5 Experimental monotonic and cyclic inelastic tensile tests of bolt assemblies.....</b>	<b>123</b>
5.1 <i>Introduction</i> .....	123
5.2 <i>European normative background</i> .....	125
5.2.1 Preloadable bolt assemblies .....	126
5.2.2 Non-preloadable bolt assemblies .....	127
5.3 <i>Bolt assembly features</i> .....	127
5.3.1 Preloadable bolt assemblies .....	127
5.3.2 Non-preloadable bolt assemblies .....	130
5.4 <i>Experimental activity</i> .....	131
5.4.1 Investigated parameters .....	131
5.4.2 Experimental test set up .....	135

5.4.3 Variable amplitude cyclic loading protocol..... 137

5.4.4 Constant amplitude cyclic loading protocol..... 138

5.5 *Experimental results* ..... 139

5.5.1 Monotonic bolt assembly response..... 140

5.5.2 Linearized monotonic stress-strain curves ..... 144

5.5.3 Normalized stress-strain curves..... 149

5.5.4 Ductility ..... 153

5.5.5 Variable amplitude cyclic bolt assembly response ..... 154

5.5.6 Constant amplitude cyclic bolt assembly response..... 156

5.6 *Finite element modelling* ..... 160

5.6.1 Background ..... 160

5.6.2 Modelling of HR assemblies ..... 163

5.6.3 Modelling of HV assemblies..... 169

5.6.4 Modelling of SB assemblies..... 172

5.6.5 Modelling of T-stub response with HR and HV assemblies ..... 175

5.7 *Conclusive remarks* ..... 184

**Chapter 6 Parametric numerical analysis of flush end-plate beam-to-column joints** ..... 187

6.1 *Introduction* ..... 187

6.2 *Framework of the study*..... 189

6.2.1 Proposed ductility criteria..... 189

6.2.2 Parametric variables..... 192

6.2.3 Finite element modelling..... 196

6.2.4 Validation of the FE modelling..... 200

6.2.5 Strain rate effects ..... 201

6.2.6 Fracture initiation in plates and welds ..... 206



6.2.7 Moment-rotation response curves .....	207
6.3 Results.....	210
6.3.1 Monotonic column loss action – strong axis column configuration..	210
6.3.2 Monotonic column loss action – weak axis column configuration ...	228
6.3.3 Cyclic bending followed by monotonic column loss action.....	232
6.4 Consequences for design.....	254
6.4.1 Joints under monotonic column loss action.....	254
6.4.2 Joints under cyclic action and subsequent column loss action .....	257
6.5 Conclusive remarks .....	260
<b>Chapter 7 Nonlinear dynamic analysis of MRF structures under column loss scenarios.....</b>	<b>265</b>
7.1 Introduction .....	265
7.2 Framework of the study.....	266
7.2.1 Generalities.....	266
7.2.2 Investigated parameters .....	266
7.2.3 Design assumptions .....	268
7.2.4 Monitored parameters .....	269
7.2.5 Analysis methodology .....	272
7.2.6 Modelling assumptions .....	284
7.3 Results.....	318
7.3.1 Baseline robustness .....	318
7.3.2 Post seismic robustness .....	369
7.4 Consequences for design.....	415
7.4.1 Current design methodology.....	415
7.4.2 New performance based progressive collapse methodology proposal .....	416

TABLE OF CONTENTS

7.5 *Conclusive remarks* ..... 440

**Chapter 8 General conclusions and perspectives..... 445**

8.1 *Conclusions* ..... 445

8.2 *Implications for design and contribution to the future revision of EN 1991-1-7*  
..... 451

8.3 *Personal contributions* ..... 454

8.4 *Open questions and further research* ..... 457

**REFERENCES..... 461**

**Appendix A Moment resisting frame member cross sections ..... 477**

**Appendix B Generation of the structures in Seismostruct..... 491**

**Appendix C Proposal for a new EN 1991-1-7 Annex E ..... 522**

**Appendix D Detailing rules justification..... 543**

# NOTATIONS

## Lowercases

$a$	<i>Distance between the centre of an external row bolt and the end-plate edge</i>
$a_{DAZ}$	<i>Acceleration of the directly affected zone</i>
$a_{gR}$	<i>Reference peak ground acceleration on type A ground</i>
$b$	<i>Width of the cross section</i>
$b_{eff}$	<i>Effective width of the composite slab</i>
$c$	<i>Depth of the washer face</i>
$d$	<i>Depth of the straight zone of the web</i>
$d_a$	<i>Diameter of the unthreaded bolt shank</i>
$d_b$	<i>Nominal diameter of the bolt</i>
$d_d$	<i>Bolt assembly displacement at <math>F=F_y</math></i>
$d_f$	<i>Diameter of the washer face</i>
$d_r$	<i>Interstorey drift displacement</i>
$d_y$	<i>Bolt assembly yielding displacement</i>
$e$	<i>Bolt head or nut width across corners</i>
$f$	<i>Frequency of vibration</i>
$f_b$	<i>Mean normalized vertical compressive strength of the masonry unit</i>
$f_m$	<i>Average compressive strength of mortar</i>
$f_k$	<i>Mean vertical characteristic compressive strength of masonry</i>
$f_y$	<i>Yield strength</i>
$f_{y,k}$	<i>Characteristic yield strength</i>
$f_{y,k,bolt}$	<i>Bolt material characteristic yield strength</i>
$f_{y,u,bolt}$	<i>Bolt material ultimate yield strength</i>
$f_{ym}$	<i>Average yield strength</i>
$f_u$	<i>Ultimate strength</i>
$g$	<i>Gravitational acceleration</i>
$g_k$	<i>Characteristic value of the permanent load</i>
$h$	<i>Depth of the cross section</i>
$k$	<i>Thickness of the bolt head</i>
$k_{Assembly}$	<i>Bolt assembly stiffness</i>
$k_{softening}$	<i>Rate of bolt assembly response strength softening</i>

## NOTATIONS

$k_{v,i,MRF}$	<i>Initial elastic vertical frame stiffness</i>
$l_{eff}$	<i>Effective length of the equivalent T-Stub</i>
$l_{hinge}$	<i>Length of the plastic hinge</i>
$m$	<i>Thickness of the nut</i>
$p$	<i>Thread pitch or distance between consecutive bolt rows</i>
$p_k$	<i>Characteristic value of the dead load</i>
$q$	<i>Behaviour factor</i>
$q_k$	<i>Characteristic value of the variable load</i>
$r$	<i>Radius of root fillet</i>
$s$	<i>Bolt head or nut width across flats</i>
$t$	<i>Thickness</i>
$t_{ep}$	<i>End-plate thickness</i>
$t_f$	<i>Flange thickness</i>
$t_{min,Mode2}$	<i>Minimum end-plate thickness to induce a failure mode 2 according to the proposed design criterion</i>
$t_{max,Mode2}$	<i>Maximum end-plate thickness to induce a failure mode 2 according to the proposed design criterion</i>
$t_r$	<i>Action rise time</i>
$u_{CC}$	<i>Storey horizontal displacement of the frame with façade claddings</i>
$u_{CN}$	<i>Storey horizontal displacement of the bare frame</i>
$u_{hor,max}$	<i>Maximum horizontal storey displacement</i>
$u_{dyn,equil,damaged}$	<i>Static displacement in equilibrium after stabilisation</i>
$u_{dyn,max,damaged}$	<i>Maximum dynamic displacement at the zero kinetic energy condition</i>
$u_{DAZ}$	<i>Displacement of the directly affected zone</i>
$u_i$	<i>Vertical displacement at step <math>i</math> of the pushdown analysis</i>
$u_{u,damaged}$	<i>Displacement at collapse</i>
$\bar{u}^{pl}$	<i>Effective plastic displacement for the ductile damage model</i>
$t_w$	<i>Web thickness</i>
$v_{b,0}$	<i>Basic wind velocity</i>
$v_{DAZ}$	<i>Velocity of the directly affected zone</i>
$w$	<i>Spacing between the centres of bolts in the same bolt row</i>
$z$	<i>Lever arm</i>

## Uppercases

$A_b$	Nominal area of the bolt shank
$A_{be}$	Effective area of the threaded shank
$A_d$	Accidental design action
$A_{eff}$	Effective bolt shank area
$A_{nom}$	Nominal bolt shank area
$A_{risk}$	Area at risk of collapse
$A_{tol}$	Tolerable area at risk of collapse
$B$	Bolt force in the T-Stub model
$B_{t,Rd}$	Design tensile resistance of the bolt
$C$	Strain rate constant
$CoV$	Coefficient of Variation
$D$	Damage
$D_{nom}$	Bolt nominal diameter
$DLF_0$	Base value of the Dynamic Load Factor
$E$	Young's modulus
$E_{Barron\&Bickford}$	Shank elastic modulus according to Barron and Bickford (1998)
$E_{eq}$	Equivalent shank elastic modulus
$E_{i,masonry}$	Initial elastic modulus of the masonry panel
$F$	Force applied to the T-Stub
$F_{stat}$	Static gravity load in the column prior to notional removal
$F_{p,Rd}$	Design resistance of the connected plate
$F_{t,Rd}$	Design resistance of the bolt
$F_{T,2}$	T-Stub resistance in failure mode 2
$F_{T,3}$	T-Stub resistance in failure mode 3
$F_{u,damaged}$	Ultimate capacity of the structural system in the damaged configuration
$F_y$	Yielding force
$G$	Shear modulus
$H$	Interstorey height
$I_{rob}$	Risk based robustness index
$K_b$	Bolt elastic stiffness
$K_e$	Elastic distortional stiffness of the column web panel
$K_E$	Stiffness of the smooth part of the shank

## NOTATIONS

$K_{eq}$	<i>Bolt assembly elastic stiffness</i>
$K_p$	<i>Post yield distortional stiffness of the column web panel</i>
$K_{tg}$	<i>Stiffness of the threads in the bolt grip</i>
$K_Z$	<i>Stiffness of the threaded part of the shank</i>
$Q$	<i>Prying force in the T-Stub</i>
$L$	<i>Span of the beam (or length or characteristic length of the finite element)</i>
$L_0$	<i>Reference length</i>
$L_s$	<i>Length of the bolt shank</i>
$L_{tg}$	<i>Length of the threaded zone included in the bolt's grip</i>
$M$	<i>Applied bending moment</i>
$\dot{M}$	<i>Variation of bending moment in time</i>
$M_{\theta, chord}$	<i>Bending resistance of the first cycle at chord rotation <math>\theta</math></i>
$M_{connection}$	<i>Bending moment in the connection</i>
$M_{j, EC3}$	<i>Joint bending resistance prediction according to EN 1993-1-8</i>
$M_{j, pin, EC3}$	<i>Joint bending resistance limit for nominally pinned classification according to EN 1993-1-8</i>
$M_{j, sec, \theta}$	<i>Joint bending resistance at secant rotation demand <math>\theta</math></i>
$M_p$	<i>Plastic bending resistance</i>
$M_P$	<i>Plate plastic bending resistance in a T-Stub</i>
$M_{pl, beam}$	<i>Beam plastic resistance in bending</i>
$M_{pl, Rd}$	<i>Design plastic bending resistance of the plate</i>
$M_{u, P.C.}$	<i>Post cyclic action ultimate joint bending strength</i>
$M_{u, I.U.}$	<i>Ultimate bending strength of the initially undamaged joint</i>
$N$	<i>Number of storeys (or number of cycles at failure)</i>
$N_p$	<i>Plastic axial resistance</i>
$N_{PC, N}$	<i>Maximum estimated catenary force for progressive collapse</i>
$R_s(u)$	<i>Static joint resistance at displacement <math>u</math></i>
$S$	<i>Span</i>
$S_d$	<i>Design spectral acceleration</i>
$S_{j, ini}$	<i>Joint initial elastic bending stiffness</i>
$S_{j, ini, EC3}$	<i>Joint initial elastic bending stiffness prediction according to EN 1993-1-8</i>
$S_{j, N, ini}$	<i>Joint initial elastic axial stiffness</i>
$S_{j, pin, EC3}$	<i>Joint initial elastic bending stiffness limit for nominally pinned classification according to EN 1993-1-8</i>

$S_{j,sec,\theta, chord}$	Secant joint stiffness at $\theta_{chord}$
SD	Standard deviation
T	Vibration period (or stress triaxiality state)
$T_i$	Internal tie design force
$T_m$	Mean period
$T_n$	Period of vibration of the $n^{th}$ Eigen mode
$T_p$	Peripheral tie design force (or predominant period)
$V_p$	Column web panel plastic shear strength
$V_y$	Column web panel shear yield strength
W	Section modulus
$W_{int}$	Internal energy
$W_{ext}$	External work done
Y	Length of the threaded shank outside the nut
Z	Length of the threaded shank in the connected plates

### Lowercase Greek letters

$\alpha$	Parameter for the computation of $\lambda_1$ and $\lambda_2$ in EN 1993-1-8 or strain hardening parameter according to Krawinkler (1978) for the column web panel model
$\alpha_n$	$n^{th}$ alfa parameter of the proposed constitutive law for the equivalent HV shank
$\alpha_{cr}$	Minimum force amplifier for the elastic critical buckling load
$\beta_1$	Convergence limit for the Newton-Raphson procedure
$\beta_n$	$n^{th}$ beta parameter of the proposed constitutive law for the equivalent HV shank
$\gamma$	Specific weight (or Ramberg-Osgood transition parameter for the column web panel model)
$\gamma_{ov}$	Material overstrength factor
$\gamma_{PC,N}$	Adjustment factor for maximum catenary force in progressive collapse
$\gamma_{sh}$	Strain hardening factor
$\gamma_y$	Column web panel yield distortion
$\delta$	Logarithmic decrement of damping
$\delta_{vert}$	Vertical displacement
$\delta_D$	Dynamic load factor reduction factor for the design scenario
$\delta_N$	Dynamic load factor reduction factor for the number of storeys

## NOTATIONS

$\varepsilon$	Strain
$\varepsilon_f$	Ductile plate fracture strain
$\varepsilon_y$	Yielding strain
$\varepsilon_{eng}$	Engineering strain
$\varepsilon_{Norm}$	True strain normalised to Criterion 1
$\varepsilon_{p,critical}$	Average critical plastic strain
$\varepsilon_{true}$	True strain
$\varepsilon_{true,plastic}$	True plastic strain
$\varepsilon_{true,plastic,u}$	Ultimate true plastic strain
$\varepsilon_u$	Ultimate strain
$\bar{\varepsilon}_0^{pl}$	Equivalent plastic strain at the onset of damage
$\bar{\varepsilon}_f^{pl}$	Equivalent plastic strain at failure
$\dot{\varepsilon}^*$	Dimensionless plastic strain rate
$\dot{\varepsilon}$	Strain rate
$\dot{\varepsilon}_0$	Reference quasi-static strain rate
$\zeta$	Damping ratio
$\theta$	Rotation
$\theta_A$	Rotation normalisation factor for catenary action
$\theta_{beam}$	Beam rotation
$\theta_{chord}$	Chord rotation
$\theta_{column}$	Column rotation
$\theta_{connection}$	Connection rotation
$\theta_p$	Rotation normalisation factor for flexure
$\theta_{p+A}$	Rotation normalisation factor for flexure and catenary action
$\theta_{u,P.C.}$	Post cyclic action ultimate joint rotation capacity
$\theta_{u,I.U.}$	Ultimate rotation capacity for the initially undamaged joint
$\mu$	Average value
$\nu$	Poisson coefficient
$\sigma$	Standard deviation
$\sigma_{dyn}$	Dynamic strength
$\sigma_{eng}$	Engineering stress
$\sigma_{eq}$	Von Mises equivalent stress



$\sigma_H$	<i>Hydrostatic pressure stress</i>
$\bar{\sigma}_{Norm}$	<i>True stress normalised to Criterion 1</i>
$\sigma_{Residual}$	<i>Residual stress</i>
$\bar{\sigma}_{Stat}$	<i>Quasi-static strength</i>
$\sigma_{True}$	<i>True stress</i>
$\phi$	<i>Beam rotation</i>
$\phi_{CM/C}/\phi_{CN}$	<i>Ratio of reduction of rotational demand due to claddings</i>
$\phi_{j,avail col.loss}$	<i>Available joint rotation capacity</i>
$\phi_{j,req col.loss}$	<i>Required joint rotation capacity under column loss action</i>
$\phi_{max,PS}$	<i>Maximum post seismic joint chord rotational demand under column loss action</i>
$\phi_{IU}$	<i>Maximum joint chord rotational demand under column loss action for the initially undamaged scenario</i>
$\psi$	<i>Live load combination factor</i>
$\psi_1 Q_k$	<i>Frequent value of the variable action Q</i>
$\psi_2 Q_k$	<i>Quasi permanent value of the variable action Q</i>
$\omega$	<i>Angular velocity</i>

### Uppercase Greek letters

$\Delta$	<i>T-Stub displacement</i>
$\Delta_A$	<i>Beam elongation inducing beam section tensile yielding</i>
$\Delta_B$	<i>Bolt elongation for the T-Stub model</i>
$\Delta_p$	<i>Mid-span vertical displacement inducing beam section plastic bending moment</i>
$\Delta W$	<i>Energy balance</i>
$\Gamma\theta_u$	<i>Ultimate rotation ratio</i>
$\Gamma M_u$	<i>Ultimate bending strength ratio</i>
$\Phi$	<i>T-Stub plate rotation</i>
$\Omega$	<i>Margin of safety</i>

**Abbreviations**

ALARP	As Low As Reasonably Possible
ALA	Alternative Loadpath Analysis
ALM	Alternative Loadpath Method
CBF	Concentrically Braced Frame
CC	Consequence Class
CFS	Cold Formed Steel
CoV	Coefficient of Variation
CPS	Civil Protection Service
CWP	Column Web Panel
DAZ	Directly Affected Zone
DCR	Demand-to-Capacity Ratio
DIF	Dynamic Increase Factor
DOF	Degree Of Freedom
EBF	Eccentrically Braced Frame
EC	Eurocode
FE	Finite Element
FEA	Finite Element Analysis
FEM	Finite Element Method
FEP	Flush End-Plate
GSA	General Services Administration (Guidelines)
IPB	Internal Primary Beam
ISB	Internal Secondary Beam
LIF	Load Increase Factor
LPS	Large Panel System
LSP	Linear Static Procedure
LVDT	Linear Variable Displacement Transducer
MRF	Moment resisting frame
NDP	Nonlinear Dynamic Procedure
NSP	Nonlinear Static Procedure
OLS	Ordinary Least Squares
PEEQ	Equivalent Plastic Strain

PGA	Peak Ground Acceleration
PPB	Perimeter Primary Beam
PPC	Proneness to Progressive Collapse
PRA	Preliminary Robustness Assessment
RI	Rupture Index
RIF	Residual Influence Factor
RSR	Residual Strength Ratio
SDOF	Single Degree Of Freedom
SLS	Serviceability Limit State
SMCS	Stress Modified Critical Strain
SRSS	Square Root of Sum of Squares
UFC	United Facilities Criteria
ULS	Ultimate Limit State
US	United States (of America)



## Chapter 1 Introduction

### 1.1 Relevance and scope

The importance of steel structures in buildings has increased significantly in Europe and throughout the world in the last decades, owing to two combined beneficial aspects: i) the excellent mechanical properties of steel as a material, which combines slender lightweight elements with high levels of resistance, enabling to obtain structural elements of reduced dimensions but also large spans; ii) the construction process which is based on the assembly of standardized elements that are fabricated in shop, thus allowing for noticeable time and cost reductions when compared to other materials. In addition, such constructive procedures enable great control over the quality of the welding process used to interconnect elements. Concurrently, structures can be designed to be split into parts later to be assembled at the construction site by means of simple bolting, thus reducing significantly execution times and risks associated with construction procedures.

Given the particular mechanical characteristics of steel, it is often combined with other materials, from which result composite materials that take advantage of steel's good performance in tension, and associate it with other materials that present, for example, good performance under compression, thus creating a new range of composite materials that are well adjusted to different design requirements. Finally, steel is nearly 100% recyclable, rendering it one of the best structural materials when considering the reduction of environmental impacts.

Steel structures have been increasingly adopted in seismic areas throughout Europe, due to advances in research in the last decades that allowed for a better understanding of the behaviour of steel structures under seismic actions, taking

advantage of ductility and exploiting material non-linearity. Design codes presently aim to achieve economical design by exploiting the post elastic regime and dissipative behaviour, in which inelastic deformations can be accommodated under seismic action, by taking advantage of material ductility. As stated by Elghazouli (2009), this procedure is performed by assigning a structural behaviour factor that reduces the forces resulting from the elastic response spectra. The evaluation of the capacity of the structure is based on a predefined plastic mechanism, also designated as failure mode, while assuring that sufficient ductility is provided to the structure in plastic zones, and adopting overstrength factors in other regions, that must remain in the elastic domain.

The design of steel structures to resist seismic actions can be performed by adopting different structural frame systems, regarding their behaviour under seismic actions, namely moment resisting frame (MRF), concentrically braced frame (CBF) and eccentrically braced frame (EBF). The MRF, in particular, are designed according to the principle weak beam/strong column, as shown in Figure 1.1, by which the structure resists lateral actions by forming plastic hinges in the beams, rather than in the columns, providing a favourable performance in terms of deformation and second order effects, characterized by high levels of ductility.

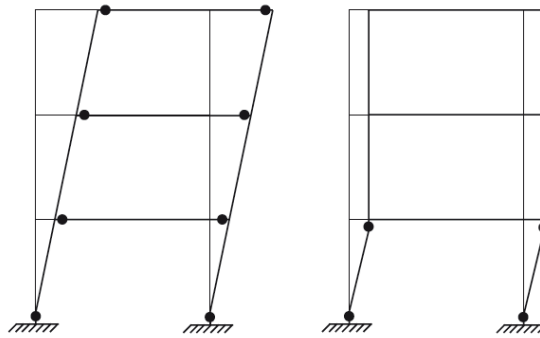


Figure 1.1: Moment Resisting Frame - weak beam/strong column and weak column/strong beam behaviour

Due to its simplicity of construction, good integration with building architecture and functionality, well known structural behaviour and reduced economical costs, the MRF structure typology is often adopted in zones of moderate/high seismicity for low/medium rise buildings.

On May 16th 1968, the lighting of a match sparked a gas explosion on the 18th floor of a 22-story tower block located in the east London area and known as Ronan Point tower. This explosion blew out the load bearing flank walls and removed the vertical support for the four floors above, causing a partial structural collapse. This event triggered the first ever introduction in regulations of disproportionate collapse preventive measures, which have since then undergone some revision and evolution in Europe.

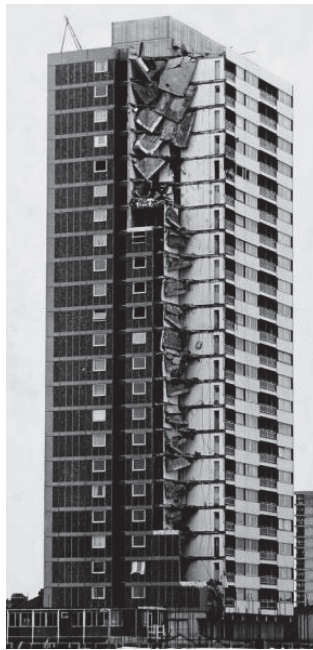


Figure 1.2: Ronan Point Tower partial collapse

Since the Ronan Point Tower partial collapse in 1968 (see Figure 1.2), several other case studies such as the collapse of the skywalks of the Kansas City Hyatt Regency Hotel in 1981 (see Figure 1.3a)), the L’Ambiance Plaza collapse in 1987 (see Figure 1.3b)), the Alfred P. Murrah Federal Building collapse in 1995 (see Figure 1.3c)) or the Jackson Landing Skating Rink collapse in 1996 (see Figure 1.3d)) have put in evidence how aspects such as the lack of structural integrity (Ronan Point), the inexistence of structural redundancy (Hyatt Hotel), the insufficiency of slab reinforcement (L’Ambiance Plaza), the insufficient member resistance to withstand an alternate load path (Alfred Murrah Building) or the lack of horizontal bracing (Jackson Skating Rink) can lead to full structural collapses and loss of human life (National Institute of Standards and Technology, 2007). These case studies stress the importance of analysing structural robustness to prevent progressive collapses and have raised

questions regarding the adequacy of building regulations and of current knowledge of structural behaviour under extreme events (Canisius, Sorensen, & Baker, 2007).

In this sense, the research community is currently developing significant efforts to study the different aspects of structural robustness, in order to improve building regulations, aiming to reduce to ALARP levels the occurrence of progressive collapses. To that end, the study of full building structures accounting for the contribution of all structural members is fundamental to understanding how aspects such as the structural system, the behaviour of connections, non-structural member contribution or the presence of façade claddings can contribute to prevent progressive collapse.



Figure 1.3: Case studies of progressive collapse (National Institute of Standards and Technology, 2007): a) Kansas City Hyatt Regency Hotel; b) L'Amiance Plaza; c) Alfred P. Murrah Federal Building; d) Jackson Landing Skating Rink

The robustness of steel frames is currently evaluated, among other methods, by a standard analysis case involving instantaneous column loss, which serves to determine the capacity of structures to internally redistribute loads in new load paths and to arrest a progressive collapse. This method for assessing robustness was designed in order to be threat-independent, since column loss can arise from many different scenarios, such as car collision, gas explosion, fire or malicious intent.



To this sense, in the wake of an earthquake, scenarios of gas explosions or fire are extremely likely to occur, leading to situations where structures that have endured damage following an earthquake, may suffer a column loss due to fire or to an explosion near a column. Such structures, due to an existing damage level due to the seismic action, may be noticeably prone to progressive collapse.

This doctoral thesis thus aims at studying the residual post seismic structural robustness of moment resisting frame steel structures. The importance of this study relates to the fact that structural robustness is typically evaluated in undamaged structures, whereas in damaged structures, the levels of robustness may differ significantly from the starting levels. The evaluation of robustness in post seismic scenarios may prove crucial in the arrest of progressive collapse and may ultimately contribute to the safeguard of human lives in the face of rare catastrophic events. The study of robustness will be conducted considering column loss for both structures that have and that have not been designed to sustain seismic action, hence enabling to have a broader perspective on the assessment of existing structures, both recent and old. The conclusions extracted from this study are believed to present a significant contribution to the present state of knowledge regarding the robustness of damaged structures and the effectiveness of seismic detailing in the arresting of a progressive collapse. Concurrently, the contribution of other significant factors to seismic robustness will be evaluated, namely the contribution of the secondary “gravity” frame and non-structural façade cladding resistance under column loss. The role of beam-to-column joints, and in particular of full-strength joints and partial-strength flush end-plate joints will be analyzed and the contribution of the latter type in terms of stiffness and resistance to the structural response will be evaluated. For what concerns the contribution of claddings to stop the propagation of a progressive collapse, it has thus far been disregarded, but recent studies have indicated that its contribution may be decisive in the arresting of certain column loss scenarios.

## 1.2 Objectives

The main objective of this doctoral thesis is the study further to column loss of steel moment resisting frames, for both initially undamaged and post-seismic scenarios, considering the contributions of secondary “gravity” frame members and

non-structural façade claddings. The obtained results will enable to characterise structural response under different peripheral column loss scenarios and to determine whether moderate seismic actions introduce damage levels capable of reducing the building structure's resistance to progressive collapse. The data retrieved from the conducted Nonlinear Dynamic Analysis will also enable to quantify the maximum dynamic rotational demand on connections, as well as Demand-to-Capacity ratios for different structural components, hence allowing to quantify the proneness of different structural typologies to progressive collapse. The assessment of the effectiveness of the contribution of claddings to the arrest of a progressive collapse further to column loss is also an objective of the present study since these elements are typically disregarded. To this aim, the façade cladding panels are numerically modelled and calibrated to experimental results from literature, hence enabling to account for their contribution to progressive collapse arrest. The results obtained will also be evaluated aiming at proposing a design methodology and detailing rules based on structural performance, which may contribute to the future revision of the EN 1991-1-7 Annex A. The structural response further to a column loss, namely the degree of residual elasticity in the directly affected zone will serve as the base to establish a procedure for the intervention of the Civil Protection Services in cases of structures damaged by column loss.

Another very important objective of the present study is the characterisation of the response of secondary “gravity” frame joints to column loss action, in particular of bolted flush end-plate beam-column joints. To this end, a parametric numerical study based on calibrated models is conducted, in which joint response is analysed under column loss action and column loss following cyclic bending, so as to assess how resistance to column loss is affected by cyclic bending induced by seismic action. The conducted finite element simulations are aimed at determining how different connection parameters influence moment-rotation response, so as to potentially propose a viable design criterion to maximise resistance to column loss action. The investigation of the variation of the Dynamic Increase Factor with rotational demand under column loss action and the effect of the different connection parameters is also an important objective, since insufficient data is currently available regarding this topic for the flush end-plate joint typology.

### 1.3 Structure of the thesis

The present thesis describes the body of work conducted to investigate the topic of the post seismic robustness of MRF steel structures. To that end, an introduction to the investigated topics is initially presented in Chapter 1, so as to provide some background and brief indications regarding current design methods. The gap in knowledge pertaining to absence of studies on post-seismic robustness is identified and the the objectives of the research to be conducted are introduced.

Considering that the topics investigated in the scope of the present thesis encompass different aspects of structural mechanics, ranging from the micro level (e.g. bolt assembly cyclic inelastic response; flush end-plate joint response to column loss action) to the macro level (e.g. structural response to column loss; seismic response of moment frames), a literature review is presented in Chapter 2 so as to evaluate previous research conducted on topics relevant to the work to be developed. In particular, various aspects related to robustness codes and progressive collapse design methodologies, as well as experimental, numerical and analytical robustness studies are presented and discussed. In addition, considering that, on the one hand, the contribution of secondary frame beam-column joints is considered for the robustness assessment and that, on the other hand, the flush end-plate (FEP) joint typology is widely adopted for secondary frame connections (for which reason it was considered for the present study), an evaluation of conducted research on the behaviour of FEP joints was found to be essential. Furthermore, some background information pertaining to claddings is provided, highlighting the potential importance of the contribution of these non-structural elements to system robustness.

The description of the set of MRF structures to be analysed in the robustness assessment is subsequently presented in Chapter 3, in which the parametric variables and analysis cases are defined, as well as the design procedure and all relevant design assumptions, namely concerning actions and finite element modelling.

Successively, a preliminary robustness assessment is conducted, in order to provide an initial “picture” of the resistance to progressive collapse of the selected set of frames. Considering that different analysis techniques are used here, the collected data will serve as a baseline/benchmark for the detailed robustness assessment and

also to identify subsets of frames with lower robustness. The preliminary robustness assessment is described in Chapter 4.

From this point, the present thesis builds on from the detailed study of micro level components, namely bolt assemblies, to beam-to-column joints and ultimately to the macro level of the full MRF structure. To this end, the behaviour of preloadable bolt assemblies under cyclic tensile action in the inelastic range is investigated through experimental tests, as described in Chapter 5. The obtained results provide the base for developing accurate modelling criteria for bolt components under monotonic and cyclic actions, which may influence joint performance under column loss action.

Subsequently, the developed bolt modelling criteria are incorporated into the development of finite element models of flush end-plate (FEP) beam-to-column joints, which is the adopted typology for the connections of the secondary “gravity” frame. Simulations are carried out, as described in Chapter 6, under column loss action and under cyclic bending followed by column loss action, in order to determine the influence of key connection parameters on joint moment-rotation response.

Finally, the moment-rotation results from the FEP joint study are used to calibrate nonlinear springs to simulate secondary “gravity” frame beam-to-column joint response under cyclic bending and column loss action. The panel infill type elements used to numerically model the façade claddings are calibrated to experimental results from literature. These modelling assumptions/procedures, as well as the detailed description of the analysis methodology for the detailed robustness assessment for both initially undamaged and post-seismic scenarios is presented in Chapter 7. The obtained results are presented and consequences for design for progressive collapse are discussed. In particular, design guidelines and special requirements are also proposed to enhance the robustness of steel buildings on the basis of the structure’s proneness to progressive collapse.

The general conclusions and future research perspectives are presented in Chapter 8.

## Chapter 2 Literature review

### 2.1 Introduction

In this chapter a literature review on topics that are relevant to the development of the work presented in this thesis is presented.

The historical context leading to the early development of design rules for avoiding disproportionate collapse is presented, along with the subsequent evolution of robustness codes and design requirements in Europe and in the U.S.A. A discussion of the design approaches is presented, as well as a description of different methodologies for quantifying the probability of a progressive collapse and structural robustness.

The evaluation of the state-of-the-art concerning structural robustness was conducted and several important experimental, analytical and numerical robustness studies are presented, highlighting different factors that influence connection or system resistance to progressive collapse. These studies provided an important contribution to determine the analysis methodologies for the work developed in the present study.

A section of this chapter is dedicated to the topic of the behaviour of flush end-plate joints, given that this joint typology was selected for the connections of the secondary “gravity” frame, hence constituting a key aspect of the research conducted in this thesis. In this sense, the joint modelling approach designated as the Components Method which is described in EN 1993-1-8 (CEN, 2005) is presented and limitations to its application to the case of joints under column loss action are discussed in light of results from experimental and numerical studies from literature. The evaluation of available studies on FEP joint behaviour has enabled to identify a gap in knowledge concerning joint response under column loss action. The experimental data results on

FEP joints collected in this literature review serves as basis for calibrating numerical finite element models, as well as to identify typical joint failure modes.

Considering that the influence of the claddings on frame robustness is one of the objectives of the present thesis, some studies on this topic are also referenced in this chapter, highlighting the potential of these non-structural to contribute to progressive collapse arrest.

## **2.2 Robustness codes and design approaches**

The introduction of disproportionate collapse preventive measures in regulations began after an incident involving the partial collapse of a 22-storey tower block located in the east London area and known as Ronan Point tower. The Ronan Point tower was part of a wave of cheap, affordable pre-fabricated houses built in the 60's, which employed a structural system called Large Panel System building (or LPS). The system was based on the prefabrication of large concrete structural panels cast off-site, later to be lifted into position with a crane and joined together by means of on-site bolting. Construction started in 1966 and was completed in 1968.

On May 16th 1968, the lighting of a match sparked a gas explosion on the 18th floor, which blew out the load bearing flank walls, removing the vertical support for the four floors above. Because the LPS building system relied significantly on gravity's contribution to the global building stability, it is believed that the joints that tied the vertical walls to the floor slabs were the main structural weakness, eventually causing the progressive collapse of the whole south-east corner of the building.

In the wake of the Ronan Point collapse, UK authorities made major changes to building regulations in order to introduce design rules to prevent the disproportionate collapse situations (Centre for the Protection of National Infrastructure, 2011). The changes to regulations were first introduced in 1970 for England and Wales through the 5th Amendment to the Building Regulations 1970, commonly referred to as "fifth amendment", although separate rules were also in existence for the Greater London area. Since 1985, the tolerability of risk has been defined through the Approved Document A of the UK Building Regulations. The 5th Amendment of each edition of the Approved Document A contained rules regarding the design for disproportionate collapse.

The following text is intended to describe the evolution of regulations and design recommendations in Europe, regarding design against disproportionate collapse, and to synthesize this information, so that such evolution can easily be understood.

### ***2.2.1 Comparative analysis of design approaches and detailing requirements for structural robustness***

Some evolution took place in terms of regulations and codes in order to provide structural engineers with design methods that would introduce some level of robustness in building design, enabling the structure to sustain localised failure without the occurrence of a disproportionate collapse. The data presented in Table 2.1 summarizes the evolution that took place in terms of code robustness requirements in Europe.

Through analysis of Table 2.1, it can be concluded that the basic design approach for robustness has not evolved much throughout the different regulations. A quick analysis shows that the main evolution was introduced through tying provisions and risk assessment. Several design methodologies have not been changed since the very first regulations, such as the provision for alternative loadpaths, the concept of limiting the damage extension in plan and vertically, and where this condition cannot be met, design the elements as “key elements” for a specific design load case in order to design by providing continuity between different structural elements. The evolution of code requirements in the US is presented in Table 2.2.

Table 2.1: Evolution of code robustness requirements in Europe

	Building Regulations 1970 5 <sup>th</sup> Amendment (The Building Regulations 1970 (S.I. 1970/109), 1970)	Building Regulations 1985 Approved Document A: 1985 edition (The Building Regulations 1985 (S.I. 1985/1065), 1985)	Building Regulations 1991 Approved Document A: 1992 edition (The Building Regulations 1991 (S.I. 1991/2580), 1991)	Building Regulations 2000 Approved Document A: 2004 edition incorporating 2004 amendments (The Building Regulations 2000 (S.I. 2000/2531), 2000)	Eurocode 1 Part 1-7 Annex A (CEN, 2006)
ALTERNATIVE LOADPATH	•	•	•	•	•
NOTIONAL ELEMENT REMOVAL	•	•	•	•	•
KEY ELEMENT DESIGN	• (34 kPa)	• (34 kPa)	• (34 kPa)	• (34 kPa)	• (34 kPa)
HORIZONTAL DAMAGE EXTENSION LIMIT	• (lesser of 15% storey area or 70 m <sup>2</sup> )	• (lesser of 15% storey area or 70 m <sup>2</sup> )	• (lesser of 15% storey area or 70 m <sup>2</sup> )	• (lesser of 15% storey area or 70 m <sup>2</sup> )	• (lesser of 15% storey area or 100 m <sup>2</sup> )
VERTICAL DAMAGE EXTENSION LIMIT	• (removed element storey + immediately adjacent storeys)	• (removed element storey + immediately adjacent storeys)	• (removed element storey + immediately adjacent storeys)	• (removed element storey + immediately adjacent storeys)	• (removed element storey + immediately adjacent storeys)
HORIZONTAL TYING	•	•	•	•	•
VERTICAL TYING			•	•	•
SYSTEMATIC RISK ASSESSMENT				•	•
BUILDING CLASSES				•	•
APPLICABILITY	Buildings of 5 or more storeys	Buildings of 5 or more storeys and public buildings with spans exceeding 9m	Buildings of 5 or more storeys and public buildings with spans exceeding 9m	All buildings	All buildings



Table 2.2: Evolution of code robustness requirements in the U.S.

	ASCE-7 (Structural Engineering Institute, 1998)	New York City Building Code (New York City Department of Buildings, 2003)	GSA Progressive Collapse Analysis and Design Guidelines: 2003 (U.S. General Services Administration, 2003)	Unified Facilities Criteria UFC 4-023- 03: July 2005 (United States of America Department of Defense, 2005)	Unified Facilities Criteria UFC 4-023- 03: July 2009 with change 1 (United States of America Department of Defense, 2009)
ALTERNATIVE LOADPATH	•	•	•	•	•
NOTIONAL ELEMENT REMOVAL	•	•	•	•	•
KEY ELEMENT DESIGN	• (36 kPa)	• (36 kPa)		• (Ductility requirements)	• (Ductility requirements)
HORIZONTAL DAMAGE EXTENSION LIMIT		• (lesser of 20% floor area or 100 m <sup>2</sup> )	• (smaller of adjacent bays' area and 180 m <sup>2</sup> for edge columns and 360 m <sup>2</sup> for interior columns)	• (lesser of 15% floor area or 70 m <sup>2</sup> for perimeter column and lesser of 30% floor area or 140 m <sup>2</sup> for interior column )	• (no failure of floors)
VERTICAL DAMAGE EXTENSION LIMIT		• (3 storeys)	• (failure only on the floor directly above the removed element)	• (no failure of floor beneath the removed element)	• (no failure of floors)
HORIZONTAL TYING	•	•		•	•
VERTICAL TYING	•	•		•	•
SYSTEMATIC RISK ASSESSMENT					•
BUILDING CLASSES / BUILDING RISK CLASSIFICATION			•	•	•
CONSIDERATION FOR DYNAMIC EFFECTS			•	•	•
PROVISIONS FOR DUCTILITY IN CONNECTIONS			•	•	•
APPLICABILITY	All buildings	All buildings	All buildings	All buildings	All buildings

Through analysis of Table 2.2, it can be concluded that the evolution of robustness requirements for buildings wasn't as "linear" as in the European case. In the US case, different regulations were established by different institutions, and the event of modern era terrorist strikes such as the attack on the World Trade Centre towers precipitated the evolution of robustness requirements in buildings.

Several concepts and methodologies remain similar to the ones adopted originally in European regulations. However, there has been some considerable evolution and improvement in robustness requirements. A comparison can be made between the most relevant regulations for Europe and US, concerning the subject of structural robustness as presented in Table 2.3.

Table 2.3: Comparison between state-of-the-art code robustness requirements in Europe and in the U.S.

	Eurocode 1 Part 1-7 Annex A (CEN, 2006)	Unified Facilities Criteria UFC 4-023- 03: July 2009 with change 1 (United States of America Department of Defense, 2009)
ALTERNATIVE LOADPATH	•	•
NOTIONAL ELEMENT REMOVAL	•	•
KEY ELEMENT DESIGN	• (34 kPa)	• (Ductility requirements)
HORIZONTAL DAMAGE EXTENSION LIMIT	• (lesser of 15% storey area or 100 m <sup>2</sup> )	• (no failure of floors)
VERTICAL DAMAGE EXTENSION LIMIT	• (removed element storey + immediately adjacent storeys)	• (no failure of floors)
HORIZONTAL TYING	•	•
VERTICAL TYING	•	•
SYSTEMATIC RISK ASSESSMENT	•	•
BUILDING CLASSES / BUILDING RISK CLASSIFICATION	•	•
CONSIDERATION FOR DYNAMIC EFFECTS		•
PROVISIONS FOR DUCTILITY IN CONNECTIONS		•
APPLICABILITY	All buildings	All buildings

Both the Eurocode 1 (EC1) (CEN, 2006) and the United Facilities Criteria (UFC) 2009 (United States of America Department of Defense, 2009) use a building categorization system, based on building collapse consequences, as a way to assess the

building's tolerable risk of structural collapse. The EC1 takes into account risk factors such as number of storeys, building occupancy and building usage, for the definition of the building's consequence class, which is then used to define the recommended strategies to provide an acceptable level of robustness. It also uses four consequence classes, namely, classes 1, 2a, 2b and 3, relating to low, medium and high consequence classes. The UFC uses a building categorization system based on five occupancy categories, I through V, taking into account risk factors such as building occupancy, building function and criticality and economic asset value. Similarly to the EC1, the occupancy category determines the design requirements for robustness. For the EC1 consequence class 3, a systematic risk assessment is required, taking into account both foreseeable and unforeseeable hazards. Further guidance for this analysis is given in the Annex B of the same document, which describes the general framework for the risk analysis. Complementary information on the modelling of events such as vehicle impact, ship impact and internal explosions is also given in Annexes B through D.

The UFC considers that *'due to the limited database of progressive collapse events (from deliberate attack, vehicle impact, natural causes, etc), it is not possible to reasonably assess the probability of occurrence for a specific hazard or group of hazards. Therefore, the risk assessment reduces to a consideration of consequences...'*. For this reason, the UFC's preferred approach for risk assessment is the categorization through occupancy categories which translate indirectly the consequences of a collapse. However, when a quality assurance plan for progressive collapse is required, for occupancy category IV, the UFC mentions that the building requires that the design be based on the results of a systematic risk assessment, but provides no further information on how to perform this analysis.

The Alternative Loadpath Method remains still one of the best ways to introduce robustness in a structure, assuring that the loss of a single loadbearing element does not cause a disproportionate collapse, and for this reason, this methodology is adopted in both regulations. The EC1 states only that *'the building should be checked to ensure that upon the notional removal of each supporting column...the building remains stable and that any local damage does not exceed a certain limit'*, with no further definition of the analysis methodology and no specification of the limit for local damage being provided. The UFC establishes a comprehensive methodology based on the concepts of Force-controlled action and Deformation-controlled action, followed by

the determination of the m-factors for each component of the structure, and subsequent determination of the lowest m-factor value, which will then be factored to calculate the Load Increase Factor or Dynamic Increase Factors to be used in the analysis of the whole structure. The consideration for the dynamic effects in the UFC is made, either through factoring of load applied in the directly affected zone by a LIF or a DIF, for linear and nonlinear static analysis respectively or implicitly in the nonlinear dynamic procedure.

As to provisions for ductility in connections, the UFC provides an inventory of common connection types in building structures and corresponding allowable m-factor values, which will lead to the determination of the LIF/DIF. This enables the designer to choose or adjust the type of structural connections, in order to obtain a certain value for the LIF/DIF which will lead to a more or less dissipative structural behaviour. The EC1 does not provide any indication for consideration of dynamic effects or any provisions for ductility in connections.

Both regulations use vertical and horizontal tying requirements, as a means to supply the structures with minimum robustness levels, although using different expressions for the calculation of tie forces. These differences will be further studied in this document.

Damage extension limits are also indicated in both codes, even though they differ substantially in terms of base philosophy. For the EC1, the logic of compartmentalization still subsists from the time of the first regulations as the preferred approach, whereas in the UFC a new approach has been taken, which moves away from the compartmentalization approach, and is based on the premise of the non-collapse of floors. According to the UFC, *'no damage to the floor is allowed... as the floor system, beams, and girders in the bays directly above the removed column can be designed to not fail, as is done for the bays in the floors above the removed column location'*.

In terms of Key Element Design, the EC1 prescribes the use of the value for the accidental design loading pressure of 34 kPa, first introduced in the Building Regulations 1970, which is to be applied in any direction to members or attached components. This remains a simple methodology to ensure a certain degree of continuity between structural elements. The UFC prescribes that certain key or critical elements must be designed for specific loads, according to an indirect design approach named Enhanced Local Resistance. This is intended to provide a certain level of

protection for perimeter columns, by increasing the flexural resistance of columns by a given factor, as well as increasing the shear capacity of the columns and connections, in order to guarantee that the shear capacity is greater than the flexural capacity, in order to ensure that the failure mode will be ductile.

Out of all the European and US regulations analysed, the conclusion can be drawn that the Unified Facilities Criteria UFC 4-023-03: July 2009 with change 1 presents the most complete set of procedures aimed at reducing the potential of progressive collapse in structures.

## **2.3 Discussion on design concepts**

### ***2.3.1 Building risk classification***

The different perceptions of the acceptability of risk by individuals and decision-makers, gives way to different perspectives on how available resources should be spent in order to reduce risk. In general the former are risk-averse, while the latter are risk-neutral. Individuals' acceptance of risk is considered to be based mostly on the perception of risk, rather than on the probability of occurrence. The definition of the required approaches for robustness design needs therefore to take into account public perception of risk and tolerability of collapse.

The building regulations have translated these concerns through a classification system that categorises structures, by taking into account risk factors such as occupancy level or structure type and use. Its usefulness and purpose is to adequately balance the requirements for public safety with the respective costs. Typically, the attribution of a building risk category takes into account different risk factors such as population at risk, building occupancy type, evacuation time, building purpose, type of construction, structural protective measures, building age and state of conservation. In general, the classification systems implicitly account for these factors. In European regulations, building risk classes were only introduced in The Building Regulations 2000, through a 4 class system, comprising classes 1, 2A, 2B and 3, where Class 1 was a low risk class that did not imply the adoption of robustness requirements, Classes 2A and 2B represented respectively medium-low and medium-high risk buildings, and Class 3 high risk buildings, for which systematic risk analysis was required.

The Eurocode 1 Part 1-7 Annex A (CEN, 2006), minor amendments aside, maintained the category system proposed in The Building Regulations 2000. In this system, the classification of a given structure is heavily dependent on number of storeys, building type and occupancy. As for the US regulations, building risk classification was adopted also as a way of defining appropriate robustness prescriptions for different types of structures, and is present in such regulations as the GSA guidelines of 2003 (U.S. General Services Administration, 2003) or the 2005 (United States of America Department of Defense, 2005) and 2009 (United States of America Department of Defense, 2009) versions of the UFC. In the case of the 2009 version of the UFC, the tolerability of risk is expressed through five different Occupancy Categories, which depend mostly on occupancy and building function.

Unlike the Eurocode 1, the classification system of the UFC 2009 does not depend on the number of storeys or specific considerations regarding the dimensions of the building, but incorporates however economic loss as a factor, which will likely be an important factor for risk-neutral decision makers. If considering for example a 10 storey residential building, to which, according to the EC1, would correspond Consequence Class 2b, consistent with medium-high level of consequences, the robustness design requirements would include either horizontal tying, vertical tying and effective anchoring of suspended floors to walls, or, alternatively, checking for structural stability under notional removal of load-bearing elements. In this case, for the first set of robustness design requirements, no quantitative assessment is truly made to assure that a progressive collapse can be arrested, and so, if a collapse does occur, its consequences can therefore be dependent on the number of floors affected by the collapse. In this sense, the EC1's factoring of the number of storeys of the building into the classification of a building seems to take into account this fact, despite that, for medium-high risk structures, alternative loadpath analysis and design should not be an optional design approach.

The factoring of the number of storeys can always be considered as a safe side approach, in the sense that, for higher buildings, the design requirements for robustness are greater than for lower ones, since the assurance that the structure can withstand notional element removal, does not imply that it shall necessarily avert a disproportionate collapse when faced with any given initiating event. By introducing more robustness requirements through classifying the structure in a higher

consequence class due to a higher number of storeys, more robustness is introduced into the structural system.

For the structures with high risk and high consequences, the EC1 maintained the approach first set out on The Building Regulations 2000, thus requiring systematic risk analysis to account for both foreseeable and unforeseeable hazards. Risk analysis provides the building owner with an extremely powerful tool for informed decision-taking about key aspects of building design, that go from defining the frequency of building maintenance, to basic definition of the structural system type. Such decisions can largely influence the robustness performance of the global building structure and may enable to adequately optimize the robustness performance, taking both into account owner's requirements and minimum requirements, defined by public authorities. Although some general guidance for risk analysis is provided in Annex B of the Eurocode 1 Part 1-7, it is basically oriented towards calculating risk for decision making, thus not providing much guidance in terms of defining an event tree and assigning probabilities to the occurrence of both foreseeable and unforeseeable extreme events, which would enable robustness quantification.

Because the exhaustive definition of an event tree associated to a meaningful assignment of probabilities to each event is the only way to properly take advantage of such a powerful tool of analysis, its implementation remains currently largely impractical for structural design, therefore requiring the event tree definition to be simplified, rendering the analysis less accurate.

Although both classification systems account for economic loss associated to building collapse, the EC1 does not mention this explicitly, but implicitly instead through examples of building types given for each consequence class. For decision makers, that are typically risk-neutral, a quantitative evaluation of the economic loss associated with collapse could prove to be of value for decision making.

Despite the fact that the UFC and the EC1 target different types of buildings, in the sense that the UFC is intended to provide design criteria for military projects, whereas the Eurocode 1 is mainly directed at civilian projects, the introduction of a quantitative economic factor to the building categorization can surely provide a better basis for supported decision making, regardless of the obvious advantages of having a simple classification system, as the one adopted in the case of both the UFC and the EC1. The specification of a quantitative type method for building risk classification

could complement the existing classification system, namely in cases where, due to a given structure's particularities, its classification proves to be difficult.

### 2.3.2 Tie force method

The Tie Force Method is one of the three currently employed methods and is prescribed in regulations as a way of introducing a certain level of robustness in structures. The method was originally introduced in regulations as a direct response to the Ronan Point collapse, which was induced by a gas explosion originating inside the building. The typical layout of the different types of ties is present schematically in Figure 2.1.

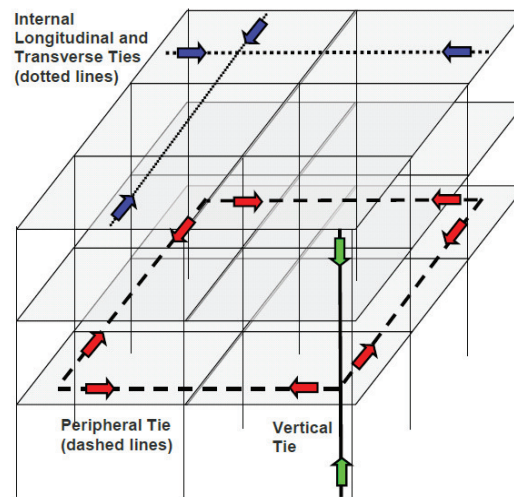


Figure 2.1 Tie forces in a framed structure

Horizontal tying is considered to allow the floors to carry loads to undamaged zones of the structure through large displacement membrane or catenary action, enabling the establishment of alternative load paths. The vertical tying requirements serve to provide mechanical continuity between structural elements, for cases of possible load reversal caused by explosions, which exert vertical upwards directed pressure upon the slabs. This method ensures a minimum level of continuity between structural elements, and is therefore particularly well suited for explosion type accidental loads, despite the fact that the introduction of continuity can also lead to counterproductive results, when it comes to introducing robustness into a structure. This occurs in cases where the structural elements adjacent to the directly affected zone do not present sufficient resistance to support the load increase in the alternative load



path. There is, nevertheless, a general consensus on the fact that tying requirements contribute to increase the levels of robustness in structures.

The main limitations of the Tie Force Method are related to the non-quantifiable increase in robustness, the counterproductive effect on structural robustness if adjacent elements to the directly affected zone are not capable of resisting the new internal force distribution and the fact that, in general, connections do not present sufficient rotation capacity for members to develop membrane/catenary action. Because this methodology does not take into account the initial robustness of structures, or the attained levels after the introduction of the ties, it appears to be more suited for low risk structures as a prescriptive measure, rather than for high risk ones, that require deterministic quantifiable methodologies, to deal with specific loads or events.

The strategy of ensuring mechanical continuity between members as a standalone measure presents disadvantages for structural robustness, in the sense that if the adjacent members to the directly affected zone cannot be proven to withstand the new internal force distribution subsequent to member loss, the mechanical continuity can lead to reducing the levels of structural robustness.

Tie force provisions, in general, provide a positive contribution for structural robustness, but its advantages are best exploited when alternative loadpath analysis is also performed, in order to ascertain adjacent member resistance. This prevents the occurrence of a “drag effect”, by which a local damage or collapse “drags” the rest of the structure into a global collapse, which corresponds to the very definition of a disproportionate collapse. In cases where the alternative loadpath analysis is not performed, a compartmentalization strategy could serve to better limit the extension of the local collapse.

The calculation of the design tying forces according to the latest applicable regulations depends on the dead and live loads acting on the floors and on the span and its calculation is straightforward.

The UFC 2009 (United States of America Department of Defense, 2009) presents, for Occupancy Class II, which is deemed to not present substantial hazard to human life or significant economic loss, a design strategy that considers alternatively tie forces or alternative path method, but not simultaneously. This approach is consistent with the fact that the adoption of Tie Force requirements as a standalone measure to

introduce a minimum level of robustness in a structure is clearly best suited for low risk structures.

As for the EC 1-1-7 (CEN, 2006), even for the upper medium risk class such as Consequence Class 2b, the design for robustness can be made through tying methods, or alternatively, through alternative loadpath methods, despite the fact that the former is prescriptive and the latter is a quantitative method. A negative side to these prescriptions is that these design approaches do not lead to the same level of structural robustness. This approach does not seem as consistent as the UFC's, in the sense that it allows tie force requirements as a standalone requirement for structures with relatively high risk to human life or economic loss. The UFC's approach appears thus to better tackle the weak points of the Tie-Force methodology, by taking advantage of the non-quantifiable increase in robustness that is guaranteed through mechanical continuity between members, while assuring through alternative loadpath analysis, that the remaining structural members have sufficient resistance under the new internal force distribution.

A comparison between different codes in terms of internal and peripheral horizontal design tie forces is presented in Table 2.4 and it is easily perceivable that there is great disparity between values for floor loads and for design tie forces.

Table 2.4: Comparison between horizontal design tie forces for interior and peripheral ties according to different codes

CODE	Internal tie design force $T_i$ (kN/m, unless stated)	Peripheral tie design force $T_p$ (kN/m, unless stated)	Floor load $p$ (kN/m <sup>2</sup> )
Eurocode 1 Part 1-7 Annex A (framed structures)	$T_i = \max\{0.8pL; 75kN\}$	$T_p = \max\{0.4pL; 75kN\}$	$p = DL + \psi LL$
BS 5905-1 (2000)	$T_i = \max\{0.5pL; 75kN\}$	$T_p = \max\{0.25pL; 37.5kN\}$	$p = 1.4DL + 1.6LL$
Unified Facilities Criteria UFC 4- 023-03: July 2009	$T_i = 3pL$	$T_p = 6pL$	$p = 1.2DL + 0.5LL$
Unified Facilities Criteria UFC 4- 023-03: January 2005	$T_i = \max\{0.5pL; 75kN\}$	$T_p = \max\{0.25pL; 37.5kN\}$	$p = 1.2DL + 1.6LL$

L - Greater of the distances between the centres of columns, frames or walls;  
DL - Dead load in kN/m<sup>2</sup>;  
LL - Live load in kN/m<sup>2</sup>;  
 $\Psi$  - Live load factor which depends upon the considered type of accidental action.

The fact that the required tie forces to develop catenary action greatly depend on the type of material and type of construction, alongside the fact that tie forces are a prescriptive method that cannot translate into a quantifiable increase in robustness explains partially the variability in the design tie forces. In order to illustrate the difference between tying requirements, an example is given in Figure 2.2.

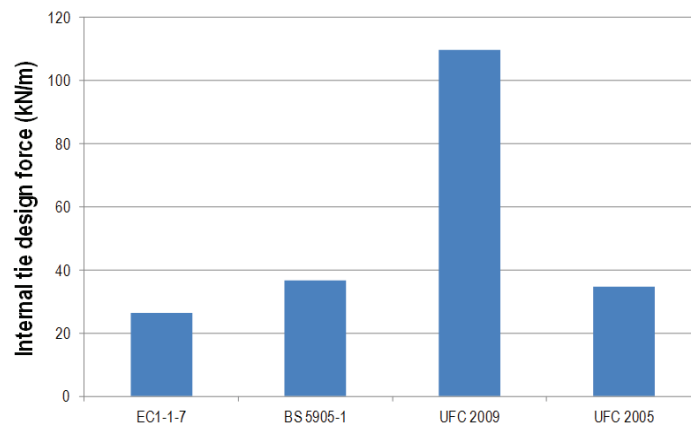


Figure 2.2: Internal horizontal tie design forces (for  $L=6\text{m}$ ,  $DL=3\text{kN/m}^2$  and  $LL=1\text{kN/m}^2$ ) according to different codes

The fact that the UFC 2009 requires internal tie design forces of about triple the values prescribed in other regulations relates to the fact that, as stated in the UFC 2009, *“Finite element analyses were also performed to determine the dynamic effects created by the sudden loss of column support; the results of these analyses were used to modify the Tie Force equations”*. In addition, the UFC 2009 assumes a new conceptual approach regarding tie forces, namely that *“one goal of the revised Tie Force approach is to remove the Tie Forces from the flexural members, which typically are not capable of sustaining the large amount of deformation associated with catenary and diaphragm action”*.

As for vertical design tie forces, all analysed codes require that the vertical ties must be capable of resisting a tensile force equal to the largest vertical load received from any one storey, using the appropriate tributary area and floor load.

### 2.3.3 Tolerable area at risk of collapse

The concept of imposing limits on the tolerable area at risk of collapse has served as a way to compartmentalize the damages from structural collapse, and therefore to indirectly limit the risk of loss of human life. This approach is directly related to the concept of disproportionality of collapse in the sense that a collapse is

deemed disproportional when the occurrence of a local damage spreads from element to element, resulting in the collapse of a disproportionately large part of the structure.

The typically adopted approach involving tolerable area at risk of collapse is based on the limitation of the areas of the bays affected by the notional removal of a single load bearing element, and on the assumption that the collapse does not extend further than the immediately adjacent storeys. Another compartmentalization strategy that could also be pursued differs from the ones currently adopted in regulations, by dividing the structure into independent structural systems, acting as “structural fuses” that could stop collapse from spreading to other bays and zones of the structure. In each independent structural zone, the design and structural detailing could take into account robustness requirements to provide for ways to arrest a progressive collapse. The “structural fuse system” acts through fuse planes and can be an efficient design procedure for simultaneously large and low buildings, where the consequences of a collapse involving the full height of the building are far smaller than in the case of a tall building. Despite the fact that the currently preferred approach assumed in the state-of-the-art regulations is oriented towards arresting a collapse, rather than concentrating on limiting its extension, this approach poses nevertheless as a simple alternative design methodology for attaining robustness in low and large buildings, with relatively low occupancy and economic value.

In the latest decades, the fast development of the construction materials, constructive technologies and structural analysis software has led to a clear tendency towards the increase of structural spans, through the use of lightweight structures combined with high strength materials. This has had a reflexion in terms of code prescriptions for tolerable areas at risk of collapse, in the sense that the latest regulations have displayed a tendency to augment these limits, so as to keep in line with currently adopted values for spans in buildings. A comparison between tolerable areas at risk according to different codes is presented in Table 2.5.

In terms of European regulations, the EC1 is the first to increase the limit from 70 m<sup>2</sup> to 100 m<sup>2</sup>, which was justified for the reason stated above, whereas the latest US regulation has assumed a clearly more conservative hypothesis, that does not allow for floors to collapse. Assuming the base hypothesis that the notional removal of a single loadbearing element affects only the immediately adjacent bays, and that the collapse does not extend further than those bays, this implies that for a peripheral column, the

damages are limited to two bays, whereas the loss of an interior column implies that four adjacent bays shall be affected. In the case of buildings with constant spans in both directions, the area at risk for a peripheral column is double the one for an internal column, which justifies the adoption of two separate limits for peripheral and interior columns.

Table 2.5: Comparison between tolerable areas at risk of collapse according to different codes

CODE	Tolerable area at risk of collapse for interior column (m <sup>2</sup> )	Tolerable area at risk of collapse for peripheral column (m <sup>2</sup> )
Eurocode 1 Part 1-7 Annex A	100m <sup>2</sup> or 15% of the floor area (whichever is smaller)	
BS 5905-1 (2000)	70m <sup>2</sup> or 15% of the floor area (whichever is smaller)	
Unified Facilities Criteria UFC 4-023-03: July 2009 with change 1	No damage to floors allowed	
Unified Facilities Criteria UFC 4-023-03: January 2005	140m <sup>2</sup> or 30% of the floor area (whichever is smaller)	70m <sup>2</sup> or 15% of the floor area (whichever is smaller)

The EC1 and the BS 5950-1 (British Standards Institution, 2000) adopted the one limit approach, whereas the UFC 2005 uses two separate values. By adopting the one limit value approach for both internal and peripheral columns, the loss of a peripheral column will not likely condition the design the definition of the area at risk, and therefore the two limit approach seems better adjusted for the definition of the limits for the areas at risk of collapse. As previously mentioned, the UFC 2009 does not allow for floor collapse since it states that *“the floor system, beams, and girders in the bays directly above the removed column can be designed not to fail, as is done in the bays in the floors above the removed column location”*. By not indicating any values for tolerable areas at risk and therefore allowing large spans, the UFC 2009 is more flexible in terms of column layout, but draws away from the formerly adopted philosophy for structural robustness, in the sense that there is no compartmentalization of damages.

Considering that the UFC 2009's methodology is aimed at arresting a progressive collapse and does not allow for floor collapse, the simultaneous imposition of limitations on the tolerable area at risk of collapse would represent a seemingly redundant and unnecessary safety measure. However, structural robustness can often be attained through redundancy, and in this case, because scenario independency is assumed for analysis through notional loadbearing element removal, it cannot explicitly account for all types of accidental events, but merely introduces a certain degree of robustness into the structural system.

The limitation of area at risk of collapse can pose as a redundant prescription according to the UFC 2009, but redundancy remains also a way to achieve robustness, and consequently, the adoption of this type of prescription can always be considered good engineering practice, in the sense that it is a safe-side measure. It is considered that in cases where the limits for areas at risk of collapse exceed the limit values, third party review of the structural design for robustness should be required, placing special emphasis on the revision of the detailing of the connections, splice zones and support condition for the elements that will resist the tie forces induced by membrane/catenary action. If the assumption of non-collapse of floors is made, then floors could be designed as primary or secondary elements, according to whether they are considered to transmit tie forces or not, but must in both cases be checked for their capacity to withstand the necessary displacements/rotations induced during the arrest of a collapse. By requiring third party review for structural solutions with larger spans and larger areas at risk, the design should become more onerous, in the sense that more time shall be required to complete the robustness analysis, which seems adequate for solutions that present higher risk. Conversely, by adopting simpler structural solutions with smaller spans and smaller areas at risk that are within the allowable limits, a more robust solution is achieved, and therefore less need for robustness analysis should be required, resulting in a faster and simpler design process, which is consistent with lower levels of risk.

An alternative design approach, which could comprise limits for areas at risk of collapse, while allowing alternatively the exceeding of these limits, only if independent third party review of the design is adopted, would allow for more flexibility in the design. In European regulations, before the Eurocodes, the limit value for the area at risk of collapse was of 70m<sup>2</sup>, which for the case of a peripheral column, implies

affecting only two structural bays with about 6m x 6m spans for example. The EC1 introduced a larger limit, by allowing up to 100m<sup>2</sup>, which for a peripheral column, represents roughly two bays of 7m x 7m spans. For the US regulations, the UFC 2005 presented two separate limits of 70m<sup>2</sup> and 140m<sup>2</sup> for peripheral and interior columns respectively, basically adopting the same values as those taken in European regulations before the EC1, but introducing two separate limit values. However, in the 2009 version of the same regulation, the concept of area at risk ceased to exist, in the sense that no floor collapse is allowed. GSA guidelines (U.S. General Services Administration, 2003), on the other hand, although having been published earlier, allow for bigger values of areas at risk, namely of 180m<sup>2</sup> and 360m<sup>2</sup> for peripheral and interior columns respectively, which roughly correspond to bays of 9.5m x 9.5m spans. These values allow for greater flexibility in the design and are more in line with contemporary span requirements for steel structures in buildings. In general, regulations have evolved in the sense of allowing for bigger areas at risk, to allow for some flexibility in the design of buildings. The differences are shown in Figure 2.3 for internal columns.

The imposing of strict limitations on the maximum areas at risk of collapse goes against the current trend of taking advantage of high resistance materials that allow for lighter structures and bigger spans. Although not being explicitly stated as such, according to the EC1 for example, the structural designer can currently choose to avoid designing with smaller spans to verify the condition of the maximum area at risk, simply by designing structural elements as key elements, and therefore complying with the required architectural constraints. This option can prove to be economic in terms of design, in the sense that it does not require retrofitting to the original design. Simply assuming from the start that certain elements shall be designed as key elements therefore may save significant design time. This tends to indicate that the currently adopted limit values in European regulation might require some further adjustment, to keep up with current construction constraints.

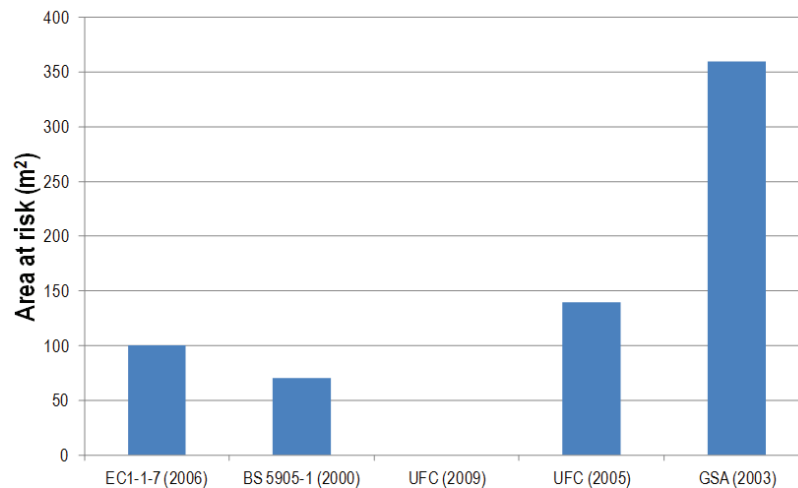


Figure 2.3: Area at risk of collapse for internal columns according to different codes

It should be noted however, that the key element approach was idealized in the aftermath of the Ronan Point collapse, which was caused by a gas explosion, meaning that this approach was mostly intended to provide a certain degree of continuity between structural elements. By simply providing continuity between elements, by designing for an accidental action characterized by a certain level of pressure applied in any direction, no analysis is performed on whether the collapse can be arrested or not, and thus, the risk of collapse and respective consequences are not truly mitigated, despite the fact that a certain degree of robustness might have been introduced into the structural system.

The key element approach does not therefore present a direct rapport with the concept of disproportionality of a collapse, and hence, when the structural layout is such that the maximum areas at risk of collapse are exceeded, alternative loadpath analysis should be required, alongside with independent third-party review, which would serve to demonstrate that the collapse can be arrested, therefore not endangering people and goods in a disproportional way. This can be particularly pertinent in the cases of certain types of structures, such as industrial buildings or large warehouse structures, which tend to be inherently non-robust structures, where the simple avoidance of the limits for areas at risk of collapse can be particularly problematic. By not going against the current trend of adopting light structural materials in large span structures, but simply adjusting to it through imposing alternative loadpath analysis in cases where the limits for areas at risk are exceeded,



the regulations could provide a better adjusted methodology to the structural design, while simultaneously assuring adequate performance in terms of robustness.

In terms of vertical damage extension limits, as shown in Table 2.1, the European regulations have systematically kept the same approach since the first introduction of provisions for avoidance of disproportionate collapse in The Building Regulations 1970, which limited the occurrence of failures to the floor of which the removed member forms part, plus the storeys directly above and below. As shown in Table 2.2, the US regulations have evolved in a different way towards progressively reducing the allowed vertical damage extension to the point of non-collapse of floors, which in order to be achieved requires alternative loadpath analysis. This is consistent with the fact that, when no limitations on the tolerable areas at risk of collapse are imposed, alternative loadpath analysis is required.

#### ***2.3.4 Key element design***

The key element methodology was introduced into regulations in the Building Regulations 1970 (The Building (Fifth Amendment) Regulations 1970 (S.I. 1970/109), 1970), as a response by authorities to the collapse of the Ronan Point tower building, which was triggered by a gas explosion. Because it was concluded that the collapse was partially due to the structural system, which presented little continuity between structural elements. The method's original intent was hence to provide for a prescriptive design methodology that would introduce minimum levels of robustness into the structures.

After its introduction, this methodology has not since evolved in European regulations, and the methodology is still simply limited to the requirement that structural elements be designed to be able to sustain an accidental design action, applied in horizontal and vertical directions, one direction at a time, to the member and any attached components. The recommended value for the action, according to the EN 1991-1-7 Annex A is of  $A_d=34$  kN/m<sup>2</sup>, which has also remained unchanged since the 1970's. In terms of the US regulations, the key element method, or specific local resistance method, according to US terminology was first implemented in the same way as in the UK. In 2003, the GSA guidelines introduced a methodology that did not include the key element approach, whereas later, in the 2005 and 2009 versions of the UFC, a new approach to the specific local resistance method was introduced. For the

2005 version of the UFC, the new approach, named Specific Local Resistance (SLR) and described in the chapter Additional Ductility Requirements, applicable for medium and high level risk categories, consisted in prescribing that the design of all the perimeter ground floor columns be such that the uniform lateral load that defines the shear capacity be greater than the load associated with the flexural capacity. In the 2009 version of the UFC, the SLR method, here named Enhanced Local Resistance (ELR), prescribes an increase in shear and flexural capacities of the peripheral ground and first floor columns, and the number of columns required to be designed according to ELR criteria are dependent upon the building's occupancy category.



Figure 2.4: Partial collapse of the Ronan Point tower

The Enhanced Local Resistance method consists of the following steps: i) determination of the baseline flexural resistance (i.e., the as-designed flexural resistance of the column); ii) checking that the connections are capable of withstanding the shear forces associated with the baseline flexural resistance; iii) checking that the connections between the columns and the lateral force resisting system can transmit the reactions associated with the baseline flexural resistance; iv) checking that the lateral force resisting system can resist the reactions associated with the baseline flexural resistance. For occupancy category IV, which presents the highest consequences associated to a collapse, the enhanced flexural resistance must be determined by performing the following steps: i) calculating the baseline flexural resistance considering the design of the structure when only gravity loads are

considered; ii) calculating the existing flexural resistance, using the design after performing the Alternate Path procedure, which already accounts for lateral loads; iii) calculating the enhanced flexural resistance as the larger of the existing flexural resistance and 2 times the baseline flexural resistance; iv) checking that the shear resistance of the column is greater than the shear capacity associated with the enhanced flexural resistance.

The requirements of the 2005 and 2009 versions of the UFC are thus aimed at insuring that the failure mode for the perimeter columns be ductile and in a flexural mode, as opposed to a brittle failure, typical of shear induced failure. It should be noted that for US regulations, namely the United Facilities Criteria, the Specific Local Resistance and the Enhanced Local Resistance methods are deemed as direct design approaches, whereas the Eurocode's approach can be better described as prescriptive design, and therefore, an indirect design method. According to the UFC 2009, the Enhanced Local Resistance procedure is not an alternative to the Alternate Path method for occupancy categories associated with substantial risk to human life or significant economic loss. The ELR can only be applied alternatively to Alternate Path method for buildings that present low hazard to human life.

Except for occupancy categories I and II, generally before applying the ELR method, the UFC states that the Alternate Path method must be first completed for all required elements, which implies that the structure possesses already the capacity to arrest a progressive collapse, therefore rendering the ELR as a simple method for guaranteeing that the column failure mode is ductile, hence providing supplementary protection to the structural elements and reducing the probability and extension of the initial damage.

A comparison can be made between the European and the US approaches, by comparing the respective most recent codes, namely the EN 1991-1-7 and the UFC 2009. According to the EC1, even for medium-high consequence classes, key element design can be performed without the previous structural design involving Alternative Loadpath Analysis. In these cases a quantitative analysis is not performed and only indirect design method is used, therefore not guaranteeing that the structure can arrest a progressive collapse. According to the UFC 2009, at the exception of situations involving low risk for human life, key element design can only be applied after Alternative Loadpath Analysis, which assures that the structure possesses adequate

resistance to disproportionate collapse. The US approach seems to present a better conjugation of the two methods, in the sense that for medium-high risk buildings, a quantitative analysis is mandatory, therefore assuring a priori that the collapse can be arrested, and rendering the key element method simply as a way to improve structural response to column loss.

As to scenario dependency of the key element design, the EC1 can be considered to be scenario dependant, since the 34kPa design accidental force was originally calibrated in the 1970's to the Ronan Point collapse and its value has since remained unchanged. The UFC 2009 key element design approach appears to focus more on accidental events with impact on vertical loadbearing elements located on the ground floor and first floor of the façades, which can be related to fire, vehicle collision or explosions. The UFC presents therefore some scenario dependency as well, since it concentrates on reinforcing specific parts of the structure, while not accounting directly, for example, for the case of an internal gas explosion.

The reinforcing of the peripheral columns' shear capacity to exceed the associated relevant flexural resistance can be regarded as good engineering design, since it renders the failure modes ductile and reduces the risk of a disproportionate collapse. A design methodology could incorporate, in addition to this criterion, the design for an accidental explosion, modelled by an equivalent static pressure, for all elements that exceed the maximum area at risk of collapse criteria, and that are therefore, by definition, key elements.

In general, the merits of the current key element method for the European approach lie in the fact that minimum levels of robustness are introduced into the structure, and for both European and US approaches, the application of the method is simple. In the case of low risk structures, key element design not accompanied by Alternative Loadpath Analysis can be a simple, adequate and efficient way of designing. However, the method also presents some disadvantages in its most recent versions, namely that for the European case, it is a non-quantitative method, that can be counterproductive in cases where the introduction of continuity is not accompanied by an Alternative Loadpath Analysis that assures that the local failure will not induce a global one, through a "drag effect" caused by the tying. In the current version of the EN 1991-1-7, even for consequence class 2b, corresponding to medium-high consequence levels, it is possible that an element that presents an associated area at risk

of collapse that exceeds the allowed maximum value can be solely designed as a key element, without performing an Alternative Loadpath Analysis. In this case, since the regulation allows key element design as an alternative to Alternative Loadpath Analysis, it is natural that for reasons related to economy and simplicity in terms of design, the former be systematically adopted, which may ultimately lead to structural solutions with reduced robustness.

Because key elements are by definition structural elements which, in case of failure, lead to a disproportionate collapse, they have a cliff-edge effect on the structural response and therefore should be the object of very careful design. Because of this fact, regulations should clearly state that this method should only be used as a last resort, and only in cases where no change to the layout of loadbearing elements is possible, rendering it impossible to prevent exceeding the maximum area at risk of collapse criteria. In addition to this, for the reasons previously stated, key element design should be performed only after completion of an Alternative Loadpath Analysis, except for structures with low risk for human life. One of the difficulties related to the strengthening of structural elements is the fact that it is inherently threat specific, or also said, scenario dependant. The value of 34kPa for the design accidental load can still be traced back to the prevention of collapse induced by internal gas explosions. The UFC 2005, for example, states that the initiating event being unknown, the strengthening of structural elements is not intended to directly limit the initial damage, but merely to reduce the risk of casualties. Although the UFC 2009 methodology may seem aimed at reducing the potential consequences arising from an explosion, fire or vehicle collision in the perimeter of the building and only on the first two floors, the principle of guaranteeing that column failure is ductile for structural elements is a scenario-independent prescription, and is therefore well adjusted to the general case where the initiating event cannot be defined. A good design methodology could therefore take advantage of combining both ductility prescriptions as well as the design accidental action, to better cover the possible diversity of characteristics of the different initiating events.

### ***2.3.5 Alternative Loadpath Method***

The alternative loadpath method is a quantitative method of asserting structural response under a scenario of loss of resistance of a loadbearing element. By using the method for different element removal scenarios, the capacity of the structure to redistribute internal forces by providing alternative loadpaths is evaluated. The determination of the new internal force distribution after member loss enables all the elements of the structure to be checked for sufficient residual capacity in terms of resistance or ductility. In this way, structural components can be designed to resist the imposed actions, arresting the progression of the damages, and thus avoiding a disproportionate collapse.

The method can be considered the most powerful tool available to evaluate a structure's resistance to disproportionate collapse since it remains the only deterministic way of assessing robustness under element loss scenarios, enabling to directly design structures for accidental events. One of the main advantages of the method is that different analysis methods can be employed, with different levels of complexity, enabling the designer to choose to employ for example a nonlinear dynamic procedure (NDP) analysis, in order to access the time domain behaviour of the structure under a given scenario, or simply to use a linear static procedure (LSP) with an appropriate load increase factor (LIF), to estimate the maximum dynamic displacement. The alternative loadpath method can also take into account a multiplicity of factors in order to better model structural response, among which are, for example, geometric and material non-linearity, dynamic amplification, consideration of different mechanisms to resist collapse, strain rate enhancement, debris-induced dynamic effects and connection behaviour.

The method presents also some disadvantages that should be taken into account, namely, that in order for the structural analysis to be thorough, many element loss scenarios must be considered, to cover, as much as possible the effects of initiating events occurring in any given point in the structure. Given that, for each scenario, all structural elements must be checked for resistance and ductility requirements, the total number of checks to be performed may become time consuming, unless these checks can be performed in an automated way through a finite-element software or post-processor. It can also be mentioned as a disadvantage of the method that it needs to account for a number of factors to be able to correctly reproduce structural response,

often requiring either a relatively high degree of understanding of structural behaviour, either the availability of data on structural behaviour of elements under large displacements. Despite these disadvantages, the Alternative Loadpath Method (ALM) remains currently the sole quantitative method for asserting structural robustness.

### ***2.3.6 Scenario dependency modelling***

In terms of risk mitigation procedures, two different approaches can be used, according to the nature of the extreme event. The first approach is scenario dependant and is more suitable for foreseeable hazards, whereas the second approach is more suitable for unforeseen hazards and is scenario independent.

The first approach, as stated, is more adequate to foreseeable hazards, such as fire, earthquake, impact, gas explosion or extreme climatic event, for which some data about the probability of occurrence is available. The process begins with the estimation of the probabilities of occurrence and magnitudes of each hazard, which will then be used in the assessment of the subsequent damaged structural states, and respective probabilities. Next, casualties and economic loss estimation is performed for each damaged state. Finally, the risk mitigation measures are assessed to check if the residual risk has been reduced to a level considered As Low As Reasonably Possible (ALARP), which implies demonstrating that the cost involved in reducing the risk further would be grossly disproportionate to the benefit gained. The risk is ultimately checked to be within the tolerable region of risk, above which risk is deemed unacceptable.

The second approach is more suitable for unforeseeable hazards characterized by very low probabilities, for which the occurrence probability cannot be easily defined, such as explosions caused by terrorist attacks. According to this methodology, the structural reliability is required to be above a specified limit, when the structure is in a damaged state, typically caused by the loss of resistance of a load-bearing structural element. A scenario independent analysis can thus be performed, i.e. the damaged structure is assessed through the notional removal of a structural element, not accounting therefore for the characteristics of the triggering event. The target structural reliability is then specified, for example, in terms of a duration for which the

structure must resist a specified loading, or a non-collapse condition. If the structure complies with the required level of reliability, the risk level is deemed tolerable.

## 2.4 Probability of a progressive collapse

The progressive collapse of a structure depends on factors such as structure geometry and location and magnitude of the initiating event, for which the probability of a progressive collapse  $P(F)$  is given by the following expression (COST, 2011):

$$P(F) = P(F|DH) \cdot P(D|H) \cdot P(H) \quad (2.1)$$

where,

$P(H)$  represents the probability of a given hazard  $H$ ,

$P(D|H)$  represents the probability of local damage  $D$  as a result of hazard  $H$  and

$P(F|DH)$  represents the probability of failure  $F$  of the structure as a result of the local damage  $D$ , by hazard  $H$ .

The formula in Eq. (2.1) is composed of three factors, and it is apparent that there are two partial probabilities that can be influenced by design, and one that cannot, the latter being related to the probability of occurrence of a given hazard, which cannot be influenced by the decision making process that occurs during the design stages of the structure. Considering now the partial probabilities  $P(D|H)$  and  $P(F|DH)$  upon which the design process has power of influence, these are respectively related to element local behaviour and to global system behaviour. The design prescriptions that fall outside the scope of systems robustness are usually related to the safety check of elements against local failure and do not take into account structural behaviour after the occurrence of a given local damage. The evaluation of robustness is therefore focused on the analysis of the probability of failure upon the occurrence of a local damage.

## 2.5 Risk assessment

The risk assessment can be performed by establishing an event tree to model the events that have the potential to damage the structure. An example of an event tree is shown in Figure 2.5, where an exposure before damage  $EX_{BD}$  occurs, which presents the potential to cause damage to the system. After the exposure to a given initiating



event, if no damage occurs, as is represented by the branch  $\bar{D}$ , the risk analysis is complete and zero consequences result from the exposure. If damage occurs, then a variety of damage states may result, which are represented in Figure 2.5 by the branch marked as  $D$ . For each damaged state, two outcomes may result, which are represented by the system failure branch  $F$ , to which are associated direct and indirect consequences, or by the no system failure branch  $\bar{F}$ , to which are associated only direct consequences.

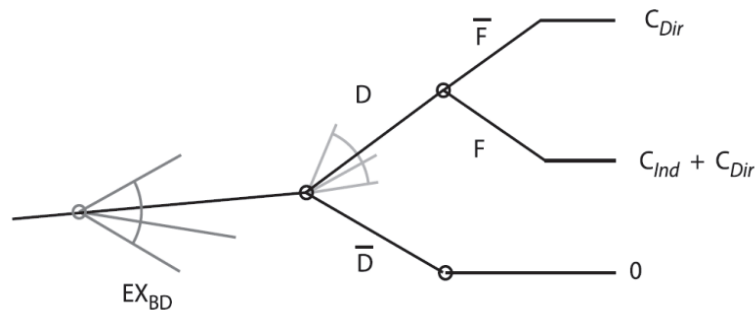


Figure 2.5: Event tree for robustness quantification

The direct consequences are those that directly result from the exposure, which may correspond to more than one damaged component. The indirect consequences include all other costs that are not included in the direct consequences, such as economical loss from affected functionality. The risk based robustness index is determined by considering the relevant exposures and defining both the damage scenarios, as well as the probabilities associated to the occurrences of damage and to the occurrence of system failure as a result of local damage. The direct and indirect consequences must also be estimated for every scenario. The risk analysis framework is based on Eq. (2.2), as presented by Baker *et al.* (2008), which accounts for risk contributions from local damages and global damages, leading to direct and indirect consequences, respectively.

$$R = \sum_i \sum_j C_{dir,ij} \cdot P(D_j | EX_i) \cdot P(EX_i) + \sum_k \sum_i \sum_j C_{ind,ijk} \cdot P(S_k | D_j \cap EX_i) \cdot P(D_j | EX_i) \cdot P(EX_i) \quad (2.2)$$

where,

- $i$  damage scenario
- $j$  system component

$C_{dir,ij}$	consequence (cost) of damage (local failure) $D_j$ due to exposure $EX_i$
$C_{ind,ij}$	consequence (cost) of comprehensive damages (follow-up/indirect) $S_k$ given local damage $D_j$ due to exposure $EX_i$
$P(EX_i)$	probability of exposure $EX_i$
$P(D_j   EX_i)$	probability of damage $D_j$ given exposure $EX_i$
$P(S_k   D_j \cap EX_i)$	probability of comprehensive damages $S_k$ given local damage $D_j$ due to exposure $EX_i$

Structural robustness is related to the probability  $P(\text{collapse} | D_j \cap EX_i)$ , and the objective of correct design for robustness is to achieve a balance between a suitable structural system with the appropriate levels of robustness, and the costs associated to the design options that enable to achieve such levels. The optimal design decision should minimize the sum of the costs of mitigating measures and the total risk  $R$ .

## 2.6 Robustness indexes

The quantification of robustness may be attained through different approaches. According to Sorensen *et al.* (2009), the approaches to define a robustness index can be divided into three categories with decreasing complexity:

- A risk based robustness index based on a complete risk analysis where the consequences are divided in direct and indirect risks,
- A probabilistic robustness index based on probabilities of failure of the structural system for an undamaged structure and a damaged structure and
- A deterministic robustness index based on structural measures.

### 2.6.1 Risk based robustness index

A risk based robustness index was proposed by Baker *et al.* (2008). In this work it is stated that “a robust system is considered to be one where indirect risks do not contribute significantly to the total system risk”. An index of robustness  $I_{rob}$  is proposed, which measures the fraction of the total risk resulting from direct consequences.

$$I_{rob} = \frac{R_{Dir}}{R_{Dir} + R_{Ind}} \quad (2.3)$$

where  $R_{Dir}$  and  $R_{ind}$  are the direct and indirect risks associated, and the robustness index  $I_{rob}$  may assume values that range from 0 to 1, with larger values indicating larger robustness. This robustness index presents some characteristics that should be mentioned. First, it measures only the relative risk due to direct consequences. In this sense, a system with very high direct risk may be deemed robust according to this index. This requires that the acceptability of the direct risk be determined separately and based on other criteria. Typically, direct risks can be controlled through the code based limit states, which evaluate direct risks with high precision, when compared to the estimation of indirect risks. A second and noteworthy characteristic of this robustness index is that it will depend not only on the failure probabilities of damaged states, but also on the relative probabilities of the various damaged states occurring. This means that for a building that presents a low failure probability for a single column removal scenario, if it is deemed likely that an exposure could cause the loss of two columns and the structure is vulnerable to that damage, then the structure could be considered non-robust.

### 2.6.2 Probabilistic robustness index

Probabilistic robustness quantification measures related to structural redundancy were presented by Frangopol & Curley (1987) and Fu & Frangopol (1990) cited in Sorensen *et al.* (2009). The reliability-based robustness index  $RI$  is defined in Eq. (2.4):

$$RI = \frac{P_{f(damaged)} - P_{f(intact)}}{P_{f(intact)}} \quad (2.4)$$

where  $P_{f(damaged)}$  is the probability of failure for a damaged structural system and  $P_{f(intact)}$  is the probability of failure of an intact structural system. The index provides a measurement of the robustness/redundancy of the structural system, and assumes value in the range from 0 to infinity, with smaller values indicating higher levels of robustness.

### 2.6.3 Deterministic robustness index

A simple and practical deterministic measure of robustness and redundancy is the Residual Influence Factor (or *RIF* - value) cited in Sorensen *et al.* (2009). The Reserve Strength Ratio (*RSR*) is defined as:

$$RSR = \frac{R_c}{S_c} \quad (2.5)$$

where  $R_c$  represents the characteristic value of the base shear capacity and  $S_c$  is the design load corresponding to collapse. The full loss of functionality of a structural member  $i$  is measured by the *RIF* - value, which is defined as follows:

$$RIF_i = \frac{RSR_{fail,i}}{RSR_{intact}} \quad (2.6)$$

where  $RSR_{intact}$  is the reserve strength ratio for the intact structure and  $RSR_{fail,i}$  is the reserve strength ratio of the structure when member  $i$  is removed. The *RIF* - value assumes values in the interval from 0 to 1, with larger values indicating larger robustness.

Other measures of robustness were presented by Starossek and Haberland (2008) such as a stiffness-based measure, a damage based measure and an energy-based measure. The stiffness based measure was introduced by Haberland (2007) cited in Starossek and Haberland (2008) and resorts to the static stiffness matrix. The calculation of the stiffness-based measure of robustness is calculated according to the following expression:

$$R_s = \min_j \frac{\det K_j}{\det K_0} \quad (2.7)$$

where:

$R_s$  is the stiffness-based measure,

$K_0$  is the active stiffness matrix of the intact structure and

$K_j$  is the active stiffness matrix of the structure after removal of a structural element or connection  $j$ .

This measure is not normalized, leaving therefore room for improvement in order to render it into an intelligible and manageable value, contained within a specific range. For simple frame structures, results indicate a low correlation between the loss of structural elements and the robustness measure  $R_s$ , indicating that it does not allow for a clear differentiation between robust and non-robust structures.

The damage-based approach to robustness is based on the quantification of damage progression caused by an initial damage. One possible formulation is:

$$R_d = 1 - \frac{p}{p_{lim}} \quad (2.8)$$

where

$R_d$  is the damage-based robustness measure,

$p$  is the maximum extent of additional damage (maximum damage progression) caused by the assumed initial damage  $i_{lim}$  and

$p_{lim}$  is the acceptable damage progression.

For the quantification of robustness, several quantities may be used to quantify damage extent such as masses, volumes, areas or costs. If the assumed initial damage and acceptable damage progression have been defined *a priori*, it is possible to calculate the measure of robustness. However, the dependence upon the assumed initial damage can be removed by using an integral measure:

$$R_{d,int} = 1 - 2 \int_0^1 [d_{max}(i) - i] di \quad (2.9)$$

where

$R_{d,int}$  is the damage-based integral robustness measure,

$d_{max}(i)$  is the maximum extent of total damage caused by and including the initial damage  $i$ , based on the corresponding comparative value of the intact building, and

$i$  is the extent of initial damage based on the intact building.

The possible scenarios of damage progression  $d(i)$  are shown in Figure 2.6.

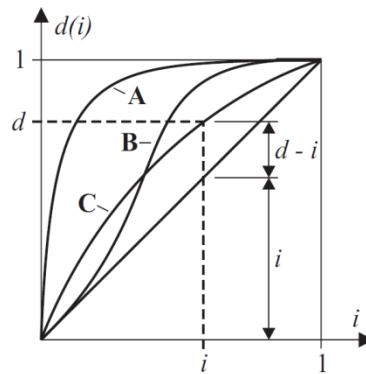


Figure 2.6: Damage based robustness measure - damage evolution

Three curves A, B and C are marked on Figure 2.6, where the curve marked A represents the damage progression which characterizes a non-robust building, given that a small initial damage leads to an extensive total damage, curve marked B represents the behaviour of a relatively robust structure given that for small initial damage, the maximum extent of total damage  $d(i)$  is low, and only for large initial damages does the structure display significant damage progression and curve C presents an intermediate behaviour between those characterized by curves A and B. Considering that the damage-based integral robustness measure is given by the area between the curves defined by the functions  $f(i)=d(i)$  and  $f(i)=i$ , the robustness values for curves B and C should be similar. However, this indicates that the robustness measure does not factor in the higher importance of the damage progression when initiated by small initial damage. However, this can be solved by simply weighing the initial damages and re-normalizing the measure to a 0 to 1 value range.

Another way of measuring robustness is through energy-based measures, which present a good balance between easiness to calculate and expressiveness. One energy-based formulation compares the energy released by the initial failure and the energy required for a progressive collapse. The expression of the measure is given in Eq. (2.10).

$$R_e = 1 - \max_j \frac{E_{rj}}{E_{s,k}} \quad (2.10)$$

where

- $R_e$  is the energy-based robustness measure,  
 $E_{r,j}$  is the energy released by the initial failure of a structural element  $j$  and available for the damage of the next structural element  $k$  and  
 $E_{s,k}$  is the energy required for the failure of the next structural element  $k$ .

The determination of the parameter  $E_{r,j}$  presents some difficulties, namely, since it can be both under or overestimated. The estimation of the released energy can be easily made for certain types of collapses, such as structures collapsing under a pancake effect, where the majority of energy will result from the kinetic energy resulting from the transformation of potential energy. However, for other types of collapses, the released energy may be difficult to quantify since only the portion of the energy which contributes to the damage of the next structural element should be considered. This measure should therefore be preferably used in the analysis of pancake-effect or domino-effect collapses, where the estimation of released energy is both simple and relatively accurate.

## 2.7 Robustness studies

### 2.7.1 Experimental robustness studies

Several experimental tests have been conducted by the U.S. Department of Defense (DoD) in the wake of numerous terrorist attacks, in order to improve the design of buildings to resist disproportionate collapse as reported by Stevens *et al.* (2011). The performed tests addressed connection performance, blast tests to beam-to-column joints and blast tests on wood structures. The results obtained from these tests have been translated into the updating of the UFC guidelines.

Field experiments and numerical simulations were conducted by Song and Sezen (2013) in order to investigate the progressive collapse potential of an existing steel frame building. The experiment was performed on an existing four story moment frame built in 1950, which presented a rectangular floor plan with a 3x9 column distribution. Four first story columns were consecutively removed. Numerical simulations were performed using linear static analysis with a LIF of 2.0, and nonlinear dynamic analysis.

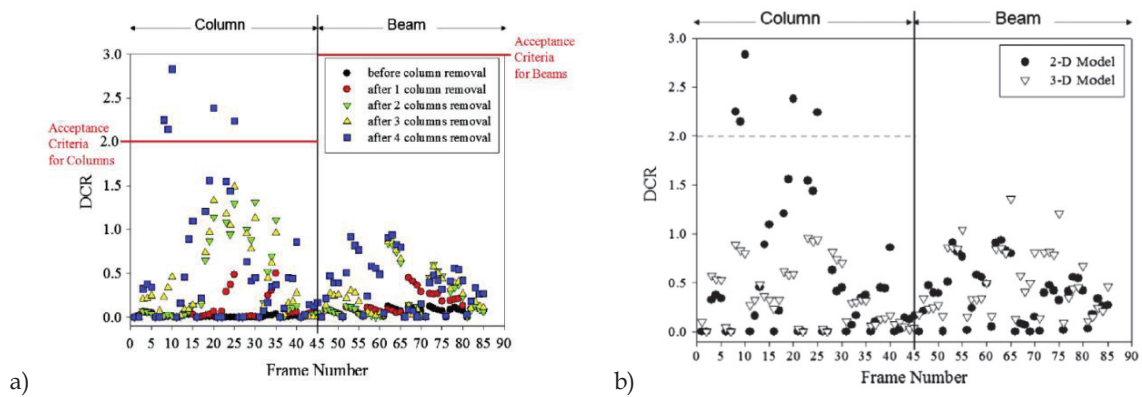


Figure 2.7: Experimental test by Song and Sezen (2013): a) Change in DCR values for each frame member; b) Comparison of DCR values determined from 2D and 3D linear static analysis after removal of four columns

An experimental study of two full scale beam-column assemblies by Lew *et al.* (2013) was conducted to define the response under column removal scenarios. The analysed assemblies represent portions of the exterior MRF of two ten storey steel frame buildings. One specimen had welded unreinforced flange and bolted web connections, whereas the second specimen had reduced beam section connections. The test results showed that the rotational capacities of both connections under monotonic column displacement are about twice that based on seismic test data.

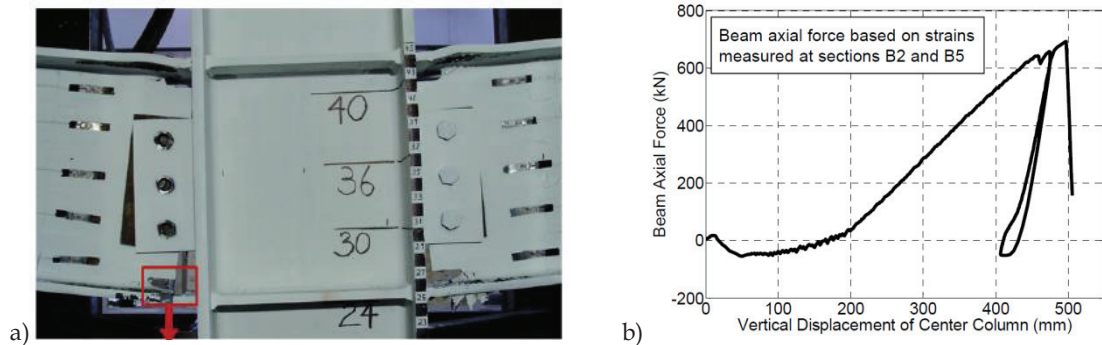


Figure 2.8: Lew *et al.* (2013) experimental test of WUF-B specimen: a) Failure mode; b) Axial force in beam vs. centre column displacement

It was verified that columns were more impacted than beams and that only upon the removal of the fourth column was the GSA 2003 (U.S. General Services Administration, 2003) acceptance criteria for columns not verified. For beam elements, even after the removal of 4 columns, the DCRs were below the allowed value of 3.0. Results indicated that 2D linear static analysis may underestimate the demands for beams. The 3D models displayed lower maximum displacements than 2D models for



both linear static and nonlinear dynamic analysis. The comparison between linear static and nonlinear static analysis showed a ratio between calculated displacements of about 1.5, indicating that the LIF of 2.0 led to overly conservative results. It was concluded that the 3D models were more accurate than the 2D models, because the former can avoid overly conservative solutions by accounting for 3D effects, such as the contribution of transverse beams to the overall resistance of the frame.

The adequacy of sudden column loss as an idealization of local damage caused by a realistic explosion event was investigated by Jahromi *et al.* (2012). This study involved the large scale testing of a typical composite floor system with corrugated steel sheeting in a prototype steel frame building and its comparison with developed computational models. The connections in the prototype frame were double angle and shear tabs and the lateral frame restraint was provided by a stiff restraining beam that circumscribed the specimen and that enabled for the activation of the membrane action.

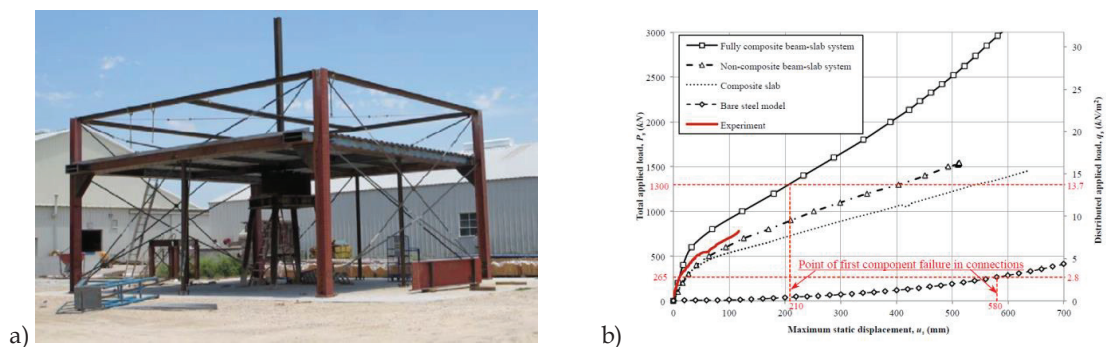


Figure 2.9: Jahromi *et al.* (2012) experimental test: a) Test specimen setup; b) Nonlinear static response of examined floor systems under uniformly distributed load

Results from tests showed that the floor system presented substantial capacity to resist the design loads, resisting approximately an applied load 1.6 times the prescribed progressive collapse load without exhibiting any significant damage. The floor system resisted a sudden column loss for a dynamic amplification factor of 1.6 as assessed by simplified nonlinear dynamic analysis.

The behaviour of composite beam-to-column joints under a middle-column-removal scenario was researched by Yang *et al.* (2015) and component based models were proposed for composite web cleat and for flush endplate connections taking into account failure criteria. It was verified that the component based models may provide acceptable predictions for composite joint behaviour for column removal.

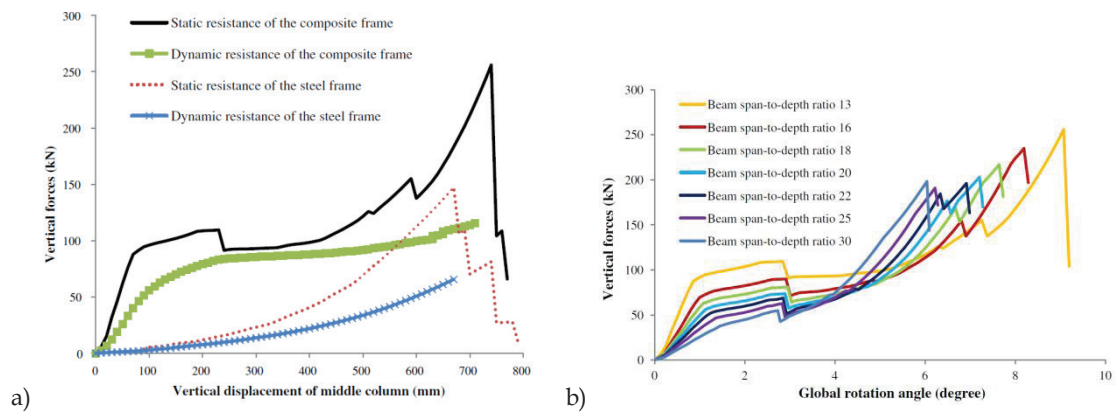


Figure 2.10: Experimental tests by Yang *et al.* (2015): a) Dynamic effects of steel and composite frames under a sudden-column-removal scenario; b) Effect of beam span-to-depth ratio in composite frame models

A subsequently conducted parametric study was carried out to investigate the effect of reinforcement ratios, profile decking and composite slabs, in which the component based joint models were incorporated. The obtained results showed that the increase of the reinforcement ratio leads to higher load resistances both at flexural stage and at catenary action stage, whereas the presence of profile decking can only increase resistance at the flexural stage, since no significant difference was observed at large deformations for models with and without the presence of decking. The static ultimate resistance of steel frames was found to be lower than that of the composite frame, although both can fully develop catenary action. The results stressed the importance of the beam span-to-depth ratio on the frame behaviour under column loss.

### 2.7.2 Analytical robustness studies

A simplified model for axially restrained beams subject to extreme loading was proposed by Izzudin (2005), which predicts the static response under ambient and elevated temperatures, accounting for elasto-plastic bending behaviour and plastic tensile catenary action. The main model assumptions were: simply supported ends with axial elastic restraint applied at cross section centroid, elastic-perfectly plastic cross section behaviour, plasticity governed by the mid span plastic hinge and linear plastic N-M interaction at the plastic hinge. The model was validated against nonlinear FE analysis and proved to provide good prediction accuracy.

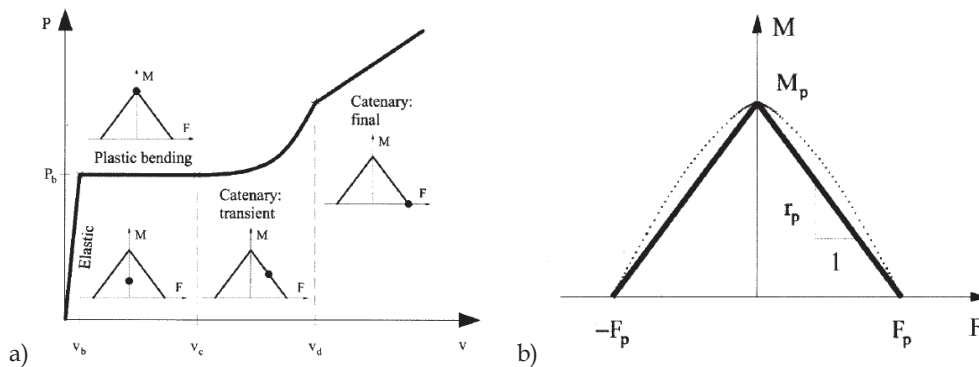


Figure 2.11: a) Four stages of elasto-plastic response; b) Plastic interaction between axial force and bending moment (Izzudin, 2005)

The blast modelling in relation to progressive collapse was extensively addressed by Marchand and Alfawakhiri (2004) and several topics such as blast effects, resistance to blast and local extreme loads, and progressive collapse mitigation strategies were presented and discussed. The mitigation measures presented include the code approaches to achieve structural robustness such as tie forces, alternate load path method, as well as other general design strategies involving connection detailing.

The subject of mitigating risk from progressive collapse was studied by Ellingwood (2006), who proposed a framework for addressing low probability/high consequence. Strategies for risk mitigation were indicated and the constraints for their implementation in design codes were identified and discussed.

A simplified assessment framework was proposed by Izzudin *et al.* (2008) which enables to assess robustness at different levels of idealisation. The procedure involves three main stages consisting on the determination of the nonlinear static response, the assessment of the maximum dynamic response through energy balance and the ductility assessment. The approach assumes that sudden column loss produces similar effects to the sudden application of gravity loads on the directly affected part. Initially, since the gravity forces exceed the static resistance, the differential work done is transformed into kinetic energy; for greater levels of deformation, the opposite occurs and kinetic energy decreases; considering response dominated by a single deformation mode, the maximum dynamic displacement is achieved for the zero kinetic energy condition, i.e., when the work done by the gravity loads equals the energy absorbed by the structure.

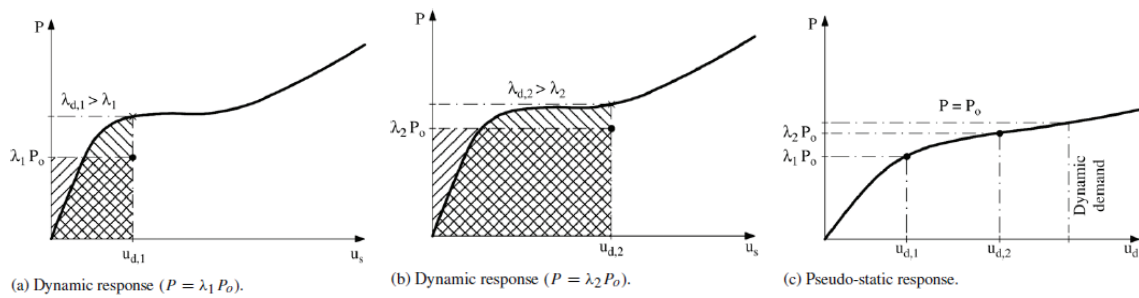


Figure 2.12: Simplified dynamic assessment and definition of the pseudo-static response (Izzudin *et al.* 2008)

The computation of the maximum dynamic response therefore takes into consideration the highly nonlinear structural response involving the elastic phase, yielding, plastic stage and catenary stage. A single measure of robustness was proposed consisting of the system pseudo-static capacity, which compares to the applied gravity loading to establish the limit state. The applicability of this framework was verified by Vlassis *et al.* (2008) by means of a case study consisting of column removal in a framed composite building structure. It was concluded for the investigated structures that the bare steel beams were prone to progressive collapse, even though they were code compliant, and that tie force design alone did not guarantee the required levels of robustness to avoid progressive collapse.

The structural response of steel frames under column loss was investigated by Hai (2009), which proposed an analytical model for the directly affected part. The global structure is substituted by the substructure of the directly affected part by adopting the appropriate springs to model the interaction at the boundaries.

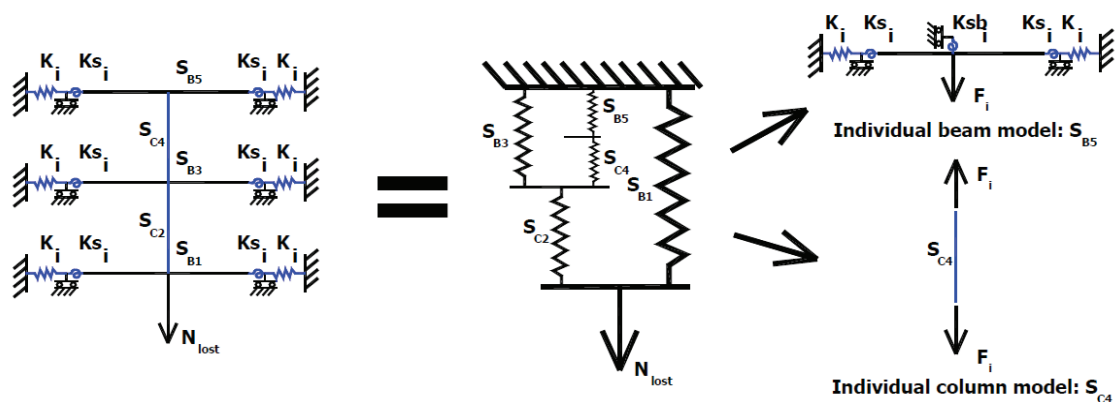


Figure 2.13: Equivalent beam analytical model (Hai, 2009)

It was concluded that the directly affected part's behaviour is complex and depends on many parameters such as the configuration of the frame, location of the damage. The behaviour of the directly affected part was found to be primarily linked to the behaviour of the equivalent beam. The proposed analytical model which describes the behaviour of the different elements of the directly affected part was compared to FE models shown to be able to predict structural behaviour under column loss with an acceptable level of accuracy. The approximations of this model include elastic-perfectly plastic material behaviour and neglecting the elongation of the members for the first calculation step.

Analytical Load Increase Factors (LIFs) and Dynamic Increase Factors (DIFs) were compared by to the empirical formulae recommended in the UFC 2009 Guidelines (United States of America Department of Defense, 2009) by Tsai (2012). The collapse resistance of a column removed structure was obtained and its performance under allowable loading was compared to the acceptance criterion of the UFC 2009. The comparison of the empirical and analytical expressions showed that the analysed empirical based LIFs obtained by Stevens *et al.* (2008) formulae differ from the analytical LIFs, although approximately consistent with Marchand *et al.* (2009) LIFs for steel frames. It was observed that the post yield stiffness ratio may significantly influence the LIFs, and positive values of the stiffness ratio were found to induce smaller LIFs and a nonlinear variation of LIFs with the ductility demand. Regarding the DIFs, a comparison showed that analytical values were approximately consistent with those from Stevens *et al.* and Marchand *et al.* expressions for steel structures, and that DIFs are influenced by the post-yield stiffness ratio in the sense that positive values of the ratio lead to greater DIFs for larger ductility values.

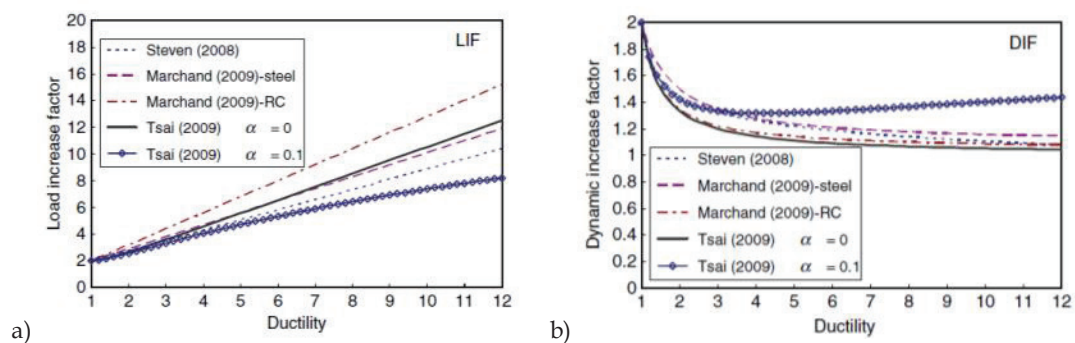


Figure 2.14: a) Comparison of the empirical and analytical LIFs; b) Comparison of the empirical and analytical DIF's (Tsai, 2012)

Pseudo static approach was found to be reasonably conservative and approximated to the real values. In terms of DIFs, both the empirical and analytical formulae were found to underestimate in certain cases the DIFs under low to medium ductility demands. Regarding non-zero post yield stiffness ratio values, it was verified that both LIFs and DIFs predicted by the analytical formula are quite close to the exact values, which is not true for the empirical expressions. It was concluded that using the Linear Static Procedure with empirical LIFs from the UFC 2009 will lead to conservative ductility demands and that the Nonlinear Static Procedure with DIFs may overestimate the allowable loading.

An analytical method for the prediction of the collapse mechanism of a steel frame under corner column loss at different floor heights was presented by Gerasimidis (2014), which established critical ductility curves for each column removal scenario. The results have showed that different collapse mechanisms are produced for different column removal locations along the height of the building structure. Typically, when column removal is performed at the lower zones, the failure tends to be governed by column buckling, whereas for removals in the upper zones, failure is governed by flexural failure of the beam elements above the removed column. Results have also indicated that vertically irregular frames are more prone to column buckling collapse modes.

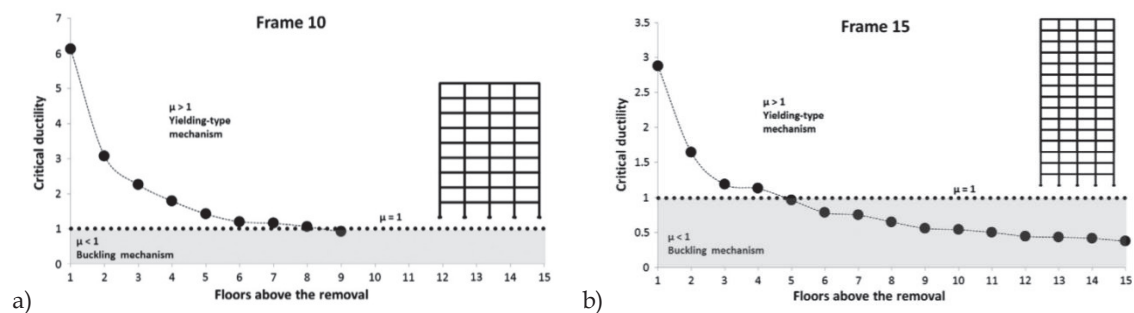


Figure 2.15: a) Ductility limit state graph for frame 10; b) Ductility limit state graph for frame 15 (Gerasimidis, 2014)

A complete analytical procedure for assessing the response of a 2D frame under column loss was proposed by Huvelle *et al.* (2015) which predicts the force-displacement behaviour of the structure and estimates the load redistribution throughout the different identified phases that characterize structural behaviour under column loss, in order to check if the structure can prevent the progressive collapse. The analytical model uses as inputs the M-N interaction curves for the plastic hinges, the

stiffness of the horizontal spring which models the response of the indirectly affected zone and the spring that models the axial stiffness of a plastic hinge submitted to simultaneous bending and axial forces. It was assumed that the indirectly affected part remains elastic, as well as the horizontal restraints that enable for the development of the catenary action. The proposed model was validated against numerical and experimental results and shown to be able to provide a good approximation.

### 2.7.3 Numerical robustness studies

An analytical procedure was developed by Comeliau *et al.* (2010) to predict the structural response of steel and composite plane frames under column loss and taking into account membrane effects.

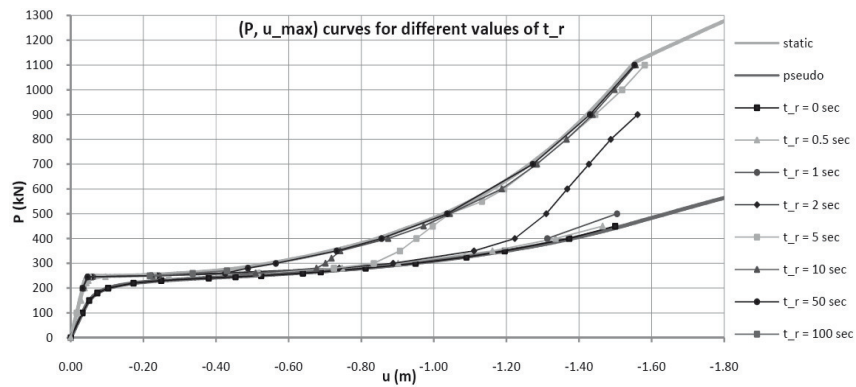


Figure 2.16: Influence of rise time on load-displacement behaviour (Comeliau *et al.* 2010)

The conducted numerical simulations enabled to highlight the influence of parameters such as the first natural period  $T$ , loading conditions and duration of column loss  $t_r$  considering a ramp function leading to the total loss of column capacity. A method was proposed for quantifying the maximum dynamic displacement under a given loading.

Extreme loading conditions such as that induced by explosions due to bombs was the object of a study by Ngo *et al.* (2007) in which a detailed description of blast phenomena and dynamic structural response of various elements is presented. Different methods for estimating blast loads and structural response were also described and the study highlighted the importance of considering extreme loading conditions for high risk buildings, indicating that design prescriptions in terms of ductility levels should be made available to improve building performance.

A numerical parametric study on the progressive collapse of multi storey composite frame buildings was conducted by Fu (2010) addressing parameters such as the strength of structural steel, strength of concrete and reinforcement mesh size. 20 storey composite buildings with bracing systems were analysed, considering full composite action and taking into account concrete cracking. This study concluded that although plasticity is typically assumed to develop in the beam, considering the beam sizes used in current design practice, after column removal the beam may still be in the elastic range. The cross bracing system was found to be less vulnerable to progressive collapse. An increase in the steel mesh was found to lead to increased rotational capacity, although for steel beams still in the elastic range, given that no plastic hinges are formed, the catenary effect is not significantly mobilized.

The load resisting capacity of composite steel-concrete floors subjected to column loss was addressed by Alashker and El-Tawil (2011) that developed a design oriented model for computing floor resistance under the premise that floor collapse is resisted through membrane action in the slab and catenary action in the steel beams. The comparison with the numerical simulation results showed that the model was able to reasonably reproduce the system behaviour, despite the assumed simplifications.

In order to measure the robustness performance of structures, Khandelwal and El-Tawil (2011) have used the pushdown analysis method to determine the residual system capacity and to determine the collapse modes of damaged structures and results showed that the structures designed for higher seismic risk present improved robustness due to the presence of reduced beam sections and stringer columns. The DIFs computed in accordance with the UFC 2009 were found to provide a better fit than those given in GSA 2003.

A numerical study on the progressive collapse of a multistorey building by Kwasniewski (2010) investigated the behaviour of a specific existing building using NDA according to GSA 2003 guidelines, having concluded that the crucial parts in the FE simulation are the beam-to-column connections and the composite slab modelling.

The influence of modelling assumptions in the collapse response of structures such as 2D versus 3D modelling, members response and use of macromembers was investigated by Alashker *et al.* (2011). Results pointed to significant differences between 2D and 3D models due to floor system contribution and it was concluded that 2D



modelling does not necessarily lead to conservative results. 3D analysis was found to be required in order to rigorously investigate robustness.

A numerical study of beam-column joints subjected to catenary action was devised by Yang and Tan (2012), in which six beam-column joints with six different types of connections were analysed. The rotational capacities of the different types of connections under catenary action were determined and are reproduced in Table 2.6 and design recommendations were indicated regarding connection acceptance criteria under column loss scenarios.

Connection type	DOD [2]/ASCE 41 [23] (radians)	Current simulation results (radians)
Web cleat	$\theta = 0.1125 - 0.0027d_{bg}^a$	$\theta = 0.1745 - 0.0033d_{bg}$
Fin plate	$\theta = 0.0502 - 0.0015d_{bg}$	$\theta = 0.1172 - 0.0034d_{bg}$
Flush end plate	0.015	0.15
TSWA (12 mm)	0.035	$\theta = 0.214 - 0.0077 d^b$

<sup>a</sup>  $d_{bg}$  = depth of bolt group, inch.  
<sup>b</sup>  $d$  = depth of beam, inch.

Table 2.6: Comparison of connection rotation capacities between the current simulation results and DoD/ASCE 41 (Yang and Tan, 2012)

This study concluded that connection depth has a significant influence on the behaviour of beam-to-column joints under column removal scenarios and that improving bolt arrangement in flush end-plate connections can significantly increase the load carrying and rotational capacity. This study also concluded that the current acceptance criteria for rotational capacity for steel joints are probably too conservative since only flexural resistance is considered.

The blast resistance of structures designed according to seismic design criteria was addressed by Parisi and Augenti (2012) for the case of reinforced concrete framed buildings. Two sets of building structures were analysed, the first set consisting of structures designed for earthquake resistance according to the EN 1998-1 and the second set was designed only for gravity loads according to older codes. Global pushdown analysis was performed on 3D structures for columns failing under blast scenarios, characterized by local pressure-impulse analysis. Conclusions point to the fact that seismic design criteria did not provide sufficient robustness against blast scenarios.

The progressive collapse capacity of earthquake-resistant steel moment frames under column failure was investigated by Ferraioli *et al.* (2014) using pushdown analysis. The NSP results were compared with the results from incremental NDA and

the DIF for pushdown analysis was determined as being in the range from 1.25 to 1.30 for the investigated structures. It was concluded that the investigated frames presented a high potential for progressive collapse.

The development of multiple post flexural resisting mechanisms in reinforced concrete structures was investigated by Botez *et al.* (2014) using NSP and NDA procedures. The studied mechanisms were the compressive arc action, catenary action and Vierendeel action. Results showed that all mechanisms can be accurately modelled using distributed plasticity formulations and that simplified sub-structures may be adopted in some cases without significant loss of precision.

The progressive collapse behaviour for different types of seismic connections was addressed by Kim and Kim (2009) in which Reduced Beam Section (RBS), Welded Cover Plated Flange (WCPF) and Welded Unreinforced Flange - Welded Web (WUF-W) connection types were studied. The NSP pushdown results indicated that the yield strength is highest in structures with WCPF connections, and lowest in structures with RBS connections. In structures designed for moderate seismicity, the load factors at yield are less than 1 for structures with RBS connections, implying high potential for progressive collapse. It was concluded that WUF-W/WCPF connections are safe for progressive failure and that structures designed for high seismicity turned out to be safer under sudden column loss.

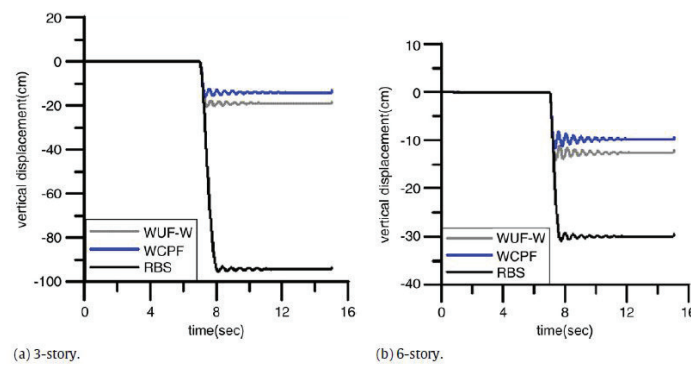


Figure 2.17: Vertical deflection time histories for structures designed for moderate seismic load (Kim and Kim, 2009)

The behaviour of double angle shear connections for structural robustness was investigated by Liu *et al.* (2012) and results showed that these connections present large rotation capacity and also that they are able to sustain higher loads when compared to the analysed set of shear tab connections.

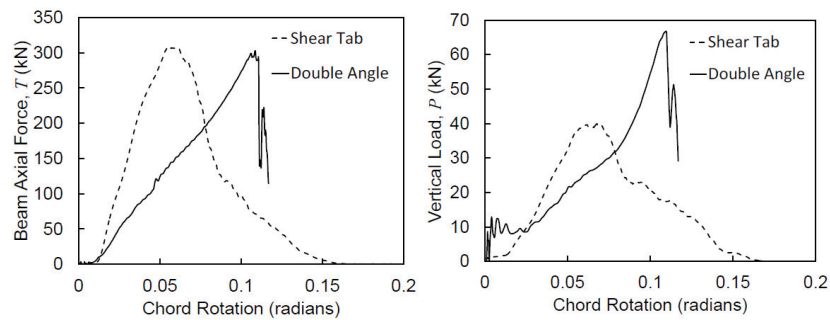


Figure 2.18: Beam axial force and total vertical load versus chord rotation for shear tab and double angle subassemblies (Liu *et al.* 2012)

A computational investigation conducted by Sadek *et al.* (2013) to simulate the response of two beam-column assemblies with welded unreinforced flange with bolted web connections and with reduced beam section connections showed that the ultimate fracture of the connections in both assemblies was due to combined axial and flexural stresses. The results also showed that the moment connections were capable of developing a significant fraction of the cross section capacity of the beams.

Pushdown analysis was used by Lu *et al.* (2012) to perform an assessment of resistance to progressive collapse of framed structures using both deterministic pushdown analysis and random pushdown analysis taking into account random system properties. Robustness was measured using both deterministic and reliability-based indexes. Results show that the loading scheme for simulating column loss and instant of column removal, different load steps and the effects of the proportionally increased loading pattern have no effect on the failure mode but may influence the ultimate load carrying capacity of the structure. It was also verified that the robustness assessment using the deterministic based index is consistent the assessment with the reliability-based index.

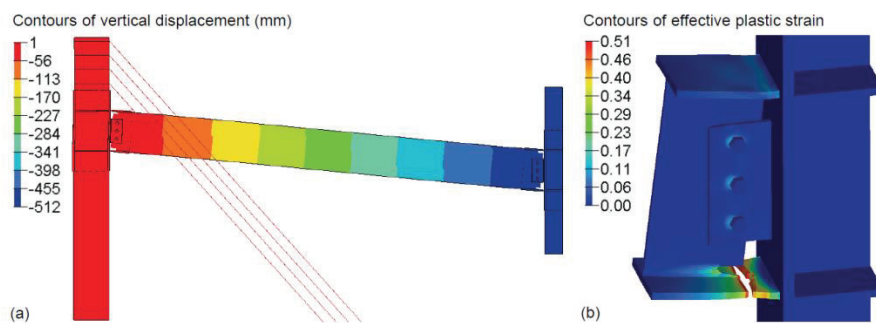


Figure 2.19: Detailed model results for the WUF-B specimen: a) deflected shape at a centre column; b) failure mode at a connection to centre column (Sadek *et al.* 2013)

A probabilistic robustness assessment of steel moment frames was performed by Xu and Ellingwood (2011) and uncertainties in collapse demands and on the resisting capacity of the connections were modelled probabilistically. The dominant connection failure mode by weld fracture in the beam flange to column flange zone was modelled using a J-integral formulation of fracture demand and characterized probabilistically. The connection response was validated against data from the SAC Project following the Northridge earthquake and robustness was assessed according to the requirements given in the UFC (2009) and according to a system reliability analysis using nonlinear dynamic analysis. Results from this study indicate that for steel frames designed according to pre-Northridge detailing may not meet the integrity requirements under a column loss scenario. It was also concluded that uncertainties in connection behaviour were found to not have a significant impact on robustness.

A new empirical method for the calculating the dynamic increase factor formulation for nonlinear static analysis of building frames was proposed by Liu (2013) which defines the DIF as a function of the maximum ratio between the factored moment demand under original unamplified static gravity loads and the factored plastic moment capacity, for all the beams in the zone above the removed column.

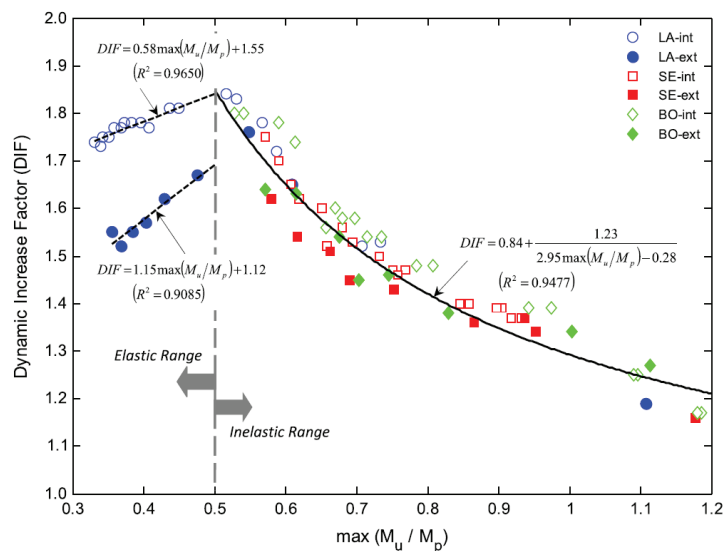


Figure 2.20: Dynamic increase factor as a function of  $\max(M_u/M_p)$  (Liu 2013)

It was found that for values of  $(M_u/M_p)$  smaller than 0.5, the damaged frame responds elastically, and the DIF values inferior to two are due to the geometrical nonlinearity of the damaged frame. For values of  $(M_u/M_p)$  greater than 0.5, frames

typically respond in the inelastic domain and the larger the ratio, the smaller the DIF values and the more likely the frame will respond inelastically, indicating that material nonlinearity is predominant over geometric nonlinearity. The proposed DIF formulation may be used with nonlinear static analysis, to avoid using the more complex nonlinear dynamic analysis, although the extension of these findings may be limited due to the small number of structures on which the study was based.

The catenary action contribution to robustness was investigated by McConnell *et al.* (2015), who conducted a parametric study of steel beams with different connection idealizations, characterized by parameters such as beam size, connection type and axial stiffness of the surrounding frame. A procedure for normalizing the joint rotations for disparate beams based on the flexural and axial stiffnesses of the beams was introduced, which was shown to be effective up to capacities compatible with the full development of beam tensile resistance.

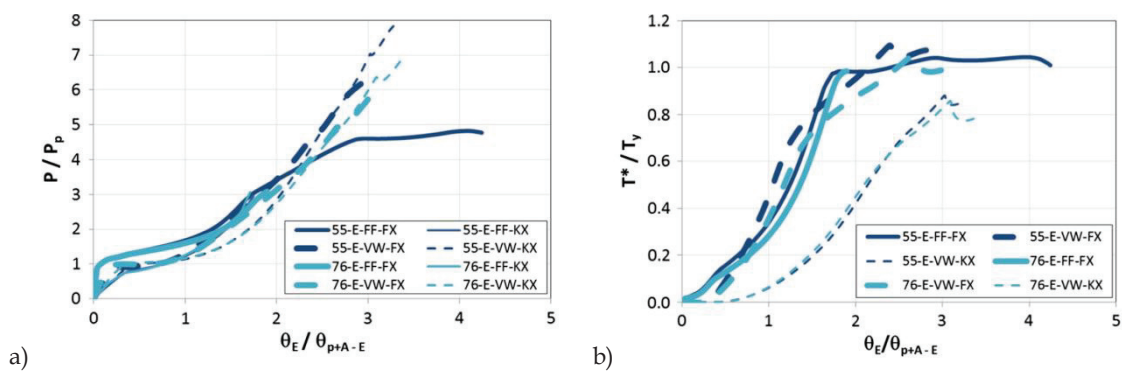


Figure 2.21: a) Normalized load versus end rotation normalized by  $\theta_{p+A}$ ; b) Effective normalized axial force versus end rotation normalized by  $\theta_{p+A}$  (McConnell *et al.* 2015)

This methodology was concluded to be suitable for future connection rotation benchmarks. The influence of residual stresses and geometric imperfections was also investigated and results showed that geometrical imperfections can decrease the load carrying capacity and increase the flexural demand, while the residual stresses presented negligible influence on joint response.

## 2.8 Flush end-plate joint behaviour

In this section a review of literature concerning the topic of the behaviour of FEP joints is presented. The fact that only the FEP joint type is discussed here is due to the fact that this was the selected joint typology for the secondary “gravity” frame beam-to-column joints. In this sense, available research from literature on this topic is

presented here, hence providing background for the analysis and finite element modelling to be conducted in this thesis.

### ***2.8.1 Components method modelling***

The monotonic moment-rotation behaviour of joints can be approximately predicted through the Components Method described in the EN 1993-1-8 (CEN, 2005) which quantifies joint resistance, stiffness and rotation capacity, based on the characteristics of each of the active connection components. The principles of the Components Method are based on the research by Zoetemeijer (1983), later continued by other researchers, who described the behaviour and refined the accuracy of the mechanical behaviour of further components. The accuracy of the method relies heavily on the accurate description of the basic components, on the assembly process and on the interaction between components. It is assumed that component properties are independent, but such assumption is not entirely accurate, since not all components truly display this characteristic, but interact and influence other components' behaviour instead.

The application of the Components Method can be summarized in the following steps:

- Determination of the path of forces in the connection that are in equilibrium with the applied forces;
- Identification of all the active basic components in terms of strength and stiffness (the list of possible components is presented in table 6.1 of the EN 1993-1-8);
- Evaluation of the mechanical properties / model of each one of the individual components (resistance, stiffness and rotation capacity);
- Assembly of the components;
- Evaluation of connection resistance, stiffness and rotation capacity;
- Classification of the joint.

The basic components are presented in Table 2.7.

Table 2.7: Components method basic joint components (CEN, 2005)

Component Number	Description
1	Column web panel in shear
2	Column web in transverse compression
3	Column web in transverse tension
4	Column flange in bending
5	End-plate in bending
6	Flange cleat in bending
7	Beam or column flange and web in compression
8	Beam web in tension
9	Plate in tension or compression
10	Bolts in tension
11	Bolts in shear
12	Bolts in bearing (on beam flange, column flange, end-plate or cleat)
13	Concrete in compression including grout
14	Base plate in bending under compression
15	Base plate in bending under tension
16	Anchor bolts in tension
17	Anchor bolts in shear
18	Anchor bolts in bearing
19	Welds
20	Haunched beam

An example of the components for a bolted flush-end plate beam-to-column connection is presented in Figure 2.22.

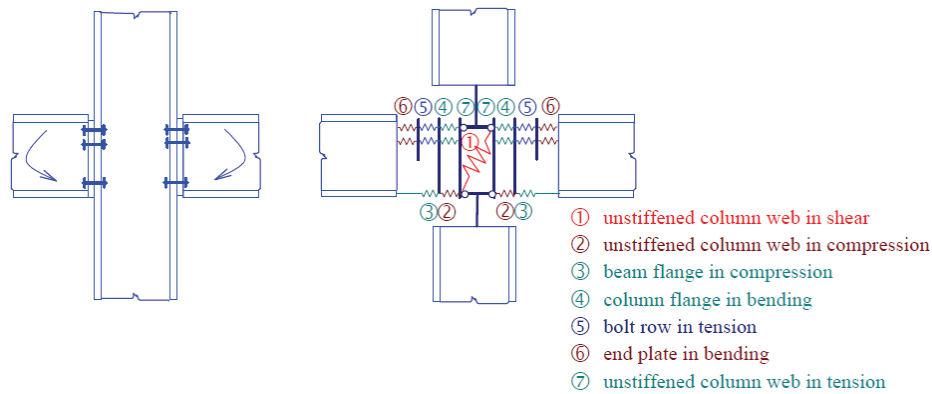


Figure 2.22: Components method - components in a bolted flush end-plate beam-to-column connection

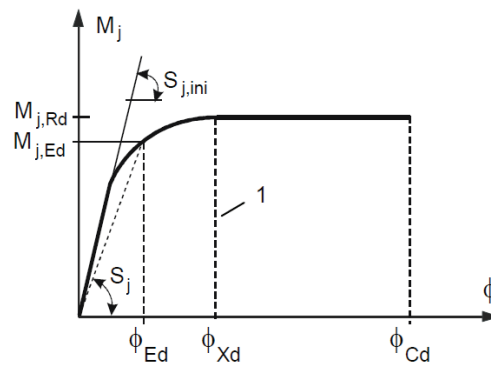


Figure 2.23: Components method joint moment-rotation curve (CEN, 2005)

The assembly of the components enables the evaluation of the joint's stiffness and strength by means of a moment-rotation curve, described in the EN 1993-1-8 (CEN, 2005) and presented in Figure 2.23.

The first part of the diagram is linear and characterized by an initial stiffness. However, it is noticeable that for low levels of bending moment below the resisting bending moment, the curve deviates from the linear elastic line and assumes lower values of stiffness due to local plasticity caused by stress concentrations and residual stresses. In the EN 1993-1-8 (CEN, 2005), the behaviour is assumed linear elastic up to 2/3 of the resisting design bending moment  $M_{j,Rd}$ , characterized by an initial stiffness  $S_{j,ini}$ . Upon reaching 2/3 of  $M_{j,Rd}$ , the stiffness is reduced until moment resistance is reached. The prediction of the joint's rotational capacity is still being researched and only deemed-to-satisfy rules are provided, i.e. rules to limit brittle failure in bolts or welds. In order to proceed with the determination of the design resistance of a bolted end-plate beam-to column joint, the evaluation of the mechanical properties of each



one of the individual components must be performed. In the case of T-stub components, the EN 1993-1-8 evaluates three different collapse mechanisms, where:

- Type 1 - Complete yielding of the flange;
- Type 2 - Bolt failure with yielding of the flange;
- Type 3 - Bolt failure.

The design tension resistance  $F_{t,Rd}$  of a T-stub flange varies according to the collapse mechanism type and is given for each type by the following expressions, considering that prying forces may develop in modes 1 and 2:

$$F_{T,1,Rd} = \frac{4M_{pl,1,Rd}}{m} \quad (2.11)$$

$$F_{T,2,Rd} = \frac{2M_{pl,2,Rd} + n \sum F_{t,Rd}}{m+n} \quad (2.12)$$

$$F_{T,3,Rd} = \sum F_{t,Rd} \quad (2.13)$$

where,  $M_{pl,1,Rd}$  and  $M_{pl,2,Rd}$  are the design bending moments for mode 1 and 2 effective lengths respectively, which are calculated based on bolt geometry, individual and group behaviour of bolt rows, and circular and non-circular failure patterns, and  $F_{t,Rd}$  is the design tension resistance of a single bolt. The T-stub failure modes are presented in Figure 2.24.

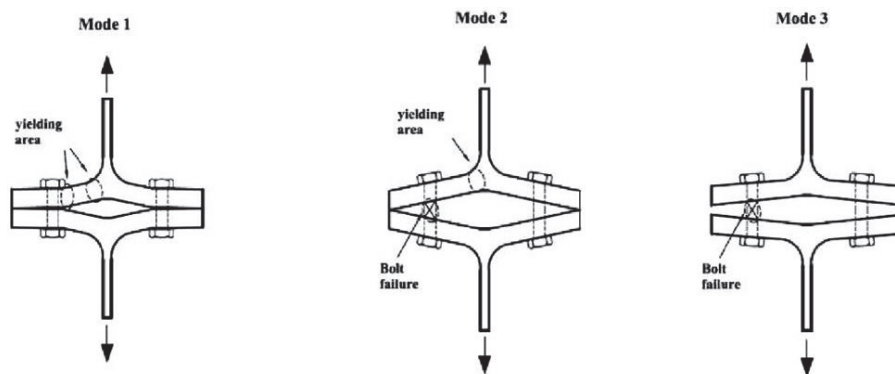


Figure 2.24: T-stub failure modes

After the determination of the mechanical properties of each one of the basic components, the design resistance of the joint  $M_{j,Rd}$  may be determined from:

$$M_{j,Rd} = \sum_r h_r F_{tr,Rd} \quad (2.14)$$

where:

- $F_{tr,Rd}$  is the effective design tension resistance of bolt-row  $r$ ;  
 $h_r$  is the distance from bolt row  $r$  to the centre of compression;  
 $r$  is the bolt-row number.

The effective design tension resistance of a bolt-row taken as an individual bolt row or as part of a group of bolt rows, shall be reduced below the value of  $F_{t,Rd}$  to account for potential reduced resistance of the column web in tension, column flange in bending, end-plate in bending and beam web in tension. Furthermore, the effective design tension resistance of a bolt-row shall be further reduced, in order to insure that for all bolt-rows taken up to and including a given bolt-row  $r$ , the sum of the design bolt tension resistance  $\sum F_{t,Rd}$  does not exceed the design resistance of the column web in compression  $F_{c,wc,Rd}$ , the design resistance of the beam flange and web in compression  $F_{c,fb,Rd}$  or the design resistance of the column web in shear  $V_{wp,Rd}$  divided by the  $\beta$  factor (as defined in clause 5.3 of the EN 1993-1-8). A final reduction should be performed in cases where the effective design tension resistance  $F_{tx,Rd}$  of one of the previous bolt-rows  $x$  is greater than  $1.9 F_{t,Rd}$ . The effective design tension resistance  $F_{tr,Rd}$  for bolt row  $r$  should be reduced in order to verify that it does not exceed the value of  $F_{tx,Rd} h_r / h_x$ , where  $h_x$  is the distance from bolt-row  $x$  to the centre of compression, and  $x$  is the bolt row farthest from the centre of compression that has a design tension resistance greater than  $1.9 F_{t,Rd}$ . For the case of bolted end-plate connections, the centre of compression is considered to be in line with the mid-thickness of the compression flange of the beam.

The calculation of the rotational stiffness of the joint is based on the flexibilities of its basic components, each represented by an elastic stiffness coefficient. For an acting bending moment  $M_{j,Ed}$  lower than  $M_{j,Rd}$ , the rotational stiffness of the joint  $S_j$  is given by the following expression:

$$S_j = \frac{Ez^2}{\mu \sum_i 1/k_i} \quad (2.15)$$

where:

- $E$  is Young's modulus;  
 $z$  is the lever arm (given in Figure 6.15 of the EN 1993-1-8);

$k_i$  is the stiffness coefficient for the basic joint component  $i$ ;

$\mu$  is the stiffness ratio  $S_{j,ini}/S_j$ .

For end-plate joints with two or more bolt-rows in tension, the basic components related to all of these bolt rows should be represented by a single equivalent stiffness coefficient  $k_{eq}$  determined by the following expression.

$$k_{eq} = \frac{\sum_r k_{eff,r} h_r}{z_{eq}} \quad (2.16)$$

where:

$h_r$  is the distance from bolt row  $r$  to the centre of compression;

$k_{eff,r}$  is the effective stiffness coefficient for bolt-row  $r$  taking into account the stiffness coefficient  $k_i$  for the basic components;

$z_{eq}$  is the equivalent lever arm.

The effective stiffness coefficient  $k_{eff,r}$  for bolt row  $r$  should be determined is given by:

$$k_{eff,r} = \frac{1}{\sum_i 1/k_{i,r}} \quad (2.17)$$

where:

$k_{i,r}$  is the stiffness coefficient representing component  $i$  relative to bolt-row  $r$ .

The equivalent lever arm  $z_{eq}$  can be calculated in accordance with the following expression:

$$z_{eq} = \frac{\sum_r k_{eff,r} h_r^2}{\sum_r k_{eff,r} h_r} \quad (2.18)$$

Regarding the estimation accuracy of the method, a wide comparison between the predicted and experimental values of the joint rotational behaviour was presented by Faella *et al.* (2000) and it was concluded that the Eurocode 3 approach led to an overestimation of the joint rotational stiffness while underestimating bending moment capacity in most cases. Recently, a study devoted to the characterisation of web panel components in bolted end-plate joints by Augusto *et al.* (2016) has evaluated the

behaviour of joints both globally and in terms of local components, concluding that the adopted modelling strategy can be used for extracting the force-deformation response of components.

The method's applicability to predict joint response when submitted to dynamic actions is a very important issue, since it would allow to better understand structural response to seismic actions. In the context of the present study, the behaviour of partial strength joints under seismic and column loss actions is to be investigated, for which reason some background to this topic is therefore introduced in this section, namely different studies that have been conducted on this topic in recent years.

Regarding the applicability of the method to connections subjected to dynamic actions, according to da Silva *et al.* (2003), the applicability of the formulation depends on the parameter to be determined. In this sense, the initial rotational stiffness  $S_{j,ini}$  and the moment capacity  $M_{j,Rd}$  can be used for the case of dynamic actions. The rotational capacity cannot be predicted by the method but results from extensive experimental tests have led to the conclusion that the rotation capacity of connections subjected to dynamic actions is approximately half the one resulting from monotonic loading conditions.

A research on the cyclic modeling of bolted beam-to-column connections was performed by Latour *et al.* (2011), aiming at the prediction of cyclic joint response by using the framework defined in the EN 1993-1-8 for monotonic loading. Results indicated the possibility of extending the component approach to cyclic loading conditions, although further research efforts are still required to improve the accuracy of the force-displacement behaviour of joint components.

A study regarding the ultimate behaviour of bolted beam-to-column connections under cyclic actions was conducted by Iannone *et al.* (2011) in order to assess the possibility of using the component approach as a design tool to govern the location of the dissipative elements by imposing the weakest component. This hypothesis was confirmed by experimental results. Furthermore, aiming to investigate the possibility of extending the components approach to predict the cyclic rotational response of beam-to-column joints, experiments were conducted, demonstrating that the overall dissipation capacity of joints can be obtained as the sum of the energy dissipated by the single joint components. Results indicated that the extension of the

component approach under monotonic loads to cyclic loading can be carried out, provided that components are adequately characterized in terms of cyclic force-displacement behaviour.

Another study conducted by Augusto *et al.* (2016) evaluated the cyclic behaviour of web panel components in bolted end-plate joints, which characterised the global joint response as well as the dissipative components, providing an extraction procedure for the cyclic force-displacement response of the column web panel.

The above mentioned studies indicate that the extension of the use of the components method to predict cyclic joint rotational behaviour can provide an approximate estimation, although research efforts will still be required to improve prediction accuracy.

The study of the arrest of a progressive collapse is heavily dependent upon the establishment and efficacy of the catenary/membrane effect. To this sense, end connections of steel members in the directly affected zone are typically subjected to combined bending moment and axial forces. An adequate prediction model of joint behaviour should therefore take into consideration how tensile forces affect joint response. The EN 1993-1-8 (CEN, 2005) states that the design moment resistance of a beam-to-column joint can be determined using the Components Method approach, provided that the axial force in the connected member does not exceed 5% of the design tensile resistance of its cross section. In cases where the axial force in the connected beam exceeds this value, a conservative method is provided considering linear interaction between axial force and bending moment as given by the following expression:

$$\frac{M_{j,Ed}}{M_{j,Rd}} + \frac{N_{j,Ed}}{N_{j,Rd}} \leq 1 \quad (2.19)$$

where  $M_{j,Rd}$  is the design bending moment resistance of the joint, assuming no axial force, and  $N_{j,Rd}$  is the axial design resistance of the joint, assuming no applied bending moment. This approach can yield conservative results and an alternative approach was developed by Jaspart *et al.* (1999), based on the extension of the Components Method, where the components are used evaluated under no axial load and then assembled in a

modified procedure to calculate joint stiffness and resistance. A comparison between the EN 1993-1-8 linear interaction method and the proposed alternative method is presented in Figure 2.25.

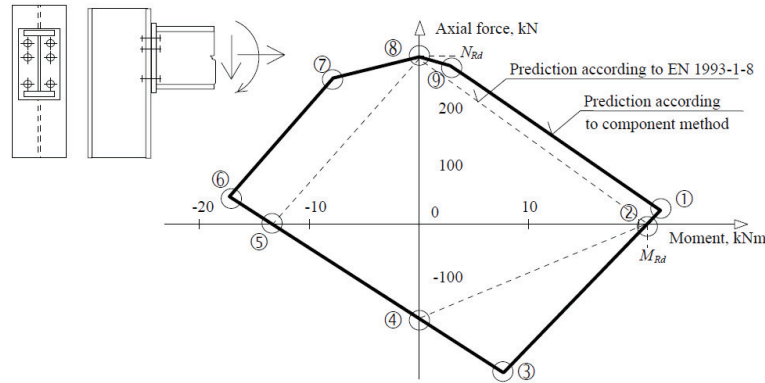


Figure 2.25: Components Method - M-N interaction curve comparison between linear interaction and Components Method (Jaspart *et al.* 1999)

Both proportional and non-proportional loading can be considered, but for progressive collapse situations further to column loss, only proportional moment-axial loading pattern is relevant. By recurring to the concept of effective rigid area, the position of the neutral axis can be derived through equilibrium equations. To what concerns the rotational stiffness of the connection, it can be determined based on the deformation of the components.

### 2.8.2 Experimental studies

An experimental investigation was conducted by Boorse (1999) in order to evaluate the inelastic rotation capability of flush end-plate connections under seismic loading, in which seven specimens were tested using slow cyclic loading. The verified failure modes included fracture at the end-plate to weld interface (see Figure 2.26a) , as well as flange-to-endplate weld fracture (Figure 2.26b)).

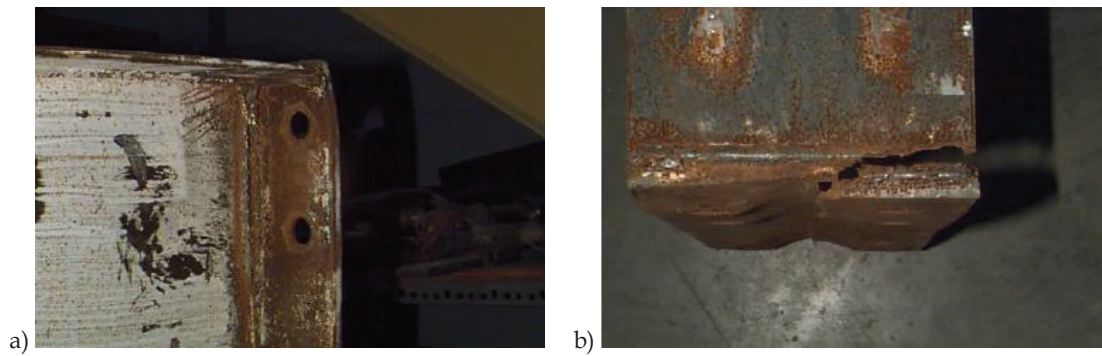


Figure 2.26: a) Web-to-End-Plate Weld Fracture - F2-3/4-3/8-16; b) Flange-to-End-Plate Weld Fracture - F2-3/4-3/8-16 (Boorse, 1999)

Result showed that nearly all specimens exhibited inelastic rotations higher than 0.01 radians and that connections designed with larger pitches allowed for more yielding of the endplate. In general the wide pitch connection specimens exhibited nearly double the rotation capacity when compared to the equivalent tight pitch configurations.

Aribert *et al.* (2004) conducted tests on “simple” beam-to-column joints, including 4 tests on bolted flush endplate joints and discussed design aspects and their impact on global structural analysis. Observed failure modes included bolt failure near the tension flange, fillet weld failure at the endplate and fillet weld failure combined with bolt dethreading.

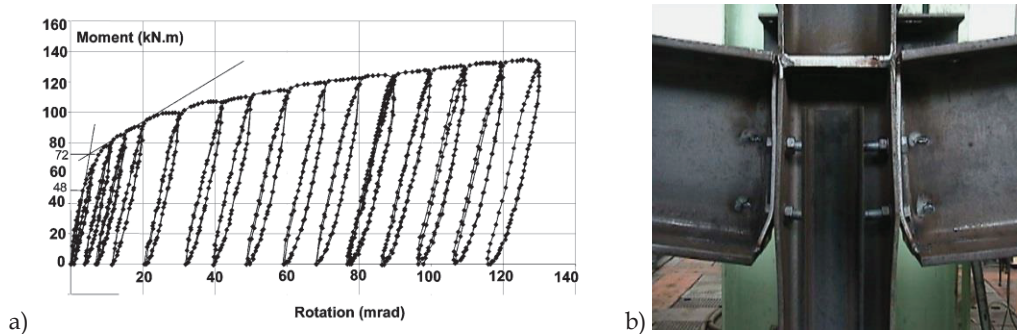


Figure 2.27: a) Moment-rotation curve of test EP2; b) Test EP2 rupture of the fillet weld connecting the endplate (Aribert *et al.* 2004)

The experimental values were compared to the prediction given in the EN 1993-1-8 (CEN, 2005) and it was found that the initial stiffness prediction values were significantly higher than the experimental values. The observed experimental rotation capacity was clearly superior to the rotation corresponding to the maximum deflection of  $l_b/50$  often adopted in literature to validate rigid-plastic analysis, which for a simply supported beam corresponds to 40 mrad. It was concluded that when high ductility

levels are required, great attention should be paid to the fabrication details, namely for what concerns the welds.

An experimental study conducted by da Silva *et al.* (2004) on extended end-plate joints analyzed the possibility of extending the component method philosophy for combined bending moment and axial force. Test results indicated that axial force significantly influenced structural behaviour, as shown in Figure 2.28.

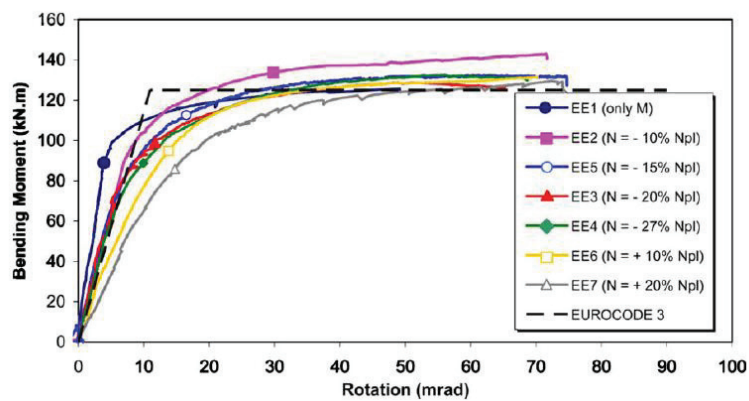


Figure 2.28: Effect of axial forces - Experimental moment versus rotation curves for varying axial loads (da Silva *et al.* 2004)

The simple extension of the method developed for pure bending was found to not be valid, since loading history may cause pronounced shifts in the neutral axis positions and since components must present different behaviour in tension and in compression. Additionally it was concluded that the concept of tension and compressions zones for components is no longer possible since the model must consider all possible components.

An experimental investigation on high strength steel moment connections with end-plates was conducted by Girão Coelho and Bijlaard (2007) comprising tests on two flush end-plate specimens and one extended end-plate, in order to characterize the nonlinear behaviour, to verify the validity of the EC3 specifications and to quantify the ductility of these connections. Results showed a good agreement in terms of resistance between the experimental values and the EN 1993-1-8 prediction whereas in terms of stiffness, the prediction/test values varied within the range from 1.59 to 1.75, showing that the code overestimates this property. In terms of ductility, results show ductility indexes varying between 3.0 and 3.8 associated to joint rotation capacities varying from



37 to 46 mrad. This study has also showed that the welding details did not play an important role in the joint deformation behaviour.

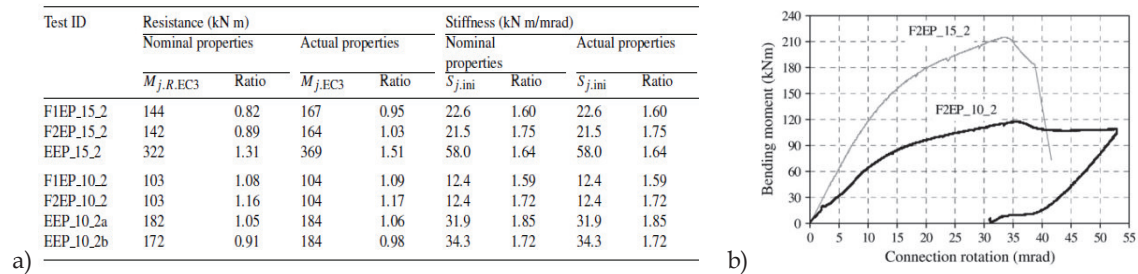


Figure 2.29: a) Comparison of Eurocode 3 predictions with experiments; b) Experimental flush end-plate response for 10mm and 15mm thick end-plates (Girão Coelho and Bijlaard, 2007)

An experimental study conducted by Broderick and Thomson (2002) on the seismic behaviour of flush end-plate joints consisting on 2 monotonic tests and 6 cyclic tests was performed on joint specimens using different end-plate thicknesses, beam sections and bolt sizes and grades, to ensure all three T-stub failure modes would occur.

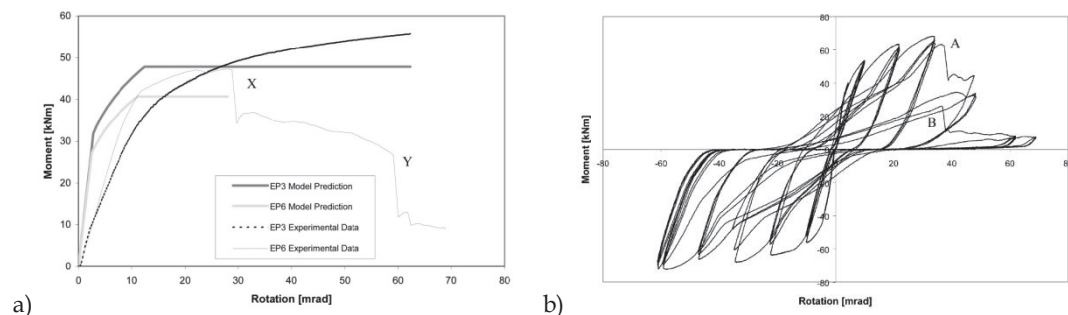


Figure 2.30: a) Comparison of experimental and predicted moment-rotation characteristics; b) Moment-rotation relationship for specimen EP2 (Broderick and Thomson 2002)

Results showed high levels of ductility for T-stub mode 1 failures, as well as for mode 2 failures, although lower for the latter. Failure modes 2 and 3 were governed by bolt failure, and mode 3 presented the lowest level of ductility. An interesting feature of the cyclic moment-rotation curves was observed, i.e., the increase in stiffness observable at large inelastic displacements, related to the plastic deformation of the end-plate. The prediction model of the EC3 was found to not be accurate, since it overestimated stiffness in nearly all tests by factors ranging from 1.56 to 3.97, leading to low values of rotation at yield. The predicted ultimate bending moment, however, provided a good fit to the experimental results, with differences of about 15% for most cases. The failure modes displayed by individual joints were correctly predicted. The

consequences for design purposes of the difference between real and predicted behaviour may lead to larger than predicted frame natural periods leading to overly conservative design forces and larger than predicted story drifts. The error in moment capacities may render column capacity design checks unsafe, while leading also to uneconomical design. The use of flush end-plate joints in seismic resistant frames is considered to be likely limited to areas of low-to-medium seismicity. It was observed that the joints with the highest moment capacities (i.e., mode 3 joints) display the lowest rotation ductility.

The behaviour of flush endplates joints under elevated temperatures was the subject of experimental and numerical investigations by Yu *et al.* (2011) for which the coupled effect of tying forces and large rotations was analysed.

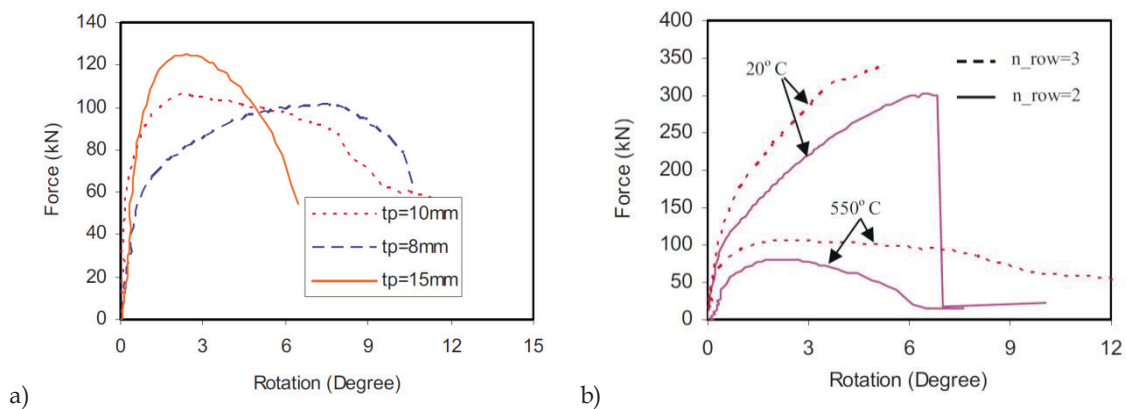


Figure 2.31: a) Effect of endplate thickness; b) Effect of number of bolt rows (Yu *et al.*, 2011)

The endplate thickness was shown to have an effect on connection response, with thicker endplates corresponding to enhanced resistance but reduced ductility. The results have shown that flush endplate connections present a relatively stiff response when compared to other types of simple connections. For the investigated specimens, at low temperature, failure was found to be controlled by the end plate, which developed a shear fracture close to the weld.

### 2.8.3 Numerical studies

The moment-rotation behaviour of flush end-plate connections was predicted by Abolmaali *et al.* (2005) through the development of Ramberg-Osgood and Three-Parameter Power model equations. FE models were developed and verified according experimental tests from literature and were curve fitted according to the two models in

order to obtain the defining parameters and both modelling techniques were found to predict experimental  $M-\phi$  curves with a good fit.

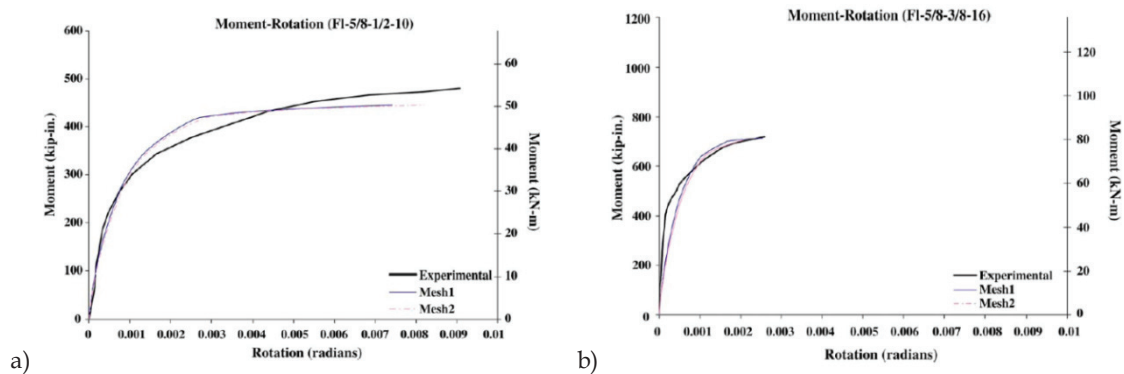


Figure 2.32: Comparison of experimental and numerical moment-rotation curves a) Case FI-5/8-1/2-10; b) Case FI-5/8-3/8-16 (Abolmaali *et al.*, 2005)

A numerical study on the effect of the axial force on the behaviour of flush end-plate joints was conducted by Goudarzi *et al.* (2012), showing that the application of tensile axial load on the beam caused a decrease in ultimate bending capacity, but that a compressive load applied to the beam caused an increase in the ultimate bending capacity of the connection for low compression values, followed by the decrease in connection capacity due to the buckling of the compressed flange, for higher compression loads.

A series of numerical simulations was conducted by Yang and Tan (2012) on different types of steel beam-to-column joints subjected to catenary action induced by middle column loss, including flush endplate joints.

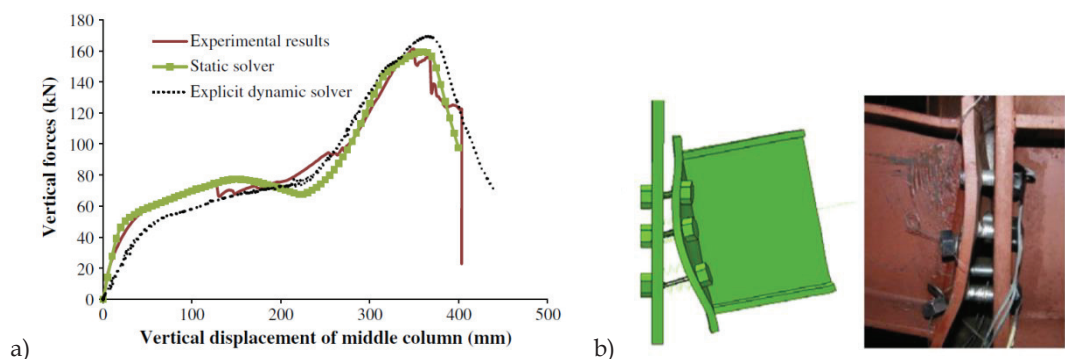


Figure 2.33: a) Comparison of FE simulations to test data of flush endplate connection; b) Failure modes of the static solver numerical simulation and of the experimental test (Yang and Tan, 2012)

The impact of the number of bolt rows in the joint response was investigated. Results showed that when bolt rows increased from 3 to 4, an increase of the first peak load was achieved given the increase in flexural resistance, but at large displacements,

the second peak load only produced a small increment compared to the first peak load value. Instead, for the 3 bolt row configuration, the second peak increase was very significant. Considering the same beam cross section, it was verified that the bolt located at the beam centroid improves resistance under catenary action.

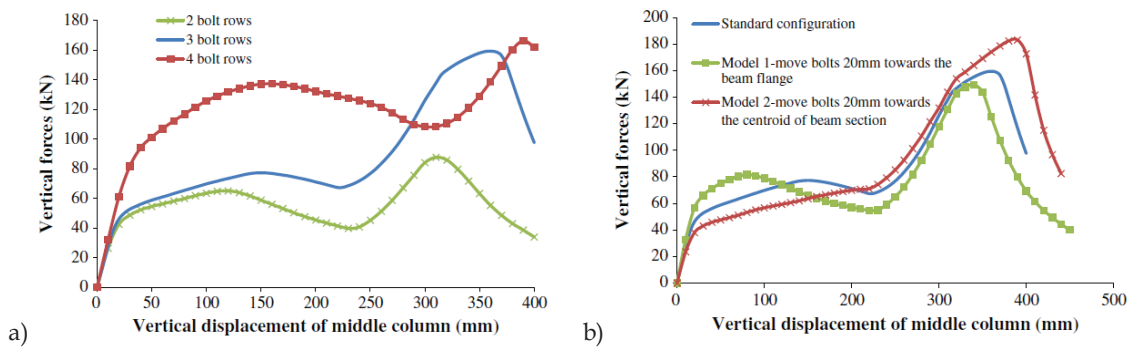


Figure 2.34: a) Effect of bolt rows for flush endplate connections; b) Effect of bolt arrangement for flush endplate connections (Yang and Tan, 2012)

The influence of bolt configuration was also investigated and results showed that moving the bolts closer to the centroid of the beam cross section led to improved resistance and ductility at the large deformation stage. The rotation capacities of the investigated joints were compared to code prescriptions. The simulation results yielded a total rotation (elastic rotation + plastic rotation) value of 150 mrad for the flush endplate connections, which compares to much smaller values of plastic rotational capacity given in the ASCE/SEI 41-06 (ASCE, 2006), hence indicating that the code values are likely too conservative, since they are based on experimental tests on joints under seismic loads. Since only pure flexural action contributes to seismic resistance, and since under column loss the catenary action significantly increases rotation capacity (by a factor of approximately 3), the smaller values prescribed in the code cannot apply directly.

## 2.9 Claddings

The study conducted by Farazman *et al.* (2012) investigated the contribution of unreinforced masonry infill panels to the robustness of steel framed buildings subject to sudden column loss. The infill panels were modelled according to the ultimate failure mode and confinement due to the frame. A simplified approach was proposed, in order to determine the contribution of the infill panel in isolation of the surrounding

frame and the net nonlinear response of the panel was obtained as the difference between the response of an infilled frame and a frame with no infill.

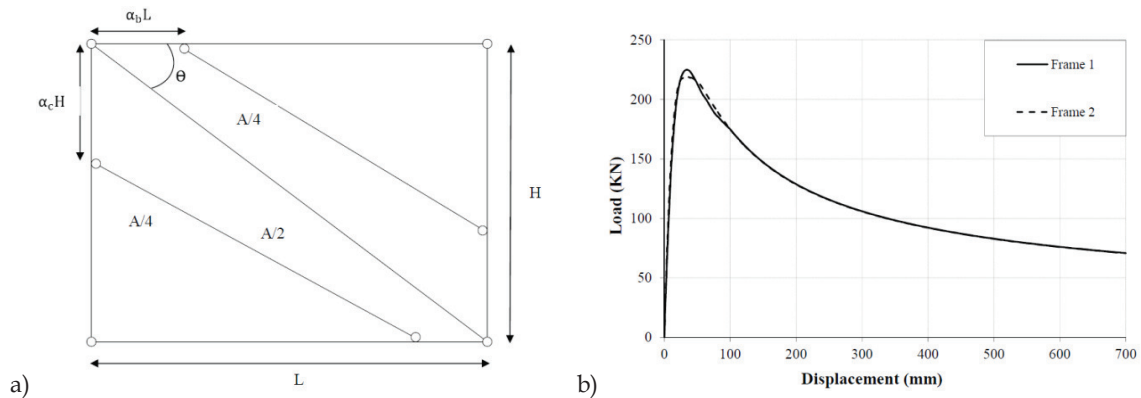


Figure 2.35: a) Geometry of the three strut model; b) Net nonlinear static response of the panel for different frame stiffness values (Farazman *et al.*, 2012)

It was concluded that the panel net response remained unaffected, allowing by superposition to determine the influence of panels on the pseudo-static resistance to column loss. Due to the brittle nature of panels, the maximum pseudo-static response may be obtained before the ductility limit is reached, in which case the resistance is given by the maximum value for dynamic displacements up to the ductility limit. Robustness was concluded to be governed by the additional contributions of the panels, rather than by the ductility of the connections on the floor system, meaning that in such cases, additional connection ductility brings no additional benefits in terms of robustness. The calculated DCR indicated that even for single leaf panels with openings, the contribution for robustness is significant. For panels without openings, the pseudo-static resistance is enhanced to an extent where even a bare steel frame without composite action fulfils the robustness requirements. It was concluded that clearly infill panels should be considered in robustness assessment and design.

The cyclic behaviour of masonry infill panels in steel frames was investigated by Markulak *et al.* (2013) through experimental tests on three types of masonry under quasi-static cyclic loading.

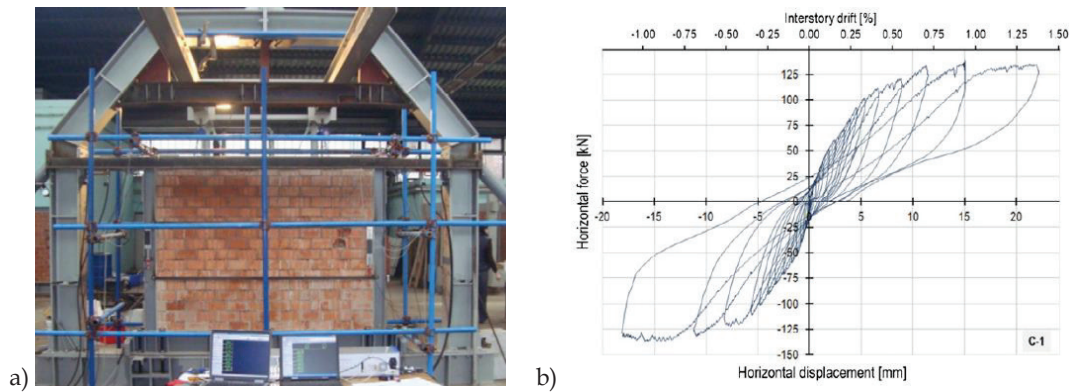


Figure 2.36: a) Test set-up for perforated clay block masonry; b) Hysteresis loops for the perforated clay block masonry C-1 (Markulak *et al.*, 2013)

The results from this study concluded that the load carrying capacity of steel frames infilled with perforated clay blocks was higher for values of up to 1% lateral drift while the ultimate lateral load capacity was 10% smaller than that for aerated blocks. The infilled frames with clay perforated blocks retained their carrying capacity up to drift values of 1.7% and their lateral stiffness was found to be 40% higher. The amount of dissipated hysteretic energy was 6.7 times higher than that of the bare steel frame, highlighting the importance of the contribution of these elements for structural behaviour under cyclic actions.

## **Chapter 3 Definition of parametric study and design of frames**

### **3.1 Introduction**

Following the literature review, the next step in the present study consisted in identifying the relevant variables for the parametric numerical study of the residual post seismic robustness of moment resisting frame steel buildings. This required the definition of the structural typologies to be designed and the characterization of the robustness analysis cases to be studied.

The definition of materials, structural layouts, actions, action combination criteria and limit state verification criteria enabled to subsequently perform the required linear static analysis to design the structures of the buildings as defined for the parametric study. A more detailed description and justification of the definition of the parametric variables, analysis cases, design assumptions and methodologies and numerical models is presented in this chapter.

### **3.2 Parametric variables and analysis cases**

#### ***3.2.1 Parametric variables***

The parametric variables were selected in order to be representative of a large number of realistic structures. Several parametric variables were identified, to which values were attributed based on the relevance that such parameters may hold regarding the robustness study to be conducted. The list of the considered parametric variables and corresponding values is presented in Table 3.1.

As for fixed parameters for the linear elastic design of the set of structures, all floor systems were considered as composite, the column base connections were taken as pinned, beam-to-column connections belonging to the moment resisting frames were taken as full strength rigid and beam-to-column connections not belonging to the moment resisting frames were considered pinned.

To unequivocally identify each structure, a labelling system was created, that establishes the correspondence between the structure's name and its unique set of parametric variables. An example of a structure label is given by the code N8-H3-S6-CL-T4x4-DE, where N indicates the number of storeys, H is the interstorey height, S is the bay span, C is the cladding type, T is the type of bay plan layout and D is the lateral force design scenario.

Table 3.1: Parametric numerical study - variables and admissible values

PARAMETRIC VARIABLE	ADMISSIBLE VALUES	CASES
(N) Number of storeys	4; 8	2
(H) Interstorey height	3m (3.5m between gr. and 1 <sup>st</sup> floor); 4m (4.5m between gr. and 1 <sup>st</sup> floor)	2
(S) Bay span	6m; 10m	2
(C) Façade claddings*	None (N); Brick masonry (M - for wind designed frames); Cold formed steel "X" bracing (C - for seismically designed frames)	2
(T) Bay plan layout	3x5; 4x4; 5x4	3
(D) Lateral force design scenario	Wind designed (W) ; Seismic + Wind designed (E)	2
(L) Column removal scenario	XZ façade (L); XY façade (S); Corner (C)	3

\* - Not modelled in the preliminary robustness assessment

### 3.2.2 Analysis cases

The designed structures will be analysed under different column loss scenarios, for both undamaged and damaged conditions, where the latter corresponds to the structure after sustaining damage induced by seismic action. Regarding the column loss location, three different peripheral scenarios have been considered, with column removals for the corner column, long façade column and short façade column. For each plan location for the column removal, the section of column to be removed is the one defined between the ground level and the first storey.



### 3.3 Design assumptions

#### 3.3.1 Structural solution

##### 3.3.1.1 Foundations

The type of foundation considered was a continuous slab, in order to guarantee that the horizontal displacements at the bases of the columns are equal. For each peripheral column, small concrete walls acting as struts were added to restrain horizontal translational displacements at a height of 1m above the top of the foundation slab. The adopted solution is presented in Figure 3.1.

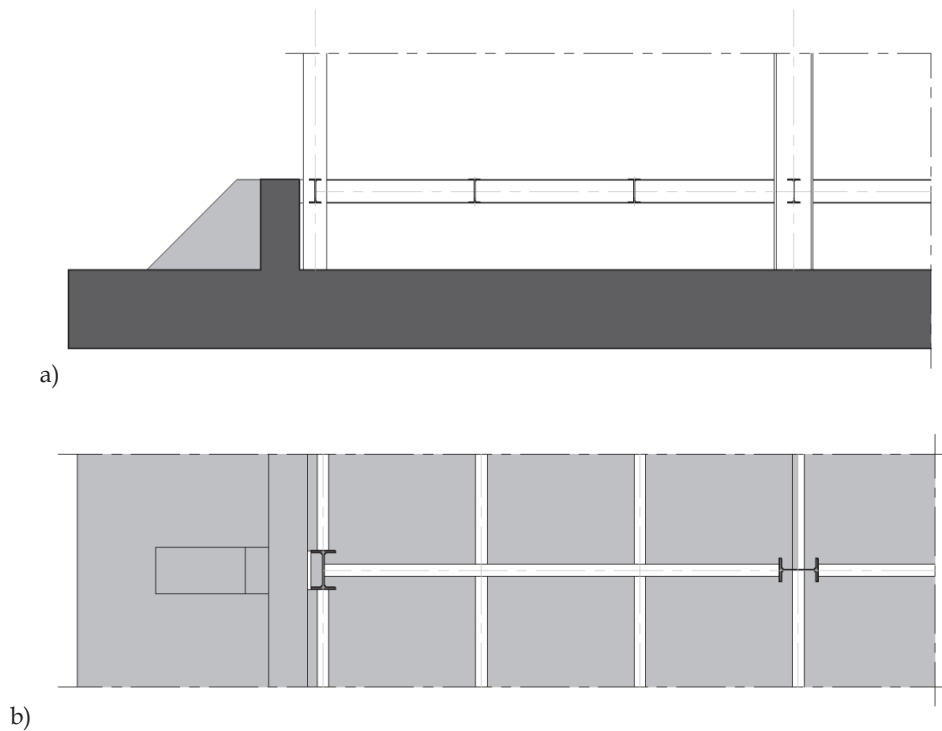


Figure 3.1: Building foundation type: a) elevation; b) plan view

##### 3.3.1.2 Superstructure

###### 3.3.1.2.1 Floor system

The building's floor system is composed of a pavement in profiled steel sheeting composite slab, supported by secondary steel beams with composite action and 2m spacings, idealised as perfectly pinned for design purposes. The secondary beams are supported by primary steel beams with composite action that transfer the loads to the steel columns. The adopted steel sheeting is a standard construction

product, commonly adopted in steel-concrete composite pavements. Its main geometric characteristics are presented in Figure 3.2.

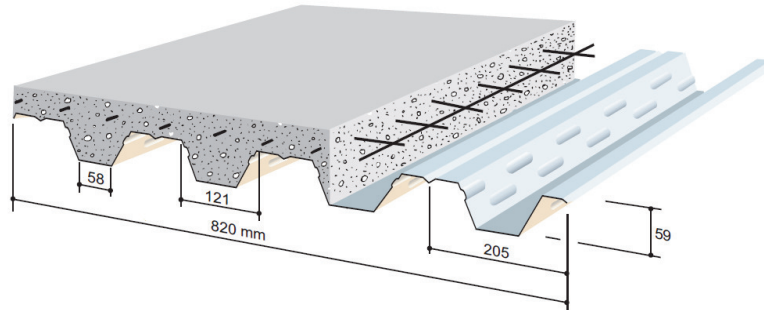


Figure 3.2: Composite floor system - steel sheeting geometry

A thickness of 0.75mm was adopted for the steel sheeting, and a total height of 10 cm was considered for the composite floor. The verification of the Ultimate Limit States was performed in accordance with tables supplied by the manufacturer for maximum admissible loads, considering deflection limitations for the construction and final stages.

### 3.3.1.2.2 Beams

The floor is supported by secondary and primary steel beams with composite action. The standard layout of the beams is displayed in Figure 3.3.

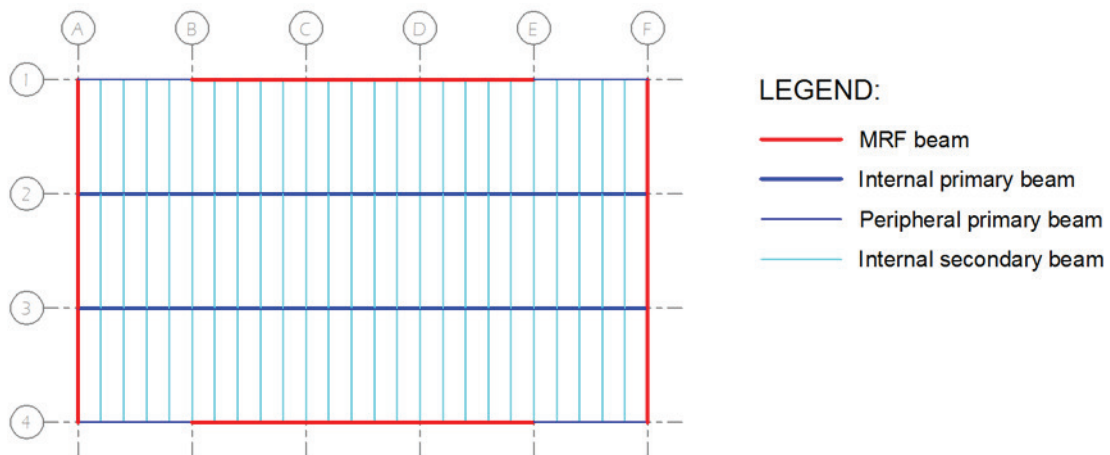


Figure 3.3: Example of floor beam layout and beam types

In the example shown the secondary beams are marked in light blue, the primary beams in dark blue and the beams that make up the moment resisting frame

(MRF) are marked in red. The beams marked in light and dark blue were designed for gravity loads only, whereas the beams marked in red, which belong to the moment resisting frames, were designed for both vertical and horizontal loads. The beams designed for gravity loads were considered as pinned at both ends for design purposes, whereas the connections at the extremities of the beams of the MRF were considered as full-strength rigid. For the design, all beams were considered as unpropped during the constructive stage, with lateral torsional restraints at the ends only and studs welded through the profiled steel sheeting. An important characteristic for the design of the beams belonging to the MRF is that they were designed to not take advantage of composite action, by disconnecting the beams from the composite floor system at the beam ends, in accordance with the procedure described in clause 7.7.5 of the EN 1998-1 (CEN, 2004), which states that the plastic resistance of a composite beam may be computed taking into account only the steel section, if the slab is disconnected from the steel frame in a circular zone around the column with a diameter  $2b_{eff}$ , where  $b_{eff}$  is the larger of the effective widths of the beams connected to that column. In this sense the lateral resisting structure is an all-steel structure and may be analysed and designed as such. The beams were designed considering IPE, HEA or HEB sections only.

#### 3.3.1.2.3 Columns

The columns that make up the structure are steel columns and are considered to have full-strength rigid connections at column splices and pinned connections at the base. In terms of geometry, the columns present a first section between the foundation level and the ground level with a 1m length. The column section between the ground floor and the first elevated is characterized by an interstorey height that is 0.5m longer than the interstorey height between all other elevated floors. The columns were designed considering HEA or HEB sections only.

#### 3.3.1.2.4 Moment resisting frames

The lateral resisting structure is made up of moment resisting frames located at the peripheral zones of the structures, in order to reduce the effects of torsional Eigen modes. Three different floor plan layouts variations were considered for the parametric study, as described above, and for each layout, the location of the MRFs was selected in

order to maximize structural resistance while trying to maintain an adequate balance with the potential buildings costs. In Figure 3.4 the location of the MRFs for each type of considered layout is highlighted in red.

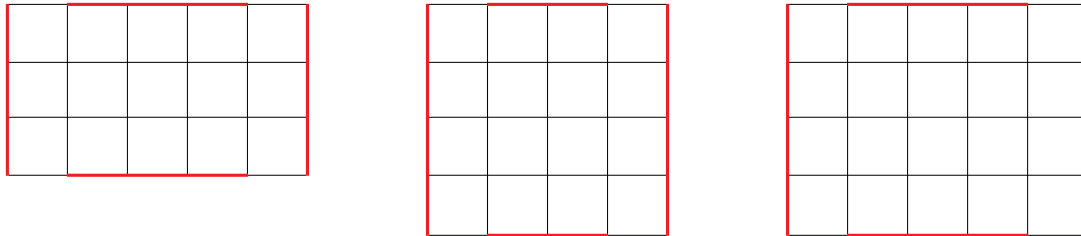


Figure 3.4: Moment resisting frame locations for the floor plan layouts

For each layout, a total of four MRFs were adopted, with two MRFs distributed along the  $x$  direction and two along the  $y$  direction. The MRFs were defined so as not to intersect in a common node, resulting in simpler connections and in a more simple and intelligible structural behaviour. For the particular case of the 8 storey structures with 10m span designed for seismic actions, for which the design was not feasible under the above mentioned design assumptions, a full 3D moment resisting frame was considered. In this sense, all nodes were designed to be moment resisting and column cruciform cross sections were considered which are symmetrical about the main axes and are built up by welding a pair of steel wide flange profiles.

### 3.3.2 Materials

The materials considered in the structural design are presented in Table 3.2.

Table 3.2: Materials

ELEMENT	MATERIAL
Steel in profiled sheeting	S 320 GD
Concrete in composite floors	C30/37
Steel in beams	S355
Steel in columns	S355 or S460

Steel grade S355 was assumed for all column members except for two cases, where S460 was adopted, namely the 5×4 and 4×4 seismically designed (DE) structures

with 8 storeys, in order to satisfy the strength requirements for N-M-V interaction at Ultimate Limit State.

### 3.3.3 Actions

The quantification of permanent actions and live loads was done in accordance with the EN 1990 (CEN, 2005) and the EN 1991-1-1 (CEN, 2002). The wind loads were determined according to the EN 1991-1-4 (CEN, 2005) and the seismic design action was quantified in accordance with the EN 1998-1 (CEN, 2004).

#### 3.3.3.1 Permanent structural actions

Concrete elements	$\gamma = 25 \text{ kN/m}^3$
Steel elements	$\gamma = 77 \text{ kN/m}^3$
Composite slab	$1.7 \text{ kN/m}^2$

#### 3.3.3.2 Permanent non-structural actions

##### Ground Floor:

Floor	$0.4 \text{ kN/m}^2$
Facade	$0.5 \text{ kN/m}^2$
Internal partition walls	$0.8 \text{ kN/m}^2$

##### Elevated storeys:

Floor	$0.4 \text{ kN/m}^2$
Facade	$0.5 \text{ kN/m}^2$
Suspended ceiling	$0.2 \text{ kN/m}^2$
Internal partition walls	$0.8 \text{ kN/m}^2$

##### Roof storey:

Insulation system	$1.0 \text{ kN/m}^2$
Facade	$0.5 \text{ kN/m}^2$
Suspended ceiling	$0.2 \text{ kN/m}^2$

### 3.3.3.3 Live loads

Ground floor	Category D1	4.0 kN/m <sup>2</sup>
Elevated storeys	Category B	3.0 kN/m <sup>2</sup>
Roof storey	Category H	0.4 kN/m <sup>2</sup>

### 3.3.3.4 Wind loads

For the determination of the design wind loads, the basic wind velocity  $v_b$  was calculated through the expression given in clause 4.2(2)P of the EN 1991-1-4 (CEN, 2005). The values of the basic wind velocity depend on the value of the fundamental value of the basic wind velocity  $v_{b,0}$ , which is given in the National Annexes. In this sense, it was considered in accordance with the Portuguese National Annex that the structure is located in the most unfavourable wind zone in Portugal, which is designated as zone A. In this zone the fundamental value of the basic wind velocity  $v_{b,0}$  is equal to 30m/s. For the design, it was considered that the terrain category is category III, which is representative of suburban areas. The choice of the terrain category III is related to the fact that designing a structure for strong wind loads can provide the structure with an exaggerated level of robustness that is not representative of buildings. The exposure factor was considered according to the Figure NA-4.2 of the Portuguese National Annex of the EN 1991-1-4 (CEN, 2005) and the structural coefficient  $c_s c_d$  was taken as 1.

### 3.3.3.5 Seismic action

Regarding the definition of the seismic action, the following base hypotheses were assumed:

- Seismic action Type 1 ( $a_{gR}=2.45 \text{ m.s}^{-2}$ ) and Type 2 ( $a_{gR}=2.45 \text{ m.s}^{-2}$ ),
- Soil type C,
- Importance class II,
- Ductility Class DCH and
- Behaviour factor  $q = 5 \times (\alpha_u / \alpha_1) = 5 \times 1.3 = 6.5$ .

The reference ground acceleration values used correspond to an acceleration of 0.25g, which was deemed representative of moderate seismicity zones. The expressions

used to generate the spectra were the ones indicated in clause 3.2.2.5 of the EN 1998-1 (CEN, 2004). The design response spectra considered are presented in Figure 3.5.

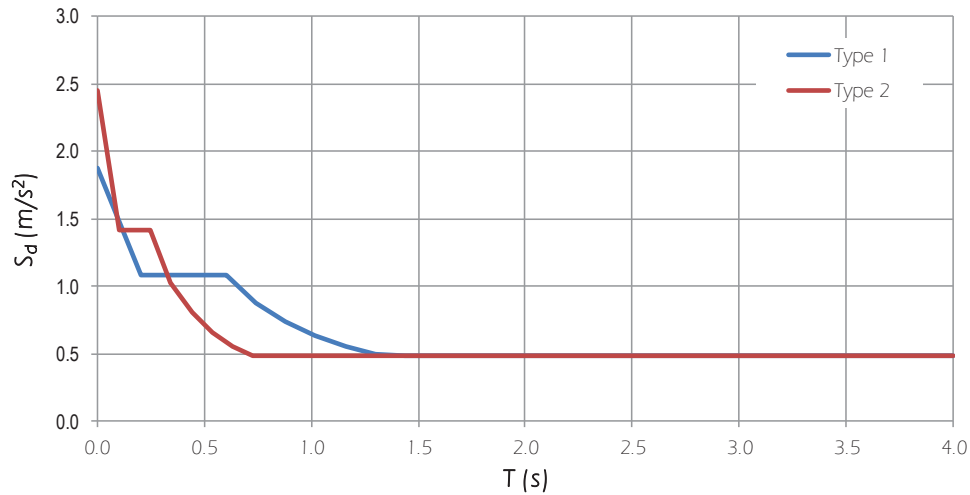


Figure 3.5: Horizontal design acceleration response spectra

For limit state verifications, the following assumptions were considered:

- Displacement behaviour factor  $q_d$  assumed equal to behaviour factor  $q$  (for  $T > T_C$ ),
- $d_r \nu \leq 0.01h$  (Damage limitation requirement considering that non-structural elements do not interfere with structural deformations),
- $\nu=0.5$  (Importance Class II) and
- $f_{y,max} \leq 1.1\gamma_{ov}f_y$  (for the steel in dissipative zones).

### 3.3.4 Imperfections and 2<sup>nd</sup> order effects

The imperfections for global analysis of the frames were introduced in the form of horizontal forces, equivalent to the global initial sway imperfections, as given in clause 5.3.2 of the EN 1993-1-1 (CEN, 2005). Taking into account that each storey was modelled as a diaphragm, the total horizontal force on a given storey  $\phi N_{Ed}$  can therefore be applied at each level considering a total axial force  $N_{Ed}$  that corresponds to the sum of the vertical forces of all the columns on that floor.

According to clause 5.2.1 of the EN 1993-1-1 (CEN, 2005), the 2<sup>nd</sup> order effects should be considered if they increase the actions effects significantly, or modify significantly the structural behaviour. These effects can be neglected if the following criterion is satisfied for an elastic analysis:

$$\alpha_{cr} = \frac{F_{cr}}{F_{Ed}} \geq 10 \quad (3.1)$$

The buckling analysis was performed on the Finite Element program, in order to determine the buckling modes and corresponding  $\alpha_{cr}$  parameters, and geometrically nonlinear analysis was performed for the wind designed structures in cases where the criterion was not met. In the case of seismic designed structures, 2<sup>nd</sup> order effects were considered through 2<sup>nd</sup> order effects multipliers for elements at each storey level.

### 3.3.5 Modelling

The modelling and analysis of the set of structures for the numerical parametric study was performed in the finite element software SAP 2000 v14 (CSI, 2009). To this end, one-dimensional finite elements were used to numerically model the structures.

In terms of restraints, the nodes at the bases of the columns were considered as pinned, with restrained translations degrees-of-freedom (DOF) along the global axis  $x$ ,  $y$  and  $z$ , and free rotation DOFs in all directions.

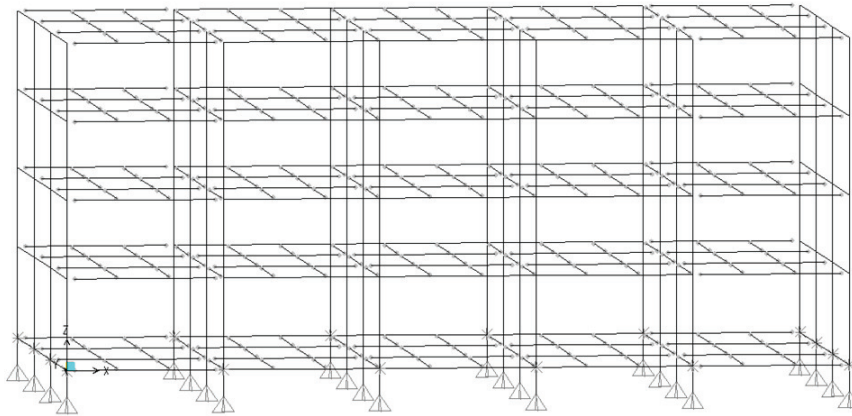


Figure 3.6: Finite element model for structural design (example)

The nodes of the columns at ground level along the periphery were considered as fixed, i.e., with restrained translational DOFs along the global  $x$  axis for columns belonging to the façade that develops along the  $y$  axis, and restrained translational DOFs along the  $y$  axis for columns belonging to the façade that develops along the  $x$  axis, in order to model the restraining effect of the concrete strut-walls in the peripheral zones of the building.



The fact that the composite slabs are connected to all the composite beams through shear connectors causes the floors to act as diaphragms. To model such effect, diaphragm constraints were introduced to all nodes belonging to a given storey, imposing equal translational DOFs to all joints along the  $x$  and  $y$  axis directions.

Regarding interior connections between elements, namely beam-beam splices or column-column splices, they were modelled with full continuity between elements. Regarding beam-to-column connections, the ones appertaining to the MRF were modelled with full continuity, i.e., as full strength rigid connections, whereas the beam-to-column connections of the gravity designed zones of the floor structure were modelled as pinned, as were the connections at the base of the columns.

### **3.4 Conclusive remarks**

In this chapter, the process that led to the design of the MRF steel structures has been described. The parametric variables of the study and corresponding values were defined, and the analysis cases for robustness were presented.

The design assumptions and methodologies were also presented, and a description of the structural solutions was provided, along with the materials, actions and combination criteria.

The set of structures designed according to the principles defined in this chapter was subsequently subjected to a preliminary robustness assessment, in order to identify structural subsets and properties that display low robustness, as described in Chapter 4.



## Chapter 4 Preliminary robustness assessment

### 4.1 Introduction

Seismic design rules currently implemented in modern codes (e.g. the EN 1998-1) aim at conceiving structures with adequate local and global ductility to guarantee the formation of an overall dissipative mechanism. This implies that dissipative zones (e.g. the beams in case of moment resisting frames) should be able to develop plastic hinges rotating until the collapse mechanism is completely developed without reducing their moment capacity, thus assuring the required redistribution of bending moments. The plastic deformation of ductile beams is characterized by strain hardening, which is responsible for the development of bending moments larger than the plastic bending strength. Therefore, according to hierarchy criteria, non-dissipative elements (namely connections and columns) should be designed to resist the maximum bending moment experienced by the beams. Consequently this philosophy leads to frames with strong column/weak beam assemblies. On the contrary, low/medium rise steel moment resisting frame (MRF) structures designed for lateral wind actions only, are typically characterized by a weak column/strong beam typology. It is thus evident that these two design philosophies should influence differently the structural robustness in case of progressive collapse.

The present chapter is dedicated to a preliminary robustness assessment of the set of MRF structures described in Chapter 3, aiming at quantifying structural robustness of steel MRFs under column loss scenarios and at assessing the efficacy of seismic detailing on arresting a progressive collapse under different column loss scenarios, considering simplified modelling assumptions regarding plastic hinge behaviour and secondary structure joint response. To this end, a numerical parametric

study based on both nonlinear static and nonlinear dynamic analysis is carried out on the set of reference frames and results are presented and discussed hereinafter.

## 4.2 Background

A study by El-Tawil *et al.* (2014) showed that imposing a ductile damage pattern is favourable since it increases the structural capacity against progressive collapse. However, the required level of detailing to improve the building robustness in case of column loss scenarios is still an open issue. In recent years, a large number of studies have been carried out on structural robustness and the progressive collapse of structures, as well. Izzudin *et al.* (2008) proposed a framework for evaluating robustness based on the computation of the system pseudo-static capacity. Pushdown analysis was also used in studies conducted by Lu *et al.* (2012) concluding that failure modes were correctly determined using pushdown analysis and that robustness can be quantified using the residual reserve strength ratio. The loss of stability induced progressive collapse modes were studied by Gerasimidis (2014). Numerical studies by Dinu *et al.* (2015), Khandelwal *et al.* (2008) and Hayes *et al.* (2005) showed that frames designed using seismic design provisions may improve robustness. Khandelwal *et al.* (2008) also concluded that layout and system strength significantly influence robustness and Jahromi (2009) verified that the response under column loss is dominated by a single mode. The importance of the three-dimensional effects on dynamic response was addressed by Song and Sezen (2013) and Alashker *et al.* (2011), concluding that 2D modelling does not necessarily lead to conservative results and that 3D analysis is required to rigorously investigate robustness. The influence of column loss action rise time was investigated by Comeliau *et al.* (2010) and a method for quantifying the maximum dynamic displacement for planar frames was proposed. An analytical method based on critical ductility curves was proposed by Gerasimidis (2014) to predict the collapse mechanism for the case of a corner column loss. A study by Fu (2010) showed that for many beams designed according current design practice, no plasticity is developed and catenary effect is not developed. The influence of different types of connections on robustness was investigated by Kim and Kim (2009). Formisano *et al.* (2015) highlighted that both full strength and rigid connections allow achieving satisfactory robustness levels, whereas semi-rigid ones exhibit inferior performance although providing adequate behaviour when they are full strength.

Studies by Ruth *et al.* (2006) and Song and Sezen (2013) showed that a dynamic increase factor (DIF) of 2.0 is overly conservative and that more economic design can be achieved. A new DIF to amplify the gravity loads within the bays that are immediately affected by a suddenly removed element was proposed by Liu (2013) which takes into account the specific level of gravity loads. Starossek and Haberland (2008) addressed the subject of robustness measures.

The effectiveness of seismic detailing according to EN 1998-1 (CEN, 2004) on improving structural robustness is still under discussion, and although there is some consensus that seismic detailing might be beneficial (Hayes *et al.*, 2005, Khandelwal *et al.*, 2008, Taewan and Jinkoo, 2009), quantification of this effect is still required. Adopting capacity design principles alone as a prescriptive measure for improving robustness presents shortcomings similar to prescriptions given by other codes (e.g. EN 1991-1-7 (CEN, 2006), UFC 2009 (United States of America Department of Defense, 2009) for addressing robustness, such as the “Tie Force Method” or the “Key Element Design”, which aim at assuring minimum levels of structural continuity and robustness.

### 4.3 Framework of the study

#### 4.3.1 Investigated parameters

In this chapter, a subset of 48 different building structures with varying number of storeys, interstorey height, span, bay configuration and design lateral loads (i.e. wind or earthquake) was used to perform a preliminary robustness assessment. The values of the parametric variables are those previously defined in Table 3.1, where the non-structural façade claddings were not modelled, in accordance with typical structural design assumptions.

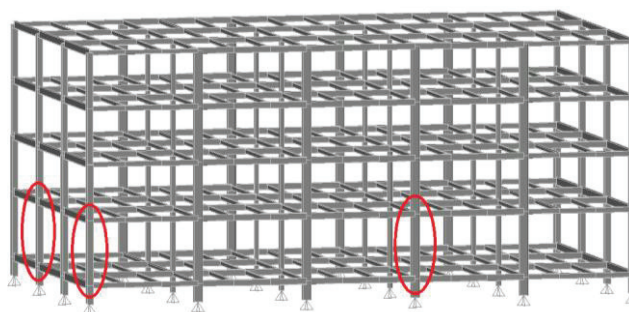


Figure 4.1: Column removal location scenarios

As shown in Figure 4.1, three column removal location scenarios were analysed for each structure (see also Table 3.1), namely: i) internal column along the XZ façade (LL); ii) internal column along the YZ façade (LS); iii) corner column (LC). The positions of column loss were defined in accordance with the UFC 2009 (United States of America Department of Defense, 2009), considering in all cases that the section to be removed is located between the ground level and the first storey.

#### **4.3.2 Design assumptions**

The materials and action definition considered for the preliminary assessment are those defined in sections 3.3.2 and 3.3.3, respectively. The verification checks and the requirements for seismic design are in accordance with EN 1993-1-1 (CEN, 2005) and EN 1998-1 (CEN, 2004), respectively.

Since the influence of joint detailing is out of the scope of this preliminary assessment, the beam-to-column joints of the MRFs were assumed as full strength rigid connections in all examined cases, whereas the joints in the secondary frame were modelled as perfectly pinned, as previously stated in Section 3.3.5.

Horizontal in-plane bracings were assumed to guarantee a diaphragmatic behaviour of each floor, which was conceived in order to avoid any composite behaviour with all (both primary and secondary) beams (i.e. all steel solution). Structures designed for the load scenario DE were conceived to resist both gravity and seismic actions and were subsequently verified against wind actions and redesigned whenever necessary, while maintaining compliance with the seismic design requirements (i.e. strong column - weak beam). Conversely, structures designed for the load scenario DW were conceived to resist solely gravity and wind actions in order to satisfy all limit states according to EN 1993-1-1. In this case, the dimensions of columns were directly obtained from elastic analysis and no hierarchy of resistance was considered, thus leading to strong beam-weak column frames.

Considering that the accidental action combination indicated in EN 1991-1-7 (CEN, 2006) factors the wind action by 0, the only horizontal loading applied to the MRFs corresponds to the initial sway imperfection which is accounted for by a system of equivalent horizontal forces, as indicated in EN 1993-1-1 (CEN, 2005).

On the basis of the above described actions, in order to highlight the design overstrength of the frame that influences the structural robustness, the margins of

safety  $\Omega$  at both serviceability limit state (SLS) and ultimate limit state (ULS) were also calculated for all examined frames as follows:

$$\Omega = \frac{R-E}{E} \quad (4.1)$$

where  $R$  is alternatively the displacement limit at SLS or the design factored strength at ULS of structural members, while  $E$  is the maximum effect induced by design actions, respectively at either SLS or ULS.

The average margin of safety factors for the analysed frames is summarized in Table 4.1 and Table 4.2. As it can be recognized, the beams of MRFs designed against either DW or DE lateral load scenarios are characterized by the higher  $\Omega_{\text{ULS}}$  values, which is due to the need to satisfy drift limitation and overall stability requirements. On the contrary, the beams of gravity load resisting frames are characterized by the lower  $\Omega_{\text{ULS}}$  values, because their design was mainly influenced by lateral torsional buckling verification checks for the constructional phase condition. This issue also explains large  $\Omega_{\text{SLS}}$  values. The columns of MRFs designed under DE scenario are characterized by low  $\Omega_{\text{ULS}}$  values, because of capacity design requirements. Also the gravity resisting columns are characterized by small safety margin. Conversely, the columns belonging to MRFs designed under DW scenario have the larger  $\Omega_{\text{ULS}}$  values, owing to the need to control lateral drifts. Finally, full strength joints were assumed for MRFs, characterized by safety margins ranging from 0.22 to 0.45 (N.B. lower for wind design frames and larger for seismic resisting structures). Pinned joints were considered for gravity load frames, with by safety margins ranging from 0.11 to 0.28, being the lower values for long span.

Table 4.1: Average margin of safety factors  $\Omega$  for moment frame elements

N	S	D	$\Omega_{SLS}$	$\Omega_{ULS,beam}$	$\Omega_{ULS,column}$	$\Omega_{ULS,joint}$
-	m	-	-	-	-	-
4	6	W	0.08	1.51	1.03	0.22
		E	0.15	0.81	0.29	0.39
	10	W	0.14	0.13	0.71	0.24
		E	0.07	0.17	0.06	0.41
8	6	W	0.05	2.08	0.51	0.26
		E	0.19	1.10	0.12	0.43
	10	W	0.14	1.32	0.07	0.27
		E	0.18	0.61	0.05	0.45

Table 4.2: Average margin of safety factors  $\Omega$  for secondary gravity frame elements

Element	S	$\Omega_{SLS}$	$\Omega_{ULS}$	$\Omega_{ULS,joint}$
-	-	-	-	-
Primary internal beam	6	0.88	0.23	0.19
	10	0.32	0.19	0.12
Primary perimeter beam	6	0.76	0.29	0.28
	10	0.24	0.35	0.11
Secondary internal beam	6	7.82	0.22	0.23
	10	14.00	0.22	0.14
Secondary perimeter beam	6	6.89	0.20	0.20
	10	11.50	0.30	0.13
Internal column	6	-	0.22	-
	10	-	0.04	-

### 4.3.3 Monitored parameters

The Alternative Load-path Method (ALM) is widely used to evaluate the robustness of steel frames ((U.S. General Services Administration, 2003); (United States of America Department of Defense, 2005); (United States of America Department of Defense, 2009) and is generally combined with a threat independent approach, characterized by instantaneous column loss, to evaluate the capacity of structures to internally redistribute loads and to arrest a progressive collapse. However, ALM does not provide further information about the reserve capacity of the structural system Khandelwal *et al.* (2008) and, consequently, does not allow distinguishing between structures with large and negligible reserve capacities. Hence, it is essential to adopt measures of robustness that provide a measurement of the system's sensitivity to localized failure. As highlighted by Starossek and Haberland (2008), none among the



methods used to assess robustness can be considered as the most effective or suitable in all cases, since different types of collapse mechanisms can be better described by using specific measures.

Robustness measures may be subdivided into two groups, namely local and global robustness measures. The former type evaluates robustness locally through demand-to-capacity ratios, whereas the latter type expresses global robustness through a ratio between the load capacity of the damaged structure and the nominal gravity loads (El-Tawil *et al.*, 2014). Several approaches to measuring robustness have been proposed by different authors, as previously described in section 2.6. In this study, a deterministic global robustness measure was adopted, namely the Residual Strength Ratio (*RSR*) of the system evaluated as follows:

$$RSR = \frac{F_{u,damaged}}{F_{dyn,damaged}} \quad (4.2)$$

where ( $F_{u,damaged}$ ) is the ultimate capacity of the structural system in the damaged configuration and ( $F_{dyn,damaged}$ ) is the equivalent dynamically amplified force (see Figure 4.2) for which the system reaches equilibrium in the damaged state, which is obtained as shown in Figure 4.3.

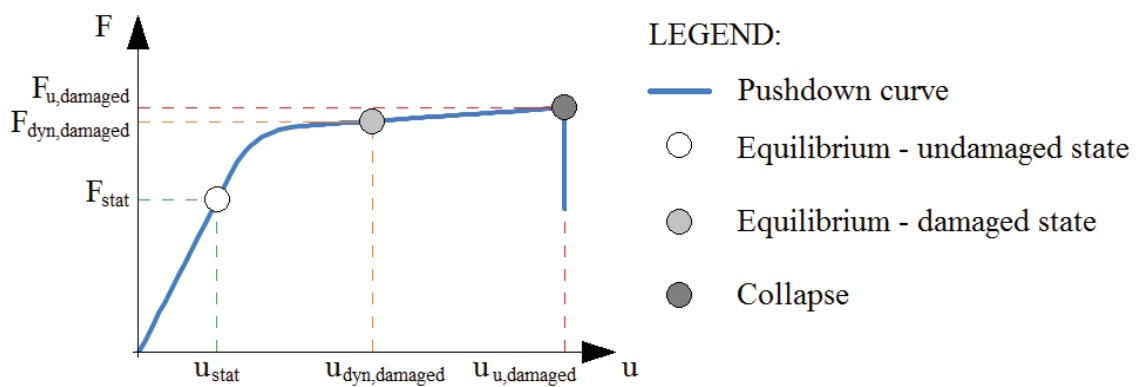


Figure 4.2: Schematic representation of static and dynamic equilibrium for a generic pushdown curve

It should be noted that *RSR* given in Eq. (4.2) differs from the index used by Lalani and Shuttleworth (1990) because these Authors assumed their redundancy index as the ratio between collapse and design loads.

The capacity of a system to respond to a column loss action in the plastic range by taking advantage of global ductility can be expressed by the Dynamic Load Factor

(*DLF*) which accounts for inertial and nonlinear effects (United States of America Department of Defense, 2009) and is given by the following ratio:

$$DLF = \frac{F_{dyn,damaged}}{F_{stat}} \quad (4.3)$$

where ( $F_{dyn,damaged}$ ) is the equivalent dynamically amplified force for which the system reaches equilibrium in the damaged state and ( $F_{stat}$ ) is the value of the static gravity loads on the resisting element prior to notional removal (see Figure 4.2).

In order to assess the system's reserve displacement capacity, the Residual Ductility Ratio (*RDR*) was considered as ductility measure. This parameter is given as the following ratio:

$$RDR = \frac{u_{u,damaged}}{u_{dyn,damaged}} \quad (4.4)$$

being ( $u_{u,damaged}$ ) the system's displacement immediately prior to global collapse and ( $u_{dyn,damaged}$ ) the equivalent dynamic displacement at equilibrium.

#### **4.3.4 Analysis methodology**

##### *4.3.4.1 Pushdown analysis*

For pushdown analysis, both material and geometrical nonlinearities were accounted for. In addition, the internal force distribution in the element to be removed was initially determined in accordance with the accidental load combination given in the EN 1991-1-7 (CEN, 2006), and the column segment was replaced by the equivalent reactions. Subsequently, increasing vertical displacements were imposed to the node to which equivalent column reaction forces were applied, hence generating the vertical force-displacement pushdown curve.

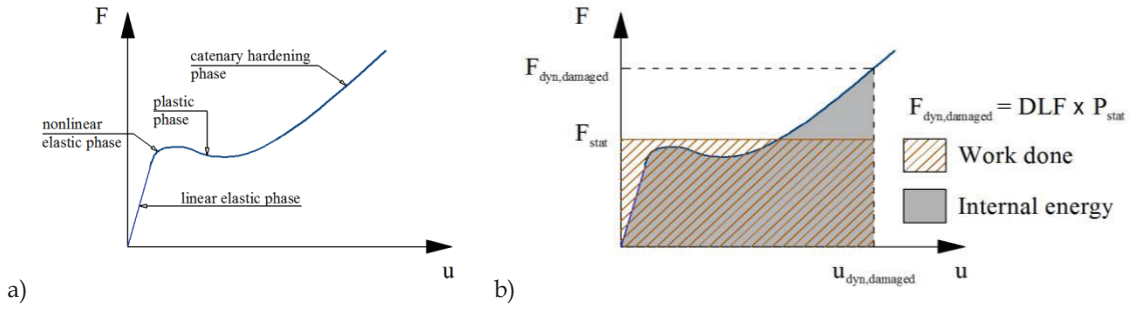


Figure 4.3: Typical nonlinear static structural response according to (Izzudin, Vlassis, Elghazouli, & Nethercot, 2008)

The procedure adopted to assess structural robustness by means of pushdown analyses was the energy balance method proposed by Izzudin *et al.* (2008). This methodology allows computing the system pseudo-static capacity by imposing a zero kinetic energy condition, and consists of three stages: i) Determination of the nonlinear static response of the structure under gravitational loading; ii) Simplified dynamic assessment through energy balance to establish the maximum dynamic response; iii) Ductility assessment of the connections. The computation of the response implicitly assumes that the directly affected zone behaves as a Single Degree of Freedom (SDOF) system, which is considered a reasonable hypothesis for robustness assessment purposes (Jahromi, 2009). The structural response under column loss is characterized by an initial linear elastic phase, followed by a nonlinear phase due to geometric and material nonlinearity, and finally by an eventual hardening phase due to catenary effect, or alternatively by a softening phase due to buckling or failure of structural elements. The typical nonlinear static structural response is presented in Figure 4.3.

The application of the energy balance method requires the computation of the external work done (which is equal to the axial force in the column prior to removal times the total vertical displacement at each step of the pushdown analysis) and the computation of the internal energy (which is given by integral of the Force-Displacement system response curve) for all vertical displacement values.

The external work done  $W_{ext}$  and the internal energy  $W_{int}$  at the vertical pushdown displacement  $u_i$  are given by:

$$W_{ext} = F_{stat} \times u_i \quad (4.5)$$

$$W_{int} = \int_0^{u_i} F(u) du \quad (4.6)$$

Equilibrium in the damaged configuration is achieved by imposing the zero kinetic energy condition, which is obtained when the energy balance is equal to zero, i.e., when the work done is equal to the internal energy:

$$\Delta W = W_{ext} - W_{int} = 0 \quad (4.7)$$

$$F_{stat} \times u_i - \int_0^{u_i} F(u) du = 0 \quad (4.8)$$

The displacement value  $u_i$  for which the condition indicated in Eq. (4.8) is verified corresponds to the equivalent dynamic displacement at equilibrium  $u_{dyn,damaged}$  defined in Figure 4.3b). For the cases in which the energy balance is not obtained, the zero kinetic energy condition is therefore not reached and global structural collapse occurs.

#### 4.3.4.2 Nonlinear dynamic analysis

For the nonlinear dynamic analysis (NDA), a threat independent approach was adopted by considering a pseudo-instantaneous column removal. The load combination used for pushdown analysis was also considered for NDA, namely the accidental load combination described in EN 1991-1-7. In the first step, the equivalent reaction forces at the column end for the accidental load combination were determined. Subsequently, the gravity and the column equivalent reaction loads were applied according to a ramp function as shown in Figure 4.4. GSA 2003 guidelines (U.S. General Services Administration, 2003) recommend assuming a time interval  $t_r$  for the decreasing ramp function equal to or smaller than 1/10 of the natural vibration period of the structure. In order to verify the applicability of the recommended  $t_r$  value for the threat-independent analysis, a sensitivity study on column removal action rise time was carried out, which concluded that a rise time  $t_r = 0.01s$  was suitable to perform the analyses.

The NDAs were performed accounting for both geometrical and material nonlinearities, and using the Hilber-Hughes-Taylor alpha method (CSI, 2009) with an alpha coefficient equal to 0 and a time step of 0.01s for the direct integration method. In order to avoid overdamping, Rayleigh tangent damping ratio  $\zeta = 2\%$  was considered for a frequency of 1Hz and for the structure's natural frequency of vibration in the damaged configuration. The applicability of the assumed value for the damping ratio

was also verified by performing a sensitivity analysis for the examined column removal scenarios.

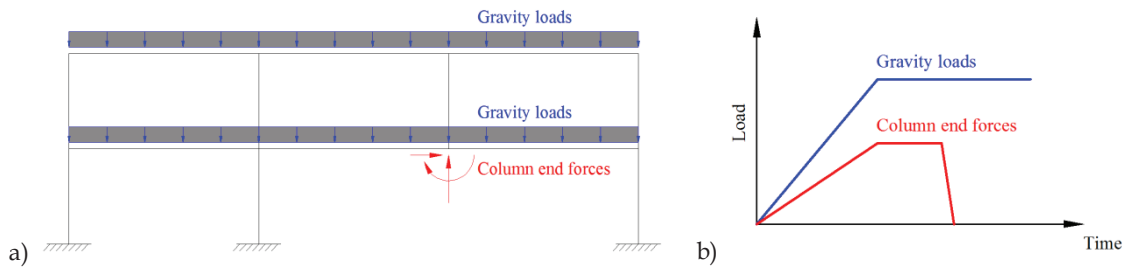


Figure 4.4: Gravity and column loss load time history application for NDA

The type of vibration mode after column loss (i.e either multiple or single vibration mode dominated behaviour) was also extracted from NDA response curves, and the joint rotation demands at the equilibrium condition in the damaged configuration were determined, as well.

#### 4.3.5 Modelling assumptions

The numerical models of the structures for the preliminary robustness assessment were developed using the software SAP 2000 (CSI, 2009). Geometric nonlinearities were taken into account according to the P-Delta formulation with large displacements. Material nonlinearity was modelled through a lumped plasticity formulation. The plastic hinge response curves and the relevant acceptance criteria were derived according to FEMA 356 (American Society of Civil Engineers (ASCE), 2000). Although the parameters provided by FEMA 356 refer to cyclic loading and despite the fact that modelling criteria given by UFC 2013 (United States of America Department of Defense, 2013) are specifically derived for pushdown analysis, the response of the examined beam-to-column joint is better described by the relationship provided by FEMA 356 (see Figure 4.6a). This is due to the fact that UFC 2013 does not provide modelling criteria specifically devoted to simulate the behaviour of full strength bolted moment connections which was the typology considered within this study.

The beams of both MRF and gravity resisting spans are all-steel members, because no composite action was considered with the floor that is simply supported by the steel girders. The diaphragmatic behaviour is guaranteed by the presence of in-plane bracing at floor level. The beam-to-column joints of the MRF beams were

modelled as full-strength rigid joints, while the gravity designed beams were considered as perfectly pinned at both ends. Since the behaviour of the joints of both MRF and secondary frames plays a key role in determining the frame robustness, the validity and consistency of the above described modelling assumptions were verified against finite element analysis (FEA) of beam-to-column joint sub-assemblies, which were selected according to the sub-structuring procedure depicted in Figure 4.5.

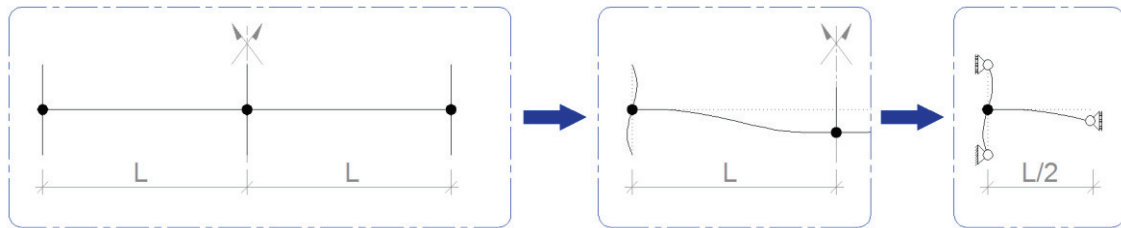


Figure 4.5: Substructure selection for joint modelling validation

For what concerns the joint typologies, bolted joints with extended endplate, rib stiffeners and additional column web panel configurations were considered for MRF, while flush endplate beam-to-column joints were assumed for the secondary structure, since both joint configurations are widely used in European practice. The joints have been designed according to the EN 1993-1-8 (CEN, 2005) and EN 1998 (CEN, 2004) for all beam-column assemblies of the frames reported in . Hereinafter, for briefness sake, the results from FEAs are described and commented for the most representative joints. In particular, the assembly consisting of an IPE 600 beam and an HEB 500 column was found to be representative of the MRF, because it is the one characterized by the deeper beam, thus potentially developing the larger catenary action on the connection. For the secondary structure, the results obtained for a flush endplate joint with an IPE 220 beam connected to an HEB 500 column are shown, because this joint is characterized by the weaker connection among those of all gravity resisting joint assemblies.

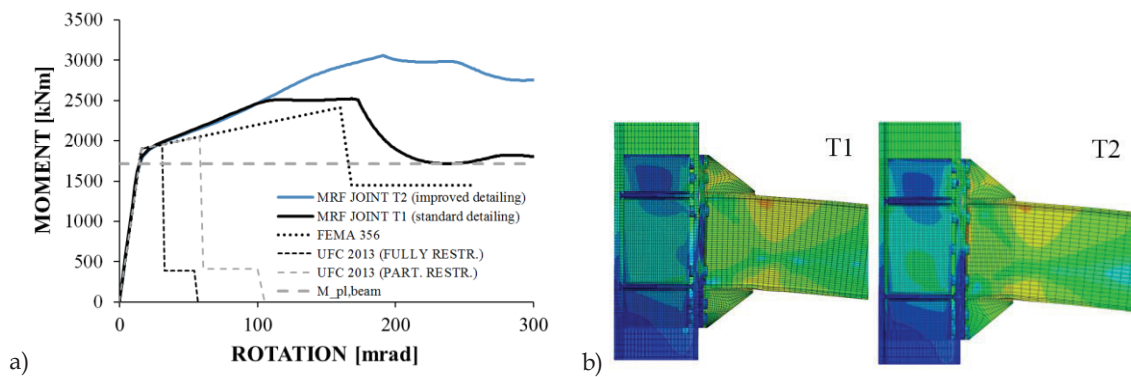


Figure 4.6: MRF joints under column loss action: a) Moment – chord rotation response; b) Deformed shapes (chord rotation = 100 mrad)

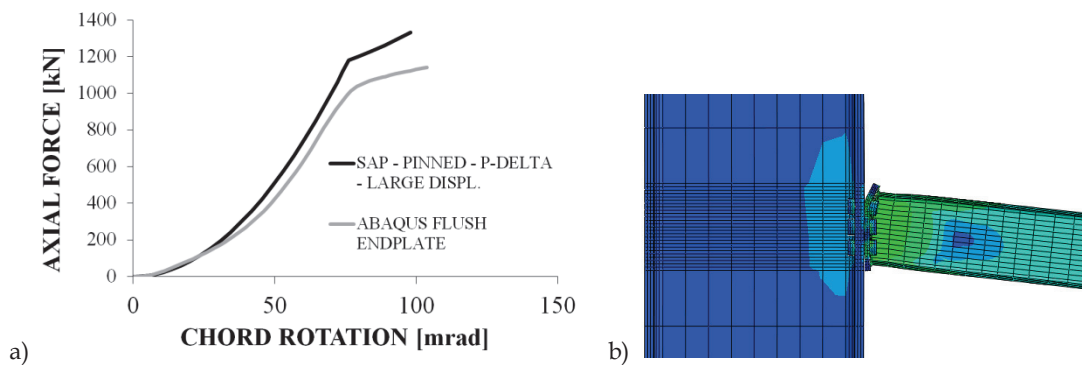


Figure 4.7: Gravity load resisting joint under column loss action: a) Axial force – chord rotation response; b) Deformed shape (chord rotation = 100 mrad)

The finite element models were developed using Abaqus ver. 6.13 (Dassault, 2013). The finite element type C3D8I (an 8-node linear brick, incompatible mode) was adopted for steel beams, columns and high strength bolts. This element was selected because it can effectively avoid shear-locking phenomenon (comparing with element C3D8R), which could significantly affect the initial stiffness of connection. Steel yielding was modelled by means of the von Mises yield criteria and plastic hardening was represented using a nonlinear kinematic and isotropic hardening. The external restraints were simulated by slaving to reference points (RP) the nodes belonging to the end cross sections of the beam and column. Contact phenomena were modelled considering the general contact algorithm using a Coulomb friction model. A penalty friction formulation was adopted and a friction coefficient of 0.3 was adopted.

Considering that the MRF beam-to-column joints are subjected to important catenary forces following column loss actions, two MRF joint configurations were analysed, namely a joint with standard detailing (T1) and a joint with improved detailing (T2) consisting of an additional bolt row in the middle of end plate (namely in

the horizontal axis of symmetry). The moment - chord rotation response curves for MRF joint types T1 and T2 are presented in Figure 4.6a, and compared with the plastic hinge response according to FEMA 356, UFC 2013 and the beam plastic bending moment  $M_{pl,beam}$ , the latter computed in accordance with the EN 1998-1 (CEN, 2004). In addition, the joint deformed shapes at an imposed chord rotation equal to 100 mrad are shown in Figure 4.6b.

As it can be noticed, both T1 and T2 joints are full strength and exhibit satisfactory response under column loss action, with bending strength being higher than the beam plastic capacity  $M_{pl,beam}$  even at very large rotations. The improved detailing of T2 has a beneficial effect under column loss actions, especially for chord rotation values higher than 100 mrad. The adopted FEMA 356 compliant response curve for plastic hinges shows a good agreement with the response of the T1 type joint (with standard detailing that is the type assumed for the examined structures), thus validating the adopted assumptions for MRF joints. The joint type T2 is out of the scope of this numerical study on building frames but it has been considered as a viable solution to improve joint performance if very large rotation demands are expected (Tartaglia *et al.*, 2016). Figure 4.7 shows the comparison between the SAP model axial force-chord rotation response curve with that obtained from FEA of the flush endplate joint. As it can be observed, the adopted model adequately reproduces the catenary action developed in the joint under column loss action, thus allowing deeming the joint response of the secondary beams sufficiently accurate for simulation.



## 4.4 Results

### 4.4.1 Pushdown analysis results

The overall response curves obtained from pushdown analyses are plotted in Figure 4.8 for the examined column loss scenarios (e.g. long façade, short façade and corner, respectively).

The comparison of pushdown results allowed the identification of three types of global failure mechanism, namely:

- Type I            characterized by high ductility due to the distribution of plasticity throughout the beam elements of the directly affected zone;
- Type II           characterized by poor ductility and typically conditioned by brittle column failure between the ground floor and the first storey;
- Type III          semi-ductile and generally characterized either by column failure in the segment between the last elevated storey and the roof or by simultaneous failure in beam and column members.

In terms of force-displacement response, Type I failure mode develops significant plasticity and achieves high ductility with large ultimate displacements; Type II failure mode presents linear elastic behaviour followed by sudden brittle failure associated to reduced ultimate displacements; frames with Type III failure develop an intermediate mechanism characterized by an initial plastic response followed by an early drop of resistance, after which a small plastic plateau is generally observed followed by full collapse at moderate ultimate displacements.

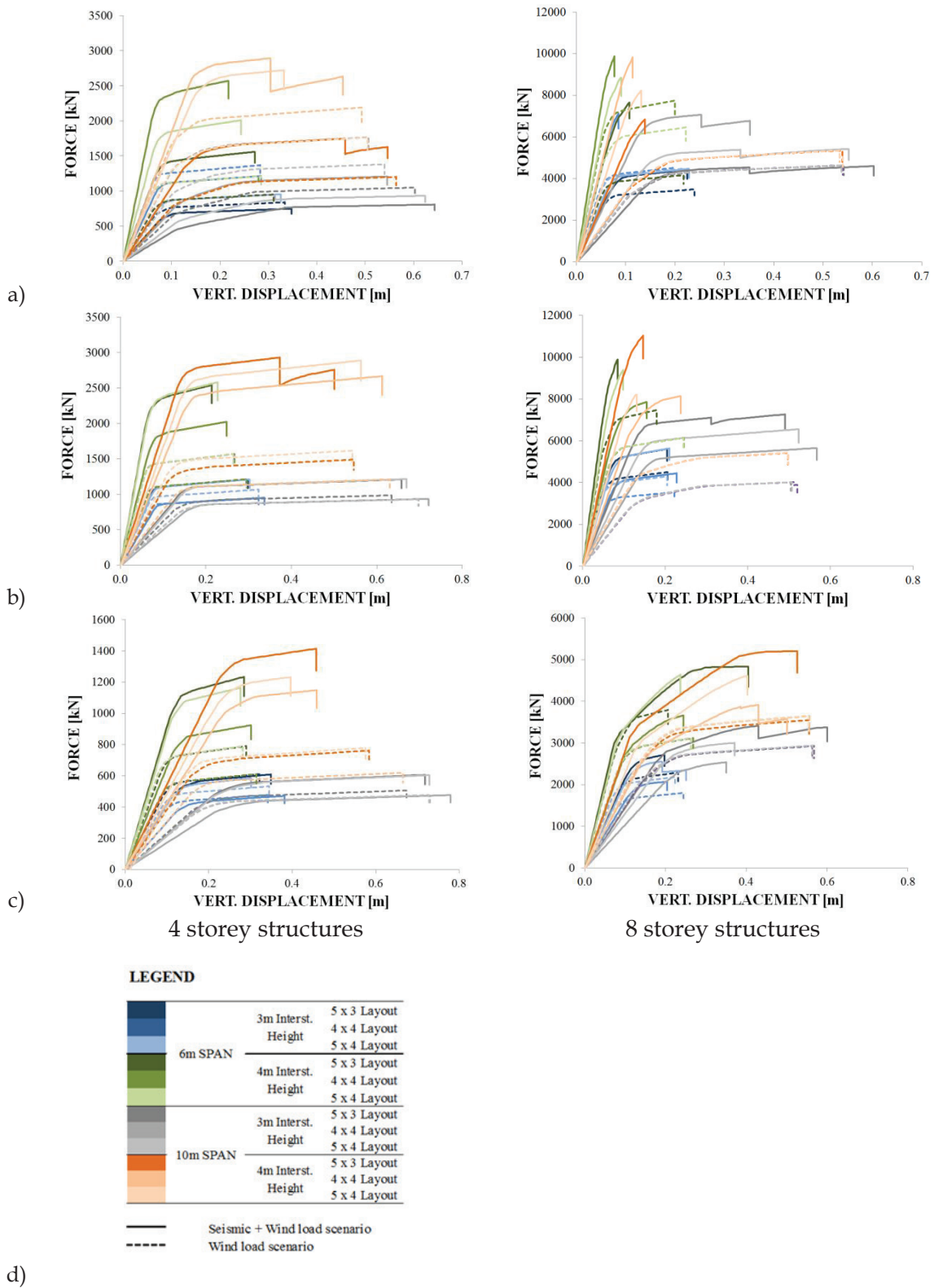


Figure 4.8: Pushdown curves for column removal in long façade (a), short façade (b), corner (c) and (d) legend

The typical plastic hinge distribution and response curve types are presented in Figure 4.9.

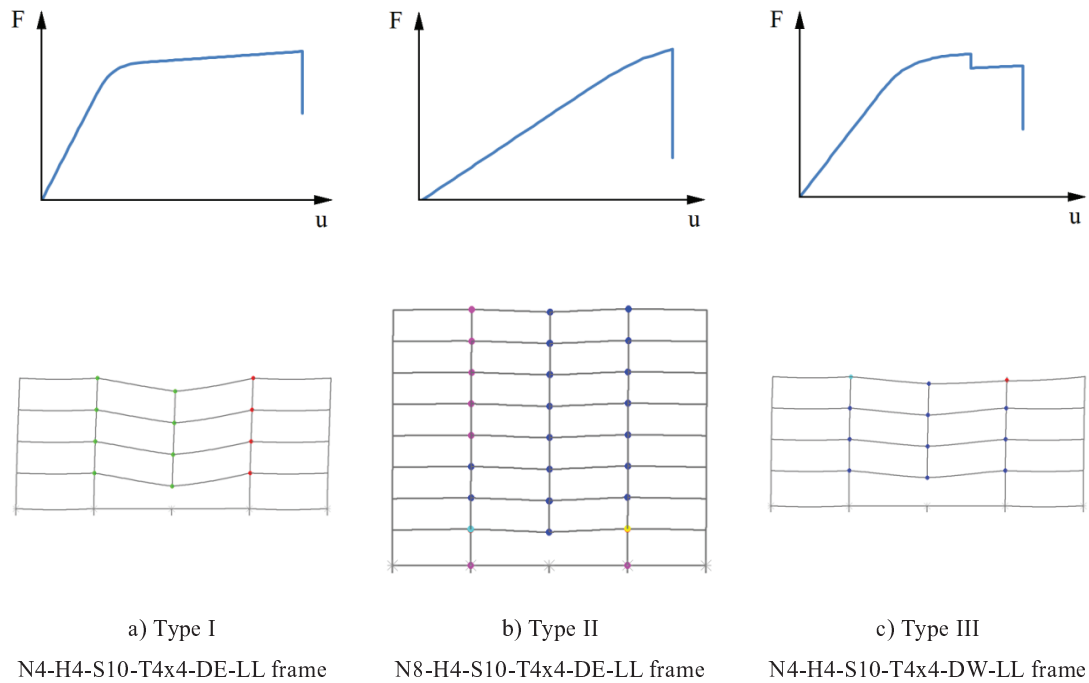


Figure 4.9: Identified failure mechanisms and corresponding plastic hinge distribution

The distribution of occurrence per failure type was analysed and results showed that the ductile Type I failure was observed for 94% and 61% of 4-storey and 8-storey buildings, respectively, while the corresponding occurrence of Type II failure was the 1% and 31%, highlighting that 8-storey structures are more susceptible to less ductile collapse modes. For what concerns the influence of the lateral load design scenario, all seismically designed structures presented ductile failure (i.e. mode Type I), whereas for the strong beam - weak column structures, 44% of failures were semi-ductile (i.e. mode Type III), or brittle (i.e. mode Type II).

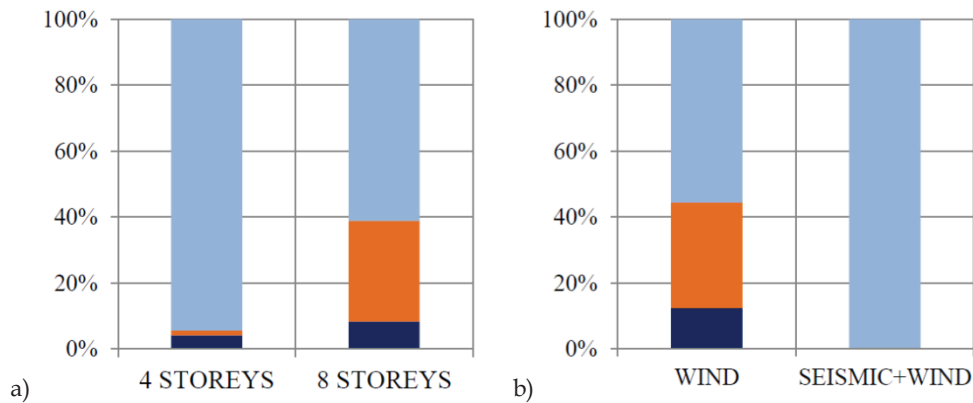


Figure 4.10: Failure mechanism occurrence distribution

#### 4.4.1.1 Residual strength ratio

The minimum acceptable *RSR* value for a structure is 1.0, which occurs when the equivalent dynamically amplified force for which the system reaches equilibrium in the damaged state  $F_{dyn,damaged}$  is equal to the ultimate capacity of the structural system in the damaged configuration  $F_{u,damaged}$  (see Eq. (4.2)). For cases in which the internal energy did not balance the work done, equilibrium was not reached and the *RSR* was taken as 0, indicating zero residual strength.

The *RSR* values for the 4 storey structures are presented in Figure 4.11 for the 6m span and 10m span structures. The analyses showed that the long span structures exhibit the lower values of *RSR*, with failure occurring in several cases, whereas no failures were observed for short span structures. These results are mainly due to two aspects: the longer is the span, the larger is the resultant of vertical loads requiring redistribution, and the larger is the demand on beam-to-column assemblies in terms of bending and catenary actions, as well.

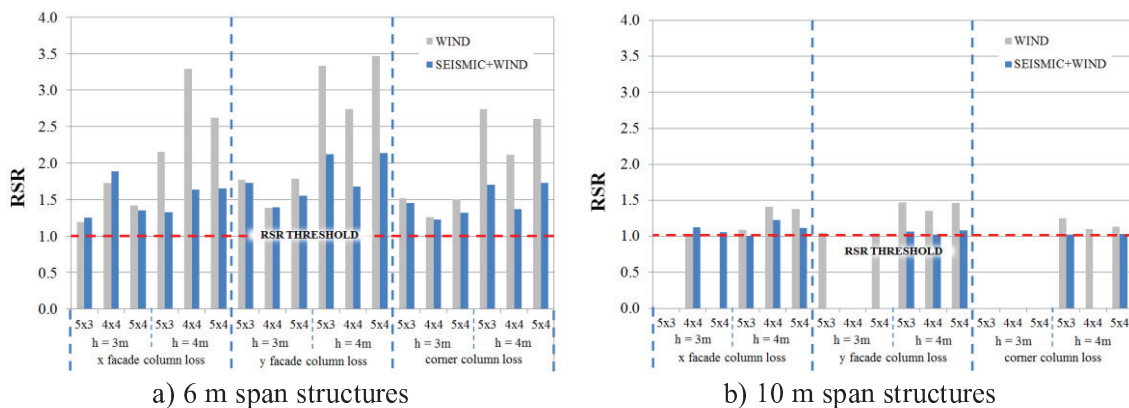


Figure 4.11: Residual Strength Ratios - 4 storey frames

As a general remark, all examined 4-storey structures characterized by deeper beams develop Type I overall failure mode, which mobilises the Vierendeel mechanism in the alternative load path, thus experiencing high ductility. Considering that wind designed structures present beams with larger cross sections dimensions, their capacity is comparatively higher than that of the seismically designed structures. Higher values of *RSR* were also observed for buildings with taller interstorey height. Once again, this result depends on the dimensions of girder cross section, which are deeper for taller buildings due to the need to limit storey drifts.

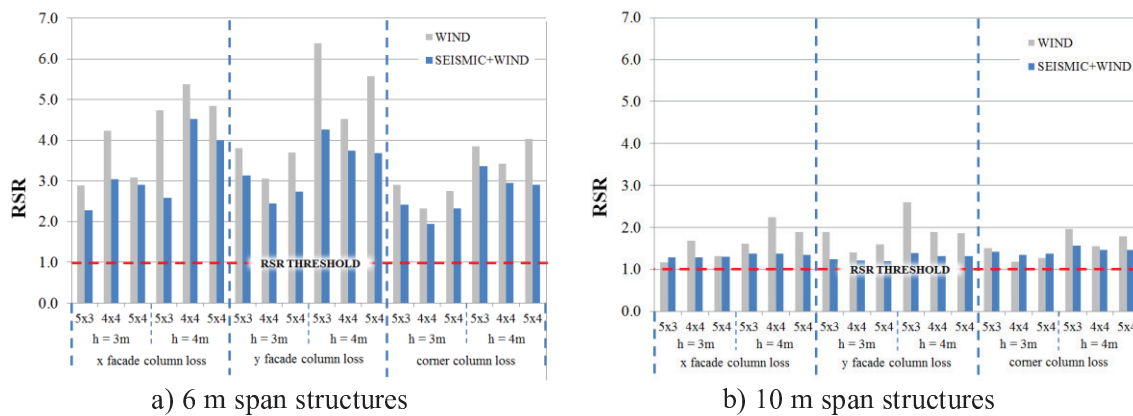


Figure 4.12: Residual Strength Ratios - 8 storey frames

The *RSR* values for the 8-storey structures are presented in Figure 4.12. Similarly to 4-storey frames, also in this case the ratios for the 10m span frames are close to 1.0, whereas 6m span frames provide larger robustness levels.

For both 4- and 8-storey frames, numerical results highlighted that the position of column loss scenario may influence *RSR*, especially for the cases of corner column loss that are characterized by lower robustness due to limited redistribution capacity. In addition, bay layout plays an important role. Indeed, structures with planar MRFs composed of few heavy elements (e.g. 4×4 bay layout in the x-z plan) are characterized by higher robustness levels. The number of spans belonging to the directly affected zone appreciably influences the frame robustness, as well.

In order to highlight the influence of seismic detailing on frame robustness, the *RSR* of seismic designed MRFs (i.e. weak beam – strong column) are compared to those of wind designed structures (i.e. strong beam – weak column) as depicted in Figure 4.13.

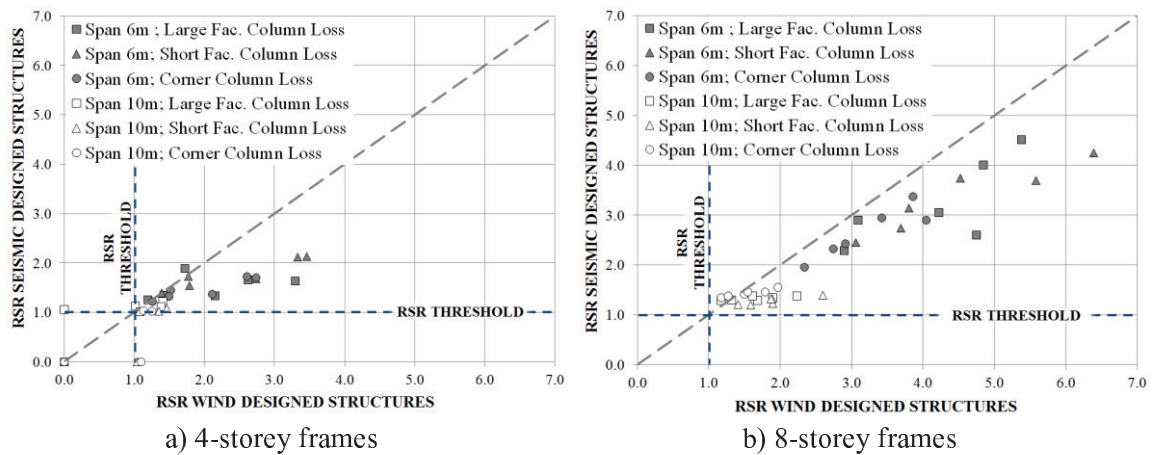


Figure 4.13: Residual Strength Ratio comparison

The *RSR* distribution outlines that the wind designed structures generally provide higher robustness, especially for the case of 8-storey frames. It is interesting to observe that seismic designed structures present smaller scatter of *RSR* than wind designed frames. This feature depends on the occurrence of failure modes. Indeed, all EC8 compliant MRFs are characterized by a Type I mechanism, while the set of wind design MRFs experienced all three types of failure modes. However, although seismic detailing provisions enforced a global ductile failure mode in all cases, it is not possible to find a direct correlation between adopting seismic provisions and enhanced robustness.

#### 4.4.1.2 Dynamic load factors

The *DLF* values were computed according to Eq. (4.3) in order to estimate the capacity of structures to exploit ductility in arresting a progressive collapse. In order to clarify the results described hereinafter, it should be noted that a *DLF* equal to 2.0 represents a purely elastic response, and a value equal to 1.0 corresponds to a theoretically rigid-plastic response, while a zero value corresponds to structural collapse. In non-collapsed cases, *DLF* values range from 1.0 to 2.0.

Figure 4.14 reports the distribution of *DLF* for 6m and 10m span structures, highlighting the role of the main investigated variables, like the column loss scenarios, the type of design lateral load and the number of storeys. As it can be observed, numerical results show that the majority of the 6m span structures respond to column loss in the elastic domain (i.e. *DLF* = 2.0) and are capable of arresting the progressive collapse, as indicated by the absence of collapsed structures (i.e. *DLF* = 0.0). Only some

of the 6m span 4-storeys frames exhibit *DLF* slightly below 2.0, whereas for the 8-storey structures, all frames are in the elastic range, thus confirming the beneficial role of a large number of resisting elements above the zone directly affected by column loss. Figure 4.14a also shows that frames' lateral load design scenario for 6m span frames does not influence *DLF*. The feature that short span frames essentially remain elastic implies that no permanent damage/deformation is sustained by the structure out of the parts directly affected by the column loss. In this sense, notwithstanding eventual localized damage (i.e. induced by the event which triggers the loss of column resistance), the required repairing interventions on the damaged frame are limited and can be made with reduced economical cost, since it mainly involves restoring the frame to its original position and replacing the damaged column segment.

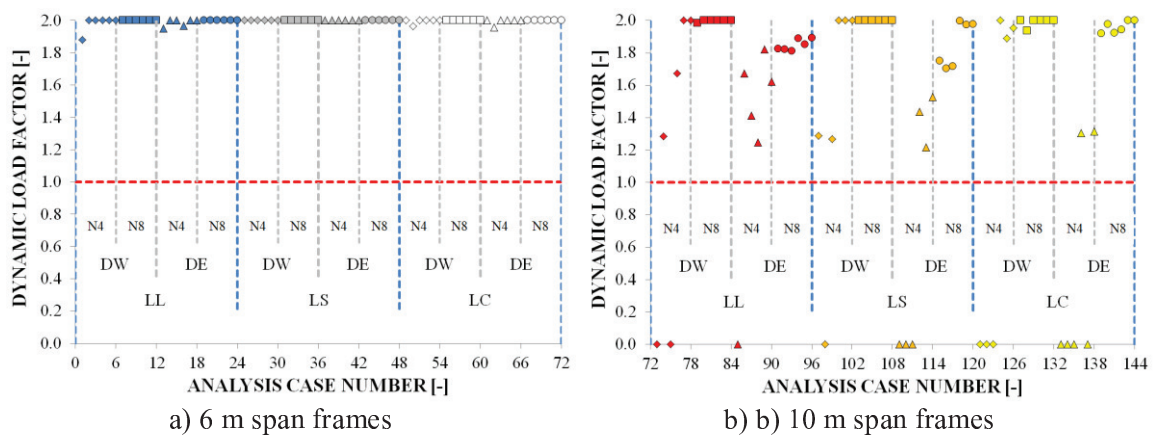


Figure 4.14: Dynamic Load Factor values by column removal scenario (LL, LS, LC), lateral load design scenario (DW, DE) and number of storeys (N4, N8)

The results for long (i.e. 10 m) span frames are reported in Figure 4.14b) and clearly show that several cases require the exploitation of frame ductility to arrest the collapse. Differently from the short span structures, for several cases, *DLFs* range between 1.0 and 2.0. As observed for the *RSR*, the reason explaining the differences in performance between the 10m span frames and the 6 m span ones can be found in the larger resultant of vertical loads requiring redistribution, which corresponds to larger demand on beam-to-column assemblies. Indeed, the examined long span frames considering column removal at building corner (namely with the smaller tributary area in the directly affected zone) are characterized by better performance with a pseudo-elastic response ( $DLF \approx 1.9-2.0$ ). It is also interesting to note that, differently from the previous set of buildings, seismic design criteria appreciably influences the performance of long span structures, which exhibit a larger capability to develop

favourable plastic mechanism than the corresponding wind designed frames. Regarding the number of storeys, consistently with the results obtained for 6m span buildings, also for this set of frames, the 8-storey *MRFs* show the better performance. In particular, *DLF* values are close to 2.0 for all wind designed structures, while ranging from 1.7 to 2.0 for seismic designed frames.

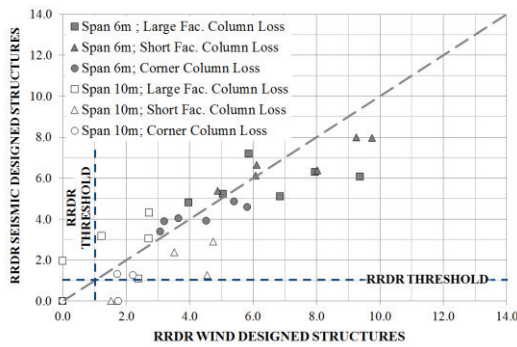
These results indicate that short span frames tend to remain elastic after the column loss, whichever design criteria is taken into account, whereas long span frames can require the development of plastic internal distribution to arrest progressive collapse. Therefore, the obtained results indicate that assuming for all cases a *DLF* equal to 2.0, as suggested in the GSA 2003 (U.S. General Services Administration, 2003) could be excessively conservative.

#### 4.4.1.3 Residual ductility ratio

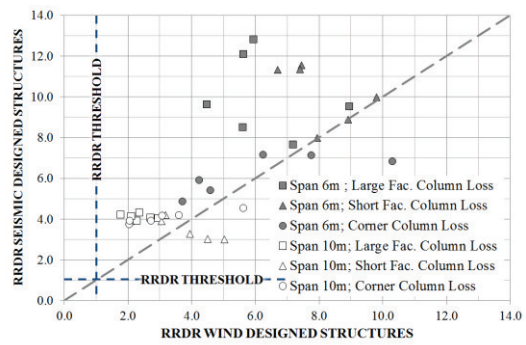
The *RDR* were computed according to Eq. (4.4) and the corresponding results are depicted in Fig. 15 for the 4- and 8-storey structures. In order to interpret the data, it should be clarified that values equal to 0 represent structures for which equilibrium subsequent to column loss was not reached and a value of 1 represents the threshold value for the ductility factor, corresponding to the case in which the maximum dynamic displacement equals the ultimate displacement of the damaged system. As a general remark, it should be noted that *RDR* is strongly related to the type of failure mode, whose occurrence depends on the examined set of structures.

The 4-storey frames present the lower *RDR*, with similar values for both seismic and wind designed structures. This may be explained by the fact that for low rise wind designed buildings, Type I failure modes are the majority of cases (i.e. the 89% of the total, while Type II are the 3% and Type III the 8%), meaning that collapse is typically controlled by the Vierendeel action, namely the ductility is governed by beam behaviour.





a) 4-storey frames



b) 8-storey frames

Figure 4.15: Residual Ductility Ratio comparison

The 8-storey frames experience the lower *RDR* for wind designed structures, as shown in Figure 4.15, since these structures are significantly susceptible to less ductile failure modes (i.e. failure mode types II and III). Conversely seismically designed structures are capable of developing a ductile failure mechanism (i.e. failure mode type I).

#### 4.4.2 Nonlinear dynamic analysis results

##### 4.4.2.1 Damping sensitivity

The performance sensitivity to the damping ratio  $\zeta$  was assessed by analysing the structural response in the damaged state for  $\zeta$  ranging from 0% to 10%. The results of this study are presented in Figure 4.16 for the most representative frame (namely that highlights the larger sensitivity to this parameter) that is the 4-storey seismically designed 5x4 bay frame with 3m interstorey height and 6m span (N4-H3-S6-T5x4-DE), considering the long façade removal (single-mode dominated response) and the corner removal (multiple-mode dominated response).

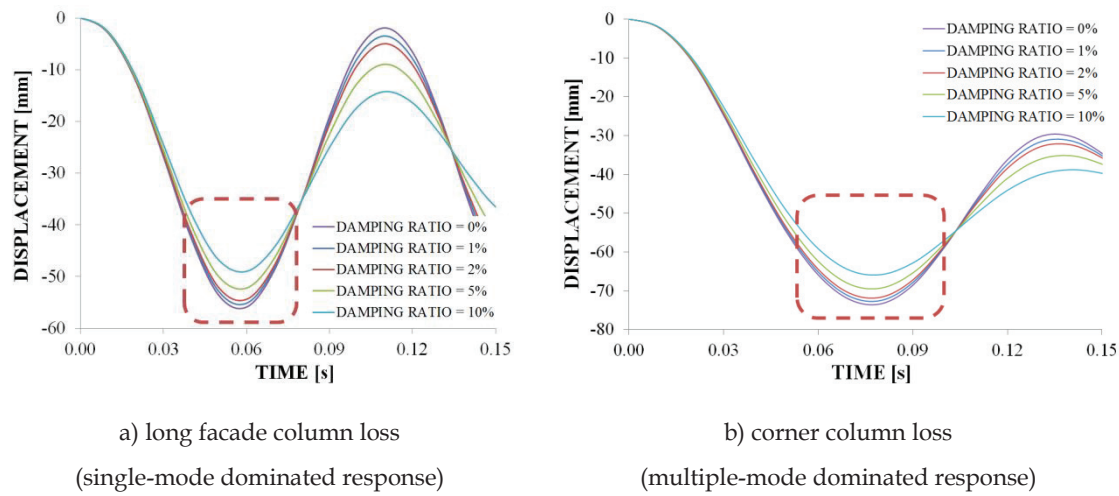


Figure 4.16: Effect of damping on the displacement time-histories of the N4-H3-S6-T5x4-DE frame

The obtained results indicate that the effect of damping on the reduction of the maximum dynamic displacement is moderate for low damping ratios. Indeed, for  $\zeta=2\%$ , which is the value adopted for NDAs of the parametric study shown in the following Sections, limited reduction of the maximum displacement response was observed (e.g. the reduction is equal to 3.3% for the long façade column removal and 2.3% for the corner column removal), thus confirming that the adopted damping ratio yields conservative predictions of the dynamic behaviour. For larger damping ratios (e.g.  $\zeta \geq 5\%$ ), the reduction of the maximum dynamic displacement is significant especially for multiple-mode dominated response, with reduction of displacements of approximately 10% for  $\zeta=10\%$ .

#### 4.4.2.2 Column loss time sensitivity

As described in Section 4.3.4, the application of the column loss action was numerically simulated by introducing a decreasing ramp function with finite rise time (see Figure 4.4), for which the response of an undamped SDOF is essentially governed by two parameters (Chopra, 1995; Comelgau *et al.*, 2010), namely,  $p_0$  which is the amplitude of the applied force, and  $t_r/T_n$  where  $t_r$  is the action rise time of the ramp function and  $T_n$  is the period of the Eigen mode in the elastic domain. According to the GSA 2003 (U.S. General Services Administration, 2003) the action rise time should be equal to or smaller than 1/10 of the natural vibration period of the structure.

Since the natural vertical frequencies of the investigated structures do to not exceed 10 Hz, the rise time compliant to GSA 2003 can be assumed equal to 0.01s. In

order to verify the effectiveness of this assumption and to ascertain the influence of the action rise time on the maximum dynamic displacement, a sensitivity analysis was conducted for different values of  $t_r$ , ranging from 0.005s to 2s. The results of this study are shown in Figure 4.17 and Figure 4.18 for two seismically designed 4-storey frames, namely N4-H3-S6-T5x4-DE (i.e. 4-storey 5x4 bay frame with 3m interstorey height and 6m span) and N4-H4-S10-T5x4-DE (i.e. 5x4 bay frame with 4m interstorey height and 10m span), respectively.

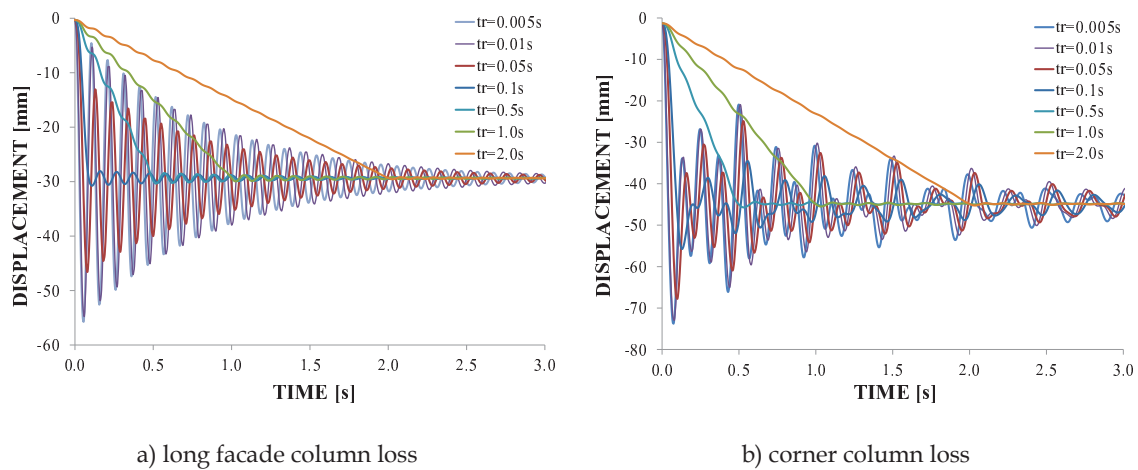


Figure 4.17: Vertical displacement time history as a function of  $t_r$  for the N4-H3-S6-T5x4-DE frame

Figure 4.17 clearly shows that for short span frames the maximum dynamic displacement is very sensitive to  $t_r$ , especially to values under 0.5s that is threshold value separating the static from the dynamically amplified responses. Indeed, for  $t_r$  greater than 0.5s, maximum displacements tend to the static solution for both façade and corner column loss. This transition behaviour was also shown by Comeliau *et al.* (2010). It is interesting to observe that the final equilibrium displacements are equal for all values of  $t_r$ , implying that the frame remains elastic, as confirmed by the *DLF* value of 2.0 previously obtained from the pushdown analysis.

For the long span frame case shown in Figure 4.18, a similar threshold is observed in terms of  $t_r$ , and for values smaller than 0.5s significant dynamic amplification can be observed. Given that this structure responds in the post-yield domain, the final equilibrium displacement varies with the maximum dynamic displacement, and therefore with  $t_r$ . Hence, in such cases, the selection of the rise time significantly affects the final equilibrium position of structures that do not remain elastic.

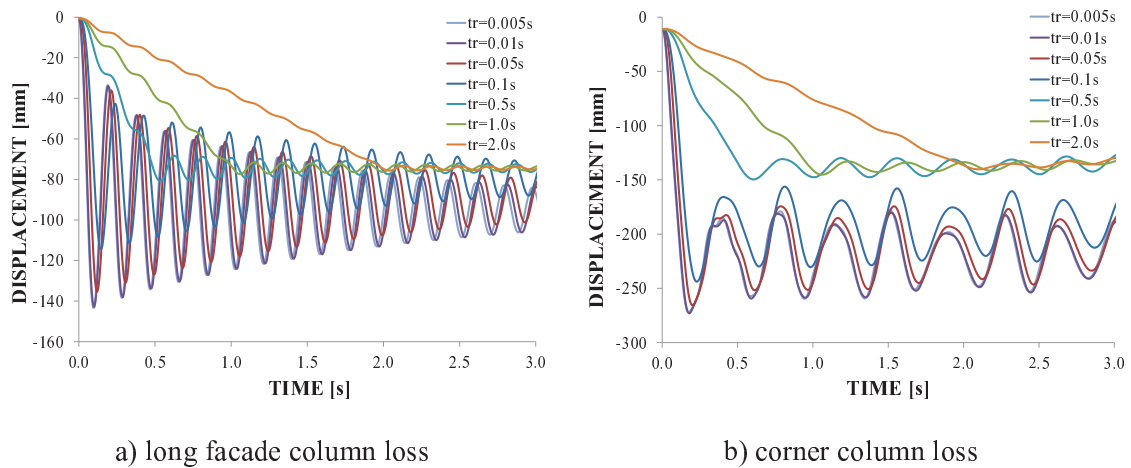


Figure 4.18: Vertical displacement time history as a function of  $t_r$  for the N4-H4-S10-T5x4-DE frame

The relationship between the maximum dynamic displacements and the action rise time is reported in Figure 4.19, showing that the value of  $t_r$  prescribed by GSA guidelines (corresponding to  $t_r=0.01$  s in the examined cases) is suitable. A smaller value for  $t_r$  does not significantly improve result accuracy but requires significant additional computational effort. Therefore, the value recommended by the GSA 2003 was adopted for the dynamic analyses shown hereinafter, since it provides a fair balance between result accuracy and computational effort.

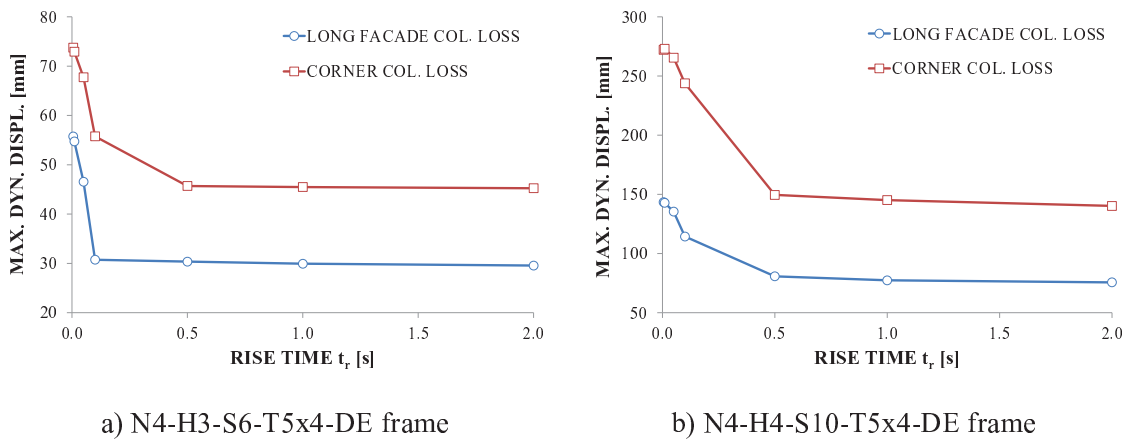


Figure 4.19: Variation of the maximum dynamic displacement with rise time

#### 4.4.2.3 Displacement time-history under column loss

The nonlinear dynamic response to the three considered column loss scenarios is illustrated in Figure 4.20 for the cases of the 4-storey seismically designed frames, with 3m interstorey height and 6m span (N4-H3-S6-DE), for the 5×3 and the 4×4 bay layout configurations.

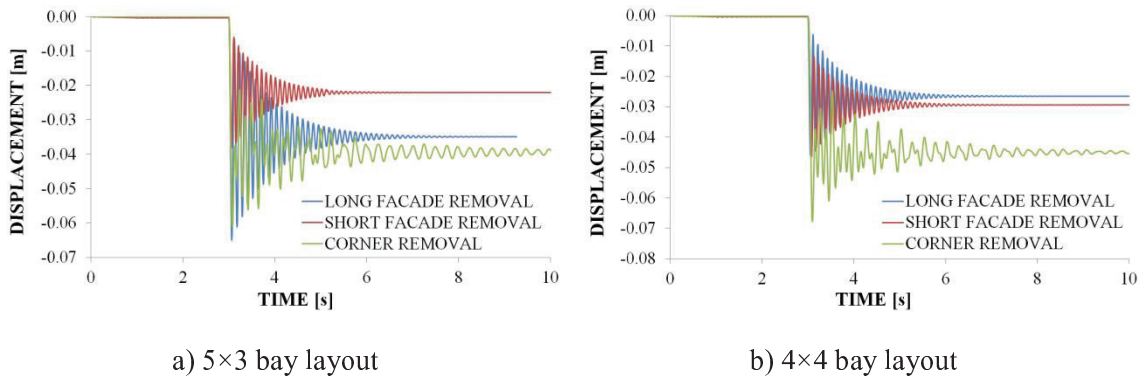


Figure 4.20: Time history response of the N4-H3-S6-DE frame under different column loss scenarios

As depicted in Figure 4.21, the cases subjected to corner column removal experienced a response dominated by multiple vibration modes, consistent with a MDOF system vibrating in a non-resonant condition, whereas for the majority of cases exposed to façade removal, the response was consistent with that of a SDOF system.

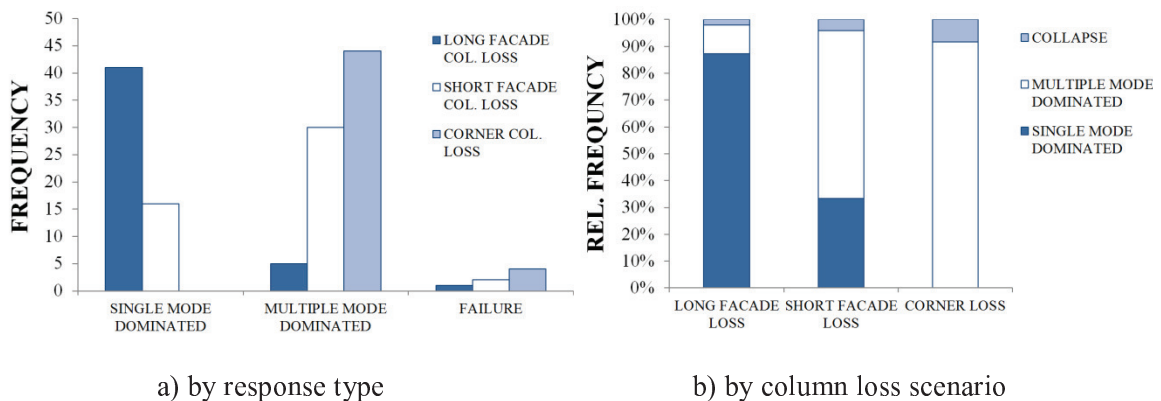


Figure 4.21: Column loss structural response

This different vibrational response is due to a particularity of the structures. Indeed, in all examined frames the corner columns belong to MRF in one direction and to secondary structural beams on the other, which translates into large stiffness variations, causing the response to be dominated by multiple vibration modes. It should also be highlighted that in several façade removal cases, the position of the removed column is offset from the centre of the façade and multiple-mode dominated responses occurred in some cases. However, most long façade removal cases resulted in single-mode dominated responses, which is due to the fact that the long façade MRFs are generally composed of elements with higher stiffness and resistance than

those of the short façade, thus providing a stabilizing effect under column loss that enforces the structure to have a single-mode response.

#### 4.4.2.4 Pushdown vs. nonlinear dynamic analysis

The explicit influence of dynamic effects was quantified by comparing the maximum displacements obtained from combined pushdown/energy balance method to those given by NDAs. The results shown in Table 4.3 for the 6 m and 10 m span frames indicate that NDA leads to smaller maximum dynamic displacement values than pushdown analysis. By grouping results by column removal scenario (see Table 4.4) it can be recognized that the cases for long façade column removal exhibit the smaller mean ratio, which is due to the dynamic response of those cases that is basically single-mode dominated, rendering the NDA results more similar to those obtained from pushdown analysis. On the contrary, for both short façade and corner removal cases, higher values of the  $u_{dyn,damaged,Pushdown}/u_{dyn,damaged,NDA}$  ratios were obtained due to the multiple-mode dominated response.

Table 4.3: Pushdown vs. NDA: maximum dynamic displacement ratios related to span

Span [m]	Column removal scenario [-]	Lateral load scenario [-]	Number of storeys [-]	$u_{\text{dyn,damaged,Pushdown}}/u_{\text{dyn,damaged,NDA}}$		
				$\mu$ [-]	$\sigma$ [-]	CoV = $\sigma/\mu$ [%]
6	L	W	4	1.07	0.03	2.9
		E	8	1.12	0.04	3.3
			4	1.07	0.01	1.2
		S	E	8	1.14	0.01
	4			1.22	0.04	3.1
	W		8	1.26	0.06	4.6
			4	1.13	0.01	0.6
	C	E	8	1.16	0.01	1.1
			4	1.35	0.12	8.7
		W	8	1.30	0.02	1.5
			4	1.24	0.03	2.6
	10	L	E	8	1.19	0.02
4				1.23	0.29	23.5
W			8	1.08	0.01	1.1
			4	1.37	0.38	27.4
S		E	8	1.13	0.02	1.9
			4	1.28	0.12	9.2
		W	8	1.28	0.05	4.2
			4	1.36	0.21	15.2
C		E	8	1.14	0.03	2.5
			4	1.17	0.01	0.8
		W	8	1.33	0.06	4.7
			4	1.58	0.02	1.6
		E	8	1.17	0.02	1.4

Considering all examined cases (i.e. non-collapsed structures only), the average ratio  $\mu$  is equal to 1.21, and the standard deviation  $\sigma$  is equal to 0.15, with a coefficient of variation CV = 12.1%.

Table 4.4: Pushdown vs. NDA: maximum dynamic displacement ratios related to column loss scenario

Column removal location [-]	$u_{\text{dyn,damaged,Pushdown}}/u_{\text{dyn,damaged,NDA}}$		
	$\mu$ [-]	$\sigma$ [-]	CoV [%]
Long facade	1.14	0.18	15.7
Short facade	1.22	0.10	8.3
Corner	1.27	0.11	8.7
Total (all cases)	1.21	0.15	12.1

It is worth highlighting that the pushdown analyses correctly predicted all failure modes that were recognized with NDA. However, given that NDAs led to smaller maximum dynamic displacement values, some structures that collapsed according to the nonlinear static procedure, survived with the NDA. This occurred in six cases of 4-storey - 10m span frames (namely: N4-H3-S10-T5x3-DG-LC, N4-H3-S10-T5x3-DE-LL, N4-H3-S10-T5x3-DE-LS, N4-H3-S10-T5x4-DG-LL, N4-H3-S10-T5x4-DG-LC, N4-H4-S10-T4x4-DE-LC), characterized by very low *RSR* values and for which small variations of maximum dynamic displacement are critical in averting collapse.

This result points out the importance of explicitly considering the dynamic effects, especially for structures with intrinsically low robustness, such as low rise - large span frames.

#### *4.4.2.5 Rotation demand at equilibrium*

In order to assess the level of rotation required to arrest a progressive collapse, maximum total chord rotations at damaged state equilibrium were computed. For the investigated frames, the span of the MRF beams is equal to the span of the secondary beams. Hence, the rotation demand on secondary structure joints is equal to the rotation demand on MRF joints. The total rotation demands obtained from the NDAs are presented in Figure 4.22 and Figure 4.23 for the 4- and 8-storey frames, respectively. Results show that the maximum rotation demands for 10m span frames are significantly higher than for 6m span ones. For the 4-storey frames, maximum values of 64.1 mrad and 17.4 mrad were obtained for the 10m and 6m span frames, respectively. Hence, rotation demand is approximately 3.7 times larger because long span frames resist collapse predominantly via catenary action.



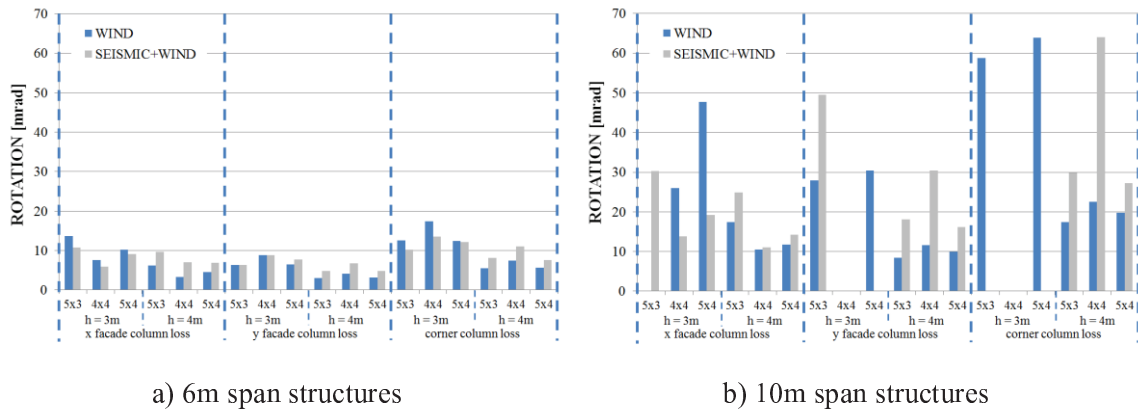


Figure 4.22: Total chord rotation demand for 4 storey structures

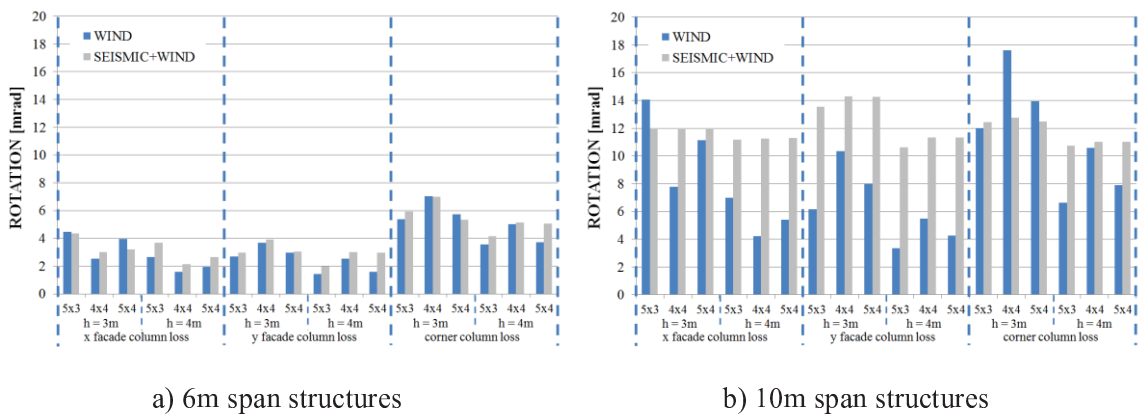


Figure 4.23: Total chord rotation demand for 8 storey structures

A similar pattern is observed for the 8-storey structures, although with a smaller difference due to the greater robustness of these structures. For the 8-storey structures the maximum rotation demand was 7.0 mrad for 6m span and 17.6 mrad for 10m span frames (approximately 2.5 times higher).

These results highlight the high levels of joint rotational demand induced by column loss, for which joint detailing rules are not currently available in European codes. In the opinion of these Authors, similarly to what done for seismic resistant connections, there is a need for further studies in order to develop prequalification procedures for joints under column loss scenario.

## 4.5 Simplified prediction model for DFL

The numerical results discussed in the previous Sections show that the  $DLF$  depends on the number of storeys ( $N$ ) and on the lateral load design scenario ( $D$ ). Therefore, a simplified method to estimate  $DLF$  values for MRF structures is proposed on the basis of the following equation:

$$DLF = DLF_0 \cdot \delta_N \cdot \delta_D \quad (4.9)$$

The proposed expression factors the influence of the number of storeys ( $N$ ) and of the lateral load design scenario ( $D$ ) on the base value  $DLF_0$ , which corresponds to the  $DLF$  for a system responding in the elastic range ( $DLF_0 = 2.0$ ). The influence of the number of storeys and of the design scenario is accounted for by the reduction factors  $\delta_N$  and  $\delta_D$  respectively. The reduction factor  $\delta_N$  was computed as the ratio between  $DLF$  values for 4 and 8 storey frames, whereas the reduction factor  $\delta_D$  was computed as the ratio between the  $DLF$  values for the seismic + wind designed (DE) and wind designed (DW) structures, as follows:

$$\delta_N = DLF_{N4}/DLF_{N8} \quad (4.10)$$

$$\delta_D = DLF_{DE}/DLF_{DW} \quad (4.11)$$

where  $DLF_{N4}$  and  $DLF_{N8}$  are the dynamic load factors for 4 and 8 storey frames respectively, whereas  $DLF_{DE}$  and  $DLF_{DW}$  are the values for the seismic + wind designed (DE) and wind designed (DW) structures, respectively. For 8 storey structures  $\delta_N$  is equal to 1, and for wind designed structures  $\delta_D$  is equal to 1. The coefficients of proposed prediction model are presented in Table 4.5.

The accuracy of the proposed model with respect to the numerical results is depicted in Figure 4.24, showing that it is generally satisfactory with little dispersion for most cases, predicting the dynamic amplification with reasonable accuracy (e.g. the scatter is smaller than 10% for 95% of examined cases). Indeed, only in 4 cases out of the 144 analysed cases the error was higher than 20%.

Table 4.5: Proposed simplified prediction model for DLF

Bay span	Number of storeys	Lateral load design scenario	Interstorey height	$DLF_0$	$\delta_N$	$\delta_D$	$DLF_{MODEL}$	Improve detailing?
S	N	D	H					
[m]	[-]	[-]	[m]	[-]	[-]	[-]	[-]	[-]
6	4	Wind	3	2.00	1.00	1.00	2.00	No
		Seismic+wind	4					
	8	Wind	3					
		Seismic+wind	4					
10	4	Wind	3	2.00	0.64	1.00	1.28	Yes
		Seismic+wind	4		0.97		1.95	
	8	Wind	3		0.85	1.00	1.70	
		Seismic+wind	4		0.74	0.74	1.09	
10	8	Wind	3	2.00	1.00	1.00	2.00	No
		Seismic+wind	4					
	8	Wind	3					
		Seismic+wind	4					

The points missing in Figure 4.24 correspond to those cases where structures collapsed and therefore no  $DLF$  value could be computed. It should be noted that the larger dispersion was recognized for structures with low residual robustness, namely for seismically designed 4 storey - 10m span frames, where the adoption of improved joint detailing (i.e. type T2 shown in Figure 4.6) is recommended in order to significantly improve the joint capacity under catenary action.

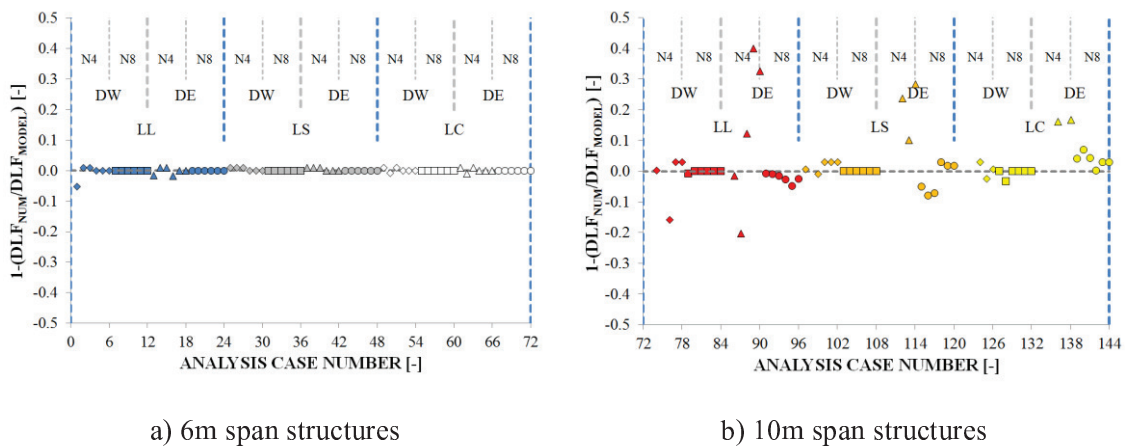


Figure 4.24: Comparison of the prediction accuracy of the proposed model and numerical results for  $DLF$

However, it is important to highlight that further studies are necessary to verify both effectiveness and generality of the proposed simplified model.

## 4.6 Conclusive remarks

A parametric study based on pushdown and NDA was carried out to investigate the influence of seismic design criteria on the robustness of steel MRF structures for three column loss scenarios. To this aim, 144 cases were examined, representative of two sets of 24 frames alternatively designed to resist either seismic action or wind action.

The numerical results showed that structures designed according to the design requirements given by EN 1998-1 exhibit values of Residual Strength Ratio (*RSR*) lower than those obtained by frames designed according to EN 1991 and EN 1993, with lower dispersion as well.

Consistently, the former structures are characterized by the same overall failure mode, while the latter showed three types of global collapse mechanisms providing different ductility levels and *RSR*. However, although seismic design criteria allow predicting and controlling the failure modes under column loss, seismic resistant steel MRF structures do not generally guarantee levels of robustness compatible with arresting progressive collapse.

Provided that joints are able to resist to catenary actions, the analyses highlighted that both strength and stiffness of girders are crucial for improving robustness. Indeed, the better performance was provided by strong beam - weak column structures (i.e. non-seismic design frames), which are mostly characterized by elastic response after column loss, thus implying that these frames do not experience permanent deformation/damage, and enabling the feasibility to repair the frame. This satisfactory behaviour was also recognized for short span (i.e. 6 m) frames designed for seismic actions, which are the cases characterized by the larger beam-to-column stiffness ratios.

Whichever the adopted design requirements, (either seismic or non-seismic) the results showed that structures with larger number of storeys experienced higher values of robustness, indicating that the number of elements mobilized through Vierendeel action is a key parameter in arresting a progressive collapse. On the contrary, the low *RSR* experienced by the 4-storey long span (i.e. 10m) span frames highlights that this particular structural configuration needs improved detailing to avoid collapse subsequent to column loss.

Feasible improved detailing may be achieved by adopting deeper girders than those strictly necessary to satisfy design code requirements, combined with improved MRF girder-to-column joint detailing. If bolted joints are used, performance can be improved by introducing supplementary bolt rows in the mid-height of the end-plate (i.e. in the beam's neutral axis) that are generally missing for joints designed to resist solely bending and shear. Moreover, the joints should be conceived to provide a rotation capacity larger than the demand that varies with structural configuration and column loss scenario. Indeed, low-rise and long span frames are characterized by the larger rotation demand. The average total rotation demands for joints are equal to 8.1 mrad and 26.2 mrad for the 4-storey 6m and 10m frames, respectively, while 3.7 mrad and 10.3 mrad are observed for 8-storey 6m and 10m frames, respectively.

Since joint detailing rules for avoiding progressive collapse are not currently provided by European codes, further studies are necessary in this field. With this regard, in the opinion of the Authors, prequalification procedures should be introduced in order to develop adequate design rules for steel beam-to-column joints under column loss scenario.

The non-linear dynamic analyses have also enabled to identify two types response, namely single and multiple-mode dominated. All corner column removal cases showed multiple-mode response, whereas for the façade removal scenarios the response was mostly single-mode type. The average displacements obtained from NDAs are smaller than those given by pushdown analyses combined with the energy balance method, in the range between 14 to 27%, depending on the column removal scenario and failure mode. A simplified prediction model for the Dynamic Load Factor was also proposed, taking into account frame span, number of storeys and lateral load design scenario. The accuracy of the proposed model was shown to be satisfactory with scatter lower than 10% for 95% of the analysed cases. However, further study is necessary to verify its effectiveness and generality.

The preliminary robustness assessment presented in this chapter has thus enabled to determine the MRF configuration subsets that are most prone to collapse following a column loss event. This data constituted the basis for the selection of the structure typologies to be analysed for the detailed robustness analysis.

Given that many different structural elements contribute to the complexity of structural behaviour of the directly affected zone (DAZ) under column loss actions, such elements are required to be explicitly modelled in order to realistically simulate structural behaviour. This is the case for the secondary gravity frame joints, which are typically considered as perfectly pinned for design purposes.

In order to accurately simulate secondary frame joint behaviour, an experimental study on the tensile behaviour of bolt assemblies was initially conducted in order to determine the strength and stiffness degradation of bolt assemblies for the full range of tensile strain up to failure. The data collected from these experimental bolt tests was subsequently used as input for the numerical modelling of secondary frame joints, hence allowing to determine joint behaviour under simultaneous tensile and bending actions. The conducted monotonic and cyclic experimental tests on pre-loadable and non pre-loadable bolt assemblies are presented in Chapter 5.

## Chapter 5 Experimental monotonic and cyclic inelastic tensile tests of bolt assemblies

### 5.1 Introduction

Bolted joints are widely adopted in European practice due to both their effectiveness and the relatively low constructional costs over welded connections, especially for on-site erection and if holes are punched rather than drilled. Indeed, whichever is the welding procedure, welds are more burdensome. In case of manual metal arc welding, welds are time-consuming and labour intensive, while capital intensive in the case of the automatic welding processes. In addition, there are the costs of weld inspection by ultrasonic or radiographic or dye penetrant testing, which contribute to increase the constructional costs that can become higher (and source of delay) if the controls on weld fail. On the contrary, making holes (either using banks of drills on an automatic machine) and fastening on-site is relatively quick and cheaper.

Design procedure for bolted beam-to-column joints should be consistent with the adopted hypotheses and methodologies of analysis. The EN 1993-1-8 (CEN, 2005) allows predicting the response of bolted joints by means of the “Components Method” which breaks down the joint into its main mechanical components, characterizing their strength and stiffness.

The bolts are key components significantly influencing the joint response in terms of strength, stiffness and ductility. For high-strength pre-loadable bolts, EN 1993-1-8 (CEN, 2005) does not distinguish between the types of bolt assemblies (intended as system made of bolt head, shank and nut) available in European market. However, the type of bolt assembly and its associated failure mode may severely affect the joint behaviour in post-yield domain.

European standards for design (e.g. EN 1993-1-1 (CEN, 2005) and EN 1993-1-8 (CEN, 2005)) and fabrication (e.g. EN 1090-1 (CEN, 2008) and EN 1090-2 (CEN, 2008)) of structural steelwork allow the use of two categories of high strength bolts for structural applications, namely i) non-preloadable (ordinary) and preloadable (High Strength Friction Grip) bolts. Most steel structures designed for execution class 2 (i.e. consequence class 2 and service category 1) according to EN 1090 (CEN, 2008) use non-preloaded structural grade 8.8 bolts, since they are more economical than preloadable fasteners, due to their lower unitary cost and reduced assembly time. According to EN 15048 (CEN, 2007) non-preloadable high strength bolts are indicated with the special marking "SB" (i.e. Structural Bolting). Indeed, steel contractors and minor steelwork companies tend to use non-preloadable SB bolts even for seismic resistant structures, when no clear requirements are stated by the designers, especially for private contracts. Therefore, according to the Author's knowledge and experience in the structural design field, in both Portugal and Italy there are a number of existing steel structures designed in seismic areas and erected using non-preloadable SB bolts for both primary and secondary structural components. This bolt category should not be tightened with the preloading force recommended in Eurocode 3 and, if removed, it allows re-using the fasteners, since no plastic strain was introduced in the threaded shank during the assembling.

Conversely, preloadable bolts should not be re-used after removal due to the large plastic deformations introduced in the threaded zone during tightening. Different codes (i.e. EN 14399-3 (CEN, 2005) and EN 14399-4 (CEN, 2005)) and requirements are used for preloadable bolts, mainly due to the different properties of the standardized products available in European market, where two different bolt assemblies are mostly used, namely the British/French system HR (acronym of "High Resistance") and the German system HV (German acronym of "Hochfeste Bolzen mit Vorspannung", which in English is "high resistance bolts for pretension"), which mainly differ for the type of failure mode under pure tensile force (Johnson, 2014) in terms of both residual strength and deformation capacity at collapse. Typically, the failure mode of HR bolt assemblies is characterized by shank necking in the treaded part, whereas the failure mode of the HV system is characterized by nut stripping without shank necking.

Both the inelastic deformation capacity and the existence of residual strength of bolt assemblies directly influence the capacity of equivalent T-Stub connections to



develop mode 2 rather than mode 3 failure and the associated rotational capacity. Bolt assembly response may also influence the structural behaviour under column loss scenarios (Kwasniewski, 2010), thus highlighting the importance of their refined modelling for accurate structural assessment.

The most of existing analytical and finite element studies on bolted joints are based on analytical force-deformation (or stress-strain) curves formerly derived for US bolt assemblies (e.g. Abel, 1993; Sherbourne and Bahaari, 1997; Bickford and Nassar, 1998; Swanson, 1999; Mays, 2000; Wade, 2006). On the contrary, at the Author's knowledge, limited data and relevant analytical response curves are available for European high-strength bolt assemblies.

The study described in the present chapter is devoted to investigating the non-linear response and the failure modes of the European high strength bolts commonly used in European market of steel constructions, namely SB, HR and HV bolt assemblies. To this aim, an experimental program was carried out in the laboratory of Department of Structures at University of Naples "Federico II".

The main test results are described and discussed by comparing the mechanical response in terms of force-displacement and the equivalent shank true stress - strain behaviour. The bolt assembly response to variable and constant amplitude cyclic actions is also presented, hence enabling to characterize the damage induced by cyclic actions in plastic range for seismic applications. Simplified assumptions for both finite element and analytical modelling of bolt assemblies are also presented, in order to allow accounting for the deformability of the main components of bolt assembly for all stages of axial response. Finally, some design considerations are drawn on the basis of the obtained results.

## 5.2 European normative background

The EN 1993-1-1 (CEN, 2005) establishes the general basis for the design of steel structures according to the safety levels defined in the EN 1990 (CEN, 2005) and covers the topics of resistance, usage, durability and fire resistance. These structural codes constitute the most up-to-date European regulations on steel structural design and in Europe all new structures should comply with the indicated calculation methodologies and verifications.

For what concerns the execution of steel structures, the EN 1090 (CEN, 2008) are a set of standards regulating the fabrication and assembly of metal (i.e. steel and aluminium) structures and establish the requirements for the “CE” (i.e. “Conformité Européenne”, meaning European Conformity) labelling according to the Construction Products Regulation. The EN 1090 specifies requirements for structures designed according to all parts of the EN 1993 standards and comprises three parts, namely: i) Part 1, which establishes the requirements for conformity assessment of structural components; ii) Part 2, which establishes the requirements for the execution of steel structures; iii) Part 3, which describes the technical requirements for the execution of aluminium structures. The EN 1090-2 (CEN, 2008) provides recommendations regarding the use of bolt assemblies and the relevant constructional features, namely concerning tightening methods for preloaded and non-preloaded assemblies, preparation of surfaces, geometrical tolerances, inspection and testing. This standard also introduces the concept of execution class as a reliability indicator, which is related to a set of execution requirements for the whole structure, for individual components and for component details.

### **5.2.1 Preloadable bolt assemblies**

The EN 14399-1 (CEN, 2005) establishes the requirements for pre-loadable high strength bolt assemblies, in terms of tolerances, mechanical properties of the assembly components (i.e. matching bolt, nut and necessary washers) and durability. The connection systems must be selected according to the EN 14399-3 (CEN, 2005) for the case of HR assembly systems, or in accordance with the EN 14399-4 (CEN, 2005) for HV systems, as shown in Table 5.1. The mechanical properties at ambient temperature of the carbon steel alloys that constitute the examined bolt assemblies should be compliant to EN ISO 898-1 (CEN, 1999). This standard provides the physical and mechanical characteristics in elastic and plastic range. For steel grade 10.9, the standard indicates a characteristic yield stress  $f_{y,k}=900$  N/mm<sup>2</sup> and a characteristic ultimate stress  $f_{u,k} = 1000$  N/mm<sup>2</sup>.

Table 5.1: Systems of bolt/nut/washer assemblies (CEN, 2005)

Type of requirement	Bolt/nut/washer assembly System HR	Bolt/nut/washer assembly System HV
Bolt / nut assembly	EN 14399-3	EN 14399-4
Marking	HR	HV
Steel grade	8.8 / 8    10.9 / 10	10.9 / 10
Washers	EN 14399-5 or EN 14399-6	EN 14399-5 or EN 14399-6
Marking H		H
Suitability test for preloading	EN 14399-2	EN 14399-2

### 5.2.2 Non-preloadable bolt assemblies

The EN 15048 establishes the requirements for non-preloadable SB bolt assemblies and it is composed of two parts: 1) EN 15048-1 (CEN, 2007) defines the requirements for the components of the bolt/nut/washer assembly for non-preloadable structural bolting and for the assemblies themselves, as well as the requirement of the SB (Structural Bolting) special marking in bolts and nuts; 2) EN 15048-2 (CEN, 2007), which specifies the suitability testing procedures that are necessary to ensure that the tensile resistance of non-preloadable structural bolting assemblies (i.e. bolts and nuts) meet the strength requirements of EN 1993-1-8 (CEN, 2005).

## 5.3 Bolt assembly features

### 5.3.1 Preloadable bolt assemblies

Bolt assemblies are typically preloaded in order to ensure the rigidity of the bolt assembly and to reduce the influence of dynamic loads on the fatigue life of the bolts. The assemblies must be correctly tightened, since premature failure can arise both from under tightening, as well as from over-tightening (Brown *et al.*, 2008; Lulak *et al.*, 1974).

For preloadable bolts, tightening is accounted for calculation (e.g. for predicting the stiffness of bolt rows according to EN 1993-1-8 (CEN, 2005)) and during

construction. As discussed previously, two types of preloadable bolts are admitted by European standards, namely HV and HR bolts.

The HR system should comply with EN 14399-3 (CEN, 2005). It uses thick nuts and long lengths of thread to obtain a failure mode due to plastic elongation of the unthreaded zone of the shank, as shown in Prinz *et al.*, 2014). This system is less sensitive to overtightening during the bolt preloading. Indeed, it is immediately detectable if shank failure occurs due to excessive preloading. HR bolts are available in both 8.8 and 10.9 grades and in a range of diameters from M12 to M36. The main geometric properties of HR and HV systems are shown in Figure 5.1, and the relevant nominal geometric properties for the HR bolt and nut are given in Table 5.2 and Table 5.3, respectively.

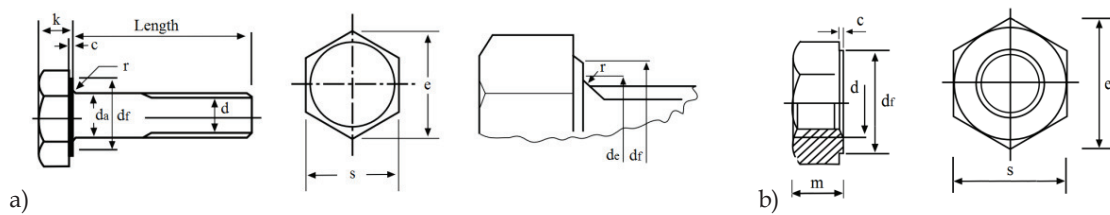


Figure 5.1: HR and HV system geometry: a) bolt; b) nut (CEN, 2005)

Table 5.2: HR system – bolt nominal geometric properties (CEN, 2005)

Nominal size	Pitch of thread	Diameter of unthreaded shank		Width across flats		Width across corners	Diameter of washer face	Depth of washer face		Radius under head	Transition diameter	Thickness of head	
d	p	da	mm	s	mm	e	df	c	mm	r	de	mm	k
-	coarse pitch	max.	min.	max.	min.	min.	min.	max.	min.	min.	max.	max.	min.
M12	1.75	12.70	11.30	22.00	21.16	23.91	20.10	0.8	0.4	1.2	15.20	7.95	7.05
M16	2.00	16.70	15.30	27.00	26.16	29.56	24.90	0.8	0.4	1.2	19.20	10.75	9.25
M20	2.50	20.84	19.16	32.00	31.00	35.03	29.50	0.8	0.4	1.5	24.40	13.40	11.60
M22	2.50	22.84	21.16	36.00	35.00	39.55	33.30	0.8	0.4	1.5	26.40	14.90	13.10
M24	3.00	24.84	23.16	41.00	40.00	45.20	38.00	0.8	0.4	1.5	28.40	15.90	14.10
M27	3.00	27.84	26.16	46.00	45.00	50.85	42.80	0.8	0.4	2.0	32.40	17.90	16.10
M30	3.50	30.84	29.16	50.00	49.00	55.37	46.60	0.8	0.4	2.0	35.40	19.75	17.65
M36	4.00	37.00	35.00	60.00	58.80	66.44	55.90	0.8	0.4	2.0	42.40	23.55	21.45

Table 5.3: HR system – nut nominal geometric properties (CEN, 2005)

Nominal size	Pitch of thread p	Width across flats s		Width across corners e	Diameter of washer face d <sub>r</sub>	Depth of washer face c		Thickness of nut m	
		mm	mm	mm	mm	mm	mm	mm	mm
	- coarse pitch	max.	min.	min.	min.	max.	min.	max.	min.
M12	1.75	22.00	21.16	23.91	20.10	0.8	0.4	10.80	10.37
M16	2.00	27.00	26.16	29.56	24.90	0.8	0.4	14.80	14.10
M20	2.50	32.00	31.00	35.03	29.50	0.8	0.4	18.00	16.90
M22	2.50	36.00	35.00	39.55	33.30	0.8	0.4	19.40	18.10
M24	3.00	41.00	40.00	45.20	38.00	0.8	0.4	21.50	20.20
M27	3.00	46.00	45.00	50.85	42.80	0.8	0.4	23.80	22.50
M30	3.50	50.00	49.00	55.37	46.60	0.8	0.4	25.60	24.30
M36	4.00	60.00	58.80	66.44	55.90	0.8	0.4	31.00	29.40

The characteristics of HV system are codified in the EN 14399-4 (CEN, 2005). This system uses thinner nuts than those used for HR assemblies, combined with shorter threads. As a consequence, this assembly typically experiences a failure mode characterized by full plastic deformation of the threads with stripping of the nut out of the shank. Figure 5.2 clearly shows the different stages of the thread stripping mechanism.

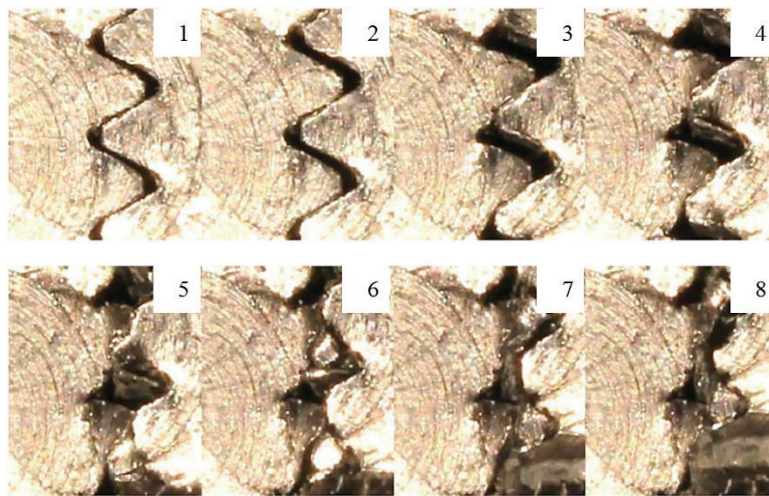


Figure 5.2: Different stages of the thread stripping process (Johnson L. , 2014)

It should be noted that this type of failure mode is beneficial in terms of residual resistance. Indeed, after de-threading, the bolt is still capable of acting as non-preloaded assembly. However, the weakness of the thread zone implies that HV system is significantly sensible to overtightening, because the failure by plastic deformation of the threads can be easily activated without any clear perception. The available diameters for HV assemblies range from M12 to M36 and, differently from

HR, only grade 10.9 is available. The geometric features of the bolt and nut for the HV system are defined in Figure 5.1 and their relevant nominal geometric properties are given in Table 5.4 and Table 5.5, respectively.

Table 5.4: HV system – bolt nominal geometric properties (CEN, 2005)

Nominal size	Pitch of thread	Diameter of unthreaded shank		Width across flats		Width across corners	Diameter of washer face	Depth of washer face		Radius under head	Transition diameter	Thickness of head	
d	p	d <sub>a</sub>	s	e	d <sub>f</sub>	c	r	d <sub>e</sub>	k				
-	-	mm	mm	mm	mm	mm	mm	mm	mm	mm	mm	mm	mm
	coarse pitch	max.	min.	max.	min.	min.	min.	max.	min.	min.	max.	max.	min.
M12	1.75	12.70	11.30	22.00	21.16	23.91	20.10	0.6	0.4	1.2	15.20	8.45	7.55
M16	2.00	16.70	15.30	27.00	26.16	29.56	24.90	0.6	0.4	1.2	19.20	10.75	9.25
M20	2.50	20.84	19.16	32.00	31.00	35.03	29.50	0.8	0.4	1.5	24.00	13.90	12.10
M22	2.50	22.84	21.16	36.00	35.00	39.55	33.30	0.8	0.4	1.5	26.00	14.90	13.10
M24	3.00	24.84	23.16	41.00	40.00	45.20	38.00	0.8	0.4	1.5	28.00	15.90	14.10
M27	3.00	27.84	26.16	46.00	45.00	50.85	42.80	0.8	0.4	2.0	32.00	17.90	16.10
M30	3.50	30.84	29.16	50.00	49.00	55.37	46.60	0.8	0.4	2.0	35.00	20.05	17.95
M36	4.00	37.00	35.00	60.00	58.80	66.44	55.90	0.8	0.4	2.0	41.00	24.05	21.95

Table 5.5: HV system – nut nominal geometric properties (CEN, 2005)

Nominal size	Pitch of thread	Width across flats		Width across corners	Diameter of washer face	Thickness of nut	
d	p	s	e	d <sub>f</sub>	m		
-	-	mm	mm	mm	mm	mm	mm
	coarse pitch	max.	min.	min.	min.	max.	min.
M12	1.75	22.00	21.16	23.91	20.10	10.00	9.64
M16	2.00	27.00	26.16	29.56	24.90	13.00	12.30
M20	2.50	32.00	31.00	35.03	29.50	16.00	14.90
M22	2.50	36.00	35.00	39.55	33.30	18.00	16.90
M24	3.00	41.00	40.00	45.20	38.00	20.00	18.70
M27	3.00	46.00	45.00	50.85	42.80	22.00	20.70
M30	3.50	50.00	49.00	55.37	46.60	24.00	22.70
M36	4.00	60.00	58.80	66.44	55.90	29.00	27.70

### 5.3.2 Non-preloadable bolt assemblies

The grade 8.8 SB bolting system should comply with the EN 15048-1 (CEN, 2007) standard. These bolts are available in European market with different sizes from M12 to M36. The mechanical properties at ambient temperature of the carbon steel alloys that constitute the bolt assemblies should be compliant to EN ISO 898-1 (CEN, 1999). This standard provides the physical and mechanical characteristics in elastic and plastic range. For steel grade 8.8, which is the most commonly used for structural

applications, the standard indicates a characteristic yield stress  $f_{y,k}=640 \text{ N/mm}^2$  and a characteristic ultimate stress  $f_{u,k}=800 \text{ N/mm}^2$ .

The main geometric properties of the SB system are shown in Figure 5.3, and the relevant nominal geometric properties for both bolt and nut of the available diameters are given in Table 5.6.

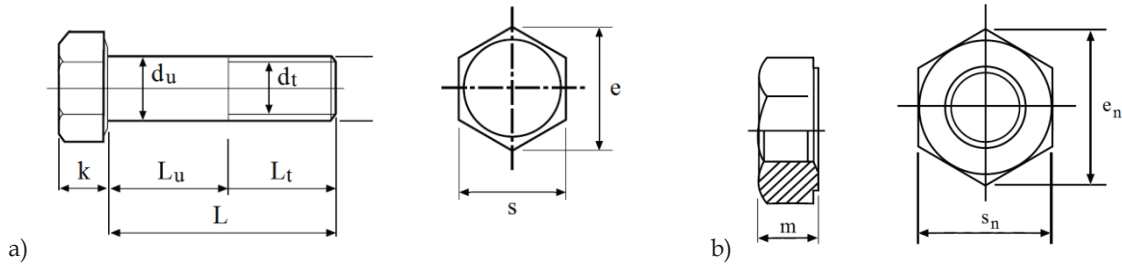


Figure 5.3: SB system geometry: a) bolt; b) nut

Table 5.6: SB system – bolt and nut nominal geometric properties (CEN, 2007)

Nominal diameter	Bolt head width across flats		Bolt head width across corners	Thickness of bolt head		Nut width across flats		Nut width across corners	Thickness of nut	
	s	e		k	s <sub>n</sub>	e <sub>n</sub>	m			
d	[mm]	[mm]	[mm]	[mm]	[mm]	[mm]	[mm]	[mm]	[mm]	[mm]
[-]	max.	min.	min.	max.	min.	max.	min.	min.	max.	min.
M12	18.00	17.57	19.85	7.68	7.32	18.00	17.57	21.10	10.80	10.37
M16	24.00	23.16	26.17	10.29	9.71	24.00	23.67	26.75	14.80	14.10
M20	30.00	29.16	32.95	12.85	12.15	30.00	29.16	32.95	18.00	16.90
M24	36.00	35.00	39.55	15.35	14.65	36.00	35.00	39.55	21.50	20.20
M30	46.00	45.00	50.85	19.12	18.28	46.00	45.00	50.85	25.60	24.30
M36	55.00	53.80	60.79	22.92	22.08	55.00	53.80	60.79	31.00	29.40

## 5.4 Experimental activity

### 5.4.1 Investigated parameters

The main aim of the experimental study presented hereinafter is to investigate the influence of the type of bolt assembly on the monotonic and cyclic responses under tensile forces. In particular, HR, HV, HV with double nut and SB assemblies were tested and three different diameters were examined in order to investigate the possible scale effects on the bolt response. A detailed description of the conducted tests is presented in Table 5.7 and Table 5.8 for the pre-loadable and non-pre-loadable specimens respectively, where the parameters of variations are also shown.

Table 5.7: Experimental programme for preloadable bolt assemblies

Bolt type	Number of nuts	Loading protocol	Amplitude	Nominal bolt diameter	No. of Tests	Specimen designation
[-]	[-]	[-]	[-]	[mm]	[-]	[-]
HR	1	Monotonic	-	16	1	#1
				2	#2	
				20	1	#3
				2	#4	
				24	1	#5
				2	#6	
		Variable	16	1	#7	
			2	#8		
			20	1	#9	
			2	#10		
			24	1	#11	
			2	#12		
		Cyclic	16	-	1	#13
					2	#14
					3	#15
			20	Constant	1	#16
					2	#17
					3	#18
			24	Constant	1	#19
					2	#20
					3	#21
HV	1	Monotonic	-	16	1	#22
				2	#23	
				20	1	#24
				2	#25	
				24	1	#26
				2	#27	
		Variable	16	1	#28	
			2	#29		
			20	1	#30	
			2	#31		
			24	1	#32	
			2	#33		
		Cyclic	16	-	1	#34
					2	#35
	3				#36	
	20		Constant	1	#37	
				2	#38	
				3	#39	
	24		Constant	1	#40	
				2	#41	
				3	#42	
				1	#43	
	2	Monotonic	-	16	2	#44
				1	#45	
				20	2	#46
				1	#47	
				24	2	#48
1				#49		
1				#49		
Cyclic	Variable	-	16	1	#49	



Bolt type	Number of nuts	Loading protocol	Amplitude	Nominal bolt diameter	No. of Tests	Specimen designation
[-]	[-]	[-]	[-]	[mm]	[-]	[-]
					2	#50
				20	1	#51
					2	#52
				24	1	#53
					2	#54
					1	#55
				16	2	#56
					3	#57
			Constant	20	1	#58
					2	#59
					3	#60
				24	1	#61
					2	#62
					3	#63

Table 5.8: Experimental programme for non-preloadable bolt assemblies

Loading protocol	Amplitude	Nominal bolt diameter	Test number	Specimen designation
[-]	[-]	[mm]	[-]	[-]
Monotonic	-	16	1	#1
			2	#2
		20	1	#3
			2	#4
		24	1	#5
			2	#6
Cyclic	Variable	16	1	#7
			2	#8
		20	1	#9
			2	#10
		24	1	#11
			2	#12
	Constant	16	1	#13
			2	#14
			3	#15
		20	1	#16
			2	#17
			3	#18
24	1	#19		
	2	#20		
	3	#21		

The geometry of each bolt assembly was accurately measured prior to testing, in order to determine the actual dimensions of each component. The measured dimensions are presented in Figure 5.4 and the corresponding values (i.e. average  $\mu$ , standard deviation SD and coefficient of variation CoV) are reported in Table 5.9 and

Table 5.10. The values for the normalised thread height are also presented in Table 5.10, showing that this parameter does not vary linearly with bolt nominal diameter.

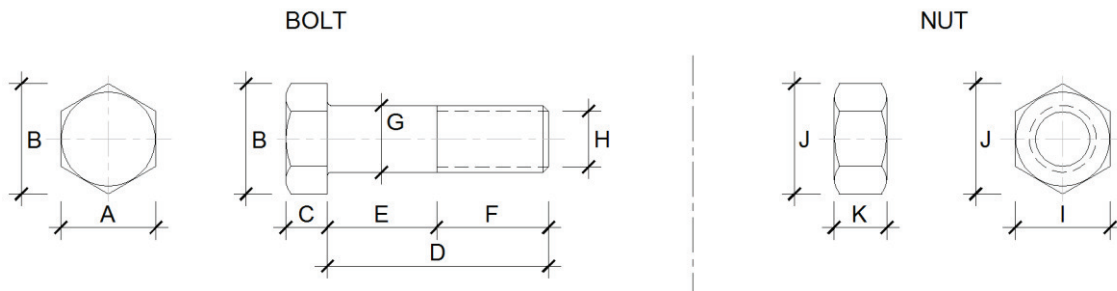


Figure 5.4: Schematic representation of the measured bolt assembly geometry

Table 5.9: Geometric properties of bolt head and nut of tested specimens

Bolt type	Nominal bolt diameter	Head width across flats			Head width across corners			Thickness of the head			Nut width across flats			Nut width across corners			Thickness of the nut		
		A			B			C			I			J			K		
		[mm]	[mm]	[mm]	[mm]	[mm]	[mm]	[mm]	[mm]	[mm]	[mm]	[mm]	[mm]	[mm]	[mm]	[mm]	[mm]	[mm]	[mm]
[-]	[mm]	$\mu$	SD	CoV	$\mu$	SD	CoV	$\mu$	SD	CoV	$\mu$	SD	CoV	$\mu$	SD	CoV	$\mu$	SD	CoV
HR	16	27.1	0.1	0.3%	30.7	0.0	0.1%	11.2	0.1	1.0%	26.5	0.1	0.2%	30.3	0.1	0.2%	14.4	0.1	0.4%
	20	31.8	0.0	0.1%	36.3	0.1	0.2%	13.2	0.0	0.1%	31.5	0.1	0.2%	35.9	0.0	0.0%	17.5	0.0	0.3%
	24	40.4	0.0	0.1%	46.2	0.1	0.1%	16.2	0.0	0.2%	40.7	0.0	0.1%	46.3	0.0	0.1%	21.0	0.1	0.5%
HV	16	26.9	0.0	0.1%	30.6	0.0	0.1%	10.1	0.1	0.9%	26.8	0.0	0.1%	30.4	0.0	0.0%	13.0	0.0	0.1%
	20	31.8	0.0	0.1%	36.4	0.0	0.1%	13.4	0.0	0.2%	31.8	0.0	0.1%	36.2	0.0	0.0%	16.2	0.1	0.5%
	24	40.6	0.1	0.2%	46.4	0.1	0.1%	16.2	0.0	0.3%	40.7	0.0	0.1%	46.3	0.0	0.1%	19.9	0.1	0.4%
SB	16	23.8	0.0	0.1%	27.2	0.0	0.1%	10.4	0.0	0.3%	23.8	0.0	0.0%	27.2	0.0	0.1%	14.6	0.0	0.1%
	20	29.7	0.0	0.0%	34.0	0.0	0.1%	13.3	0.1	0.8%	29.3	0.0	0.1%	33.6	0.0	0.1%	17.5	0.0	0.2%
	24	35.6	0.1	0.2%	40.8	0.0	0.1%	15.5	0.1	0.6%	35.2	0.0	0.1%	40.4	0.1	0.1%	20.8	0.0	0.1%

Table 5.10: Geometric properties of the bolt shank of tested specimens

Bolt type	Nominal bolt diameter	Length			Unthreaded shank length			Threaded shank length			Diameter of the unthreaded shank			Diameter of the threaded shank			Normalised thread height (G-H)/G
		D			E			F			G			H			
		[mm]	[mm]	[mm]	[mm]	[mm]	[mm]	[mm]	[mm]	[mm]	[mm]	[mm]	[mm]	[mm]	[mm]	[mm]	
[-]	[mm]	$\mu$	SD	CoV	$\mu$	SD	CoV	$\mu$	SD	CoV	$\mu$	SD	CoV	$\mu$	SD	CoV	[mm]
HR	16	99.2	0.1	0.1%	56.3	0.4	0.6%	43.2	0.4	0.9%	15.8	0.2	1.1%	14.0	0.0	0.2%	0.114
	20	109.0	0.3	0.3%	61.0	0.5	0.9%	48.5	0.8	1.7%	19.4	0.0	0.1%	17.2	0.0	0.1%	0.113
	24	119.9	0.1	0.1%	57.3	0.1	0.1%	62.6	0.2	0.3%	23.4	0.0	0.0%	20.6	0.1	0.5%	0.120
HV	16	99.8	0.2	0.2%	69.9	0.3	0.4%	30.0	0.4	1.2%	15.6	0.0	0.2%	14.0	0.0	0.2%	0.103
	20	109.5	0.5	0.5%	70.7	0.2	0.2%	38.7	0.4	0.9%	19.4	0.0	0.1%	17.3	0.1	0.3%	0.108
	24	119.4	0.2	0.2%	73.0	0.2	0.3%	46.6	0.3	0.6%	23.5	0.0	0.2%	20.6	0.1	0.7%	0.123
SB	16	109.7	0.2	0.1%	67.2	0.1	0.2%	42.6	0.1	0.3%	15.4	0.0	0.1%	13.7	0.0	0.1%	0.110
	20	110.0	0.1	0.1%	57.7	0.1	0.1%	52.3	0.0	0.0%	19.8	0.0	0.2%	17.0	0.0	0.2%	0.141
	24	120.0	0.2	0.2%	57.7	0.1	0.1%	62.3	0.2	0.3%	23.9	0.0	0.2%	20.4	0.0	0.1%	0.146

The average geometrical properties are compared in Figure 5.5a, while the parameters  $C$ ,  $E$ ,  $Z$ ,  $K$  and  $Y$  are defined in Figure 5.5b. In detail, the length of the threaded part inside the connected plates ( $Z$ ) is the parameter mostly influencing the initial stiffness and the elongation of the bolt.

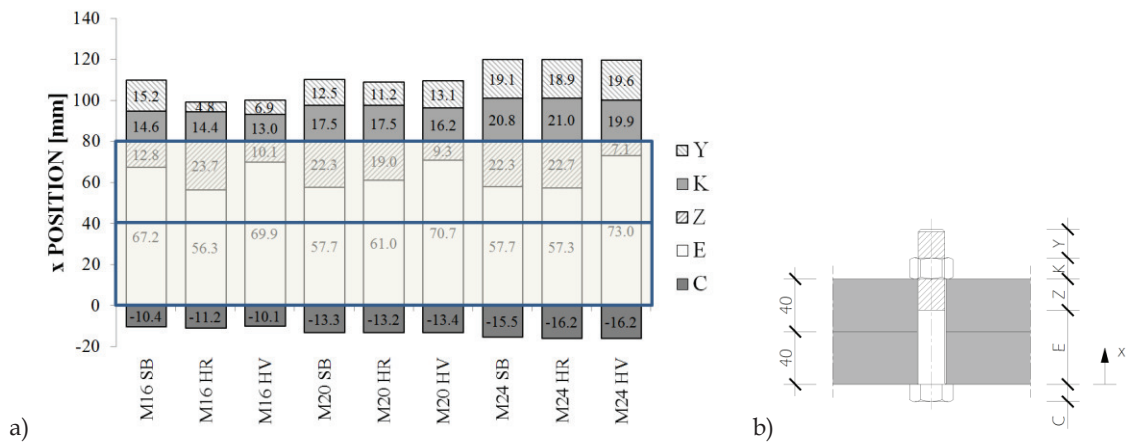


Figure 5.5: a) Bolt assembly geometry comparison; b) Bolt assembly geometry definition

For HR assemblies, it is possible to observe that the M20 bolts have a smaller value of  $Z$  (i.e. 19.0mm) than those for M16 and M24 bolts. On the contrary, the length  $Z$  of HV bolts inversely decreases with the nominal diameter. Another distinguishing feature is the thickness of the nut, which is smaller for HV bolts. Consequently, the nut and the threaded shank zones result as the weaker components of this assembly. For SB bolts, the M16 specimen is characterized by the shorter  $Z$  length (i.e. 12.8 mm), while both M20 and M24 have the same length (i.e. 22.3 mm).

#### 5.4.2 Experimental test set up

Pseudo-static monotonic, cyclic variable amplitude and constant amplitude tests were carried out using a universal electro-mechanical MTS testing machine (see Figure 5.6a). The maximum load, the bolt elongation and the types of failure mode were monitored for each test. Tests were carried out under displacement control in tension and under force control in compression with a minimum force threshold equal to 5 kN in order to avoid the transmission of compression loads to the experimental setup.

The tension force was applied to the bolts by means of test fixtures consisting of a couple of steel casings pulled by the test machine, according to ISO 3800:1993 (ISO, 1993). It should be noted that the ISO 3800:1993 allows using two types of test fixtures for axial load testing of bolts, namely: i) fixture with insert; ii) fixture without insert. The first type uses removable inserts to enable testing of bolts with different diameters using the same test fixture, as adopted in Shahani and Shakeri (2015); the second type does not use a removable insert and only one bolt diameter can be tested per test fixture. For the present study, test fixtures without insert were adopted.

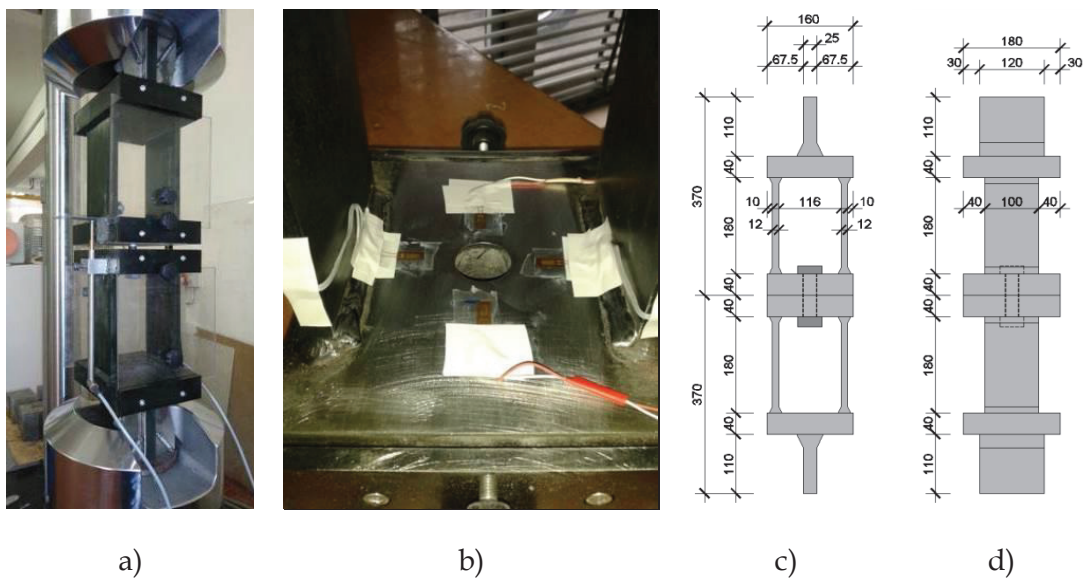


Figure 5.6: Experimental test set up: a) steel casings with installed LVDTs; b) 40 mm thick plates with strain gages; c) dimensions - front view; d) dimensions - side view

Three sets of two steel built-up casings were specifically conceived to carry out the tests on M16, M20 and M24 assemblies, having the same geometry (see Figure 5.6c,d), except for the diameter of the hole where the bolts are inserted, namely 18 mm, 22 mm and 26 mm for the M16, M20 and M24 diameters, respectively.

The bolt elongation was measured by means of a couple of linear variable displacement transducers (LVDT) with a displacement range of  $\pm 50$  mm, which provide the relative displacements between the two steel plates of the casings connected by the bolt assembly, as shown in Figure 5.6a. These plates were designed to have thickness values compliant with those required by ISO 3800 (ISO, 1993) and also in order to have bending deformations smaller than the accuracy of displacement transducers (i.e.  $\pm 0.002$  mm), thus producing a negligible source of error on the

measurement of the experimental data. This assumption was also verified experimentally by means of 4 strain gages, located on the surface of plates as shown in Figure 5.6b. The measured data confirm that the strains at the peak applied force are about  $\varepsilon_y/100$  (being  $\varepsilon_y$  the steel yielding strain) and the corresponding bending displacements are smaller than 1/1000 mm. The bolt assemblies were hand tightened with wrenches, inducing tensile forces within the range of 20 - 30 kN, as indicated by the test machine.

#### 5.4.3 Variable amplitude cyclic loading protocol

The loading protocol for variable amplitude cyclic tests was defined ad-hoc by adapting the procedure for cyclic protocol described in ECCS recommendations (ECCS, 1986). In particular, the applied displacement history was conceived to have bolts permanently under tension throughout the duration of the test. The protocol consists of sequences of three cycles at increasing strain amplitudes. Each set of three cycles is characterized by a maximum imposed strain value and by a minimum strain equal to zero. In order to avoid the transmission of compression forces in unloading phase, force-controlled unloading was adopted with a 5 kN minimum tensile force threshold. The adopted cyclic loading protocol is presented in Figure 5.7.

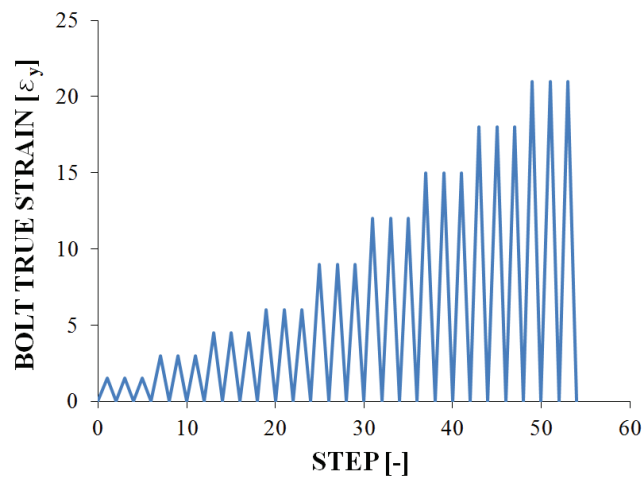


Figure 5.7: Variable amplitude cyclic loading protocol

It should be noted that the displacement history of the loading protocols were derived from the corresponding expected strain into the bolt assembly formerly determined from the monotonic testing data.

#### 5.4.4 Constant amplitude cyclic loading protocol

Low cycle fatigue tests were conducted in order to determine the  $\epsilon$ - $N$  bolt assembly fatigue curves, being  $\epsilon$  the maximum imposed strain in plastic field at each cycle and  $N$  the number of cycles around that value.

Each constant amplitude cyclic loading protocol was characterized by a maximum strain (which was determined according to the corresponding actuator displacement vs. bolt strain curve, as indicated in Table 5.11) in the loading phase and by a minimum applied tensile force threshold equal to 5 kN in the unloading phase.

Table 5.11: Constant amplitude loading protocol list

Bolt assembly type [-]	Number of nuts [-]	Nominal diameter [mm]	Maximum applied strain [-]	Maximum Actuator displacement [mm]	
HR	1	16	$3\epsilon_y$	3.09	
			$4\epsilon_y$	3.95	
			$5\epsilon_y$	4.82	
		20	$3\epsilon_y$	4.16	
			$4\epsilon_y$	4.32	
			$5\epsilon_y$	4.68	
	24	$3\epsilon_y$	5.52		
		$4\epsilon_y$	6.58		
		$5\epsilon_y$	7.65		
		1	16	$1.5\epsilon_y$	1.59
				$2.2\epsilon_y$	1.81
				$3.0\epsilon_y$	2.42
20	$1.5\epsilon_y$		3.44		
	$2.2\epsilon_y$		3.91		
	$3.0\epsilon_y$		4.02		
24	$1.5\epsilon_y$	5.67			
	$2.2\epsilon_y$	6.14			
	$3.0\epsilon_y$	6.26			
	HV	16	$2\epsilon_y$	2.13	
			$3\epsilon_y$	3.09	
			$4\epsilon_y$	3.95	
20		$2\epsilon_y$	3.90		
		$3\epsilon_y$	4.16		
		$4\epsilon_y$	4.32		
24	$2\epsilon_y$	4.42			
	$3\epsilon_y$	5.52			
	$4\epsilon_y$	6.58			
SB	1	16	$3\epsilon_y$	2.67	
			$4\epsilon_y$	3.44	
			$5\epsilon_y$	4.21	

Bolt assembly type [-]	Number of nuts [-]	Nominal diameter [mm]	Maximum applied strain [-]	Maximum Actuator displacement [mm]
		20	$3\varepsilon_y$	5.13
			$4\varepsilon_y$	6.19
			$5\varepsilon_y$	7.25
		24	$3\varepsilon_y$	8.14
			$4\varepsilon_y$	9.27
			$5\varepsilon_y$	10.32

Since bolt assemblies have different features, each of them was characterized by a set of loading protocols, one per considered strain amplitude (as summarized in Table 5.11). As it can be observed, HR and SB bolts were tested under the larger strain amplitudes, while smaller amplitudes were applied for HV and HV with 2 nut assemblies. These differences depend on the ductility and ultimate displacement capacity displayed in the monotonic tests. Indeed, SB and HR bolts are the most ductile, HV with 2 nuts have slightly smaller displacement capacity prior necking and HV assemblies are characterized by an early drop of resistance after yielding. In addition, initial tests on HV assemblies showed that the cyclic actions lead very quickly to nut stripping, thus rendering the shank surface flat and smooth and enabling the cyclic action to go on indefinitely without achieving any cracks or fatigue failure.

## 5.5 Experimental results

The experimental response curves were corrected to account for the initial preloading force with a 3 step procedure as illustrated in Figure 5.8. Indeed, the curve identified as Step 0 is the original average response given by the LVDTs. The curve identified as Step 1 is obtained by extending the initial linear elastic branch of the Step 0 curve until the point of zero force. The “actual” corrected curve is identified as Step 2, which is obtained by shifting the Step 1 curve to the zero of the plot reference axes.

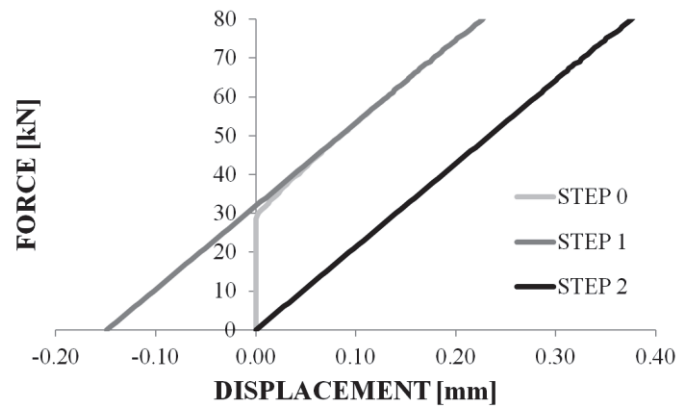


Figure 5.8: Monotonic Force-Displacement response curve correction process

The experimental results are presented hereinafter in terms of force-displacement curves and relevant failure modes. Subsequently, piece-wise linear models of the force-displacement response curves are provided, thus enabling to quantify and to compare the characteristics of the tested specimens. The linearized force-displacement curves are also converted to both engineering and true stress - strain curves. This procedure enables to obtain a simplified piece-wise stress-strain relationship that can be implemented into finite element models (FEM) to simulate the equivalent response of bolt assembly.

### 5.5.1 Monotonic bolt assembly response

#### 5.5.1.1 HR bolt assemblies

The different stages of the test conducted on an M16 HR Cl. 10.9 assembly are shown in Figure 5.9. Bolt shank elongation is observed throughout the test until failure occurs by shank failure in the threaded zone located between the bolt head and the nut. The failed nut and attached shank are retrieved at the end of the test on the plate located below the nut.





Figure 5.9: Monotonic test of the M16 HR Cl. 10.9 assembly at different stages

The response curves for the tested HR assemblies are shown in Figure 5.10a,b,c for the M16, M20 and M24 diameters, respectively. The response curves are characterized by an initial linear elastic segment, followed by the transition to the plastic domain, after that a softening branch can be observed due to bolt shank necking in the threaded part with corresponding reduction of tensile strength until failure. The onset of softening branch occurs for displacement values ranging between 1.5 and 2 mm, with similar softening rates for all diameters. The failure occurs for displacement values from 4.8 to 7.2 mm; M24 bolt presents the smaller displacements at failure.

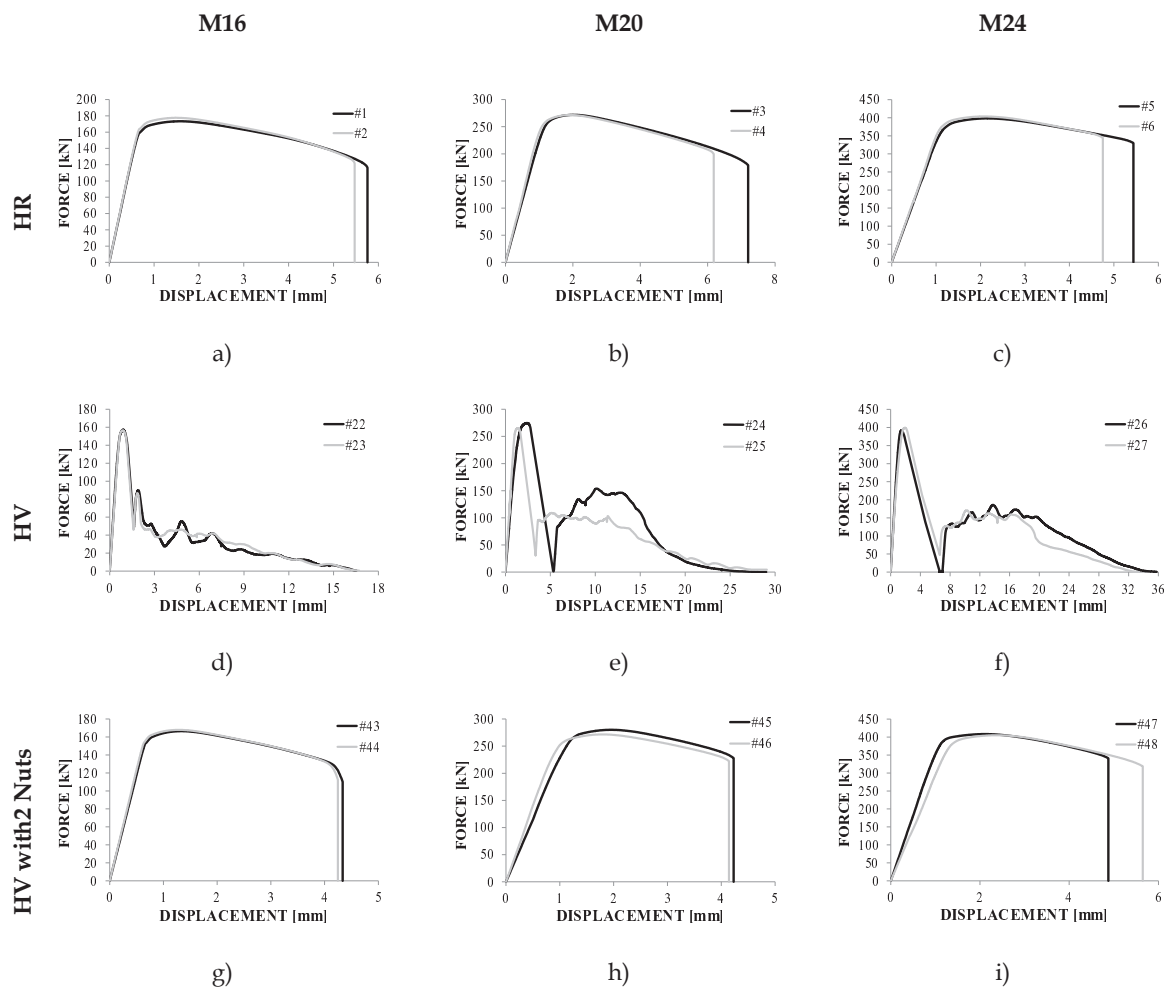


Figure 5.10: Force-displacement response curves for the monotonic tests – preloadable bolt assemblies

### 5.5.1.2 HV bolt assemblies

The different stages of a monotonic test conducted on an HV Cl. 10.9 assembly are shown in Figure 5.11. During the conduction of the test, the progressive thread stripping of the assembly can be observed by the threads that fall onto the plate located below the nut. The test ends with the full de-threading of the assembly and consequent separation of the nut.

The experimental responses for HV assemblies are shown in Figure 5.10d,e,f. Differently from HR assemblies, the failure mode of HV bolts was the nut stripping. The experimental response curves of HV assemblies are characterized by an initial linear elastic response, followed by a very limited transition to the plastic regime, afterward the bolt resistance suddenly drops, due to the failure of the threads, to about 30 to 40% of the peak strength. The post-peak strength corresponds to the stripping

resistance of the crests screwed into the nut. Therefore, each tooth of the curve corresponds to the failure of the corresponding crest of the threaded part.

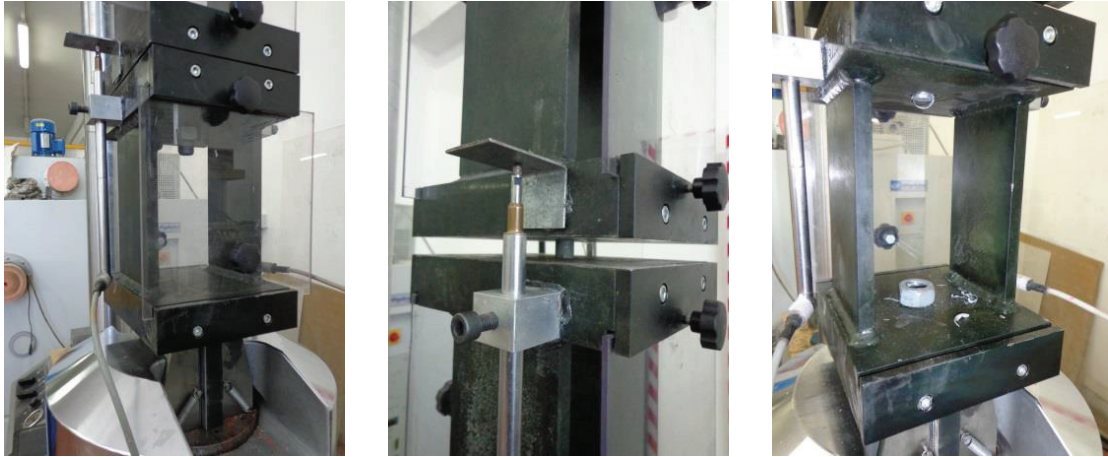


Figure 5.11: Monotonic test of the M20 HV Cl. 10.9 assembly at different stages

Tests clearly showed sudden slips between the nut and the shank when the crest failure occurred. It is interesting to observe that the residual post peak strength is sustained for an additional displacement of about 10 mm, after which the strength decreases with an approximately constant rate up to zero, when the nut is extracted.

#### 5.5.1.3 HV bolt assemblies with 2 nuts

The force-displacement responses for the tested HV assemblies with 2 nuts are presented in Figure 5.10g,h,i for the M16, M20 and M24 cases respectively. As it can be observed, these specimens show a response curve very similar to those of HR assemblies. Hence, adding of a second nut is effective to shift the failure mode from de-threading to shank necking in the threaded zone near the nuts. Test results show that the onset of softening occurs for displacements ranging from about 1.5 mm to 2 mm and similar softening rates are displayed for varying bolt nominal diameters. However, the values of displacements corresponding to the failure are smaller than those of HR bolts, ranging from 4.1 mm to 5.6 mm.

#### 5.5.1.4 SB bolt assemblies

The different stages of a test conducted on an SB Cl. 8.8 assembly are shown in Figure 5.12. During the conduction of the test, bolt shank elongation is observed until failure occurs by shank failure in the threaded zone located between the bolt head and

the nut. The failed nut and attached shank are retrieved at the end of the test on the plate located below the nut.

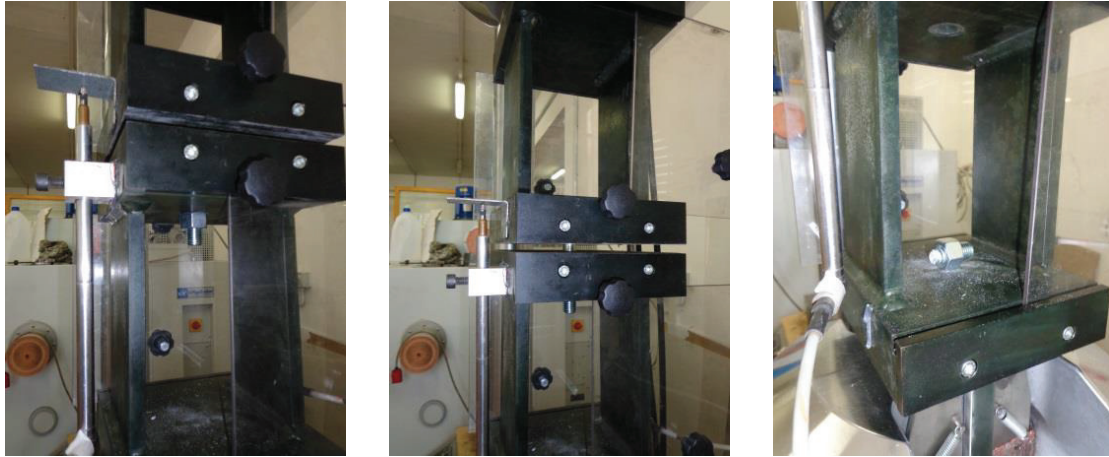


Figure 5.12: Monotonic test of the M16 SB Cl. 8.8 assembly at different stages

The response curves of the tested SB assemblies are shown in Fig. 4a, b and c for the M16, M20 and M24 diameters, respectively. The response curves are characterized by an initial linear elastic segment, followed by the transition to the plastic domain; after that a softening branch can be observed due to bolt shank necking in the threaded part. The onset of softening branch occurs for displacement values around 2 mm, with similar softening rates (around -13 kN/mm) for all tested diameters. The failure displacement experimentally observed ranges from 6.4 mm to 7.9 mm, with M20 bolt assemblies showing the larger values.

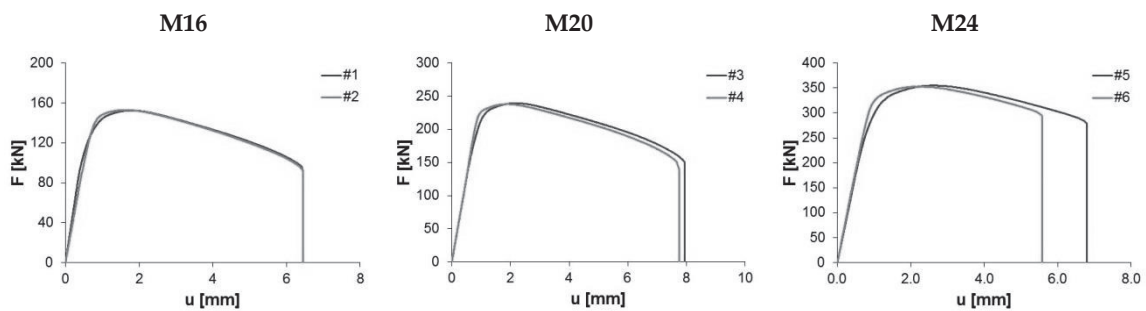


Figure 5.13: Force-displacement response curves for the monotonic tests – non-preloadable bolt assemblies

### 5.5.2 Linearized monotonic stress-strain curves

The experimental force-displacement curves were approximated by using a piece-wise linear model, as exemplified in Figure 5.14 for M16 HR and HV assemblies, which is composed by the following parts: i) a first segment that corresponds to the

linear elastic stage; ii) a second segment represents the transition from elastic to plastic response that was obtained equating the areas between the linearized and original curves; iii) a third segment which characterizes the plastic plateau zone with zero hardening; iv) a fourth segment that models the softening in its initial phase; v) a fifth segment which corresponds to a stage with more pronounced softening (HR bolts) or to a sudden drop in resistance caused by the first thread failure (HV bolts); vi) a sixth segment that models the bolt failure (HR bolts) or the residual force plateau (HV bolts); vii) a seventh segment that provides the final residual force softening stage (for HV bolts only).

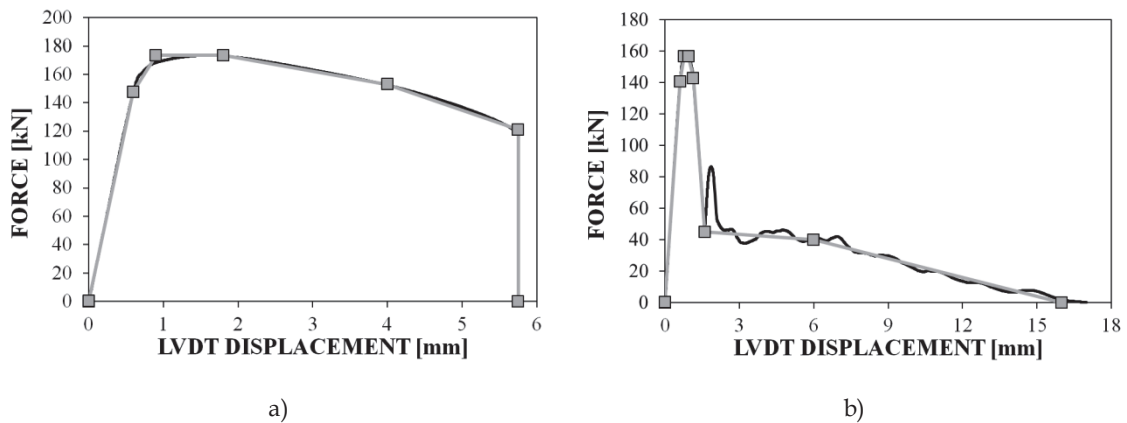


Figure 5.14: Monotonic force - displacement experimental curve and piece-wise linear approximation: a) M16 HR (#1); b) M16 HV (#23)

After linearization of experimental response curves through the described methodology, the response of bolts was converted into engineering stress-strain curves (i.e. the stress was computed by dividing the applied force by the initial effective tensile shank area, while the equivalent strain was computed by normalizing the measured average relative displacement to the reference length), and subsequently converted into true stress - true strain curves according to the following expressions:

$$\sigma_{true} = \sigma_{eng}(1 + \varepsilon_{eng}) \quad (5.1)$$

$$\varepsilon_{true} = \ln(1 + \varepsilon_{eng}) \quad (5.2)$$

This process has enabled to perform comparisons between different assemblies, so as to determine the effect of the analysed variables.

### 5.5.2.1 Effect of bolt assembly type

The influence of bolt type is highlighted in Figure 5.15, which clearly shows that different types of assemblies lead to great differences in terms of bolt performance, which may significantly influence the ductility of T-stub failure mechanisms involving bolts in tension (e.g. failure modes 2 and 3).

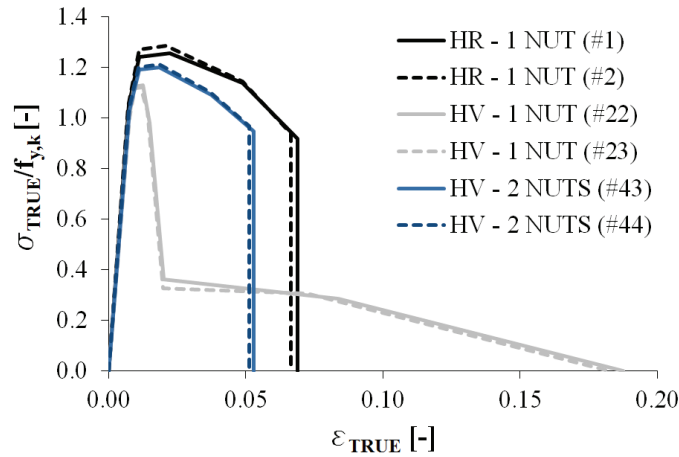


Figure 5.15: Effect of type of bolt assembly for the case of M16

In the comparison presented in Figure 5.15 for the preloadable assemblies, HV type exhibits a sudden drop of resistance at a strain about 1.4%. However HV bolts can provide large deformation capacity up to their full collapse, while keeping a residual tensile strength. Moreover, since the plastic deformations concentrate on the crests of the threaded zone, the shank is in elastic range, thus HV can reasonably provide their full shear capacity even at very large axial deformation.

### 5.5.2.2 Effect of nominal diameter

The effect of the nominal diameter in the equivalent bolt assembly response was analysed by superposing the average true stress (normalized to the relevant characteristic yield stress) – true strain response curves for the three analysed diameter values, as shown in Figure 5.16, where the standard deviation around the average response was also computed.

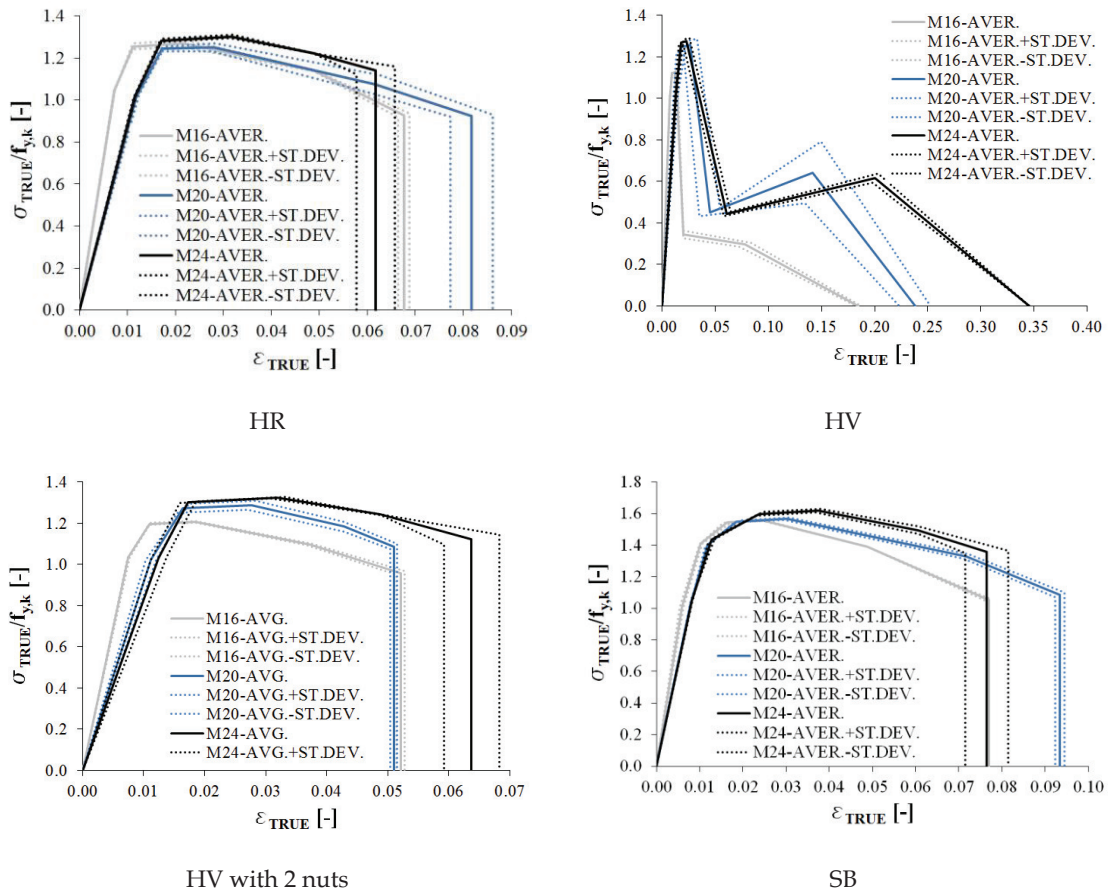


Figure 5.16: Effect of nominal bolt diameter on normalised true stress – true strain curves

The role of bolt diameter in HV assemblies is different than in HR bolts. Indeed, in the latter type the peak stress is almost insensitive to the diameter variation, while for HV the M16 specimens are characterized by an equivalent peak stress 15% smaller than that of the M20 and M24. Moreover, the M16 residual stress plateau is characterized by slight softening behaviour, whereas M20 and M24 bolts exhibit hardening behaviour in the post peak range. This feature can be explained by the different dimensions of the crests of the treaded zone, which are larger and stronger for increasing diameters. The variation of the residual stress  $\sigma_{RESIDUAL}$  throughout the plateau for M16, M20 and M24 assemblies is shown in Figure 5.17, where “Plateau End 1” corresponds to the point at the start of the equivalent plateau and “Plateau End 2” corresponds to its end point.

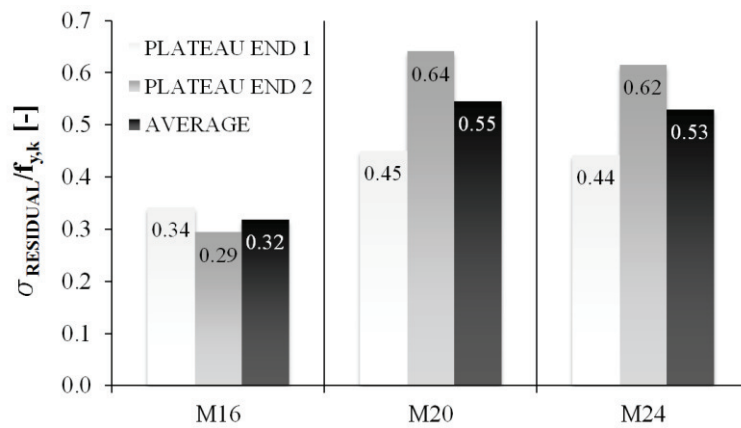


Figure 5.17: Stress plateau: resisting stress to nominal HV bolt yield stress ratios

Assuming that the residual stress plateau is maintained until the nut slips by a relative displacement value equal to the length  $Y$  (defined in Figure 5.5b), after which point the nut is not fully in contact with the shank, the correlation between the strain range of the residual stress plateau and the parameter  $Y$  was examined as shown in Figure 5.18, where it can be observed that the strain range increases with both  $Y$  and the bolt nominal diameter. An exponential regression was represented, showing good agreement with the data, although further testing is required to improve the quality of the fit.

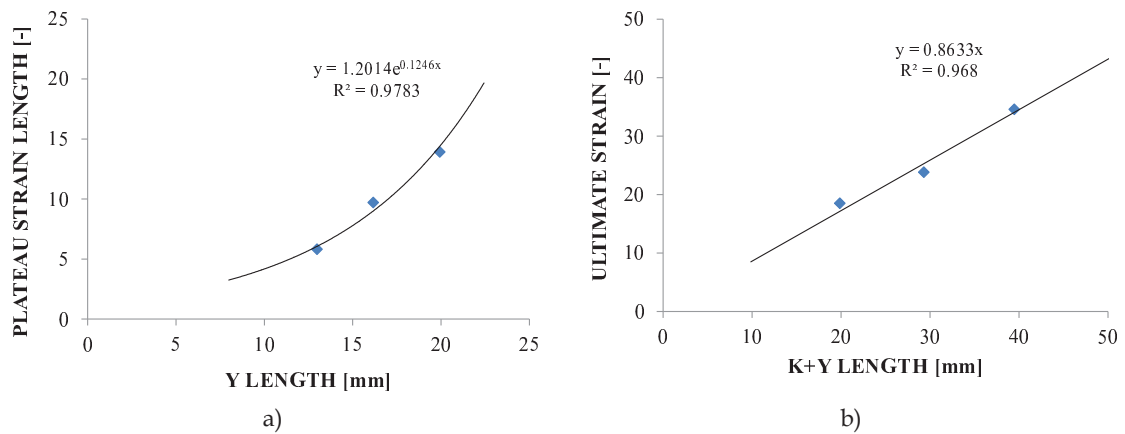


Figure 5.18: HV assemblies: a) Variation of the residual plateau strain length with the parameter  $Y$ ; b) Variation of the average assembly ultimate strain with the parameter  $K+Y$

The final softening segment is characterized by similar softening rate values and the ultimate strain at assembly collapse is obtained when the nut slipping is equal to  $K+Y$ , where  $K$  and  $Y$  are defined in Figure 5.5b, namely corresponding to the nut removal. As shown by the good correlation depicted in Figure 5.18b for the tested M16,



M20 and M24 HV assemblies, the  $K+Y$  geometrical parameter is a good predictor of the ultimate strain of HV assemblies.

The comparison for the HV assemblies with 2 nuts is presented in Figure 5.16c. The difference in terms of stiffness is likely due to a reduced deformability of the threaded zone for the M16 case. The peak resisting stress is similar for the M20 and M24, with the M16 displaying smaller overstrength. Similarly to HR assemblies, results show some variability in terms of ultimate strain, with the M24 assembly attaining the highest ultimate strain value, although associated to large dispersion.

For what concerns SB type assemblies, as seen in Figure 5.16d, some differences in terms of initial stiffness can be observed. In particular, M16 assemblies exhibit higher values than M20 and M24. This feature can be easily explained considering that the portion of the smooth shank length is longer for M16 than for the other cases. The bolt diameter showed reduced influence on the peak stress, since it is almost insensitive to the diameter variation. In particular, average peak stresses values of 997, 1003 and 1037 N/mm<sup>2</sup> were measured for the M16, M20 and M24 assemblies. The ratio between these values and the characteristic ultimate tensile stress (i.e. 800 N/mm<sup>2</sup> as indicated in EN ISO 898-1 (CEN, 1999)) yields overstrength values ranging from 1.25 to 1.30, which are in good accordance with the value for the material overstrength factor  $\gamma_{ov}=1.25$  provided in EN 1998-1 (CEN, 2004).

Regarding the ultimate strain, the experimental results showed some differences with the bolt diameter. The higher ultimate strain value observed for M20 assemblies is due to the  $E$  and  $Z$  dimensions (where  $E$  is defined in Figure 5.4 and  $Z$  is the length of the threaded shank inside the connected plates) that do not progressively increase with nominal diameter.

### 5.5.3 Normalized stress-strain curves

Two different criteria were considered to normalise the linearized average true stress – true strain curves. The first criterion, henceforth designated as Criterion 1, consists in normalizing the true stress by the characteristic yield stress and the true strain by the corresponding yield strain obtained from the linearized curves. The second criterion, henceforth designated as Criterion 2, normalises the true stress and the true strain by means of the relevant yield stress and strain computed directly from

the experimental curves, according to the ECCS methodology (ECCS, 1986). The stress-strain curves normalised according to both criteria are presented in Figure 5.19.

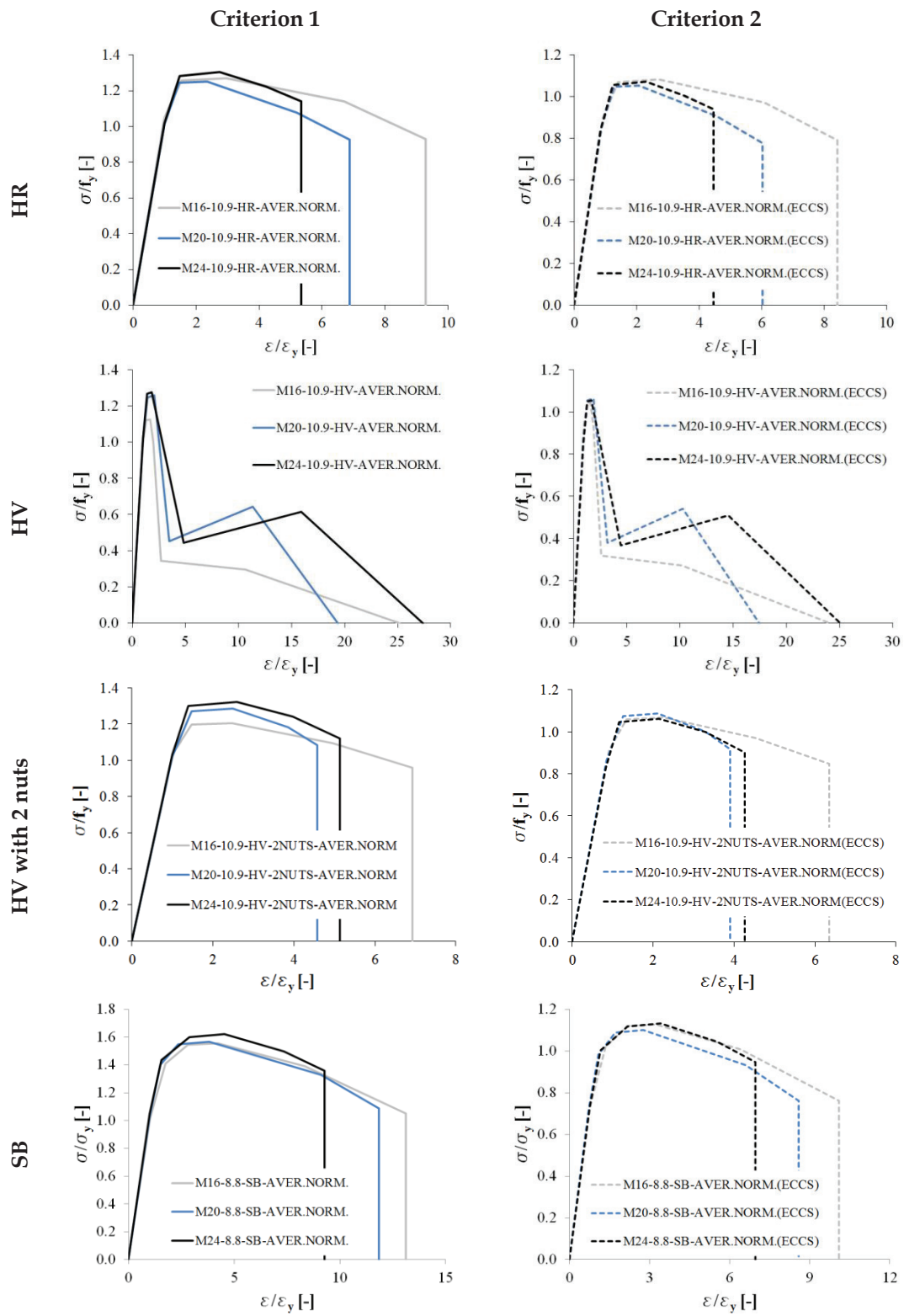


Figure 5.19: Normalised true stress - true strain curves

5.5.3.1 HR assemblies

The results for the normalised stress-strain curves for HR assemblies according to the two selected criteria presented in Figure 5.19 show that the shank nominal diameter influences neither the transition from the elastic range to the plastic range, nor the rate of softening branch. In terms of peak stress, Criterion 1 yields at peak values of  $\sigma/f_y$  equal to about 1.25, namely higher than the characteristic ultimate-to-yield stress ratio (e.g. for steel grade 10.9 this ratio is equal to  $f_{u,k}/f_{y,k} = 1000/900 = 1.11$ ). According to Criterion 2, the peak  $f_u/f_y$  values are closer to 1.1. Nonetheless, significant differences are observed in terms of ultimate strain by varying the bolt diameter. However, in the opinion of the Author, Criterion 1 is more suitable for practical applications being directly related to the characteristic value of yield strength. Thereby, the equations for the segments of the response curves of HR assemblies normalised by Criterion 1 are presented in Table 5.12.

Table 5.12: Equations for true stress true strain response curves normalized according to Criterion 1 – HR assemblies

Segment	$\sigma_{Norm} = m \epsilon_{Norm} + b$											
	M16				M20				M24			
	m	b	domain		m	b	domain		m	b	domain	
[-]	[-]	[-]	$\epsilon_{min}$	$\epsilon_{max}$	[-]	[-]	$\epsilon_{min}$	$\epsilon_{max}$	[-]	[-]	$\epsilon_{min}$	$\epsilon_{max}$
1	1.047	0.000	0.000	1.000	1.016	0.000	0.000	1.000	1.019	0.000	0.000	1.000
2	0.388	0.659	1.000	1.536	0.503	0.513	1.000	1.453	0.558	0.460	1.000	1.475
3	0.010	1.241	1.536	2.970	0.008	1.232	1.453	2.356	0.015	1.261	1.475	2.742
4	-0.035	1.372	2.970	6.701	-0.061	1.395	2.356	5.201	-0.054	1.451	2.742	4.224
5	-0.082	1.692	6.701	9.289	-0.090	1.544	5.201	6.882	-0.073	1.532	4.224	5.335

5.5.3.2 HV assemblies

The normalised curves for the Cl. 10.9 HV assemblies are shown in Figure 5.19 and as it can be observed, according to Criterion 1, the computed stress ratios  $\sigma/f_y$  are close to 1.3 for the M20 and M24, and around 1.1 for the M16 case, whereas the stress ratios are slightly smaller than 1.1 for all diameters according to Criterion 2. The equations for segments of response curves normalised by Criterion 1 are presented in Table 5.13.

Table 5.13: Equations for true stress true strain response curves normalized according to Criterion 1 - HV assemblies

Segment	$\sigma_{\text{Norm}} = m \epsilon_{\text{Norm}} + b$											
	M16				M20				M24			
	m	b	domain		m	b	domain		m	b	domain	
[-]	[-]	[-]	$\epsilon_{\text{min}}$	$\epsilon_{\text{max}}$	[-]	[-]	$\epsilon_{\text{min}}$	$\epsilon_{\text{max}}$	[-]	[-]	$\epsilon_{\text{min}}$	$\epsilon_{\text{max}}$
1	0.989	0.000	0.000	1.000	1.019	0.000	0.000	1.000	1.016	0.000	0.000	1.000
2	0.471	0.518	1.000	1.279	0.551	0.469	1.000	1.414	0.626	0.390	1.000	1.402
3	0.010	1.108	1.279	1.668	0.017	1.223	1.414	2.052	0.017	1.244	1.402	1.812
4	-0.748	2.372	1.668	2.714	-0.561	2.409	2.052	3.492	-0.276	1.774	1.812	4.825
5	-0.006	0.359	2.714	10.657	0.024	0.366	3.492	11.352	0.016	0.368	4.825	15.901
6	-0.020	0.510	10.657	25.192	-0.080	1.548	11.352	19.386	-0.054	1.469	15.901	27.367

### 5.5.3.3 HV assemblies with 2 nuts

For the HV assemblies with 2 nuts the normalisation results shown in Figure 5.19 exhibit some differences in terms of ultimate strains at failure, with the M20 assemblies displaying smaller normalised strains. The stress ratios  $\sigma/f_y$  range from 1.20 to 1.32 for Criterion 1 and from 1.06 to 1.09 for Criterion 2; the  $\sigma/f_y$  ratios for Criterion 2 are in good agreement with the nominal ultimate-to-yield stress ratio which is equal to 1.11. The equations for segments of response curves normalised by Criterion 1 are presented in Table 5.14.

Table 5.14: Equations for true stress true strain response curves normalized according to Criterion 1 - HV assemblies with 2 nuts

Segment	$\sigma_{\text{Norm}} = m \epsilon_{\text{Norm}} + b$											
	M16				M20				M24			
	m	b	domain		m	b	domain		m	b	domain	
[-]	[-]	[-]	$\epsilon_{\text{min}}$	$\epsilon_{\text{max}}$	[-]	[-]	$\epsilon_{\text{min}}$	$\epsilon_{\text{max}}$	[-]	[-]	$\epsilon_{\text{min}}$	$\epsilon_{\text{max}}$
1	1.033	0.000	0.000	1.000	1.022	0.000	0.000	1.000	1.031	0.000	0.000	1.000
2	0.353	0.679	1.000	1.463	0.529	0.494	1.000	1.472	0.702	0.329	1.000	1.387
3	0.010	1.182	1.463	2.472	0.015	1.250	1.472	2.492	0.016	1.280	1.387	2.587
4	-0.044	1.316	2.472	4.950	-0.076	1.476	2.492	3.853	-0.059	1.475	2.587	3.962
5	-0.070	1.442	4.950	6.933	-0.134	1.698	3.853	4.585	-0.103	1.648	3.962	5.137

### 5.5.3.4 SB assemblies

Results show that the shank nominal diameter influences neither the transition from the elastic range to the plastic range, nor the softening rate of the softening branch. In terms of peak stress, the adopted criterion yields peak values of  $\sigma/f_y$  around 1.6 for Criterion and slightly lower than 1.2 for Criterion 2. The equations for the segments of the normalised response curves are presented in Table 5.15 and the normalised stress-strain curves are presented in Figure 5.19.

Table 5.15: Equations for true stress true strain response curves normalized according to Criterion 1 – SB assemblies

Segment	$\sigma_{Norm} = m \epsilon_{Norm} + b$											
	M16				M20				M24			
	m	b	domain		m	b	domain		m	b	domain	
[-]	[-]	[-]	$\epsilon_{min}$	$\epsilon_{max}$	[-]	[-]	$\epsilon_{min}$	$\epsilon_{max}$	[-]	[-]	$\epsilon_{min}$	$\epsilon_{max}$
1	1.007	0.000	0.000	1.000	1.029	0.000	0.000	1.000	1.050	0.000	0.000	1.000
2	0.530	0.478	1.000	1.756	0.748	0.281	1.000	1.497	0.698	0.352	1.000	1.552
3	0.129	1.181	1.756	2.817	0.174	1.140	1.497	2.356	0.123	1.244	1.552	2.885
4	0.009	1.519	2.817	4.216	0.012	1.521	2.356	3.826	0.013	1.561	2.885	4.541
5	-0.041	1.729	4.216	8.330	-0.045	1.741	3.826	9.099	-0.044	1.823	4.541	7.358
6	-0.070	1.975	8.330	13.139	-0.089	2.136	9.099	11.850	-0.072	2.027	7.358	9.277

### 5.5.4 Ductility

The ductility of the different bolt assemblies was computed from the experimental curves as the ratio  $d_d/d_y$ , where  $d_y$  is the displacement at yielding and  $d_d$  is obtained by intersecting the response curve with the horizontal straight line  $y = F_y$  (see Figure 5.20a). The computed values for the average assembly ductility are shown in Figure 5.20b).

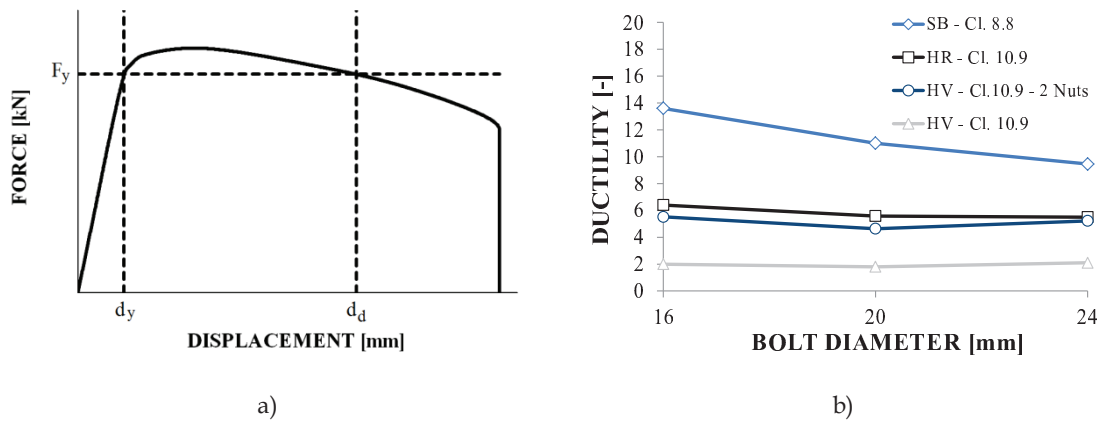


Figure 5.20: Bolt assembly ductility: a) Parameter definition; b) Influence of bolt diameter and type on ductility

The values displayed in Figure 5.20b) (which are also presented tabular format in Table 5.16) indicate that the type of bolt significantly affects the assembly ductility. HV assemblies present very low values of ratio  $d_d/d_y$ , since the first thread failure occurs for very small displacements. However, it should be noted that this definition of ductility disregards the additional reserve of displacement capacity that HV assemblies can provide up to the removal of the nut.

Table 5.16: Average bolt assembly ductility and failure modes

Nominal bolt diameter [mm]	Bolt class [-]	Bolt type [-]	Number of nuts [-]	Failure mode [-]	Ductility $d_q/d_y$ [-]
16	8.8	SB	1	Shank necking	13.6
16	10.9	HR	1	Shank necking	6.4
16	10.9	HV	1	Thread stripping	2.0
16	10.9	HV	2	Shank necking	5.5
20	8.8	SB	1	Shank necking	11.0
20	10.9	HR	1	Shank necking	5.6
20	10.9	HV	1	Thread stripping	1.8
20	10.9	HV	2	Shank necking	4.6
24	8.8	SB	1	Shank necking	9.5
24	10.9	HR	1	Shank necking	5.5
24	10.9	HV	1	Thread stripping	2.1
24	10.9	HV	2	Shank necking	5.2

The obtained results show that non-preloadable SB bolts display higher ductility when compared to preloadable HR assemblies, which in turn display similar values to the HV with 2 nuts assemblies, showing that adding a second nut to an HV assembly does not significantly reduce ductility since the failure mode is shifted to the bolt shank. When increasing bolt diameter from 16 mm to 24 mm, ductility was found to decrease. This effect is more noticeable for SB assemblies where ductility is reduced by 19% and 30%, when transitioning from 16 mm to 20 mm and from 16 mm to 24 mm, respectively.

### 5.5.5 Variable amplitude cyclic bolt assembly response

The response curves for the tested assemblies are presented in Figure 5.21 for M16, M20 and M24 diameters, respectively. For the case of HR assemblies, results show that the experimental cyclic response curves practically overlap with the corresponding monotonic response curves for all tested diameters. Therefore, the adopted cyclic loading pattern does not detrimentally affect the HR bolt assembly response until bolt failure.

For HV assemblies the monotonic and the cyclic responses exhibit similar behaviour, although some differences can be observed in the residual post-peak zone due to local failure of crests and crushing of threads inside the nut. In general, as for HR assemblies, the cyclic loading does not impair the overall bolt assembly response both in terms of resisting stress and of ultimate displacement in comparison to the monotonic response.

The cyclic loading response of the HV assemblies with 2 nuts is consistent with the response under monotonic loading, since no significant strength degradation or deformation capacity reduction occurs. Some variability in terms of ultimate deformation can be observed, although this is partly due to small differences in the stiffness of the elastic branch, which depends on geometry of gripped threads.

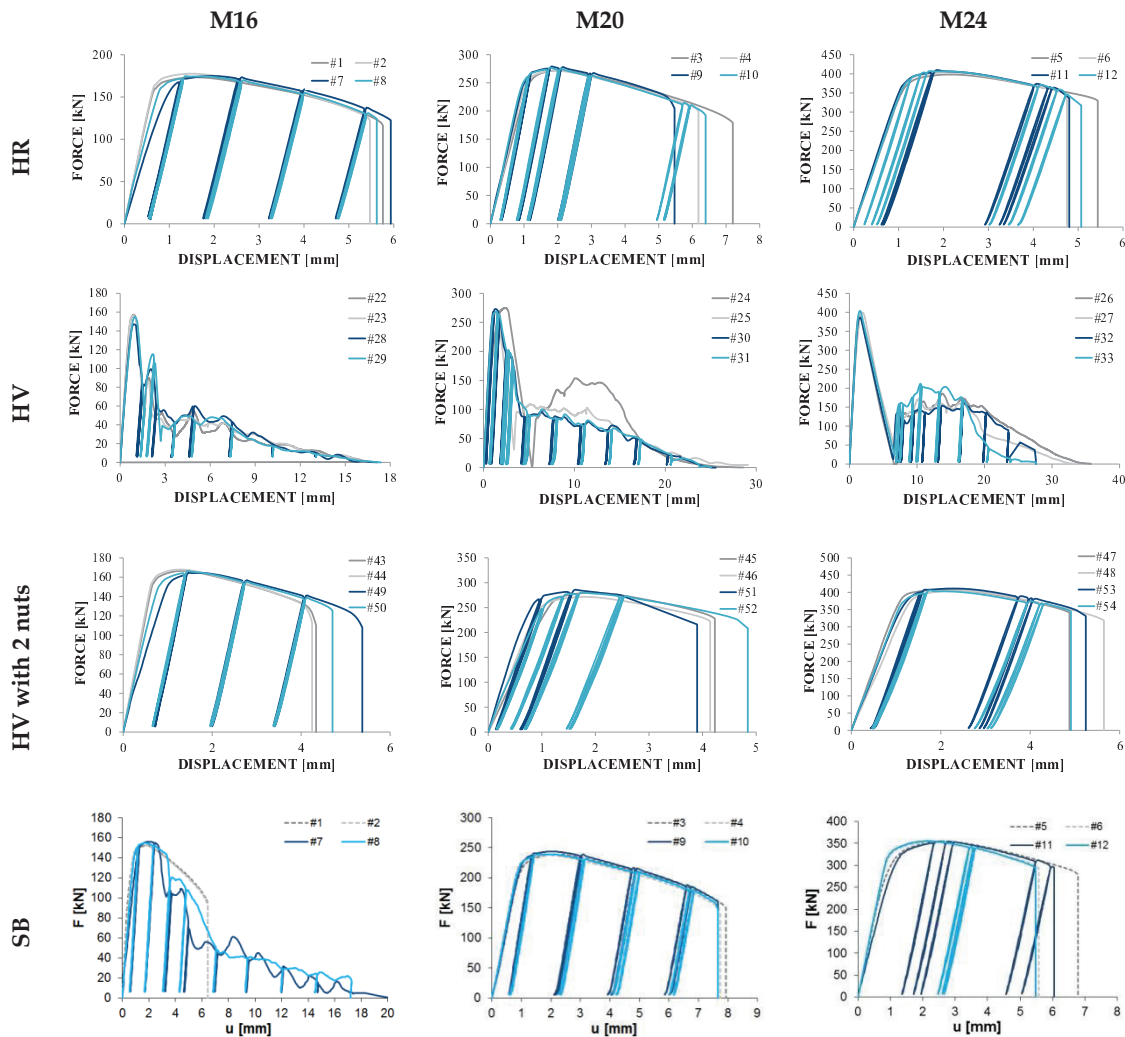


Figure 5.21: Monotonic - cyclic variable response comparison

For the SB assemblies results show that the cyclic response of M16 is substantially different from the behaviour of both M20 and M24. Indeed, both the failure mode (i.e. shank tearing) and the envelope of the cyclic response curves for the M20 and M24 assemblies mostly coincides with the monotonic response curves (see Figure 5.21), even though the failure displacement of M24 given under cyclic loading showed is slightly smaller than that obtained from monotonic test. On the contrary, M16 assemblies are significantly affected by cyclic loading. Indeed, as shown in Figure

5.21, the M16 SB under cyclic loading failed by nut stripping (see Figure 5.22a), while shank tearing occurred in monotonic tests.

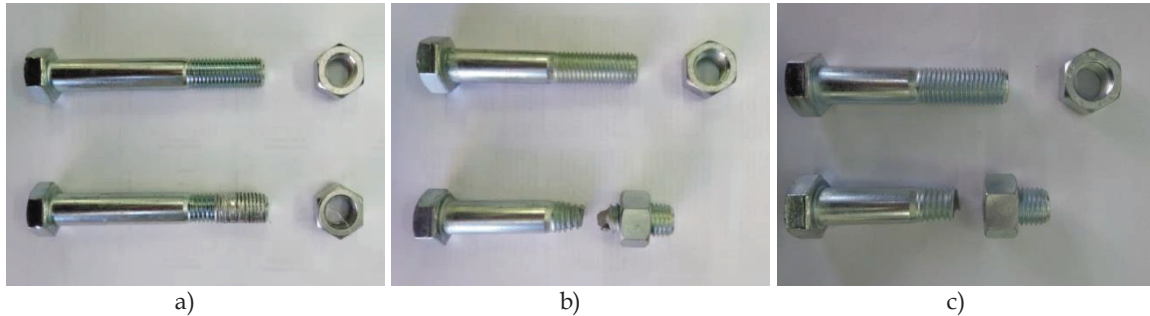


Figure 5.22: Comparison between undamaged SB assemblies and specimens retrieved after the variable cyclic tests: a) M16 (specimen #7); b) M20 (specimen #10); c) M24 (specimen #11)

As a consequence, the M16 envelope response curves differ from those obtained in the monotonic tests. The tensile strength of the former dropped for displacements ranging between 2.5 mm and 3.3 mm, but the assemblies continued to cycle with low residual strength levels up to complete removal of the nut (i.e. thread-stripping process, which is typical for HV bolts as indicated in Johnson (2014)). This phenomenon was due to the imposed cyclic deformation that induced and cumulated plastic strain into the crests of the threaded zone of the shank.

The difference of the type of failure mode depends on the local strength of the threaded zone that is influenced by the dimensions of the crests. In the examined cases the normalised thread height (see Table 5.10 and Figure 5.4), i.e. the depth of the crests ( $G-H$ ) normalized to the net diameter parameter ( $G$ ) of the treaded zone, varies with the diameter. In particular  $(G-H)/G$  is larger and almost equal in value (i.e. equal to 0.141 and 0.146, respectively) for M20 and M24, while it is smaller (i.e. about 0.110) for M16.

### 5.5.6 Constant amplitude cyclic bolt assembly response

The assessment of the low fatigue resistance of bolt assemblies was performed by imposing constant amplitude displacement cycles (see Section 5.4.4) and measuring the number of cycles  $N$  until failure was achieved, hence allowing determining the  $\varepsilon-N$  curves.

HR and HV with two nuts showed typical fracture failure into the threaded zone of the shank at the section between bolt and nut, as also observed in elastic



fatigue tests on GR. 8.8. bolts by Shahani and Shakeri (2015), whose aspect is characterized by several ratchet marks along the thread radius. Figure 5.23a) depicts the experimental response curve of a HV with two nuts specimen.

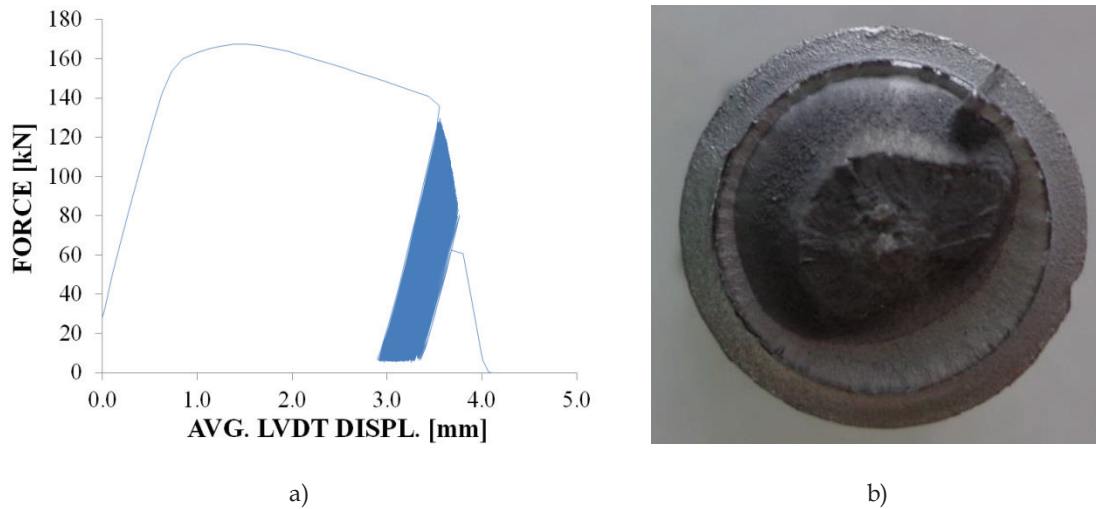


Figure 5.23: Constant amplitude cyclic test on M16 HV with 2 nuts: a) applied force vs time series; b) fatigue fracture

As it can be observed, during the test the applied force progressively reduces due to the propagation of cracks (i.e. with reduction of the shank effective area) until failure. Figure 5.23b) shows the flat fracture with seashore-like marks due to the propagation of cracks followed by the roughest final fracture.

HV assemblies (i.e. with one nut) did not exhibit any cracks and fatigue fracture. Indeed, owing to the occurrence of thread stripping failure, the portion of the threaded zone subjected to the relative slip of the nut is rendered smooth cycle by cycle, thus flattening the crests. Under this condition, the assembly indefinitely cycles without failing. Hence, the tests on HV specimens were interrupted after about 300000 cycles. The force-displacement response curve for a M16 HV assembly is shown in Figure 5.24a), while Figure 5.24b) shows the specimen after the test, where the smoothed surface of threaded zone of the shank due to the nut stripping can be observed. This feature made unfeasible the determination of  $\varepsilon$ - $N$  curve for HV assemblies.

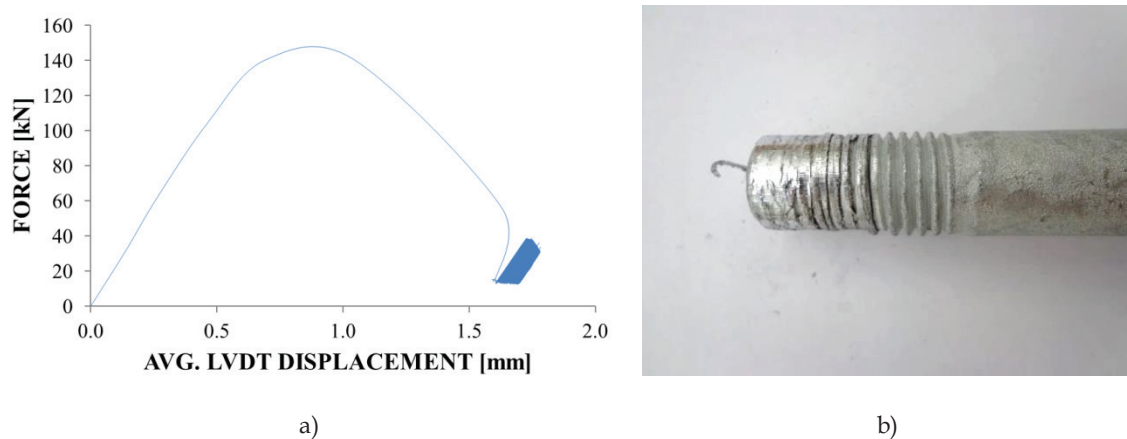


Figure 5.24: Constant amplitude cyclic test on M16 HV: a) applied force vs time series; b) bolt after test and forced nut extraction

SB assemblies, similarly to the HR and HV with 2 nuts cases, showed typical fracture failure in the threaded zone of the shank between bolt head and nut, as observed in elastic fatigue tests on Gr. 8.8. bolts by Shahani and Shakeri (2015). Figure 5.25a) depicts the experimental response curve of a M24 specimen.

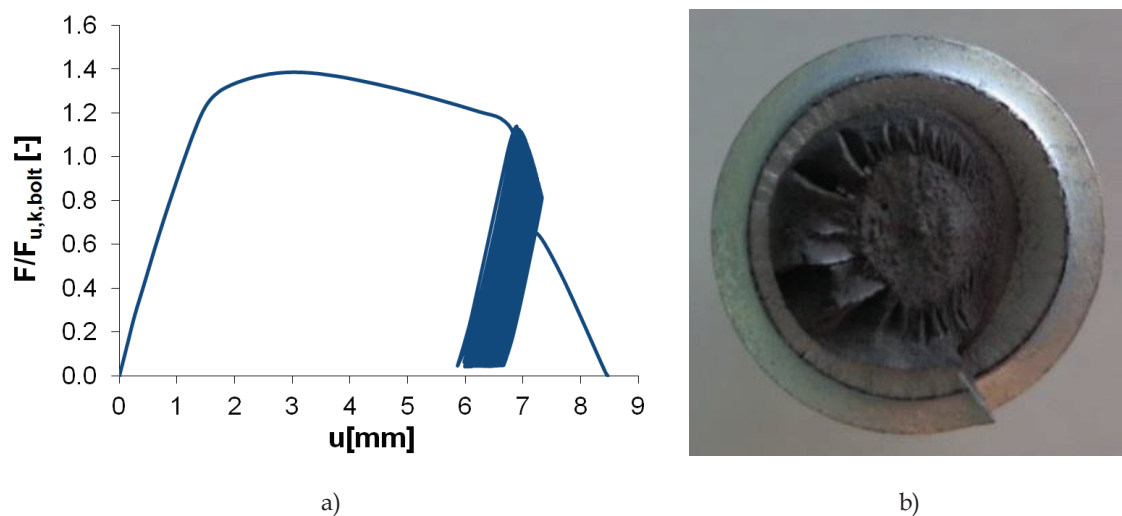


Figure 5.25: Constant amplitude cyclic test on M24 SB: a) applied force vs time series normalised to ultimate characteristic force; b) fatigue fracture

As it can be observed, during the test the applied force progressively reduces due to the propagation of cracks (i.e. with reduction of the shank effective area) until failure. Figure 5.25b) shows the flat fracture with seashore-like marks due to the propagation of cracks and the final fracture zone at the centre.

The low-cycle fatigue endurance till the failure of the bolts is expressed in terms of  $\varepsilon$ - $N$  curves, which were obtained by linear regression of experimental data having expressed the number of cycle  $N$  in logarithmic scale.

The low cycle fatigue curves for HR and HV with 2 nuts assembly types are presented in Figure 5.26, where  $R^2$  coefficients close to 1 guarantee a satisfactory fitting of the test results. It is interesting to observe that in both assemblies the fatigue resistance inversely increases with the diameter, namely being larger for the smaller diameters. This feature can be explained considering that larger size of the crests (which increase with the diameter of the shank) of the threaded zone corresponds to an increase of the stress concentration factor. The lower accuracy of the regression lines for HV with two nuts is due to the larger dispersion of experimental results, especially for M24, which can be explained considering that the couple of nuts were tightened consecutively, inducing different stress distribution into the threaded zone.

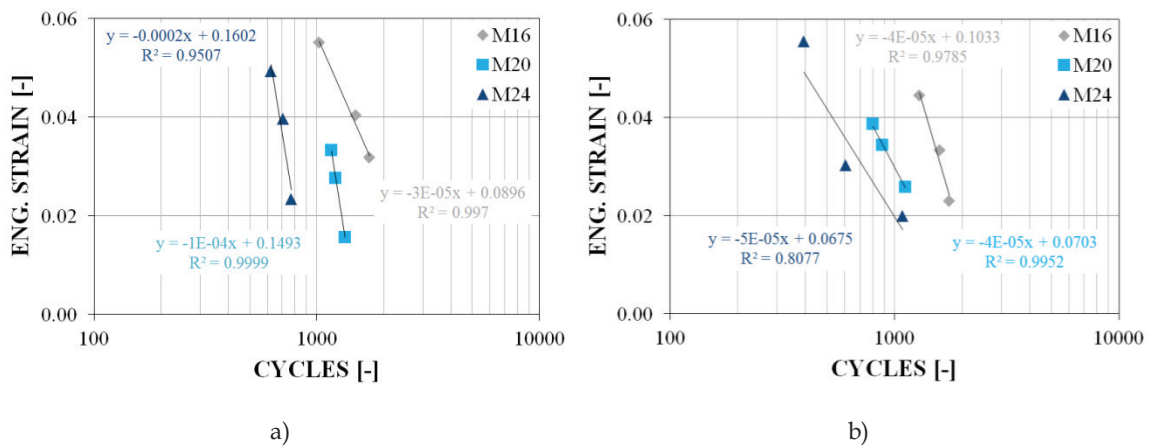


Figure 5.26: Fatigue resistance at constant engineering strain: a) HR bolt assemblies; b) HV with 2 nuts bolt assemblies

For the case of SB assemblies, the minimum number of cycles corresponding to bolt failure is relatively high and 10 times larger than the number of cycles observed by Čermelj *et al.* (2015) for the crack initiation into welded beam-to-column joints made of European IPE, HEA and HEB profiles under seismic condition. This finding may suggest that low-cycle fatigue of SB bolts could not impair the cumulated ductility of bolted joints under seismic action. However, further tests on bolted sub-assemblages will be necessary to verify this issue.

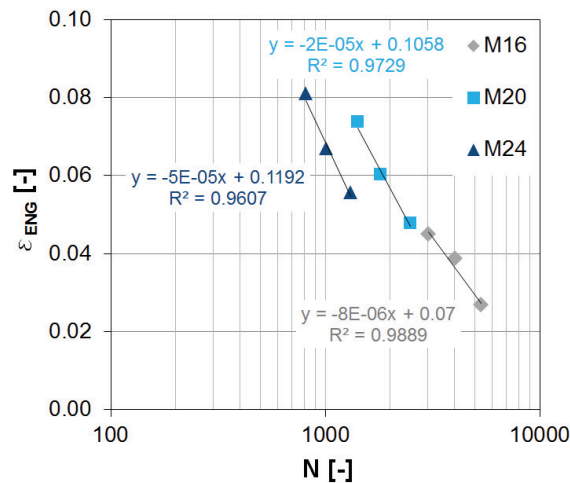


Figure 5.27: Fatigue resistance at constant engineering strain of SB bolt assemblies

It was also observed that fatigue resistance inversely increased with the diameter, namely being larger for smaller diameters. This feature can be explained considering that to a larger size of the crests (which increase with the diameter of the shank) of the threaded zone may correspond to an increase of the stress concentration factor.

## 5.6 Finite element modelling

### 5.6.1 Background

The modelling of tensile response until failure of bolt assemblies is fundamental to ensure the accuracy of numerical results obtained by means of finite element analysis of steel bolted joints. Most of analytical and numerical studies proposed effective modelling assumptions for US bolt assemblies (Abel, 1993; Sherbourne and Bahaari, 1997; Bickford and Nassar, 1998; Swanson, 1999; Mays, 2000; Wade, 2006). Recently, Prinz *et al.* (2014) proposed a trilinear stress-strain relationship to simulate the material behaviour of HR bolts used for bolted beam-column joints. The bolt ultimate strength is taken as 17% higher than the yield strength, and the yield plateau extends indefinitely. The post-elastic transition branch is characterized by a stiffness value equal to  $0.63E$ , being  $E$  the elastic modulus of the steel. However, the fact that the elastic branch presents a stiffness of 210 GPa indicates that the presented model pertains only to the shank deformability itself and does not account for other possible sources of deformability that contribute to the total assembly deformability, such as the threads. Since HV bolts are heavily dependent on deformations developing into the

threaded zone of the shank, the numerical model should account for this additional source of deformability.

A more refined multi-linear model for bolts was given by Swanson and Leon (2011), where the bolt response was derived from experimental tension test and schematized by four linear segments. The first branch simulates the bolt behaviour prior to overcoming pretension, the second segment represents the linear elastic response, the third segment models the onset of yielding (taken at 85% of the tensile capacity) and finally the fourth mimics the behaviour in plastic range. The elastic stiffness of the bolt  $K_b$  was computed according to Bickford and Nassar (1998) and Swanson (1999) as follows:

$$\frac{1}{K_b} = \frac{f \cdot d_b}{A_b \cdot E} + \frac{L_s}{A_b \cdot E} + \frac{L_{tg}}{A_{be} \cdot E} + \frac{f \cdot d_b}{A_{be} \cdot E} \quad (5.3)$$

where  $f$  is a correlation factor taken as 0.55,  $d_b$  is the nominal diameter of the bolt,  $A_b$  is the nominal area of the bolt shank,  $A_{be}$  is the effective area of the threaded shank,  $L_s$  is the length of the bolt shank,  $L_{tg}$  is the length of the threaded portion included in the bolt's grip and  $E$  is the steel modulus of elasticity.

In order to avoid obtaining excessive values for the ultimate bolt elongation, this model limits elongation according to the following expression:

$$\delta_{fract} = \frac{0.90 \cdot B_n \cdot L_s}{A_b \cdot E} + \varepsilon_{fract} \left( L_{tg} + \frac{2}{n_{th}} \right) \quad (5.4)$$

where  $\varepsilon_{fract}$  is the fracture strain;  $B_n$  is the tensile capacity of the bolt;  $n_{th}$  is the number of threads per unit length of the bolt.

The modelling approach showed by Swanson and Leon (2001) describes the most important stages of bolt response, allowing to capture accurately the softening due to the shank necking. More recently, Hanus *et al.* (2011) proposed a model to simulate also the bolt softening by using an equivalent force-displacement relationship in tension. This model is characterized by an elastic branch, a nonlinear transition segment and a bilinear descent branch.

A more refined approach was adopted by Pavlovic *et al.* (2015), which used a plasticity curve to define the hardening material behaviour, coupled with a damage

initiation criterion and a damage evolution law to reproduce softening and failure. However, this method requires very detailed modelling of bolt assembly geometry, including the geometrical modelling of the treads on the shank and into the nut and the relevant surface interactions, thus requiring significant computational effort for the FE analysis of a single bolt. Therefore, unless required for a very specific and detailed application, the adoption of such a model is less convenient for quick and effective FE analysis of bolted joints. On the contrary, the use of multi-linear constitutive law to simulate the bolt mechanical behaviour, when a sufficient number of segments is considered, can effectively describe all stages of bolt assembly response with a significant limitation of corresponding computational effort.

In order to highlight the accuracy of existing multi-linear models (N.B. early developed for US bolts) given by Abel (1993), Sherbourne and Bahaari (1997), Swanson (1999) and Mays (2000) to predict the behaviour of European high strength preloadable bolts, their relevant force-displacement response curves obtained from both analytical and finite element analysis performed with Abaqus 6.14 (Dassault, 2013) were compared to the corresponding experimental curves obtained in this study.

Figure 5.28a) depicts the comparison between the analytical predictions given by different authors to the piece-wise linear approximated response curves of M24 both HV and HR, while Figure 5.28b) shows the comparison between results from finite element analyses incorporating models by different authors and the experimental results. As it can be observed, the examined formulations overestimate the initial stiffness of European bolt assemblies, in line with the consideration that the threaded zones of EU bolts differ from US and its contribution to axial deformability varies, as well. In addition, the modelling assumptions by these authors satisfactorily match the softening rate of HR assembly, while largely mispredict the post-yielding response of HV bolts. This comparison highlights that better refinement is necessary to accurately simulate European high strength bolts. Hence, in the following Sections, modelling assumptions are proposed and verified against presented experimental results.

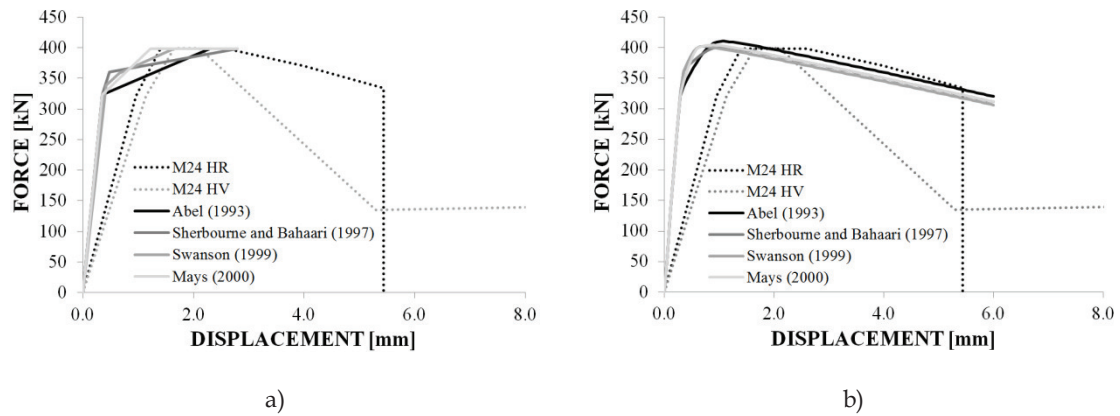


Figure 5.28: Force-displacement response comparison between European piece-wise linear approximated and modelling assumptions by different authors for M24 HR and M24 HV assemblies: a) analytical response curves; b) numerical response curves

### 5.6.2 Modelling of HR assemblies

#### 5.6.2.1 Simplified model with equivalent shank

Finite element models of HR assemblies were carried out using Abaqus (Dassault, 2013). The finite element model is shown in Figure 5.29a). The finite element type C3D8R (an 8-node linear brick type element with reduced integration and hourglass control) was used to discretize the model. In order to avoid shear locking and hourglass, more than three layers of finite elements across the thickness were adopted. The numerical analysis was conducted using a single step in which monotonically increasing displacements were imposed to the nut until reaching a target displacement corresponding to assembly failure.

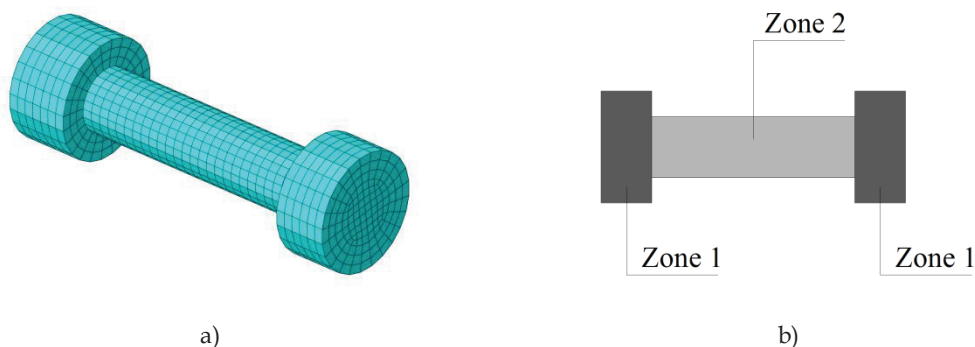


Figure 5.29: Modelling of HR assembly: a) finite element model ; b) main components

The equivalent geometry of HR bolts is made up of a single continuous element composed of two zones, as shown in Figure 5.29b), each of them characterized by

different mechanical properties. Both bolt head and nut (i.e. corresponding to Zone 1) are modelled using a linear elastic material constitutive law with  $E=210$  GPa and Poisson coefficient  $\nu=0.3$ . The shank (i.e. corresponding to zone 2) was modelled by meshing a solid cylinder having the nominal circular gross area of the bolt, where the plastic behaviour of the assembly is concentrated.

Zone 2 should account for both elastic deformability of the shank and the plastic behaviour of the assembly, as well. The equivalent elastic modulus of the shank is calibrated from the experimental curves, from which the stiffness of the assembly  $K_{eq}$  is subsequently derived. Considering the smooth part of the shank, the threads and threaded portion included in the bolt's grip (i.e. the threads inside the nut) as a system of three springs working in series, as follows:

$$\frac{1}{K_{eq}} = \frac{1}{K_E} + \frac{1}{K_Z} + \frac{1}{K_{tg}} \quad (5.5)$$

where the stiffness of the smooth part of the shank  $K_E$  and the stiffness of the threaded part of the shank  $K_Z$  are calculated on the basis of the theory of elasticity, then the stiffness of threads in the bolt grip  $K_{tg}$  can be derived solving Eq. (5.5). Thus, rearranging Eq. (5.5) and expanding each term, the equivalent shank elastic modulus  $E_{eq}$  can be obtained as follows:

$$E_{eq} = \left( \frac{1}{K_E} + \frac{1}{K_Z} + \frac{1}{K_{tg}} \right)^{-1} \times \frac{E+Z}{A_{nom}} \quad (5.6)$$

$$E_{eq} = \left( \frac{E}{E_s A_{nom}} + \frac{Z}{E_s A_{eff}} + \frac{1}{K_{tg}} \right)^{-1} \times \frac{E+Z}{A_{nom}} \quad (5.7)$$

where  $E$  is the length of the smooth part of the shank (as defined in Figure 5.5);  $Z$  is length of the threaded shank (as defined in Figure 5.5);  $A_{nom}$  is nominal shank area;  $A_{eff}$  is effective shank area.

The equivalent shank stiffness and elastic modulus for the examined HR bolts (that have  $E+Z$  length of the shank equal to 80mm) are shown in Table 5.17, where it can be recognized that the equivalent experimental elastic modulus  $E_{eq}$  is smaller than the elastic shank modulus  $E_{Barron\&Bickford}$  computed according to Eq. (5.3).

Table 5.17: HR equivalent shank model elasticity modulus values



Bolt assembly type	Nominal diameter	Smooth shank length	Threaded shank length	Nominal shank area	Effective shank area	Stiffness smooth shank.	Stiffness threaded shank	Stiffness grip zone	Assembly stiffness	Equivalent elastic modulus	Equivalent elastic modulus from Eq. (3)
[-]	D [mm]	E [mm]	Z [mm]	A <sub>nom</sub> [mm <sup>2</sup> ]	A <sub>eff</sub> [mm <sup>2</sup> ]	k <sub>E</sub> [N/mm]	k <sub>Z</sub> [N/mm]	k <sub>g</sub> [N/mm]	k <sub>Assembly</sub> [N/mm]	E <sub>eq</sub> [N/mm <sup>2</sup> ]	E <sub>Barron&amp;Bickford</sub> [N/mm <sup>2</sup> ]
HR	16	56.3	23.7	201	157	749965	1391139	1009579	328651	130766	157420
	20	61.0	19.0	314	245	1081532	2707895	697631	366659	93369	152080
	24	57.3	22.7	452	353	1657971	3265639	1355818	607191	107375	144196

The plasticity model was calibrated on the basis of monotonic tests described in Section 5.5.1. The constitutive law to be applied to zone 2 is characterized by the multi-linear stress-strain curve shown in Figure 5.30a), and the coordinates of each point (i.e. P1 through P5) are computed according to Table 5.18. As it can be noted, the maximum normalised stress ratio  $\sigma_{true}/f_{y,k,bolt}$  values are around 1.0, being the shank modelled with its nominal diameter. By modelling the shank with its gross area, the true stress values are scaled down to simulate fictitiously the bolt strength. Softening is defined by a single segment between points P3 and P4. The ultimate plastic strain  $\epsilon_{P4}$  is given from quadratic interpolation curve of experimental results as shown in Figure 5.30b).

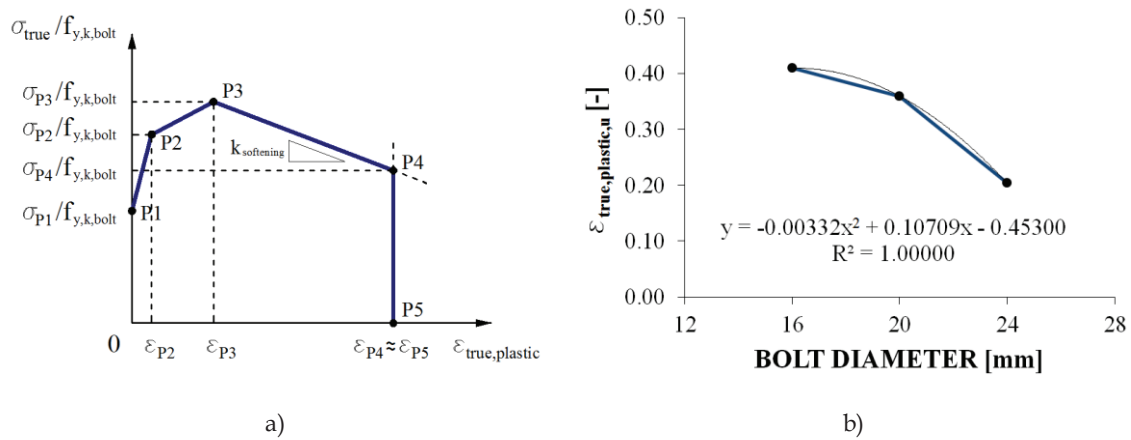


Figure 5.30: a) Proposed simplified HR equivalent bolt shank model; b) Variation of ultimate true plastic strain with bolt nominal diameter

Table 5.18: Proposed constitutive law for HR equivalent shank

POINT	$\epsilon_{true,plastic}$	$\sigma_{true}/f_{y,k,bolt}$
[-]	[-]	[-]
P1	0.000	0.931
P2	0.005	0.988
P3	0.017	1.008
P4	$-3.32E-3 D_{nom}^2 + 0.10709 D_{nom}^2 - 0.453$	$k_{softening} \epsilon_{true,plastic,P4} + 1.0136$
P5	$\epsilon_{P4} + 0.001$	0.000
$k_{softening} =$		-0.3328

The comparison between the experimental and the calibrated numerical bolt force-displacement response curves is presented in Figure 5.31, showing that the equivalent bolt shank model is capable of accurately reproducing all stages of the bolt response, including the softening associated to shank necking leading up to assembly failure.

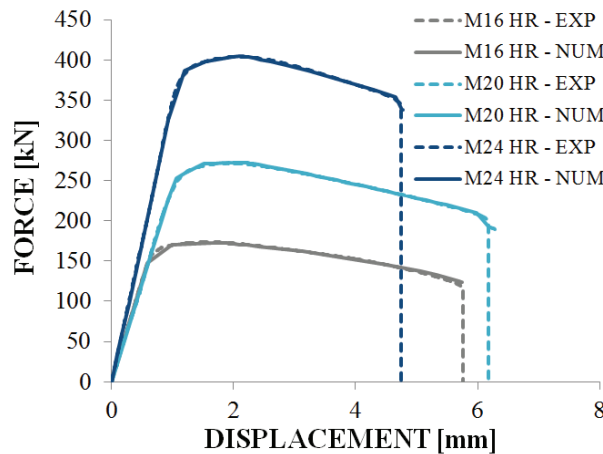


Figure 5.31: Experimental vs numerical response comparison - equivalent shank model - HR assemblies

### 5.6.2.2 Ductile damage model

Both initial stiffness and failure mode of HR bolts can be simulated using a more refined approach. With this regard, bolt geometry was also modelled with two different diameters along the shank, corresponding to the smooth part and that corresponding to the equivalent area of the threads. This assumption allows directly obtaining the initial stiffness of the bolt with good accuracy. In addition, modelling the transition of diameter along the shank enforces the failure in the threaded zone as

verified in experimental tests. The ductile failure was simulated using progressive damage model (Dassault, 2013), which accounts for damage initiation, softening, crack initiation and progression as shown in Figure 5.32, where point  $D=0$  corresponds to the damage initiation point, the dashed curve represents the undamaged material response and the continuous line after point  $D=0$  represents the material softening.

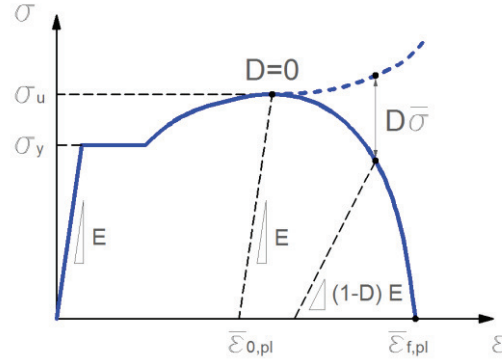


Figure 5.32: Progressive ductile damage model

The formulation for ductile damage included in the Abaqus (Dassault, 2013) software package was adopted, requiring the definition of the generic undamaged material response curve, damage initiation criterion and damage evolution law. The equivalent plastic strain at the onset of damage  $\bar{\epsilon}_0^{pl}$  is dependent on strain rate and stress triaxiality  $T$ , defined as the ratio between the hydrostatic pressure stress (or isotropic stress)  $\sigma_H$  and the Von Mises equivalent stress  $\sigma_{eq}$ , defined as:

$$\sigma_H = \frac{\sigma_{xx} + \sigma_{yy} + \sigma_{zz}}{3} \quad (5.8)$$

$$\sigma_{eq} = \sqrt{\frac{(\sigma_{xx} - \sigma_{yy})^2 + (\sigma_{yy} - \sigma_{zz})^2 + (\sigma_{zz} - \sigma_{xx})^2 + 6(\tau_{xy}^2 + \tau_{yz}^2 + \tau_{zx}^2)}{2}} \quad (5.9)$$

The adopted undamaged material plasticity curve was based on the properties used by Pavlovic *et al.* (2015) for grade 10.9 bolt assemblies, multiplied by a stress scaling factor to compensate for material overstrength. Equal damage initiation criteria were adopted for the calibration of the M16, M20 and M24 assemblies. The adopted undamaged response curve and damage onset criterion curves are shown in Figure 5.33.

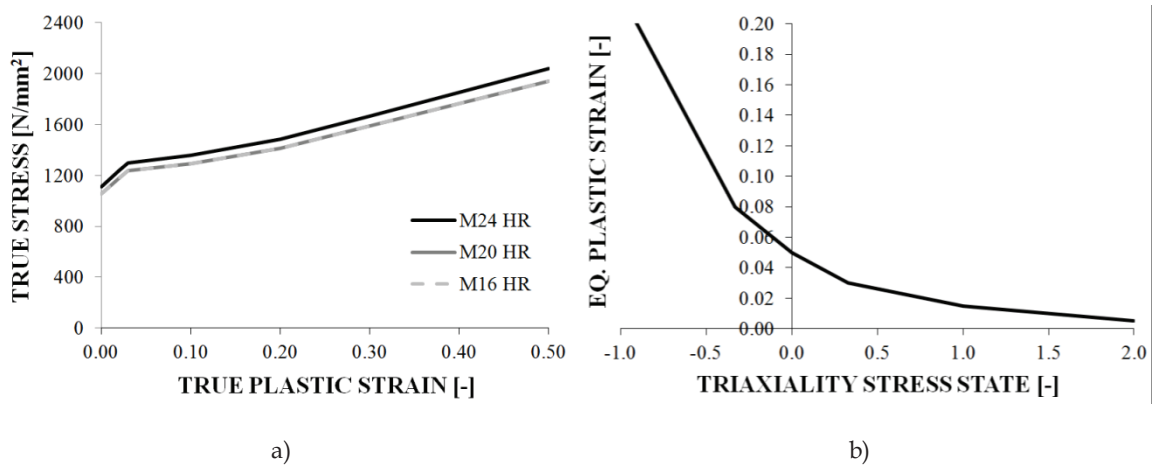


Figure 5.33: a) undamaged material constitutive law; b) equivalent plastic strain vs triaxiality stress state according to (Pavlovic *et al.*, 2015)

A linear damage evolution law based was assumed, with the effective plastic displacement  $\bar{u}^{pl}$  defined as the product of the equivalent plastic strain at failure  $\bar{\epsilon}_f^{pl}$  by the characteristic length  $L$  of the finite element. The calibrated curves for the damage parameter  $D$  as a function of  $\bar{u}^{pl}$  are shown in Figure 5.34a), while the validated curves for the equivalent plastic strain at failure  $\bar{\epsilon}_f^{pl}$  as a function of bolt nominal diameter are shown in Figure 5.34b), for a characteristic finite element length  $L = 2$  mm.

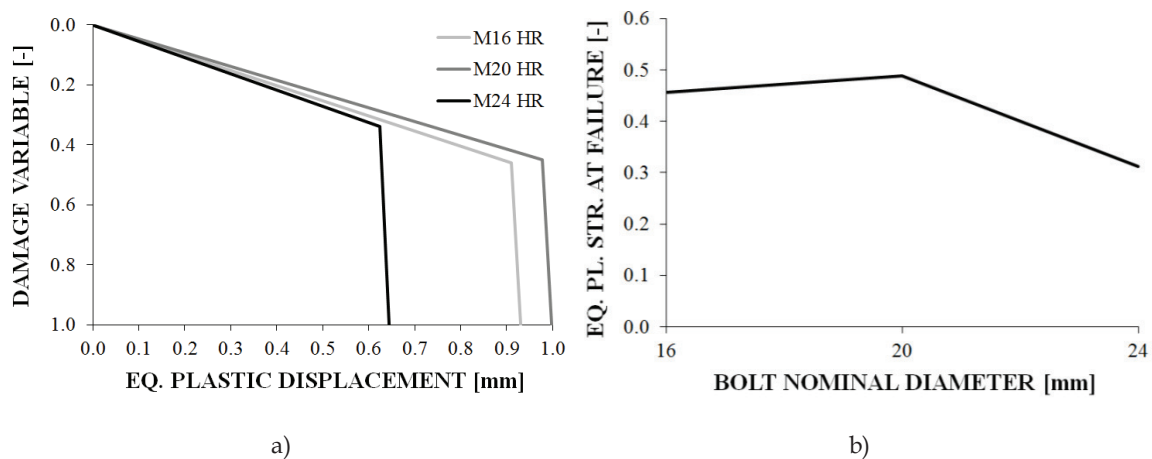


Figure 5.34: a) damage evolution law; b) equivalent plastic strain at failure

The calibrated curves show that the damage evolution is similar by varying bolt diameters, consistently with the similar softening rates exhibited in experimental tests. Similar equivalent plastic displacement values were obtained for the M16 and M20

assemblies, while for the M24 a significant reduction was observed, coherently with the reduced ultimate displacement displayed in the experimental tests.

The force-displacement comparison between experimental and the calibrated numerical progressive damage model response is shown in Figure 5.35a) and the numerical model for the M24 assembly after fracture is presented in Figure 5.35b).

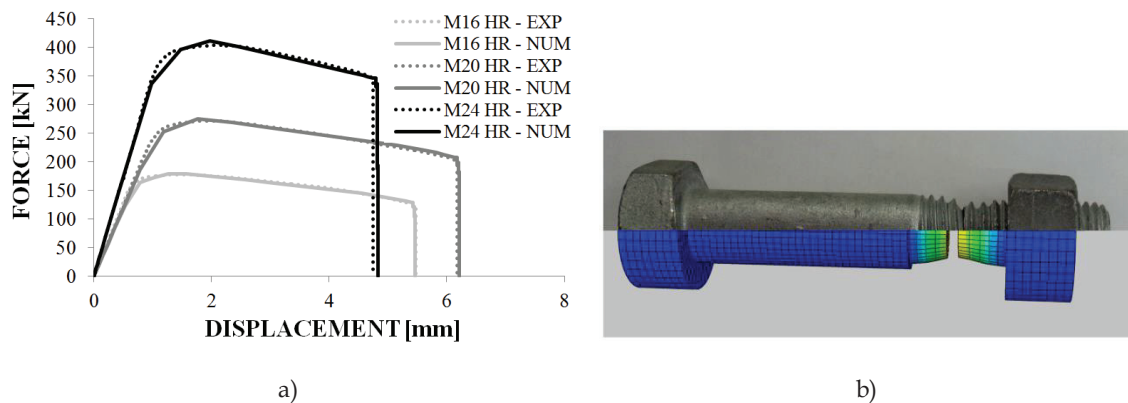


Figure 5.35: a) comparison between numerical damage model and experimental force-displacement response; b) M20 failed specimen and model after fracture

The calibrated progressive damage models are capable of accurately capturing damage initiation, softening and failure mode, although requiring significant computational effort for simulating a single assembly. Hence, this modelling strategy appears to be suitable for application in small size models and to predict crack initiation and propagation patterns. For more complex models including a large number of bolt assemblies and for large scale parametric studies for which computational time is a key factor, a more simplified approach may be more advantageous.

### 5.6.3 Modelling of HV assemblies

The modelling assumptions described for HR bolts are not effective for HV assemblies, because their failure is characterized by the nut stripping that cannot be effectively simulated by an equivalent plastic failure as for the shank necking. Hence, a different modelling strategy was adopted. The geometry of HV assembly was sub-structured into three main parts: i) the nut, modelled by solid finite elements; ii) the bolt, comprising head and shank, modelled with solid finite elements; iii) a fictitious one-dimensional wire finite element connected to the head and the nut as shown in Figure 5.36a) to simulate the nut stripping. The model uses one-dimensional wire type

finite elements to simulate the behaviour of the shank and three-dimensional solid elements to model the bolt head and shank, as well as the nut. This choice allows overcoming problems of local shank necking by adopting a zero Poisson ratio value for the cross section of the wire element, to which a nonlinear material constitutive law function is assigned in order to account for the different stages of the HV assembly response.

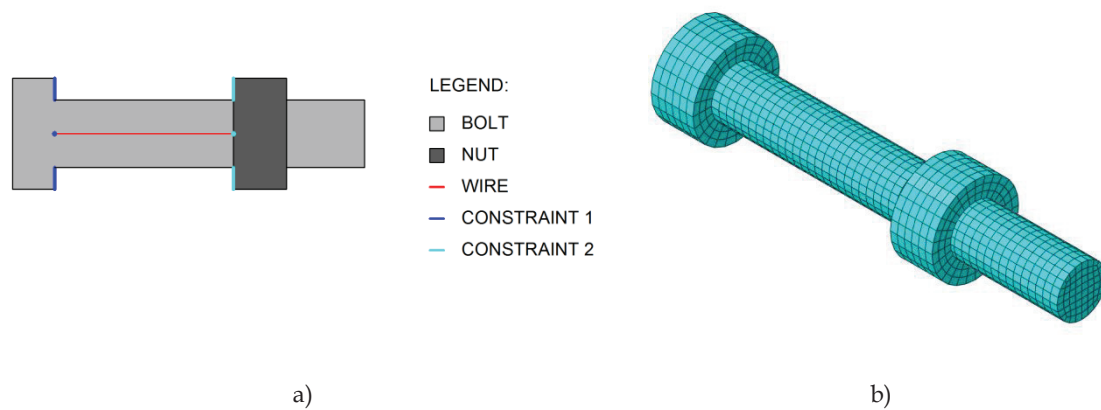


Figure 5.36: HV assembly modelling: a) main components; b) finite element model

As for HR assemblies, the geometry of the shank was modelled by meshing a solid cylinder having the nominal circular gross area of the bolt. The nut geometry corresponds to a hollow cylinder with its internal diameter equal to the bolt nominal diameter. One end of the wire is connected to the nut through a rigid body constraint which only allows longitudinal translation of the nut along the direction defined by the wire. In addition, the second end of the wire was connected to the internal surface of the bolt head by a rigid body constraint. Hard contact without friction was defined between the nut's internal surface and the solid finite elements of the bolt shank, since all resistance opposing the nut slip is accounted for in the constitutive law of the wire. C3D8R finite elements were used for the solid parts of the model, which are characterized by a linear elastic behaviour with elastic modulus  $E=210$  GPa and Poisson coefficient  $\nu=0.3$ . The equivalent elastic modulus of the shank was determined as for HR assembly and the experimental and calculated values are reported in Table 5.19.

Table 5.19: HV equivalent shank model elasticity modulus values

Bolt assembly type	Nominal diameter	Smooth shank length	Threaded shank length	Nominal shank area	Effective shank area	Stiffness smooth shank.	Stiffness threaded shank	Stiffness grip zone	Assembly stiffness	Equivalent elastic modulus	Equivalent elastic modulus from Eq. (3)
	D	E	Z	A <sub>nom</sub>	A <sub>eff</sub>	k <sub>E</sub>	k <sub>Z</sub>	k <sup>g</sup>	k <sub>Assembly</sub>	E <sub>eq</sub>	E <sub>Barron&amp;Bickford</sub>
[-]	[mm]	[mm]	[mm]	[mm <sup>2</sup> ]	[mm <sup>2</sup> ]	[N/mm]	[N/mm]	[N/mm]	[N/mm]	[N/mm <sup>2</sup> ]	[N/mm <sup>2</sup> ]
HV	16	69.9	10.1	201	157	604049	3264356	511924	255411	101625	163259
	20	70.7	9.3	314	245	933146	5532258	386791	260568	66353	155945
	24	73.0	7.0	452	353	1301394	10440845	539119	367774	65118	149883

As it can be observed, the elastic stiffness of HV assemblies is lower than that of HR (see Table 5.17), due to the lower stiffness of the treads in the grip zone.

A zero Poisson coefficient value was associated to the wire element and its nonlinear behaviour consists in a multi-linear constitutive law that resists solely in tension for relative displacements between the bolt head and the nut. The proposed equivalent multi-linear material response curve was derived from the stress-strain curves presented in Section 5.5.1 and it is shown in Figure 5.37a), while the equations of each segment are reported in Table 5.20. The comparison between the experimental and the calibrated numerical bolt force-displacement response curves is presented in Figure 5.37b), showing that the proposed modelling strategy is suitable for capturing the highly nonlinear behaviour of HV assemblies.

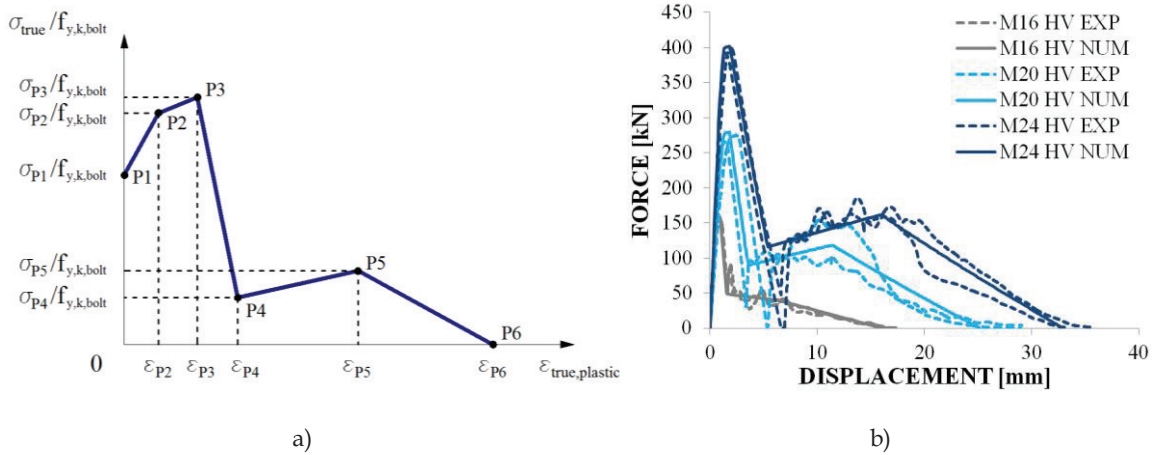


Figure 5.37: a) Proposed simplified HV equivalent bolt shank model; b) comparison between experimental and numerical response curves

Due to the variability of the experimental curves when nut stripping occurs, two monotonic experimental curves for each assembly diameter are plotted in Figure 5.37b) to verify the accuracy of the proposed modelling assumptions.

Table 5.20: Proposed constitutive law for HV equivalent shank

POINT	$\epsilon_{\text{true,plastic}}$	$\sigma_{\text{true}}/f_{y,k,\text{bolt}}$
[-]	[-]	[-]
P0	0	0.7867
P1	$0.0023 \alpha_1$	$0.9808 \beta_1$
P2	$0.0089 \alpha_2$	$0.9878 \beta_2$
P3	$0.0502 \alpha_3$	$0.2999 \beta_3$
P4	$\epsilon_{P3} + \alpha_4$	$0.2999 \beta_3 + \beta_4 / f_{y,k,\text{bolt}} (\epsilon_{P4} - \epsilon_{P3})$
P5	$\alpha_5$	$\beta_5$

$\alpha_1 = 0.4$  if  $D = 16$  ;  $\alpha_1 = 1.0$  if  $D > 16$   
 $\beta_1 = 0.893$  if  $D = 16$  ;  $\beta_1 = 1.0$  if  $D > 16$   
 $\alpha_2 = \alpha_1$  ;  $\beta_2 = \beta_1$   
 $\alpha_3 = 0.1091 * D - 1.4$   
 $\beta_3 = -8.411E-3 * D^2 + 3.431E-1 * D - 2.443$   
 $\alpha_4 = 6.711E-3 * D - 4.585E-2$   
 $\beta_4 = 1000 * (-5.558E-2 * D^2 + 2.406 * D - 2.485E1)$   
 $\alpha_5 = 4.087E-4 * (K+Y)^2 - 1.228E-2 * (K+Y) + 2.825E-1$   
 $\beta_5 = 1E-4$   
 $D \equiv$  Shank nominal diameter;  $K+Y$  defined in Figure 5.5b)  
 $D, K, Y$  in mm  
 $f_{y,k,\text{bolt}} \equiv$  bolt characteristic yielding stress

## 5.6.4 Modelling of SB assemblies

### 5.6.4.1 Simplified model with equivalent shank

The modelling of SB assemblies according to the equivalent shank model was performed according to the methodology described in Section 5.6.2.1 for HR assemblies. The equivalent shank stiffness and elastic modulus for the examined SB (that have an  $E+Z$  length of the shank equal to 80 mm) are presented in Table 5.21, showing that the equivalent experimental elastic modulus  $E_{eq}$  is smaller than the elastic shank modulus  $E_{Barron\&Bickford}$  computed according to Eq. (5.3).

Table 5.21: SB equivalent shank model elasticity modulus values

Bolt assembly type	Nominal diameter	Smooth shank length	Threaded shank length	Stiffness smooth shank.	Stiffness threaded shank	Stiffness grip zone	Assembly stiffness	Equivalent elastic modulus	Equivalent elastic modulus from Eq. (5.3)
[-]	D [mm]	E [mm]	Z [mm]	$k_E$ [N/mm]	$k_z$ [N/mm]	$k_{tg}$ [N/mm]	$k_{\text{Assembly}}$ [N/mm]	$E_{eq}$ [N/mm <sup>2</sup> ]	$E_{Barron\&Bickford}$ [N/mm <sup>2</sup> ]
SB	16	67.2	12.8	628319	2575781	334022	201062	80000	162065
	20	57.7	22.3	1143387	2307175	429221	274889	70000	150808
	24	57.7	22.3	1646478	3324215	564590	373221	66000	144336



The plasticity model was calibrated on the basis of monotonic tests described in Section 5.5.1. The constitutive law to be applied to zone 2 is characterized by the multi-linear stress-strain curve adopted for HR assemblies and presented in Figure 5.30a), and the coordinates of points P1 through P5 are given in Table 5.22.

Table 5.22: Proposed constitutive law for SB equivalent shank

POINT	$\epsilon_{true,pl}$	$\sigma_{true}/f_{y,k,bolt}$
[-]	[-]	[-]
P1	0.000	1.062
P2	0.005	1.193
P3	0.020	1.261
P4	$-1.065E-2 D_{nom}^2 + 0.3907 D_{nom} - 3.009$	$k_{softening} \epsilon_{true,pl,P4} + 1.2681$
P5	$\epsilon_{true,pl,P4} + 0.001$	0.001
$k_{softening} = -0.3643$		

As it can be noted, the maximum normalised stress ratio  $\sigma_{true}/f_{y,k,bolt}$  values are around 1.26. The ultimate true plastic strain  $\epsilon_{true,pl,P4}$  is given from quadratic interpolation of experimental results. The comparison between the experimental and the calibrated numerical bolt force-displacement response curves is presented in Figure 5.38a), showing that the equivalent bolt shank model is capable of accurately reproducing all stages of the bolt response, including the softening associated to shank necking (see Figure 5.38b) leading up to assembly failure.

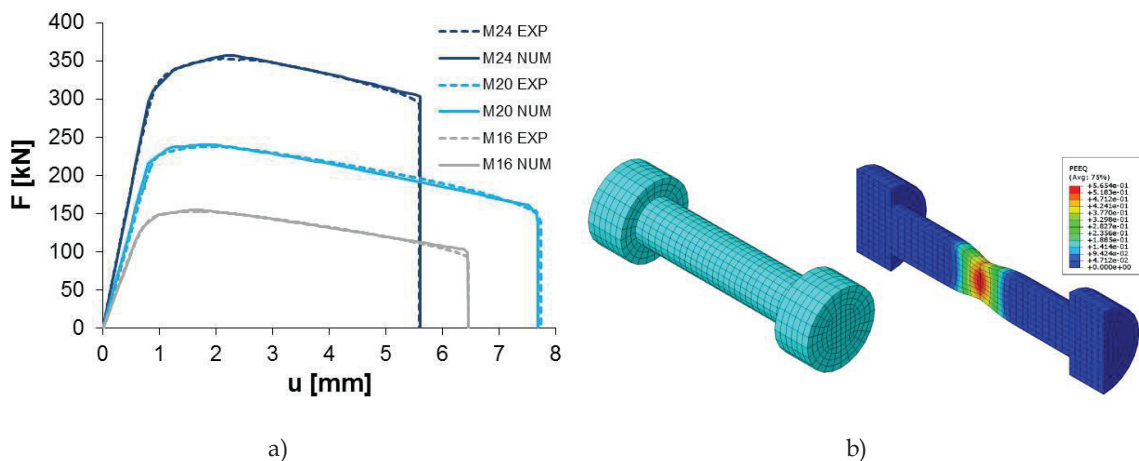


Figure 5.38: a) Experimental vs numerical response comparison - equivalent shank model - SB assemblies; b) M20 model and plastic equivalent strain PEEQ contour plot with shank necking prior to failure

### 5.6.4.2 Ductile damage model

The modelling assumptions for the SB assembly ductile damage modelling are the same as those adopted for HR assemblies and described in Section 5.6.2.2. The adopted undamaged response curves and damage onset criterion curve are shown in Figure 5.39.

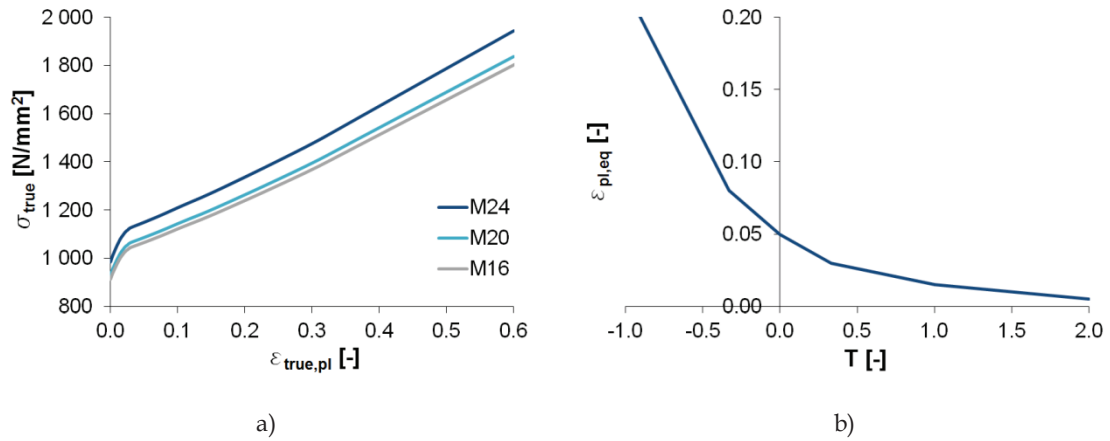


Figure 5.39: a) undamaged material constitutive law; b) equivalent plastic strain vs triaxiality stress state according to Pavlovic *et al.* (2015)

A linear damage evolution law was assumed and the calibrated curves for the damage parameter  $D$  as a function of  $\bar{u}^{pl}$  are shown in Figure 5.40a), and the equivalent plastic strain at failure is presented in Figure 5.40b) as function of bolt diameter, for an average characteristic finite element length  $L = 2$  mm.

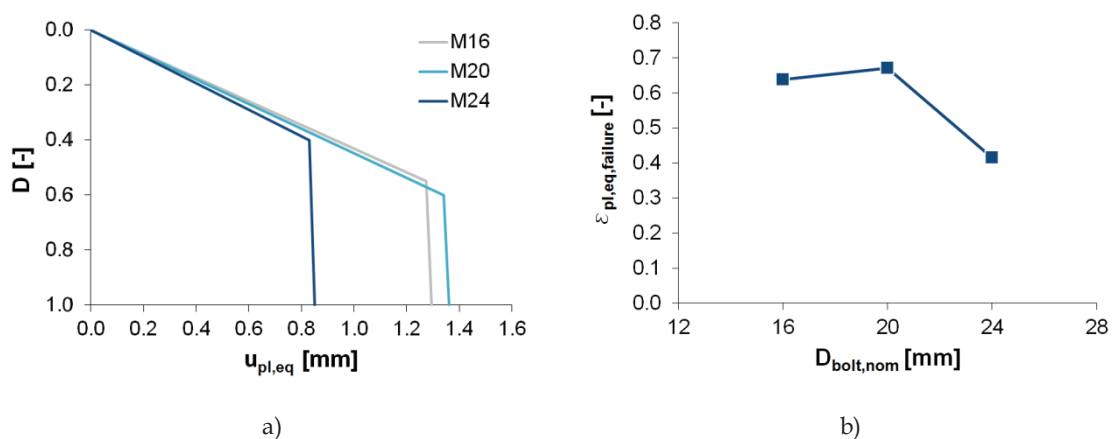


Figure 5.40: a) damage evolution law; b) equivalent plastic strain at failure

The calibrated curves show that the damage evolution law is similar for different bolt diameters, consistently with the similar softening rates exhibited in experimental tests. Similar equivalent plastic displacement values were obtained for

the M16 and M20 assemblies, while for the M24 a significant reduction was observed, coherently with the reduced ultimate displacement displayed in the experimental tests. The force-displacement comparison between experimental and the calibrated numerical progressive damage model response is shown in Figure 5.41a) and the numerical model for the M20 assembly after fracture is presented in Figure 5.41b).

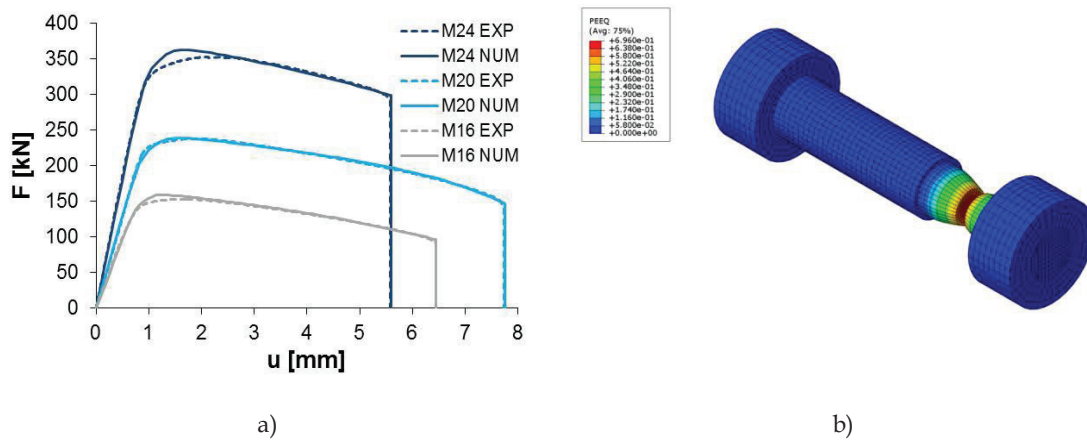


Figure 5.41: a) comparison between numerical damage model and experimental force-displacement response; b) M20 assembly numerical model after fracture

The calibrated progressive damage models are capable of accurately capturing damage initiation, softening and failure mode, although requiring more computational effort than the simplified models like the equivalent shank model.

### 5.6.5 Modelling of T-stub response with HR and HV assemblies

#### 5.6.5.1 Analytical modelling

The T-stub model is widely used to predict the behaviour of tension zones in bolted joints, and its deformation capacity is often the most important source of deformation of the joint. In light of the differences in terms of force-displacement response between the HV and the HR type assemblies shown in the previous Sections, the T-stub response may be significantly affected by the selection of the type of bolt assembly if its failure is either mode 2 (i.e. bolt failure with yielding of the flange shown in Figure 5.42b) or mode 3 (i.e. bolt failure only shown in Figure 5.42c). In order to examine this issue, the analytical 2D models shown in Figure 5.44 were used, considering either HR or HV, alternatively.

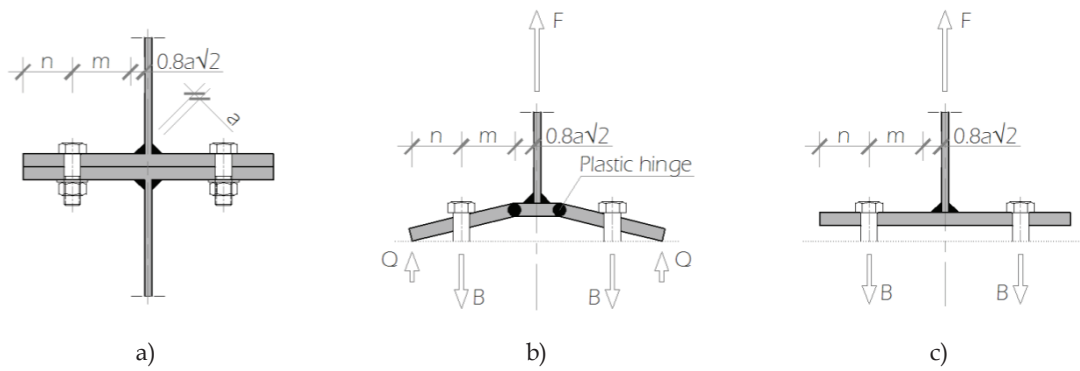


Figure 5.42: T-stub: a) Geometry; b) Mode 2 failure mechanism; c) Mode 3 failure mechanism

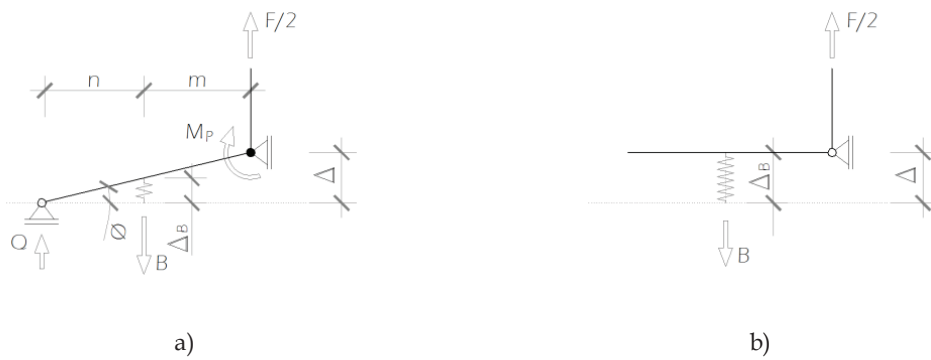


Figure 5.43: 2D simplified analytical models: a) Mode 2; b) Mode 3

The geometry of the T-stub used in this example is shown in Figure 5.44 and it was extracted from a secondary structure flush endplate joint designed for the gravity resisting part of the multi-storey building frames described in Chapter 3 of this dissertation. All beam, column and end-plate are made of S355 steel grade and the average yield stress  $f_{ym} = 444\text{MPa}$  was used for this calculation example.

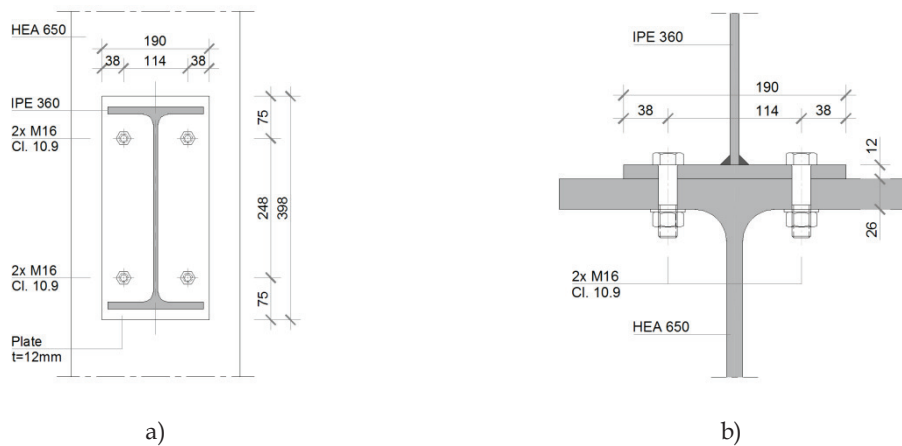


Figure 5.44: Flush endplate joint: a) joint geometry; b) t-stub geometry

The following hypotheses were assumed for the 2D analytical models: i) the plates are axially rigid; ii) the flush end-plate presents rigid-perfectly plastic behaviour in bending; iii) the stress-strain responses for the M16 HR and HV bolt assemblies corresponds to the average curves presented in Figure 5.16; iv) the plastic hinges formed at the endplate exhibit indefinite rotational capacity. The mode 2 response curves were derived by increasing displacements  $\Delta$  imposed to the T-stub and the corresponding bolt elongation  $\Delta_B$  was calculated based on a rigid body translation/rotation of the endplate (see Figure 5.44a). The bolt strain was computed as the ratio between the elongation  $\Delta_B$  and the initial bolt length and the corresponding resisting stress was determined from the stress-strain curves for M16 assemblies presented in Figure 5.16, and subsequently converted to bolt assembly resisting axial force  $B$ . The resistance  $F_{T,2}$  of the T-stub in mode 2 was computed by solving the moment equilibrium equation at the point of application of the prying force  $Q$ , and by imposing the force on the bolt assembly  $B$ , as follows:

$$\sum M_Q = 0 \quad (5.10)$$

$$F/2 \times (n + m) - M_p = B \times n \quad (5.11)$$

$$F = \frac{2}{n+m} (B \times n + M_p) \quad (5.12)$$

This equation can be re-written according to the nomenclature of the EN 1993-1-8 as follows:

$$F_{T,2} = \frac{2 \times M_p + 2 \times B \times n}{m+n} \quad (5.13)$$

$$F_{T,2} = \frac{2M_p + n \Sigma F_{t,Rd}}{m+n} \quad (5.14)$$

where  $M_p$ ,  $n$  and  $m$  are defined in Figure 5.42 and Figure 5.43. For the mode 3 response, the T-stub resistance is equal to the strength of bolts, namely equal to  $2B$ .

The T-stub response curve results are presented in Figure 5.45, where the T-stub force  $F$  is normalised to the T-stub's total bolt characteristic yielding force  $\Sigma F_{y,k,bolt}$ . For values of imposed displacement  $\Delta$  smaller than 0.4 mm, the T-stub mode 2 analytical response is practically identical for both HR and HV assemblies. For HR type, at displacements larger than 0.4mm the T-stub can sustain tensile forces close to its peak

resistance, whereas the case with HV exhibits significant reduction of strength even though the ultimate displacement capacity is about three times larger. The analytical  $F-\Delta$  response of the mode 3 was computed from the bolt assembly stress-strain curves and presents a similar behaviour but with smaller deformation capacity, since the endplate does not contribute to the T-stub deformation capacity.

In this calculation example, the critical mode for HR type is the mode 2, exhibiting the smaller capacity. For HV assemblies the T-stub behaves in mode 2 up to displacement equal to 0.6 mm; beyond such threshold, the mode 3 curve exhibits smaller strength, showing critical mode in bolts failure. Therefore, the high nonlinearity of the bolt response deeply affects the failure mode of T-stubs equipped with HV assemblies, resulting highly dependent on the applied displacement.

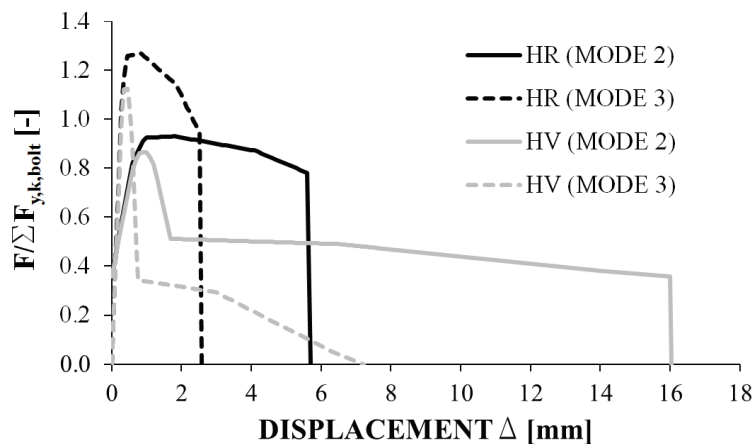


Figure 5.45: T-stub force-displacement response for the HR and HV type assemblies in modes 2 and 3

This feature becomes more important for bolted joints with several bolt rows evaluated according to components method provided in the EN1993-1-8 (CEN, 2005). Indeed, the components method assumes perfectly plastic behaviour of the T-Stub strength, which might differ from the actual behaviour of HV assemblies. Therefore, computing the T-stub failure mode based on nominal properties can be unsafe when HV assemblies are adopted, since both the strength and the failure mode are affected by the applied displacement.

This simple calculation example highlights that the design of joints should properly account for the type of bolt assembly, which should be selected by explicitly taking into account rotation and strength demands. In addition, the analysed example

shows that HV bolt assemblies can be suitable for the design of joints that should behave as nominally pinned with high rotation capacity. Conversely, the use of HR type assemblies is more appropriate for semi-rigid type joints, whose rotational demand is smaller and larger stiffness is required.

#### 5.6.5.2 Numerical modelling

The T-stub is a widely used model to predict the behaviour of tension zones in bolted joints. In order to highlight the differences in T-stub response using HR or HV bolt assembly types, numerical FE models were developed on two T-Stub joints, whose geometry is depicted in Figure 5.46a), alternatively designed according to EN1993-1-8 (CEN, 2005) to exhibit either mode 2 or mode 3.

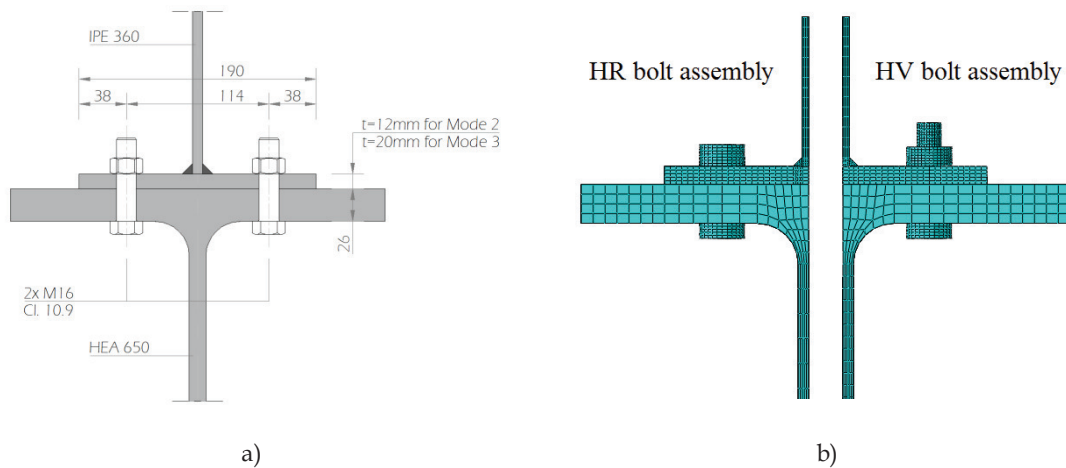


Figure 5.46: T-stub definition: a) geometry; b) FE models for HR and HV cases

The two FE models that were created to compare the T-stub response with HR and HV bolt assemblies are presented in Figure 5.46b), where only half T-stub was modelled, by taking advantage of symmetry conditions. The analyses were carried out in a single step using dynamic implicit analysis with a linear ramp function to apply displacements up to failure. Steel grade S355 with yield stress  $f_y = \gamma_{ov} \times f_{y,k} = 1.25 \times 355 = 444 \text{ N/mm}^2$  (where  $\gamma_{ov}$  is the overstrength factor provided in EN 1998-1), is used for end-plate, column and beam. Contact was modelled using a Coulomb friction model with a friction coefficient equal to 0.3. Finite element type C3D8R was used to model all parts of the analysed T-stubs. The adopted bolt modelling techniques for HR and HV assemblies are those described in previously in Sections 5.6.2 and 5.6.3, respectively. For the T-Stub with HV bolts, the sudden transition from failure mode 2 to mode 3

which was predicted by the analytical model from D'Aniello *et al.* (2016) described in Section 5.6.5.1, was found to introduce a pulse associated to the sudden loss of strength, which led to numerical difficulties and to some internal force fluctuation in the wire element. This computational problem can be overcome by reducing the degree of meshing in the wire element so as to limit the transverse vibration effects on the wire. This option did not lead to any loss of accuracy of the results, since the wire finite element is solely active in pure tension.

The failure modes for the T-Stubs designed for mode 2 with HR and HV assemblies are shown in Figure 5.47a) and Figure 5.47b) and the different stages leading up to failure of T-Stubs with HR and HV bolt assemblies are presented in Figure 5.47c) and Figure 5.47d).

For the case with HR bolts (see Figure 5.47c)), the T-Stub evolves in failure mode 2 up to bolt fracture, as predicted by the analytical model. Instead, the case with HV bolts exhibits a more complex behaviour as shown in Figure 5.47d), which starts with a failure mode 2 configuration for shank yield displacements (Stage 2) and subsequently evolves to mode 3-like (Stage 3) up to the complete extraction of the nut (Stage 4).

Figure 5.48a) depicts the comparison between the numerical force-displacement response of T-Stub with HR bolts and the analytical prediction developed by D'Aniello *et al.* (2016) and described in Section 5.6.5.1, which used a 2D model with axially rigid plates and rigid-perfectly plastic end-plate in bending, it is possible to verify that the failure mode was correctly predicted by the analytical models and that the Abaqus model is consistent in terms of strength with the analytical mode 2 prediction. The EN 1993-1-8 (CEN, 2005) prediction is also shown as a bi-linear model representing initial stiffness and strength capacity, assuming  $f_y = 444 \text{ N/mm}^2$  for members and the bolt ultimate stress from experimental tests.

A significant difference can be observed in terms of ultimate displacement for the HR case, which is due to several reasons. Indeed, the actual bending behaviour of the end-plate is not rigid-plastic, as assumed in the analytical model and likewise, the end-plate is not axially rigid as also assumed in the analytical model. This is substantiated by the fact that the end-plate strain hardening partially compensates for the bolt softening, hence resulting in the numerical model showing a smaller softening rate when compared to the analytical mode 2 curve. Furthermore, as seen in



Fig. 13(c), the nut rotates, implying that the bolt is not under pure tension as assumed in the analytical model, enabling the rotation of the end-plate. Finally, the Abaqus 3D model clearly shows that the deformed shape at failure differs from that assumed by the 2D analytical calculation.

Indeed, finite element analysis shows that prior to bolt failure, only the central part of the endplate is in contact with the column flange. In addition, as observed in Stage 3 of Figure 5.47c), while bolt fracture is occurring the endplate is no longer in contact with the column flange, implying prying forces equal to zero, hence reducing the demand on the bolt and enabling to achieve a larger displacement at collapse. In addition, the bending of endplate edges contributes to reduce stiffness and to increase the ultimate displacement. Finally, the EN 1993-1-8 prediction overestimates the stiffness, while providing good agreement in terms of ultimate strength.

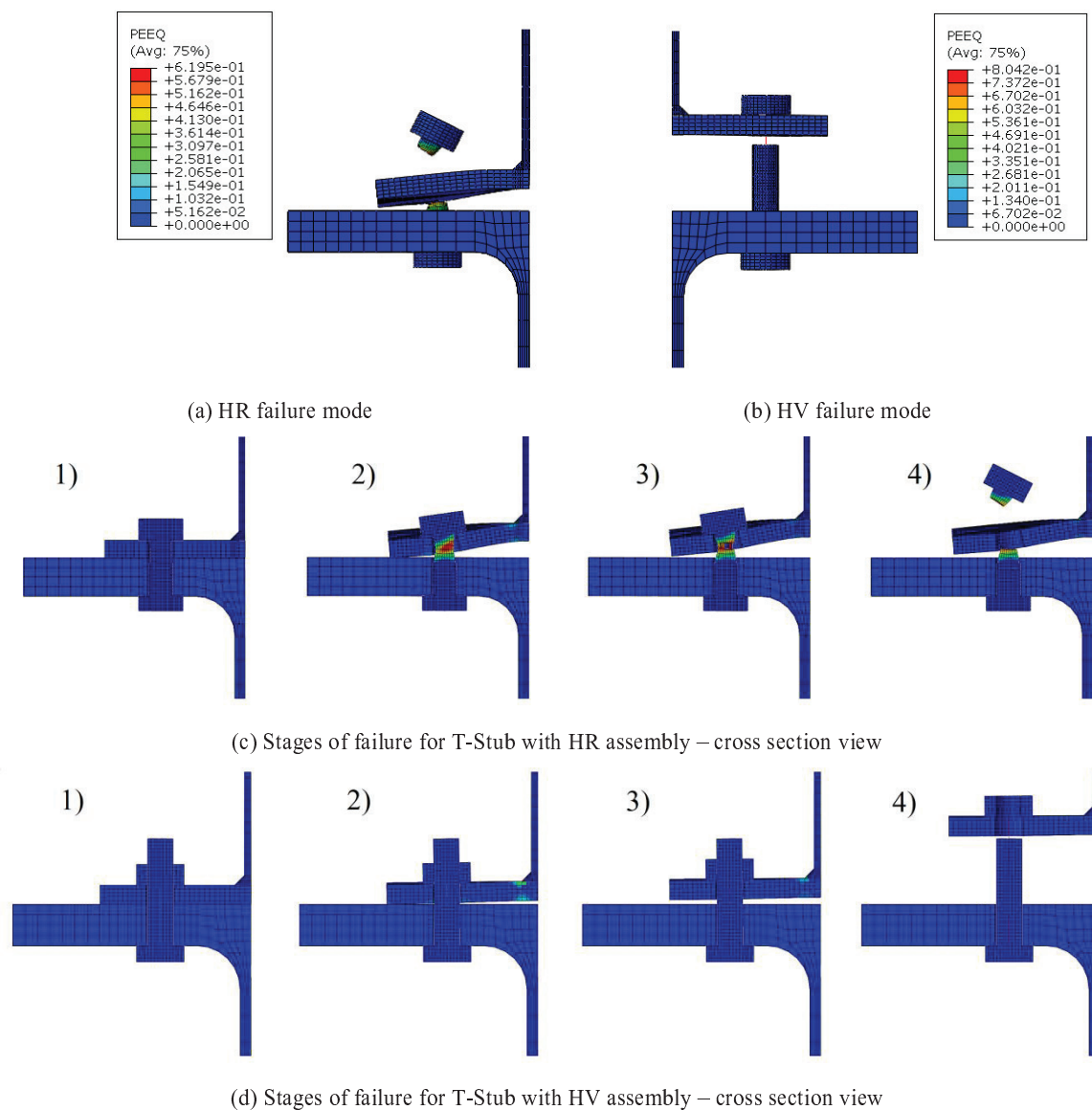


Figure 5.47: T-stub failure modes

The comparison between numerical and analytical T-Stubs theoretically designed for mode 2 with HV assemblies is presented in Figure 5.48b). According to the analytical prediction, mode 2 is the failure mode up to a T-Stub displacement of 0.61 mm (to which corresponds a tensile force of 225 kN), after which mode 3 is activated. The numerical model response in Figure 5.48b) shows good agreement with the analytical prediction for mode 2. Also in this case, differences between FEM and analytical predictions are due to modelling assumptions, as previously described for the case with HR bolts. The loss of strength in the numerical model occurs for a 2.4 mm displacement, after which the T-Stub transitions to failure mode 3, as recognisable by the correspondence in terms of strength

with the mode 3 analytical curve. For the T-Stub with HV assemblies, the transition to mode 3 leads to a better agreement with the analytical predictions, since end-plate strain hardening, nut rotation and partial end-plate contact with the column flange do not occur to the same extent as in mode 2 failure. The ultimate displacement for the FE model is higher than mode 2 prediction mostly due to difference in terms of initial stiffness. As for HR bolts, the EN 1993-1-8 prediction overestimates initial stiffness and does not account for strength reduction leading to potentially unsafe predictions of T-Stub response.

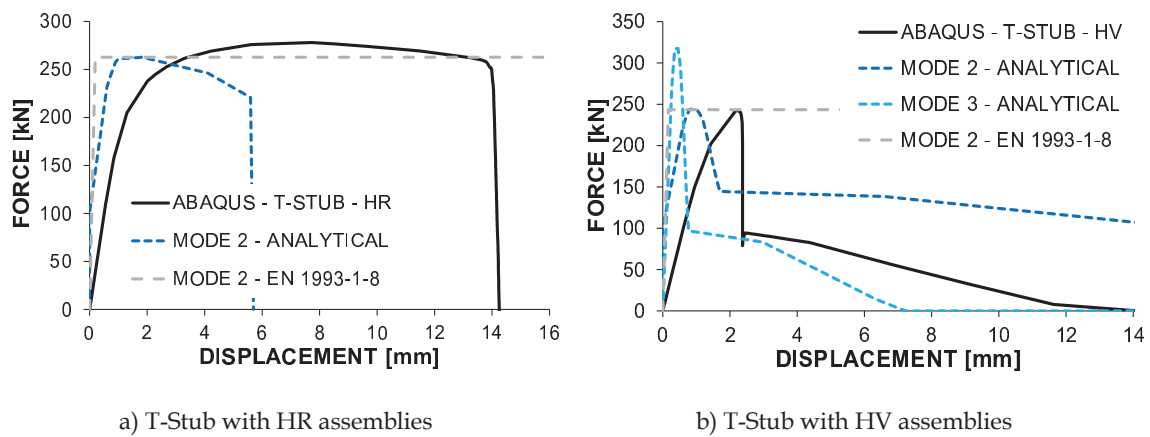


Figure 5.48: Force-displacement comparison between numerical model and analytical models from D'Aniello *et al.* (2016)

In order to assess the T-Stub response in mode 3 with the proposed HR and HV modelling criteria, two other FE models were developed based on the geometry shown in Figure 5.46a), but with an end-plate thickness equal to 20 mm. The FE models are shown in Figure 5.49a) and Figure 5.49b). The comparison in terms of force-displacement response curves between analytical and numerical T-Stub models with HR assemblies is presented in Figure 5.49c), where the numerical model clearly displays lower stiffness and larger displacement at failure. As for the former cases designed for mode 2, the difference of initial stiffness is due to the end-plate that is not perfectly rigid as assumed by the analytical model. Furthermore, finite element models exhibit the yielding of welds and end-plate, which also contribute to reduce the stiffness.

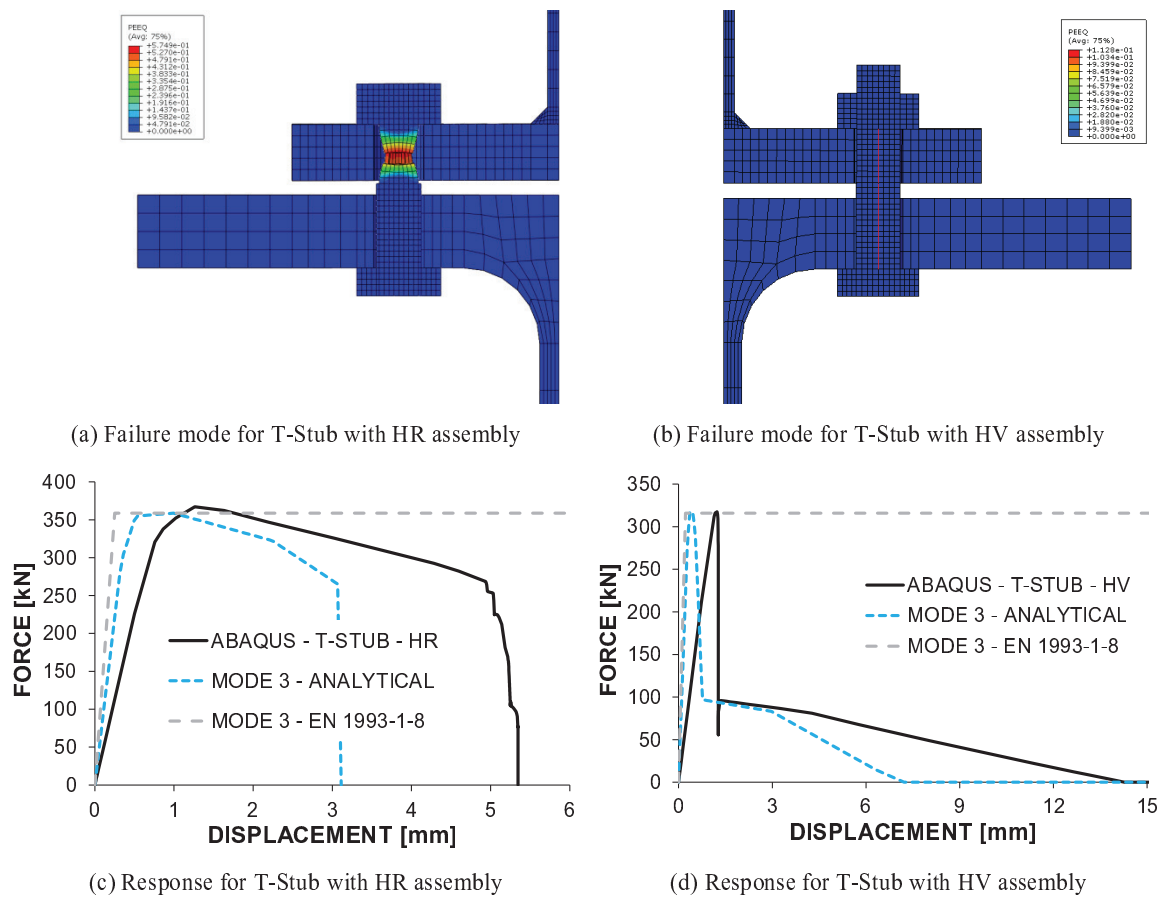


Figure 5.49: T-Stub models with mode 3 failure - failure modes and comparison to (D'Aniello, Cassiano, & Landolfo, 2016) analytical prediction model

This result is also in line with the experimental results on endplate beam-to-column joints Broderick and Thomson (2002), Aribert *et al.* (2004) and Girão Coelho and Bijlaard (2007), which showed that EN 1993-1-8 can significantly overestimate the initial stiffness of bolted joints. Since the bolts are key components to determine joint stiffness, these considerations highlight that the formulation for the stiffness coefficient of bolts in tension provided by EN 1993-1-8 could be improved in a future revision, in order to account for the type of bolt assembly.

## 5.7 Conclusive remarks

In this chapter the results of an experimental campaign devoted to characterize the monotonic and cyclic tensile behaviour of both European preloadable and non-preloadable bolts commonly used for structural applications, namely HR, HV and SB

bolts, were described and discussed. In the light of the obtained results some conclusive remarks were drawn.

Failure modes were identified for all tested bolt assemblies and results showed that HR and SB types are characterized by shank necking failure, whereas nut stripping occurs for HV bolt assemblies. It was verified also that adding a double nut to an HV assembly shifts failure mode from nut stripping to shank necking.

The shape of the force-displacement response curves of HR and HV with two nuts and SB assembly types are characterized by an initial linear elastic segment, followed by nonlinear transition to the plastic regime and onset of softening due to shank necking until failure.

The response curve of HV assemblies was found to significantly differ from that of the HR and HV with 2 nuts, since it is characterized by an initial linear elastic segment, followed by a very short plastic yield plateau, after which the resistance suddenly drops up to a residual strength ranging between 30 % to 40% of the peak strength until very large displacements. The HV strength drops to zero when the nut is fully removed from the shank.

Bolt diameter was found to bear little influence on the ductility of HR, HV and HV with 2 nuts bolt assemblies, while having greater influence on SB type, with ductility decreasing for increasing bolt diameters.

The results from the conducted variable amplitude cyclic tests showed that for all types of bolt assembly, the force-displacement response is not affected by the cyclic loading protocol, namely no reduction in terms of strength and deformation capacity was observed.

Constant amplitude cyclic tests were conducted to assess the low cyclic fatigue resistance of bolt assemblies and results showed that the localised thread crushing in HV assemblies leads to flattening the crests of the threads, which enables this type of assembly to cycle indefinitely without achieving failure. For bolt assemblies characterized by shank necking failure such as the HR and HV with two nuts,  $\epsilon$ - $N$  curves were determined and results showed that the smaller is the bolt diameter, the larger is its low cyclic fatigue resistance. The HR type was found to exhibit slightly higher fatigue resistance than the HV with two nuts type.

Based on the experimental results, simplified assumptions for finite element modelling of HR and HV bolt assemblies were developed and the comparison with experimental results confirmed the accuracy of the proposed models.

The influence of bolt assembly on bolted joints was discussed using a simple calculation example based on 2D analytical model of a T-stub. The strength and analytical response curves of failure modes 2 and 3 were derived by taking into account the actual response curves of HR and HV bolt assemblies. This comparison showed that computing the T-stub failure mode based on nominal properties can be unsafe when HV assemblies are adopted.

The design of bolted joints should therefore take into account the bolt assembly type and the required rotation demand, in order to ensure that joint performance is consistent with specific requirements. With this regard, HV bolt assemblies can be suitable for joints that should behave as nominally pinned, whereas HR type assemblies can be more appropriate for semi-rigid type joints.

The bolt assembly behaviour and FE modelling presented in the present chapter have enabled to determine numerical modelling strategies that were validated against experimental results and that can effectively simulate real assembly behaviour, accounting for all stages of bolt assembly response up to failure. These bolt assembly models were subsequently used for the FE modelling of the secondary frame beam-to-column flush endplate joints. In the next chapter a study on the behaviour of flush endplate joints under column loss action and under cyclic bending action followed by column loss action is presented.

## Chapter 6 Parametric numerical analysis of flush end-plate beam-to-column joints

### 6.1 Introduction

In recent years several experimental and numerical studies were carried out to investigate structural issues related to the progressive collapse under column loss scenario, such as the behaviour of steel beam-to-column joints (Yang & Tan, 2012; Kim and Kim, 2009; Liu *et al.*, 2012; Sadek *et al.*, 2013), the overall structural response ((Xu and Ellingwood, 2011; Izzudin *et al.*, 2008; Hai, 2009; Huvelle *et al.*, 2015), the flexural behaviour of axially restrained beams (Izzudin, 2005) and full scale experimental tests involving column removals (Lew *et al.*, 2013; Song and Sezen, 2013; Jahromi *et al.*, 2012).

These studies highlighted the importance of connections on system behaviour under extreme actions. However, while the modelling of primary frame beam-to-column rigid full-strength joint behaviour has been a topic in recent studies (Kim and An, 2009; Khandelwal and El-Tawil, 2007; Lee *et al.*, 2009; Lew *et al.*, 2013; Yang and Tan, 2013), the contribution in terms of strength and stiffness of semi-rigid partial strength joints has not yet been sufficiently investigated.

This type of joints is typically used for secondary structural elements, which are generally modelled with zero stiffness and resistance and required to be checked for displacement acceptance criteria. The contribution of these elements for arresting a progressive collapse is however favourable and contributes to improve the evaluation of structural response under column loss. In addition, it may contribute to reduce conservatism in design guidelines by levelling ductility requirements in the structure.

The flush endplate joint (FEP) joint type was selected for the secondary beam-to-column joints of the secondary “gravity” frames to be analysed in 0, given that it is widely adopted in European steel construction, due to its simplicity and reduced assemblage time. This joint typology consists of a simple rectangular plate steel plate with the approximate same width and depth as those of the beam, which is fully welded to the beam end. The large variety of possible joint geometry configurations, coupled with stress concentrations or contact interaction render the FEP joint behaviour complex and highly nonlinear.

Several experimental and numerical studies have been carried out in order to investigate FEP joint response under monotonic and cyclic actions in pure bending (Boorse, 1999; Aribert *et al.*, 2004), showing that FEP joints can provide adequate rotation capacity, provided that the failure of welds and mode 3 are prevented. The possibility of extending the components method for combined bending moment and axial force was experimentally investigated by da Silva *et al.* (2004) and results indicated that axial force significantly influenced structural behaviour and that the simple extension of the method developed for pure bending was found not to be valid. An experimental investigation on high strength steel end-plate moment connections (Girão Coelho and Bijlaard, 2007) showed that EN 1993-1-8 (CEN, 2005) accurately predicts the resistance, but overestimates the stiffness experimentally obtained. An experimental investigation on the seismic behaviour of FEP joints (Broderick and Thomson, 2002) concluded that the failure modes were correctly predicted by the EN 1993-1-8 (CEN, 2005).

The response of FEP joints under bending and catenary actions has also been evaluated through some studies (Lima, 2003; da Silva, 2004; Yang and Tan, 2013), although limited data is currently available on this topic. Experimental tests on different types of bolted beam-column joints were conducted (Yang and Tan, 2013) under column removal scenarios, indicating that flush end-plate connections can experience ductile deformation and are capable of developing catenary action. The behaviour of FEP joints under normal and elevated temperatures was also recently investigated both experimentally and numerically (Yu *et al.*, 2009; Wang *et al.*, 2011). In particular, Wang *et al.* (2011) showed that catenary actions developing into the beams are limited by the deformation capacity of the FEP joints to sustain very large deflections. Guo *et al.* (2015) carried out a numerical study on composite frame with



FEP joints under column loss action, showing that progressive collapse resistance is sensitive to bolt properties. In particular, increasing bolt diameter and/or bolt fracture strain can improve the resistance against progressive collapse. Yang and Tan (2012) carried out a series of numerical simulations on different types of steel beam-to-column joints, including FEP joints, subjected to catenary action induced by column loss and they concluded that connections designed with bolt rows closer to the centroid of the beam cross section provide enhanced resistance and ductility at the large rotations, contrarily to what is generally expected under pure bending where the bolt rows are more effective if largely spaced out and located close to the beam flanges.

This concise review of existing literature about FEP joints highlights that design criteria and detailing recommendations for FEP joints under catenary actions need further investigation.

These considerations motivated the study presented in this chapter, which is aimed at investigating the rotation capacity of FEP joints and its flexural interaction with catenary forces developing under column loss and under column loss following cyclic bending, which cannot presently be directly predicted according to the EN 1993-1-8 (CEN, 2005).

To this end a numerical parametric study based on finite element analysis (FEA) was carried out and the following variables were examined: the bolt diameter, the end-plate thickness, the number of bolt rows and the type of beam section profile and the column axis orientation. The influence of the different variables on joint response and on design is discussed and a proposed design criterion to maximise joint performance under column loss action is confronted with the obtained numerical results and discussed.

## **6.2 Framework of the study**

### ***6.2.1 Proposed ductility criteria***

#### *6.2.1.1 Column loss action*

Considering that end-plate thickness determines the T-Stub failure mode and that mode 3 typically corresponds to reduced ductility (Boorse, 1999; Broderick and Thomson, 2002), both end-plate thickness (i.e. end-plate flexural strength) and bolt diameter (i.e. bolt strength) could be selected in a given range so as to mobilise both

end-plate and bolt components, thus maximising the joint performance under column loss. Hence, the range of optimal thicknesses of end-plate is bounded by the minimum and maximum values inducing mode 2.

The EN 1993-1-8 (CEN, 2005) distinguishes between circular and non circular yield line mechanisms in T-Stub flanges, which differ in terms of shape and corresponding effective lengths (Jaspart, 1991). In order to select the smallest plate thickness value inducing mode 2, the  $\beta$  value (see Figure 6.1) must be higher than 1, in order to obtain this failure mode for both circular and non circular yield patterns.

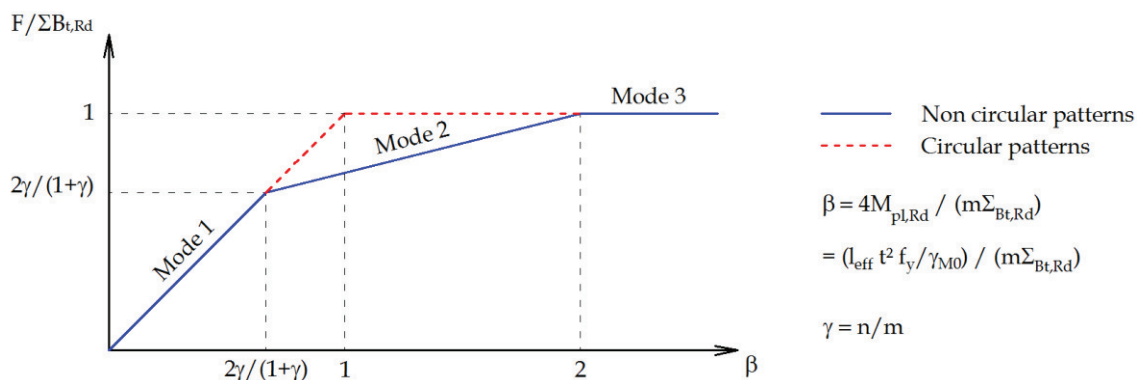


Figure 6.1: T-Stub resistance according to EN 1993-1-8 (CEN, 2005)

By adopting a single criterion for the lower mode 2 threshold and assuming  $\gamma_{M0}$  and  $\gamma_{M2}$  respectively equal to 1.0 and 1.25, the EN 1993-1-8 recommends the following ductility criterion:

$$t_{min,Mode2,EN1993:1-8} \geq 0.36 \cdot d \cdot \sqrt{\frac{f_{ub}}{f_y}} \quad (6.1)$$

The resistance of each individual bolt ( $F_{t,Rd}$ ) should therefore be greater than the resistance ( $F_{p,Rd}$ ) of the connected plates (end-plate or column flange). However, the failure strength of joints should be evaluated accounting for both the random variability of plate material and its relevant strain hardening, as follows:

$$F_{t,Rd} \geq \gamma \cdot F_{p,Rd} = \gamma_{ov} \cdot \gamma_{sh} \cdot F_{p,Rd} \quad (6.2)$$

The random material overstrength factor  $\gamma_{ov}$  in Eq. (6.2) can be taken as 1.25, as recommended by Eurocode 8, whereas the value for  $\gamma_{sh}$  is assumed as the ratio between

the ultimate stress  $f_u$  and the yield stress  $f_y$  of the plate material. For European mild carbon steel, the ratio  $f_u/f_y$  can be conservatively assumed equal to 1.5. Thus rearranging the inequality in Eq. (6.2) and introducing the EN 1993-1-8 (CEN, 2005) design equations for the strength of yield line mechanism into the end-plate and the bolt strength, the inequality can be written as:

$$\beta = \frac{4M_{pL,Rd}}{m \Sigma B_{t,Rd}} \cdot \gamma_{ov} \cdot \gamma_{sh} \geq 1 \quad (6.3)$$

$$\beta = \frac{l_{eff} t^2 f_y / \gamma_{M0}}{m \Sigma B_{t,Rd}} \cdot \gamma_{ov} \cdot \gamma_{sh} \geq 1 \quad (6.4)$$

By introducing the following 3 conditions, in line with Jaspart (1991):

$$n = 1.25m \quad (6.5)$$

$$B_{t,Rd} = \frac{0.9A_s f_{ub}}{\gamma_{M2}} = \frac{0.9 \times 0.72 \times \pi d^2 f_{ub}}{4\gamma_{M2}} \approx \frac{0.51d^2 f_{ub}}{\gamma_{M2}} \quad (6.6)$$

$$l_{eff} = 2\pi m \text{ (circular pattern)} \quad (6.7)$$

where  $d$  is the nominal bolt diameter, it is possible to derive a simple criterion as follows:

$$\beta = \frac{2\pi m t^2 f_y / \gamma_{M0}}{\frac{2 \times 0.51 d^2 f_{ub}}{\gamma_{M2}}} \cdot \gamma_{ov} \cdot \gamma_{sh} \geq 1 \quad (6.8)$$

$$t^2 \geq \frac{2m \cdot 0.51 d^2 f_{ub} \cdot \gamma_{M0}}{\gamma_{M2} \cdot 2\pi m \cdot f_y \cdot \gamma_{ov} \cdot \gamma_{sh}} \quad (6.9)$$

$$t \geq \sqrt{\frac{2m \cdot 0.51 d^2 f_{ub} \cdot \gamma_{M0}}{\gamma_{M2} \cdot 2\pi m \cdot f_y \cdot \gamma_{ov} \cdot \gamma_{sh}}} \quad (6.10)$$

Further simplifying it is finally possible to revise the ductility condition of EC3-1-8 as follows:

$$t_{min, Mode2} \geq \frac{0.40 \cdot d}{\sqrt{\gamma_{ov} \gamma_{sh}}} \cdot \sqrt{\frac{\gamma_{M0} f_{ub}}{\gamma_{M2} f_y}} = 0.26 \cdot d \cdot \sqrt{\frac{f_{ub}}{f_y}} \quad (\leq t_{min, EN1993:1-8}) \quad (6.11)$$

The upper bound value of thickness can be determined in order to avoid mode 3, namely imposing the following inequality:

$$\beta = \frac{l_{eff} t^2 f_y / \gamma_{M0}}{m \sum B_{t,Rd}} \cdot \gamma_{ov} \cdot \gamma_{sh} \leq 2 \quad (6.12)$$

Considering that the threshold between mode 2 and mode 3 depends on the non-circular yield line pattern, the inequality in Eq.(6.12) can be re-arranged, yielding the expression for the maximum end-plate thickness inducing mode 2. In this case, the strain hardening parameter  $\gamma_{sh}$  is assumed equal to 1.0, since in failure mode 3 the end-plate remains elastic.

In order to keep safety margin from mode 3, the maximum thickness for mode 2 ( $t_{max,Mode2}$ ) given by Eq.(6.12) is factored by 0.9. In addition, considering that the threshold between mode 2 and mode 3 depends on the non-circular yield line pattern, the inequality in Eq.(6.12) is re-arranged as follows:

$$t_{max,Mode2} \leq 0.9 \frac{1.35 \cdot d}{\sqrt{\gamma_{ov} \gamma_{sh}}} \cdot \sqrt{\frac{\gamma_{M0} \cdot f_{ub}}{\gamma_{M2} \cdot \alpha \cdot f_y}} = 1.15 \cdot d \cdot \sqrt{\frac{0.8 \cdot f_{ub}}{\alpha \cdot f_y}} \quad (6.13)$$

which represents the upper bound criterion for the thickness of end-plate. In light of these considerations, the range of thickness [ $t_{min,Mode2}; t_{max,Mode2}$ ] defined by Eq.(6.11) and Eq.(6.13) is proposed as a ductility criterion to improve the robustness of FEP joints. Hereinafter, the effectiveness of this criterion is discussed on the basis of the results obtained by finite element analyses.

#### 6.2.1.2 Cyclic bending followed by column loss action

The proposed ductility criteria for column loss action was also confronted with results from cyclic bending followed by column loss, in order to verify if the same criteria can be effective in this case.

### 6.2.2 Parametric variables

The parametric variables selected for the FEP joint parametric numerical study cover a comprehensive array of realistic configurations of FEP joint. For this reason, the beam-to-column assemblies and the variation of relevant parameters are extracted from first storey spans of a set of 48 steel moment resisting frames designed according to Eurocodes and analysed under column loss (Cassiano *et al.*, 2016) (see Chapter 4).

S355 steel grade is assumed for beams, columns and end-plates, while high-strength grade 10.9 is considered for bolts.

Since the beam and the connection are the elements that mostly characterize the performance of FEP joints under catenary action, in this parametric study the column profile is kept constant, while the beam and the connection are varied. The cross section of the column is assumed as the most commonly adopted in the set of reference frames (Cassiano *et al.*, 2016) and equal to HEA 650. The beams are designed using both IPE and HEA type sections, with depth ranging from 220 mm to 500 mm.

The adopted parameters and the relevant variations are reported in Table 6.1, where the relative orientation between the beam and the column (corresponding to parametric variable C) is analysed for two different scenarios, i.e. the cases in which the column is mobilised in bending around the strong axis (CS) and around the weak axis (CW). For the cyclic bending followed by column loss, only the CS case was investigated. The following label code is used to identify each joint:

**R**<sub>(number of bolt rows)</sub>-**D**<sub>(bolt diameter)</sub>-**T**<sub>(thickness of end-plate)</sub>-**S**<sub>(beam profile, either I or H)</sub>-**C**<sub>(column orientation)</sub>

Figure 6.2a) and Figure 6.2b) show the main geometric features of the investigated FEP joints. As it can be observed, the FEP connection oriented towards the column weak axis is bolted to a T-Stub, which is welded to the column web. The T-Stub is obtained by cutting an additional segment of the column profile along its symmetry axis. Furthermore, in Figure 6.2c) and Figure 6.2d) the analysed joint configurations are characterised in terms of normalised bending and tensile strength-stiffness distributions.

Table 6.1: FEP joint parametric variable definition

Parameter	Symbol	Examined Values	Units
Number of bolt rows	R	{ 2 ; 4* }	[-]
Bolt diameter**	D	{ 16 ; 20 ; 24 }	[mm]
End-plate thickness	T	{ 8 ; 12 ; 16 ; 20 }	[mm]
Beam cross section	S	{ IPE 220* ; IPE 360 ; HEA 320 ; HEA 500 }	[-]
Column orientation	C	{ S (strong axis); W (weak axis) }	[-]

\* 4 bolt rows configuration is not feasible for the case with IPE 220 profile. Indeed, in order to satisfy the minimum distances recommended by EN 1993-1-8 (CEN, 2005), only in this case 3 bolt rows configuration is adopted due to small depth of IPE200

\*\* High strength bolts with grade 10.9 are adopted for all investigated diameters

The joint stiffness and strength distributions in Figure 6.2c) and Figure 6.2d) were computed from the FEP joint model in da Silva *et al.* (2004) with component response according to EN 1993-1-8 (CEN, 2005). Joints compliant with the proposed thickness range criteria defined in Eq.(6.11) and Eq.(6.13) are highlighting. For CW joints, a 3D FE model (see Figure 6.2e)) with linear elastic properties ( $E=210\text{GPa}$ ) was used to evaluate the bending and tensile stiffness of the connection between the column web and aforementioned T-stub, since no information is provided for these components in EN 1993-1-8.

In CW joints, deformation is concentrated in the column web panel which was found to be very flexible, leading to joint initial stiffness significantly lower than that shown by the corresponding CS configurations. Local column web stiffness increases with rotational/tensile demand, owing to local hardening induced by membrane effect. The low stiffness of CW joints revealed to be a key factor influencing the capacity of joints to mobilise compressive arching. Indeed, increasing the joint deformability tends to reducing the compressive arching effect, as it can be recognized by comparing CS and CW joint configurations (see Figure 6.2f)) for the case with the highest level of compressive arching (i.e. HEA 500). Results for CW joints under column loss action are presented and discussed in more detail in Section 6.3.2.

The geometric features of the examined FEP joints are reported in Table 6.2. The vertical pitch  $p$  is constant so as to equally space the bolt rows; the horizontal pitch  $w$  is assumed as the technological minimum distance, as conditioned by the fillet radius of the columns and the dimensions of bolts and corresponding washers. In order to limit brittle failures of the welds (Boorse, 1999; Aribert *et al.*, 2004; Yu *et al.*, 2011; Shaker and

Elrahman, 2014), the throat thickness of the fillet welds between beam and end-plate is assumed equal to 0.7 times the thickness of the thinnest connected plate.

Table 6.2: Flush endplate joint dimensions

<b>Beam profile</b>	<b>p (2 bolt rows)</b>	<b>p (3 bolt rows)</b>	<b>p (4 bolt rows)</b>	<b>a</b>	<b>w</b>
IPE 220	120	60	-	50	114
IPE 360	248	83	-	56	114
HEA 320	189	-	63	61	168
HEA 500	348	-	83	71	168

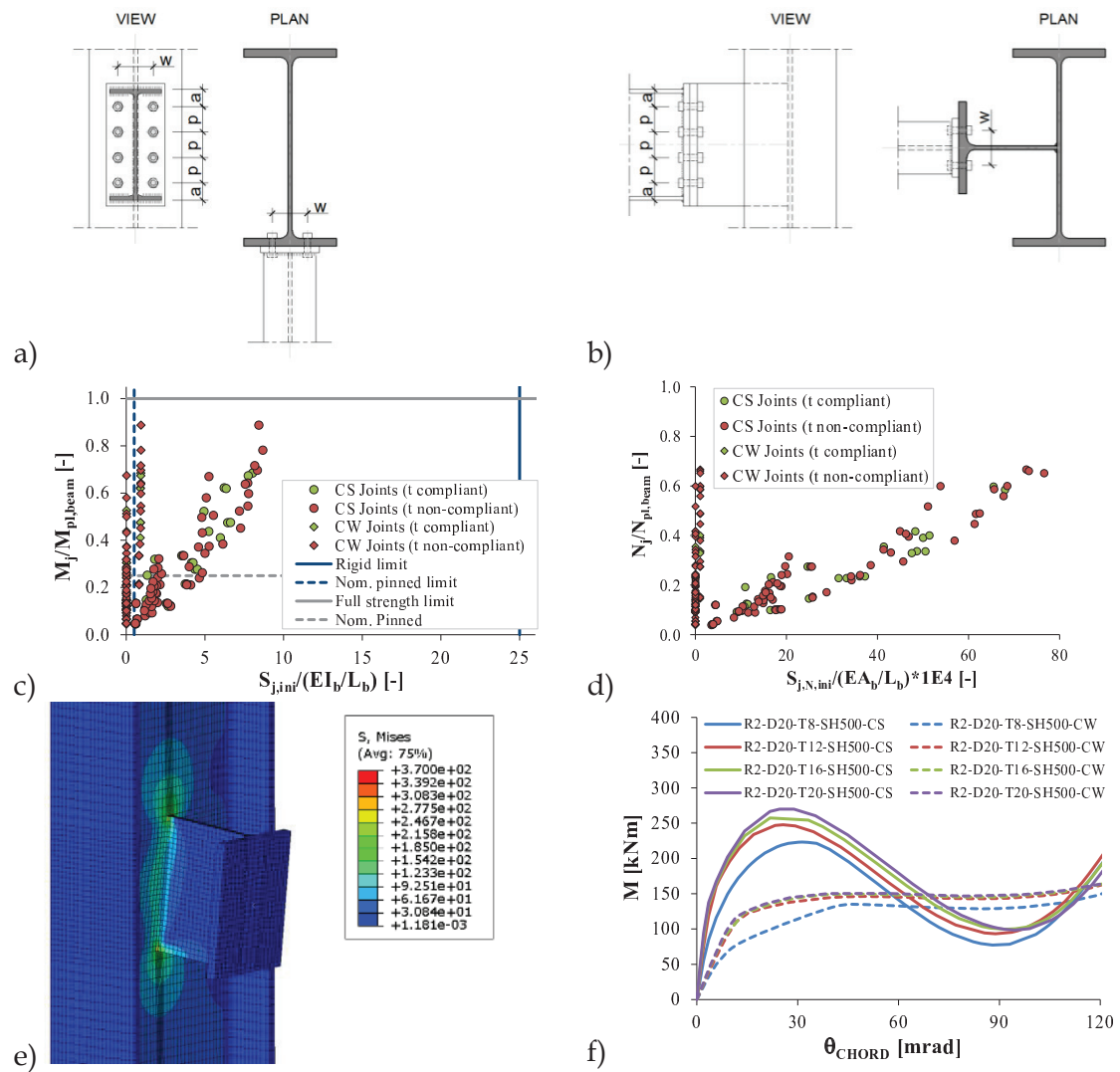


Figure 6.2: Geometry of FEP joints in bending around the column's strong (a) and weak (b) axis; joint normalised bending strength vs. stiffness (c); joint normalised tensile strength vs stiffness (d); FE model for evaluating the stiffness of CW connections, e.g. deformed shape and Von Mises stress at 50 mrad (e); Comparison in terms of Moment (M) vs chord rotation ( $\theta$ ) between CS and CW joints for R2-D20-SH500 configurations (f).

### 6.2.3 Finite element modelling

#### 6.2.3.1 Generality

Finite element models (FEM) of FEP joints (see Figure 6.3) were developed using ABAQUS ver. 6.13 (Dassault, 2013). Both mechanical and geometrical nonlinearities were considered and C3D8R elements, i.e. reduced integration 8-node linear brick elements, were used with hourglass control and a minimum of three layers of finite elements along the plate thickness in order to avoid possible shear locking problems. The structured meshing technique was assigned to obtain regular shape for



elements, especially for those elements discretizing rounded parts, e.g. bolt shanks, bolt head and nuts.

### 6.2.3.2 Material definition

S355 mild carbon steel is assumed for beam, column and end-plate. The true stress-true strain relationship adopted for the analyses is taken from the average response of available tensile coupon tests, using combined isotropic/kinematic hardening rule and also a progressive ductile damage model. This modelling strategy enables to save significant computational time since plate fracture initiation constitutes a limit state characterized by a significant drop in resistance (Wang *et al.*, 2016), after which the evolution of the residual resistance varies significantly and hence falls outside the scope of the present study. The onset of plate fracture is evaluated *a posteriori* through the Rupture Index, according to the procedure described in Section 6.2.6.

Fillet welds are modelled considering their relevant throat thickness and assuming an elastic-perfectly plastic stress-strain relationship with yield stress equal to 460MPa, which corresponds to an electrode grade A46 (as given by EN ISO 2560 (ISO, 2009)).

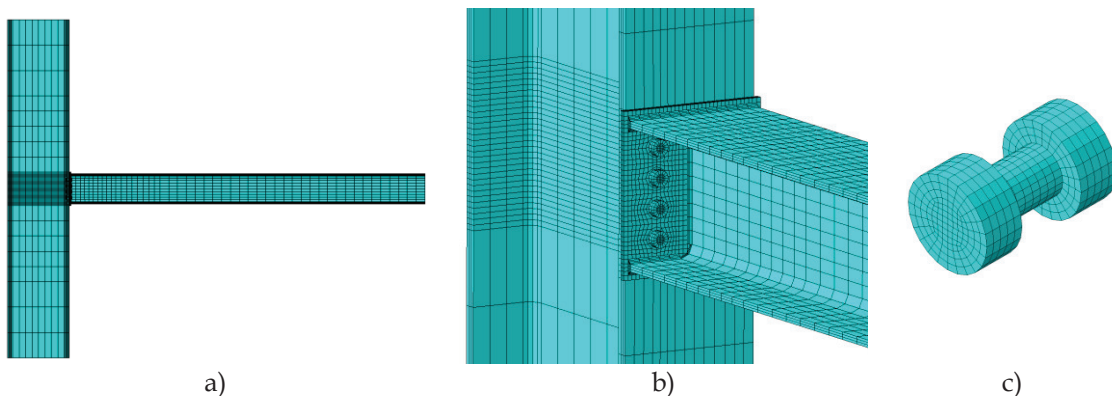


Figure 6.3: Finite element model of the R4-D20-T12-SH320-CS flush end-plate joint: a) planar view of the assembly; b) 3D view; c) detail of bolt model.

The bolts are modelled as a single part made of three partitioned zones, namely the shank, the head and the nut (see Figure 6.3c)) according to the methodology described in Section 5.6.2. 3D solid finite element models with progressive damage are used, accounting for damage initiation, softening, crack initiation and progression. The undamaged material plasticity curve and the equivalent plastic strain at damage onset curve as a function of triaxial stress state were taken from Pavlovic *et al.* (2015).

### 6.2.3.3 Contact definition

Contacts are modelled to simulate the interactions between (i) the end-plate and column flange; (ii) the bolt nuts and the surfaces of end-plate and column flange; and (iii) the bolt shanks and the holes of both end-plate and column flange. Hard contact law was adopted to simulate the unilateral contact in the normal direction of the interface between the extended end-plate and the column flange. In addition, tangent contact with “Coulomb friction” law is assumed to account for the friction between the interfaces with a slip coefficient equal to 0.3.

### 6.2.3.4 Boundary conditions

The boundary conditions are applied in order to simulate the intended structural behaviour under a column loss event according to the sub-structuring hypothesis shown in Figure 6.4.

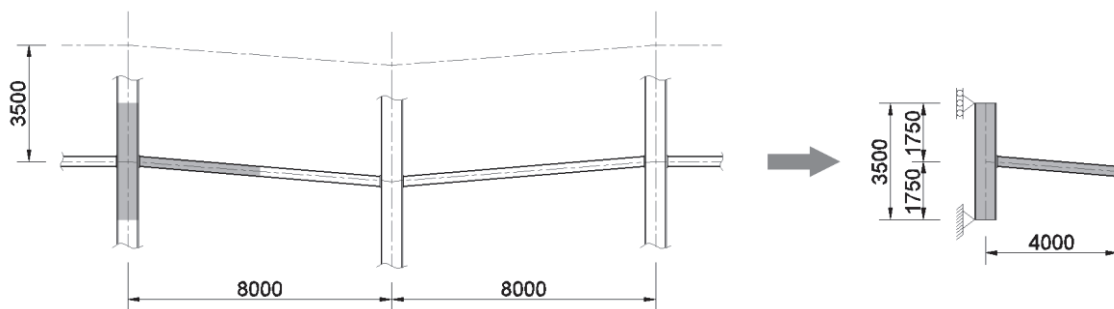


Figure 6.4: Substructure selection and beam-column joint model idealization - deformed shape under column loss action

The surface of the cross sections at both ends of the columns were tied to a reference point placed into the section centroid. The boundary conditions were applied to these reference points. In particular, the 3 translational and the torsional degrees of freedom (DOFs) were restrained at the lower end of the column, while the vertical translational DOF was released at its top end, to allow column shortening. These boundary conditions were kept constant throughout the analysis.

Initially the FEAs were carried out considering two different levels of axial force in the column: i) zero axial force; ii) 30% of the plastic strength of the column (which is larger than the maximum axial force calculated in the columns of the frame studied in Cassiano *et al.* (2016) - see also Chapter 4). However, results from FEAs showed that axial force in the column within the examined range has negligible

influence on the joint response. This assumption is in line with experimental tests by Kuhlmann *et al.* (2007). Therefore, this parameter is not discussed hereinafter.

#### 6.2.3.5 Analysis steps

The numerical analysis for the column loss action case was performed in 2 analysis steps, while the analysis for the cyclic bending followed by column loss action case was performed using 3 analysis steps.

For the former, the first step consists in the application of the EC3-compliant tightening force to the bolts using the static general procedure and taking advantage of the Abaqus (Dassault, 2013) built-in bolt preload formulation; the second step consists in simulating the column loss action, which is achieved by restraining all DOFs at the beam tip, except for the bending rotation about the strong axis of the beam and subsequently monotonically increasing the vertical displacement of the beam tip until failure using the Abaqus static general procedure.

For the latter, the first step consists in the application of the EC3-compliant tightening force to the bolts; the second step consists in imposing a cyclic bending action according to a loading protocol (see Section 6.2.3.6), which is achieved by applying vertical displacements to the beam tip; at the end of the cyclic bending step, a vertical sliding bearing is introduced at the beam tip, enabling vertical translation with simultaneous axial force restriction; the third step consists in increasing vertical displacements to the beam tip until reaching joint failure. For the second and third steps, the dynamic implicit procedure was used and vertical displacements were quasi-statically applied using an amplitude function over a 20000s time interval with a smoothing parameter of 0.025 to overcome numerical difficulties. The column loss step was simulated using the dynamic implicit procedure to quasi-statically apply increasing vertical displacements to the beam end, using a ramp function over a 1000s time interval for a maximum displacement value corresponding to 200 mrad.

#### 6.2.3.6 Cyclic loading protocol

The cyclic bending action was defined in order to be representative of the expected damage to the joint that can be induced during a seismic event. The AISC 341-05 (AISC, 2005) allows the use of connections in special moment frame beam-to-column joints subjected to seismic actions that are capable of accommodating an

interstorey drift angle of 40 mrad. Instead, the EN 1998-1 (CEN, 2004) states that for dissipative semi-rigid and/or partial strength joints the rotation capacity of the plastic hinge should not be less than 35 mrad for DCH class structures. In order to satisfy both criteria, the cyclic loading protocol was defined for a maximum interstorey drift angle  $\theta=40$  mrad (or  $\theta=4\%$ ).

The adopted cyclic loading history is based on the AISC 341-05 loading protocol (AISC, 2005), which consists of stepwise increasing deformation cycles, using  $\theta$  as the deformation parameter to control the loading history. The use of this protocol allows to introduce the exact level of damage consistent with the adopted drift angle. The loading protocol was interrupted after completing two cycles at  $\theta=4\%$  as shown in Figure 6.5.

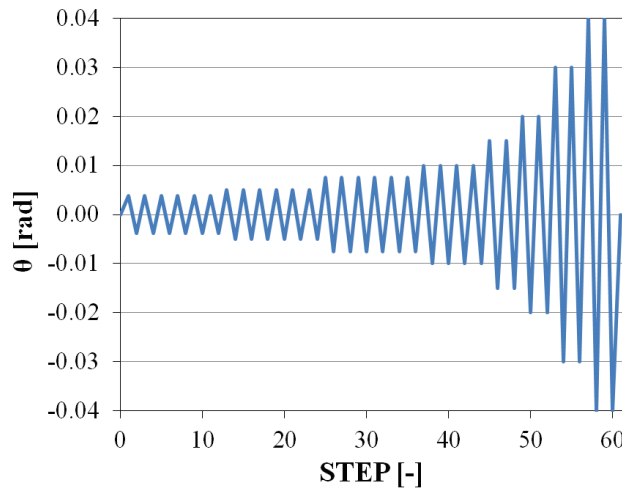


Figure 6.5: AISC 341-05 cyclic loading protocol (AISC, 2005)

#### 6.2.4 Validation of the FE modelling

The accuracy of the FE modelling of FEP joint response under cyclic actions and under column loss actions was compared with experimental results from literature.

For the case of cyclic actions, FEP joint response was compared to experimental results by Broderick and Thomson (2002) as presented in Figure 6.6a), showing that the model can correctly predict joint response for rotations up to around 35 mrad.

The accuracy of the FE modelling assumptions of FEP joints under simultaneous bending and axial forces was validated with experimental results obtained by Lima (2003). Figure 6.6b) shows the comparison between FE predictions

and experimental responses of three joints subjected to bending and varying values of axial tensile force (hereinafter given as a percentage of the plastic axial resistance of the beam), namely: i) case FE1 ( $N = 0\% N_{pl}$ ); ii) case FE8 ( $N = 10\% N_{pl}$ ) and iii) case FE9 ( $N = 20\% N_{pl}$ ).

In addition, since the ultimate resistance and ductility of the bolts largely influence the system ductility under a column loss scenario (Aribert *et al.*, 2004; Broderick and Thomson, 2002; Guo *et al.*, 2015) and the accuracy of finite element models, the modelling assumptions of bolts are validated on the basis of experimental tests on high strength bolts (D'Aniello *et al.*, 2016), described in Chapter 5 of this dissertation. As previously shown, the FE predictions satisfactorily reproduce the experimental response.

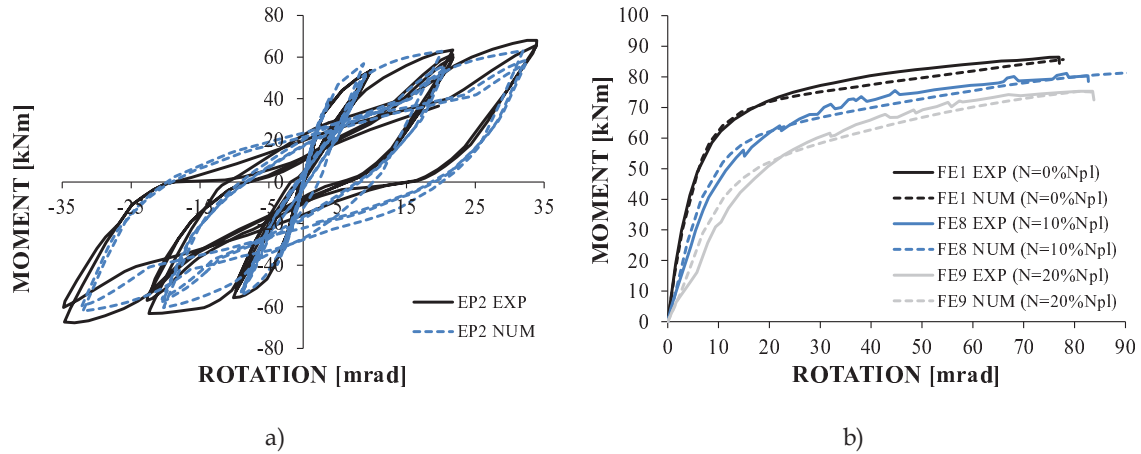


Figure 6.6: FE model validation: a) under cyclic action - case EP2 from Broderick and Thomson (2002); b) under column loss action - cases FE1, FE8 and FE9 from Lima (2003)

### 6.2.5 Strain rate effects

The influence of strain rate on the constitutive law of materials can be evaluated through the Dynamic Increase Factor (*DIF*), which is given by the ratio between dynamic strength  $\sigma_{dyn}$  and the strength under quasi-static conditions  $\sigma_{stat}$ :

$$DIF = \sigma_{dyn} / \sigma_{stat} \quad (6.14)$$

The effects of strain rate on material constitutive law can be evaluated using the Johnson-Cook model (Johnson and Cook, 1983) which is given by:

$$\sigma_{dyn} = (A + B\varepsilon^n) \cdot (1 + C \ln\dot{\varepsilon}^*) \cdot (1 - (T^*)^m) \quad (6.15)$$

where  $A$  is the quasi static yield strength;  $B$  and  $n$  represent the effects of strain hardening;  $m$  is the thermal softening fraction;  $T^*$  is a non-dimensional parameter that depends on melting and transition temperatures to account for material softening from temperature variations;  $\varepsilon$  is the equivalent plastic strain;  $\dot{\varepsilon}^* = \dot{\varepsilon}/\dot{\varepsilon}_0$  is the dimensionless plastic strain rate;  $\dot{\varepsilon}$  is the strain rate;  $\dot{\varepsilon}_0$  is the reference quasi-static strain rate ( $\dot{\varepsilon}_0 = 0.001 \text{ s}^{-1}$ ) and  $C$  is the strain rate constant.

By replacing the first term of the Johnson-Cook model by the stress-strain curve and by disregarding the third term pertaining to thermal softening, the *DIF* expression becomes:

$$DIF = (1 + C \ln\dot{\varepsilon}^*) \quad (6.16)$$

The plastic strain rate was obtained from the results of time-history analyses of frames subjected to column loss in Cassiano *et al.* (2016), from which the maximum vertical velocity of the Directly Affected Zone (DAZ)  $v_{DAZ} = 1.7 \text{ m/s}$  was derived, which corresponds to a joint chord angular velocity  $\omega = v_{DAZ} / L = 1.7 / 6 = 0.28 \text{ rad/s}$ .

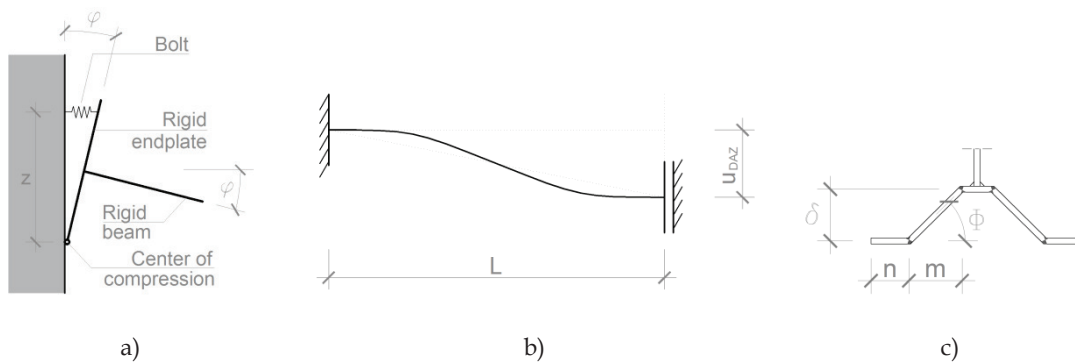


Figure 6.7: Models for simplified strain-rate assessment in joint components: a) bolt; b) beam flange in tension; c) endplate of T-stub

A simplified methodology is used to estimate the upper bound value for the strain rate in the bolts using the model shown in Figure 6.7a), which assumes that beam, end-plate and column elements are rigid and that the connection rotates around the centre of compression (i.e. the beam flange under compression), while only the top

bolt row is mobilised in tension. Under this assumption, the joint with the deeper beam (i.e. HEA 500 in the present study) maximizes the axial bolt velocity  $v_b$ . Hence, the bolt axial velocity is computed as  $v_b = \omega z = 114$  mm/s and the corresponding strain rate is computed as follows:

$$\dot{\varepsilon} = \frac{d\varepsilon}{dt} = \frac{d}{dt} \left( \frac{L(t) - L_0}{L_0} \right) = \frac{1}{L_0} \frac{dL(t)}{dt} = \frac{v(t)}{L_0} \quad (6.17)$$

where  $\dot{\varepsilon}$  is the strain rate,  $L_0$  is the reference length and  $v(t)$  is the speed of relative motion between the ends of the reference length. The bolt reference length for the case of the thinnest endplate analysed in this study ( $t=8$  mm) is given by the sum of endplate plus column flange thicknesses and is equal to  $L_0 = 34$ mm, which, for a velocity  $v(t) = v_b$  yields  $\dot{\varepsilon} = 3.4$  s<sup>-1</sup>. By adopting the strain rate constant value  $C = 0.0072$  for high strength bolts from Ribeiro *et al.* (2016), a dynamic increase factor for the bolts  $DIF_{bolt} = 1.06$  is obtained.

Experimental T-stub tests performed with M24 Cl.10.9 bolts (Pereira, 2012) which displayed failure mode 3 showed average increases of 5.6% and 2.0% in yield and maximum stresses, showing the low rate-sensitivity of T-stub failures involving the bolt. A similar conclusion is reached in Ribeiro *et al.* (2016), which states that for T-stubs in failure mode 3, no advantage can be taken in terms of strength increase due to higher strain rates. Considering furthermore that the bolt assemblies analysed in the present study were preloaded, then, until the preload force is exceeded, the assembly axial stiffness is sufficiently high so that no strain rate is effectively applied.

In order to evaluate possible strain rate enhancement effects on the beam flange zone, a simplified conservative model was considered (see Figure 6.7b), consisting of a beam fixed at both ends with an imposed displacement  $u_{DAZ}$  at one end. Considering no rotation at the beam ends, moment to vertical displacement relation is given by elastic theory:

$$M = u_{DAZ} \cdot \frac{6EI}{L^2} \quad (6.18)$$

The variation of bending moment in time is given by:

$$\dot{M} = \frac{dM}{dt} = \frac{d}{dt} \left( u_{DAZ} \cdot \frac{6EI}{L^2} \right) = \frac{6EI}{L^2} \frac{d(u_{DAZ})}{dt} = \frac{6EI}{L^2} v_{DAZ} \quad (6.19)$$

According to elastic theory, in pure bending, strain can be related to the applied bending moment:

$$\sigma = \varepsilon E \quad (6.20)$$

$$\frac{M}{W} = \varepsilon E \quad (6.21)$$

$$\varepsilon = \frac{M}{EW} \quad (6.22)$$

Differentiating Eq. (6.20) with respect to time and replacing Eq. (6.22) in Eq. (6.20), the strain rate at beam flange of the end section of the beam is given by:

$$\dot{\varepsilon} = \frac{d\varepsilon}{dt} = \frac{\dot{M}}{EW} = \frac{6EIv_{DAZ}}{EWL^2} \quad (6.23)$$

For the beam cross sections analysed in the present study, the beam flange strain rates, evaluated through the simplified model, range from  $0.03s^{-1}$  (for the IPE 220) to  $0.07s^{-1}$  (for the HEA 500). The strain rate enhancement on S355 steel in Ribeiro *et al.* (2016) can be assessed by computing the corresponding *DIF*. By adopting the strain rate constant value for mild steel  $C = 0.0039$  from Ribeiro *et al.* (2016), the maximum dynamic increase factor in the beam flange equals  $DIF_{beam\ flange} = 1.02$ .

For the endplate element assessment, a simplified model was used (see Figure 6.7c), where the endplate was assumed to deform in mode 1, in accordance with the Components Method described in (CEN, 2005). Beam, column and bolts were assumed as rigid and joint rotation was assumed equal to beam rotation, with the connection rotating around the intersection between the line defined by the compressed beam flange (i.e., the centre of compression) and the external column flange face. Equivalent T-stubs were computed for the range of analysed beam cross sections and for the thinnest analysed endplate thickness case ( $t=8$  mm). The beam rotation  $\varphi$  and the T-stub rotation  $\Phi$  can be related to the T-stub displacement  $\delta$  through variables  $z$  and  $m$  as:



$$\varphi = \frac{\delta}{z} \quad (6.24)$$

$$\Phi = \frac{\delta}{m} \quad (6.25)$$

where  $z$  is the lever arm and  $m$  is the T-stub dimension as defined in (CEN, 2005). By equalling  $\delta$  from Eq. (6.24) and Eq.(6.25) and solving with respect to  $\Phi$ :

$$\Phi = \frac{\varphi z}{m} \quad (6.26)$$

Differentiating Eq.(6.26) with respect to time yields:

$$\dot{\Phi} = \frac{d\Phi}{dt} = \frac{d}{dt} \left( \frac{\varphi z}{m} \right) = \frac{\dot{\varphi} z}{m} = \frac{\omega z}{m} \quad (6.27)$$

Considering that the T-stub deformation is concentrated on the plastic hinges and that the plastic hinge length  $l_{hinge}$  is equal to the endplate thickness  $t_{ep}$ , then the endplate plastic hinge rotation  $\Phi$  is given by:

$$\Phi = \frac{\Delta l}{\frac{t_{ep}}{2}} = \frac{2\varepsilon l_{hinge}}{t_{ep}} = 2\varepsilon \quad (6.28)$$

Differentiating Eq.(6.28) with respect to time, equalling to Eq.(6.27) and solving with respect to  $\dot{\varepsilon}$  yields:

$$2\dot{\varepsilon} = \frac{\omega z}{m} \quad (6.29)$$

$$\dot{\varepsilon} = \frac{\omega z}{2m} \quad (6.30)$$

For the analysed cross sections, the strain rate ranges from 0.48 to 0.91 s<sup>-1</sup>, to which correspond *DIFs* ranging from 1.02 to 1.03 for a strain rate constant  $C = 0.0039$ .

The computed *DIF* values for the bolts, beam flange and endplate show that little strain enhancement effect is induced by the column loss action, even when adopting very conservative models which are nonetheless able to provide an order of magnitude of the dynamic amplification effect. The effect of strain rate sensitivity for moderate rates as those induced by frames subjected to column loss, was shown in

Pereira (2012) to be less significant at component level than at material level and to fade out with higher levels of structural idealisation. Given that *DIF* values are close to 1 in all cases, strain rate enhancement was considered to have a very small effect on joint response and was therefore disregarded for the present study.

### 6.2.6 Fracture initiation in plates and welds

The fracture initiation depends on a set of variables such as initial material imperfections, actual stress triaxiality and direction of rolling (El-Tawil *et al.*, 1999). In this study a simplified method is used, namely the fracture initiation into the plates and welds is estimated by means of the plastic equivalent strain index (*PEEQ*).

The threshold value at fracture initiation of *PEEQ* is determined from the Rupture Index (*RI*) reported in literature. *RI* is defined as the ratio between the plastic equivalent strain index *PEEQ* and the ductile fracture strain  $\varepsilon_f$ , multiplied by the material constant *a* (El-Tawil *et al.*, 1999), as follows:

$$RI = a \frac{PEEQ}{\varepsilon_f} = \frac{PEEQ}{\exp(-1.5T)} \quad (6.31)$$

where the *PEEQ* value that causes fracture can be obtained for a given stress triaxiality condition. The strain at ductile fracture initiation according to Hancock and Mackenzie (1976) is given by:

$$\varepsilon_f = a \cdot \exp\left(-1.5 \frac{\sigma_H}{\sigma_{eq}}\right) = a \cdot \exp(-1.5T) \quad (6.32)$$

where  $\varepsilon_f$  is the ductile failure strain, *a* is the material constant,  $\sigma_H$  is the hydrostatic stress defined in Eq.(5.8),  $\sigma_{eq}$  is the Von Mises stress defined in Eq.(5.9) and *T* is the stress triaxiality given by the ratio between  $\sigma_H$  and  $\sigma_{eq}$ .

A study by Zangouie and Deylami (2013) reported an average value of *PEEQ* = 0.71 (associated to a coefficient of variation *CoV* = 0.25) at crack initiation of flange plate connections with beam flange thickness ranging from 9 to 20 mm. Another study by Myers *et al.* (2010) predicted fracture according to the Stress Modified Critical Strain (SMCS) (Hancock and Mackenzie, 1976) by verifying when the equivalent plastic strain at any point exceeds a critical value, according to the following expression:

$$\bar{\varepsilon}_p > \bar{\varepsilon}_{p,critical} = \alpha \cdot \exp(-1.5T) \quad (6.33)$$

Once the material-dependent toughness parameter  $\alpha$  is determined, the expression from Eq.(6.33) can be used to predict fracture initiation in structural components constructed from the same material. The experimental values for  $\alpha$  and  $T$  yielded an average equivalent plastic strain value at failure  $\varepsilon_{p,critical}=0.59$  with a  $CoV=0.24$ . Another study on ductile fracture using the SMCS criterion (Chi *et al.*, 2006) back-calculated the parameter  $\alpha$  to have a mean value of 2.6, which if applied to Eq.(6.33) along with  $T$  values at crack initiation zones yields an average critical equivalent plastic strain  $\varepsilon_{p,critical}=0.58$  with a  $CoV=0.17$ . The values obtained from these studies are consistent with the ones from Zangouie and Deylami (2013).

Considering that some variability in terms of critical *PEEQ* is verified and that the cases analysed in Zangouie and Deylami (2013) are similar to those analysed in this study, the critical plastic strain is assumed equal to 0.53 that corresponds to the average *PEEQ* value minus its standard deviation obtained from Zangouie and Deylami (2013).

$$PEEQ_{critical,low} = \mu_{PEEQ} - \sigma_{PEEQ} = 0.71 - 0.18 = 0.53 \quad (6.34)$$

The post fracture response of joint is highly influenced by the crack propagation pattern which is strongly dependent on local material and geometrical imperfections (Wang *et al.*, 2016). Therefore, post-fracture joint behaviour is not analysed in this study and the joint response curves are truncated according to adopted critical *PEEQ* criterion. This approach is consistent with design purposes since the residual post fracture resistance is conservatively not accounted for.

### 6.2.7 Moment-rotation response curves

The results obtained from finite element analysis are presented in terms of bending moment vs. chord rotation response curves. In particular, the chord rotation  $\theta_{chord}$  was computed as the sum of three contributions, namely, column rotation  $\theta_{column}$ , beam rotation  $\theta_{beam}$  and connection rotation  $\theta_{connection}$  (see Figure 6.8a)).

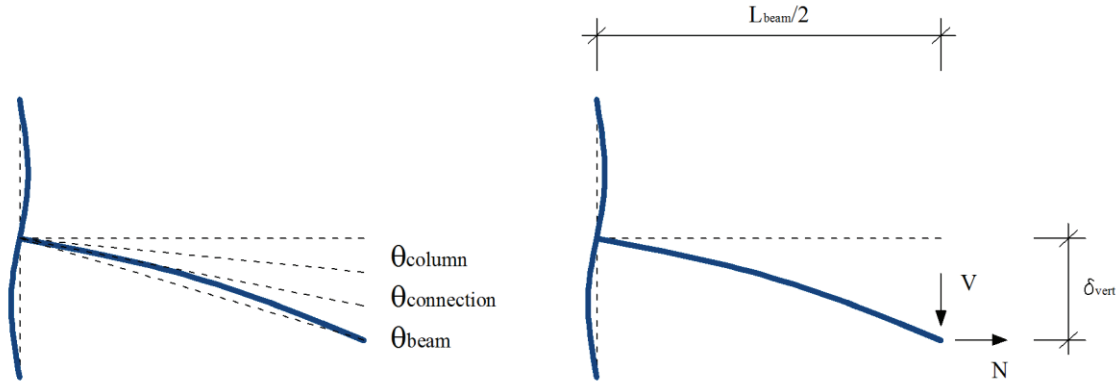


Figure 6.8: Definition of rotation contributions to joint chord rotation

The connection rotation is extracted from FEA results as the chord rotation minus the rotation contributions given by both beam and column. The column rotation is directly computed from the displacements of two points of the column at the end-plate extremity zones and beam rotation is taken as the sum of a first and second order contributions:

$$\theta_{chord} = \theta_{column} + \theta_{beam} + \theta_{connection} \quad (6.35)$$

$$\theta_{connection} = \theta_{chord} - \theta_{column} - \theta_{beam} \quad (6.36)$$

$$\theta_{connection} = \arctan(\delta_{vert}/(L_{beam}/2)) - \theta_{column} - (\theta_{beam}^I - \theta_{beam}^{II}) \quad (6.37)$$

$$\theta_{connection} =$$

$$\arctan(\delta_{vert}/(L_{beam}/2)) - \theta_{column} - \left( \arctan\left(\frac{V(L_{beam}/2)^2}{3EI}\right) - \arctan\left(\frac{N\delta_{vert}(L_{beam}/2)^2}{2EI}\right) \right) \quad (6.38)$$

The bending moment is computed on the basis of the free-body scheme shown in Figure 6.8b), as follows:

$$M_{connection} = V \left( \frac{L_{beam} - h_{column}}{2} \right) - N\delta_{vert} \quad (6.39)$$

In order to compare the performance of the investigated joints, the joint moment-rotation response was normalised as proposed by McConnell *et al.*, 2015). In particular, the bending moment was normalised by the beam section plastic bending moment  $M_p$  while the axial force was normalised to the section plastic tensile resistance  $N_p$ .

The chord rotation was normalized by a rotation factor  $\theta_{p+A} = \theta_p + \theta_A$ . The term  $\theta_p$  is the section rotation corresponding to the section plastic bending moment (see Figure 6.9a)), and  $\theta_A$  is the rotation related to the catenary action (see Figure 6.9b)). The rotation  $\theta_p$  normalises rotation in the flexural range, whereas  $\theta_A$  normalises rotation in the post flexural catenary stage.

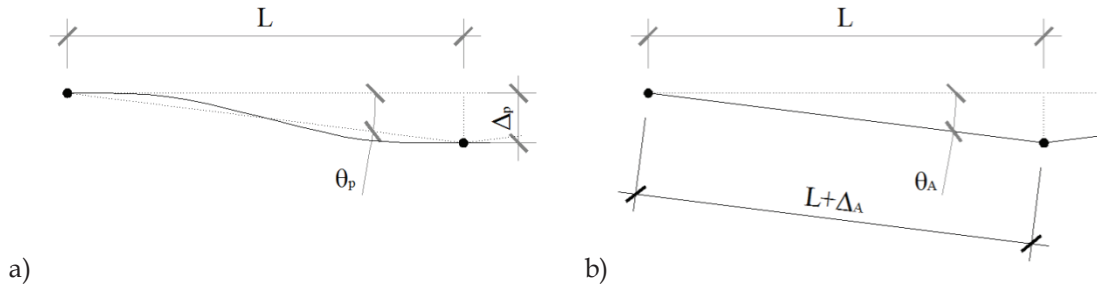


Figure 6.9: Definition of the normalisation rotation angles: a)  $\theta_p$ ; b)  $\theta_A$

For the purpose of computing the normalisation angle for the flexural range  $\theta_p$ , a simplified response in bending was considered, by taking the moment-rotation response in bending as bilinear. This simplification enables to compute the plastic rotation angle based on the elastic beam stiffness coefficient and on the value of the plastic bending moment. The vertical displacement at beam mid-span  $\Delta_p$  corresponds to the displacement required to induce the section plastic bending moment at the beam's ends, as computed from the stiffness coefficients derived from elastic beam theory:

$$\Delta_p = M_p / (6EI/L^2) \quad (6.40)$$

$$\theta_p = \arctg(\Delta_p/L) \quad (6.41)$$

$$\theta_p = \arctg\left(M_p L / (6EI)\right) \quad (6.42)$$

In order to compute the rotation  $\theta_A$ , the axial elongation  $\Delta_A$  obtained from the fully yielded section in tension condition is initially calculated; considering that the beam ends are fixed, the rotation  $\theta_A$  relative to the undeformed beam shape with a total length  $L$  can hence be determined as shown below:

$$\Delta_A = \frac{NL}{EA} \quad (6.43)$$

$$\cos(\theta_A) = \frac{L}{L + \Delta_A} \quad (6.44)$$

$$\theta_A = \arccos\left(\frac{L}{L+\Delta_A}\right) \quad (6.45)$$

$$\theta_A = \arccos\left(\frac{L}{L+\frac{NL}{EA}}\right) \quad (6.46)$$

$$\theta_A = \arccos\left(\frac{1}{1+\frac{f_y}{E}}\right) \quad (6.47)$$

As an example, for a yield stress  $f_y = 355 \text{ N/mm}^2$  and a Young's modulus  $E = 210000 \text{ N/mm}^2$ , the catenary normalising angle would assume the value  $\theta_A = 58.1 \text{ mrad}$  ( $\approx 3.33^\circ$ ).

The adopted normalisation factors  $M_p$ ,  $N_p$  and  $\theta_{p+A}$  for the analysed cases presented in Table 6.3 show that, while moment and axial force normalisation factors vary significantly with girder cross section dimensions, the rotation normalisation values vary instead within a relatively short range, given that the larger contribution to  $\theta_{p+A}$  is provided by the rotation related to the catenary phase  $\theta_A$ .

Table 6.3: Bending moment and rotation normalisation factors

Beam section	$M_p$	$N_p$	$\theta_p$	$\theta_A$	$\theta_{p+A}$
-	kNm	kN	mrad	mrad	mrad
IPE 220	106	1235	22.2	59.3	81.5
IPE 360	377	2691	13.5	59.3	72.8
HEA 320	602	4603	15.3	59.3	74.6
HEA 500	1461	7308	9.8	59.3	69.1

## 6.3 Results

### 6.3.1 Monotonic column loss action – strong axis column configuration

#### 6.3.1.1 General response

The response of a double span beam under column loss action depends on the mechanical features of the beam-to-column joints. Depending on the axial restraint stiffness of the joints and the beam depth, two inelastic response can characterize the inelastic performance of the joints, namely (i) a post-elastic response initially affected by compressive arching mechanism with subsequent catenary effects (Izzudin *et al.*,

2008) (see Figure 6.10a)) and (ii) a post-elastic behaviour solely influenced by tensile catenary action since the beginning (see Figure 6.10b)).

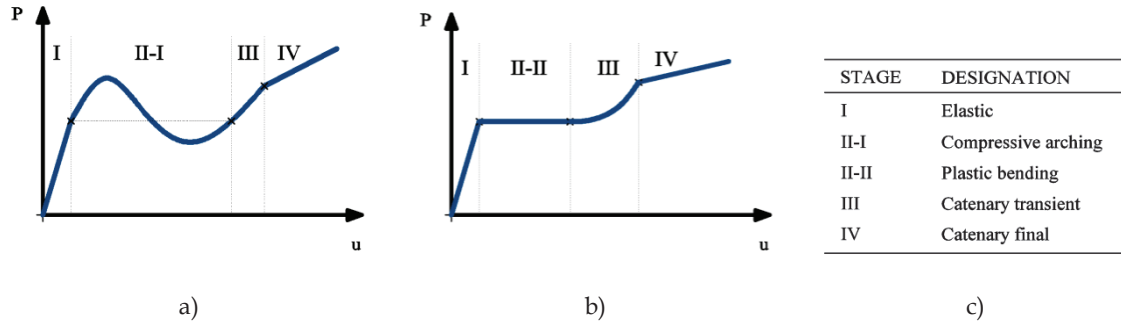


Figure 6.10: Typical joint moment-rotation response under simultaneous bending and axial force (Izzudin, *et al.*, 2008): a) initial compressive arching effect followed by tensile catenary action; b) solely tensile catenary action; c) description of each response stage

### 6.3.1.2 Influence of beam profile

The geometry of beam cross section significantly influences the response of joint assemblies in the strong axis of the column (see CS joints in Table 6.1 and Figure 6.2a)), especially at the initial response stages (i.e. for connection rotation up to 25 mrad, as shown in Figure 6.11). Beam-to-column assemblies with shallow beams (i.e. IPE 220) are characterized by the connection response shown in Figure 6.10b), namely pure tensile catenary action. On the contrary, compressive arching effect followed by catenary transient stage (i.e. mechanism depicted in Figure 6.10a)) is observed for joints with deep beams.

Since the beam-to-joint stiffness ratio affects the activation of catenary action, the shape of beam profile is also important. Indeed, HEA profiles have a higher cross section area and axial stiffness than the corresponding IPE profiles with the same depth. This feature clarifies the reason why the investigated beam-to-column assemblies with HEA beams experience arching mechanism prior to developing catenary action (see Figure 6.11). It is also interesting to observe that the catenary final stage is not achieved for the examined joint configurations, because the connections fail prior to the onset of full beam section axial plasticity. This finding is in agreement with the components method predictions presented in Figure 6.2c) and Figure 6.2d), that displayed  $N_j/N_{pl,beam}$  and  $M_j/M_{pl,beam}$  ratios lower than 1 in all cases.

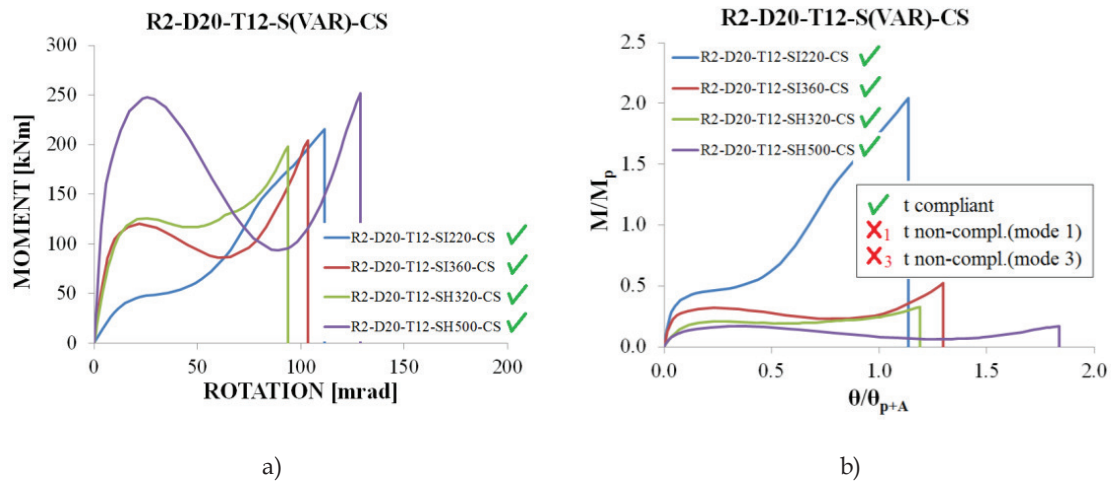


Figure 6.11: Influence of cross section type on R2-D20-T12-CS joints: a) moment vs. connection rotation; b) normalised moment vs. connection rotation

For what concerns the joints in weak axis of the column (see CW joints in Figure 6.2b) and in Table 6.1) no arching effects are observed. Indeed, as previously mentioned, the mobilisation of the compressive arching effect strongly depends on the stiffness of the column member.

The normalized moment-rotation response curves show that joints with shallow beams can develop higher  $M/M_p$  ratios increasing the relevant available rotation ductility  $\theta/\theta_{p+A}$ . Indeed, joints with IPE220 beam develop significant overstrength, with failure resistance being larger than the plastic bending moment of the beam cross section (i.e. about  $2M_p$ ), corresponding to ductility  $\theta/\theta_{p+A}$  close to 1. This type of performance is due to the catenary induced second order flexural effects, which are observed at both global and local level. In particular, in the latter case, membrane action develops into the end-plate that is bended in large deformations, owing to its larger gauge width. On the contrary, the failure of joints with HEA 500 beam occurs after arching effect is extinguished and catenary action starts developing (see Figure 6.11), with a failure moment approximately equal to  $0.2M_p$  and ductility  $\theta/\theta_{p+A}$  lower than 2.

In all cases, the failure of the joints is due to the failure of bolts and the higher normalised rotation capacity is provided by the connections having the smaller ratio between the tensile strength of all bolts and the tensile plastic strength of the beam, as is the case of joints with taller beams. For the joint configurations in Figure 6.11, the minimum mode 2 thicknesses according to Eq.(6.1) and Eq.(6.11) are equal to 10.7 mm



and 8.8 mm, respectively, implying that all joints are in mode 2. For joints with 2 bolt rows and M20 bolts, the  $N_{pl,bolts}/N_{pl,beam}$  ratio is equal to 1.02, 0.47, 0.27 and 0.17 for the IPE 220, IPE 360, HEA 320 and HEA 500 beam sections, respectively.

### 6.3.1.3 Influence of end-plate thickness

As previously stated, the compressive arching behaviour is highly dependent on joint stiffness, for which reason end-plate thickness should significantly influence joint response.

The influence of the end-plate thickness on joint response mostly depends on two features, namely the ratio between the axial stiffnesses of the beam and the connection and the type of failure mode of the bolt rows. Indeed, at the same beam depth, the stiffer is the connection (i.e. increasing the thickness of end-plate) the higher is the influence of the arching effect on the overall response of the assembly. In addition, the connections characterized by mode 1 and mode 2 (i.e. those with the larger bolt diameter) can mobilize the end-plate resistance and ductility due to formation of plastic flexural deformations, which are subsequently followed by membrane lengthening when joint rotation increases and the catenary action fully develops at global level. On the contrary, end-plate thickness has negligible influence on connections characterized by mode 3.

As discussed in the previous Section, the shape of beam profile can significantly affect the response of the joint assembly. Therefore, the influence of end-plate thickness is separately discussed hereinafter for the set of joints with either IPE or HEA sections, focusing on the cases characterized by the weaker resistance of bolts (i.e. the joints with two bolt rows).

Figure 6.12 shows the comparison between the response obtained for the set of R2-SI360-CS joints with M16 bolts and M24 bolts. As it can be noted, the joints with M16 bolts do not develop appreciable flexural overstrength (see Figure 6.12b)) and catenary action is limited by bolt failure, even though the arching effect slightly increases with the thickness of the end-plate (as shown in Figure 6.12c)), with joint-to-beam axial stiffness ratios  $S_{j,N,ini}/(EA_b/L_b)$  ranging between  $16.5 \times 10^{-4}$  for  $t = 8\text{mm}$  and  $36.2 \times 10^{-4}$  for  $t = 20\text{ mm}$ . For the joints in Figure 6.12a),b),c), the thickness criterion compliant joint is characterised by a failure mode 2 with limited plastic deformations into the end-plate, resulting in a response similar to joints with thicker end-plates and

that are clearly in mode 3. For joints with M16 bolts, the minimum thicknesses for mode 2 according to Eq.(6.1) and Eq.(6.11) are equal to 9.7 mm and 7.0 mm, respectively. The joints with M24 bolts experience ductile mechanism and the influence of the end-plate thickness is very important because it affects the shape of the moment-rotation response, the ultimate joint strength and ultimate rotation capacity.

The cases with the thinner end-plate (i.e. 8mm) show pure mode 1 with end-plate failure occurring at a chord rotation equal to 74 mrad that corresponds to a ductility capacity  $\theta/\theta_{p+A} = 0.94$ . The lower bound mode 2 thickness  $t_{min,Mode2}$  thresholds for M24 bolts given by Eq.(6.1) and Eq.(6.11) are equal to 12.9 mm and 10.5 mm, respectively, while the  $t_{max,Mode2}$  according to Eq.(6.13) is equal to 17.2mm. The joint resistance significantly improves by increasing the thickness up to 12mm, thus shifting the bolt row failure mechanism from mode 1 to mode 2. It can be noticed that joints compliant with the proposed criterion ( $t=12\text{mm}$  and  $t=16\text{mm}$ ) display the better performance in terms of both strength and rotation capacity. For the M24 case, the  $S_{j,N,ini}/(EA_b/L_b)$  ratios range between  $17.7 \times 10^{-4}$  for  $t=8\text{mm}$  and  $45.0 \times 10^{-4}$  for  $t=20\text{mm}$ .

Figure 6.12d),f) allow estimating the acting bending moment  $M$  and axial force  $N$  for a given rotational demand  $\theta$ . As it can be noted, the level of axial force developing at failure (e.g.  $0.3N_p$ ) is almost independent from the joint strength and the end-plate thickness. Additionally, the fact that collapse of the joint is determined by bolt failure in these cases led to similar axial forces at failure.

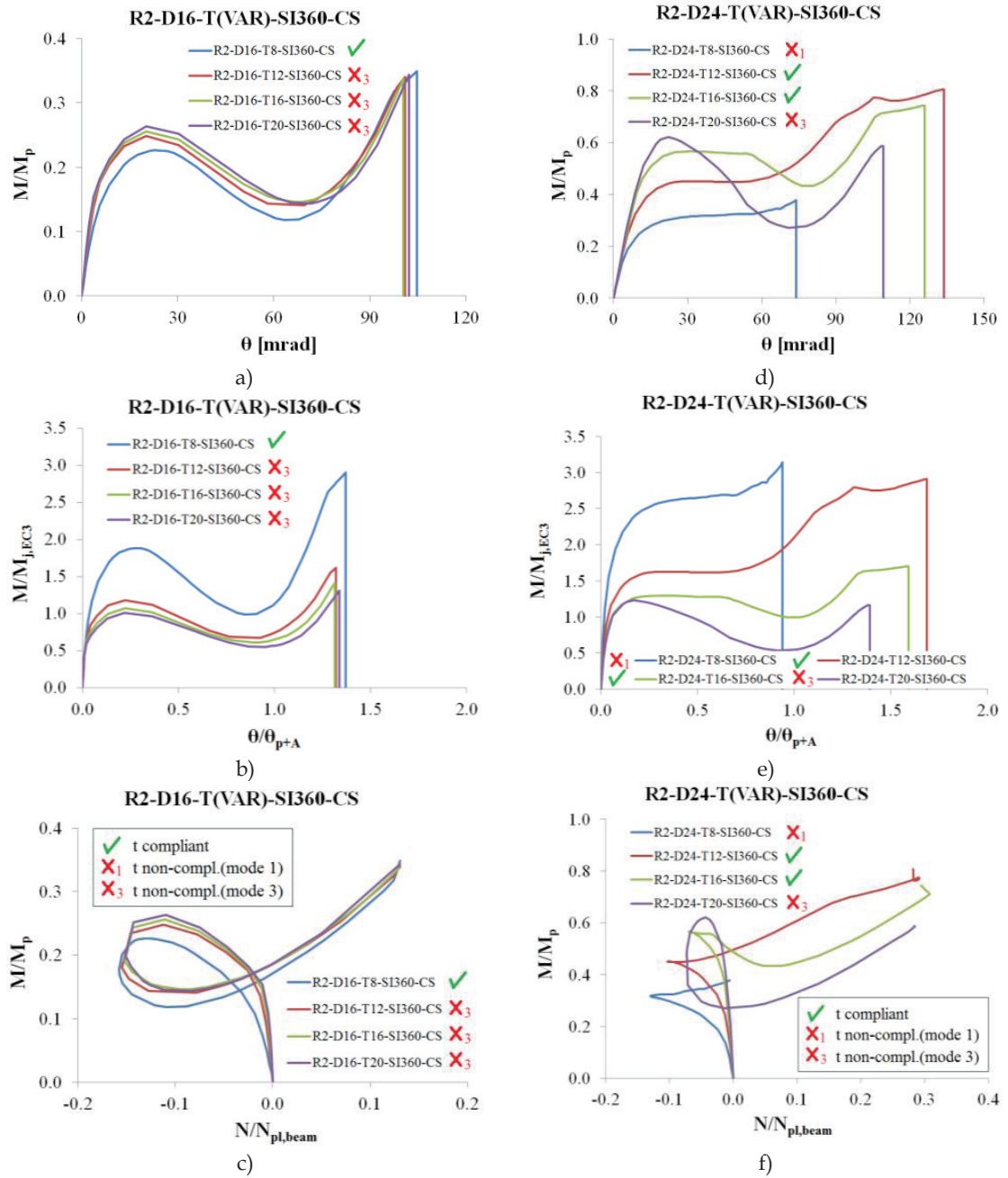


Figure 6.12: Influence of end-plate thickness on R2-SI360-CS joints with M16 bolts (a,b,c) and M24 bolts (d,e,f)

Table 6.4: Connection rotation, bending moment and axial force results for M24 bolts

BEAM SECTION	BOLT ROWS	ENDPLATE THICKNESS	$\theta_u$	$\theta_u/\theta_{p+A}$	$M_u$	$M_u/M_p$	$N_u$	$N_u/N_{p,nom,\Sigma bolts}$	$N_u/N_p$
[-]	[-]	[mm]	[mrad]	[-]	[kNm]	[-]	[kN]	[-]	[-]
IPE 220	2	8	83	1.02	216	2.04	586	0.32	0.47
		12	93	1.14	285	2.69	771	0.43	0.62
		16	119	1.46	376	3.55	946	0.52	0.77
		20	132	1.62	411	3.88	1024	0.57	0.83
	3	8	76	0.93	213	2.01	624	0.23	0.51
		12	98	1.20	309	2.92	836	0.31	0.68
		16	131	1.61	414	3.90	1014	0.37	0.82
		20	166	2.03	507	4.79	1138	0.42	0.92
IPE 360	2	8	68	0.94	142	0.38	-15	-0.01	-0.01
		12	123	1.69	304	0.81	759	0.42	0.28
		16	116	1.59	280	0.74	793	0.44	0.29
		20	101	1.39	221	0.59	761	0.42	0.28
	4	8	72	0.99	218	0.58	224	0.06	0.08
		12	147	2.02	765	2.03	1437	0.40	0.53
		16	134	1.84	732	1.94	1496	0.41	0.56
		20	131	1.80	760	2.02	1591	0.44	0.59
HEA 320	2	8	83	1.11	203	0.34	521	0.29	0.11
		12	118	1.59	345	0.57	862	0.48	0.19
		16	95	1.28	261	0.43	856	0.47	0.19
		20	98	1.31	228	0.38	747	0.41	0.16
	4	8	81	1.08	228	0.38	524	0.14	0.11
		12	138	1.86	785	1.30	1534	0.42	0.33
		16	148	1.99	822	1.36	1579	0.44	0.34
		20	141	1.89	812	1.35	1622	0.45	0.35
HEA 500	2	8	59	0.85	206	0.14	-990	-0.55	-0.14
		12	157	2.28	280	0.19	718	0.40	0.10
		16	134	1.94	223	0.15	701	0.39	0.10
		20	132	1.92	192	0.13	619	0.34	0.08
	4	8	59	0.86	253	0.17	-891	-0.25	-0.12
		12	174	2.52	689	0.47	1361	0.38	0.19
		16	157	2.27	650	0.44	1431	0.40	0.20
		20	134	1.94	559	0.38	1426	0.39	0.20

The performance of joints with shallow IPE girder (i.e. IPE 220) is substantially different from the behaviour of the joint assemblies with deep IPE beam (i.e. IPE360), as recognizable comparing Figure 6.12 to Figure 6.13. Indeed, the set of R2-SI220-CS joints are characterized by larger joint-to-beam stiffness ratios (for the M24 case,  $S_{j,N,ini}/(EA_b/L_b)$  ratios range between  $25.8 \times 10^{-4}$  for  $t = 8$  mm to  $72.7 \times 10^{-4}$  for  $t = 20$  mm) than R2-SI360-CS joints and do not exhibit compressive arching. FEM results show that the R2-SI220-CS joints exhibit failure mode 1 with deformation capacity impaired by the failure of the welds between beam flange and end-plate. For this motive, since joint failure did not occur according to one of the three T-stub failure modes, the simple application of the proposed end-plate thickness criterion does not allow to predict the optimised joint configuration. It is also worth noting that, for this set of joints, the

increase of end-plate thickness corresponds to a significant increase of moment resistance and rotation capacity (i.e. ranging from 83 to 132 mrad), as well. In particular, the connections with thicker end-plates (and corresponding thicker and stronger welds) mobilize an important membrane action into the bended portion of end-plate at each bolt row in tension. This mechanism is associated to large displacement capacity of the relevant equivalent T-stub in tension, thus explaining how rotation capacity increases with the thickness of end-plate. In addition, being the plastic engagement of the connection larger than in the previous case, the contribution of the beam elongation and the relevant axial force up to collapse increase with the end-plate thickness (see Figure 6.13c).

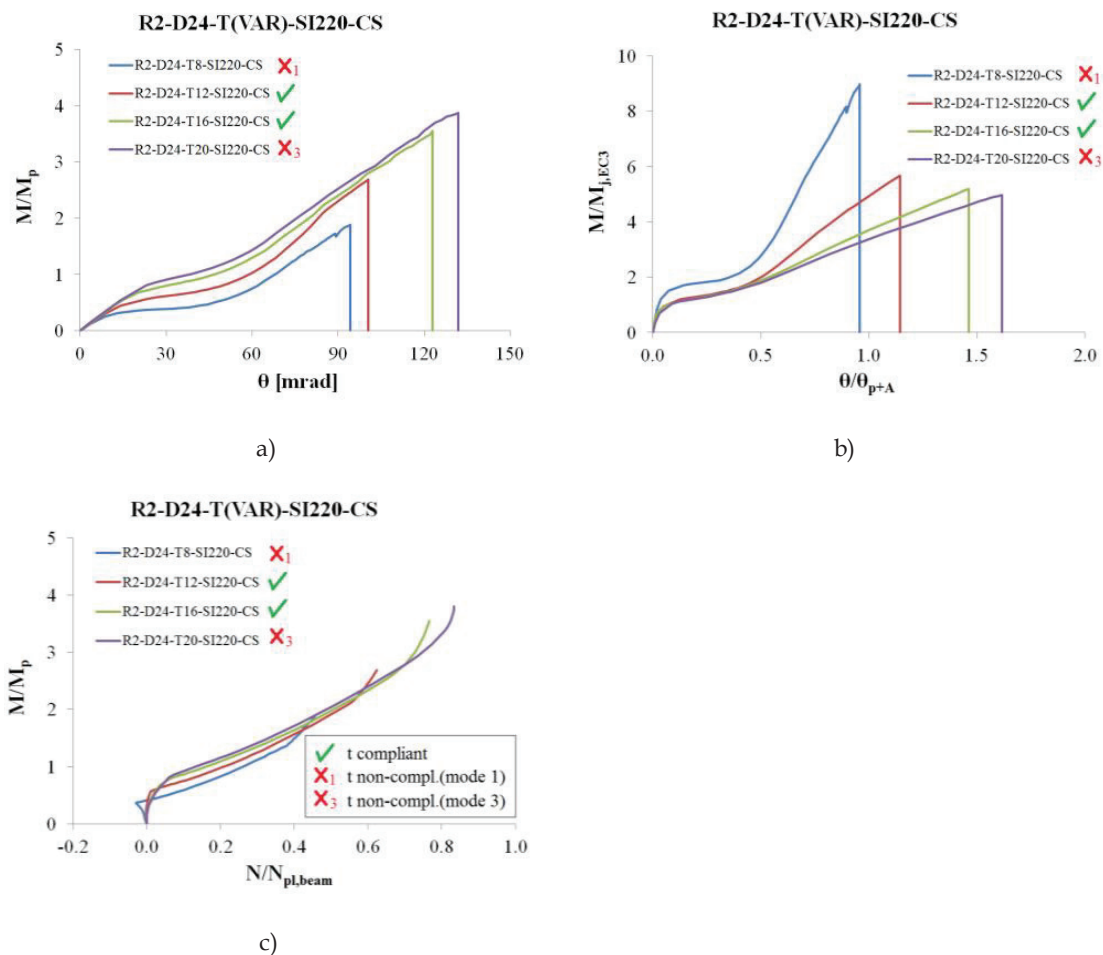


Figure 6.13: Influence of endplate thickness on R2-SI220-CS joints with M24 bolts: a) normalised connection moment vs. chord rotation; b) connection moment normalised to EC3 joint resistance vs. normalised rotation; c) normalised connection moment vs. normalised axial strength

Also for the set of joints with HEA beams, the end-plate thickness is more influential for R2-SH320-CS joints with the shallower beam profiles (i.e. HEA320),

where end-plate thickness determines whether the joint response is dominated by post yield plastic behaviour or post yield compressive arching. As shown in Figure 6.14, the cases with end-plate thickness ranging from 8 mm to 12 mm are characterized by flexural yielding and development of catenary action, with  $S_{j,N,ini}/(EA_b/L_b)$  ratios of  $4.8 \times 10^{-4}$  for  $t = 8$  mm and  $11.5 \times 10^{-4}$  for  $t = 12$  mm.

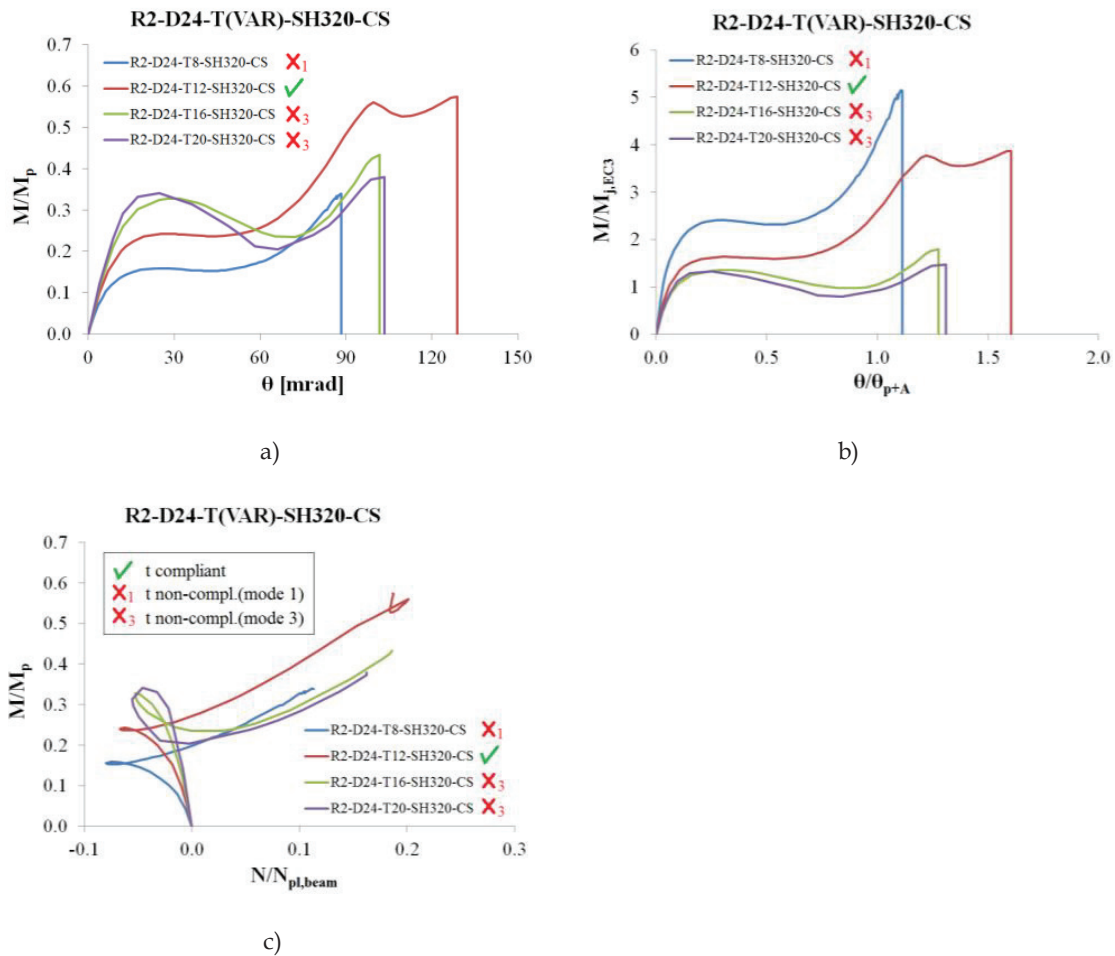


Figure 6.14: Influence of endplate thickness on R2-SH320-CS joints with M24 bolts: a) normalised connection moment vs. chord rotation; b) connection moment normalised to EC3 joint resistance vs. normalised rotation; c) normalised connection moment vs. normalised axial strength

The joint with end-plate thickness equal to 8 mm shows pure mode 1 up to failure, namely plastic deformation mostly concentrated into the end-plate and welds between end-plate and beam flange (see plastic equivalent strain  $PEEQ$  distribution in Figure 6.15), while the criterion compliant joint with end-plate thickness equal to 12 mm experiences mode 2, with plastic engagement distributed between bolts and endplate (see plastic equivalent strain  $PEEQ$  distribution in Figure 6.16).

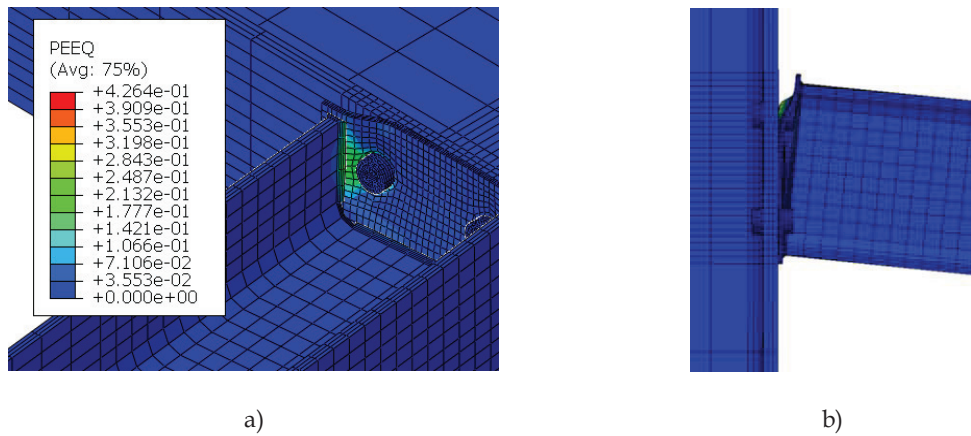


Figure 6.15: Failure mode and equivalent plastic strain PEEQ for the R2-SH320-CS with 8mm thick endplate and M24 bolts: a) perspective; b) side view

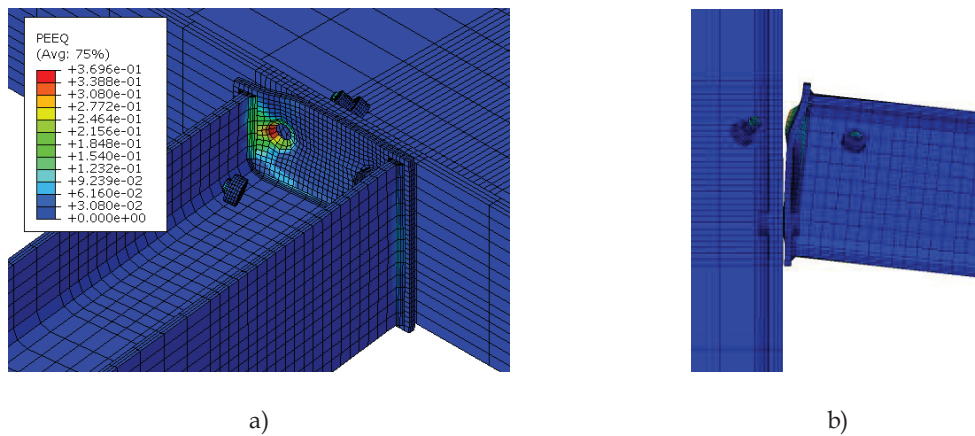


Figure 6.16: Failure mode and equivalent plastic strain PEEQ for the R2-SH320-CS with 12mm thick endplate and M24 bolts: a) perspective; b) side view

Also in this case, selecting a mode 2 compatible end-plate thickness for grade 10.9 M24 bolts, in accordance with Eq.(6.11) and Eq.(6.13) (i.e.  $t_{min,Mode2} \leq t \leq t_{max,Mode2}$ ) leads to maximising the joint capacity. The EN1993-1-8 (CEN, 2005) criterion from Eq.(6.1) yields  $t_{min,Mode2,EN1993-1-8} \geq 12.9$  mm, while Eq.(6.11) yields  $t_{min,Mode2} \geq 10.5$  mm showing the latter criterion, which accounts for material variability and strain hardening, to be more suitable in this case. For thickness values of 16mm and 20mm, the joint response is dominated by arching effect (characterised by  $S_{j,N,ini}/(EA_b/L_b)$  ratios of  $17.1 \times 10^{-4}$  for  $t = 16$  mm and  $20.2 \times 10^{-4}$  for  $t = 20$ mm) and rotation capacity is reduced because the connection collapse mechanism is shifted from mode 2 to mode 3.

The results for R2-SH500-CS joints (i.e. with HEA 500 beam) are shown in Figure 6.17, where it can be observed that the response is dominated by arching mechanism and that the rotation capacity is maximised for the joint with the criterion

compliant thickness. In particular, ultimate chord rotation values of 59 mrad, 157 mrad, 134 mrad and 132 mrad are reported for the 8mm, 12mm, 16mm and 20mm end-plate thickness configurations, respectively. In this case, the joint-to-beam tensile stiffness ratios  $S_{j,N,ini}/(EA_b/L_b)$  are equal to  $3.8 \times 10^{-4}$ ,  $9.5 \times 10^{-4}$ ,  $13.8 \times 10^{-4}$  and  $16.3 \times 10^{-4}$  for  $t$  equal to 8, 12, 16 and 20mm, respectively.

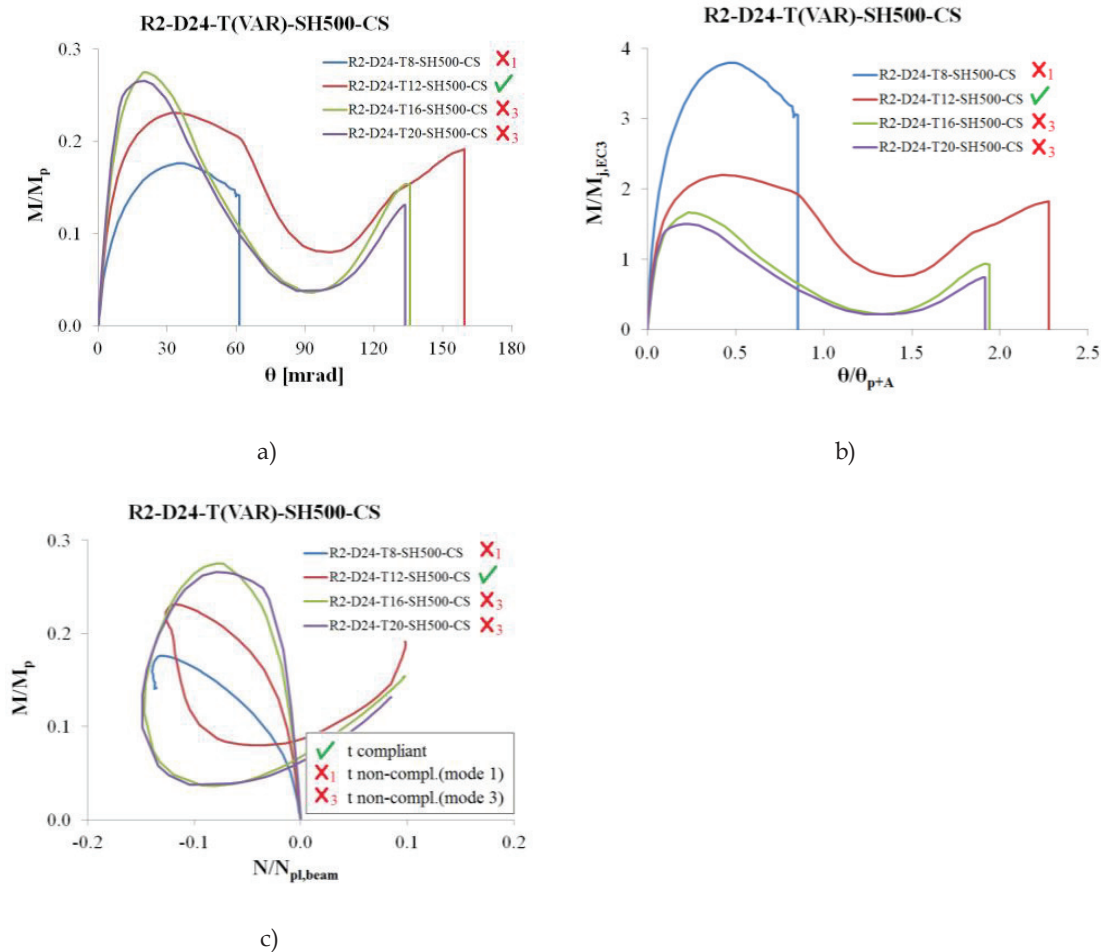


Figure 6.17: Influence of endplate thickness on R2-SH500-CS joints with M24 bolts: a) normalised connection moment vs. chord rotation; b) connection moment normalised to EC3 joint resistance vs. normalised rotation; c) normalised connection moment vs. normalised axial strength

The comparison between the normalised response curves reported in Figure 6.12, Figure 6.13, Figure 6.14 and Figure 6.17 shows that the ductility at failure (i.e.  $\theta/\theta_{p+A}$  ratios) significantly varies with endplate thickness. However, except for R2-SI220-CS joints that are characterized by collapse mode type 1 with failure due to cracking of the beam flange weld, the assemblies with 12 mm thick end-plate (which comply with the end-plate thickness range for mode 2 given defined by Eq.(6.11) and Eq.(6.13)) show the larger ductility that falls in the range 1.6 - 2.3. This feature depends



on the type of failure mode, which starts as mode 1 and subsequently involves the failure of bolts due to the hardening developed by the end-plate.

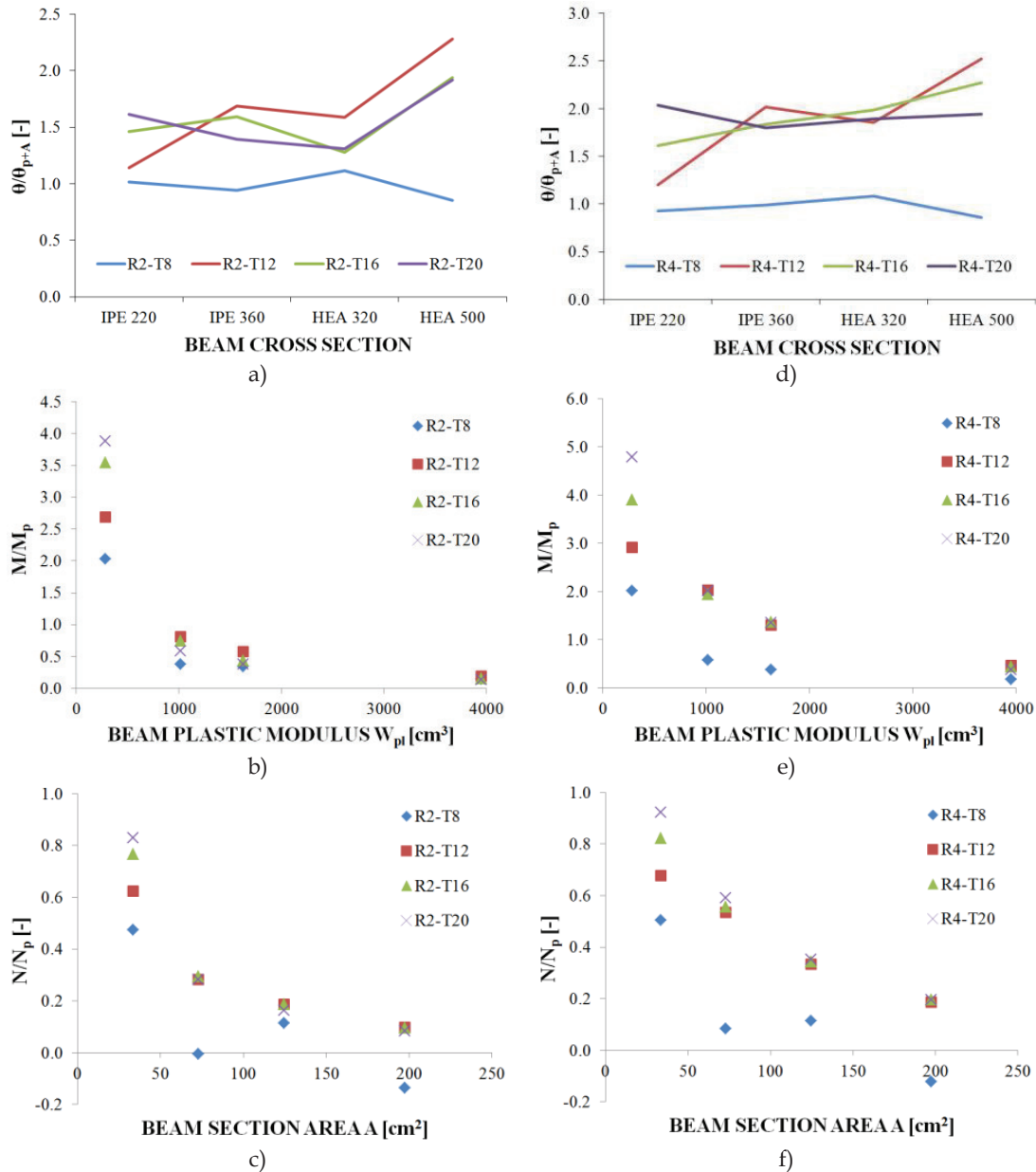


Figure 6.18: Influence of endplate thickness for M24 bolts: a) on normalised connection rotation factor  $\theta/\theta_{p+A}$  (2 rows); b) on the normalised resistance factor  $M/M_p$  (2 rows); c) on the normalised resistance factor  $N/N_p$  (2 rows); d) on normalised connection rotation factor  $\theta/\theta_{p+A}$  (4 rows); e) on the normalised resistance factor  $M/M_p$  (4 rows); f) on the normalised resistance factor  $N/N_p$  (4 rows, N.B. 3 bolt rows for IPE 220)

Figure 6.18 depicts the relationship between the normalised flexural response parameters and end-plate thickness for joints varying the number of M24 bolt rows. In particular, Figure 6.18a) shows that the joint ductility at failure is almost the same (i.e. about 1.0) for thin end-plates (i.e.  $t = 8$  mm). On the contrary, the ductility at failure

tends to increase when the end-plate thickness is in the proposed range (except for cases of premature weld failure) and when increasing the number of bolt rows. It should be noted that 12 mm thick end-plate (compliant with the proposed criterion) with either two or four bolt rows exhibit a similar trend of ductility at failure for different profiles of the beam. This result depends on the type of failure mechanism that starts as mode 1 and afterwards involves the upper bolts, owing to both hardening and membrane action developing into the end-plate. The normalised resistance of joints is plotted versus the beam profile mechanical properties in Figure 6.18(b), (c), (e), (f).

#### 6.3.1.4 Influence of bolts

The influence of bolt diameter on joints with end-plate thickness  $t = 12$  mm is shown in Figure 6.19, varying both the number of bolt rows and the type of beam profile. The comparison between the response curves for the same set of joints and among the different joint assemblies clearly highlights that the joint ultimate resistance increases with the bolt diameter. In addition, at the same beam-to-column assembly and at the same bolt diameter, increasing the number of bolt rows is beneficial to the capacity of the joint under column loss. In particular, increasing the number of bolt rows and the relevant diameter leads to increasing the connection stiffness, thus allowing to further mobilize catenary action in place of arching mechanism. In terms of the  $S_{j,N,ini}/(EA_b/L_b)$  stiffness ratio, changing from 2 to 3 bolt rows led to moderate increases of 4%, 3% and 2% for M16, M20 and M24 cases, owing to the fact that adding bolt rows also increases T-stub group effect, reducing effective lengths and leading to increased joint deformability.

Figure 6.19a) depicts the response curves for joints with IPE 220 beam, which as previously stated are characterised by premature flange-endplate weld failure. For the cases with two bolt rows, the rotation capacity  $\theta/\theta_{p+A}$  appreciably increases (e.g. about 43%) when bolt diameter varies from M16 to M20 and the corresponding normalized resistance  $M/M_p$  increases up to 111%. For the cases with three bolt rows, both  $\theta/\theta_{p+A}$  and  $M/M_p$  increase up to M20 and reduce for M24. This result depends on the connection collapse mechanism, which starts as mode 1 and ends with bolt failure for assemblies with bolt diameter up to M20, while for those with M24 bolts the failure mode mobilises the end-plate only.

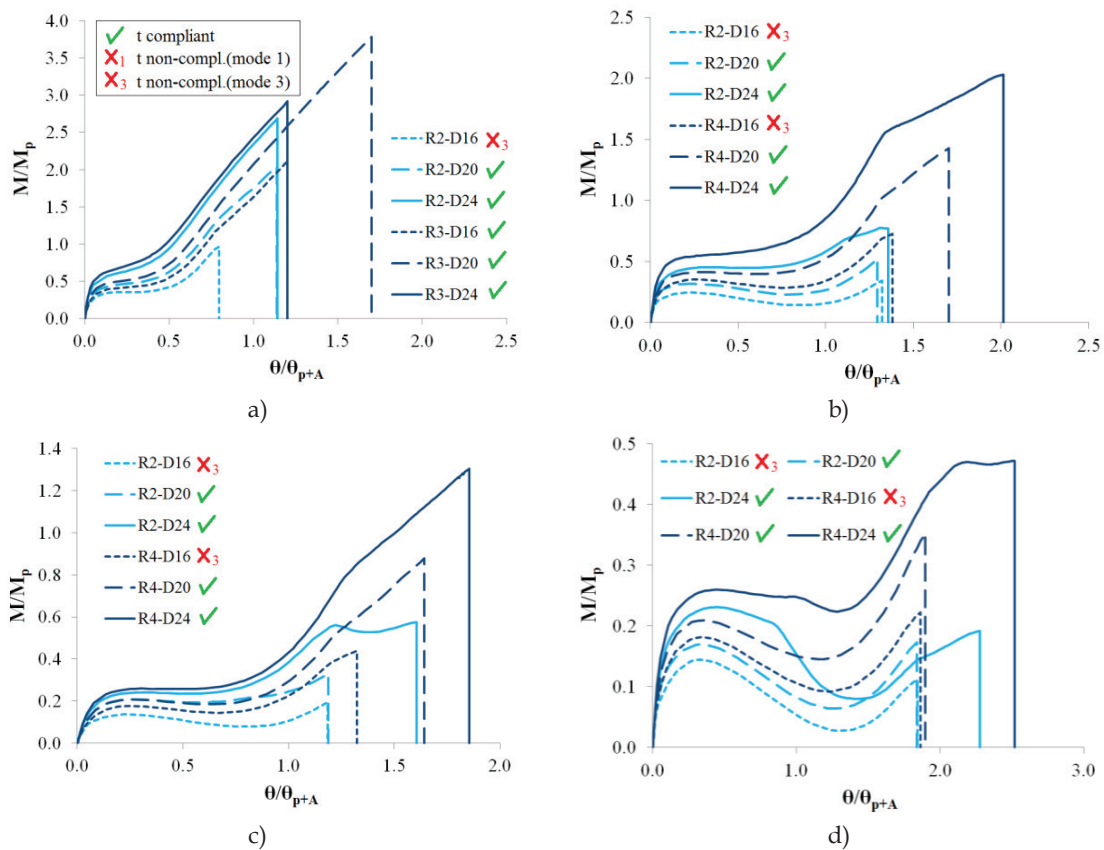


Figure 6.19: Influence of bolt diameter on normalised connection moment-rotation for endplate thickness  $t=12\text{mm}$ : a) IPE 220 beam; b) IPE 360 beam; c) HEA 320 beam; d) HEA 500 beam

The role of bolt diameter on the response of joints with either IPE 360 or HEA320 beam is very similar, as it can be noted comparing Figure 6.19b) to Figure 6.19c). Indeed, the bolt diameter influences both the type of connection failure mode and the resisting mechanism under column loss. For the IPE 360 case, results showed that by increasing from 2 to 4 bolt rows, the  $S_{j,N,ini}/(EA_b/L_b)$  stiffness ratios increased by 19%, 15% and 12%, for M16, M20 and M24 cases respectively.

The connections with the smaller bolt diameters (e.g. M16) are characterized by failure mode 3 and the joint assembly response is significantly affected by arching mechanism. Increasing the diameter (and the relevant joint stiffness), the connection behaviour improves, triggering the activation of collapse mode type 2, and enabling the catenary mechanism to be developed.

The set of joints with HEA 500 beams display significant compressive arching action (see Figure 6.19d)), which is mitigated by increasing both the bolt diameter and the number of bolt rows. As for the previous cases, the joints with M24 bolts activate the failure mode 2 failure, since end-plate thickness respects the proposed thickness

criterion, leading to substantial improvements in terms of ultimate rotation capacity and resistance. In this case, increasing from 2 to 4 bolt rows led to  $S_{j,N,ini}/(EA_b/L_b)$  ratio variations of 13%, 10% and 8% for the M16, M20 and M24 cases, respectively.

Figure 6.20 reports the FEP joint response curves varying the number of bolt rows and end-plate thickness. The comparison between the plots shows that the performance of FEP joints generally improves by selecting end-plate thickness values in the range defined by Eq.(6.11) and Eq.(6.13) and by increasing bolt diameter and number of bolt rows. Significant performance enhancement was reported when shifting from mode 1 failure (i.e. non-compliant with Eq.(6.11)) to mode 2 failure (i.e. compliant with Eq.(6.11)).

For the cases with IPE 220 beam (see Figure 6.20a)) that displayed premature weld failure, the catenary action response is not significantly improved by the number of bolt rows rather than the bolt diameter. On the contrary, the other sets of joint assemblies (see Figure 6.20b),c),d)) are substantially influenced by increasing the number of bolt rows, with improved strength and ductility. Indeed, after the failure of the upper bolt row (which is the most engaged) no resistance loss is observed thanks to the axial force redistribution through the inner bolt rows. Especially in the cases with the larger bolt diameter (i.e. M24), the thicker end-plate (i.e.  $t = 20\text{mm}$ ) and the greater number of rows (e.g. four), it is observed that the hardening developed by the membrane action into the fully yielded upper bolt row triggers off the plastic engagement into the inner rows, thus enabling their hardening and a significant joint overstrength.

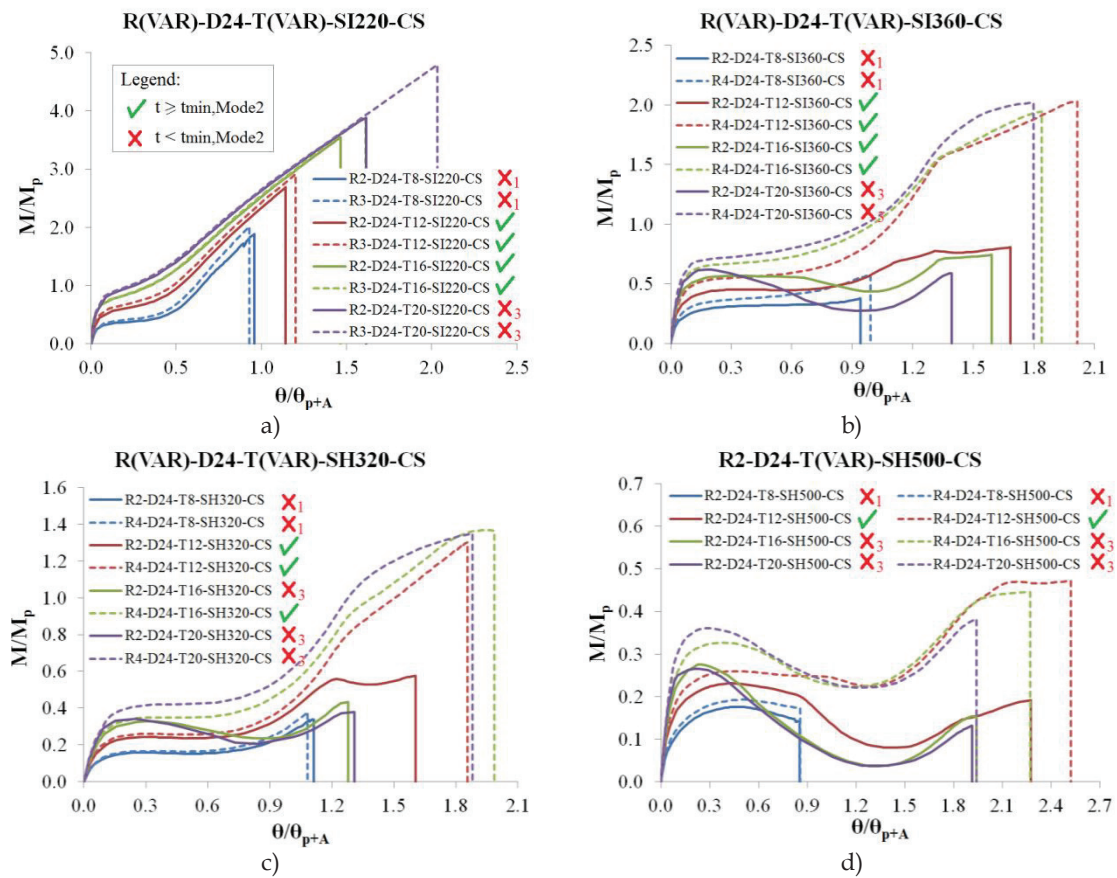


Figure 6.20: Influence of the number of bolt rows on the normalised connection moment-rotation response curve for joints with M24 bolts: a) IPE 220 beam; b) IPE 360 beam; c) HEA 320 beam; d) HEA 500 beam

This effect is clarified in Figure 6.21, where the failure modes of FEP joints with HEA 320 beam and either two or four M24 bolt rows are compared. For the 4 bolt rows configuration, after the failure of the first bolt row the tensile forces are redistributed to inner bolt rows close to the centroid of beam section, which are effective in resisting catenary actions. This example shows that disregarding or not designing inner bolt rows as currently assumed for FEP joints under conventional first order design approach is not effective to guarantee satisfactory resistance under column loss. On the contrary, adopting inner bolt rows located close to the centroid of the connection can significantly improve the joint robustness when catenary action develops.

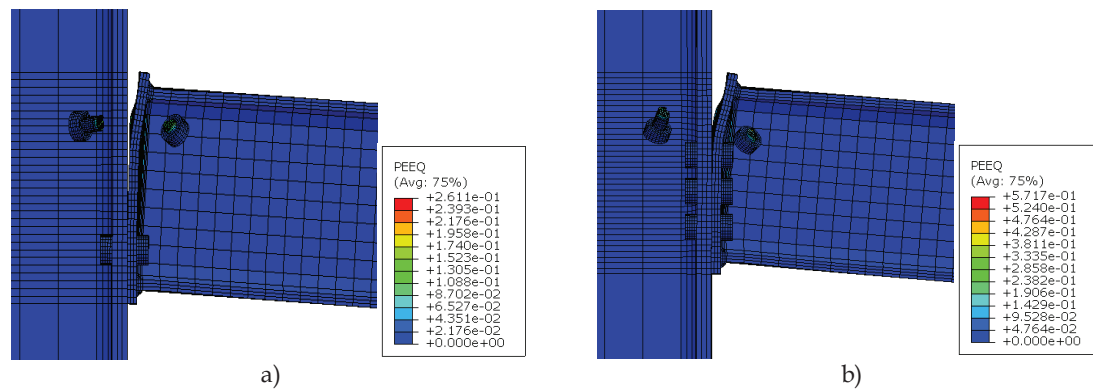


Figure 6.21: Deformed shape at first bolt row failure and equivalent plastic strain PEEQ for the HEA 320 section with  $t=16\text{mm}$  endplate joints with M24 bolts: a) 2 bolt rows; b) 4 bolt rows

For what concerns the effect of end-plate thickness, results show that for both joints with 2 and 4 bolt rows, the best performance was obtained when the end-plate thickness was compliant with the proposed criterion. Moreover, in the light of the FEM outcomes, it can be argued that to mobilise the maximum ductility provided by the end-plate deformation, it is preferable to use large bolt diameter that should be designed to have an axial strength at least equal to the mode 1 resistance of the equivalent T-stub per row, the latter evaluated considering both the random variability of the steel yield stress and the relevant hardening, in accordance with Eq.(6.11). The end-plate thickness should however be smaller than the value proposed in Eq.(6.13), to avoid reducing rotation capacity.

#### 6.3.1.5 Dynamic Increase Factor

The Dynamic Increase Factor (*DIF*) is typically defined as the ratio between the static force  $F_{stat}$  and the dynamic force  $F_{dyn}$  under the same displacement demand and it can be expressed as follows:

$$DIF = P_{stat}/P_{dyn} \quad (6.48)$$

The load-carrying capacity of the structure under dynamic loading is hence:

$$P_{dyn} = P_{stat}/DIF \quad (6.49)$$

For elastic systems under a suddenly applied load, the *DIF* is equal to 2.0, whereas ranging from 1.0 to less than 2.0 for elastic perfectly plastic systems (United States of America Department of Defense, 2009; Tsai, 2010). However, both these cases do not account for catenary action for the computation of the *DIF*.

In order to estimate the dynamic behaviour and in line with Liu *et al.* (2013) the connections are liken to a SDOF system, for which the energy balance principle states that the external work  $W_{ext}$  is equal to the strain energy stored in the specimen  $W_{int}$  when the connection reaches the maximum dynamic displacement. The energy balance equation is expressed as follows:

$$P_{dyn}u_{dyn} = \int_0^{u_{dyn}} R_{stat}(u)du \quad (6.50)$$

where  $R_{stat}(u)$  is the static connection resistance at the displacement  $u$  that is applied at beam tip. The energy balance equation is solved for all displacement values up to the connection failure, enabling to compute the corresponding *DIF* as a function of the chord rotation demand. Figure 6.22 shows that the *DIF* decreases from 2.0 to 1.0 at chord rotation equal to 60 mrad, after which the behaviour is dominated by the catenary action and *DIF* increases again up to joint failure.

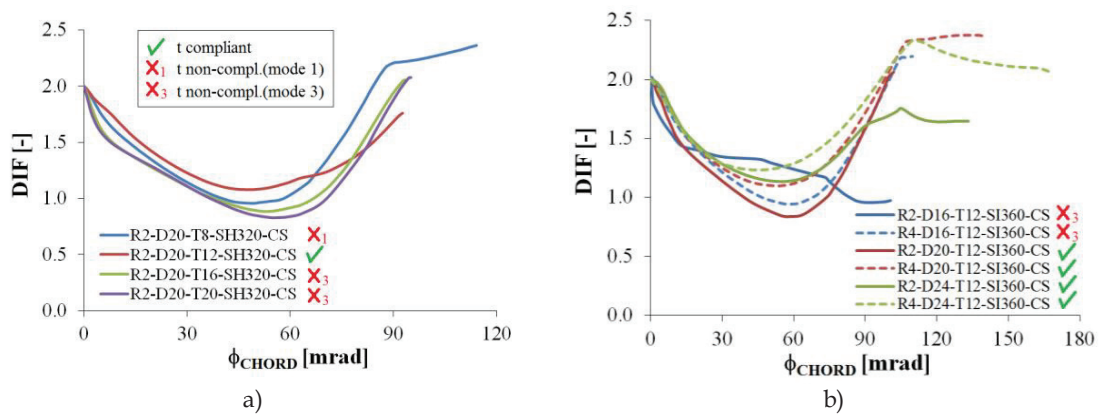


Figure 6.22: DIF vs. chord rotation demand: a) effect of end-plate thickness on joints with HEA 320 beam and 2 rows of M20 bolts; b) effect of number of bolt rows on joints with IPE 360 beam and 12mm thick end-plates

The endplate thickness has a moderate influence on the *DIF*, as shown in Figure 6.22a, whereas increasing the number of bolt rows is more influential on the *DIF* in the

catenary dominated zone ( $\phi_{chord} > 60 \text{ mrad}$ ) and prior to connection failure (see Figure 6.22b).

The influence of beam cross section on the *DIF* is depicted in Figure 6.23 for joints with either M20 or M24 bolts. The cases with IPE 220 beam with response dominated by catenary action are characterized by the larger *DIF*. Instead for joints with the larger beam profiles, e.g. HEA 500 beam, the compressive arching effect leads to very low *DIF*, with values lower than 0.5 at a rotation demand of about 85 mrad.

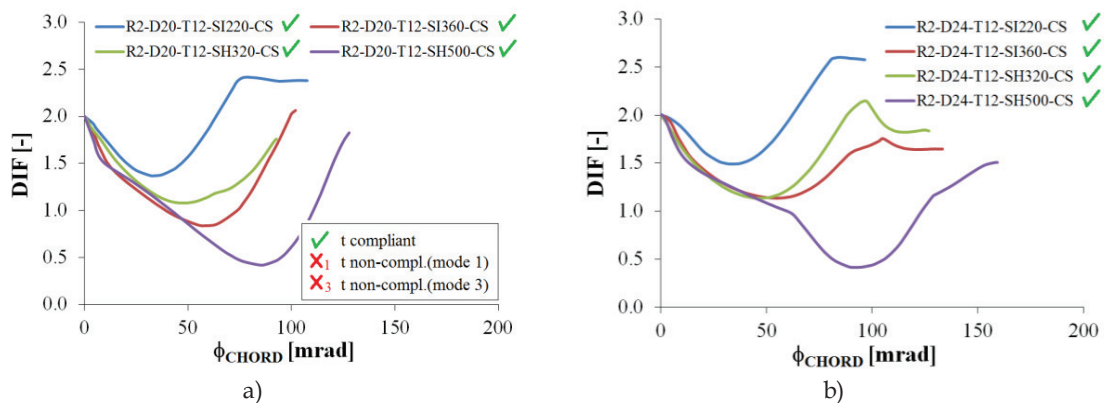


Figure 6.23: Influence of beam cross section on *DIF* vs. chord rotation demand response curve: a) joints with 2 rows of M20 bolts; b) joints with 2 rows of M24 bolts

The discontinuity observed in Figure 6.23 for the cases with HEA 500 beam corresponds to the premature failure of the upper bolt row while the assembly is still in the compressive arching stage. These results show that increasing the dimensions of the beam cross section the *DIF* reduces when the rotation demand increases. Moreover, *DIF* values at joint failure significantly vary (i.e. from 1.5 to 2.5), depending on the geometrical and mechanical features of the connection.

### 6.3.2 Monotonic column loss action – weak axis column configuration

#### 6.3.2.1 General response

The FEP joints with weak axis column configuration (see Figure 6.2b)) exhibit a non-linear performance similar to the corresponding joints with strong axis column configuration (see Figure 6.2a)). Indeed, the differences are basically due to the different contributions of the column to the chord rotation, since the column web panel behaves almost elastically under the localized transverse bending in all examined cases and considering that the damage pattern is basically concentrated into the connection.



In the CW joints the column is less stiff than in CS joints and the overall effect results in slightly larger chord displacement capacity of the joint assembly. In addition, another source of deformability relies on the welded T-stub connecting the beam to the column web, which exhibits some localised plastic deformations in the zone where it is welded to the column web, as depicted in Figure 6.24.

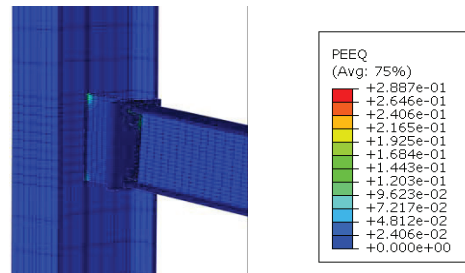


Figure 6.24: Deformed shape and PEEQ at 90 mrad chord rotation for R2-D24-T16-SI360-CW joint

### 6.3.2.2 Influence of beam profile

The influence of the beam cross section is shown in Figure 6.25 for the bigger (i.e. M24) and smaller (i.e. M16) bolts and for 12 mm thick end-plate. Similarly to the case with strong axis column, the joints with shallow and compact beams (i.e. IPE220) experience the lower ductility  $\theta/\theta_{p+A}$  at joint failure, but the higher flexural strength  $M/M_p$ , while the opposite results are observed for the joints with deeper beams (i.e. HEA 500). In addition, the comparison between Figure 6.25a) and Figure 6.25b) clearly shows that increasing bolt diameter from 16mm to 24mm increases the joint robustness under column loss.

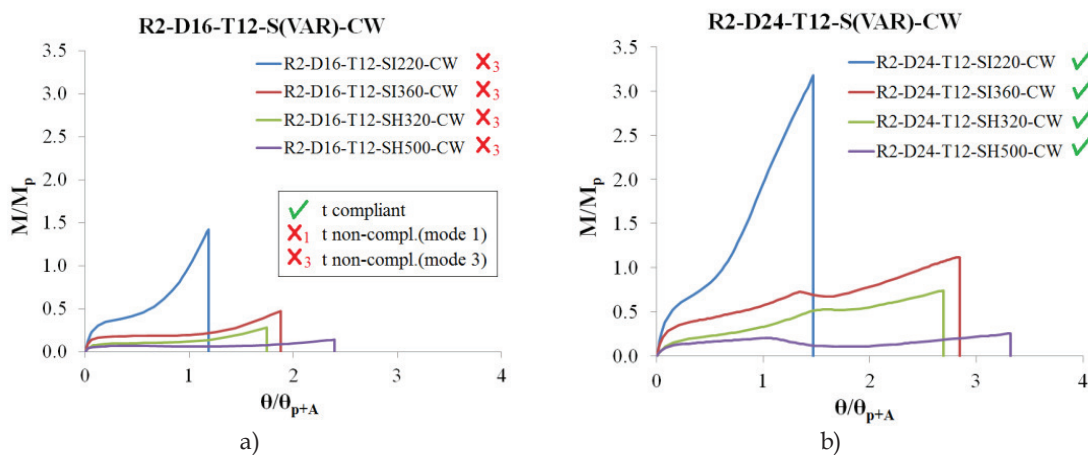


Figure 6.25: Influence of beam cross section on normalised connection moment-rotation response curve of R2-T12-CW joints : a) M16 bolt assemblies; b) M24 bolt assemblies

6.3.2.3 Influence of end-plate thickness

For the FEP joints with weak axis column configuration, the influence of end-plate thickness is negligible for the joint assemblies with the smaller bolts (i.e. M16), because of the failure mode type 3 of the relevant connections (see Figure 6.26a,b)).

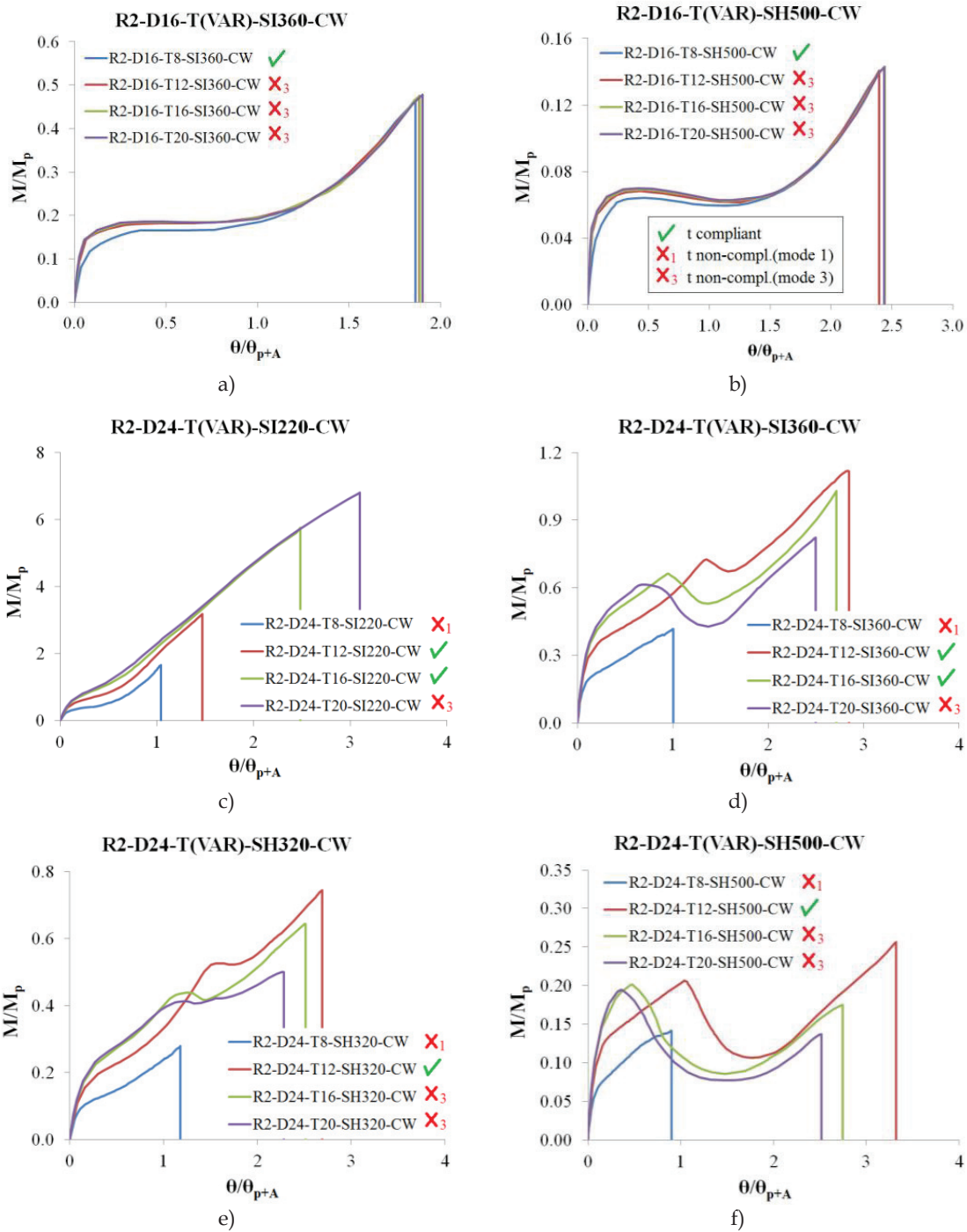


Figure 6.26: Influence of end-plate thickness on R2-CW joints with: a) M16 bolts and IPE 360 beam; b) M16 bolts and HEA 500 beam; c) M24 bolts and IPE 220 beam; d) M24 bolts and IPE 360 beam; e) M24 bolts and HEA 320 beam; f) M24 bolts and HEA 500 beam

For the  $t = 8\text{mm}$  configuration, the end-plate displayed reduced plasticity, for which reason its moment-rotation response and ultimate rotation capacity is similar to other joints that displayed mode 3 failure.

The influence of end-plate thickness is more evident for M24 bolts, where the bolt is sufficiently resistant to mobilise the full strength of end-plate. As for the CS cases, joint performance is generally maximized joints with end-plate thickness values compliant with Eq.(6.11) and Eq.(6.13), as shown in Figure 6.26d),e),f). The maximum normalised connection rotation capacities  $\theta/\theta_{p+A}$  at joint failure for the cases with IPE 220, IPE 360, HEA 320 and HEA 500 beam are equal to 3.1, 2.8, 2.7 and 3.3, which correspond to connection rotations equal to 253 mrad, 205 mrad, 201 mrad and 229 mrad respectively.

#### 6.3.2.4 Influence of bolts

Regarding the influence of bolt diameter and number of bolt rows, numerical results indicate that increasing the number of bolt rows significantly increases resistance and the rotation capacity, as shown in Figure 6.27. It is also interesting to compare Figure 6.19 and Figure 6.20 to Figure 6.27, where it can be observed that CW joints experience twice larger displacement capacity at failure than CS joints. This feature depends on both the larger elastic rotation of the column and the plastic contribution of the welded T-stub constituting the connection.

It is also worth noting that CW joints with HEA500 beam are less affected by arching mechanism as respect to the corresponding CS assemblies, with also larger ductility and flexural overstrength due to catenary action developing since the beginning of the nonlinear response.

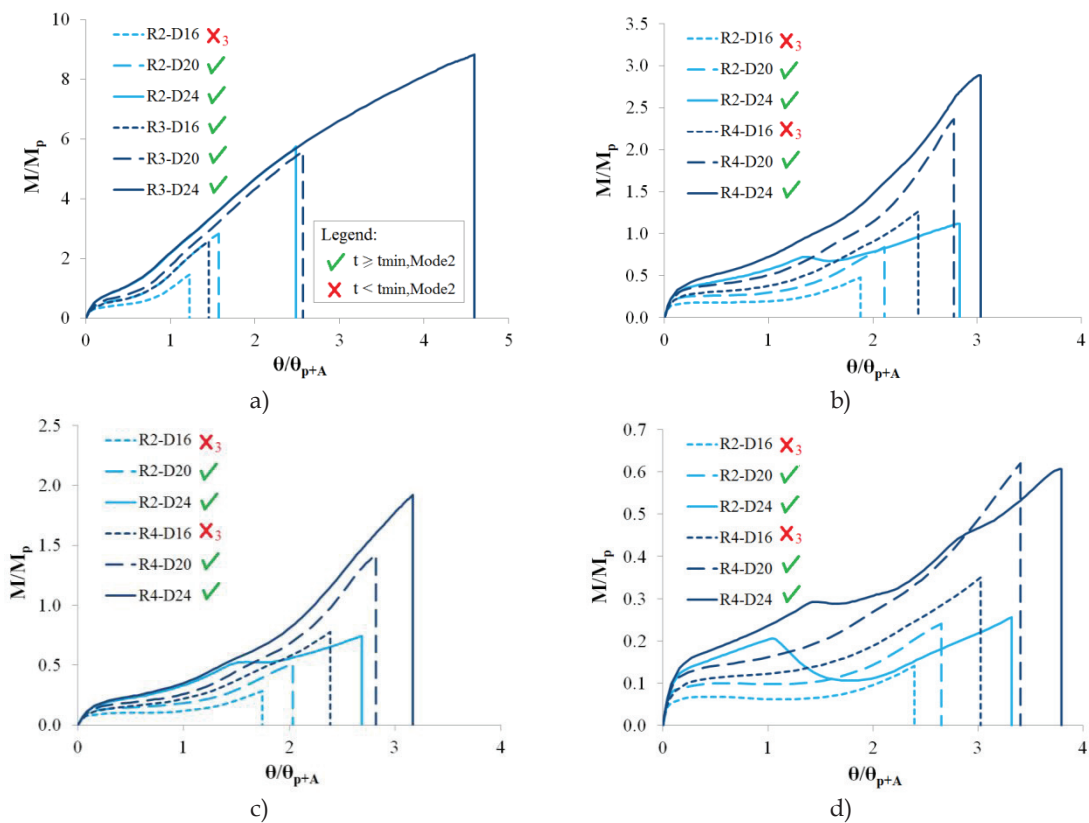


Figure 6.27: Influence of bolt diameter and number of bolt rows on normalised connection moment-rotation: a) IPE 220 beam section and end-plate thickness  $t=16\text{mm}$ ; b) IPE 360 beam and end-plate thickness  $t=12\text{mm}$ ; c) HEA 320 beam and end-plate thickness  $t=12\text{mm}$ ; d) HEA 500 beam and end-plate thickness  $t=12\text{mm}$

### 6.3.3 Cyclic bending followed by monotonic column loss action

The results here presented and discussed focus on two aspects of FEP joint response, namely: i) response to cyclic actions; ii) post cyclic response to column loss action. Regarding the former, performance assessment is discussed in terms of performance levels, to determine which joint configurations are capable of sustaining rotation demands compatible with global structural deformation under seismic action. Results regarding post seismic column loss are presented and compared to the undamaged joint performance of CS type joints (see Table 6.1) shown in Section 6.3.1 and in Cassiano *et al.* (2016), hence enabling to quantify the robustness reduction induced by the cyclic bending action.

### 6.3.3.1 Response to cyclic bending action

The cyclic joint response was found to vary with joint configurations, due to the development of different T-stub modes which mobilise different joint components. For increasing rotational demands, stiffness is progressively reduced due to the overcoming bolt preload and to the spread of plasticity. Adopting thin endplates induces T-stub mode 1 deformation, characterized by significant plasticity in the endplate zone and large hysteretic loops. Instead, thicker endplates shift response to modes 2 and 3, in which bolts are plasticized. The transition in hysteretic behaviour is shown in Figure 6.28a), where the Components Method (CEN, 2005) predicts mode 1 failure for  $t=8\text{mm}$ , mode 2 for  $t=12\text{mm}$  and  $t=16\text{mm}$ , and mode 3 for the  $t=20\text{mm}$  case. Premature plate fracture initiation was found to occur in many cases with thin endplates and wide bolt horizontal pitch. This was the case for 8 and 12 mm plates in Figure 6.28a), in which beam-endplate weld zone fracture was verified, limiting joint rotation to around 20 and 30 mrad, respectively. Joints in mode 3 were found to display low energy dissipation capacity, due to plasticisation being concentrated in the bolts (some plasticisation was also verified in the welds). Tensile forces coupled with bending action induced by endplate-bolt rotation compatibility were found to lead to partial bolt plasticisation (see Figure 6.28b), hence yielding low hysteretic energy dissipation. The thickness criteria compliant joint in this case is seen to display some energy dissipation capacity.

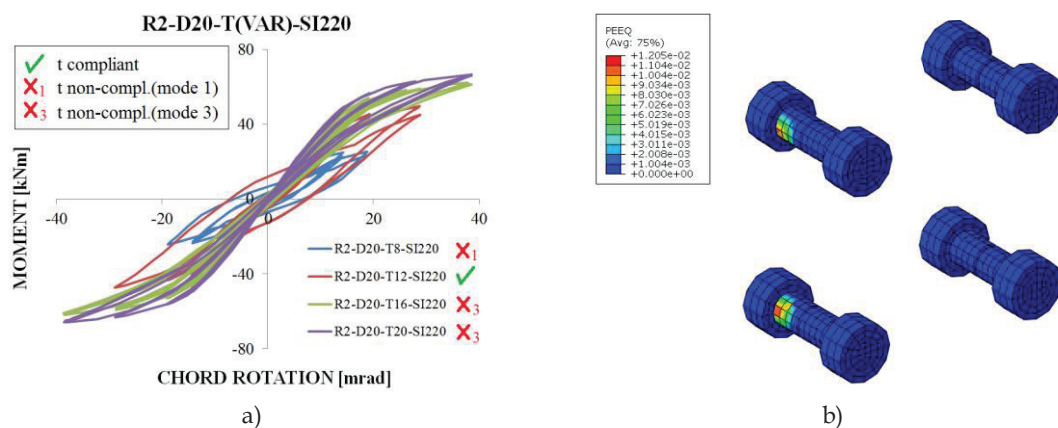


Figure 6.28: Cyclic joint response for the R2-D20-SI220 joints: a) moment - chord rotation response for varying endplate thickness; b) partial bolt plasticisation in mode 3 for the  $t=20\text{mm}$  endplate at the end of the cyclic loading protocol

### 6.3.3.1.1 Influence of endplate thickness

The endplate thickness was found to be a key factor in determining the T-sub behaviour and joint hysteretic response. Although thin endplates lead to T-stub mode 1 response, with significant energy dissipation and large hysteretic loops, elevated endplate flexibility also led to high stress concentrations in the beam flange-endplate weld zone (see Figure 6.29). This early fracture prevented these joints from resisting the full cyclic loading protocol. Conversely, thicker endplates can reduce endplate - beam flange rotation, reducing concentrated stresses and preventing fracture initiation.

Significant hardening behaviour was displayed by 8mm thick endplate joints, due to the nonlinear hardening effect of the S355. The effect of endplate thickness on joints with 2 bolt rows and IPE 360 beam cross section is presented in Figure 6.30 for the M16 and M20 bolt assemblies.

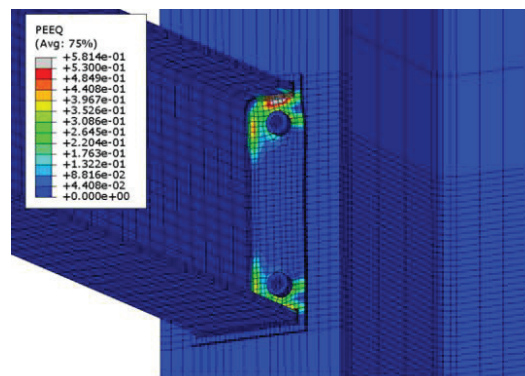


Figure 6.29: PEEQ distribution at plate fracture initiation - R2-D20-T8-SI360 joint

The results for M16 assemblies in Figure 6.30a) show early fracture for the 8mm case, limiting connection rotation at 27 mrad. For  $t \geq 12\text{mm}$ , bolts sustain plastic elongation and resistance drops to zero following load reversal. At high rotational demand, softening occurs and for the  $t=20\text{mm}$  case (T-stub in mode 3) it is coupled with early bolt failure at 10.3 mrad.

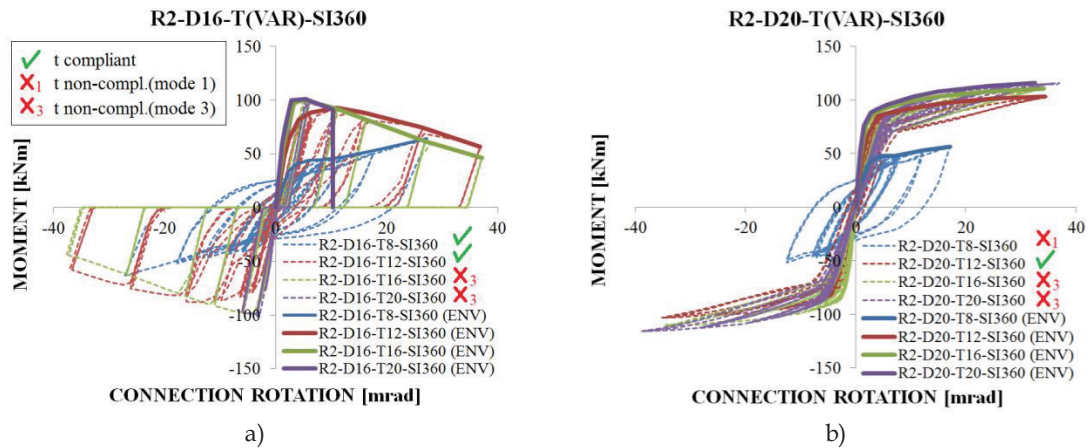


Figure 6.30: Effect of endplate thickness on R2-SI360 joints : Moment - connection rotation and cyclic envelope curves: a) M16 bolt assemblies; b) M20 bolt assemblies

For the M20 assemblies, Figure 6.30b) shows that for  $t=8\text{mm}$ , rotation capacity is further reduced with respect to the corresponding M16 case, with crack initiation at 17 mrad. For joints in T-stub modes 2 and 3 ( $t>8\text{mm}$ ), energy dissipation is small, since bolt plasticization is partial and involves a small material volume (see Figure 6.28b). The M24 assemblies displayed similar behaviour. The comparison between M16 and M20 in Figure 6.30 graphs shows no softening for the M20 case. Bending resistance predictions according to EN 1993-1-8 (CEN, 2005) were found to be accurate for joints in T-stub modes 1 and 2, whereas for mode 3 cases, resistance was lower than predicted. This is ascribable to bolts being subjected to combined bending and axial force (see Figure 6.28b), whereas the prediction is based on pure tensile resistance instead. In general, for joints with M16 bolts, adopting thicker endplates leads to bolt softening at high rotational demands, for which case resistance was found to be lower than the EN 1993-1-8 (CEN, 2005) prediction. This suggests that not accounting for bolt softening in FEP joint design may be contrary to safety at high rotational demands and for the case of small bolt diameter. The ductility criterion compliant joints are seen here to be able to resist the cyclic loading without bolt failure, although limited rotation capacity is available for the D16-T8 case due to early fracture initiation.

The moment-rotation envelope curves for joints with HEA 500 beam section and M16 and M20 bolts are presented in Figure 6.31. For the sake of clarity, a vertical drop to zero moment represents bolt failure and an interrupted curve without vertical drop is indicative of plate fracture initiation. Results for M16 assemblies show that only  $t=12\text{mm}$  and  $t=16\text{mm}$  joints were capable of sustaining rotations up to 40 mrad, albeit

associated with severe strength reduction to about 40% to 50% of predicted resistance. For M20 bolts,  $t=8\text{mm}$  and  $t=12\text{mm}$  joints are predicted in mode 1,  $t=16\text{mm}$  in mode 2 and  $t=20\text{mm}$  in mode 3. For  $t=8\text{mm}$ , fracture was initiated prior to hardening onset, at  $M/M_{j,EC3}=1.07$ ; for  $t=12\text{mm}$ , a ratio  $M/M_{j,EC3}=0.97$  was obtained; the  $t=16\text{mm}$  and  $t=20\text{mm}$  cases displayed  $M/M_{j,EC3}$  ratio values of 0.89 and 0.75, respectively. These ratios are smaller than 1 due to the fact that bolts are only partially plasticized. This stands in contrast with the prediction assumption of uniform tensile stress  $f_{u,b}$  in the effective bolt shank area. The D16 criteria compliant joint in Figure 6.31a) is seen to display a performance in line with expected resistance levels but is limited by weld fracture initiation, pointing to the fact that improving weld detailing could also improve joint resistance, enabling it to withstand up to 40 mrad chord rotations. The criteria compliant joint in Figure 6.31b) displayed very good behaviour in terms of both resistance, which is seen to be in line with EC3 prediction, but also sufficient rotation capacity to withstand the imposed cyclic loading.

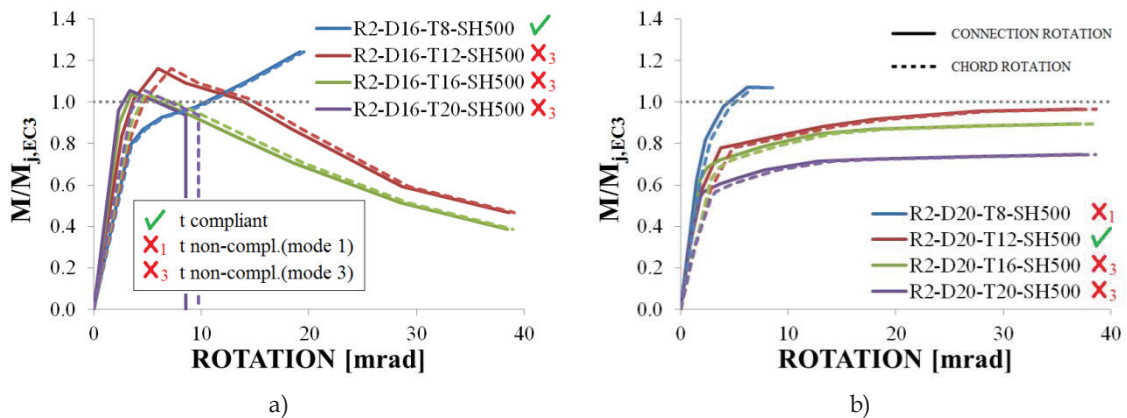


Figure 6.31: Effect of endplate thickness on R2-SH500 joints : Cyclic envelope curves - bending moment normalised to EC3 prediction versus connection rotation: a) M16 bolt assemblies; b) M20 bolt assemblies

For other beam cross sections with M16 bolts, early plate failure was verified for all  $t=8\text{mm}$  cases and also for the IPE 220 with a  $t=12\text{mm}$ . Indeed the large bolt horizontal pitch to beam flange width resulted in high stress concentration at the intersection between the tip of the beam flange and the endplate, leading to premature joint failure. In this sense, although joints with large bolt horizontal pitch may display an efficient behaviour under monotonic column loss as seen in Section 6.3.1 and in Cassiano *et al.* (2016) due to local catenary effect, when subjected to cyclic actions, premature fracture occurs and limits joint performance. In general, endplate thickness



influences the suitability of FEP joints to withstand cyclic actions. In this sense, the required rotational demand should be taken into account for the joint design namely by selecting an appropriate endplate thickness. Simply choosing a thicker endplate may present the disadvantage of not enabling hysteretic energy dissipation.

### 6.3.3.1.2 Influence of bolt diameter

The influence of bolt diameter on joint response is coupled with the endplate thickness, since these variables determine the T-stub mode. As shown in Figure 6.32 and Figure 6.33 for joints with IPE 360 and HEA 320 beams respectively, for the cases of  $t=8\text{mm}$  and  $t=8\text{mm}$ , increasing bolt diameter leads to higher resistance coupled with a rotation capacity reduction, namely when increasing from M20 to M24 assemblies. No rotation capacity reduction owing to fracture initiation was verified for  $t>12\text{mm}$ . Bolt failure was verified only for the R2-D16-T20-SI360 joint case.

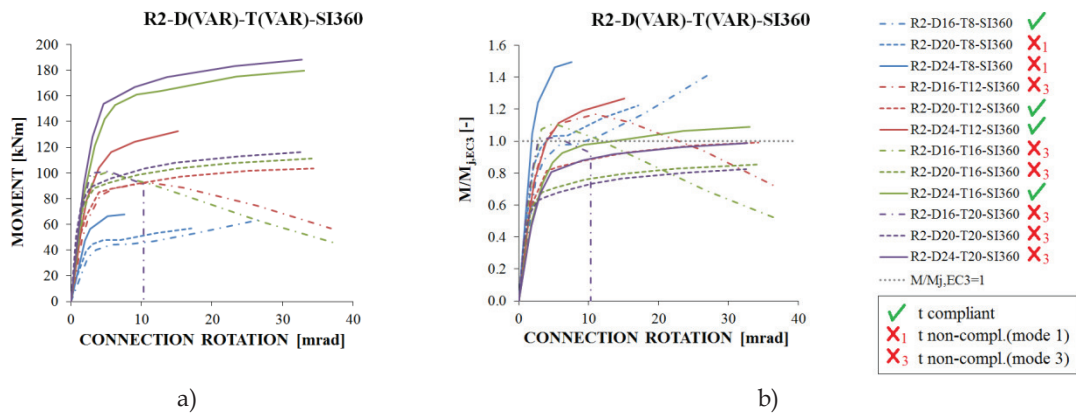


Figure 6.32: Effect of bolt diameter on the cyclic envelope curves of R2-SI360 joints: a) moment – connection rotation; b) bending moment normalised to EC3 prediction vs. connection rotation

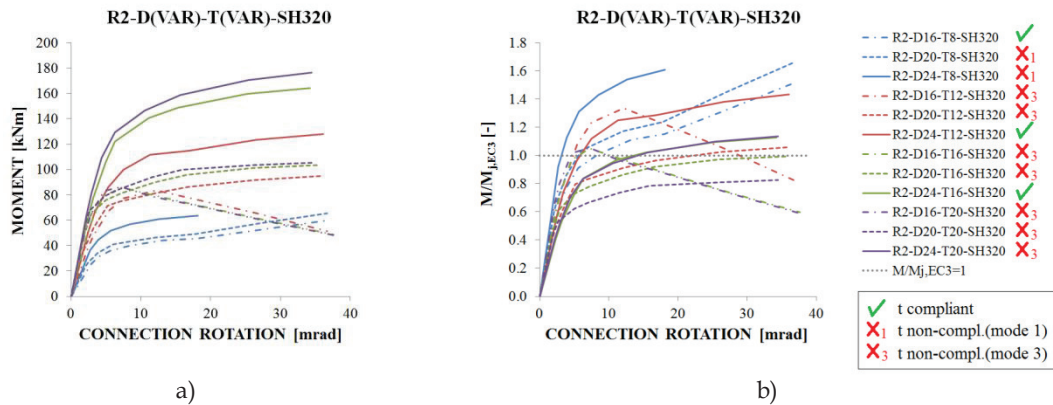


Figure 6.33: Effect of bolt diameter on the cyclic envelope curves of R2-SH320 joints: a) moment – connection rotation; b) bending moment normalised to EC3 prediction vs. connection rotation

In terms of strength ratios  $M/M_{j,EC3}$ , results show that values close to or slightly higher than 1 are obtained in most cases, which indicates that the EN 1993-1-8 (CEN, 2005) prediction leads to safe resistance-wise design. This was however not the case for joints with M16 bolts, which display significant softening leading to  $M/M_{j,EC3} < 1$  at 40 mrad chord rotation, potentially leading to unsafe design. This can be avoided by designers by adopting bolt assemblies with higher nominal diameters when designing FEP joints for seismic actions. For the other case in which bending resistance was lower than the predicted value, namely for M20 assemblies with 16 or 20mm thick endplates, bolts were found to be partially plasticized. However, when transitioning from M20 to M24 bolts, the strength increase compensates for this effect and the  $M/M_{j,EC3}$  ratio values at 40 mrad are close to 1. The evaluation of the plasticity distribution in the bolt shank requires however further testing, namely experimental, to confirm these findings.

Criteria compliant joints in Figure 6.32 and Figure 6.33 are seen to generally display adequate rotation capacity and strength levels in line with EC3 predicted resistance, whenever weld fracture initiation does not occur.

#### 6.3.3.1.3 Influence of bolt rows

Adopting additional bolt rows was shown to stabilise joint response due to the redistribution of internal forces after the yielding of the first bolt row. For M16 bolts, increasing from 2 to 4 bolt rows reduces softening, namely up to about 20 mrad, while providing for increases in strength for all values of rotational demand, as shown in Figure 6.34. Although joints with M24 bolts are seen to display reduced rotation capacity as seen in Figure 6.33b), the effect of increasing the number of bolt rows is positive both in terms of strength and rotation capacity. The results show that joints respecting the proposed ductility criterion, namely those using M24 bolts, may be especially affected by early weld fracture initiation due to the higher rotation demand on the end-plates, resulting in higher stress concentrations in the welds.

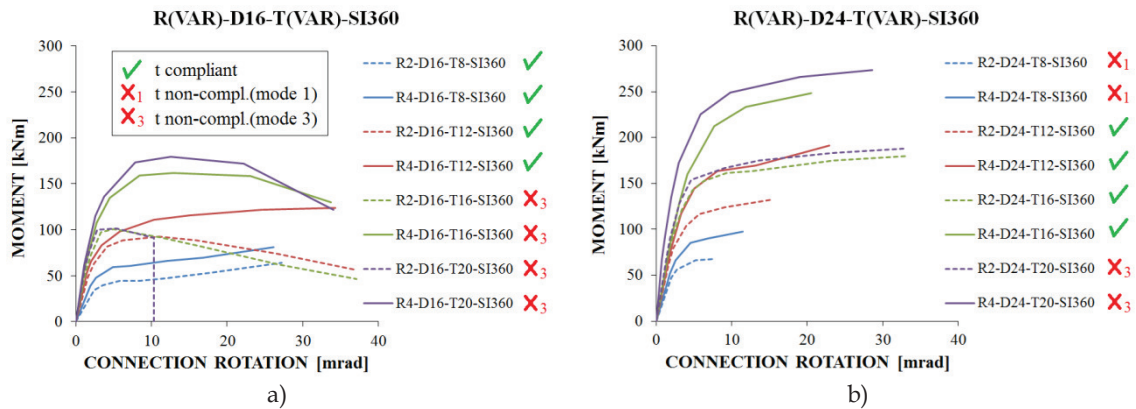


Figure 6.34: Effect of number of bolt rows on the cyclic envelope curves of joints with IPE 360 beam sections: a) M16 bolt assemblies; b) M24 bolt assemblies

#### 6.3.3.1.4 Performance levels

Secondary structure beam-column joints are required to comply with displacement acceptance criteria. The EN 1998-1 (CEN, 2004) states that the secondary structure connections should maintain resistance while accommodating for the displacements induced by seismic action; however this code also limits the lateral stiffness contribution of these elements, so that the hypotheses of disregarding secondary structure strength and stiffness remain valid. It is thus important to assess which FEP joint configurations can avoid premature failure while assuring nominally pinned behaviour according to the EN 1993-1-8 (CEN, 2005) classification limits. To this end, joint response was classified using performance levels, in order to provide for an understanding of strength and stiffness evolution for increasing rotational demand. To quantify joint stiffness degradation, the stiffness ratio between the joint secant stiffness at chord rotation  $\theta$  and the initial joint stiffness prediction according to the EC3 [5] were computed for  $\theta$  equal to 0%, 1%, 2%, 3% and 4%. The stiffness ratios were computed for the secant stiffness displayed at the first cycle for each  $\theta$  value.

Analysis results were divided into 5 performance levels STF1 through STF5 (see definition in Table 6.5). The results for joints with 2 bolt rows are presented in Table 6.5, showing that stiffness degradation is more severe for configurations with small bolt diameter combined with thick endplates, typically yielding performance level STF5 at 3% chord rotation (i.e.  $S_{sec,\theta, chord}/S_{j,ini,EC3} < 0.2$ ). Indeed, joints with M16 bolts tend to display less than 20% of the initial predicted stiffness at  $\theta=4\%$ . For joints with M20 bolts, several cases of STF4 at  $\theta=4\%$  rotation were reported, namely for the larger beam

sections within the IPE or HEA types. For joints with M24 bolts, STF4 performance level at  $\theta=3\%$  and  $\theta=4\%$  highlight the importance of adopting larger bolts for retaining some degree of the initial stiffness under cyclic actions.

Table 6.5: Stiffness ratios, classification and performance levels – joints with 2 bolt rows

R	D	T	S	Stiffness Ratio					Stiffness Classification				
				$S_{j,sec,\theta, chord} / S_{j,ini, EC3}$					$S_{j,sec,\theta, chord} / S_{j,pin, EC3}$				
-	-	-	-	$\theta=0\%$	$\theta=1\%$	$\theta=2\%$	$\theta=3\%$	$\theta=4\%$	$\theta=0\%$	$\theta=1\%$	$\theta=2\%$	$\theta=3\%$	$\theta=4\%$
2	8	1220	I220	0.96	0.72	0.42	0.31	0.25	7.19	5.37	3.14	2.31	1.86
			I360	0.85	0.40	0.24	0.19	0.16	4.54	2.13	1.27	1.03	0.87
			H320	1.73	1.00	0.57	0.44	0.38	2.38	1.38	0.78	0.60	0.52
			H500	1.10	0.49	0.31	0.00	0.00	1.34	0.60	0.38	0.00	0.00
	12	1220	I220	0.76	0.65	0.47	0.33	0.00	9.33	8.02	5.73	4.02	0.00
			I360	0.79	0.52	0.26	0.14	0.08	6.48	4.27	2.14	1.19	0.68
			H320	1.32	0.96	0.48	0.28	0.16	3.65	2.65	1.32	0.76	0.45
			H500	1.01	0.47	0.19	0.09	0.05	2.43	1.14	0.46	0.21	0.12
	16	1220	I220	0.70	0.62	0.50	0.36	0.24	10.21	9.05	7.32	5.25	3.55
			I360	0.80	0.57	0.21	0.11	0.06	7.43	5.28	1.97	0.99	0.56
			H320	1.22	0.81	0.35	0.19	0.11	4.41	2.93	1.27	0.68	0.42
			H500	1.00	0.38	0.14	0.07	0.04	3.01	1.14	0.42	0.21	0.12
	20	1220	I220	0.71	0.63	0.54	0.36	0.22	10.92	9.81	8.29	5.59	3.37
			I360	0.82	0.52	0.00	0.00	0.00	7.90	5.08	0.00	0.00	0.00
			H320	1.21	0.74	0.31	0.17	0.10	4.85	2.95	1.23	0.68	0.41
			H500	0.98	0.34	0.00	0.00	0.00	3.22	1.13	0.00	0.00	0.00
	20	1220	I220	1.04	0.82	0.48	0.00	0.00	7.98	6.28	3.69	0.00	0.00
			I360	1.02	0.45	0.24	0.00	0.00	5.73	2.52	1.38	0.00	0.00
			H320	2.00	1.10	0.60	0.47	0.40	2.81	1.55	0.85	0.66	0.57
			H500	1.63	0.58	0.00	0.00	0.00	1.92	0.69	0.00	0.00	0.00
	20	12	I220	0.76	0.69	0.50	0.37	0.00	9.82	8.93	6.47	4.75	0.00
			I360	0.83	0.52	0.27	0.19	0.14	7.25	4.52	2.36	1.64	1.27
			H320	1.45	0.95	0.51	0.36	0.28	4.20	2.76	1.49	1.06	0.82
			H500	1.24	0.49	0.25	0.18	0.13	3.14	1.23	0.64	0.44	0.34
	20	16	I220	0.69	0.64	0.50	0.39	0.29	10.70	9.96	7.76	6.12	4.52
			I360	0.81	0.49	0.25	0.19	0.14	8.11	4.88	2.55	1.88	1.35
			H320	1.29	0.73	0.43	0.30	0.23	4.98	2.84	1.65	1.17	0.89
			H500	1.03	0.39	0.21	0.14	0.11	3.34	1.25	0.68	0.46	0.35
	20	1220	I220	0.67	0.57	0.48	0.37	0.28	11.17	9.56	8.04	6.20	4.74
			I360	0.82	0.45	0.25	0.18	0.14	8.59	4.75	2.66	1.87	1.47
			H320	1.21	0.69	0.41	0.28	0.22	5.22	2.96	1.78	1.19	0.94
			H500	1.17	0.38	0.20	0.13	0.10	4.19	1.36	0.72	0.47	0.36
	24	8	I220	1.17	1.02	0.62	0.00	0.00	9.03	7.88	4.77	0.00	0.00
			I360	1.12	0.57	0.00	0.00	0.00	6.36	3.25	0.00	0.00	0.00
			H320	2.44	1.37	0.76	0.00	0.00	3.47	1.94	1.08	0.00	0.00
			H500	1.53	0.00	0.00	0.00	0.00	1.92	0.00	0.00	0.00	0.00
	24	12	I220	0.78	0.76	0.61	0.43	0.00	10.38	10.07	8.06	5.68	0.00
			I360	0.88	0.63	0.35	0.00	0.00	7.96	5.72	3.18	0.00	0.00
			H320	1.61	1.15	0.66	0.47	0.37	4.77	3.41	1.96	1.40	1.09
			H500	1.20	0.61	0.00	0.00	0.00	3.13	1.59	0.00	0.00	0.00
24	16	I220	0.69	0.68	0.59	0.45	0.00	11.02	10.89	9.43	7.29	0.00	
		I360	0.82	0.67	0.40	0.27	0.21	8.60	7.04	4.25	2.80	2.16	
		H320	1.38	1.12	0.66	0.46	0.36	5.52	4.50	2.64	1.84	1.44	
		H500	1.10	0.60	0.34	0.23	0.18	3.72	2.04	1.13	0.77	0.59	
24	20	I220	0.66	0.65	0.58	0.46	0.36	11.39	11.32	10.07	8.04	6.33	
		I360	0.81	0.67	0.38	0.26	0.20	9.04	7.44	4.23	2.93	2.26	
		H320	1.33	1.04	0.61	0.43	0.34	5.97	4.70	2.74	1.94	1.52	
		H500	1.07	0.56	0.31	0.23	0.17	4.05	2.11	1.18	0.86	0.63	

Stiffness Performance Levels

Colour	Level	$S_{sec,\theta, chord} / S_{j,ini, EC3}$
White	STF1	>1.00
Light Blue	STF2	0.80-1.00
Medium Blue	STF3	0.50-0.80
Dark Blue	STF4	0.20-0.50
Black	STF5	0.00-0.20

Stiffness Classification

Colour	Classification	$S_{sec,\theta, chord} / S_{j,pin, EC3}$
Light Grey	Semi rigid	>1.00
White	Nom, pinned	0.00-1.00
Black	Failure	0.00

Several cases of fracture initiation leading to joint failure ( $S_{j,sec,\theta,chord}/S_{j,ini,EC3}=0$ ) were seen to occur for joints with  $t=8\text{mm}$  endplates, highlighting the severity of the damage induced by the cyclic action which leads to reduced joint capacity. For joints with M24 bolts, response is characterized by smaller stiffness degradation, with most non-failed joints displaying performance level STF4 at 4% chord rotation. The stiffness of FEP joints at varying chord rotations was also compared to the stiffness limit provided in EN 1993-1-8 (CEN, 2005) so as to determine if FEP joints are capable of behaving as nominally pinned, as is typically assumed for structural design. Results in Table 6.5 show that joints undergo significant stiffness degradation, namely for joints with small bolt diameters.

Regarding joint stiffness classification according to EN 1993-1-8 (CEN, 2005), results showed that at low rotational demand, joint stiffness is typically much higher than the semi rigid - nominally pinned stiffness threshold, implying that FEP joints generally behave as semi-rigid at low  $\theta$ . Instead, for increasing rotation demand, stiffness degradation leads to  $S_{j,sec,\theta,chord}/S_{j,pin,EC3}$  ratios closer to 1 (i.e. nominally pinned). This is more evident for joints with M16 bolts, which display higher stiffness degradation, than for the M20 and M24 cases, which tend to behave semi-rigid joints, even at  $\theta=4\%$ . Results also show that joints with smaller beam cross sections are more prone to behaving as semi-rigid, whereas those with larger beam sections tend to behave as nominally pinned.

Results for R4 joints (3 rows for the IPE 220 case) are presented in Table 6.6, highlighting the reduction in stiffness degradation due to the additional bolt rows. Indeed, at  $\theta=4\%$  the majority of non-failed joints display performance level STF4 (i.e.  $0.2 < S_{j,sec,\theta,chord}/S_{j,ini,EC3} < 0.5$ ). Regarding stiffness classification,  $S_{j,sec,\theta,chord}/S_{j,pin,EC3}$  ratios are higher for the R4 cases, which have higher propensity to behave as semi-rigid joints.

Table 6.6: Stiffness ratios, classification and performance levels – joints with 4 bolt rows

R	D	T	S	Stiffness Ratio					Stiffness Classification					
				$S_{j,sec,\theta,chor,d}/S_{j,ini,EC3}$					$S_{j,sec,\theta,chor,d}/S_{j,pin,EC3}$					
				$\theta=0\%$	$\theta=1\%$	$\theta=2\%$	$\theta=3\%$	$\theta=4\%$	$\theta=0\%$	$\theta=1\%$	$\theta=2\%$	$\theta=3\%$	$\theta=4\%$	
4*	20	16	8	I220	1.04	0.82	0.48	0.35	0.00	7.33	5.81	3.36	2.47	0.00
				I360	1.03	0.58	0.33	0.25	0.00	5.29	2.96	1.67	1.30	0.00
				H320	2.01	1.18	0.68	0.53	0.44	2.49	1.47	0.84	0.65	0.54
				H500	1.37	0.66	0.39	0.00	0.00	1.56	0.76	0.45	0.00	0.00
			12	I220	0.78	0.69	0.53	0.37	0.27	9.33	8.28	6.38	4.39	3.27
				I360	0.88	0.60	0.35	0.24	0.19	7.03	4.78	2.79	1.95	1.48
				H320	1.47	1.10	0.61	0.44	0.32	3.77	2.82	1.57	1.11	0.82
				H500	1.17	0.68	0.35	0.22	0.15	2.72	1.58	0.81	0.51	0.35
			16	I220	0.71	0.65	0.55	0.41	0.30	10.28	9.35	7.86	5.86	4.39
				I360	0.85	0.70	0.43	0.28	0.17	7.80	6.47	3.94	2.53	1.56
				H320	1.34	1.09	0.66	0.46	0.32	4.57	3.71	2.25	1.55	1.08
				H500	1.14	0.72	0.33	0.19	0.08	3.35	2.11	0.98	0.57	0.24
			20	I220	0.70	0.64	0.56	0.42	0.31	10.79	9.89	8.68	6.48	4.84
				I360	0.85	0.73	0.44	0.29	0.15	8.23	7.03	4.30	2.78	1.47
				H320	1.31	1.03	0.68	0.46	0.28	5.04	4.00	2.64	1.77	1.08
				H500	1.13	0.68	0.30	0.16	0.07	3.66	2.21	0.97	0.52	0.23
			8	I220	1.10	0.96	0.54	0.00	0.00	7.94	6.91	3.91	0.00	0.00
				I360	1.14	0.63	0.35	0.00	0.00	5.97	3.29	1.85	0.00	0.00
				H320	2.24	1.31	0.75	0.60	0.00	2.81	1.65	0.95	0.75	0.00
				H500	1.48	0.73	0.00	0.00	0.00	1.71	0.84	0.00	0.00	0.00
			12	I220	0.77	0.74	0.57	0.41	0.00	9.62	9.22	7.06	5.06	0.00
				I360	0.90	0.68	0.40	0.00	0.00	7.47	5.69	3.30	0.00	0.00
				H320	1.70	1.23	0.71	0.49	0.38	4.36	3.14	1.83	1.27	0.97
				H500	1.28	0.71	0.38	0.27	0.20	3.07	1.70	0.91	0.65	0.49
			16	I220	0.70	0.67	0.56	0.44	0.34	10.62	10.15	8.50	6.67	5.11
				I360	0.86	0.68	0.44	0.31	0.24	8.27	6.56	4.19	3.00	2.30
				H320	1.45	1.06	0.73	0.51	0.37	5.13	3.76	2.59	1.80	1.32
				H500	1.14	0.69	0.39	0.27	0.21	3.51	2.11	1.19	0.84	0.64
			20	I220	0.68	0.65	0.56	0.43	0.34	11.10	10.57	9.20	7.02	5.50
				I360	0.85	0.68	0.44	0.31	0.24	8.66	6.98	4.53	3.20	2.45
				H320	1.34	1.02	0.69	0.51	0.39	5.44	4.13	2.79	2.07	1.58
				H500	1.27	0.64	0.38	0.26	0.20	4.37	2.20	1.32	0.90	0.69
			8	I220	1.25	1.17	0.73	0.00	0.00	9.12	8.59	5.37	0.00	0.00
				I360	1.31	0.82	0.00	0.00	0.00	6.94	4.33	0.00	0.00	0.00
				H320	2.88	1.69	0.94	0.00	0.00	3.62	2.13	1.18	0.00	0.00
				H500	1.90	0.00	0.00	0.00	0.00	2.22	0.00	0.00	0.00	0.00
			12	I220	0.82	0.80	0.65	0.48	0.00	10.37	10.21	8.30	6.14	0.00
				I360	0.97	0.82	0.50	0.36	0.00	8.23	6.94	4.24	3.07	0.00
				H320	1.84	1.39	0.81	0.59	0.47	4.93	3.73	2.15	1.59	1.25
				H500	1.42	0.85	0.45	0.00	0.00	3.47	2.08	1.10	0.00	0.00
			16	I220	0.71	0.71	0.63	0.48	0.00	10.95	10.95	9.82	7.51	0.00
				I360	0.89	0.81	0.57	0.41	0.00	8.78	8.00	5.59	4.05	0.00
				H320	1.56	1.29	0.86	0.62	0.47	5.65	4.68	3.13	2.25	1.71
				H500	1.28	0.87	0.51	0.35	0.26	4.04	2.75	1.60	1.09	0.83
			20	I220	0.67	0.67	0.61	0.49	0.40	11.35	11.34	10.28	8.23	6.68
				I360	0.87	0.79	0.57	0.40	0.31	9.10	8.33	5.98	4.26	3.28
				H320	1.46	1.24	0.90	0.66	0.50	6.07	5.14	3.73	2.73	2.09
				H500	1.24	0.86	0.52	0.37	0.28	4.37	3.05	1.85	1.30	1.00

Stiffness Performance Levels

Colour	Level	$S_{j,sec,\theta,chor,d}/S_{j,ini,EC3}$
White	STF1	>1.00
Light Blue	STF2	0.80-1.00
Medium Blue	STF3	0.50-0.80
Dark Blue	STF4	0.20-0.50
Black	STF5	0.00-0.20

Stiffness Classification

Colour	Classification	$S_{j,sec,\theta,chor,d}/S_{j,pin,EC3}$
Light Grey	Semi rigid	>1.00
White	Nom. pinned	0.00-1.00
Black	Failure	0.00

\*) 3 bolt rows in the case of IPE 220 sections

The evolution of joints bending strength under cyclic action was quantified using strength ratios  $M_{\theta, chord}/M_{j, EC3}$ , that measure the relation between the resistance of the first cycle at rotation  $\theta$  and the resistance prediction according to the EN 1993-1-8 (CEN, 2005), and that were subsequently divided according to strength levels STR1 through STR5 (see definition in Table 6.7). Additionally, strength classification with respect to partial strength - nominally pinned strength threshold from EN 1993-1-8 (CEN, 2005) was computed using the ratio  $M_{j, sec, \theta}/M_{j, pin, EC3}$ , where  $M_{j, sec, \theta}$  is the joint strength at rotation demand  $\theta$ , and  $M_{j, pin, EC3}$  is the strength threshold.

Results in Table 6.7 show significant strength degradation for joints with small bolt diameters coupled with thick endplates. Indeed, for joints with M16 bolts and  $t \geq 16\text{mm}$ , strength reduction at  $\theta=4\%$  is considerable, highlighting that bolt softening effect reduces joint capacity, potentially leading to unsafe design. Fracture initiation condition was verified for several cases with thin endplates ( $t=8\text{mm}$ ), with the higher number of cases being verified for joints with higher bolt diameters, due to the higher rotational demand on plates. The best performance was obtained for joints with M20 bolts, which displayed fewer failure cases and also good correspondence with predicted strength at  $\theta=4\%$ , typically displaying levels STR1 and STR2. For M24 bolts, joints displayed  $M_{\theta, chord}/M_{j, EC3} > 1$  (performance level STR1) immediately prior to failure.

Joints with compact beam sections and large bolt diameters were found to be more prone to partial-strength behaviour. Joints with  $t=8\text{mm}$  generally behaved as nominally pinned ( $M_{j, sec, \theta}/M_{j, pin, EC3} < 1$ ) even at low rotation demands, whereas for  $t \geq 12\text{mm}$  the more compact IPE 220 and IPE 360 beam sections tended to behave as partial-strength, as opposed to HEA 320 and HEA 500 that displayed strength ratios lower than 1.

For 4 bolt row configurations, strength ratios at 3% and 4% rotational demand are higher when compared to 2 bolt row joints. In particular, significant improvement was verified for joints with M16 bolts, which were typically STR1 (excluding fracture initiation or bolt failure cases), showing that increasing the number of bolt rows improves joint performance for joints with small bolt diameter. For joint with M20 or M24 bolts, at  $\theta=4\%$ , strength ratios are in general greater than 1.




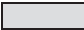






Table 6.7: Strength ratios, classification and performance levels – joints with 2 bolt rows

R	D	T	S	Strength Ratio				Strength Classification				
				$M_{\theta, \text{chord}}/M_{j, \text{Rm}, \text{EC3}}$				$M_{\theta, \text{chord}}/M_{j, \text{pin}, \text{EC3}}$				
				$\theta=1\%$	$\theta=2\%$	$\theta=3\%$	$\theta=4\%$	$\theta=1\%$	$\theta=2\%$	$\theta=3\%$	$\theta=4\%$	
2	20	8	I220	0.84	0.98	1.08	0.00	0.72	0.84	0.93	0.00	
			I360	0.98	1.17	1.41	0.00	0.47	0.56	0.68	0.00	
			H320	1.01	1.15	1.33	1.51	0.27	0.30	0.35	0.40	
			H500	0.97	1.24	0.00	0.00	0.18	0.23	0.00	0.00	
		12	I220	0.69	0.99	1.06	0.00	1.06	1.53	1.62	0.00	
			I360	1.11	1.12	0.94	0.72	0.94	0.94	0.79	0.60	
			H320	1.23	1.24	1.05	0.82	0.51	0.51	0.44	0.34	
			H500	1.09	0.87	0.59	0.47	0.35	0.28	0.19	0.15	
		16	I220	0.67	1.09	1.17	1.04	1.21	1.97	2.12	1.89	
			I360	1.11	0.91	0.69	0.51	1.06	0.87	0.66	0.49	
			H320	1.05	0.90	0.74	0.60	0.57	0.49	0.40	0.32	
			H500	0.95	0.70	0.51	0.39	0.35	0.26	0.19	0.14	
		20	I220	0.60	1.02	1.04	0.83	1.31	2.23	2.26	1.81	
			I360	1.02	0.00	0.00	0.00	1.07	0.00	0.00	0.00	
			H320	1.05	0.88	0.73	0.59	0.57	0.48	0.40	0.32	
			H500	0.94	0.00	0.00	0.00	0.34	0.00	0.00	0.00	
		24	8	I220	0.96	1.12	0.00	0.00	0.83	0.96	0.00	0.00
				I360	1.03	1.22	0.00	0.00	0.51	0.60	0.00	0.00
				H320	1.08	1.24	1.45	1.66	0.28	0.33	0.38	0.44
				H500	1.07	0.00	0.00	0.00	0.19	0.00	0.00	0.00
			12	I220	0.60	0.91	0.99	0.00	1.14	1.72	1.89	0.00
				I360	0.84	0.93	0.97	0.99	0.93	1.03	1.08	1.10
				H320	0.83	0.96	1.03	1.06	0.49	0.57	0.61	0.63
				H500	0.83	0.92	0.96	0.97	0.35	0.39	0.40	0.41
	16		I220	0.53	0.86	0.93	0.99	1.26	2.05	2.22	2.37	
			I360	0.71	0.80	0.83	0.85	0.98	1.10	1.14	1.18	
			H320	0.78	0.92	0.97	0.99	0.54	0.64	0.67	0.69	
			H500	0.79	0.87	0.88	0.90	0.38	0.41	0.42	0.43	
	20		I220	0.65	0.77	0.86	0.91	1.81	2.15	2.39	2.52	
			I360	0.68	0.77	0.80	0.82	1.02	1.15	1.20	1.23	
			H320	0.67	0.78	0.81	0.83	0.57	0.66	0.69	0.70	
			H500	0.67	0.72	0.74	0.75	0.39	0.42	0.42	0.43	
	8		I220	1.24	1.52	0.00	0.00	1.05	1.28	0.00	0.00	
			I360	1.49	0.00	0.00	0.00	0.72	0.00	0.00	0.00	
			H320	1.43	1.61	0.00	0.00	0.38	0.42	0.00	0.00	
			H500	0.00	0.00	0.00	0.00	0.00	0.00	0.00	0.00	
	12		I220	0.71	1.06	1.21	0.00	1.34	2.02	2.29	0.00	
			I360	1.19	1.27	0.00	0.00	1.32	1.41	0.00	0.00	
			H320	1.12	1.28	1.38	1.43	0.66	0.76	0.82	0.85	
			H500	1.15	0.00	0.00	0.00	0.48	0.00	0.00	0.00	
	16	I220	0.53	0.92	1.08	0.00	1.46	2.52	2.95	0.00		
		I360	0.86	0.99	1.06	1.09	1.51	1.74	1.86	1.91		
		H320	0.84	1.02	1.10	1.13	0.81	0.99	1.06	1.09		
		H500	0.94	1.02	1.07	1.09	0.62	0.68	0.71	0.72		
	20	I220	0.47	0.87	1.04	1.09	1.48	2.72	3.25	3.41		
		I360	0.81	0.92	0.96	0.99	1.63	1.85	1.95	2.00		
		H320	0.83	1.02	1.10	1.13	0.86	1.05	1.13	1.17		
		H500	0.91	1.00	1.05	1.08	0.64	0.71	0.74	0.76		

Strength Performance Levels			Strength Classification		
Colour	Level	$M_{\theta, \text{chord}}/M_{j, \text{Rm}, \text{EC3}}$	Colour	Classification	$M_{\theta, \text{chord}}/M_{j, \text{pin}, \text{EC3}}$
	STR1	>1.00		Semi rigid	>1.00
	STR2	0.80-1.00		Nom. pinned	0.00-1.00
	STR3	0.50-0.80		Failure	0.00
	STR4	0.20-0.50			
	STR5	0.00-0.20			

Table 6.8: Strength ratios, classification and performance levels – joints with 4 bolt rows

R	D	T	S	Strength Ratio				Strength Classification					
				$M_{\theta, \text{chord}}/M_{j, \text{Rm}, \text{EC3}}$				$M_{\theta, \text{chord}}/M_{j, \text{pin}, \text{EC3}}$					
				$\theta=1\%$	$\theta=2\%$	$\theta=3\%$	$\theta=4\%$	$\theta=1\%$	$\theta=2\%$	$\theta=3\%$	$\theta=4\%$		
-	-	-	-	-	-	-	-	-	-	-	-	-	-
		8	I220	0.58	0.68	0.73	0.00	0.78	0.91	0.98	0.00		
			I360	1.21	1.39	1.62	0.00	0.64	0.74	0.86	0.00		
			H320	0.54	0.61	0.72	0.80	0.29	0.32	0.38	0.42		
			H500	1.21	1.42	0.00	0.00	0.23	0.27	0.00	0.00		
		12	I220	0.67	0.97	1.08	1.06	1.10	1.60	1.78	1.74		
			I360	0.90	1.07	1.12	1.14	1.04	1.23	1.29	1.31		
			H320	1.08	1.20	1.28	1.26	0.55	0.61	0.65	0.64		
			H500	1.16	1.16	1.14	1.04	0.47	0.47	0.46	0.42		
		16	I220	0.60	1.01	1.13	1.10	1.26	2.12	2.37	2.31		
			I360	0.96	1.16	1.13	0.93	1.43	1.72	1.68	1.38		
			H320	0.95	1.21	1.25	1.16	0.69	0.88	0.91	0.84		
			H500	1.05	1.04	0.89	0.52	0.61	0.60	0.51	0.30		
		20	I220	0.52	0.91	1.02	1.01	1.33	2.33	2.62	2.60		
			I360	0.84	1.10	1.06	0.75	1.44	1.90	1.82	1.29		
			H320	0.94	1.24	1.25	1.01	0.78	1.03	1.04	0.84		
			H500	1.08	0.94	0.75	0.45	0.67	0.58	0.47	0.28		
		8	I220	0.65	0.78	0.00	0.00	0.87	1.04	0.00	0.00		
			I360	1.37	1.53	0.00	0.00	0.73	0.81	0.00	0.00		
			H320	0.60	0.68	0.82	0.00	0.32	0.36	0.43	0.00		
			H500	1.33	0.00	0.00	0.00	0.25	0.00	0.00	0.00		
		12	I220	0.48	0.75	0.82	0.00	1.20	1.86	2.03	0.00		
			I360	1.02	1.19	0.00	0.00	1.25	1.44	0.00	0.00		
			H320	0.99	1.18	1.25	1.27	0.58	0.69	0.73	0.75		
			H500	1.15	1.26	1.32	1.35	0.50	0.55	0.58	0.59		
		16	I220	0.50	0.89	1.02	1.06	1.27	2.27	2.60	2.69		
			I360	0.73	0.93	1.00	1.02	1.45	1.85	1.98	2.04		
			H320	0.87	1.12	1.25	1.23	0.72	0.92	1.03	1.01		
			H500	0.88	1.05	1.10	1.13	0.61	0.73	0.77	0.78		
		20	I220	0.49	0.83	0.99	1.03	1.41	2.39	2.83	2.96		
			I360	0.65	0.86	0.91	0.93	1.51	1.99	2.12	2.17		
			H320	0.71	0.96	1.05	1.09	0.80	1.08	1.19	1.23		
			H500	0.75	0.87	0.92	0.94	0.67	0.78	0.82	0.84		
		8	I220	0.79	1.06	0.00	0.00	1.06	1.42	0.00	0.00		
			I360	1.81	0.00	0.00	0.00	0.96	0.00	0.00	0.00		
			H320	0.78	0.86	0.00	0.00	0.41	0.46	0.00	0.00		
			H500	0.00	0.00	0.00	0.00	0.00	0.00	0.00	0.00		
		12	I220	0.56	0.90	1.00	0.00	1.38	2.23	2.48	0.00		
			I360	1.26	1.48	1.67	0.00	1.53	1.80	2.03	0.00		
			H320	0.71	0.83	0.89	0.96	0.72	0.83	0.90	0.97		
			H500	1.40	1.53	0.00	0.00	0.61	0.67	0.00	0.00		
		16	I220	0.54	0.96	1.12	0.00	1.44	2.58	3.02	0.00		
			I360	0.81	1.18	1.26	0.00	1.70	2.47	2.63	0.00		
			H320	0.71	0.96	1.03	1.05	0.91	1.22	1.32	1.34		
			H500	1.07	1.21	1.28	1.30	0.84	0.95	1.00	1.02		
		20	I220	0.39	0.78	0.93	0.98	1.40	2.76	3.32	3.48		
			I360	0.68	0.99	1.05	1.08	1.83	2.64	2.82	2.90		
			H320	0.78	1.13	1.24	1.27	1.00	1.45	1.59	1.63		
			H500	0.83	1.01	1.08	1.10	0.92	1.12	1.19	1.21		

Strength Performance Levels			Strength Classification		
Colour	Level	$M_{\theta, \text{chord}}/M_{j, \text{Rm}, \text{EC3}}$	Colour	Classification	$M_{\theta, \text{chord}}/M_{j, \text{pin}, \text{EC3}}$
	STR1	>1.00		Semi rigid	>1.00
	STR2	0.80-1.00		Nom. pinned	0.00-1.00
	STR3	0.50-0.80		Failure	0.00
	STR4	0.20-0.50			
	STR5	0.00-0.20			

(\*) 3 bolt rows in the case of IPE 220 sections

By comparing Table 6.7 to Table 6.8, results show that increasing the number of bolt rows leads joints towards partial-strength behaviour over nominally pinned, which is not the standard design assumption. Therefore, adding bolt rows leads to a trade-off between enhancing resistance and moving away from the nominally pinned assumption.

### 6.3.3.2 Response to post-cyclic column loss action

The FEP joint response under column loss subsequent to cyclic action aims at quantifying the strength and rotation capacity degradation induced by a seismic event, thus enabling to determine the joint configurations most suitable for maximising post seismic robustness. The analysis of the initially undamaged response of FEP joints was previously presented and discussed in Section 6.3.1.

#### 6.3.3.2.1 Influence of endplate thickness and bolt diameter

The results in Figure 6.35 display the cyclic response curves (thin lines) and the post-cyclic column loss response curves (thick lines) for varying endplate thicknesses for the R2-SI360 joints and for both M16 and M24 bolts. In case of failure during the cyclic loading, joints are considered to display zero resistance to column loss. Indeed, for the R2-D16-SI360 (see Figure 6.35a), no post cyclic resistance is available for the  $t=8\text{mm}$  and  $t=20\text{mm}$  cases. For the 12mm and 16mm endplate cases, damage induced by cyclic action elongates the bolt shank and the initial response under column loss is characterized by zero stiffness; once contact between plates and bolt assembly is resumed, a resistance reprise is verified. Subsequently, resistance increases until reaching peak resistance of the most solicited bolt row, after which tensile force is redistributed to the other bolt row, leading to a new increase in resistance until joint collapse is finally reached. The ultimate rotation capacities were found to be greater than 100 mrad.

For the M24 case (see Figure 6.35b), fracture initiation during the cyclic loading was verified for the  $t \leq 12\text{mm}$  cases. For  $t \geq 16\text{mm}$ , rotation capacity is mostly provided by bolts, which displayed partial shank plasticization, resulting in limited hysteretic dissipation capacity. Post cyclic behaviour displayed compressive arching, followed by catenary action stage and collapse at rotation values around 100 mrad, in line with results for the M16 assemblies.

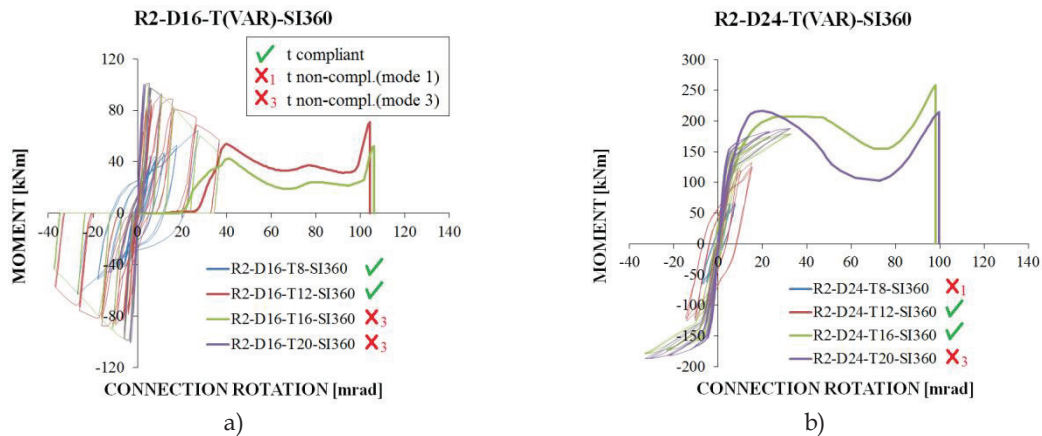


Figure 6.35: Connection cyclic and post-cyclic column loss response curves for R2- SI360 joints with: a) M16 bolts; b) M24 bolts

The effect of the cyclic action in reducing joint strength and rotation capacity is shown by comparing the undamaged joint response under column loss to the post-cyclic column loss response, as seen in Figure 6.36 and Figure 6.37 for the cases of the R2-H320 and R2-I360 joints, respectively.

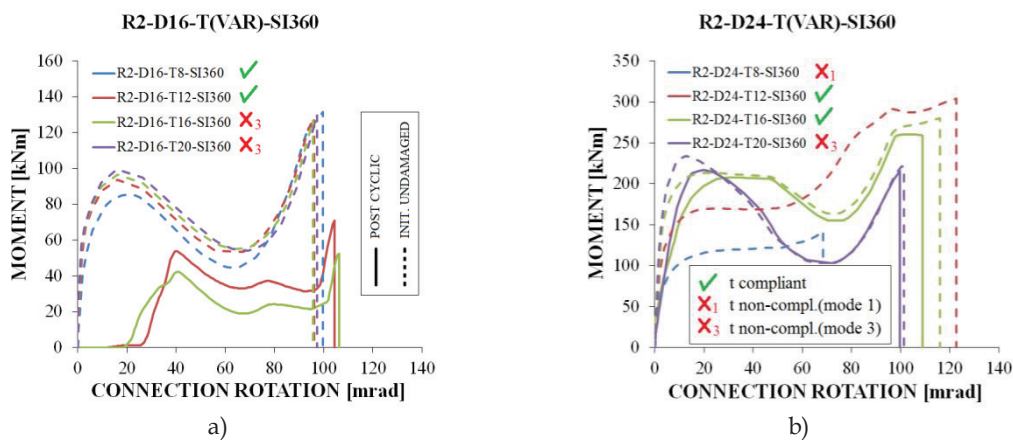


Figure 6.36: Comparison between initially undamaged and post cyclic column loss response for R2-SI360 joints with: a) M16 bolts; b) M24 bolts

In general, for joints that did not fail under cyclic action, the damage introduced by the cyclic action did not significantly affect ultimate rotation capacity. However, joint strength is significantly affected, namely for the M16 case (see Figure 6.36a and Figure 6.37a), since bolt shank elongation under cyclic action leads to loss of strength for  $\theta \leq 40$  mrad (maximum rotation in cyclic action), preventing joints from mobilising compressive arching resistance. For  $\theta > 40$  mrad and up to the end of the compressive arching stage (definition of response stages is in accordance with Izzudin *et al.*, 2008),

post-cyclic response tends towards the initially undamaged joint response; subsequently in catenary transient stage, internal force redistribution between bolts rows occurs, with the initially undamaged and post-cyclic curves diverging until joint collapse is reached. Post-cyclic bending resistance was found to be limited to approximately half that of the initially undamaged.

For joints compliant with the proposed ductility criterion, results in general show rotation capacities in exceedance of 100 mrad whenever failure under cyclic action did not occur, indicating that improving weld detailing may enable criterion compliant joints to achieve suitable post cyclic resistance to column loss action.

A comparison between the post cyclic (P.C.) and the initially undamaged (I.U.) joint responses under column loss is presented in Table 6.9 in terms of ultimate rotation and bending strength. The ultimate rotation ratio  $\Gamma\theta_u = (\theta_{u,P.C.}/\theta_{u,I.U.} - 1)$  and the ultimate bending strength ratio  $\Gamma M_u = (M_{u,P.C.}/M_{u,I.U.} - 1)$  values were computed to quantify the influence of the cyclic action on the post cyclic joint robustness. Results showed both joints with thin endplates and S1220 joints to display zero post-cyclic robustness, owing to plate fracture initiation due to high stress concentrations at the beam flange to endplate weld zone.

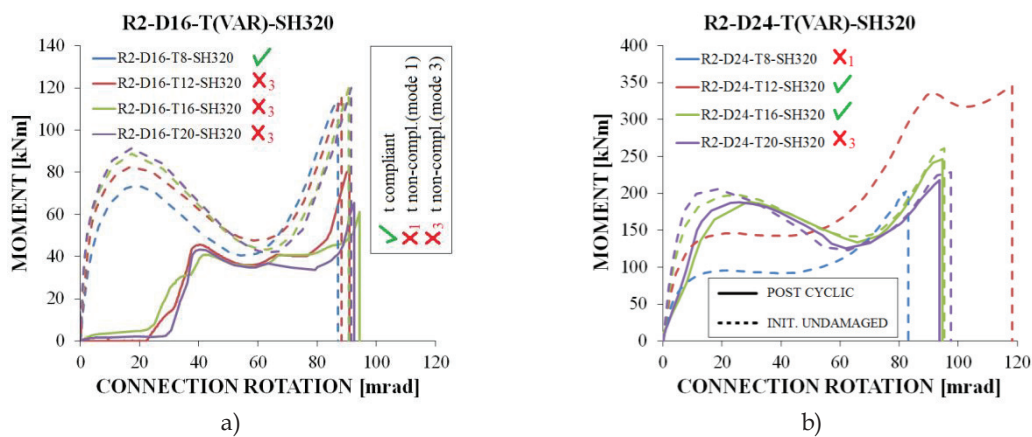


Figure 6.37: Comparison between initially undamaged and post cyclic column loss response for R2-SH320 joints with: a) M16 bolts; b) M24 bolts

Small variations in terms of ultimate rotation capacities were verified, as shown by  $\Gamma\theta_u$  ratio absolute values below 11%. Positive values of  $\Gamma\theta_u$  (i.e. post-cyclic capacity larger than initially undamaged), namely for cases with M16 bolts, are attributable to differences in moment-rotation trajectories up to failure. Indeed, for the I.U. case, M- $\theta$  trajectory is characterized by a compressive arching stage, whereas for the P.C. case,

the shanks of all bolt rows are already elongated at the start of the column loss action, hence contributing to achieve slightly higher rotational capacity.

Table 6.9: Comparison between post cyclic (P.C.) and initially undamaged (I.U.) joint column loss response - ultimate rotation and bending capacities of joints with 2 bolt rows

R	D	T	S	I.U.			P.C.			$\Gamma = (P.C./I.U.)^{-1}$	
				$\theta_u$ [mrad]	$\theta_u/\theta_{p+A}$ [-]	$M_u/M_p$ [-]	$\theta_u$ [mrad]	$\theta_u/\theta_{p+A}$ [-]	$M_u/M_p$ [-]	$\Gamma\theta_u$ [%]	$\Gamma M_u$ [%]
2	20	8	I220	96	1.18	1.38	FRACT. IN CYCLIC			-	-
			I360	100	1.37	0.35	FRACT. IN CYCLIC			-	-
			H320	87	1.17	0.19	FRACT. IN CYCLIC			-	-
			H500	124	1.80	0.11	FRACT. IN CYCLIC			-	-
		12	I220	65	0.80	0.96	FRACT. IN CYCLIC			-	-
			I360	96	1.32	0.34	104	1.43	0.19	8.6	-44.7
			H320	88	1.19	0.19	91	1.22	0.13	2.8	-30.2
			H500	127	1.84	0.11	136	1.97	0.04	7.1	-67.6
		16	I220	64	0.78	0.95	63	0.77	0.93	-1.5	-2.3
			I360	96	1.31	0.34	106	1.46	0.14	11.2	-58.8
			H320	91	1.22	0.20	94	1.27	0.10	4.0	-48.9
			H500	129	1.87	0.11	140	2.02	0.02	8.2	-79.9
	20	I220	65	0.80	0.97	65	0.80	0.94	-0.6	-3.3	
		I360	97	1.34	0.34	BOLT FAIL IN CYCLIC			-	-	
		H320	92	1.23	0.20	93	1.24	0.11	1.1	-45.5	
		H500	131	1.90	0.11	BOLT FAIL IN CYCLIC			-	-	
	24	8	I220	78	0.96	1.38	FRACT. IN CYCLIC			-	-
			I360	120	1.65	0.66	FRACT. IN CYCLIC			-	-
			H320	110	1.47	0.37	FRACT. IN CYCLIC			-	-
			H500	140	2.02	0.19	FRACT. IN CYCLIC			-	-
		12	I220	93	1.14	2.04	FRACT. IN CYCLIC			-	-
			I360	96	1.32	0.54	95	1.31	0.54	-1.0	-1.1
			H320	89	1.19	0.33	89	1.20	0.31	0.9	-5.7
			H500	127	1.84	0.17	128	1.85	0.17	0.7	0.1
16		I220	71	0.87	1.61	70	0.86	1.59	-0.5	-1.4	
		I360	98	1.34	0.55	98	1.34	0.55	0.0	-0.4	
		H320	92	1.24	0.32	92	1.23	0.32	-0.6	-1.5	
		H500	131	1.89	0.18	131	1.89	0.18	0.1	-0.2	
20	I220	70	0.86	1.60	69	0.85	1.57	-1.1	-2.0		
	I360	97	1.33	0.55	97	1.34	0.55	0.4	0.0		
	H320	94	1.26	0.33	95	1.28	0.33	1.5	1.0		
	H500	131	1.90	0.18	134	1.93	0.18	1.9	1.5		
24	8	I220	83	1.02	2.04	FRACT. IN CYCLIC			-	-	
		I360	68	0.94	0.38	FRACT. IN CYCLIC			-	-	
		H320	83	1.11	0.34	FRACT. IN CYCLIC			-	-	
		H500	59	0.85	0.14	FRACT. IN CYCLIC			-	-	
	12	I220	93	1.14	2.69	FRACT. IN CYCLIC			-	-	
		I360	123	1.69	0.81	FRACT. IN CYCLIC			-	-	
		H320	118	1.59	0.57	FRACT. IN CYCLIC			-	-	
		H500	157	2.28	0.19	FRACT. IN CYCLIC			-	-	
	16	I220	119	1.46	3.54	FRACT. IN CYCLIC			-	-	
		I360	116	1.59	0.74	109	1.50	0.69	-6.0	-7.7	
		H320	95	1.28	0.43	95	1.27	0.41	-0.5	-5.4	
		H500	134	1.94	0.15	131	1.89	0.13	-2.6	-11.6	
20	I220	132	1.61	3.87	FRACT. IN CYCLIC			-	-		
	I360	101	1.39	0.59	100	1.37	0.57	-1.6	-2.6		
	H320	98	1.31	0.38	94	1.26	0.36	-4.0	-4.5		
	H500	132	1.91	0.13	131	1.90	0.12	-0.6	-10.0		

The strength ratios  $\Gamma M_u$  displayed in Table 6.9 show resistance degradation of up to -79.9%, -5.7% and -11.6% for joints with M16, M20 and M24 bolts, respectively. The best performance was obtained for joints with M20 assemblies, since both the number of failures during the cyclic action stage, as well as the  $\Gamma\theta_u$  and  $\Gamma M_u$  ratio values are minimised. In particular, joints with M20 bolts displayed rotation ratios  $\Gamma\theta_u$  below 2% and strength ratios  $\Gamma M_u$  below 6%.

#### 6.3.3.2.2 Influence of endplate thickness and bolt diameter

As stated in Section 6.3.3.2, the high stress concentration at the intersection beam flange – endplate zone for the IPE 220 section cases, resulting from the high ratio between horizontal bolt pitch and beam flange width, constitutes a key factor in limiting joint performance under cyclic actions. This effect is reduced by adopting thicker endplates, hence shifting T-stub mode from 1 to 2 or 3, reducing endplate rotation contribution to joint rotation. The P.C. normalised values  $\theta_u/\theta_{p+A}$  in Table 6.9 and Table 6.10 indicate that joints with compact beams tend to display smaller  $\theta_u/\theta_{p+A}$  ratios, with typical values around 0.8 for IPE 220 and up to 2.0 for HEA 500. In terms of P.C. ultimate rotation  $\theta_{u,P.C.}$ , Table 6.9 shows that cross section bears influence on rotation capacity, although response is complex and other variables should be factored, namely horizontal bolt pitch. Notwithstanding, beam size correlated positively with rotation capacity.

#### 6.3.3.2.3 Influence of number of bolt rows

Comparing Table 6.9 to Table 6.10 highlights that increasing the number of bolt rows led approximately to the same number of joint failure cases under cyclic loading. For D16-T20 joints, adding bolt rows compensated for early bolt failure, since tensile force redistribution to other rows is more efficient. Although adding bolt rows led in some cases to slightly lower P.C. ultimate rotation, coupled with significant gains in ultimate resistance  $M_u$ , the general trend summarised in Table 6.11 indicates that the added redistribution capacity of 3 and 4 bolt row joints allows for higher rotation capacity.

Results show that for joints with 12mm endplates, increasing bolt rows resulted in rotation capacity variations of -4%, +20% and -9%, associated to corresponding increases in ultimate strength of +290%, +268% and +131%, for the IPE 360, HEA 320

and HEA 500 sections, respectively. For joints with  $t=16\text{mm}$ , variations in rotation capacity of -7%, -1% and -13%, coupled with resistance gains of +125%, +313% and +84% were obtained for the same cross sections.

Table 6.10: Comparison between post cyclic (P.C.) and initially undamaged (I.U.) joint column loss response - ultimate rotation and bending capacities of joints with 3 or 4 bolt rows

R	D	T	S	I.U.			P.C.			G = (P.C./I.U.) -1	
				$\theta_u$	$\theta_u/\theta_{p+A}$	$M_u/M_p$	$\theta_u$	$\theta_u/\theta_{p+A}$	$M_u/M_p$	$\Gamma\theta_u$	$\Gamma M_u$
[-]	[mm]	[mm]	[-]	[mrad]	[-]	[-]	[mrad]	[-]	[-]	[%]	[%]
4(*)	20	8	I220	104	1.28	2.12	FRACT. IN CYCLIC			-	-
			I360	129	1.77	0.94	FRACT. IN CYCLIC			-	-
			H320	127	1.70	0.57	126	1.69	0.52	-0.7	-9.4
			H500	143	2.08	0.25	FRACT. IN CYCLIC			-	-
		12	I220	98	1.20	2.10	FRACT. IN CYCLIC			-	-
			I360	101	1.38	0.72	100	1.38	0.73	-0.4	1.3
			H320	99	1.32	0.44	109	1.46	0.50	10.2	13.1
			H500	129	1.86	0.22	125	1.80	0.08	-3.3	-62.8
		16	I220	70	0.86	1.54	FRACT. IN CYCLIC			-	-
			I360	97	1.34	0.71	99	1.36	0.31	1.6	-56.2
			H320	93	1.24	0.27	93	1.25	0.42	0.9	58.0
			H500	132	1.91	0.23	122	1.76	0.04	-7.8	-81.9
	20	I220	69	0.85	1.52	78	0.96	1.83	13.4	20.1	
		I360	97	1.34	0.71	101	1.38	0.24	3.3	-65.8	
		H320	95	1.27	0.43	93	1.25	0.23	-1.5	-46.8	
		H500	132	1.91	0.23	125	1.82	0.05	-5.0	-79.8	
	20	8	I220	76	0.93	1.51	FRACT. IN CYCLIC			-	-
			I360	84	1.15	0.56	FRACT. IN CYCLIC			-	-
			H320	124	1.66	0.75	FRACT. IN CYCLIC			-	-
			H500	113	1.64	0.20	FRACT. IN CYCLIC			-	-
		12	I220	139	1.70	3.77	FRACT. IN CYCLIC			-	-
			I360	124	1.70	1.43	FRACT. IN CYCLIC			-	-
			H320	123	1.64	0.88	119	1.60	0.88	-2.5	-0.2
			H500	131	1.90	0.35	123	1.78	0.33	-6.4	-5.0
		16	I220	128	1.57	3.53	FRACT. IN CYCLIC			-	-
			I360	102	1.40	1.19	100	1.37	1.18	-1.8	-1.4
			H320	95	1.28	0.68	94	1.27	0.68	-1.0	-0.7
			H500	131	1.90	0.36	131	1.89	0.35	-0.4	-0.8
20	I220	106	1.31	3.03	108	1.33	3.06	1.7	1.1		
	I360	98	1.34	1.15	98	1.35	1.16	0.6	0.2		
	H320	96	1.28	0.69	95	1.28	0.69	-0.4	-0.8		
	H500	133	1.92	0.36	134	1.93	0.36	0.6	0.1		
24	8	I220	76	0.93	2.00	FRACT. IN CYCLIC			-	-	
		I360	72	0.99	0.58	FRACT. IN CYCLIC			-	-	
		H320	81	1.08	0.38	FRACT. IN CYCLIC			-	-	
		H500	59	0.86	0.17	FRACT. IN CYCLIC			-	-	
	12	I220	98	1.20	2.91	FRACT. IN CYCLIC			-	-	
		I360	150	2.06	2.02	FRACT. IN CYCLIC			-	-	
		H320	138	1.86	1.30	FRACT. IN CYCLIC			-	-	
		H500	182	2.63	0.43	FRACT. IN CYCLIC			-	-	
	16	I220	131	1.61	3.89	FRACT. IN CYCLIC			-	-	
		I360	134	1.84	1.94	FRACT. IN CYCLIC			-	-	
		H320	144	1.92	1.37	138	1.85	1.29	-4.0	-5.9	
		H500	160	2.32	0.44	143	2.07	0.44	-10.7	1.0	
20	I220	166	2.03	4.77	FRACT. IN CYCLIC			-	-		
	I360	131	1.80	2.02	125	1.71	1.86	-4.9	-7.8		
	H320	140	1.88	1.35	132	1.77	1.23	-5.6	-9.2		
	H500	134	1.94	0.38	130	1.88	0.35	-3.4	-8.6		

(\*) 3 bolt rows in the case of IPE 220 sections



A comparison between the damaged configurations at the end of the cyclic action for 2 and 4 bolt row joints is presented in Figure 6.38, where bolt elongation and endplate deformation are clearly noticeable. At  $\theta=4\%$ , the R4 joint in Figure 6.38b is capable of mobilising tensile resistance from the adjacent bolt row due to the action of the endplate in bending, which is required to accommodate the elongation difference between adjacent bolt rows, hence increasing joint strength. This explains the significant increase in joint strength achieved by adopting a higher number of bolt rows.

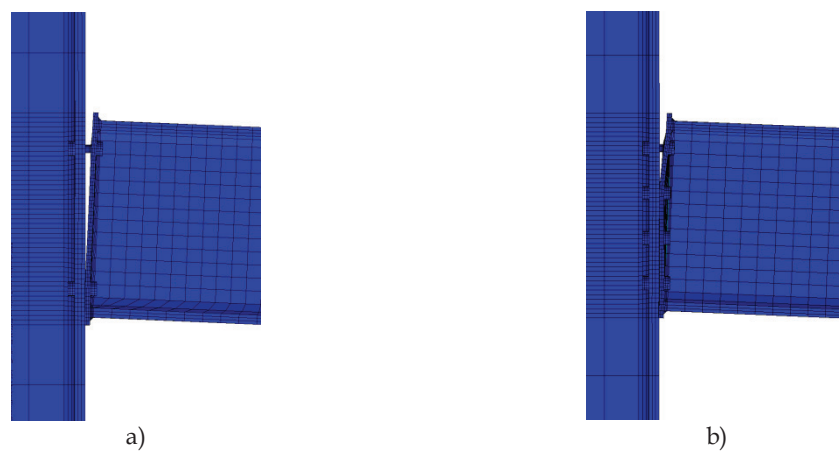


Figure 6.38: Comparison between deformed shapes at the end of the cyclic action ( $\theta=4\%$ ) of D20-T12-SH500 joints with: a) 2 bolt rows; b) 4 bolt rows

The small differences in ultimate rotation capacity  $\theta_{u,P.C.}$  between joints with 2 and 4 bolt rows can be explained by the fact that prior to failure, bolts experience softening and lose stiffness, becoming the joint's "weak link" and contributing the most to joint rotation while allowing for other components to recover their elastic deformation. Ultimate rotation capacity is therefore determined by the capacity of the bolts, which is not significantly affected by variable cyclic loading, as seen previously in Chapter 5.

Table 6.11: Influence of the number of bolt rows on the post cyclic (P.C.) ultimate rotation capacity – average, standard deviation and coefficient of variation

R	D	$\theta_{u,P.C.,AVG.}$	$\theta_{u,P.C.,ST.DEV.}$	$\theta_{u,P.C.,CoV.}$
[-]	[mm]	[mrad]	[mrad]	[-]
2	16	99.2	25.2	0.25
	20	99.9	21.1	0.21
	24	109.8	15.7	0.14
4(*)	16	106.5	15.3	0.14
	20	111.4	14.6	0.13
	24	133.4	6.4	0.05

(\*) 3 bolt rows in the case of IPE 220 sections

The effect of the number of bolt rows on the P.C. ultimate rotation capacity  $\theta_{u,P.C.}$  is summarized in Table 6.11 for all cases with non-zero P.C. robustness, showing the positive effect of increasing the number of bolt rows. In general, the analysed FEP joints that did not fail in cyclic loading were able to achieve rotation capacities in exceedance of approximately 100 mrad, although associated to a significant level of uncertainty, as highlighted by the respective coefficients of variation (CoV), ranging between 14% to 25% and 5 to 14% for R2 and R4 joints, respectively.

## 6.4 Consequences for design

### 6.4.1 Joints under monotonic column loss action

The numerical results discussed in the previous Sections enable to draw some considerations about the design of FEP joint against column loss scenarios.

The response under column loss can exhibit two different post-yield mechanisms, namely the compressive arching and catenary effect. The first mechanism is associated to high levels of resistance at low chord rotation, typically under 25 mrad, which could contribute to arrest a progressive collapse subsequent to column loss at low imposed vertical displacements. However, joint details that lead to compressive arching may be unsuitable as a design approach since it is dependent upon the stiffness of the column, which becomes negligible for small column profiles. However, the compressive arching behaviour is acceptable solely for cases involving rigid collapse-arresting mechanisms, namely when small displacements are required for arresting the progressive collapse, e.g. the case of structures with masonry claddings. On the

contrary, for most steel buildings, adopting joint configurations that achieve maximum resistance at larger displacements is more efficient because the system energy absorption capacity is maximized. In addition, the joint performance is also more coherent with the pinned behaviour assumed at design stage for secondary structural elements.

Therefore, it is more advisable to design joints able to develop the catenary mechanism maximizing energy absorption capacity. It should be noted that it is unfeasible to design FEP joint configurations able to develop the final catenary stage with the beam axial yielding, because this design objective would require adopting very heavy detailing of the connection (e.g. extremely thick end-plates and large diameter bolts), which is largely impractical and makes also difficult to guarantee a ductile failure mode of the connection. Indeed, in pure bending FEP joints exhibit the higher ductility for failure mode 1 and the lower ductility for mode 3 (Broderick and Thomson, 2002), implying that the use of thin end-plates optimizes rotational capacity. However, under column loss action the end-plate thickness should be carefully selected in order to be thin enough to provide sufficient rotational capacity for the imposed displacements to which it is subjected under column loss, while also being thick enough in order to have sufficient resistance under a column loss event. Considering that results show that the use of very thin plates leads to rotation-wise premature collapse under column loss type action, a sufficiently thick plate should be selected when designing flush endplate joints, in order to mobilize first the deformability contributions of the endplate and subsequently the plastic engagement the upper bolt rows. The proposed ductility criterion expressed by requires also that the welds between beam flange and end-plates are stronger than the connected plates. Therefore, it is recommended to use full penetration welds in place of fillet welds, which are most commonly adopted.

Besides the end-plate thickness, an important feature to improve the robustness of FEP joints is the number of bolt rows. The analyses showed that using inner bolt rows located near the centroid of the connection is a good design strategy for maximizing FEP joint resistance under simultaneous bending and tensile force. In addition, increasing the number of bolt rows allows increasing the axial stiffness of the connection that is beneficial to activate the catenary action in place of compressive arching mechanism.

The results for the tested 2 bolt row cases in terms of ultimate bending moment  $M_u$  appear to be inversely proportional to  $(W_{pl}/A)$ , namely if excluding the IPE 220 case, to which corresponds the lowest value of  $(W_{pl}/A)$  out of the analysed cross sections and that presented failure in the weld zone. For the 4 bolt row case, inverse proportionality between ultimate bending moment and  $(W_{pl}/A)$  was verified for the three cases with highest  $(W_{pl}/A)$  values (i.e., excluding the IPE 220 case which has only 3 bolt rows). The  $W_{pl}/A$  factor was selected since it provides a measure of the bending over tensile capacity ratio, which presents lower values for small beam sections such as the IPE 220 ( $W_{pl}/A=8.55\text{cm}$ ) and higher values for larger sections such the HEA 500 ( $W_{pl}/A=19.99\text{cm}$ ). The testing of further cases with different cross sections and joint detailing configurations are required to further evaluate the importance of the factor  $W_{pl}/A$ .

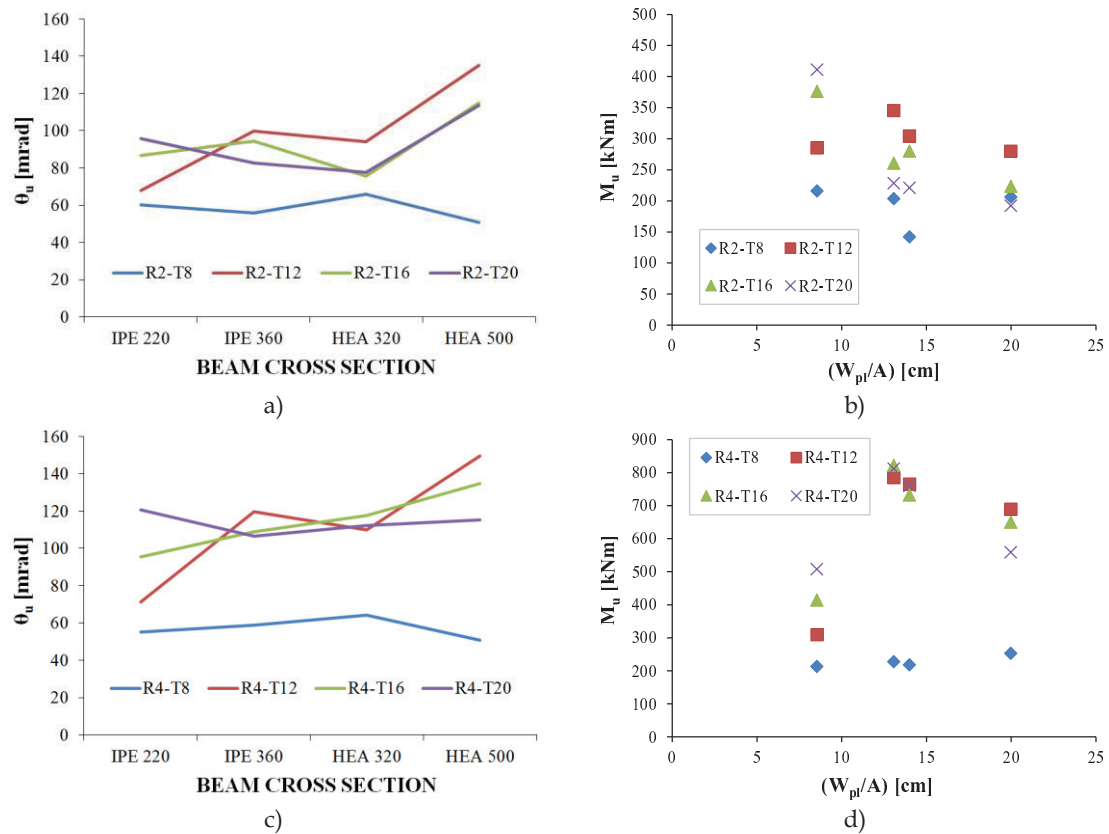


Figure 6.39: Influence of endplate thickness with M24 bolts: a) on ultimate connection rotation for the 2 bolt row case; b) on ultimate bending moment for the 2 bolt row case; c) on ultimate connection rotation for the 4 bolt row case; d) on ultimate bending moment for the 4 bolt row case

The estimation of the ultimate rotation and bending moment joint capacity of the joint can provide useful information for designers. On the one hand, the prediction

of the rotation capacity establishes a limit state, or displacement acceptance criterion, for the verification of secondary structural elements. On the other hand, the estimation of the ultimate joint resistance provides for a measure of the resistance contribution of secondary structural elements under simultaneous bending and axial force.

With this aim, the plots shown in Figure 6.12, Figure 6.13, Figure 6.14 and Figure 6.17 in terms of  $M/M_p$  as a function of  $\theta/\theta_{p+A}$  and of  $N/N_p$  can be used to determine the set of internal forces acting on the connection ( $M;N$ ) for a selected applied rotation  $\theta$ .

The joint available rotation capacity  $\phi_{j,avail|col.loss}$ , which is nearly equal to the connection rotation supply (rotation contributions from beam and column are comparatively small) can be compared to the rotational demand  $\phi_{j,req|col.loss}$  on the joints when subjected to column removal scenarios. Considering that for low- and medium-rise MRF structures the rotation demand at collapse arrest may vary within 2 mrad – 60 mrad (Cassiano *et al.*, 2016), in light of the obtained FEM results, FEP joints are suitable to sustain the rotation demand induced by the column loss without collapsing, providing also additional resistance to the primary structure for the arrest of a progressive collapse.

#### **6.4.2 Joints under cyclic action and subsequent column loss action**

The response of FEP joints under cyclic actions showed that most analysed joint configurations are capable of sustaining cyclic actions compatible with seismic events leading to chord rotations up to 4%, while maintaining resistance levels consistent with the EN 1993-1-8 (CEN, 2005) prediction. The analysis of the results has however enabled to determine joint configurations that are less suitable to be adopted in seismic areas.

Joint configurations with thin endplates ( $t=8\text{mm}$ ) were found to be not be capable of withstanding the full cyclic loading up to  $\theta=4\%$ , due to premature fracture initiation. In addition, joints with IPE 220 beams, which are characterized by high horizontal pitch to beam flange width ratio, were found to display premature failure owing to high stress concentrations at the beam flange tip zones, leading to fracture initiation. In this sense, adopting full penetration welds over the typically used fillet welds between beam flange and endplate may contribute to improve joint

performance, although experimental testing would be required to draw more definitive conclusions.

The combination of thicker endplates with small diameter bolts (namely M16) in 2 bolt row joints led to significant strength reduction at high rotational demand, due to bolt softening. This implies that FEP joint design according to the Components Method considering an elastic-perfectly plastic bolt response as seen in EN 1993-1-8 (CEN, 2005) may be contrary to safety, since bolt softening is not explicitly accounted for.

FEP joints are generally assumed to behave as perfectly pinned, hence displaying zero hysteretic energy dissipation capacity. However, significant hysteretic dissipation is reported for joints in which endplate deformation significantly contributed to joint rotation (joints in T-stub modes 1 and 2). For joints with  $t \leq 12\text{mm}$ , response is characterized by large stable loops (see Figure 6.28a); instead, for  $t \geq 16\text{mm}$ , joints displayed reduced energy dissipation since plasticization is concentrated in the bolts (partial bolt shank plasticization occurred in some cases) and hence involves reduced material volume. This difference in dissipative behaviour due to endplate thickness implies that designers can select the appropriate endplate thickness so as to induce an intended T-stub mode that maximises dissipative behaviour and joint capacity. Indeed, selecting joint typologies capable of dissipating energy may have a beneficial effect on steel structures in seismic areas, considering the scale effect provided by the high number of secondary nodes. Joint typology selection should however take into account the predicted rotation demand, since results show that joints with thin endplates are prone to premature fracture initiation at medium/low rotation levels. The adoption of the proposed ductility criteria is shown to lead to joint configurations with suitable post cyclic column loss response whenever weld fracture in cyclic bending is not an issue. The use of stronger welds may therefore lead to improvements in post cyclic response. This hypothesis is however not verified in this study and should be confirmed in future numerical or experimental tests.

The verified degradation of secant stiffness for increasing rotational demand points to joints with small bolt diameter (i.e. M16) tending to behave as nominally pinned at high rotational demands ( $\theta=3\%$  or  $\theta=4\%$ ), while remaining semi rigid for smaller demands ( $\theta=1\%$  or  $\theta=2\%$ ). Instead, joints with medium/large bolt diameters tended towards behaving as semi-rigid joints, even at  $\theta=4\%$ , hence implying they must

be explicitly modelled for structural analysis. In terms of strength classification, joints with larger beam cross sections and small bolt diameter tend to behave as nominally pinned even at  $\theta=4\%$ . Instead, joints with medium/large bolt diameters and more than 2 bolt rows displayed higher tendency to respond as partial strength joints, requiring also explicit joint modelling for global structural analysis.

The best performance in terms of compatibility with nominally pinned design assumptions (both in terms of stiffness and strength) at  $\theta=3\%$  and  $\theta=4\%$ , was obtained for joints with 2 bolt rows, small/medium bolt diameters (i.e. M16 and M20) and medium/large beam cross sections. For  $\theta \leq 2\%$ , the  $M_{j,sec,\theta}/M_{j,pin,EC3}$  ratio values are generally lower than 1 (i.e. joint is nominally pinned), but ratios  $S_{j,sec,\theta,chord}/S_{j,pin,EC3}$  are higher than 1 (i.e. joint is semi rigid).

This indicates that, in many cases, at higher rotational demand, joint behaviour is more consistent with the design assumption of disregarding secondary structure contribution, whereas for lower rotational demand, the elevated secant stiffness leads to semi rigid joint behaviour, hence requiring explicit joint modelling for structural analysis. Furthermore, considering that during a single seismic event, joints may be subjected to both low and high rotation demands, then explicit modelling of FEP beam-column joints is required for accurate structural analysis.

Since all joint failures in cyclic loading correspond to joints with zero residual joint robustness, failed joint configurations should be avoided when designing FEP joints for post seismic robustness.

The plastic elongation of small diameter bolts (i.e. M16) during the cyclic action led to near-zero initial post cyclic resistance, with resistance reprise occurring at about 40 mrad (i.e. at the maximum chord rotation in cyclic action). This implies that for joints with small bolt diameters, FEP joint contribution to collapse arrest should not be considered when collapse arrest is predicted at low displacement levels, as is case when accounting for masonry façade cladding contribution. For these joints, important reductions in ultimate strength ratios  $\Gamma M_u$  were verified, coupled with small variations in rotation capacity, implying that for large displacement collapse arrest, reduced resistance must be accounted for.

The best post cyclic performance was provided by joints with intermediate bolt diameter (i.e. M20), which displayed variations between I.U. and P.C. responses in terms of both strength and rotation capacities lower than 2%. The use of large diameter

bolts (i.e. M24), despite having led to several cases of failure under cyclic action, also led to low  $\Gamma M_u$  and  $\Gamma \theta_u$  ratios values, indicative of reduced cyclic action induced damage.

Endplate thickness greatly influences cyclic response but has a limited effect on P.C. column loss response. Since failure is determined by bolts, for which ultimate displacement is not affected by variable cyclic loading (see 0), joint ultimate capacity appears to not be significantly affected by endplate thickness and no simple correlation between endplate thickness and rotation or strength capacity was observed.

The effect of increasing the number of bolt rows is beneficial, especially for increasing P.C. ultimate strength, due to higher internal redistribution capacity and increased load path efficiency in transmitting tensile force, due to the nearness between central bolt rows and the beam section centroid. Slight increases in rotation capacity were also achieved by adding bolt rows. For design conditions requiring the adoption of small diameter bolts, adding bolt rows may constitute a good design strategy to overcome joint strength softening at high rotational demand.

The results from this parametric study indicate that post seismic joint robustness of FEP joints can be maximised by adopting more than 2 bolt rows with medium/large bolt assemblies. Structural design accounting for FEP joint contribution for post seismic progressive collapse up to 100 mrad appears to be safe according to the obtained numerical results, although some dispersion in terms of ultimate rotation capacity was reported.

## 6.5 Conclusive remarks

A comprehensive parametric study based on finite element analyses was presented and discussed in this chapter, with the aim to investigate the capacity of bolted flush end-plate joints to resist column loss action and cyclic action followed by column loss.

The analysed configurations are representative of a significant array of possible detailing arrangements and in general results show that connection failure in the catenary stage typically limits the response under simultaneous bending and axial force. The influence of mechanical and geometrical features (i.e. the column orientation, the type of beam profile, the thickness of end-plate thickness, the bolt



diameter and number of bolt rows) on joint moment-rotation response were examined and the performance response parameters were quantified through FE analysis.

The results from finite element simulations on FEP joints under monotonic column loss action have enabled to draw some conclusive remarks. In particular, the nonlinear response of FEP joints was found to exhibit two different resisting mechanisms, namely compressive arching mode and catenary action mode.

The joints with axial joint-beam stiffness ratios  $S_{j,N,ini}/(EA_b/L_b)$  lower than  $20E-4$  (i.e. those characterized by the larger beam cross sections and stiffer endplates) are characterized by compressive arching mode, which enables to mobilise significant resistance at low rotation values, that may be advantageous when joint ultimate rotational demand is small or when stiff masonry claddings are mobilised. Conversely, joints with axial joint-beam stiffness ratios  $S_{j,N,ini}/(EA_b/L_b)$  higher than  $20E-4$  (i.e. those characterized by the larger beam cross sections and stiffer endplates) are characterized by catenary action mechanism, which is very effective to accommodate large ductility demand under column loss.

The obtained results have also shown that the end-plate thickness significantly influences the joint response when large diameter bolts are adopted. Indeed, the end-plate should be thin enough to provide sufficient rotational capacity for the imposed displacements to which it is subjected under column loss, while simultaneously being thick enough in order to have sufficient resistance under a column loss event, thus enabling the transition from a type 1 to a type 2 failure mode. In this sense, a criterion to design FEP joints is proposed, consisting of adopting the larger plate thickness inducing mode 1, or the minimum plate thickness which yields mode 2, which is estimated accounting for the random variability of yield strength and the maximum hardening that the plates can develop.

Regarding joint detailing and in order to guarantee adequate the activation of membrane action in the end-plate, the welds should be stronger than the connected plates. With this regard, full penetration welds were found to be preferable to the more commonly adopted fillet welds for the FEP joint typology.

The bolt diameter and the number of bolt rows were found to substantially influence the resistance of FEP joints under column loss. In order to enhance the joint performance, it is necessary to use the larger bolt diameter and the greater number of

bolt rows compatible with the constructional limitations. Contrarily to the first order design, the inner bolt rows located close to the centroid of the connection were reported to noticeably increase the resistance and the rotation capacity under column loss. In addition, these bolt rows were found to be very important to redistribute the internal forces developing into the connection, allowing also to mobilize the catenary action under column loss.

The obtained numerical results hence point to the fact that adopting additional bolt rows near the beam section centroid, combined with large diameter bolts and a sufficiently thick endplate that engages both bolt and endplate deformation at failure is a suitable detailing strategy to achieve robust flush endplate joints under progressive collapse scenarios.

In this chapter, the joint configuration in which the beam is connected to the column's weak axis was also investigated, showing that the proposed typology displays high rotation capacity and is suitable for achieving robust joint response under column loss actions.

For what concerns FEP beam-column joint behaviour under cyclic action followed by column loss action, the study described in this chapter analysed the effect of key connection parameters and failure modes were identified. Response under cyclic action was quantified via *ad hoc* defined performance levels to quantify the strength and stiffness degradation throughout the cyclic loading. Results were compared to strength and stiffness limits for nominally pinned joints provided in EN 1993-1-8 (CEN, 2005), in order to assess FEP joint compliance with typical design assumptions of perfectly pinned behaviour. Results were also confronted in terms of the proposed ductility criterion to assess on its adequacy. Post cyclic column loss response was quantified in terms of joint moment-rotation curves and was compared to the column loss response for initially undamaged joints also described in this Chapter, hence quantifying the variation in joint robustness induced by cyclic actions. The influence of key connection parameters and consequences for design were also presented and discussed.

In light of the obtained results, some conclusive remarks were drawn. Indeed, joint response to cyclic actions was found to be influenced by joint detailing and T-stub deformation modes, which mobilise different joint components.

Adopting thin endplates (T-stub in mode 1 or 2) was found to lead to moment-rotation response characterized by large hysteretic loops with significant energy dissipation; conversely, selecting thicker endplates (T-stub in mode 3) led to plasticization being concentrated in bolts and response to display low energy dissipation capacity.

Fracture initiation in the beam flange - endplate weld zone prior to completion of the cyclic loading was reported for joints with thin endplates and fracture initiation was also verified for cases with compact beam section and large bolt horizontal pitch. The results showed adequate behaviour for joints designed according to the proposed ductility criteria, whenever weld fracture initiation in cyclic bending did not occur. The use of full penetration welds and/or thicker endplates may therefore limit concentrated stresses and prevent premature joint failure.

The rotational demand and energy dissipation capacity should be taken into consideration by designers when selecting endplate thickness to achieve intended joint performance.

Joints with small diameter bolts and thick endplates experienced severe softening at high rotational demand and resistance was reported to be significantly lower than the EN 1993-1-8 (CEN, 2005) prediction, indicating that joint design not accounting for bolt softening may be contrary to safety. Conversely, the bending resistance of FEP joints was found consistent with the EN 1993-1-8 (CEN, 2005) prediction (with the exception of joints with M16 assemblies) leading to safe resistance-wise design.

The effect of increasing the number of bolt rows was found to be beneficial in terms of both strength and rotation capacity under cyclic actions, due to increased internal force redistribution capacity subsequent to first bolt row yielding.

At low rotational demand, FEP joints behave as semi-rigid, according to the EN 1993-1-8 (CEN, 2005) classification whereas at high rotational demand, secant stiffness degradation leads to nominally pinned behaviour. Joints with compact beam sections tend to behave as semi rigid, whereas joints with larger sections tend to behave as nominally pinned and joints with 3 or 4 bolt rows displayed higher propensity to behaving as semi rigid.

In terms of joint strength, the best performance under cyclic loading was verified for joints with intermediate shank diameters (M20 bolts), which minimized

premature failure occurrences and presented good correspondence with predicted resistance at  $\theta=4\%$ . Joints with compact beam sections and higher bolt diameters generally behaved as partial-strength. Joints with thin endplates ( $t=8\text{mm}$ ) were shown to behave as nominally pinned; for  $t\geq 12\text{mm}$ , IPE 220 and IPE 360 section cases are prone to behave as partial-strength, whereas HEA 320 and HEA 500 behaved as nominally pinned. Increasing the number or bolt rows was found to enhance resistance but to also lead to partial strength behaviour.

For collapse arrest at small displacements, FEP joint contribution with small diameter bolts should be limited or disregarded, due to shank elongation under cyclic action which leads to zero initial post cyclic (P.C.) column loss resistance; instead, for collapse arrest at large displacements, joints with small bolts provide rotation capacities of approximately 100 mrad but with reduced resistance, when compared to the initially undamaged (I.U.) joint performance.

The best P.C. column loss performance was obtained for joints with intermediate diameter bolts (M20), with variations between I.U. and P.C. responses in terms of both strength and rotation capacity under 2%.

The endplate thickness was found to have a limited effect on P.C. column loss response and no correlation was found between endplate thickness and rotation or strength capacity; increasing bolt rows was shown to be highly beneficial in terms of P.C. ultimate resistance, due to improved transmission of tensile forces, although improvements in terms of rotation capacity are small. Adding bolt rows can partially compensate for joint strength softening at high rotational demand.

The findings presented in this Chapter constitute a contribution to the present body of knowledge on seismic and progressive collapse behaviour of steel beam-column joints. The obtained results provide some guidance for designers to select joint configurations that avoid premature plate fracture or bolt failure and that maximise joint performance. Considering the complexity of the phenomena that contribute to FEP joint response and the reduced amount of research and experimental data available, namely under column loss action, it is the opinion of the Author that this topic should be the subject of an experimental campaign to confirm the present findings and to provide further data to prepare guidelines for the seismic and robust design of FEP joints.

## Chapter 7 Nonlinear dynamic analysis of MRF structures under column loss scenarios

### 7.1 Introduction

In this chapter, a parametric study is conducted to assess the response of 3D MRF structures to column loss and post seismic column loss scenarios, using Nonlinear Dynamic Analysis (NDA). The contribution of the secondary gravity frame connections is taken into account by explicitly modelling the beam-to-beam and beam-to-column joints using nonlinear links. In particular, the FEP joint typology is adopted for the beam-to-column joints and the response to column loss is modelled and calibrated in accordance with the results presented in Chapter 6. The contribution of the façade claddings is also taken into account, in order to evaluate the effectiveness of these elements in reducing the maximum dynamic demand under column loss. The results from the preliminary robustness assessment presented in Chapter 4 served as the base for the selection of the most relevant analysis cases, which correspond to structural typologies with low robustness levels, as further explained in this Chapter.

These analyses are thus aimed at addressing some of the current open topics of research related to the structural robustness of steel structures. Some of the investigated parameters include the maximum rotational demands on members and connections, as well as the Demand-to-Capacity ratios of different structural members. This enables to evaluate the margins of safety under column loss, as well as to determine which are the elements that would contribute the most to enhancing overall MRF robustness through improved detailing. The assessment of the effect of the façade infill panels on reducing the maximum dynamic displacements under column loss and for such a large number of cases has not yet been conducted and can provide information regarding its adequacy as a viable collapse arresting strategy. The analysis

of the internal forces in the beams and columns of the DAZ enables to quantify the relative contribution of the different collapse arresting mechanisms, as well as to determine for MRFs, how current regulation tying forces (see Section 2.3.2) compare with the catenary forces required to arrest the progressive collapse. The assessment of the cases of collapse is also compared to the tolerable area at risk of collapse (see Section 2.3.3) defined in the EN 1991-1-7 (CEN, 2006).

By comparing the post seismic column loss response to that for the initially undamaged structures, the impact of seismically induced damaged on structural robustness is quantified. These results provide the basis for the evaluation of the level of safety and reserve capacity of MRF structures after seismic events, providing also indications regarding the safety for rescue party interventions in post seismic scenarios and regarding the necessity for installing temporary propping prior to rescue interventions.

## **7.2 Framework of the study**

### **7.2.1 Generalities**

In this Chapter, the behaviour of MRF structures is analysed under different column loss scenarios and for two states prior to notional column removal, namely: i) for the undamaged structure and ii) for the initially damaged structure, where the damage is introduced by a seismic action compatible with the design approach described in EN 1998-1 (CEN, 2004). The initially undamaged MRF structures will be subjected to column loss and their response will constitute the baseline robustness of these frames, i.e. the base with which the post seismic robustness will subsequently be compared. This will enable to quantify the effect of the design seismic action in reducing the robustness of MRF structures. The properties and characteristics of the MRF structures analysed in this Chapter are as previously described in Chapter 3.

### **7.2.2 Investigated parameters**

The set of structures considered for the robustness assessment described in this Chapter consists of the set of 96 different structures designed according to the methodology previously presented in Chapter 3. These structures vary in terms of the following parameters: number of storeys, interstorey height, span, bay configuration,

design lateral loads and façade claddings. For what concerns the baseline robustness, the full set of 96 structures was analysed under column loss for the 3 different column loss location scenarios described in Table 3.1.

As for the preliminary robustness assessment described in Chapter 4, each structure presents two MRFs per direction, while the remaining structural elements are designed to resist gravity loads only. The beam-to-column joints of the MRF were assumed to be fully rigid, whereas the secondary frame joints were modelled according to their response in bending and under column loss action, according to the modelling criteria described in Section 7.2.6.

The list of investigated parameters and corresponding values for the baseline robustness assessment, i.e. for the robustness assessment considering initially undamaged structures, can be consulted in Table 3.1.

As seen in Table 3.1, for the “Façade claddings” variable, three cases are investigated. The masonry claddings were considered only for the case of wind designed structures (i.e. DW-CM case), whereas panels with cold formed steel bracings were considered for seismic+wind designed frames (i.e. DE-CC case). This is due to the fact that, for the present study, it was considered that in Europe, many cases of steel MRF structures were designed in seismic areas in past decades, hence before seismic design codes were available. In these cases, structures were designed for gravity and wind actions only and façade claddings typically consisted of masonry. Instead, new structures in seismic zones are designed according to seismic design regulations and designers tend to use lighter façade materials, requiring smaller assembly times and employing dry assembled technology. To be consistent with this present trend, the façade cladding type considered for seismically designed frames consisted of a cold formed steel panel which is commercially available. A more complete description of the façade cladding types and properties is presented in Section 7.2.6.

The column removal scenarios considered for the robustness assessment are those indicated previously in Table 3.1. The locations of the removed columns were defined in accordance with the UFC 2009 (United States of America Department of Defense, 2009), and are the same as those shown in Figure 4.1. For all cases, the section to be removed is located between the ground level and the first storey, as previously stated in Section 3.2.2.

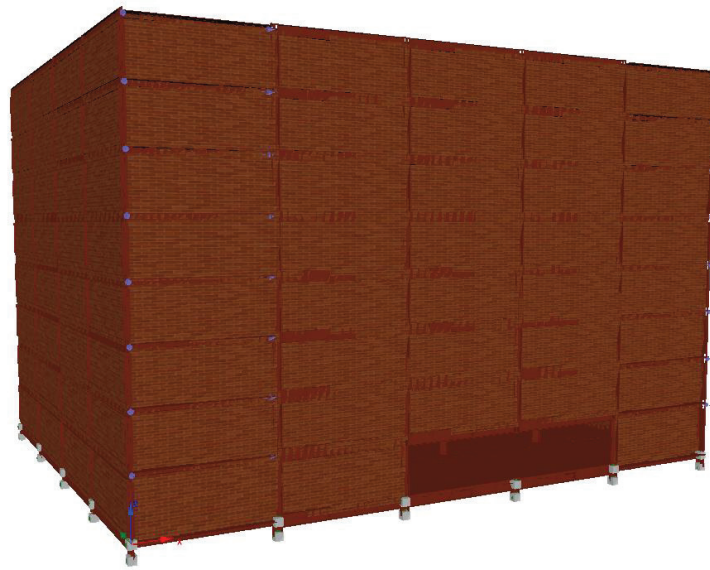


Figure 7.1: Example of an LL column removal location scenario – Case N8-H4-S10-CM-T5x4-DW-LL

The cladding elements adjacent to the removed column are also notionally removed. This hypothesis is consistent with explosion, vehicle collision or localised fire scenarios in which the adjacent façade claddings are also affected by the triggering event.

For the case of the post seismic robustness assessment, only the 4-storey frames subset was analysed since, as shown in the preliminary robustness assessment in Chapter 4, these structures inherently display lower robustness, owing to the reduced number of elements to which loads can be vertically redistributed in the directly affected zone (DAZ). Furthermore, only seismically designed frames (i.e. DE frames) were analysed for post-seismic robustness, since the wind designed frames (i.e. DW frames) are not designed for seismic action and are expected to fail, for which reason they are not analysed in this study. Since 8-storey structures under seismic action are more prone to remain elastic, due to the stringent lateral storey drift limitation criteria, no post-seismic reduction in robustness is expected, for which reason this structural subset was not analysed for post-seismic robustness.

### **7.2.3 Design assumptions**

The design assumptions are the same as those described in Section 4.3.2.



### 7.2.4 Monitored parameters

To provide an assessment of the structural performance under column loss scenarios, it is important to monitor the contribution of the different collapse resisting mechanisms (Centre for the Protection of National Infrastructure, 2011), such as: i) frame catenary action; ii) shear deformation of deep transfer beams; iii) membrane action in slabs with central column removal; iv) Vierendeel action; v) compressive arching action between composite slab and steel beams; vi) compressive strut action in façade claddings.

The adopted finite element modelling using Seismostruct (Seismosoft, 2014) directly accounts for frame catenary action, shear deformation of deep beams and Vierendeel action. Membrane action in slabs was not accounted for since the present study is devoted to assessing the robustness of the bare steel structures, which is especially relevant in cases in which the pavement is not a steel-concrete composite slab with shear interaction. Furthermore the removed columns are located in the façade which limits the contribution of the membrane action. The contribution of the compressive arching action between composite slab and steel beams is zero since the beams are disconnected from the composite slab at the ends (see also Section 3.3.1.2.2), rendering the MRF an all-steel structure. The cladding compressive strut action was quantified by explicitly modelling the façade infill panels.

To quantify the system's reserve displacement capacity, the Residual Ductility Ratio (*RDR*) was computed as shown in Eq.(4.4), where  $(u_{u,damaged})$  is the ultimate displacement (immediately prior to collapse) and  $(u_{dyn,max,damaged})$  the maximum dynamic displacement evaluated through NDA. Considering however that the maximum dynamic displacement after column loss  $(u_{dyn,max,damaged})$  typically differs from the displacement value after the structure has stabilised and reached equilibrium  $(u_{dyn,equil,damaged})$ , depending on the degree of plasticity developed in the DAZ, a ratio was introduced to quantify the development of plasticity in the DAZ as follows:

$$DOP_{DAZ} = \frac{u_{dyn,equil,damaged}}{u_{dyn,max,damaged}} \quad (7.1)$$

where  $DOP_{DAZ}$  can vary between 0.5 for a fully elastic DAZ response (similarly to a SDOF system under impulse load - see Chopra, 1995) and 1 for a perfectly plastic

behaviour. This ratio enables the quantification of the capacity of different structural typologies to mobilise plasticity for arresting the progressive collapse. Furthermore, in order to evaluate the level of safety of the structures for rescue party interventions in post seismic column loss scenarios, the system's reserve ductility relative to the final equilibrium displacement after the column loss ( $u_{dyn,equl,damaged}$ ) was also computed as follows:

$$RDD_{equil} = \frac{u_{u,damaged}}{u_{dyn,equl,damaged}} = \frac{u_{u,damaged}}{DOP_{DAZ} \cdot u_{dyn,max,damaged}} \quad (7.2)$$

The information provided by the  $RDD_{equil}$  ratio is in fact better suited to evaluate system reserve safety than the  $RDR$  evaluated for the maximum dynamic displacement, since at the time of a rescue intervention the structure will have stabilized and reserve ductility capacity should be measured from the stabilised equilibrium position ( $u_{dyn,equl,damaged}$ ) and in relation to the ultimate displacement at collapse ( $u_{u,damaged}$ ).

The ductility demand-to-capacity ratios  $DCR_{ductility}$  were also computed for MRF and secondary gravity frame members, in order to identify the structural components that should be preferably reinforced in order to enhance global structural robustness. The ductility  $DCR$  ratio for member  $i$  in structure  $j$  was computed according to the following expression:

$$DCR_{ductility,ij} = \frac{u_{dyn,damaged,j}}{u_{u,damaged,i}} \quad (7.3)$$

where ( $u_{dyn,damaged,j}$ ) is the maximum dynamic displacement (or rotation) subsequent to column removal in structure  $j$  (depends of the characteristics of structure  $j$  and of all members  $i$ ), i.e. the ductility demand, whereas ( $u_{u,damaged,i}$ ) is the ultimate displacement (or rotation) capacity of member  $i$  when subjected to column loss action (is independent of the characteristics of structure  $j$ ) i.e. the member ductility capacity. The identification of the elements with the highest  $DRC_{ductility}$  ratios is subsequently used as the base for the proposed design guidance for enhancing structural robustness in MRF structures.

The vertical velocity and acceleration of the DAZ was monitored for all analysis cases, hence enabling to determine velocity and acceleration profiles over time, from the instant of column removal to the first zero velocity condition instant. These results are particularly useful for studies on connection performance under column loss action and also to quantify strain rate effects in connections. Furthermore, the research recommendations provided by the Centre for the Protection of National Infrastructure (2011) state that the assessment of whether the column loss and the load redistribution can be assumed to occur independently has not been sufficiently researched. The acceleration data collected from the conducted numerical simulations can therefore provide valuable information regarding the timescale over which mass mobilisation occurs, which is important when considering a hazard-dependent approach. If the DAZ mass is mobilised over a timescale that is larger than the column loss action rise time, the mass can provide an apparent axial restraint on the column, enhancing resistance and reducing the likelihood of failure; conversely, if the mass is mobilised over a timescale significantly smaller than the column loss action rise time, the DAZ mass can have a drag down effect, increasing the rate at which the unbalanced load must be transferred to alternative load paths, increasing the dynamic demand on the structural elements and increasing the probability of failure. Further research into this topic would however require the conduction of simulations for different values of column loss action rise time, which falls outside the scope of the present study.

The maximum axial force, bending moment and rotation of the joints of the MRF and of the secondary structure were also monitored and maximum catenary tensile forces were compared to the values obtained via the prescriptive Tie Force Method for increasing robustness provided in the EN 1991-1-7 (CEN, 2006).

The forces in the cladding members of the DAZ were monitored in order to identify how the force is distributed in these elements after the column loss, and to quantify the relative importance of this collapse arresting mechanism in comparison to other relevant mechanisms.

## 7.2.5 Analysis methodology

### 7.2.5.1 Analysis type

The robustness assessment described in this Chapter was performed with the Seismostruct software (Seismosoft, 2014) using Nonlinear Dynamic Analysis (NDA). This analysis type is the most theoretically rigorous and complex, since it can account for material and geometrical nonlinearity, while implicitly modelling dynamic amplification effects and damping.

The geometrical nonlinearity is accounted for using the total co-rotational formulation, which is based on the exact description of the kinematic transformations associated with large displacements and three-dimensional rotations of the beam-column member (Seismosoft, 2014).

Distributed inelasticity elements were adopted, which take advantage of a fibre approach to represent cross section behaviour, where each fibre is associated with a uniaxial constitutive law. The section internal forces are subsequently determined by integration in the cross section of the response of the individual fibres. The adopted fibre model is particularly suitable for the present robustness assessment, since element hysteretic energy dissipation and N-M-V interaction are implicitly accounted for.

The NDA was performed by resorting to the Frontal solver, which is particularly suitable for sparse systems and was found to be at least 5 times faster when compared to the Skyline solver, which tends to be slower for very large models (Seismosoft, 2014). The Hilber-Hughes-Taylor numerical integration scheme was adopted to solve the system of equations of motion and in terms of damping, the mass- and stiffness-proportional Rayleigh formulation was adopted, considering tangent stiffness-proportional damping, which is considered to be the most suitable option for common structures (Seismosoft, 2014).

As shown by Alashker *et al.* (2011), 2D modelling leads to higher and unrealistic deformations owing to limited redistribution capacity. Three-dimensional modelling is therefore required to rigorously investigate system robustness, for which reason the structures were modelled in 3D, realistically simulating the load path redistribution throughout the secondary gravity frame members.

### 7.2.5.2 Material definition

The materials considered for the beams and columns of the analysed structures are those described in Section 3.3.2. The uniaxial response of steel was modelled according to the Menegotto-Pinto steel model provided in Seismostruct (Seismosoft, 2014)) and shown in Figure 7.2.

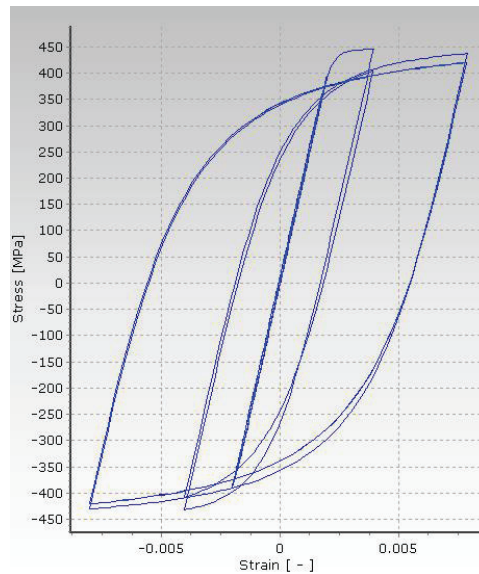


Figure 7.2: Menegotto-Pinto steel model constitutive law for S355 steel

This steel model requires the definition of ten modelling parameters to fully describe the mechanical characteristics of the material. The list of the adopted parameter values for the S355 steel using the Menegotto-Pinto model is shown in Table 7.1. The adopted yield strength value was considered equal to the nominal steel yield stress value from EN 1993-1-1 (CEN, 2005) times the  $\gamma_{ov}$  factor provided in EN 1998-1 (CEN, 2004) which is equal to 1.25, in order to account for the average material overstrength. In cases in which high strength steel was used for MRF column, the adopted material parameter values were the same as those presented in Table 7.1, at the exception of the yield stress, which was obtained by factoring the steel nominal value by the  $\gamma_{ov}$  factor.

Table 7.1: Menegotto-Pinto steel model (Seismosoft, 2014) – parameter definition for S355 steel

Material properties	Symbol	Values	Units
Modulus of elasticity	$E_s$	2.0E8	[kPa]
Yield strength	$f_y$	443750	[kPa]
Strain hardening parameter	$\mu$	0.005	[-]
Transition curve initial shape parameter	$R_0$	20	[-]
Transition curve shape calibrating coefficient	A1	18.5	[-]
Transition curve shape calibrating coefficient	A2	0.15	[-]
Isotropic hardening calibrating coefficient	A3	0	[-]
Isotropic hardening calibrating coefficient	A4	1	[-]
Fracture/buckling strain	-	0.1	[-]
Specific weight	$\gamma$	78	[kN/m <sup>3</sup> ]

For the steel-concrete composite beams of the secondary gravity resisting frame, concrete in strength class C30/37 was adopted and modelled according to the Mander *et al.* nonlinear concrete model from the Seismostruct (Seismosoft, 2014) material library. This consists of a uniaxial nonlinear formulation which assumes constant confining pressure throughout the full stress-strain range and which can effectively simulate the cyclic response of the concrete material. The material stress-strain response is shown in Figure 7.3.

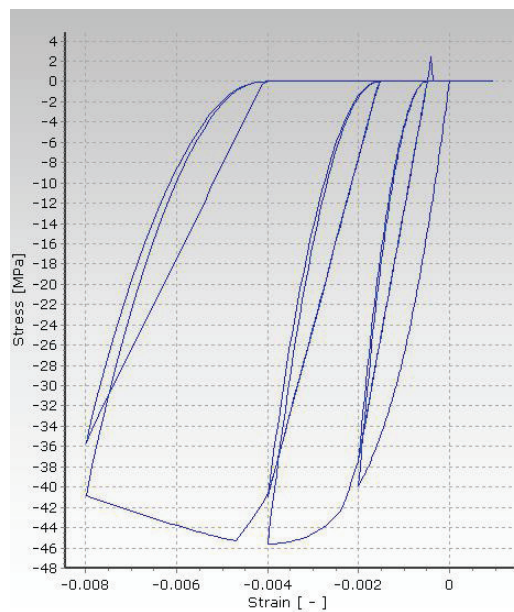


Figure 7.3: Mander *et al.* concrete model constitutive law for C30/37 concrete

The concrete property values were taken as the mean values provided in EN 1992-1-1 (CEN, 2004). The five material calibrating parameters and corresponding adopted values are presented in Table 7.2.

Table 7.2: Mander *et al.* concrete model (Seissoft, 2014) – parameter definition for C30/37 concrete

<b>Material properties</b>	<b>Symbol</b>	<b>Values</b>	<b>Units</b>
Compressive strength	$f_c$	38000	[kPa]
Tensile strength	$f_t$	2900	[kPa]
Modulus of elasticity	$E_c$	3.3E7	[-]
Strain at peak stress	$\varepsilon_c$	0.002	[-]
Specific weight	$\gamma$	24	[kN/m <sup>3</sup> ]

To model rigid one-dimensional finite elements, the Elastic material model (Seissoft, 2014) was adopted, which consists of a uniaxial material model with symmetric behaviour in tension and in compression. A modulus of elasticity value  $E=2.0E20$  kPa was adopted, after preliminary tests having shown this value to be sufficiently high so as to provide the required result accuracy, while being also sufficiently low so as to avoid numerical instability. Since this material was adopted to model fictitious elements, its specific weight was taken as  $\gamma=0$  kN/m<sup>3</sup>.

#### 7.2.5.3 Element class definition

To model all columns (i.e. both MRF and internal columns) as well as the beams of moment resisting frames, the inelastic force-based frame element type was adopted, since the modelling of these elements is critical to the robustness assessment. This element type is capable of capturing geometric and material nonlinearities and can fully account for the spread of plasticity along the member length and across the section depth. It constitutes the most accurate inelastic frame element available in the Seissoft software and it is capable of capturing inelastic behaviour along the length of the member with a single element per member. In terms of element subdivision, a total of 5 integration sections per element was considered, according to the distribution shown in Figure 7.4, where the percentages of the member length of the end and second sub-divisions were considered equal to 10% and 20% respectively.

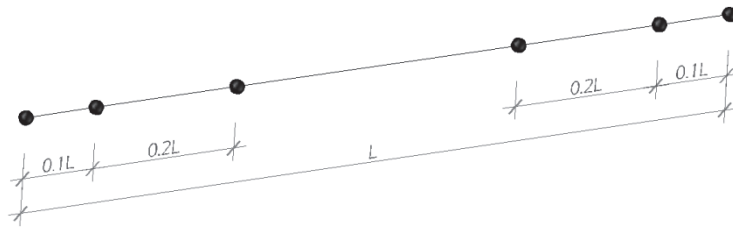


Figure 7.4: Inelastic force-based frame element – integration section distribution

For what concerns the secondary frame joints, the flush end-plate joint typology was adopted for the beam-to-column joints, whereas for the beam-to-beam joints, a web cleat joint typology was assumed. For beam-to-column FEP joints under column loss, no catenary final stage (see Figure 6.10) can be achieved, as shown previously in Chapter 6, therefore implying that the joints constitute the weak link, while the beam member remains largely elastic. This is also true for the web cleat joint configurations adopted in the present study, which were found to be nominally pinned in terms of the EN 1993-1-8 (CEN, 2005) strength classification. The beams of the gravity frame were hence modelled using elastic frame elements while the connections were modelled using nonlinear links. The detailed description of the nonlinear link modelling and calibration is presented in Section 7.2.6.

Fictitious rigid elements were modelled using the elastic frame element type .

To model the façade claddings, inelastic infill panel elements were adopted. This element type requires the input of the coordinates of four nodes to subsequently generate six strut members, where for each diagonal direction, two parallel struts carry axial load, while a third compression activated strut transfers the shear load from the top to the bottom of the panel, as illustrated in Figure 7.5.

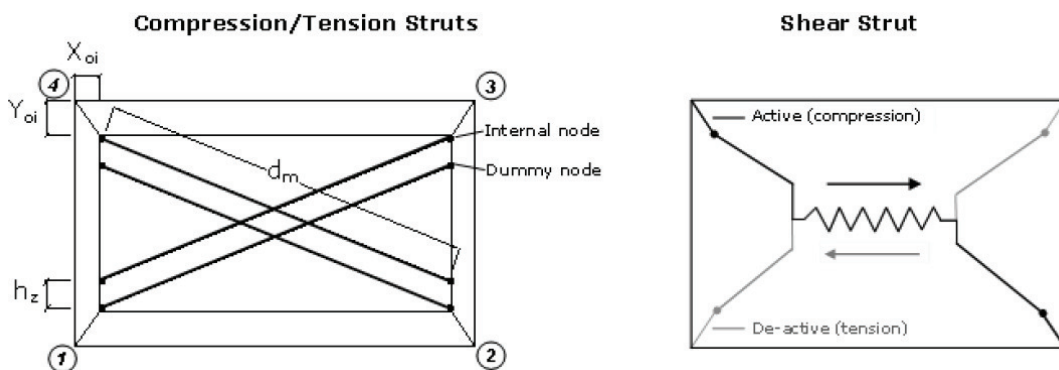


Figure 7.5: Inelastic infill panel element – strut definition (Seismosoft, 2014)



The inelastic infill panel element is extremely versatile in the sense that it allows the use of different formulations to be adopted for the characterization of the compression/tension and shear struts. The modelling of the claddings is discussed in further detail in Section 7.2.6.

Lumped mass elements were used to model the floor masses which were offset from the floor's centre of mass according to the rules provided in EN 1998-1 (CEN, 2004).

#### *7.2.5.4 Restraints*

The supports of the structure were defined so as to simulate the foundation of the MRF structures described in Section 3.3.1.1 and modelled as in the preliminary robustness assessment described in Chapter 4.

#### *7.2.5.5 Constraints*

In order to model the floor slabs, rigid diaphragms were introduced at storey level to compatibilize node translations in the X-Y plane. The constraints were applied using penalty functions with a penalty function exponent equal to  $1E10$ , which was found to be both suitable for analysis and also numerically stable.

Given that the catenary effect constitutes one the most important collapse arresting mechanisms, the introduction of a rigid diaphragm in the directly affected zone would lead to spurious column loss response. To avoid this situation, the nodes appertaining to the DAZ were not considered for the diaphragm. The axial stiffness of all joints of the DAZ was verified to be greater than that considered for the diaphragm, for which reason the model can adequately simulate response to both seismic and column loss action. Furthermore, an Eigen analysis was performed to compare the natural frequencies of vibration of models with and without DAZ nodes included in the diaphragms, which showed no differences, hence validating the adopted modelling strategy.

#### *7.2.5.6 Action definition and combination criteria*

The permanent loads which consist of the gravity loads and equivalent geometrical imperfection loads are those previously described in Section 3.3. The

variable time-history loads are input as ground accelerations applied to the restrained nodes that correspond to the foundations of the structures.

For the case of the robustness assessment of the initially undamaged frames, the ground accelerations applied to the foundation nodes are equal to zero, whereas for the post seismic robustness assessment, signals were selected to match the design EN 1998-1 (CEN, 2004) Type 1 response spectrum. In this case, the Type 2 seismic action was found to not condition the design and therefore no Type 2 seismic action was considered. For what concerns the seismic action definition, the EN 1998-1 (CEN, 2004) states that “...the seismic motion may also be represented in terms of ground acceleration time-histories and related quantities (velocity and displacement)” and also that “...the description of the seismic motion may be made by using artificial accelerograms and recorded or simulated accelerograms”.

In this study natural accelerograms records were used for structural analysis. These signals were selected using an application for the selection of earthquake ground motions designated as SeIEQ (Dias *et al.*, 2010), which allows to select records according to current seismic design code requirements, namely the Eurocode 8 and which provides record suites that are compatible with a given response spectrum. The SeIEQ tool provided a set of Type 1 accelerograms, as well as the corresponding scaling factors to render the signals compatible with the response spectra characteristics described in Section 3.3.3.5 through spectral shape matching for a given vibration period range. The general characteristics of the Type 1 earthquake records suite are presented in Table 7.3.

Table 7.3: Records for Type 1 seismic action spectral matching – general characteristics

Signal designation	Earthquake name	Year	Magnitude	Station name	Station soil $v_{s,30}$ [m/s]
T1-1	Tabas, Iran	1978	7.35	Dayhook	659.6
T1-2	Loma Prieta	1989	6.93	SF - Diamond Heights	582.9
T1-3	Chi-Chi, Taiwan	1999	7.62	ILA064	375.3
T1-4	Coyote Lake	1979	5.74	San Juan Bautista, 24 Polk St	370.8
T1-5	Chi-Chi, Taiwan	1999	7.62	TCU072	468.1
T1-6	Coalinga-01	1983	6.36	Parkfield - Gold Hill 2W	376.1
T1-7	Chi-Chi, Taiwan	1999	7.62	TCU046	465.6
T1-8	Chi-Chi, Taiwan-06	1999	6.30	CHY035	473.9
T1-9	Chi-Chi, Taiwan-03	1999	6.20	TCU138	652.9
T1-10	Chi-Chi, Taiwan	1999	7.62	HWA035	473.9

The spectral shape matching performed by the SeIEQ tool (Dias *et al.*, 2010) was optimized for the range of natural vibration periods of the analysed structures. The SeIEQ outputs regarding scaling factors and signal sampling time intervals are summarised in Table 7.4, where it should be noted that the signal scaling factors present relatively low values, ranging from 0.51 to 4.0.

Table 7.4: Records for Type 1 seismic action spectral matching –scaling factors and time steps

<b>Signal designation</b> [-]	<b>Earthquake name</b> [-]	<b>Scaling factor</b> [-]	<b>Time interval</b> [s]
T1-1	Tabas, Iran	1.43745	0.02
T1-2	Loma Prieta	3.99998	0.005
T1-3	Chi-Chi, Taiwan	4.00000	0.004
T1-4	Coyote Lake	3.87590	0.005
T1-5	Chi-Chi, Taiwan	0.51378	0.005
T1-6	Coalinga-01	3.16504	0.01
T1-7	Chi-Chi, Taiwan	2.04276	0.005
T1-8	Chi-Chi, Taiwan-06	2.38019	0.005
T1-9	Chi-Chi, Taiwan-03	2.49838	0.004
T1-10	Chi-Chi, Taiwan	3.99999	0.005

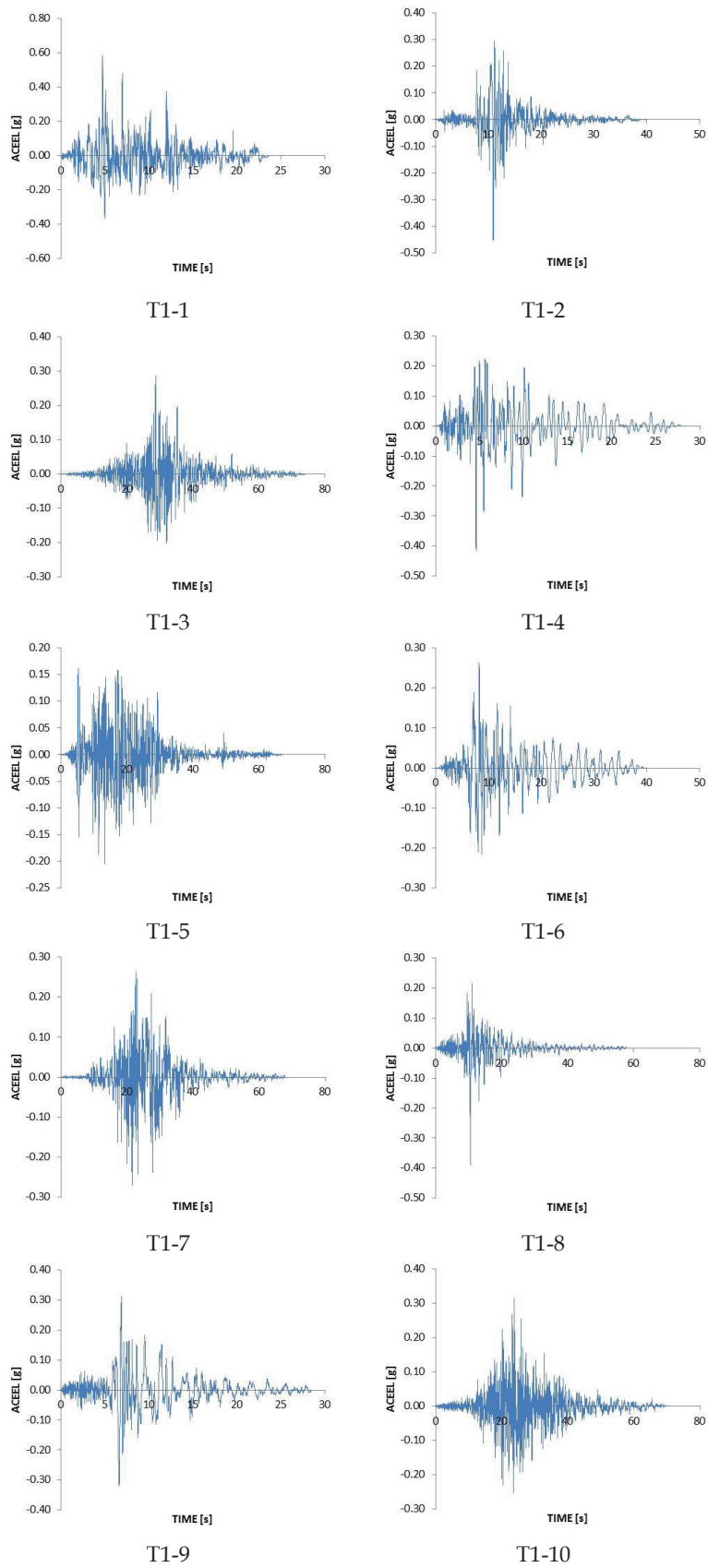


Figure 7.6: Scaled signals for Type 1 seismic action

The scaled signals for Type 1 seismic action are presented in Figure 7.6 and the target, group average and single signal response spectra generated from the signals presented in Figure 7.6 are presented in Figure 7.7, showing that the scaled signals provide for a very good fit with the target response spectra, namely in the period range corresponding to the natural periods of vibration of the analysed structures.

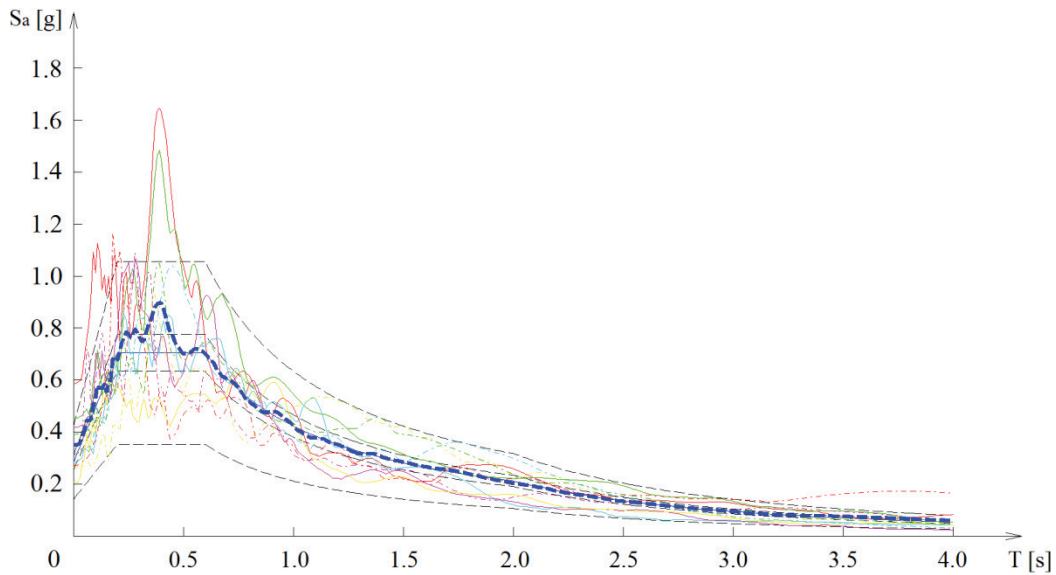


Figure 7.7: Target, group average and single signal response spectra for Type 1 seismic action

For what concerns multidirectional seismic effects, each signal was input into the  $x$ ,  $y$  and  $z$  directions, with scaling factors equal to 1 in one horizontal direction, and 0.3 in the other directions. This approach, here designated as Approach 1, enables to introduce a level of damage prior to the column loss event that is well known, quantifiable and compatible with the design action provided in EN 1998-1 (CEN, 2004).

A different approach to introducing an initial damage compatible with a realistic seismic action would also have been possible, consisting of using different signals for the  $x$ ,  $y$  and  $z$  directions, as actually occurs in reality. However this approach, here designated as Approach 2, was abandoned since it was found to lead to a set of problems related to the interpretation of the data and their relevance and usefulness for quantifying post seismic robustness. Indeed, when using set of signals registered in perpendicular directions in a seismic station, it would theoretically be possible to scale all 3 signals according to three different scaling factors, so as to match each signal's response spectrum to the design response spectrum, or even possibly to

create a procedure that would use a single scaling factor for all 3 signals and try to match the horizontal SRSS spectrum to the horizontal design spectrum. However, such an option introduces the question of how to orientate the structure in relation to the signals. In this case, it would not be possible to determine which of the horizontal direction signals would be introducing the most damage to the structure. Indeed, although using different accelerograms for different directions is more realistic, it does not allow to control to which MRF (i.e.  $x$  oriented or  $y$  oriented) is the most significant damage being introduced, nor to control the amount of damage. Paradoxically, it would be both possible and likely to introduce a set of signals in the  $x$ ,  $y$  and  $z$  directions that would introduce significant damage to the  $YZ$  plane MRFs and little to no damage to the  $XZ$  plane MRFs and then analyse the response to a column removal in a  $XZ$  façade, which would necessarily show no difference between the initially undamaged and the seismically damaged response to column loss, despite the fact that such a difference potentially exists. The methodology designated as Approach 2 was therefore found to not be suitable to evaluate the post seismic robustness as intended for this study and was therefore abandoned.

Due to the above described reasons, the methodology designated as Approach 1 was adopted and the post seismic robustness was therefore evaluated considering a seismic damage compatible with the design seismic action, which is well known and quantifiable; in all cases, the column was therefore notionally removed subsequent to the corresponding MRF having sustained maximum damage, characterized by 100% of the scaled seismic record, while the transverse MRFs were subjected to 30% of the effect of the same scaled record.

The column loss action was simulated in Seismostruct (Seismosoft, 2014) through the element connectivity feature, which allows establishing activation/de-activation times for structural elements. In this sense, after the end of the seismic action and after the structure has stabilised, the relevant column element is de-activated, effectively simulating an instantaneous column removal.

To determine the time required for the structure to stabilise, an upper bound value was initially estimated. Indeed, after sustaining the column loss action, the MRF structure response can be likened to that of a SDOF system under free under-critically damped vibration (see Figure 7.8). This regime is characterised by the equivalent

viscous damping ratio  $\zeta$ , which for typical steel structures is low and typically assumed equal to 2% for steel building frames.

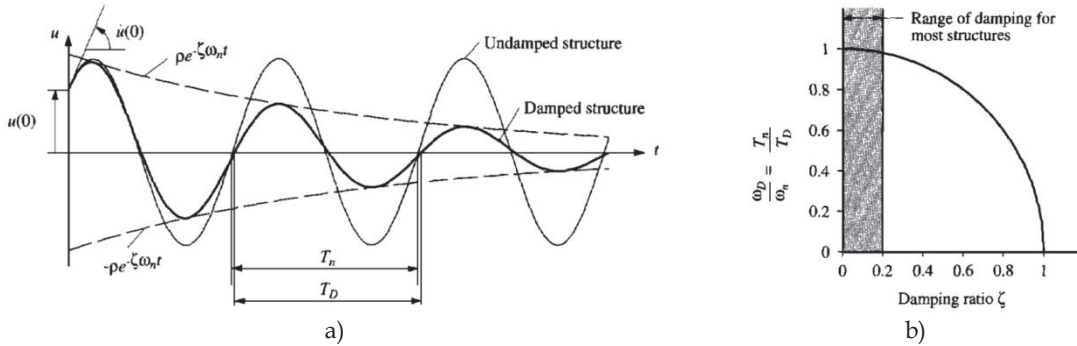


Figure 7.8: SDOF under-critically damped system (Chopra, 1995): a) effect of damping on free vibration; b) relationship between frequency and damping ratios

The equation that relates two consecutive displacement peaks  $u_i$  and  $u_{i+1}$  is given by (Chopra, 1995) as follows:

$$u_i/u_{i+1} = \exp\left(\frac{2\pi\zeta}{\sqrt{1-\zeta^2}}\right) \quad (7.4)$$

where  $\zeta$  is the damping ratio. The logarithmic decrement of damping  $\delta$  is defined as:

$$\delta = \ln(u_i/u_{i+1}) \quad (7.5)$$

Combining the two equations above, the following expression is obtained:

$$\delta = \frac{2\pi\zeta}{\sqrt{1-\zeta^2}} \quad (7.6)$$

If  $\zeta$  is small (i.e.  $\zeta < 0.2$ ), over  $j$  cycles, the approximate equation is valid:

$$\delta = \frac{1}{j} \ln \frac{u_1}{u_{j+1}} \approx 2\pi\zeta \quad (7.7)$$

The relationship between motion decrease and the number of cycles for  $\zeta=2\%$  is plotted in Figure 7.9. In order to decrease the ratio between displacement maxima to  $u_{j+1}/u_j=10\%$  a minimum of  $j_{min}=18$  cycles are required, which for a natural vibration

period  $T_{avg}=1.5s$  for example, would imply the NDA to be prolonged by  $j_{min}T_{avg}=27s$  after the column removal event, to enable the structural systems to stabilize.

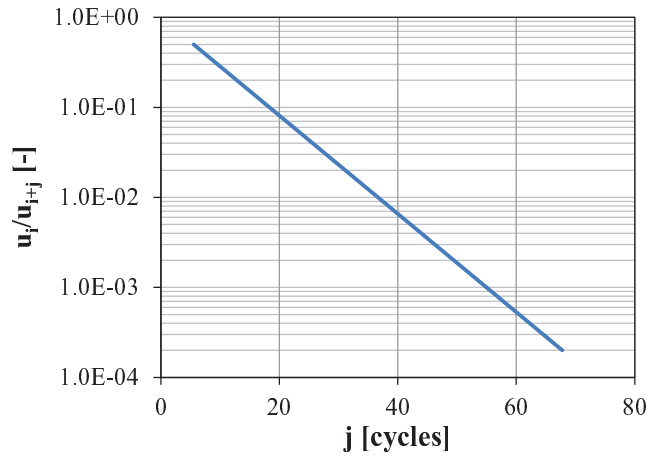


Figure 7.9: Decrease of motion  $u_i/u_{i+j}$  versus number of cycles  $j$  for  $\zeta=2\%$

This value was found to be too high, since at the end of the seismic action, both the ground motion amplitude as well as the structure’s vibration amplitude is already significantly quite low. By trial and error, an interval of 6s was found to be sufficient in most cases for the structure to stabilise and to reduce horizontal displacements to negligible values. This time interval was increased whenever it was found not to be sufficient.

In terms of action combination criteria, the Accidental load combination expression provided in EN 1991-1-7 (CEN, 2006) and previously used for the the NDA conducted in Chapter 4 of this dissertation was adopted.

## 7.2.6 Modelling assumptions

### 7.2.6.1 Foundations

The foundations were modelled according to the geometry previously defined in Section 3.3.1.1 which was composed by a continuous structural concrete slab and by small peripheric concrete struts that restrain horizontal translations at the ground storey level. An example is presented in Figure 7.10 showing the restraints marked as grey cubes, as well as the applied dynamic time-history ground accelerations marked with green arrows.



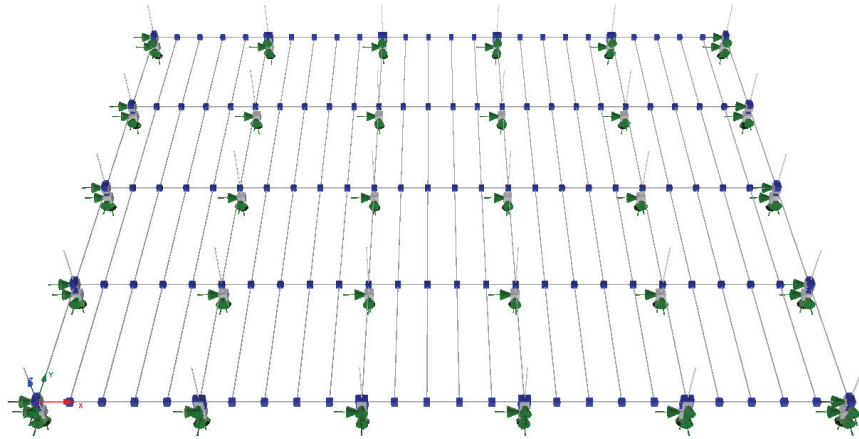


Figure 7.10: Foundation modelling for the N4-H3-S10-CN-T5x5-DW

### 7.2.6.2 Floor structure

The floor system is composed of a composite slab, which is supported by secondary steel beams with composite action and 2m spacing. The secondary beams are in turn supported by primary composite beams which transfer loads to the columns. The floor layout for the N4-H3-S10-CN-T5x5-DW structure is presented in Figure 7.11, where the secondary beams are aligned in the  $y$  direction, whereas the primary beams are aligned in the  $x$  direction (see also Figure 3.3). The web cleat joint and the flush end-plate typologies were adopted for the beam-to-beam and beam-to-column joints, respectively. In both cases, nonlinear links were used for modelling joint response, as further described in this Chapter. All modelled linear and nonlinear links are represented by blue cubic elements in Figure 7.11.

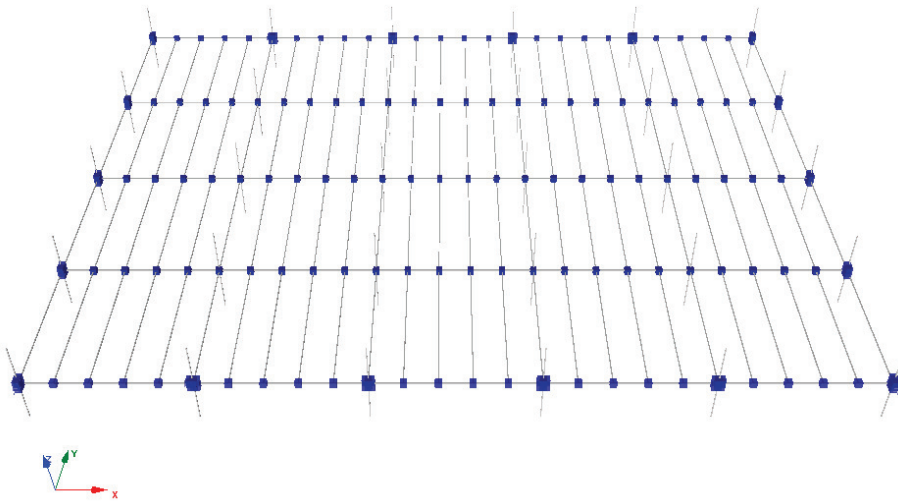


Figure 7.11: Floor structure modelling for the N4-H3-S10-CN-T5x4-DW

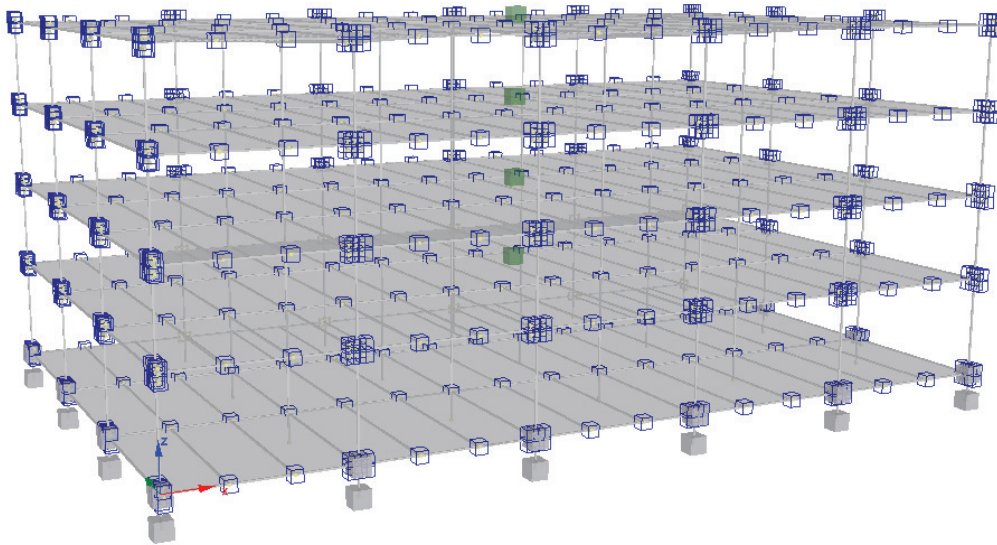


Figure 7.12: Numerical model of the N4-H3-S6-CN-T5x3-DE frame

It should be noted that the present study is not aimed at studying the effect of the composite slab in arresting progressive collapse, despite its well known relevant role. For the present study, only the role of the bare all-steel structures is evaluated and the membrane effect contribution of the concrete slab is disregarded, in accordance with the hypothesis that all composite beams are designed as simply supported, and therefore no continuity of internal forces is transmitted by the reinforced concrete slab element (the minimum rebar areas of the composite slab are hence disregarded for robustness purposes). This enables the conclusions from this work to extend to cases in which the floor structure is not a steel-concrete composite slab, as is the case, for example, of structures with timber pavements or of other cases in which the shear interaction with the steel beams is not mobilised.

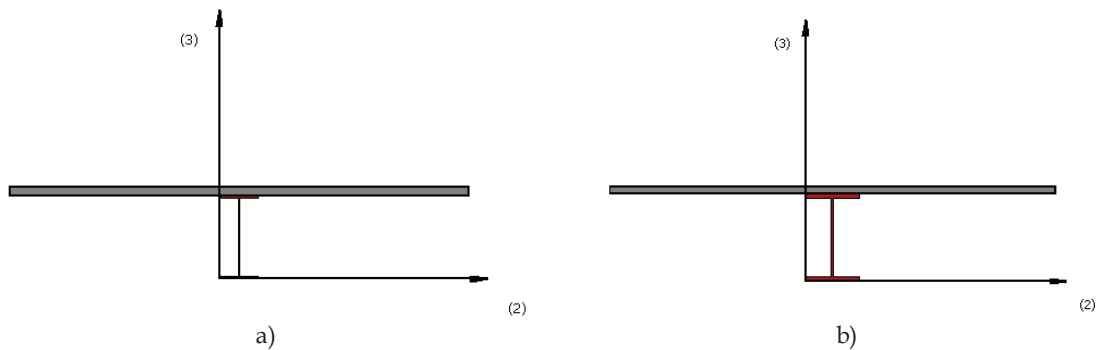


Figure 7.13: Modelling of gravity frame composite beams: a) secondary beams; b) primary beams

The composite beams were modelled with their respective effective slab width, to more accurately simulate the beam end rotations at the instant of column removal.

#### 7.2.6.3 MRF beam-to-column joints

The action of wind and seismic lateral loads introduces elevated shear forces in the column web panel (CWP) of the MRF beam-to-column joints, leading to large energy dissipation in these elements. Furthermore, the CWP deformation can supply an important part of the joint's rotation capacity (Dubina *et al.*, 2001) and significantly influence total lateral drift and base shear strength (Schneider and Amidi, 1998). Past experimental tests by Krawinkler *et al.* (1971) on beam-to-column joints have enabled to highlight several key features regarding CWP behaviour. As stated in El-Tawil *et al.* (1999), CWP zones under shear display significant post-yield strain-hardening effect coupled with very ductile behaviour, characterized by stable hysteretic loops even at large deformations. In addition, the maximum CWP shear capacity is not easily reached, since it would require a very large interstorey drift. Recent design codes such as the AISC 341-05 (AISC, 2005) or the EN 1998-1 (CEN, 2004) provide criteria for modelling and designing the CWP zone. In particular, the Eurocode 8 allows for energy dissipation within the beam-to-column joint, although limiting the CWP contribution to 30% of the plastic hinge rotation capacity. Mathematical models of the CWP shear force - distortion response have been proposed by different authors (Krawinkler, 1978; Lu *et al.*, 1988; Kim and Englehardt, 1995), which differ in terms of inelastic behaviour modelling, but that are in good agreement in terms of elastic shear stiffness  $K_e$  and yield strength in shear  $V_y$  (Gupta and Krawinkler, 1999). The monotonic shear force - shear distortion model by (Krawinkler, 1978) shown in Figure 7.14 was adopted for the present study.

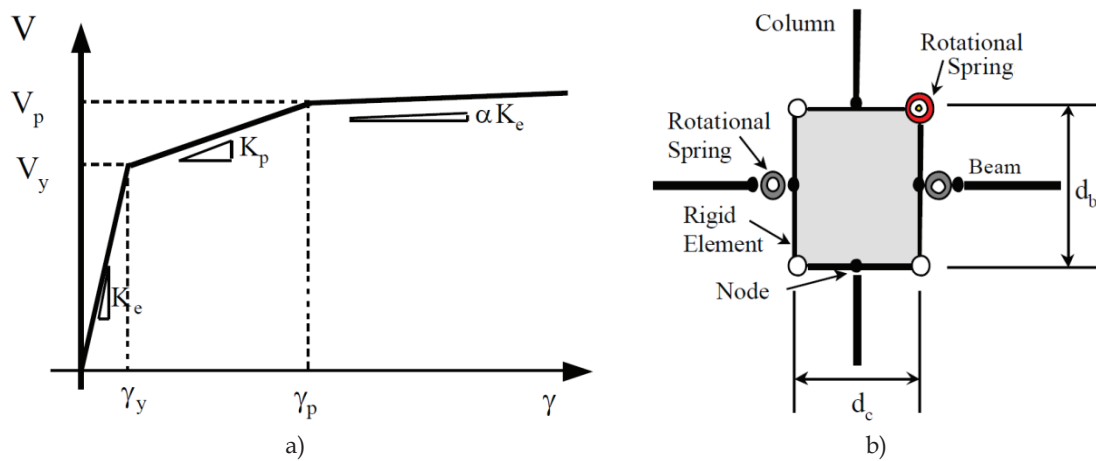


Figure 7.14: Krawinkler (1978) column web panel model cited in Gupta and Krawinkler (1999): a) trilinear shear force - shear distortion relationship; b) web panel modelling

The Krawinkler (1978) model assumes a trilinear relationship between shear force and shear distortion to simulate the different stages of the panel response, as shown in Figure 7.14a). Its implementation in finite element models can be achieved via a nonlinear rotational spring at the panel angle which controls the panel distortion moment - rotation response (see Figure 7.14b)). The panel's shear yield strength is given by:

$$V_y = \frac{F_y}{\sqrt{3}} A_{eff} = \frac{F_y}{\sqrt{3}} (0.95 d_c t_p) \approx 0.55 F_y d_c t_p \quad (7.8)$$

where  $F_y$  is the material yield strength,  $A_{eff}$  is the effective shear area,  $d_c$  is the depth of the column and  $t_p$  is the thickness of the web, including doubler plates. The yield distortion  $\gamma_y$  corresponding to  $V_y$  and the elastic stiffness  $K_e$  of the panel zone are given by:

$$\gamma_y = \frac{F_y}{\sqrt{3} \times G} \quad (7.9)$$

$$K_e = \frac{V_y}{\gamma_y} = 0.95 d_c t_p G \quad (7.10)$$

where  $G$  is the shear modulus of the column material.

After yielding, the column flanges of the panel zone are required to bend in order to accommodate the panel shear distortion, hence mobilising additional shear

resistance. The plastic shear resistance of the joint  $V_p$  was computed according to the following expression:

$$V_p = V_y \left( 1 + \frac{3K_p}{K_e} \right) \approx 0.55F_y d_c t_p \left( 1 + \frac{3b_c t_{cf}^2}{d_b d_c t_p} \right) \quad (7.11)$$

where  $K_p$  is the post yield stiffness,  $b_c$  is the width of the column flange and  $t_{cf}$  is the thickness of the column flange. The plastic resistance  $V_p$  is reached for a value of  $4\gamma_{yr}$  beyond which an appropriate value of  $\alpha$  can be adopted to model the strain hardening (see Figure 7.14a)).

The Krawinkler (1978) model was used to predict the shear force - shear distortion response, which was subsequently converted into moment-rotation, in order to be implemented into a web panel model according to the scheme shown in Figure 7.14b). The column web panel behaviour was calibrated according to experimental tests by Ciutina and Dubina (2008), namely for the test specimen *CP-R-C* which has no column web doubler plates or web reinforcements. The Seismostruct (Seismosoft, 2014) numerical model of the experimental set-up is presented in Figure 7.15a), which used the panel modelling criteria presented in Figure 7.14b) and a nonlinear rotational spring law which uses the Ramberg-Osgood hysteresis loop formulation provided in Seismostruct.

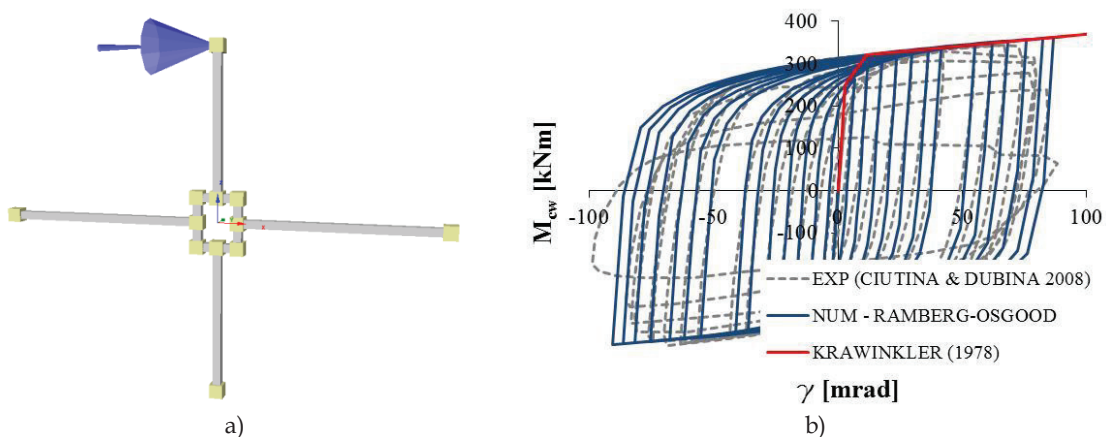


Figure 7.15: Calibration to Ciutina and Dubina (2008): a) Seismostruct model; b) comparison between experimental, numerical Ramberg-Osgood model and monotonic Krawinkler (1978) model prediction

The parameters for the Ramberg-Osgood formulation, namely the yield moment and rotation, were based on the Krawinkler model, which provided the best fit for a strain hardening parameter value  $\alpha=0.7\%$ . The Ramberg-Osgood parameter

$\gamma=10$  was found to provide the best fit to the experimental results and a convergence limit for the Newton-Raphson procedure  $\beta_1$  equal to 0.01 was found to strike a good balance between result accuracy and required computation time. The result of the numerical calibration seen in Figure 7.15b) shows good agreement between the numerical model curve and the experimental curve, indicating that the adopted modelling strategy is effective at simulating the moment-distortion response of the CWP zone.

#### 7.2.6.4 Gravity frame beam-to-beam joints

Considering that under column loss action, the gravity frame joints are unable to enter the final catenary stage, as shown previously for FEP joints in Chapter 6, the beam members typically remain in the elastic range while plasticity is developed in the joints. The joints therefore act as “structural fuses” and display highly nonlinear behaviour, which can be simulated by nonlinear link elements. For gravity frame beam-to-beam joints, the web cleat typology was selected given that it is widely adopted by designers, due to its low cost and reduced assembly time. Furthermore, its low stiffness and strength capacities imply it behaves as a nominally pinned joint, according to the EN 1993-1-8 (CEN, 2005) stiffness and strength classification and in line with typical design assumptions.

Recent experimental studies have highlighted the importance of connections for arresting progressive collapse (Taewan and Jinkoo, 2009; Yang *et al.*, 2015), implying that realistic modelling of joint contribution is key for progressive collapse analysis. In this sense, given that connections are subjected to large displacements, the connection failure criteria under dynamic loading must be defined. To this end, the behaviour of web cleat joints was initially assessed using a components model, which has enabled to characterise joint response for the six degrees of freedom required to fully define the nonlinear links, which in turn were subsequently incorporated into the full structural model in Seismostruct.

The component-based mechanical model was based on the Liu *et al.* (2015) model and was defined by initially identifying the individual components and respective equivalent nonlinear spring response and by subsequently assembling the springs, to obtain the force-displacement curve. The web cleat joint components model

is presented in Figure 7.16 and consists of five different components, arranged in two layers that correspond to the two bolt rows. The considered components were: the bolt in tension ( $bt$ ), the web angle in bending ( $wab$ ), the bolt in shear ( $bs$ ), the web angle in bearing ( $wabr$ ) and the beam web in bearing ( $bwbr$ ). The cuts on the secondary beam end allow the joint to rotate approximately  $17^\circ$  ( $\approx 297$  mrad) without contact between the webs of the beams. For what concerns the slip resistance of bolted members, non-preloadable hand-tightened bolts are the typical option for gravity frame joints, hence implying that slip resistance is very small, for which reason it was disregarded.

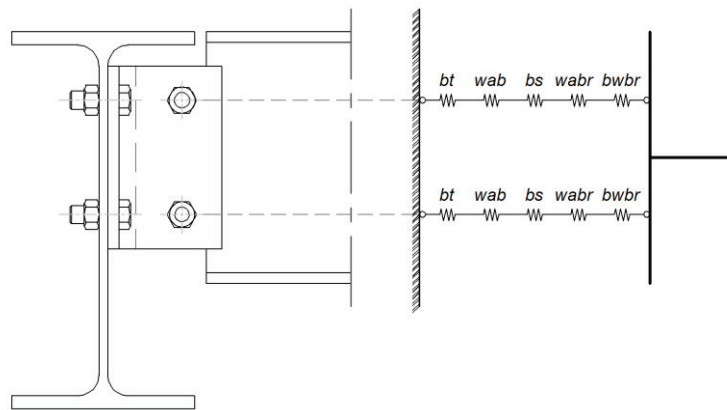


Figure 7.16: Web cleat joint model components

For what concerns strain rate enhancement effects, experimental tests on web cleat joints Liu *et al.* (2013) led to values around  $4s^{-1}$  implying that rate enhancement can be disregarded for analysis under column loss scenario.

The mechanical model for bolted angles under monotonic tensile force proposed by Yang and Tan (2012) and shown in Figure 7.17 combines the interaction between bolts and angles while respecting the observed failure modes.

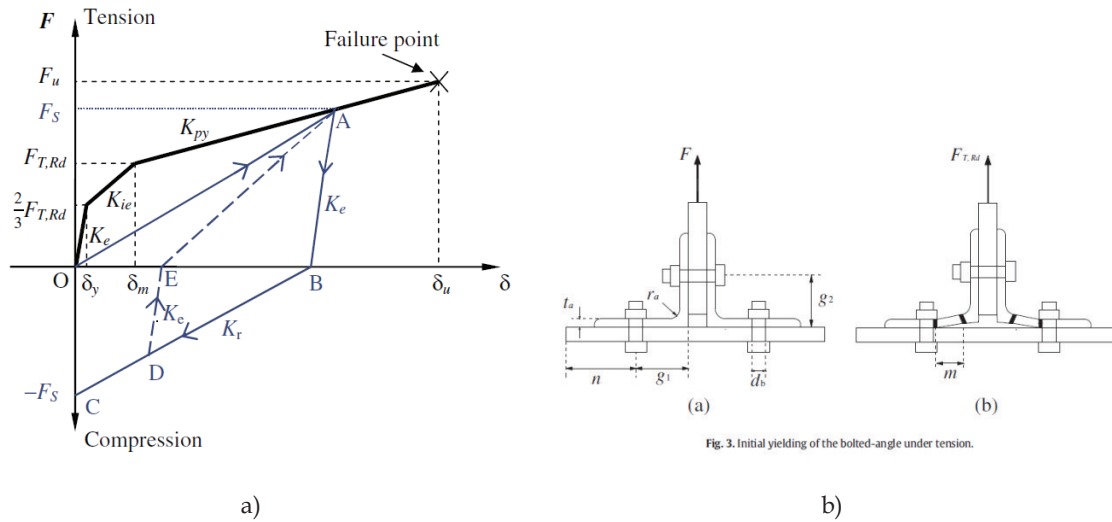


Figure 7.17: Mechanical model for bolted angles by Yang and Tan (2012): a) Force-displacement response; b) geometric properties definition

Indeed, this model combines the bolt in tension (*bt*) and web angle in bending (*wab*) components into an equivalent spring and was therefore adopted for the web cleat joint modelling. The tri-linear model is characterized by stiffnesses  $K_e$ ,  $K_{ie}$  and  $K_p$  for the elastic, transition inelastic and post-yield stages, respectively. The values for  $F_{T,Rd}$  and  $K_e$  were computed according to Faella’s model (Faella *et al.*, 2000) as follows:

$$F_{T,Rd} = \frac{4M_{y,Rd}}{m} = \frac{b_{eff,a}t_a^2f_y}{m} \tag{7.12}$$

$$K_e = \frac{0.5b_{eff,a}t_a^3E}{m^3} \tag{7.13}$$

where  $f_y$  is yield strength of the angle,  $t_a$  is the angle thickness,  $b_{eff,a}$  is the effective width of the angle and  $m$  is the distance between the two plastic hinges. The value of  $K_{ei}$  was taken as  $K_e/7$ , as recommended in Faella *et al.* (2000). The displacement at failure  $\delta_u$  was computed in accordance with the methodology proposed by Yang and Tan (2012) which accounts for interaction between bolts and angles and incorporates four failure modes as follows:

$$F_{T,Rd} = \frac{4M_{y,Rd}}{m} = \frac{b_{eff,a}t_a^2f_y}{m} \tag{7.14}$$

$$K_e = \frac{0.5b_{eff,a}t_a^3E}{m^3} \tag{7.15}$$



where  $f_y$  is yield strength of the angle,  $t_a$  is the angle thickness,  $b_{eff,a}$  is the effective width of the angle and  $m$  is the distance between the two plastic hinges. The value of  $K_{ei}$  was taken as  $K_e/7$ , as recommended in Faella *et al.* (2000). The displacement at failure  $\delta_u$  was computed in accordance with the methodology proposed by Yang and Tan (2012), which accounts for interaction between bolts and angles and incorporates four failure modes as follows:

$$\delta_u = g_1^* (1 + \varepsilon_u) \sin\left(\frac{\varepsilon_u g_1^*}{2t_a}\right) \quad (7.16)$$

$$g_1^* = g_1 - t_a - 0.8r_a + \eta d_b \quad (7.17)$$

where  $g_1$  is the horizontal gauge length,  $r_a$  is the radius of the angle fillet,  $d_b$  is the bolt diameter and  $\varepsilon_u$  is the fracture strain of the web angles taken as 0.24 according to coupon tests from Liu *et al.* (2015). The  $\eta$  coefficient, which accounts for the interaction between the strengths of angles and bolts, was determined using the expressions from Yang and Tan (2012):

$$\eta = 1.335 - 0.00242 \frac{f_{y,b} A_b b_{eff,a}}{F_{T,Rd}} \quad \text{if} \quad \frac{f_{y,b} A_b b_{eff,a}}{F_{T,Rd}} < 560 \quad (7.18)$$

$$\eta = -0.22 \quad \text{if} \quad \frac{f_{y,b} A_b b_{eff,a}}{F_{T,Rd}} \geq 560 \quad (7.19)$$

The ultimate resistance  $F_u$  corresponds to the force value obtained for a displacement  $\delta_u$  and was obtained via the incremental equation from Yang and Tan (2012) as follows:

$$F_{i+1} = F_i + [(b_{eff,a} - n d_{hole}) t_a f_u] \left( \frac{\delta_i + \Delta\delta}{\sqrt{g_1^2 + (\delta_i + \Delta\delta)^2}} - \frac{\delta_i}{\sqrt{g_1^2 + \delta_i^2}} \right) \quad (7.20)$$

in which  $F_i$  and  $\delta_i$  are the tensile force and angle displacement at iteration  $i$ ,  $\Delta\delta$  is the displacement increment,  $n$  is the number of bolts,  $d_{hole}$  is the bolt hole diameter and  $f_u$  is the ultimate angle strength. Furthermore, in order to simulate bolt fracture accounting for prying action, the resistance of the bolted angle component was limited according to the expression by Yang and Tan (2012):

$$F_u \leq \frac{2t_a b_{eff,a}}{66.67(2t_a + 0.4g_1^*)} B_{T,Rd} \quad (7.21)$$

where  $B_{T,Rd}$  is the bolt ultimate tensile resistance.

For what concerns the bolt in shear component, resistance values were computed according to the expression provided in the EN 1993-1-8 (CEN, 2005).

$$F_{V,Rd} = 0.6n_b f_{ub} A_b \quad (7.22)$$

in which  $n_b$  is the number of bolts,  $f_{ub}$  is the ultimate strength of the bolts and  $A_b$  is the area of the bolt shank. The adopted stiffness for the bolt in double shear is the same as that adopted in Liu *et al.* (2015), which is based on experimental values by Yu *et al.* (2009).

The plate in bearing component applies to both beam web and angle plates and is based on experimental results regarding the behaviour and modelling of a bolt bearing on a single plate (Rex and Easterling, 2003). This component analytical model was successfully applied to component based models for fin plate and web cleat joints (Rex and Easterling, 2003; Liu *et al.*, 2015) and was therefore adopted for the present study. The model by Rex and Easterling, 2003 provides the normalised relationship between the plate bearing force  $F_b$  and the associated bearing displacement  $\Delta_b$  as:

$$\frac{F_b}{F_{b,Rd}} = \frac{1.74\bar{\Delta}}{(1+\bar{\Delta}^{0.5})^2} - 0.009\bar{\Delta} \quad (7.23)$$

$$\bar{\Delta} = \Delta_b \beta K_i / F_{b,Rd} \quad (7.24)$$

$$F_{b,Rd} = \min\{L_e; 2.76d_b\} \times f_{up} t_p \quad (7.25)$$

where  $F_{b,Rd}$  is the nominal plate bearing resistance,  $\bar{\Delta}$  is the normalised deformation,  $\beta$  is the steel correction factor (taken as 1 for typical steel (Rex and Easterling, 2003)),  $K_i$  is the initial stiffness,  $L_e$  is the distance from bolt centre to plate edge,  $f_{up}$  is the ultimate plate strength,  $t_p$  is the plate thickness and  $d_b$  is the bolt diameter.

The initial stiffness formulation proposed by Rex and Easterling (2003) combines bending ( $K_b$ ), shearing ( $K_v$ ) and bearing ( $K_{br}$ ) stiffness values to determine the

initial stiffness ( $K_i$ ) by means of a three springs in series model, according to the following expressions:

$$K_i = \frac{1}{1/K_{br} + 1/K_b + 1/K_v} \quad (7.26)$$

$$K_{br} = 120t_p f_{yp} (d_b/25.4)^{0.8} \quad (7.27)$$

$$K_b = 32E_p t_p (L_e/d_b - 0.5)^3 \quad (7.28)$$

$$K_v = 6.67G_p t_p (L_e/d_b - 0.5) \quad (7.29)$$

in which  $f_{yp}$  is the plate yield strength and  $E_p$  and  $G_p$  are the Young and shear moduli of the steel plate. As considered in Liu *et al.* (2015), a simplified bi-linear model with symmetrical loading and unloading was adopted for modelling the plate in bearing component.

For the assembly of the different components in the spring layers shown in Figure 7.16, the force displacement response of the bolted angle component ( $bt+wab$ ) was initially compared to the capacity of the other components, the latter assumed linear elastic until reaching component capacity. For the all the adopted joint configurations, the  $bt+wab$  response was found to display lower capacity than other components, hence determining joint response and failure mode. This was also verified when applying the above described components model to a spring layer in the A90-8-50-I specimen from Yang and Tan (2012), as shown in Figure 7.18. The precision of the components model by Yang and Tan (2012) was verified against experimental results, having displayed ratios in terms of ultimate force and displacement between model and experimental test results equal to 1.05 and 0.95, respectively.

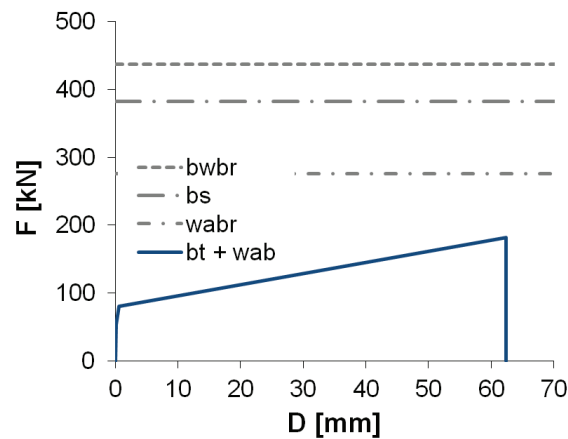


Figure 7.18: Comparison between bolted angle component (bt+wab) response and the capacity of other components in a row – specimen A90-8-50-I from (Yang & Tan, 2012)

The two equivalent springs, each corresponding to the component series shown in Figure 7.16, were assembled, hence enabling to determine joint response under bending and tensile force. By imposing increasing rotations to the joint, the displacements and corresponding forces of the two equivalent springs were computed. The joint response for drift ratios up to 4% was found to be linear elastic, which is ascribable to the very low initial stiffness that characterises web cleat joints. In this sense, under seismic action induced bending, the web cleat joints were found to respond in the elastic range; instead, under column loss action, the joint is subjected to combined bending and axial tensile force, which for small displacements is dominated by flexural behaviour, while being predominantly controlled by catenary action for large displacements, as shown in Yang and Tan (2013).

For the definition of the web cleat joint link behaviour in Seismostruct (Seismosoft, 2014), the responses of the 6 degrees-of-freedom (DOF) were defined. Joint response for the DOF in bending about the beam's strong axis was defined using the bi-linear kinematic formulation with kinematic hardening, to model elastic-plastic behaviour. The yield moment was computed when the bolted angle component reaches  $F_{T,Rd}$  (see Figure 7.17) and zero hardening was assumed to limit the bending resistance contribution; at high rotation demands, the resistance is provided by the axial force contribution that is mobilised by catenary action. For the definition of the horizontal translation DOF, a trilinear symmetric with isotropic hardening formulation was adopted, which can simulate hardening effect under large displacements up to failure. The horizontal and vertical shear DOFs were modelled using the bilinear

kinematic formulation according to the previously described shear stiffness and strength capacity of the bolt components.

For the adopted tensile and vertical shear response curve formulations, joint resistance continues to increase, even after angle failure, since the formulation provided in the Seismostruct (Seismosoft, 2014) library does not allow to model a sudden drop of resistance or negative stiffness values. In this sense, in order to clearly identify the bolted angle failure, the vertical shear DOF resistance was limited to match the vertical force which leads to bolted angle failure. This allows obtaining a zero hardening condition (i.e. approximately horizontal force-displacement segment) at bolted angle failure, which in turn enables to identify and subsequently truncate the structural response curve, since the response further to partial structural collapse falls outside the scope of the present study. The joint DOFs pertaining to beam torsion and bending about the weak axis were assumed as rigid.

The presented component characterization was based on the quasi-static response. However, an experimental study on the dynamic behaviour of web cleat connections subjected to column loss (Liu *et al.*, 2013) showed that the maximum dynamic displacement was significantly higher than the corresponding deflection under static loading. This study also showed web cleat connections to have very low energy absorption capacity under dynamic actions, resulting in a Dynamic Increase Factor (*DIF*) equal to 2.8, in exceedance of the conventional force-based *DIF* limit of 2.0 (U.S. General Services Administration, 2003). An important conclusion of the study states that since the *DIF* depends mainly on the resistance curves of the connection type, the *DIF* value can be adopted for the analysis of different span lengths. For the present study a constant force-based *DIF* value of 2.8 was adopted and the force-displacement response curves were divided by the *DIF* value, to simulate joint response under column loss action. The comparison between the experimental static (Yang and Tan, 2013), numerical dynamic (Liu *et al.*, 2013) and both static and equivalent dynamic Seismostruct nonlinear link responses are presented in Figure 7.19.

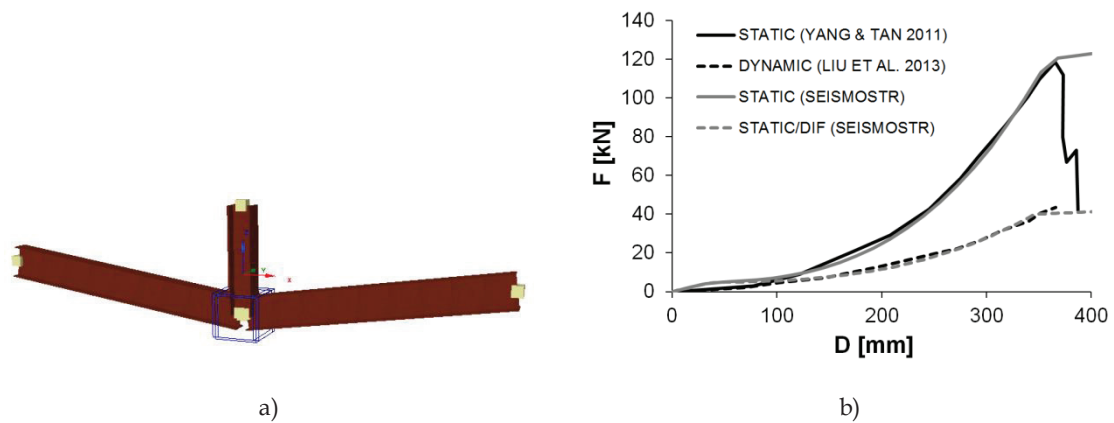


Figure 7.19: a) Seismostruct model to simulate Yang and Tan (2013) experimental test set up; b) comparison between experimental static Yang and Tan (2013), numerical dynamic (Liu *et al.*, 2013) and Seismostruct static and dynamic equivalent nonlinear link vertical force-displacement response

As shown in Figure 7.19, the adopted link definition can simulate web cleat static response under column loss at large displacements. The differences observed at low displacement values are due to the fact that response input for each DOF in Seismostruct is decoupled and that for low displacement values, the bi-linear response in bending is dominant. The response in pure bending (i.e. without axial restriction) for low displacements is intended to model the response of gravity frame joints under seismic action. Dynamic effects were considered by dividing the static curve by a constant force-based DIF=2.8. In this case, despite the fact that the DIF varies with the applied displacement, adopting a constant DIF is shown to provide good agreement with the dynamic response curve by Liu *et al.* (2013).

#### 7.2.6.5 Gravity frame beam-to-column joints

The joint response calibration was performed considering the static joint response. However, as seen for other joint typologies (Liu *et al.*, 2013), the dynamic response can significantly differ from the static one. In particular, for joints with low energy absorption capacity, force-based DIF value can be higher than 2.0, since this value is dependent on the resistance curve shape of the connection (Liu *et al.*, 2013). In order to estimate the dynamic effect, joint behaviour was treated as a Single Degree-Of-Freedom (SDOF) system (Liu *et al.*, 2013), for which the energy balance equation can be expressed as:

$$W_{ext} = W_{int} \quad (7.30)$$

$$P_d u_d = \int_0^{u_d} R_s(u) du \quad (7.31)$$

where  $W_{ext}$  is the external work,  $W_{int}$  is the internal strain energy,  $P_d$  is the dynamic resistance,  $u_d$  is the maximum dynamic displacement and  $R_s(u)$  is the static joint resistance. The force-based *DIF* (or  $DIF_P$ ) value at the maximum dynamic displacement  $u_d$  was computed as the ratio between static and dynamic strength values  $DIF_P = P_s / P_d$ .

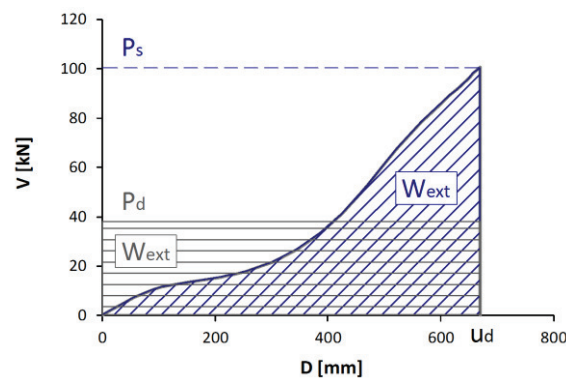


Figure 7.20: Vertical force-displacement energy balance – External work and Internal work done

The Seismostruct link response curves were therefore calibrated to the static response and subsequently divided by the  $DIF_P$ , in order to account for dynamic effects under column loss action.

#### 7.2.6.5.1 Beam to weak axis column connections

The Seismostruct link calibration for beams-to-column joints about the column's weak axis was based on the results from the parametric study on FEP joints presented in Chapter 6. For joint configurations that were not analysed in the parametric study, the response was extrapolated from the available data, according to the procedure described herein.

The FEP joint normalised moment-rotation response curves are presented in Figure 7.21a) and the ultimate bending, axial force and rotation capacities are presented in Figure 7.21b),c),d) respectively, as a function of beam section mechanical properties.

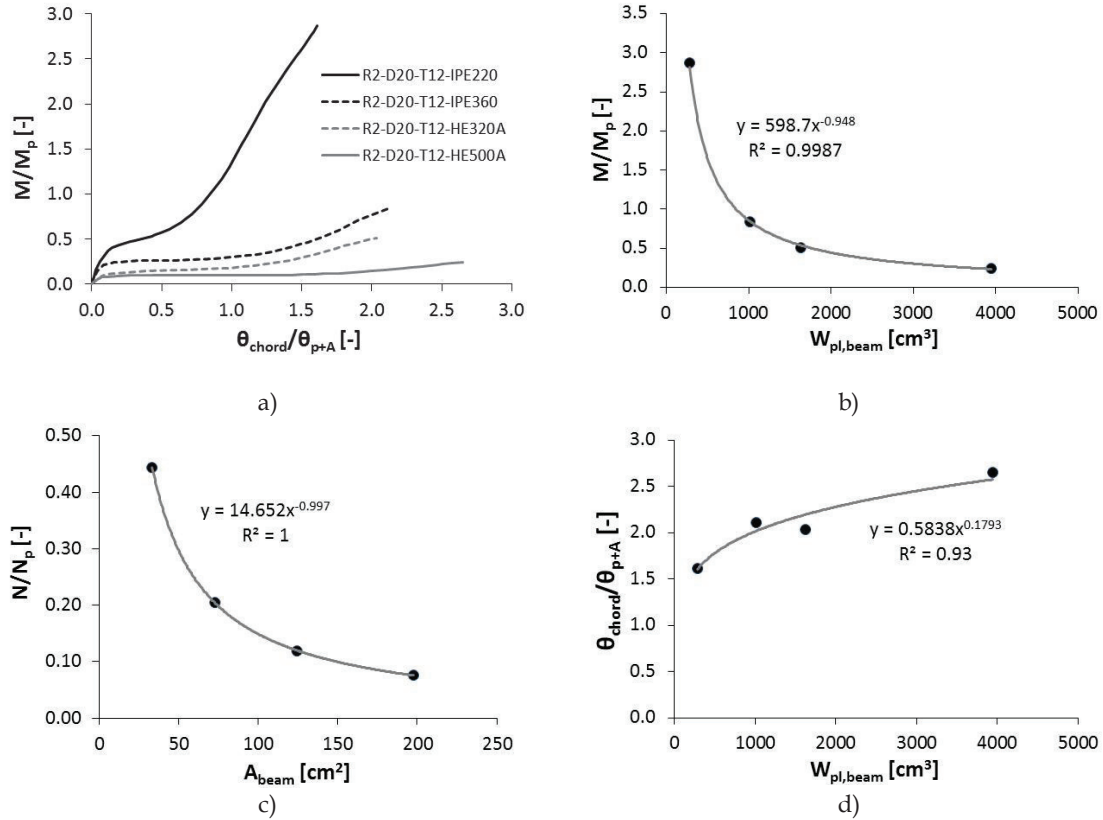


Figure 7.21: Flush endplate joint pseudo-static response under column loss: a) normalised moment-rotation; b) normalised ultimate moment vs. beam section plastic modulus; c) normalised ultimate axial force vs. beam section area; d) normalised ultimate rotation vs. beam section plastic modulus

The power regressions were used to extrapolate the ultimate joint capacity by inputting the relevant beam mechanical properties into the regression expressions shown in Figure 7.21b),c),d), enabling to compute the normalised parameters  $M/M_p$ ,  $N/N_p$  and  $\theta_{chord}/\theta_{p+A}$  at collapse, designated also as target values.

The joint moment-rotation curves were obtained through a weighted average between the two curves for the same beam section profile type. For example, to extrapolate the response of a given joint with an IPE beam section, the two IPE curves (see Figure 7.21a)) were used. The same logic goes for joints with HE type beam sections. The extrapolated normalised moment capacities for each value of  $\theta_{chord}/\theta_{p+A}$  up to joint failure (i.e. up to the target value) were computed according to the following expressions:

$$(M/M_p)_{IPE,extrapolated} = \alpha(M/M_p)_{IPE220} + (1 - \alpha)(M/M_p)_{IPE360} \quad (7.32)$$

$$(M/M_p)_{HE,extrapolated} = \alpha(M/M_p)_{HE320A} + (1 - \alpha)(M/M_p)_{HE500A} \quad (7.33)$$



The values of the  $\alpha$  parameter were determined through an iterative procedure, assuming a convergence tolerance error between the extrapolated and the target values at joint collapse of 0.05%. The extrapolated normalised axial force - rotation curves were determined according to the same procedure, replacing  $(M/M_p)$  by  $(N/N_p)$  in the two extrapolation expressions. The extrapolated FEP response curves for the IPE 240 and HE 360 B beam sections are shown in Figure 7.22.

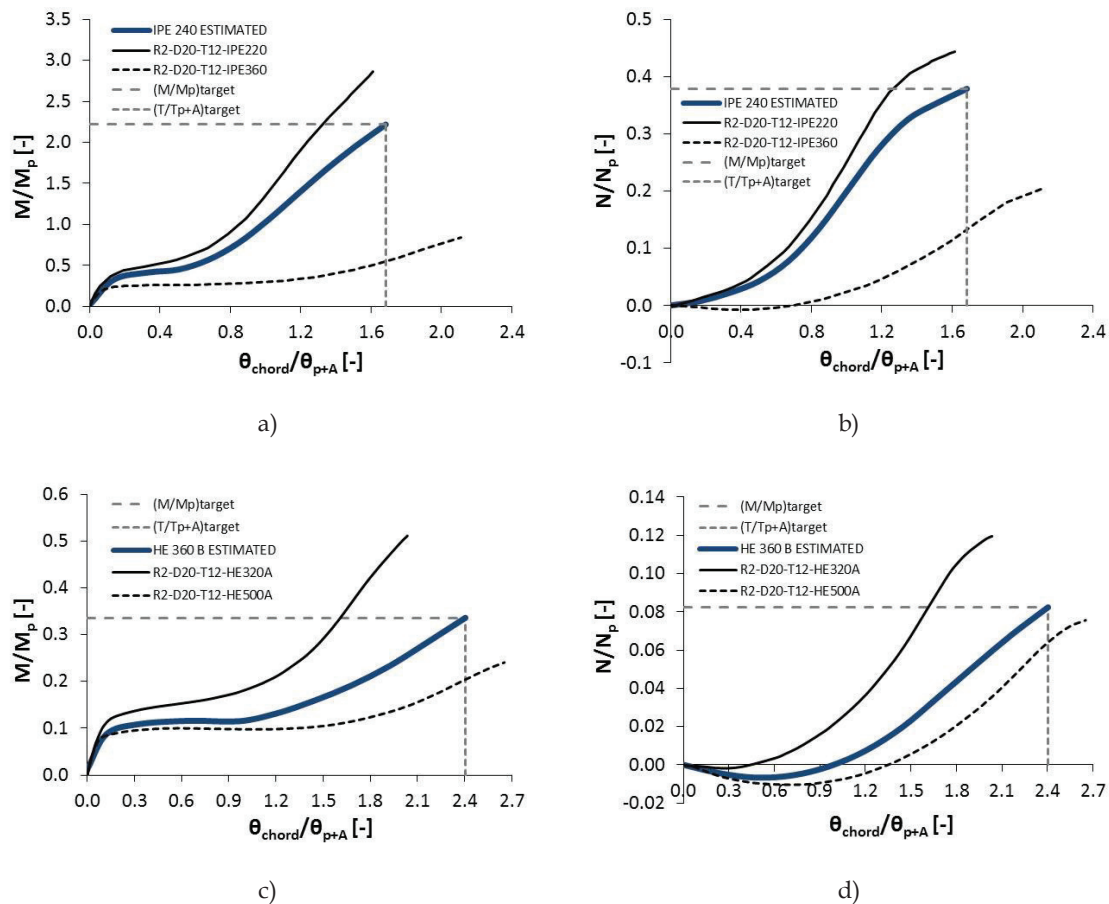


Figure 7.22: Estimated FEP joint responses for the IPE 240 and HE 360 B section cases: a) IPE 240 normalised moment - rotation; b) IPE 240 normalised axial force - rotation; c) HE 360 B normalised moment - rotation; d) HE 360 B normalised axial force - rotation

The adopted procedure ensures that the extrapolated normalised curves retain the information from the two curves from which they were derived, while displaying values of  $M/M_p$ ,  $N/N_p$  and  $\theta_{chord}/\theta_{p+A}$  at collapse equal to those provided by the power regressions expressions provided in Figure 7.21b,c,d. The normalisation factors  $M_p$ ,  $N_p$  and  $\theta_{p+A}$  are given in Table 7.5 and the non-normalised extrapolated joint  $M$ - $\theta_{chord}$  curves were subsequently determined. The curve for the case of the HE 320 A beam

section was not extrapolated since it the response curve was obtained directly from the numerical model.

Table 7.5: Normalisation factor values

Section	$M_p$	$N_p$	$\theta_p$	$\theta_A$	$\theta_{p+A}$
-	kNm	kN	mrاد	mrاد	mrاد
IPE 240	136	1447	20.3	59.3	79.6
IPE 270	179	1698	18.0	59.3	77.3
HEA 320	602	4603	15.3	59.3	74.6
HEB 360	993	6682	13.4	59.3	72.7

The extrapolated curves are presented in Figure 7.23 in both normalised and non-normalised forms.

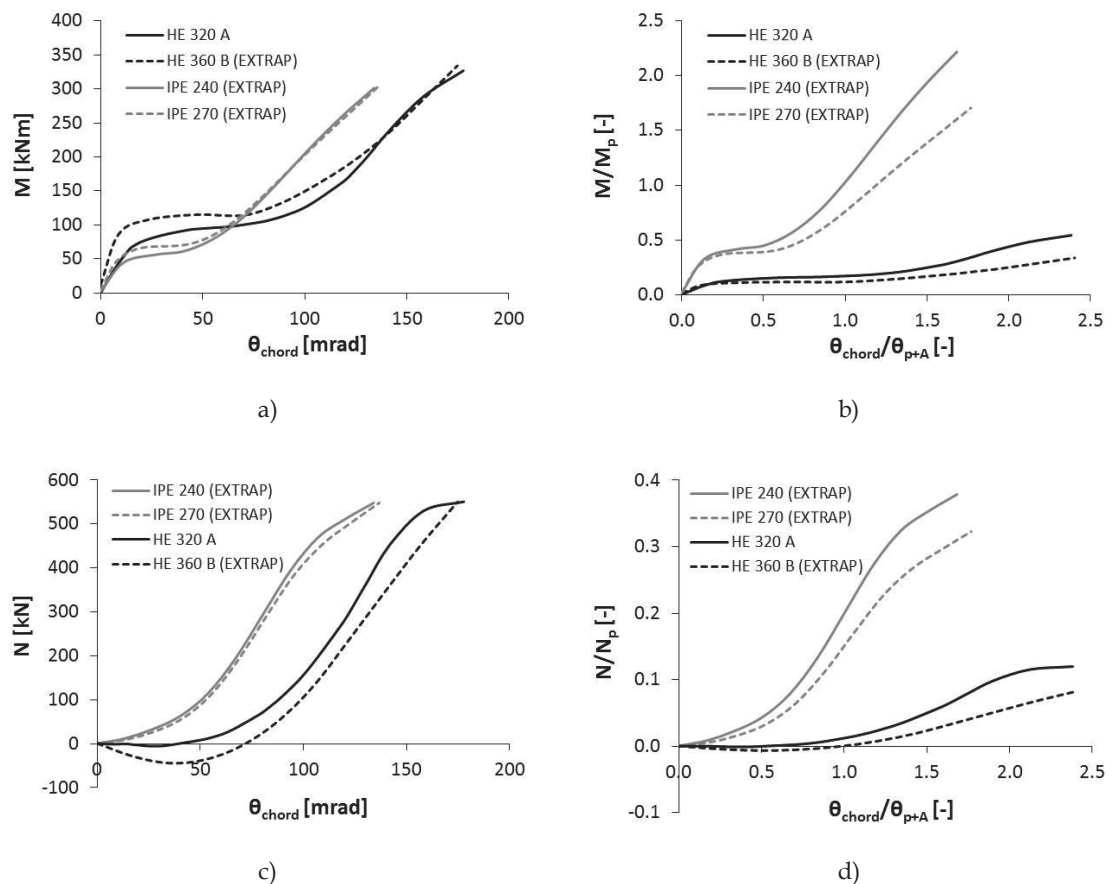


Figure 7.23: Extrapolated joint moment - rotation response curves: a) moment-rotation; b) normalised moment-rotation; c) axial force-rotation; d) normalised axial force-rotation

The six DOFs of the Seismostruct link were calibrated to the extrapolated joint response curves. Axial force and bending about the beam’s strong axis DOFs were

defined using the bilinear kinematic formulation to model elastic-perfectly plastic behaviour with zero post-yield hardening. Initial stiffness for the bending DOF was calibrated to match joint response for low rotation values and yield moment was defined to match the yielding plateau. By assuming zero hardening, the bending resistance contribution at high rotation demands was effectively limited. The link DOFs corresponding to horizontal shear, vertical shear, torsion and bending about the weak axis were defined as linear elastic with large stiffness, to simulate rigid connection conditions. The Seismostruct model for the case of the IPE 240 beam section is shown in Figure 7.24a).

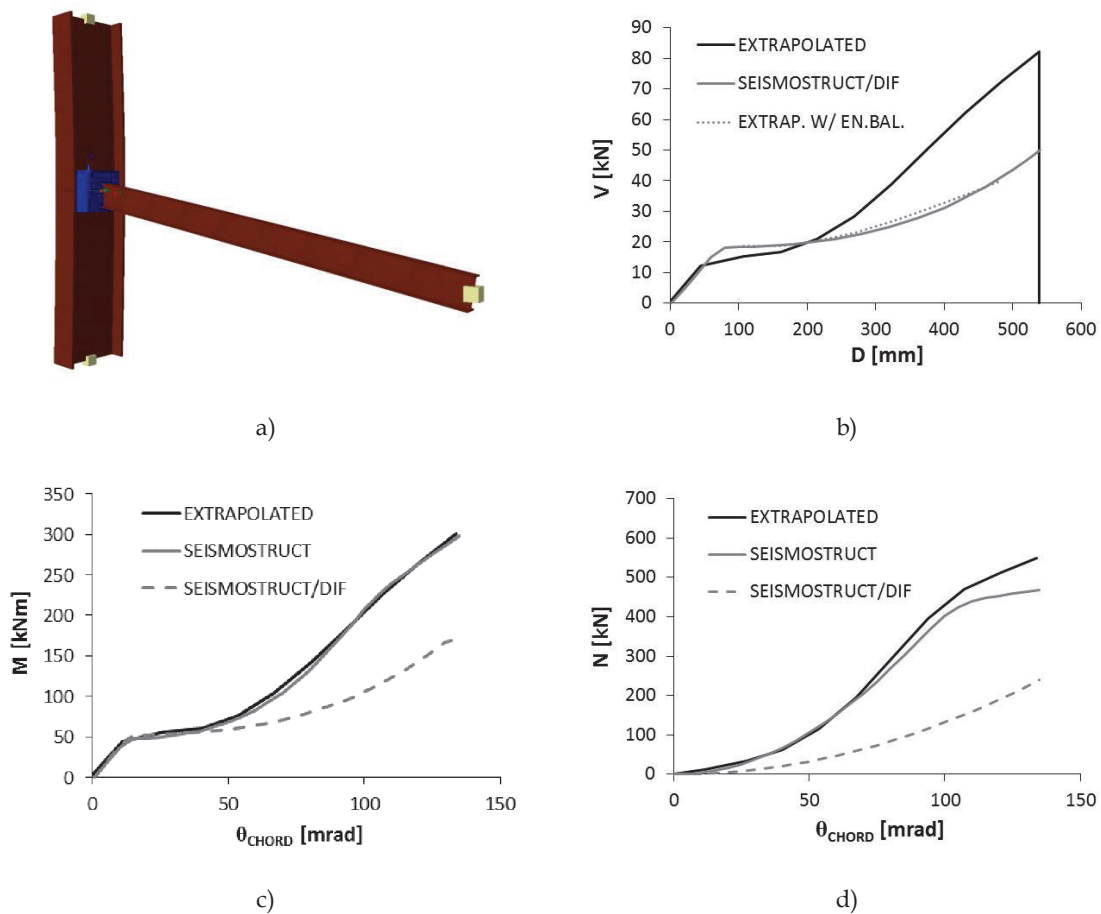


Figure 7.24: Calibration of the extrapolated IPE 240 joint: a) Seismostruct model with nonlinear link; b) vertical force – displacement static and dynamic energy balance equivalent comparison; c) static moment – rotation comparison; d) axial force – rotation static and dynamic equivalent comparison

To account for the dynamic effect, force-based DIF values were computed through energy balance and the estimated dynamic response curve was determined as seen in Figure 7.24b). The calibrated dynamic response shown in Figure 7.24b) is shown to be well adjusted to the energy balance curve. The initial elastic stiffness was

not adjusted, since this stiffness value is more coherent with the response under seismic action, and bears little influence on the overall response under column loss action. As shown in Figure 7.24c),d) the link modelling is capable of accurately simulating static joint response, yielding slightly smaller and hence conservative catenary axial force at collapse, when compared to the extrapolated response curve.

### 7.2.6.5.2 Beam to strong axis column connections

The link calibration for beam to column joints about the column's strong axis about the strong joints axis followed the same procedure as described for beam-to-column joints about the column's weak axis. Also in this case, results were taken from the parametric study from Chapter 6 and response was extrapolated for configurations not analysed in the parametric study.

The joint normalised response curves are presented in Figure 7.25a) and the ultimate bending, axial force and rotation capacities are presented in Figure 7.25b),c),d) respectively, as a function of beam section mechanical properties.

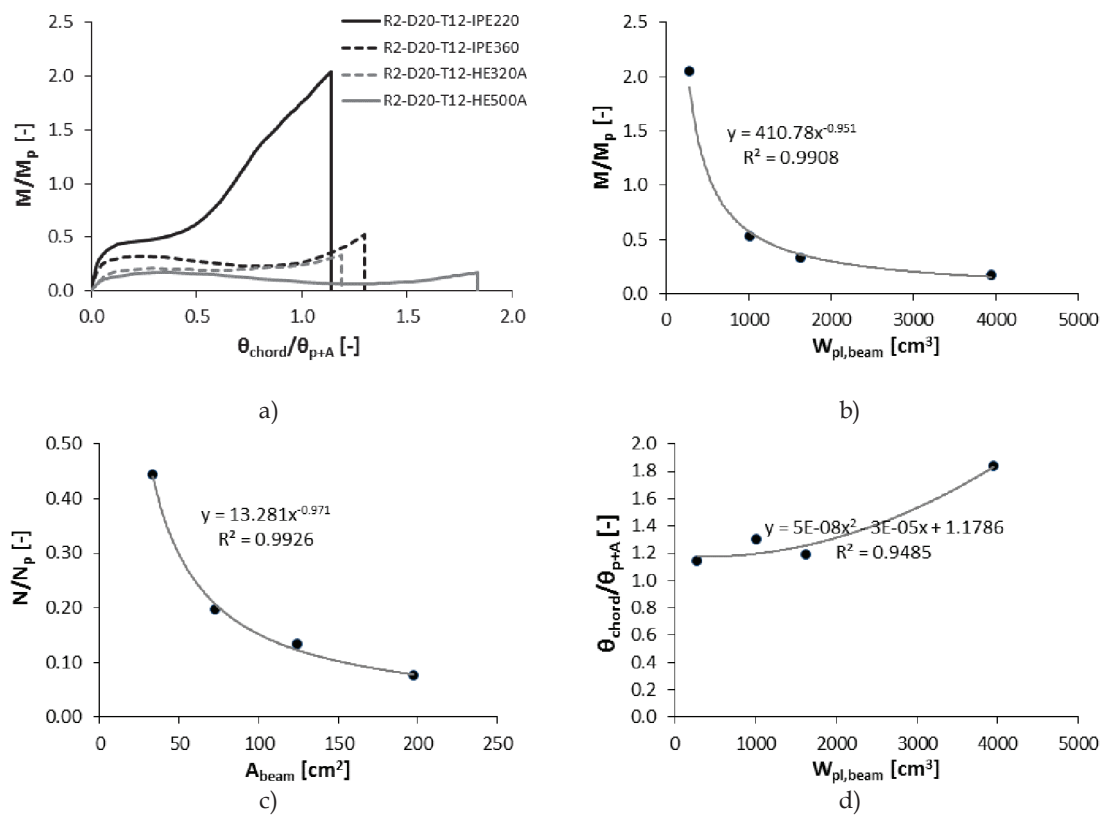


Figure 7.25: Flush endplate joint pseudo-static response under column loss: a) normalised moment-rotation; b) normalised ultimate moment vs. beam section plastic modulus; c) normalised ultimate axial force vs. beam section area; d) normalised ultimate rotation vs. beam section plastic modulus

As previously, power regressions were used to extrapolate the ultimate joint capacity, enabling to determine the target  $M/M_p$ ,  $N/N_p$  and  $\theta_{chord}/\theta_{p+A}$  values at collapse. The moment-rotation curves were obtained via a weighted average between the two curves for the same beam profile type. The extrapolated normalised moment capacities for each value of  $\theta_{chord}/\theta_{p+A}$  up to joint failure (i.e. up to the target value) were computed according to Eq.(7.32) and Eq.(7.33).

The extrapolated FEP response curves for the IPE 300 and HE 400 A beam sections are shown in Figure 7.26.

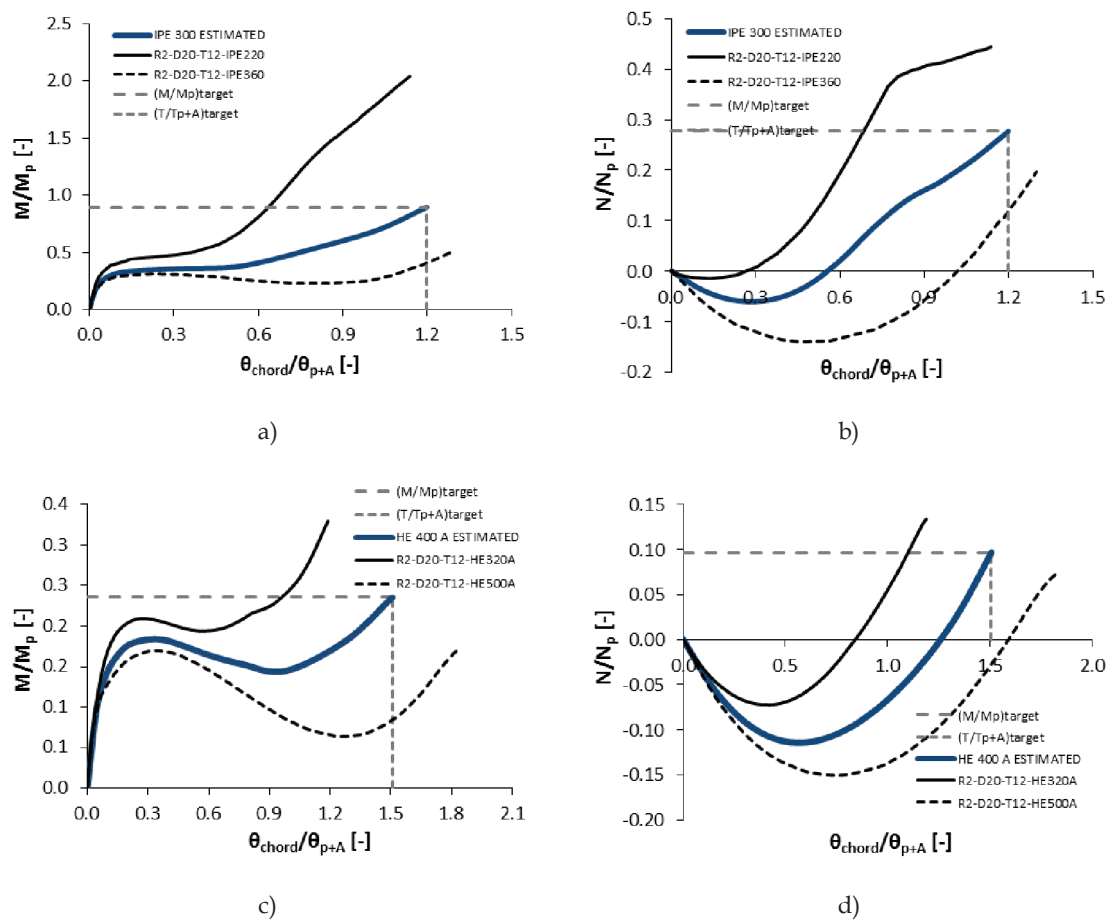


Figure 7.26: Estimated FEP joint responses for the IPE 300 and HE 400 A section cases: a) IPE 300 normalised moment - rotation; b) IPE 300 normalised axial force - rotation; c) HE 400 A normalised moment - rotation; b) HE 400 A normalised axial force - rotation

The normalisation factors  $M_p$ ,  $N_p$  and  $\theta_{p+A}$  are given in Table 7.5. The extrapolated curves are presented in Figure 7.27 in both normalised and non-normalised forms.

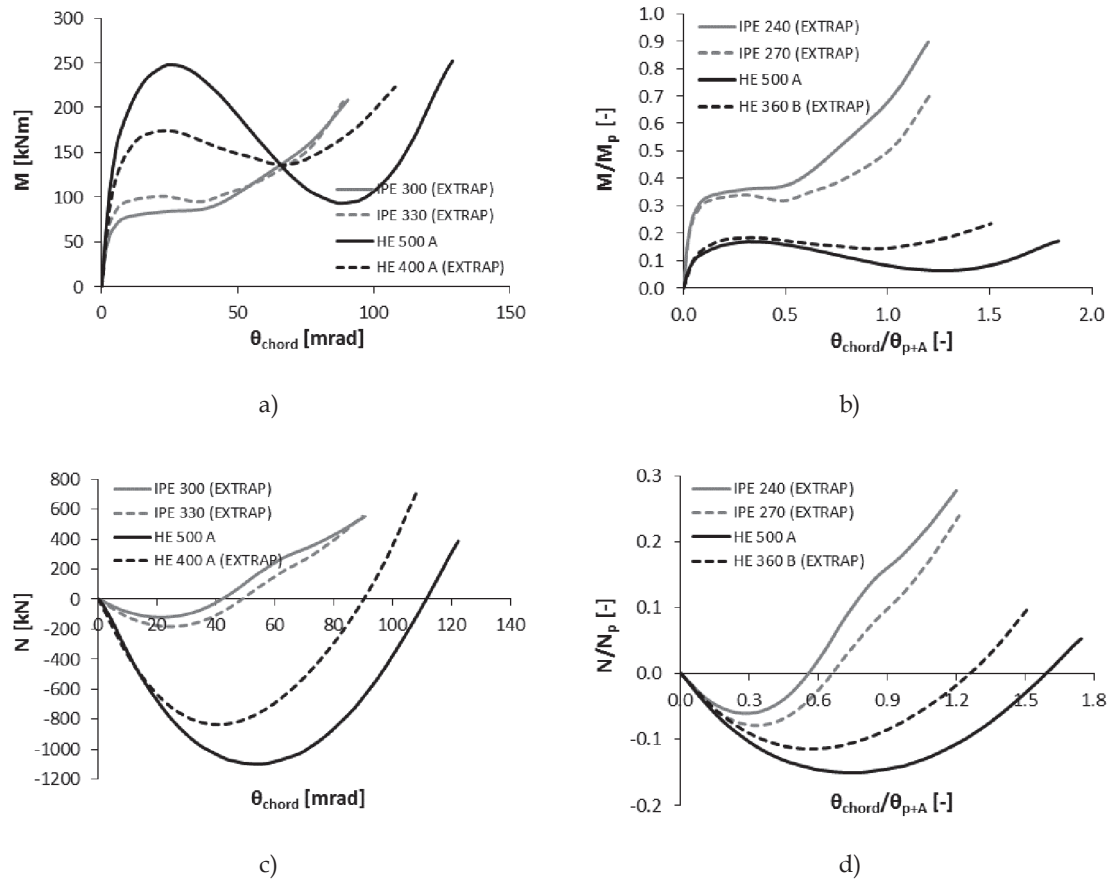


Figure 7.27: Extrapolated joint moment - rotation response curves: a) moment-rotation; b) normalised moment-rotation; c) axial force-rotation; d) normalised axial force-rotation

The DOFs of the nonlinear link were calibrated to the extrapolated joint curves. The bilinear kinematic formulation was adopted and elastic-perfectly plastic behaviour with zero post-yield hardening was assumed for axial force and bending responses. Initial stiffness was calibrated to match response for low rotation and yield moment defined to match the yield plateau. Bending resistance contribution at high rotation was disregarded, by assuming zero hardening. The horizontal shear, vertical shear, torsion and bending DOFs were defined as linear elastic with large stiffness, to simulate rigid connection conditions. The Seismotruuct model for the case of the IPE 300 beam section is shown in Figure 7.28a).

The dynamic effect was accounted for via the force-based *DIF*, which was computed through energy balance. The calibrated dynamic response in Figure 7.28b) is shown to be well adjusted to the energy balance curve.

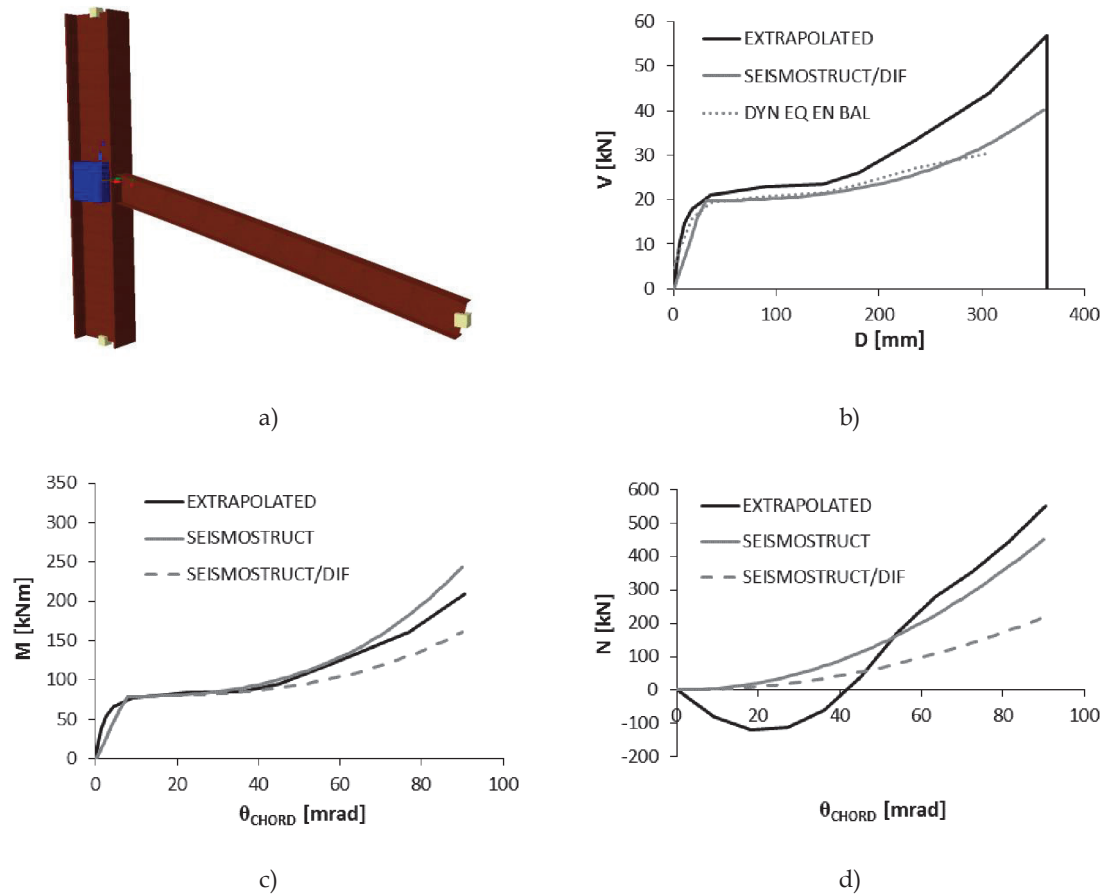


Figure 7.28: Calibration of the extrapolated IPE 240 joint: a) Seismostruct model with nonlinear link; b) vertical force – displacement static and dynamic energy balance equivalent comparison; c) static moment – rotation comparison; d) axial force – rotation static and dynamic equivalent comparison

The initial elastic stiffness was adopted as the joint stiffness in pure bending for small displacements, hence neglecting the initial compressive arching action under column loss. This provides for a suitable connection stiffness under seismic action, while under column removal, bending contribution progressively reduces as rotation demand increases, since catenary action becomes the main collapse arresting mechanism. As shown in Figure 7.28c), the adopted link modelling is capable of simulating the bending response under column, although it is not capable of modelling the compressive arching action as seen in Figure 7.28d). This is due to the fact that the extrapolated curve is derived from a 3D solid type FE model, in which this effect is implicitly modelled, whereas the Seismostruct model is based on 1D frame type FE model. This however is not a significant issue, since under cyclic action the bolts display plastic elongation (see Section 6.3.3.2) and since no compressive arching action can be mobilised up to about 40 mrad, after which a resistance reprise is verified which

approximately resumes the undamaged joint response curve. This implies that for modelling bolted FEP joints, the adopted nonlinear link modelling, which disregards compressive arching action following seismic action, is a suitable modelling strategy.

### 7.2.6.6 Claddings

#### 7.2.6.6.1 Masonry claddings

The behaviour of masonry infilled frames, which are frequently used in both northern and southern Europe, has been investigated in past decades. However, despite numerous conducted studies and recent design provisions and guidelines (e.g. EN 1998-1 (CEN, 2004)), a complete procedure for the seismic design of these structures is not yet available. A study by Markulak *et al.* (2008) has shown that infill behaviour under horizontal actions provides for an increase in frame stiffness and strength at small drift ratios. However, as the drift ratio increases, the frame/infill interface is progressively deteriorated leading to infill stiffness and strength degradation. This aspect is further illustrated in Figure 7.29.

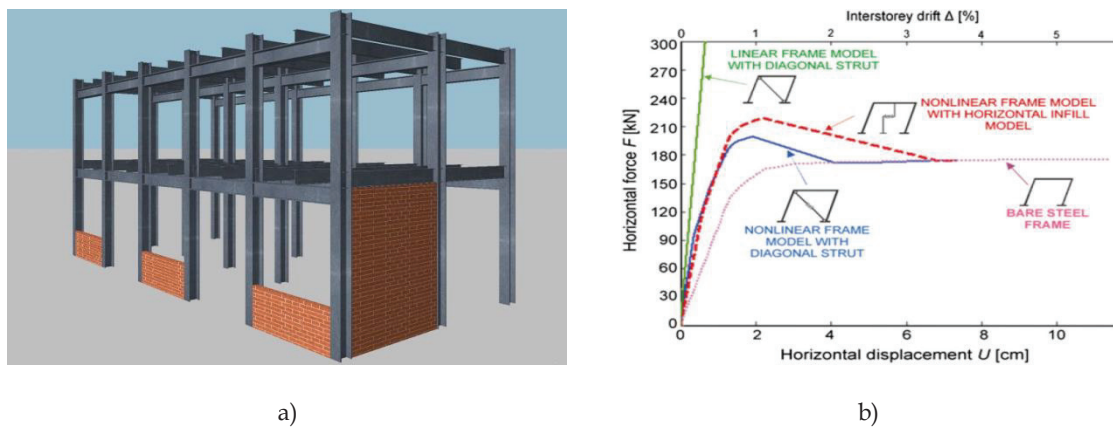


Figure 7.29: Masonry infill panels in steel frames: a) schematic representation; b) influence on the behaviour of a steel frame (Markulak *et al.*, 2008)

Unreinforced masonry infill panels have also been recently shown to significantly increase the resistance and robustness of frames under column loss action, effectively avoiding disproportionate collapse (Farazman *et al.*, 2012).

In common practice, designers typically disregard the lateral resistance contribution of infill panels which are treated as secondary non-structural elements and design is performed considering only the resistance of the bare frame. However, construction is typically not executed in accordance with this assumption and masonry



elements are in contact with the steel frame as exemplified in Figure 7.30. This situation leads to inadequate performance due to the high costs required to repair damage induced by earthquakes to walls, doors, windows and other non-structural elements.



Figure 7.30: Masonry infill panel execution detail (Markulak *et al.*, 2008)

The presence of the infill panel effectively changes the frame's response to lateral loads from a flexural behaviour to that similar to a truss girder (ASCE, 1998), characterized by the development of large forces in the diagonal strut zone. Indeed, although the diagonal strut models are commonly adopted for analysis purposes, several sources of uncertainties affect the behaviour of the masonry infills (Markulak *et al.*, 2013), namely: material properties, construction procedure, panel geometry and frame/infill interaction properties.

In the present study, the contribution of masonry claddings for robustness was considered and infill panels were modelled and calibrated according to experimental tests described in Markulak *et al.* (2013). The considered test specimen, designated C-1, consists of a one-bay, one-storey planar steel frame, infilled with perforated clay blocks characterized by  $f_b=11.8$  N/mm<sup>2</sup>,  $f_m=5.0$  N/mm<sup>2</sup> and  $f_k=1.6$  N/mm<sup>2</sup>, where  $f_b$  is the mean normalized vertical compressive strength of masonry unit,  $f_m$  is the average compressive strength of mortar and  $f_k$  is the mean vertical characteristic compressive strength of masonry, according to the EN 1996-1-1 (CEN, 2005) nomenclature. The experimental test set-up is shown in Figure 7.31a) and the geometry of the steel frame is presented in Figure 7.31b).

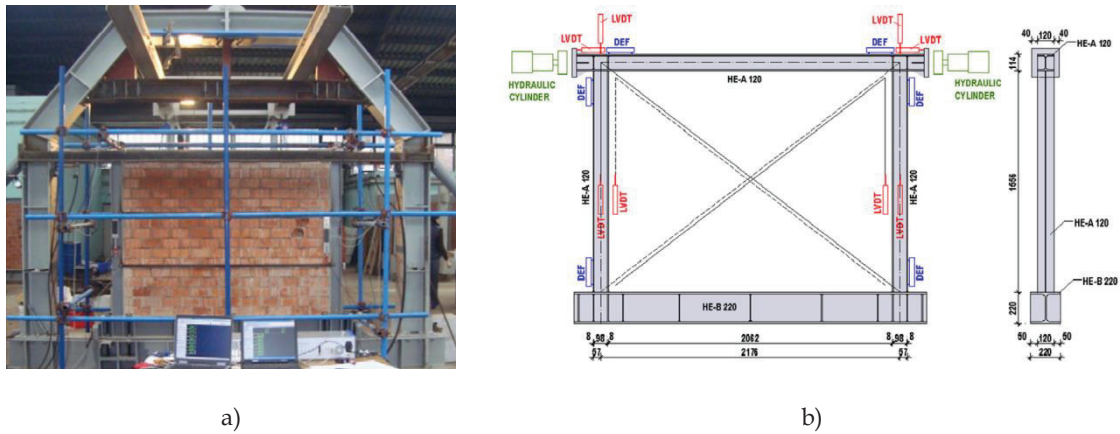


Figure 7.31: Experimental test by Markulak *et al.* (2013): a) test set-up; b) steel frame geometry

The planar frame was subjected to a series of quasi-static stepwise increasing loading cycles up to infill or frame failure according to the FEMA 461 (FEMA, 2007) testing protocols for non-structural components.

To implement the diagonal strut model for numerical analysis, the inelastic infill panel element type formulation provided in Seismostruct (Seismosoft, 2014) was adopted. This model considers each panel to be represented by six strut members, where each diagonal direction features two parallel struts that transfer axial loads between opposing panel corners, plus a third diagonal element that carries the shear load and that is activated in compression only. The infill model uses four external nodes (1 through 4) to define the contact points between the frame and the infill panel, as well as a set of dummy nodes that define the contact lengths of the frame/infill interface. The axial load struts use a masonry strut hysteresis rule, whereas the shear strut uses a bi-linear hysteresis model. The six strut inelastic infill panel model is shown in Figure 7.32.

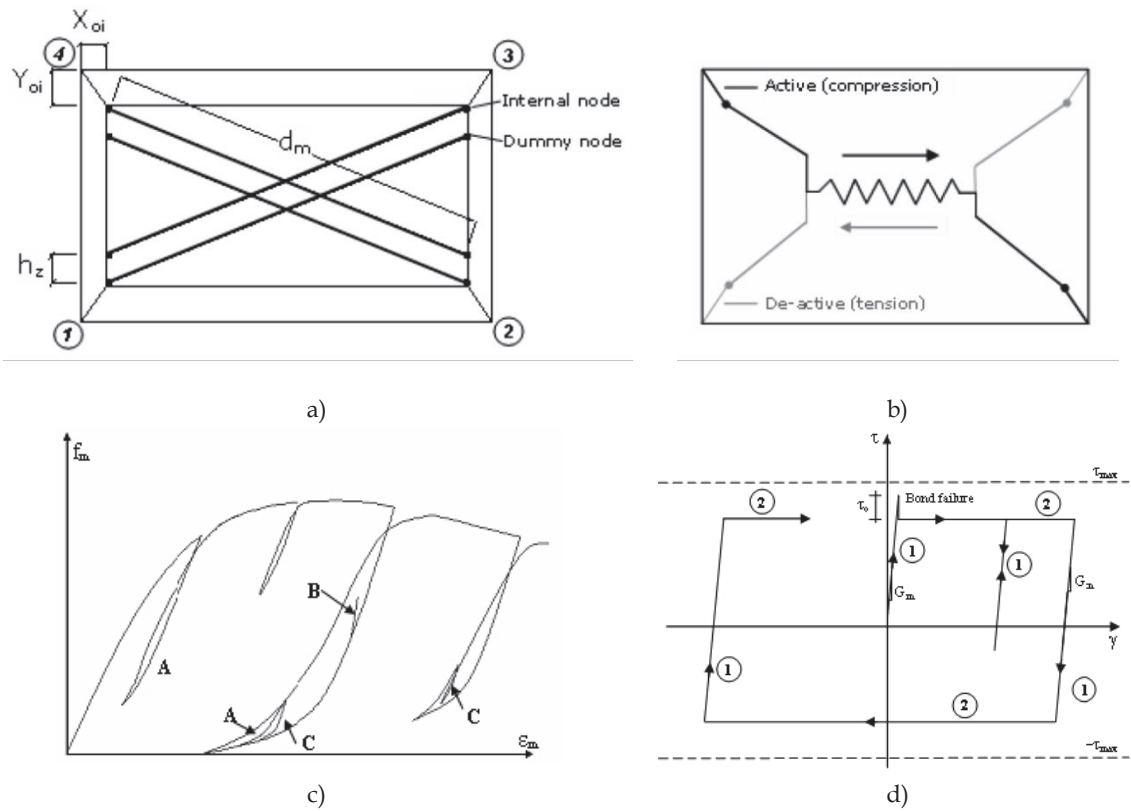


Figure 7.32: Seismostruct inelastic infill panel model (Seismosoft, 2014): a) compressions struts; b) shear strut; c) masonry strut hysteretic model; d) masonry shear strut hysteretic model

The model assumes that the strut area, which is given by the product between the panel thickness  $t$  and the equivalent width of the strut  $b_w$ , varies as a function of the axial strain, according to the function given in Figure 7.33.

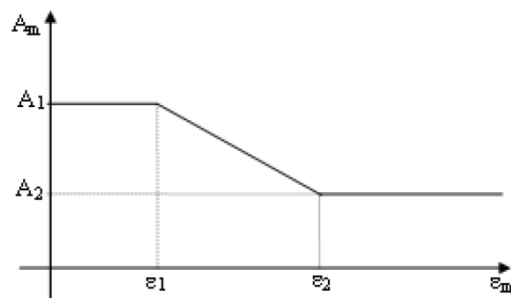


Figure 7.33: Variation of strut area with axial strain (Seismosoft, 2014)

A numerical model was developed in Seismostruct to reproduce the experimental set-up of the Markulak *et al.* (2013) test specimen C-1, which was subsequently used to calibrate the model parameters. The calibrated model general

parameters are presented in Table 7.6 and the strut and shear curve parameters are presented in Table 7.7 and Table 7.8, respectively.

Table 7.6: Inelastic infill panel element general parameters calibrated to Markulak *et al.* (2013) experimental test case C-1

Property	Value	Unit
Panel thickness	0.125	m
Out-of-plane failure drift (% of vert. panel side)	5	%
Strut area 1	0.04	m <sup>2</sup>
Strut area 2 (% of Strut area 1)	40	%
Equiv. contact length $h_z$ (% of vert. panel side)	23	%
Horizontal offset $X_o$ (% of horiz. panel side)	2.6	%
Vertical offset $Y_o$ (% of vert. panel side)	2.6	%
Proportion of stiffness assigned to shear	20	%
Specific weight	5	kN/m <sup>3</sup>

Table 7.7: Masonry strut hysteresis model curve parameters calibrated to Markulak *et al.* (2013) experimental test case C-1

Property	Symbol	Value	Unit
Initial Young modulus	$E_m$	2200000	kPa
Compressive strength	$f_{m0}$	2500	kPa
Tensile strength	$f_t$	0	kPa
Strain at maximum stress	$\epsilon_m$	0.0016	-
Ultimate strain	$\epsilon_u$	0.012	-
Closing strain	$\epsilon_{cl}$	0.004	-
Strut area reduction strain	$\epsilon_1$	0.00045	-
Residual strut area strain	$\epsilon_2$	0.0005	-
Starting unloading stiffness factor	$\gamma_{un}$	1.5	-
Strain reloading factor	$\alpha_{re}$	0.2	-
Strain inflection factor	$\alpha_{ch}$	0.7	-
Complete unloading strain factor	$\beta_a$	1.5	-
Stress inflection factor	$\beta_{ch}$	0.9	-
Zero stress stiffness factor	$\gamma_{plu}$	1	-
Reloading stiffness factor	$\gamma_{pr}$	1.5	-
Plastic unloading stiffness factor	$e_{x1}$	3	-
Repeated cycle strain factor	$e_{x2}$	1.4	-

Table 7.8: Masonry shear strut hysteresis model curve parameters calibrated to Markulak et al. (2013) experimental test case C-1

Property	Symbol	Value	Unit
Shear bond strength	$\tau_0$	380	kPa
Friction coefficient	$\mu$	0.7	-
Maximum shear strength	$\tau_{MAX}$	600	kPa
Reduction shear factor	$\alpha_S$	1.5	-

The Seismostruct model is presented in Figure 7.34a) and the comparison between the experimental and the numerical response curves is shown in Figure 7.34b).

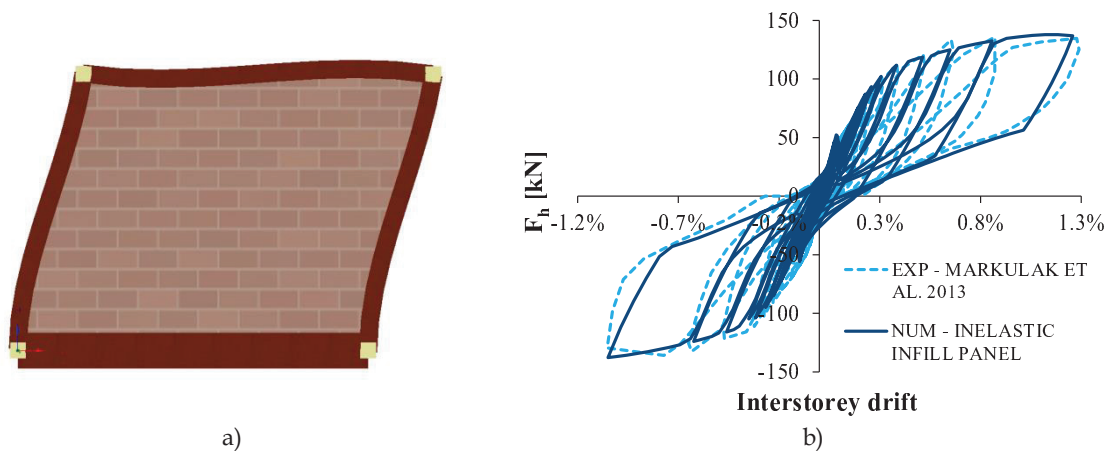


Figure 7.34: Seismostruct numerical model: a) deformed shape at 1.2% interst. drift (ampl. factor=20); b) interstorey drift - horizontal force comparison to Markulak *et al.* (2013) experimental C1 curve

The adopted infill panel modelling formulation is shown to be capable of simulating the cyclic hysteretic behaviour of infill masonry with reasonable accuracy, for which reason it was adopted for the robustness assessment.

#### 7.2.6.6.2 Cold formed steel claddings

For the case of seismically designed frames, façade claddings consisting on Cold Formed Steel (CFS) strap braced stud walls were considered. The contribution of these cladding elements to robustness was modelled and calibrated to full-scale experimental tests conducted by Iuorio *et al.* (2014). The heavy dissipative wall configuration (WHD) was selected due to its higher ultimate strength and deformation capacities and its geometrical layout and the experimental set-up are shown in Figure 7.35.

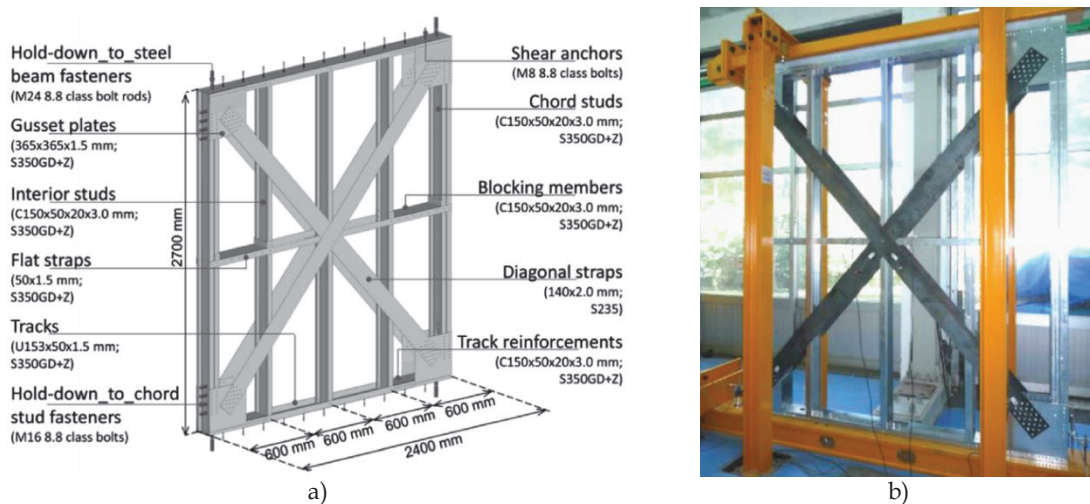


Figure 7.35: Heavy dissipative wall experimental test Iuorio *et al.* (2014): a) geometric definition; b) test set-up

The WHD specimen consists of a full scale cold formed steel (CFS) strap-braced stud wall with 2400 mm long by 2700 mm high, in which all steel members are in steel grade S350 GD, at the exception of the diagonal straps, that are in S235. The planar frame was subjected to a cyclic test characterized by a series of stepwise increasing deformation cycles, in accordance with the CUREE reversed cyclic protocol modified for CFS strap braced walls (Iuorio *et al.*, 2014), characterized by a displacement rate of 0.5 mm/s for displacements up to 7.27 mm and a rate of 2.0 mm/s for higher displacements values.

To model the CFS wall response, the inelastic infill panel element type formulation provided in Seismostruct (Seismosoft, 2014) was adopted. In this case, the multilinear polygonal hysteresis curve was adopted for the axial load strut, whereas the contribution of the shear strut was disregarded by assigning it a linear elastic response curve with zero stiffness. The inelastic infill panel element out-of-plane failure was prevented, no variation of the strut area with axial strain was considered and the adopted contact lengths  $h_z$  and offsets  $x_0$  and  $y_0$  (see Figure 7.32a) were taken as approximately zero.

A Seismostruct numerical model was hence calibrated to the WHD cyclic test from Iuorio *et al.* (2014) and the model general parameters are presented in Table 7.9, whereas the strut and shear curve calibrated parameters are presented in Table 7.10 and Table 7.11, respectively.

Table 7.9: Inelastic infill panel element general parameters calibrated to Iuorio *et al.* (2014) experimental test case WHD-C1

Property	Value	Unit
Panel thickness	0.004	m
Out-of-plane failure drift (% of vert. panel side)	100	%
Strut area 1	0.00056	m <sup>2</sup>
Strut area 2 (% of Strut area 1)	100	%
Equiv. contact length hz (% of vert. panel side)	0.1	%
Horizontal offset Xo (% of horiz. panel side)	0.1	%
Vertical offset Yo (% of vert. panel side)	0.1	%
Proportion of stiffness assigned to shear	0.001	%
Specific weight	0.001	kN/m <sup>3</sup>

 Table 7.10: Axial strut multi-linear hysteresis model curve parameters calibrated to Iuorio *et al.* (2014) experimental test case WHD-C1

Property	Symbol	Value	Unit
Initial flexural rigidity	EI	9000	kN/rad
Cracking moment (positive)	PCP	10	kNm
Yield moment (positive)	PYP	45	kNm
Yield curvature (positive)	UYP	0.02	m <sup>-1</sup>
Ultimate curvature (positive)	UUP	0.15	m <sup>-1</sup>
Post yield flexural stiffness (positive)	EI3P	0.001	(% of EI)
Cracking moment (negative)	PCN	-10	kNm
Yield moment (negative)	PYN	-45	kNm
Yield curvature (negative)	UYN	-0.02	m <sup>-1</sup>
Ultimate curvature (negative)	UUN	-0.15	m <sup>-1</sup>
Post yield flexural stiffness (negative)	EI3P	0.001	(% of EI)
Stiffness degrading parameter	HC	50	-
Ductility-based strength decay parameter	HBD	0.001	-
Hysteretic energy-based strength decay parameter	HBE	0.001	-
Slip parameter	HS	0.1	-

 Table 7.11: Shear strut model linear symmetric curve parameters calibrated to Iuorio *et al.* (2014) experimental test case WHD-C1

Property	Symbol	Value	Unit
Stiffness	k <sub>0</sub>	0.001	kN/m

The Seismostruct model is presented in Figure 7.36a) and the comparison between the experimental and the numerical response curves shown in Figure 7.36b) highlights that the numerical infill panel model can effectively simulate the cyclic response of the wall, namely the initial elastic response, the transition to the plastic

regime and the hysteretic cycling and failure, for which reason it was adopted for the robustness assessment.

For cases of MRF structures with 6m span, a set of 3 infill panels was adopted between adjacent MRF columns, whereas for the 10m span frames, a set of 5 infill panels was assumed (see Figure 7.37). To determine the behaviour of the infill panel sets, numerical models were developed in Seismostruct, for the cases with 6m and 10m spans and with 3m and 4m interstorey height, adopting panel properties as calibrated to the experimental results.

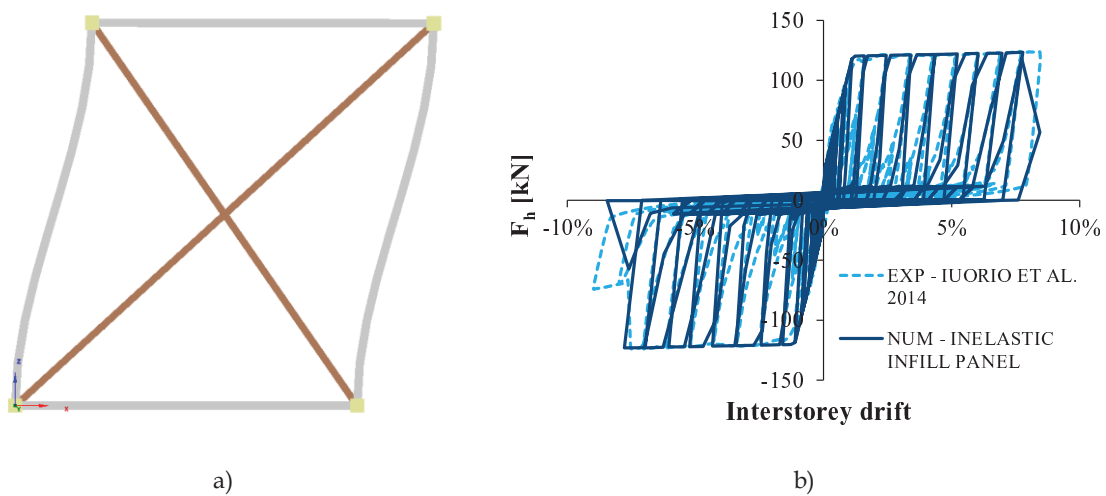


Figure 7.36: Seismostruct numerical model: a) deformed shape at 4.0% interst. drift (ampl. factor=5); b) interstorey drift - horizontal force comparison to Iuorio *et al.* (2014) experimental WHD-C1 curve

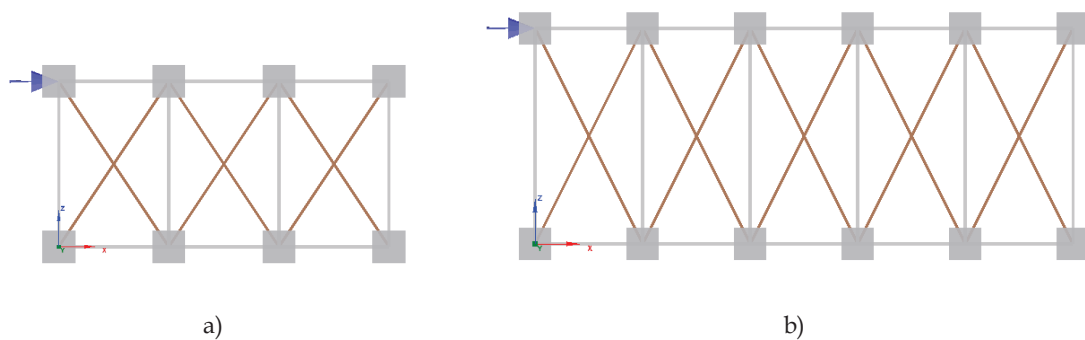


Figure 7.37: Seismostruct models of the sets of CFS infill panels: a) 6m span with 3m interstorey height; b) 10m span with 4m interstorey height

To facilitate the implementation in the numerical models while also optimizing computational time, equivalent infill panel models (see Figure 7.38) were adopted and calibrated to match the behaviour of the panel sets.



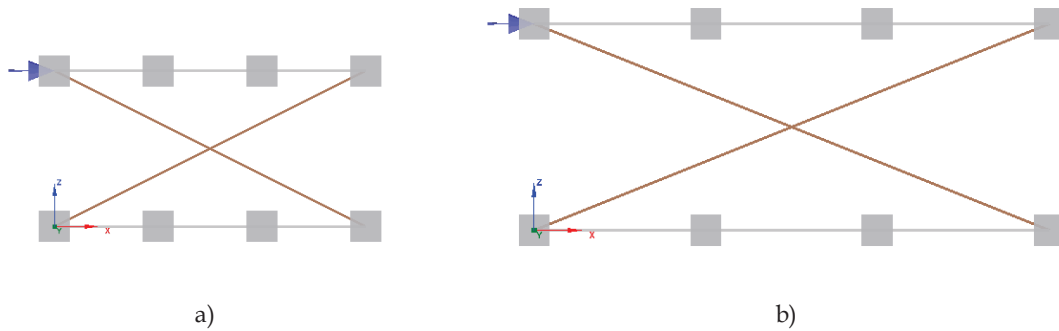


Figure 7.38: Seismostruct models of the equivalent CFS infill panels: a) 6m span with 3m interstorey height; b) 10m span with 4m interstorey height

The comparison between the response of the panel set models and the equivalent infill panel models is presented in Figure 7.39, showing that for all cases, the equivalent panel model is effective in reproducing the panel set behaviour and is therefore suitable for cladding response simulation.

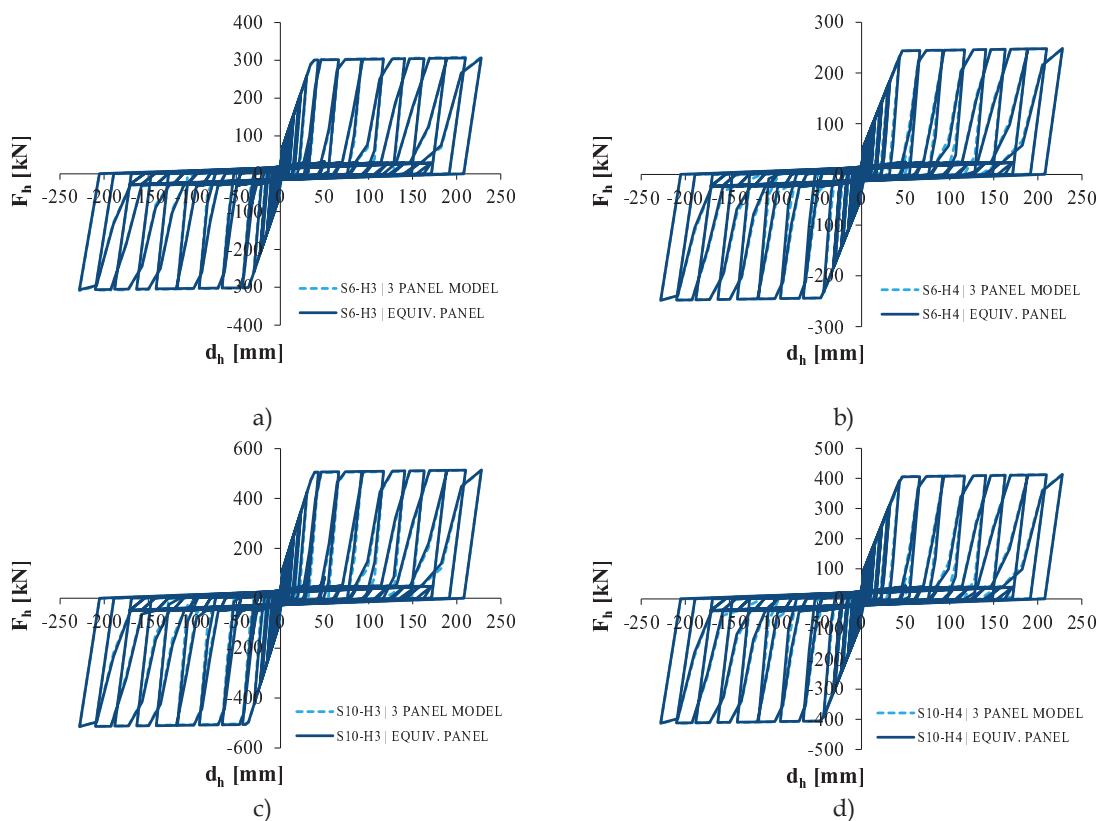


Figure 7.39: Response comparison between the panel set and the equivalent infill panel models: a) S6-H3 case; b) S6-H4 case; c) S10-H3 case; d) S10-H4 case

## 7.3 Results

### 7.3.1 Baseline robustness

#### 7.3.1.1 Sensitivity to damping

The damping ratio has been shown to be one of the most important parameters to influence the dynamic response under column loss (Kim *et al.*, 2011). In this sense, a sensitivity assessment was conducted to determine how the damping ratio  $\zeta$  influences structural response subsequent to column loss, for  $\zeta$  ranging from 1% to 10%. Two column loss scenarios were analysed, namely XZ façade and corner.

Firstly, the sensitivity analysis was conducted for a 6m span structure, namely the N4-H3-S6-T5x4-DG frame, which for  $\zeta=2\%$  displayed degrees of plasticity  $DOP_{DAZ}$  (see Section 7.2.4) of 0.57 and 0.80 for the analysed column loss scenarios, which are indicative of predominantly elastic and plastic responses, respectively. The influence of the damping ratio for the N4-H3-S6-T5x4-DG frame is presented in Figure 7.40.

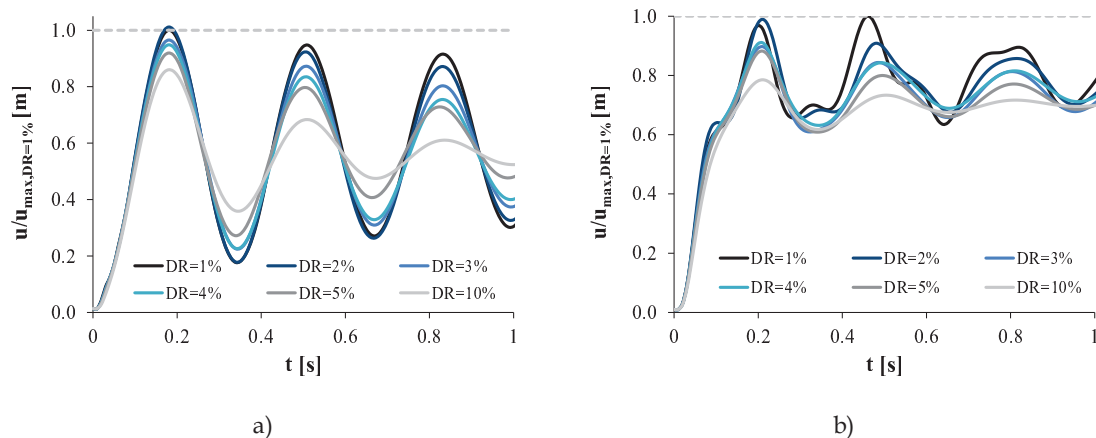


Figure 7.40: : Effect of damping on the displacement time-histories of a 6m span frame (N4-H3-S6-T5x4-DG) normalised to the maximum dynamic displacement for  $\zeta=1\%$  : a) XZ façade column removal; b) corner column removal

As seen in Figure 7.40a), when the response is predominantly elastic, the effect of damping on the maximum dynamic displacement is reduced, with  $u/u_{max,DR=1\%}$  ratio values equal to 1.00, 0.96, 0.94, 0.91 and 0.86 for damping ratios of 2%, 3%, 4%, 5% and 10%, respectively. Instead, for the corner column removal case shown in Figure 7.40b), the response is significantly more complex since the DAZ does not behave as a SDOF system, owing to the yielding of gravity frame connections which changes the DAZ stiffness. In this case, the effect of the damping is more pronounced, namely for

$\zeta > 2\%$ , with  $u/u_{max,DR=1\%}$  ratio values equal to 0.98, 0.90, 0.91, 0.88 and 0.78 for damping ratios of 2%, 3%, 4%, 5% and 10%, respectively.

For the case of long span frames, the sensitivity analysis was conducted on the N4-H3-S10-T5x3-DE frame, which for  $\zeta=2\%$  displayed degrees of plasticity  $DOP_{DAZ}$  (see Section 7.2.4 ) of 0.99 for both façade and corner column removals, which is indicative of the high degree of plasticity developed in the DAZ, as is further shown throughout this Chapter to be characteristic of long span systems.

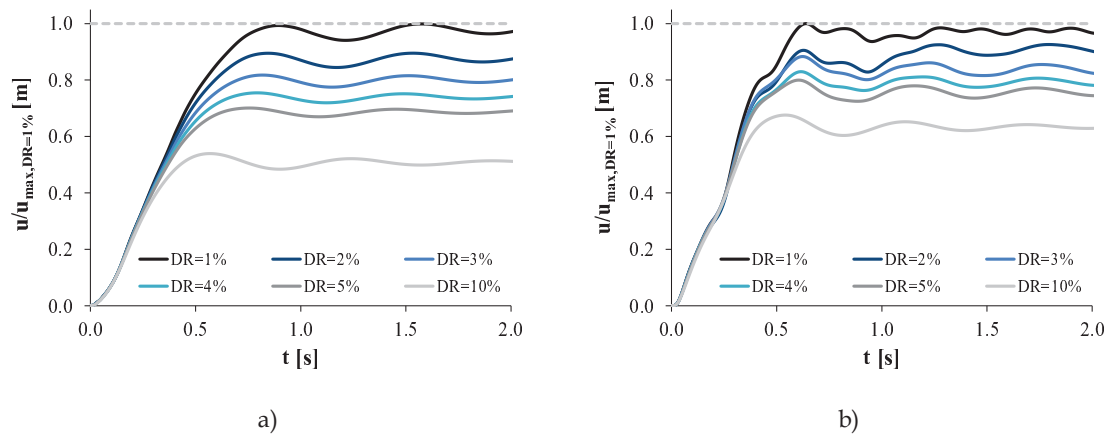


Figure 7.41: : Effect of damping on the displacement time-histories of a 10m span frame (N4-H3-S10-T5x3-DE) normalised to the maximum dynamic displacement for  $\zeta=1\%$  : a) XZ façade column removal; b) corner column removal

As seen in Figure 7.41, the effect of damping on the maximum dynamic displacement following column loss is considerably magnified when the span increases. For the façade removal, the  $u/u_{max,DR=1\%}$  ratio values equal to 0.90, 0.82, 0.75, 0.70 and 0.54 for damping ratios of 2%, 3%, 4%, 5% and 10%, respectively. Instead, for the corner removal  $u/u_{max,DR=1\%}$  values of 0.93, 0.88, 0.83, 0.80 and 0.68 are reported for damping ratios of 2%, 3%, 4%, 5% and 10%, respectively.

These results show the importance of the damping ratio as a key parameter influencing the progressive collapse arrest, namely for the case of long span frames, since differences in terms of maximum dynamic displacement can be as high as 10% between  $\zeta=1\%$  and  $\zeta=2\%$ . Given the influence of damping and in order to avoid excessive and unrealistic displacement reduction, the value of  $\zeta=2\%$  was adopted, as is typically considered for building steel frames and in accordance with the methodology adopted for the preliminary robustness assessment using NDA presented in Chapter 4.

7.3.1.2 Sensitivity to MRF beam yield strength

The yield strength variability of the MRF beams of the DAZ can greatly influence the maximum displacement demand under column loss, as reported by Kim *et al.* (2011), given that the catenary effect in the MRF beams provides a great part of the resistance to progressive collapse. In the study by Kim *et al.* (2011), the effect of randomness on key material parameters was evaluated, considering a bi-linear constitutive law for steel, for a set of structures which included a 3 storey - 6m span frame and a 10 storey - 9m span frame, both moment resisting. Results showed that the variability of MRF beam yield strength could lead to differences of up to 1.5 times in terms of vertical displacement for exterior column removals.

It was therefore concluded to be of key importance to investigate how beam yield strength variability influences displacement demand for varying span lengths. To this end, six different values were considered for the beam yield strength  $f_{y,beam}$ , namely 355, 399, 444, 488 and 533 N/mm<sup>2</sup>, corresponding to material overstrength values relative to the S355 steel nominal yield stress of 1.000, 1.125, 1.250, 1.375 and 1.500, respectively. The same two frames and column loss scenarios used for the damping sensitivity study were adopted here.

For the case of the medium span frame (N4-H3-S6-T5x4-DG frame), the influence of the beam yield strength is presented in Figure 7.42.

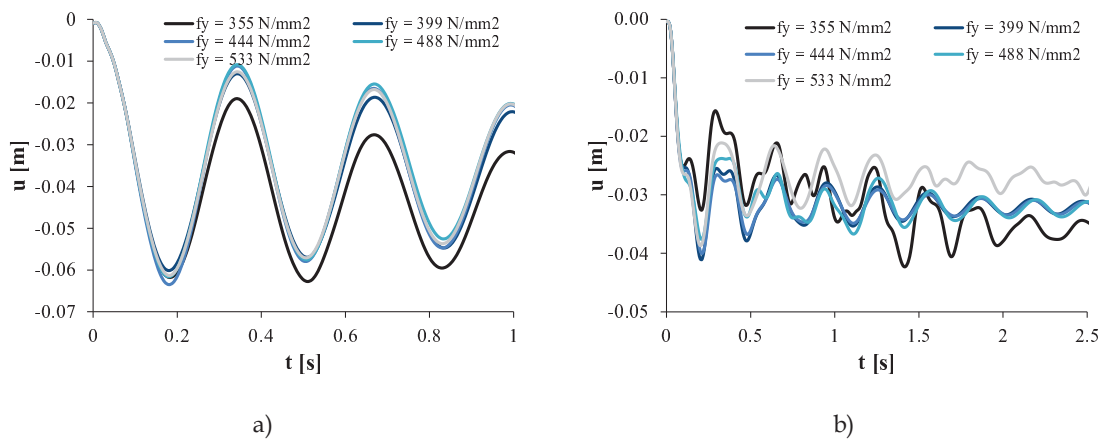


Figure 7.42: : Effect of beam yield strength variability on the vertical displacement after column loss for a 6m span frame (N4-H3-S6-T5x4-DG): a) XZ façade column removal; b) corner column removal

The effect of yield strength for the 6m span frames is shown in Figure 7.42 to be negligible for both the façade and corner column removal cases. The differences in terms of maximum dynamic displacement are inferior to 1 cm, or also put, to a chord

rotation of 1.7 mrad, having therefore no impact on the rotational demand on connections or on structural robustness.

For the case of the 10m span frame (N4-H3-S10-T5x3-DE frame), the influence of the beam yield strength is presented in Figure 7.43, showing that, unlike for 6m span frames, the beam yield strength has a great impact on the maximum dynamic displacement under column loss.

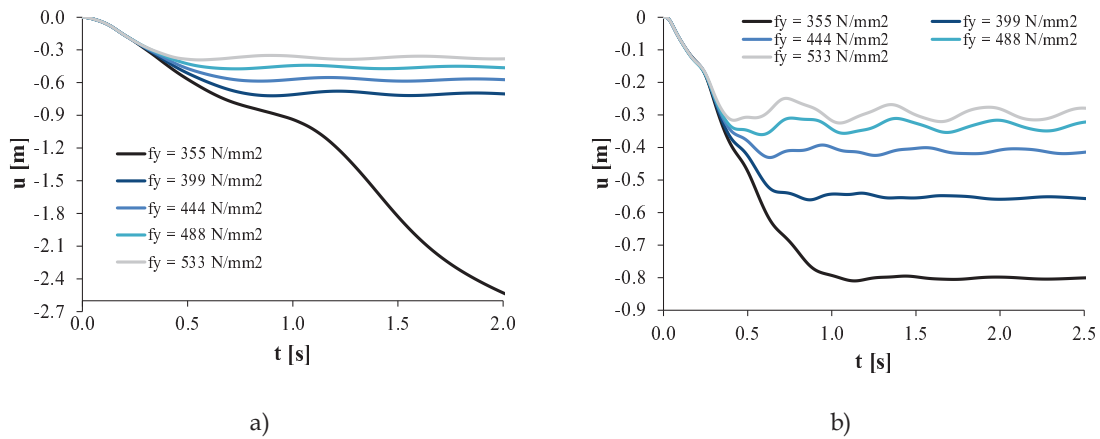


Figure 7.43: : Effect of beam yield strength variability on the vertical displacement after column loss for a 10m span frame (N4-H3-S10-T5x3-DE): a) XZ façade column removal; b) corner column removal

For the façade column loss shown in Figure 7.43a) and for  $f_y = 355 \text{ N/mm}^2$ , the progressive collapse is not arrested, contrarily to the other analysed cases. However, even for  $f_y \geq 399 \text{ N/mm}^2$ , the displacement at equilibrium  $u_{dyn, equil, damaged}$  assumes values of 0.71 m, 0.58 m, 0.46 m and 0.38 m for  $f_y$  values of 399, 444, 488 and 533  $\text{N/mm}^2$ , respectively. This stresses the great importance of this variable, since results show that displacement demand is halved when beam yield overstrength factors increases from 1.125 to 1.500. Also for the case of the corner column removal shown in Figure 7.43b), the yield strength is shown to have great impact on the post column loss response. Indeed,  $u_{dyn, equil, damaged}$  assumes values of 0.80 m, 0.56 m, 0.41 m, 0.33 m and 0.29 m for yield stress values of 355, 399, 444, 488 and 533  $\text{N/mm}^2$ , respectively. These findings are in line with those by Kim *et al.* (2011), which showed that changing the beam yield strength by 2 times its standard deviation (corresponding to a material overstrength variation of up to 24%) could lead to displacement variations by factors of approximately 1.5.

These large differences in performance are due to different degrees of plasticization of the DAZ or conversely, to the higher capacity of structures to remain in the elastic range, hence limiting irreversible plastic displacement.

For the case of structures in seismic zones, the EN 1998-1 (CEN, 2004) provides the design criteria to achieve a stable global plastic mechanism in MRF structures, in which plastic hinges are formed in the beams (or in the connections of beams to columns) but not in the columns. Therefore, when taking advantage of a structure's dissipative capacity (i.e. for structures in ductility classes DCM and DCH), a higher beam steel overstrength is unfavourable for the response to seismic actions, since it increases the probability of formation of plastic hinges in columns. Increasing robustness by increasing the beam yield strength is therefore not a suitable strategy for structures in DCM and DCH classes.

However for structures in DCL class or for non-seismically designed frames, increasing the yield strength of MRF beams remains a possible criterion for increasing robustness by decreasing the maximum dynamic demand. This can be easily implemented by designers as a progressive collapse mitigation measure, by simply increasing the steel grade of MRF beams while maintaining cross section dimensions, namely for structures with inherently low robustness, as is the case for structures with few storeys and long spans.

### *7.3.1.3 Displacement time-history under column loss*

#### *7.3.1.3.1 Low rise structures (4 storeys)*

The deformed shapes at the maximum dynamic displacement and the dynamic response of the 4-storey seismically designed frames with 3m interstorey height and a 5×3 bay configuration are presented in Figure 7.44 and Figure 7.45 respectively, for the 6m and 10m span frames.

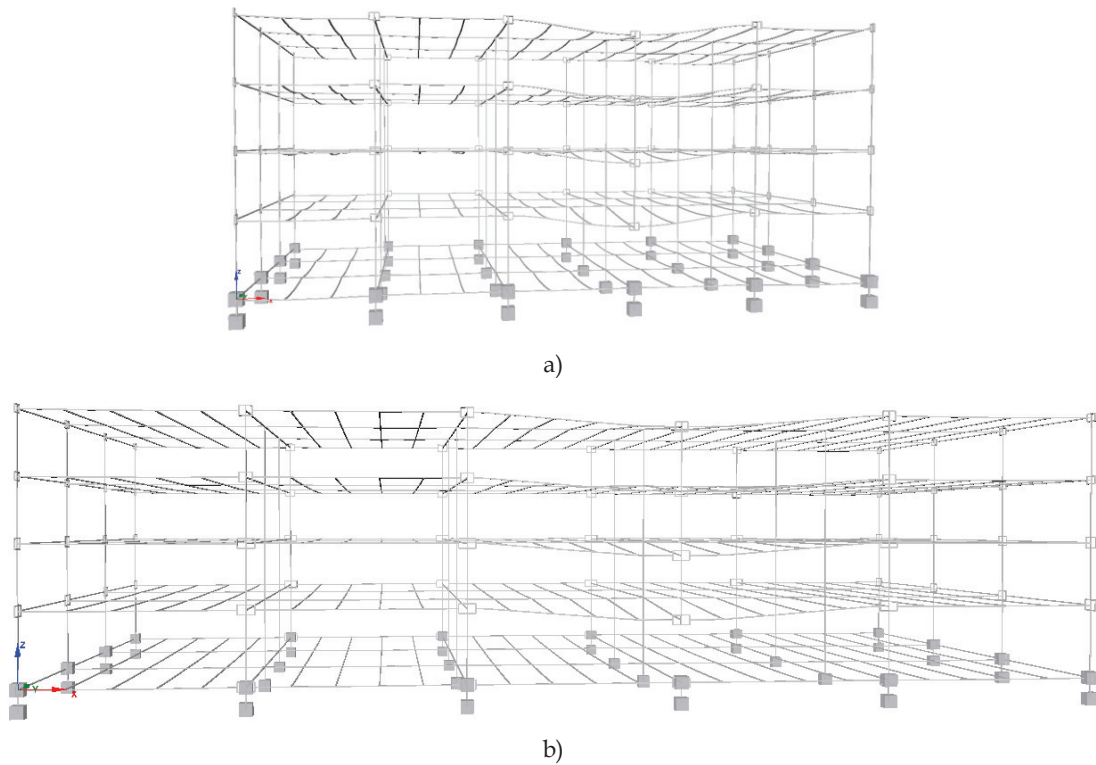


Figure 7.44: : Deformed configuration at the maximum dynamic displacement for the N4-H3-CN-T5x3-DE-LS frame: a) 6 m span frame (ampl. factor = 10.0); b) 10 m span frame (ampl. factor = 1.0)

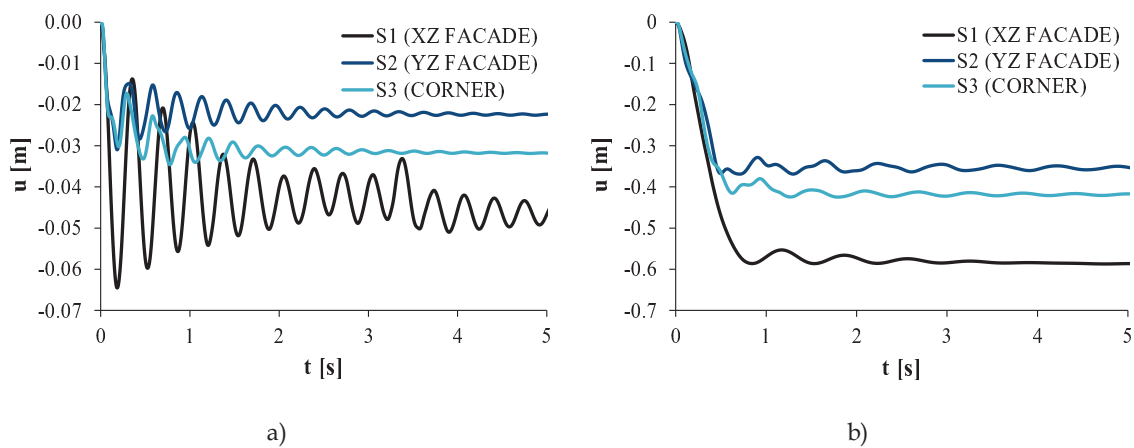


Figure 7.45: : Vertical displacement time history under column loss for the N4-H3-CN-T5x3-DE for different column loss scenarios: a) 6 m span frame; b) 10 m span frame

As it can be observed, the main difference between the 6m and the 10m span frames is the amplitude of the maximum displacement, which is approximately 10 times greater for the long span frame. Furthermore, for the 10m span frame case (see Figure 7.45b)), the maximum dynamic displacement  $u_{dyn,max,damaged}$  and the displacement at equilibrium  $u_{dyn,equl,damaged}$  are practically equal in value, implying that the DAZ is

required to develop high levels of plasticity, leading to  $DOP_{DAZ}$  values (see Eq.(7.1)) approximately equal to 1. Instead, for the 6m span frame, the response to column loss for the different removal scenarios depicted in Figure 7.45a) shows that, for scenarios S1 and S2 (i.e. façade column removals), the system preserves a degree of elasticity which leads the displacement at equilibrium to be smaller in value to the maximum dynamic displacement. In this case the  $DOP_{DAZ}$  values are equal to 0.73 for both façade removal scenarios.

As seen in Figure 7.45 for both the 6m and 10m span frames, significant differences in displacement demand are reported for different column removal scenarios, which are due to the different characteristics of the mobilised members and joints of the DAZ, as illustrated in Figure 7.46. For example, for the LL removal scenario, the collapse resistance is mainly provided by the MRF beams and respective rigid beam-to-column joints, as well as by the 10 nominally pinned beam-to-beam joints; instead for scenario LS, besides the MRF and respective beam-to-column joints, a semi-rigid FEP beam-to-column joint is mobilised, as well as 8 nominally pinned beam-to-beam joints; finally for the LC scenario (i.e. corner column removal), the moment frame and its rigid joints in the YZ façade are mobilised, whereas in the XZ façade, a semi-rigid FEP beam-to-column joint are mobilised, as well as 4 nominally pinned beam-to-beam web cleat joints.

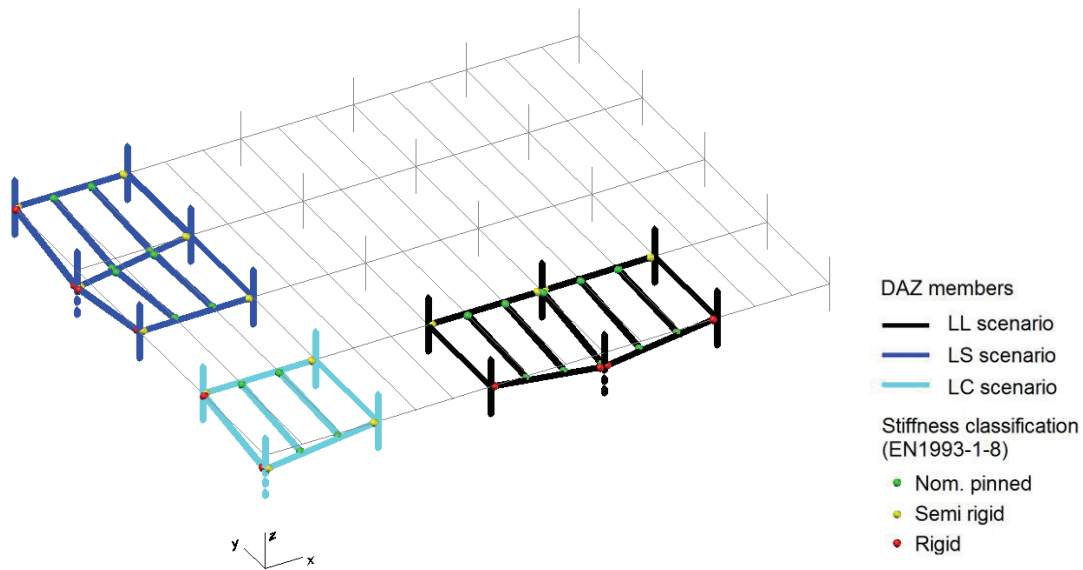


Figure 7.46: DAZ members by column loss scenario – deformed shapes and stiffness of mobilised joints



The different column loss scenarios are therefore seen to engage different floor members and connections, leading to differences in safety levels after the column loss event. Furthermore, the load to be redistributed varies depending on the removal scenario, since for the façade removal cases (i.e. LL and LS) the load to be redistributed is approximately double that for the corner removal case (i.e. LC), owing to the column influence area. In this sense, although in a corner removal the load is redistributed to XZ and YZ frames via the beams that act as cantilevers, the fact that the axial force in the removed column is also much smaller enables the structures to arrest the progressive collapse in most cases.

#### *7.3.1.3.2 Medium rise structures (8 storeys)*

For the 8 storey frames, the maximum dynamic displacements are seen to be generally smaller when compared to the corresponding 4 storey structures. This was also seen in the preliminary robustness assessment presented in Section 4.4.2, which used significantly different modelling hypotheses, namely regarding connection modelling and plasticity distribution.

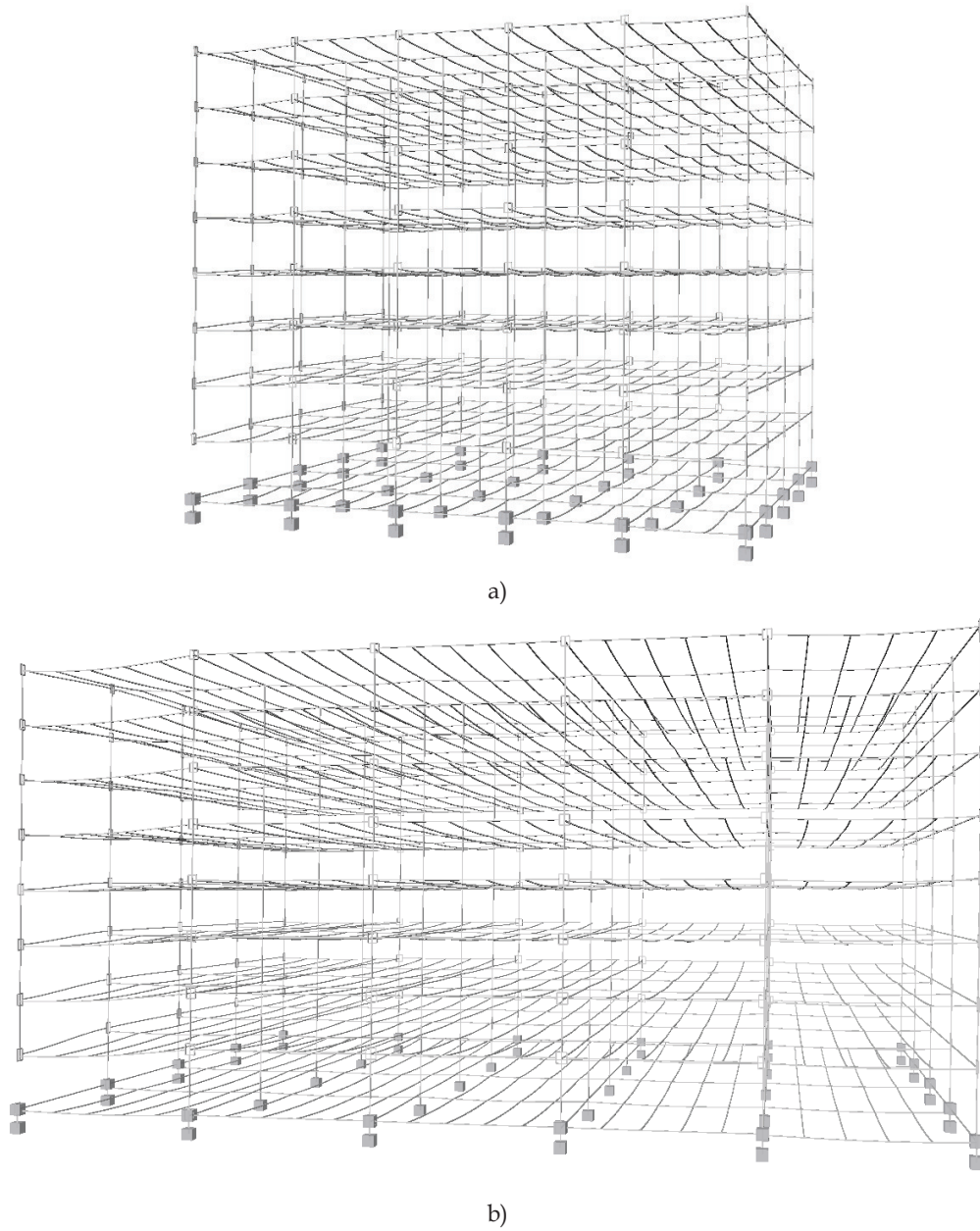


Figure 7.47: : Deformed configuration at the maximum dynamic displacement for the N8-H3-CN-T5x4-DG-LC frame: a) 6 m span frame (ampl. factor = 15.0); b) 10 m span frame (ampl. factor = 5.0)

It can therefore be concluded that, despite the fact that the axial load in the removed column (i.e. the load to be redistributed) for 8 storey frames is approximately double that of the corresponding 4 storey frames, the higher number of elements to which the load is effectively redistributed compensates for the higher axial load, resulting in smaller maximum dynamic displacements of the DAZ.

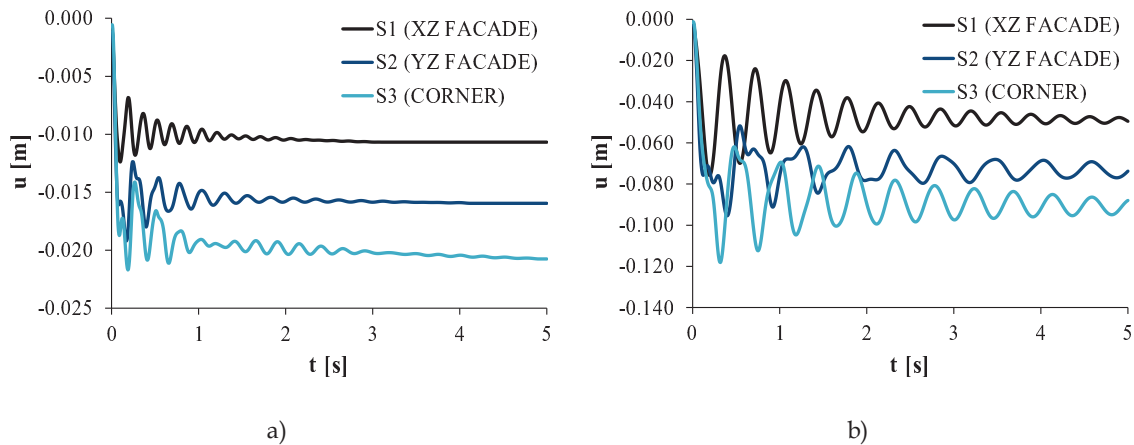


Figure 7.48: Vertical displacement time history under column loss for the N8-H3-CN-T5x4-DG for different column loss scenarios: a) 6 m span frame; b) 10 m span frame

This stresses the importance of the number of storeys above the removed column as a key parameter in terms of structural robustness. Furthermore, it is substantiated by the fact that for 8-storey frames, both for 6m and 10m span cases, as seen in Figure 7.48, the structures have the capacity to recover a part of the displacement owing to the fact that some elements of the DAZ remain elastic.

The medium rise 8-storey structures therefore display higher robustness, which translates into a higher Reserve Displacement Ductility at equilibrium ( $RDD_{equil}$ ), since part of the displacement is elastically recovered. Conversely, the lower values of Degree-Of-Plasticity of the DAZ ( $DOP_{DAZ}$ ) reported for these structures are an indicator that fewer elements sustain plastic strain, implying that repair costs for the damaged structure should be smaller. This information can be taken into consideration for risk analysis (see Section 2.5), since designing for robustness implies striking a balance between the design requirements to lower risks to a reasonable degree and the associated economical costs. Presently, the EN 1991-1-7 (CEN, 2006) only requires systematic risk assessment for buildings in Consequence Class 3.

#### 7.3.1.4 Degree of plasticity ( $DOP_{DAZ}$ )

The behaviour further to column loss is analysed here in terms of the capacity to develop plasticity in the DAZ, as measured by the  $DOP_{DAZ}$  ratio defined in Eq.(7.1). As previously stated, the ratio can vary from 0.5, for an elastic response, up to 1.0, for a fully plastic response. This ratio also provides a measure of the safety of the damaged structural system in terms of the displacement reserve capacity. In this sense, for

example, a structure that remains elastic (i.e.  $DOP_{DAZ}=0.5$ ) will recover to a displacement value in equilibrium that is equal to half the maximum dynamic displacement ( $u_{dyn,equl,damaged}=0.5*u_{dyn,max,damaged}$ ), whereas a structure with  $DOP_{DAZ}=1$  is not capable of recovering vertical displacement relative to its maximum dynamic value ( $u_{dyn,equl,damaged}=1.0*u_{dyn,max,damaged}$ ).

The ratio values for the XZ façade (LL case), YZ façade (LS case) and corner (LC case) column removal scenarios are presented in Figure 7.49, Figure 7.50 and Figure 7.51, respectively, where values of zero correspond to collapsed structures. These values are summarised in terms of average values, standard deviation and coefficient of variation in Table 7.12.

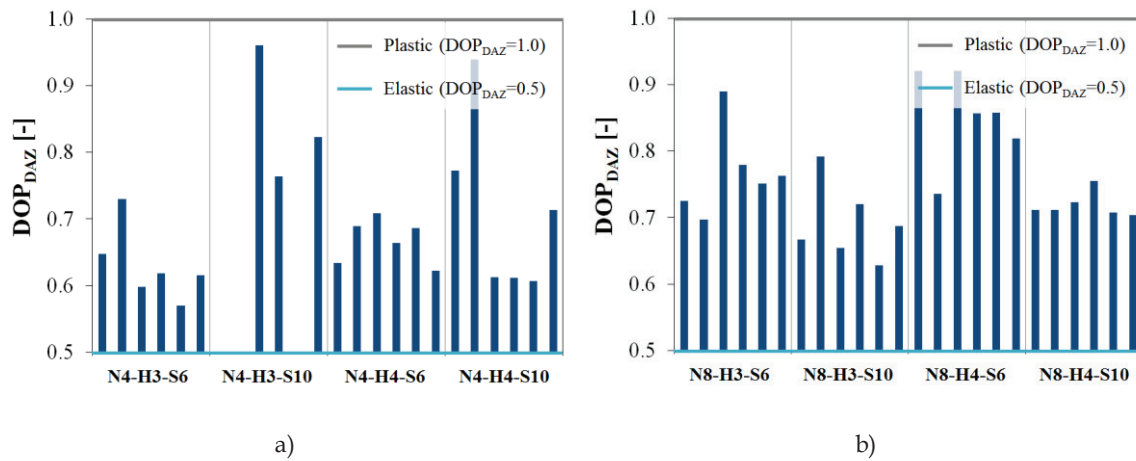


Figure 7.49: Degree-Of-Plasticity of the Directly Affected Zone  $DOP_{DAZ}$  ratios for the LL (XZ façade) column loss scenario: a) 4 storey frames; b) 8 storey frames

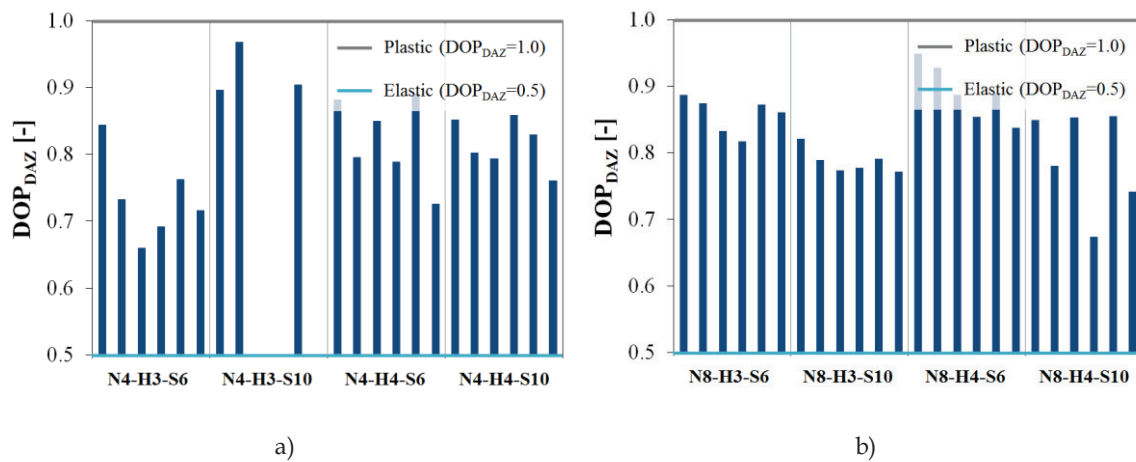


Figure 7.50: Degree-Of-Plasticity of the Directly Affected Zone  $DOP_{DAZ}$  ratios for the LS (YZ façade) column loss scenario: a) 4 storey frames; b) 8 storey frames

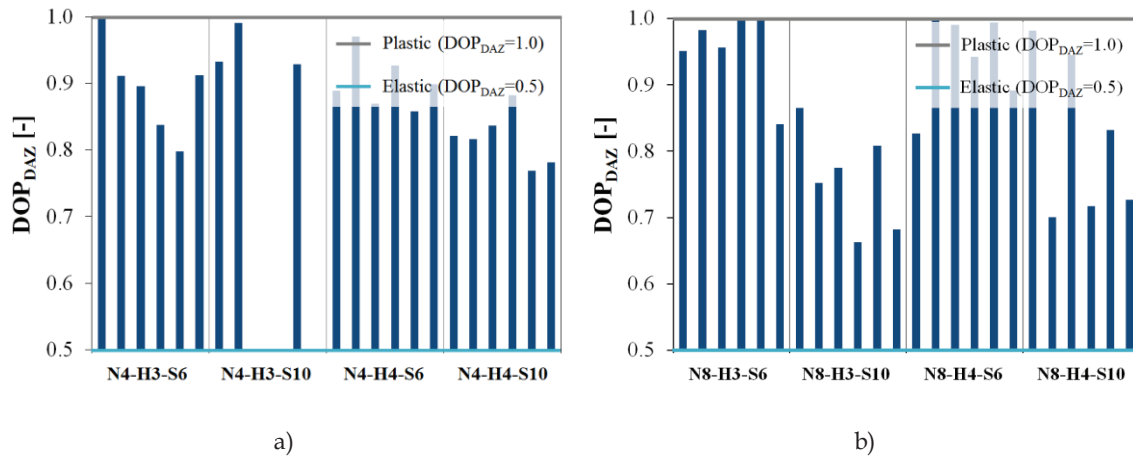


Figure 7.51: Degree-Of-Plasticity of the Directly Affected Zone  $DOP_{DAZ}$  ratios for the LC (corner) column loss scenario: a) 4 storey frames; b) 8 storey frames

The numerical results summarized in Table 7.12 show that according to the modelling strategy described in Sections 7.2.5 and 7.2.6, the structural systems are generally required to develop significant plasticity in members and connections, in order to arrest a progressive collapse, as shown by the  $DOP_{DAZ}$  ratios higher than 0.5 in all cases. This finding differs from the numerical results obtained in the preliminary robustness assessment presented in Chapter 4. Indeed, for the preliminary assessment, which was based on simplified assumptions regarding joint modelling and plasticity distribution, 6m span frames were found to respond elastically (see Table 4.5). Instead, the NDA results obtained according to the refined modelling strategy, which explicitly accounts for distributed plasticity and for the “gravity” frame joint contribution, show that in all cases some degree of plasticity is developed. On the one hand, this difference is in part ascribable to the differences in the modelling of the gravity frame joints, which were assumed as perfectly pinned (with infinite rotation capacity) for the preliminary robustness assessment; instead, for the NDA described here, secondary frame joints were explicitly modelled and calibrated to match joint response under column loss, accounting also for dynamic amplification effects. On the other hand, different MRF beam-to-column joint typologies were adopted for the preliminary and for the present robustness assessment. For the former, full strength bolted extended endplate MRF beam-to-column joints were assumed and modelled according to a lumped plasticity model based on FEMA 356 (ASCE, 2000) acceptance criteria. Instead, for the latter, MRF beam-to-column joints were assumed as welded full strength rigid

joints and modelled using a fiber based model, which accounts for distributed plasticity along the section and member length.

Table 7.12:  $DOP_{DAZ}$  ratios by number of storeys, span, interstorey height and column loss scenario - average, standard deviation and coefficient of variation values

N	S	H	L	$DOP_{DAZ}$		
				AVG	SD	CoV
[-]	[m]	[m]	[-]	[-]	[-]	[-]
4	6	3	L	0.63	0.05	0.08
			S	0.73	0.06	0.08
			C	0.89	0.06	0.07
		4	L	0.67	0.03	0.05
			S	0.82	0.06	0.07
			C	0.90	0.04	0.04
	10	3	L	0.85	0.08	0.10
			S	0.92	0.03	0.03
			C	0.95	0.03	0.03
		4	L	0.71	0.12	0.17
			S	0.82	0.03	0.04
			C	0.80	0.05	0.07
8	6	3	L	0.77	0.06	0.08
			S	0.86	0.02	0.03
			C	0.96	0.05	0.06
		4	L	0.85	0.06	0.07
			S	0.89	0.04	0.04
			C	0.94	0.06	0.07
	10	3	L	0.69	0.05	0.08
			S	0.79	0.02	0.02
			C	0.76	0.07	0.09
		4	L	0.72	0.02	0.02
			S	0.79	0.07	0.09
			C	0.82	0.11	0.14

The numerical results indicate that corner column loss cases require the development of a higher level of plasticity in the DAZ to arrest the progressive collapse in comparison to façade losses. In turn, by comparing the two façade removal cases LL (XZ façade) and LS (YZ façade), it is possible to verify that higher  $DOP_{DAZ}$  ratios are obtained for the LS case. Apart from small differences in terms of margins of safety between XZ and YZ moment resisting frame members and connections (see Eq.(4.1)), the differences in terms of degree of plasticity are attributed to the different secondary

frame systems that are activated upon column removal, as shown in Figure 7.46. For the LL case, the mobilised secondary frame joints are nominally pinned and hence more flexible, which explains the lower  $DOP_{DAZ}$  ratios. Conversely, for the LS case, the main mobilised gravity frame joints are semi-rigid partial-strength joints, which are comparatively more rigid and therefore tend to develop plasticity for lower rotational demands, leading to higher  $DOP_{DAZ}$  ratios. For the interstorey height, no correlation was found with the degree-of-plasticity. The span variable was found to influence  $DOP_{DAZ}$  ratios, namely for 4 storey frames, which have inherently lower structural robustness and which for 10m span frames display an average  $DOP_{DAZ}$  ratio increase of 11% when compared to the corresponding 6m span frames. This is due to long span systems being required to further develop catenary action and connection plasticity in order to arrest the collapse. Conversely, for 8 storey structures, which display much higher robustness due to the higher number of elements in the DAZ that are mobilised under column loss, 10m span frames display an average decrease in  $DOP_{DAZ}$  ratios of 13% when compared to 6m span frames. This difference is explained by the lateral sway limitation requirements for the 8-storey 10m span frames, which require large profiles that tend to develop less plasticity under column loss.

Structural typologies with lower  $DOP_{DAZ}$  ratios can be said to present minimum levels of safety, since it would be necessary to re-apply vertical loads to the DAZ, which is in equilibrium ( $u=u_{dyn,equl,damaged}$ ), to again reach a vertical displacement value equal to the previously reached maximum dynamic displacement ( $u=u_{dyn,max,damaged}$ ). In the absence of perfect knowledge of the capacity of all connections of the DAZ of a given real structure, as is necessarily the case for real rescue party interventions by Civil Protection Services (CPS) in column loss scenarios, a quick assessment must be made regarding the safety for intervention and the need for installing propping.

The  $DOP_{DAZ}$  ratios provide a quick estimation regarding these minimum safety levels. By breaking down the analysed frames'  $DOP_{DAZ}$  ratios by span, number of storeys, interstorey height and column loss scenario, it was possible to identify the structural typologies that display higher safety. Since these structural characteristics can be easily and quickly assessed upon arrival at the damaged structure site, the CPS can therefore rapidly correlate the key macro structural characteristics with the

expected  $DOP_{DAZ}$  values for the typology in question, hence conducting a better informed decision regarding the need for installing temporary propping.

The flow chart for decision making regarding temporary propping based on a quick visual inspection of the damaged structure is presented in Figure 7.52. By defining the high, medium and low safety levels as corresponding to typologies with average  $DOP_{DAZ}$  ratios in the ranges  $[0.50;0.60[$ ,  $[0.60;0.80[$  and  $[0.80;1.00]$ , it is possible to propose which structures should be propped. Obviously, if propping is possible/feasible, then, as an additional safety measure, it should be adopted in all cases. No high safety category was considered since all structures developed significant plasticity.

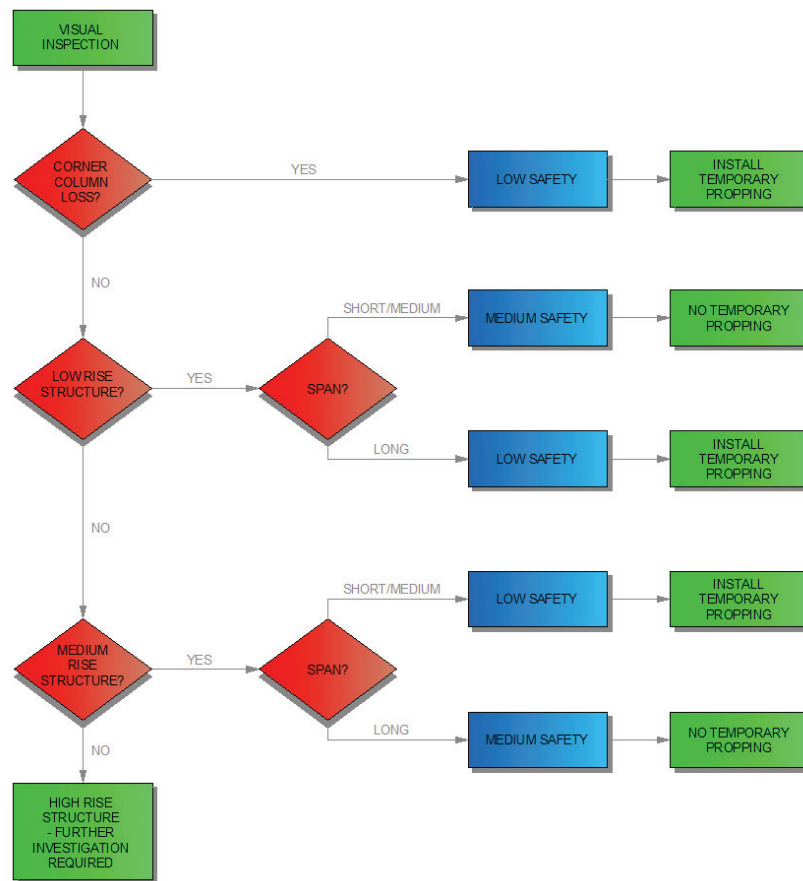


Figure 7.52: : Flow chart for minimum safety levels and temporary propping decision making based on  $DOP_{DAZ}$  ratios

While the flow chart proposed in Figure 7.52 is based on the simulation results from the present study, it can be easily adapted for structural systems other than moment frames, to incorporate data from other studies. Furthermore, the “no



temporary propping” measure can be substituted by other measures and/or further visual inspection. Since high rise structures fall outside the scope of this study (unfeasible for zones with moderate seismicity), no measures are suggested for this case. It should also be noted that no internal column loss scenario is contemplated in the flow chart. As previously stated, the degree-of-plasticity factor the ultimate vertical displacement capacity of the DAZ, which is instead accounted for by the reserve displacement ductility capacity, presented in Section 7.3.1.7.

#### *7.3.1.5 Vertical DAZ velocity and acceleration*

##### *7.3.1.5.1 Peak DAZ vertical velocity*

Under column loss action, the column above the removed member compatibilises the vertical displacements above the removed column at different storey levels, leading this zone to move as a rigid body. The characterisation of the motion of this zone in terms of peak velocity and acceleration can therefore be of significant importance for the analysis of DAZ connections under dynamic column loss action and for the quantification of strain rate effects. The conducted NDA have enabled to determine the vertical displacement – time series, from which the velocity and acceleration time series were subsequently derived. The results show that the peak velocity and acceleration values depend on key structural system features. The values for the peak vertical velocity are presented in Table 7.13.

Table 7.13: Peak vertical DAZ velocity  $v_{DAZ}$  by number of storeys, span, cladding type, interstorey height and column loss scenario – average, standard deviation and coefficient of variation

N	S	C	H	LL			LS			LC				
				AVG	SD	CoV	AVG	SD	CoV	AVG	SD	CoV		
[-]	[m]	[-]	[m]	[m/s]	[m/s]	[-]	[m/s]	[m/s]	[-]	[m/s]	[m/s]	[-]		
4	6	N	3	0.52	0.08	0.15	0.40	0.03	0.07	0.46	0.04	0.08		
			4	0.37	0.08	0.22	0.34	0.05	0.15	0.39	0.04	0.09		
		M/C	3	0.37	0.15	0.40	0.31	0.07	0.22	0.29	0.08	0.29		
			4	0.26	0.03	0.13	0.26	0.02	0.06	0.24	0.05	0.23		
		10	N	3	1.05	0.16	0.15	1.35	0.00	0.00	1.38	0.06	0.04	
				4	0.88	0.15	0.17	1.12	0.08	0.07	0.94	0.08	0.08	
	M/C		3	0.99	0.18	0.19	1.23	0.02	0.02	0.96	0.18	0.19		
			4	0.73	0.12	0.16	0.95	0.04	0.04	0.69	0.14	0.21		
	8		6	N	3	0.24	0.03	0.11	0.30	0.02	0.07	0.32	0.03	0.11
					4	0.21	0.02	0.11	0.26	0.03	0.11	0.26	0.05	0.20
		M/C		3	0.26	0.02	0.07	0.29	0.01	0.05	0.24	0.03	0.12	
				4	0.24	0.02	0.09	0.27	0.02	0.09	0.21	0.02	0.10	
10		N		3	0.76	0.10	0.13	0.88	0.14	0.16	0.81	0.04	0.05	
				4	0.60	0.20	0.33	0.67	0.06	0.09	0.69	0.04	0.05	
		M/C	3	0.67	0.07	0.10	0.75	0.18	0.23	0.65	0.15	0.22		
			4	0.46	0.05	0.12	0.58	0.09	0.15	0.52	0.14	0.26		

By analysing the NDA results, it can be verified that the column loss scenario does not significantly influence the peak velocity. Instead, results show that it is the structural configuration that influences to a higher degree the peak DAZ velocity ( $v_{DAZ}$ ). By comparing 4-storey to 8-storey frames, it can be seen that the latter presented lower  $v_{DAZ}$  values, with reductions typically around 30%. This is due to the higher inertia of the 8-storey frame DAZs, as well as to the higher robustness of these structures, which is provided by the higher number of resisting members/connections in the DAZ. The 8-storey frames therefore tend to develop less plasticity and are not required to develop significant catenary action to arrest the progressive collapse.

The span variable is also shown to greatly influence  $v_{DAZ}$  values, as 10m span frames were shown to display peak velocities 2 to 3 times higher than corresponding 6m span frames, since the axial force to be balanced following column loss is significantly higher ( $N_{S10}/N_{S6} \approx (10*5)/(6*3)=2.8$ ) and since the long span system opposes the motion mainly through catenary action, which requires the frame to undergo large displacements.

The presence of façade claddings is shown to lead to lower peak velocity values, with the effect being more pronounced for corner column loss (LC) cases. While for 4-storey 6m-span frames, the façade claddings reduced  $v_{DAZ}$  on average by 26% and 39% for façade and corner column removals respectively, for long span frames (N4-S10) the effect was found to be much less pronounced, with reductions averaging 12% and 29% for the façade and corner loss cases, respectively. For 8-storey frames, the effect of façade claddings on reducing peak velocity was found to be negligible for the N8-S6 frames under façade loss, while for the corner loss, a reduction of 23% is reported. Instead, for the N8-S10 frames, reductions are in the order of those verified for the 4-storey frames, with  $v_{DAZ}$  reductions of 16% and 22% for the façade and corner loss cases, respectively.

These results indicate that façade claddings are especially important for corner loss cases (LC), in which the much lower stiffness of the damaged structural system is partially compensated by the claddings. The efficacy of the claddings in reducing  $v_{DAZ}$  is also shown to be higher for low rise 6m span frames (N4-S6) since, on the one hand, the compressed strut inclination is more effective when the span is smaller and, on the other hand, for medium rise frames (N8) the number of resisting members and connections in the DAZ is higher providing redundancy which renders the marginal benefit from introducing façade claddings smaller.

The interstorey height is also shown to influence peak velocity, with lower values reported for frames with higher interstorey height. Indeed, for the analysed cases, the H4 frames are taller than corresponding H3 ones, leading to the adoption of deeper beam and column members to verify lateral stability requirements, resulting in higher resistance to progressive collapse.

Synthesising the results in Table 7.13 for the bare steel frames (CN cases) and despite the small but non-negligible effect of variables such as the column loss scenario or the interstorey height, the peak velocity can be seen to vary mostly according to macro structural characteristics. In this sense,  $v_{DAZ}$  values were grouped into four value zones, according to the N and S variable values, as shown in Table 7.14, where the small coefficient of variation (CoV) values indicate that the selected variables adequately describe the results.

Table 7.14: Peak vertical DAZ velocity for bare steel frames by number of storeys and span length – average, standard deviation and coefficient of variation

Storeys	Span	$v_{DAZ,AVG}$	$v_{DAZ,SD}$	$v_{DAZ,CoV}$
[-]	[m]	[m/s]	[m/s]	[-]
4	6	0.41	0.06	0.15
	10	1.12	0.19	0.17
8	6	0.27	0.04	0.14
	10	0.73	0.09	0.12

These results indicate that low rise and/or long span structures, which tend to display lower structural robustness (as seen in Chapter 4) develop higher DAZ peak velocities, since fewer and/or weaker members are available to counter the initial momentum. This trend is also verified for steel frames with façade claddings, for which the summarised results are presented in Table 7.15.

Table 7.15: Peak vertical DAZ velocity for steel frames with façade claddings by number of storeys and span length – average, standard deviation and coefficient of variation

Storeys	Span	$v_{DAZ,AVG}$	$v_{DAZ,SD}$	$v_{DAZ,CoV}$
[-]	[m]	[m/s]	[m/s]	[-]
4	6	0.29	0.04	0.15
	10	0.93	0.18	0.19
8	6	0.25	0.03	0.11
	10	0.61	0.10	0.16

These results can be compared to the peak velocity value used in the assessment of the strain rate effects in Section 6.2.5, which was derived from the preliminary robustness assessment for a subset of six seismically designed 5x3 bay structures with 6m span and with 4 or 8 storeys, for 3 different column loss scenarios. The peak DAZ velocity value assumed in Section 6.2.5 is equal to 1.7 m/s, which compares to a maximum value of 0.52 m/s for bare steel frames with 4 storeys and 6m span (see Table 7.13). This variation is due to differences in modelling assumptions, since for the preliminary robustness assessment in Chapter 4 the gravity frame joints were assumed as perfectly pinned with infinite rotation capacity, whereas for the more refined dynamic analysis presented in this chapter, the joint behaviour was explicitly modelled using nonlinear links. This finding highlights the importance of accurately modelling gravity frame members and connections according to their actual response under column loss action. In this sense, the additional stiffness contribution can prevent the DAZ from gaining momentum, leading to much lower peak velocities.

Considering that the evaluation of strain rate effects for the flush end-plate joints in Section 6.2.5 was performed on the basis of a conservative  $v_{DAZ}$  value and of joint component models leading to upper bound results, the findings in this chapter further reinforce the conclusion that the strain rate increase effect on FEP connections can be disregarded.

Since the peak velocity values were found to mostly depend on macro structural features such as number of storeys and span, rather than on other factors such as column loss location or gravity frame joint typology (see Figure 7.46), the values for bare frames and for frames with façade claddings presented in Table 7.14 and Table 7.15 respectively, can serve as a  $v_{DAZ}$  benchmark for evaluating strain rate enhancement effects on other joint typologies.

#### 7.3.1.5.2 Peak DAZ vertical acceleration

The DAZ vertical acceleration - time series were also computed from the displacement - time series, in order to determine the maximum acceleration following column loss. The values for the peak vertical acceleration are presented in Table 7.16, broken down by number of storeys (N), span (S), claddings (C), interstorey height (H) and column loss scenario (L). It should be noted that all the reported maximum values were obtained during the initial DAZ descent, for which the acceleration vector is directed downwards. In all cases, the upwards directed acceleration that is subsequently generated was found to be smaller.

In general, the trends identified for the peak velocity were also observed for the peak acceleration ( $a_{DAZ}$ ). Indeed, the peak acceleration is not greatly effected by column loss location (LL, LS or LC), while the presence of façade claddings can be seen to be more effective for corner loss scenarios, with average acceleration reductions of 20% and 5% for 4-storey and 8-storey frames, respectively. For façade removal scenarios, the presence of claddings causes relatively small changes in value to peak acceleration, and no correlation was observed for these cases.

The effect of the interstorey height for bare steel frames (CN case) was found to influence peak acceleration in the same sense as previously seen for the peak velocity. Indeed, frames with higher interstorey height require deeper members to control lateral drift, resulting in a higher initial stiffness that is more effective at counteracting the DAZ vertical motion, leading to lower  $a_{DAZ}$  values. For CN frames, peak

accelerations values for H4 frames were found to be on average 10% lower when compared to corresponding H3 frames.

Instead, for structures with façade claddings (CM or CC cases) the complex interaction and large differences in stiffness between the steel frame and the cladding struts did not lead to  $a_{DAZ}$  reductions in all cases when comparing H4 to H3 frames, as was the case for N4-S6-CM and N4-S6-CC frames. However, for N4-S10 frames, claddings reduced  $a_{DAZ}$  by 16%, whereas for N8-S6 and N8-S10, reductions averaged 5% and 4%, respectively.

It should be noted that the higher value dispersion for the N8-S10 frames is due to fact that these values reflect the behaviour of both N8-S10-DW and N8-S10-DE frames, where to the latter correspond full 3D moment resisting frames for which all beam-column joints were designed to be moment resisting with cruciform column cross sections (as described in Section 3.3.1).

The obtained NDA results point to the fact that façade claddings are most effective in reducing peak acceleration for structures with low structural robustness, as is the case for low rise long span frames, represented in this study by the N4-S10 cases. For other structural typologies, the additional redundancy provided by these elements is less effective. For medium span frames (S6), the rotational demand at equilibrium is small, as seen in the preliminary robustness assessment (see Figure 4.22a) and Figure 4.23a), hence not mobilising the resistance of claddings to a great degree. For medium rise frames (N8) the higher redundancy provided by the enhanced capacity to redistribute loads in the DAZ reduces the efficacy of the claddings, even in the case of long span frames.

Table 7.16: Peak vertical DAZ acceleration  $a_{DAZ}$  by number of storeys, span, cladding type, interstorey height and column loss scenario – average, standard deviation and coefficient of variation

N	S	C	H	LL			LS			LC				
				AVG	SD	CoV	AVG	SD	CoV	AVG	SD	CoV		
[-]	[m]	[-]	[m]	[g]	[g]	[-]	[m/s]	[m/s]	[-]	[m/s]	[m/s]	[-]		
4	6	N	3	1.50	0.15	0.10	1.61	0.12	0.07	1.59	0.11	0.07		
			4	1.24	0.11	0.09	1.48	0.13	0.09	1.43	0.04	0.03		
		M/C	3	1.27	0.20	0.16	1.40	0.07	0.05	1.19	0.12	0.10		
			4	1.76	0.73	0.41	1.50	0.18	0.12	1.19	0.09	0.08		
		10	N	3	2.20	0.36	0.17	3.56	0.13	0.04	2.98	0.03	0.01	
				4	1.98	0.27	0.14	3.12	0.12	0.04	2.60	0.07	0.03	
	M/C		3	2.40	0.23	0.09	3.15	0.22	0.07	2.53	0.14	0.05		
			4	2.02	0.18	0.09	2.73	0.11	0.04	2.04	0.05	0.02		
	8		6	N	3	1.46	0.21	0.14	1.64	0.13	0.08	1.34	0.13	0.10
					4	1.26	0.15	0.12	1.48	0.19	0.13	1.20	0.21	0.18
		M/C		3	1.65	0.17	0.10	1.58	0.10	0.06	1.19	0.10	0.09	
				4	1.48	0.17	0.12	1.41	0.15	0.10	1.27	0.32	0.25	
10		N		3	2.66	0.59	0.22	3.28	0.51	0.16	2.48	0.26	0.10	
				4	2.19	0.56	0.25	2.99	0.54	0.18	2.33	0.23	0.10	
		M/C	3	2.51	0.27	0.11	3.02	0.49	0.16	2.25	0.09	0.04		
			4	2.31	0.56	0.24	2.99	0.38	0.13	2.17	0.11	0.05		

The motion of the DAZ in terms of peak acceleration was found to correlate mostly with the number of storeys and frame span, as seen for the peak velocity. The summarised values for bare frames and for frames with claddings are shown in Table 7.17 and Table 7.18, respectively.

Table 7.17: Peak vertical DAZ acceleration for bare steel frames by number of storeys and span length – average, standard deviation and coefficient of variation

Storeys	Span	$a_{DAZ,AVG}$	$a_{DAZ,SD}$	$a_{DAZ,CoV}$
[-]	[m]	[g]	[g]	[-]
4	6	1.48	0.12	0.08
	10	2.74	0.54	0.20
8	6	1.40	0.15	0.11
	10	2.66	0.38	0.14

Table 7.18: Peak vertical DAZ acceleration for steel frames with façade claddings by number of storeys and span length – average, standard deviation and coefficient of variation

Storeys	Span	$a_{DAZ,AVG}$	$a_{DAZ,SD}$	$a_{DAZ,CoV}$
[-]	[m]	[g]	[g]	[-]
4	6	1.39	0.20	0.15
	10	2.48	0.39	0.16
8	6	1.43	0.16	0.11
	10	2.54	0.34	0.13

The summarised values show that the main variable that influences  $a_{DAZ}$  is the span, since for both bare frames and frames with claddings, the average values for 4- and 8-storey frames are very similar. The effect of span is seen to be very pronounced since acceleration values for 10m span frames range between 1.98g and 3.56g, which is approximately double that of the 6m span frames, which ranges between 1.19g and 1.76g. The higher variability in CoV values is reported for long spans, which develop higher levels of catenary action and plasticity. Nonetheless, the overall low values of CoV are indicative that structural macro characteristics defined by the N and S variables can, to a reasonable extent, predict the DAZ peak acceleration.

#### 7.3.1.6 Rotational demand

The total chord rotational demand was computed as the arctangent of the ratio between the maximum dynamic vertical displacement  $u_{dyn,max,damaged}$  and the span  $L$ . For the analysed structural typologies, since span is equal in both  $x$  and  $y$  directions, the presented values correspond to the maximum demand for both MRF and gravity frame connections.

##### 7.3.1.6.1 Four storey frames

The results for 4 storey frames are presented in Figure 7.53 and Figure 7.54 for bare steel frames (CN) and for frames with façade claddings (CM or CC).



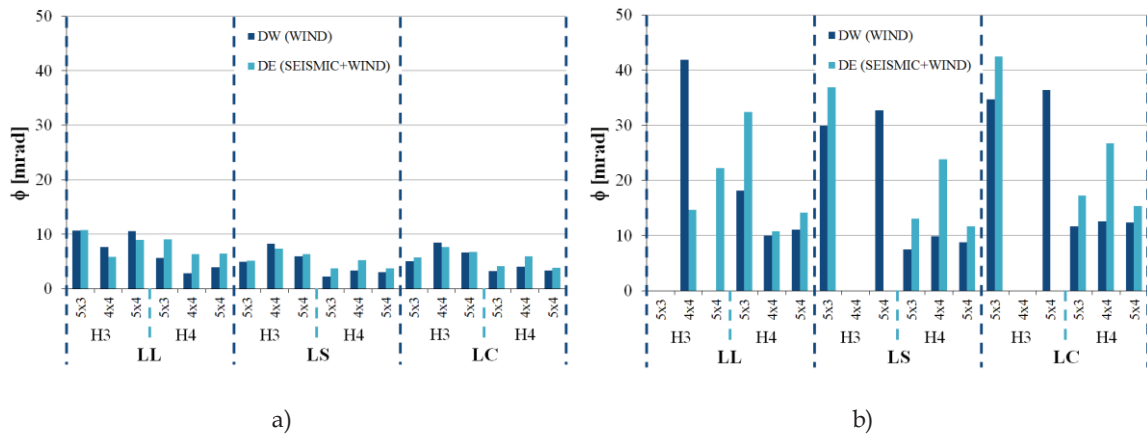


Figure 7.53: Maximum dynamic total chord rotation demand for 4 storey (N4) bare steel (CN) structures: a) 6m span frames; b) 10m span frames

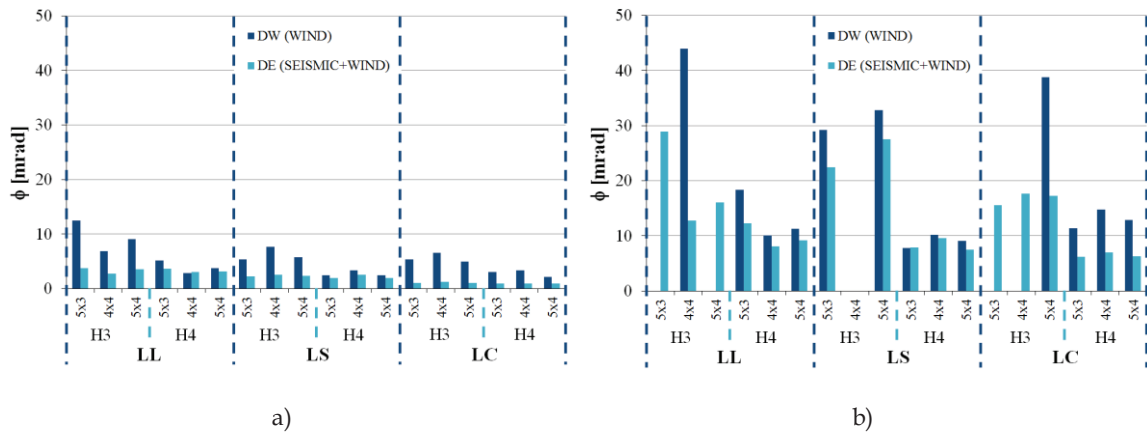


Figure 7.54: Maximum dynamic total chord rotation demand for 4 storey (N4) structures with façade claddings (CM/CC): a) 6m span frames; b) 10m span frames

The results for 4 storey bare steel frames (N4-CN) presented in Figure 7.53 show how span affects the rotational demand. Indeed, for 6 m span frames, the demand is generally below 10 mrad, whereas for structures with 10 m spans, demand can go up to around 40 mrad, although generally not being higher than 20 mrad for non collapsed cases.

The results for 6m span frames from Figure 7.53a) can be compared to those from the preliminary robustness assessment NDA (see Chapter 4), in particular to results in Figure 4.22a). This comparison shows that rotational demand results are very similar, namely for façade column loss cases (LL and LS), with average differences of 0.6 mrad and 1.0 mrad for the LL and LS cases, respectively. Instead, for the corner column loss (LC case), the refined NDA described in this Chapter, which accounts for

secondary frame connection contribution, leads to rotational demand values that are smaller by factors ranging from 0.40 to 0.60.

For the 10 m span frames, the comparison between results from Figure 7.53b) and Figure 4.22b) shows average rotation differences for non collapsed structures of 3.3 mrad and 4.1 mrad for the LL and LS removal scenarios, respectively, while for the corner removal case (LC), the refined NDA led to demands smaller than those from the preliminary robustness assessment (PRA) by factors ranging from 0.42 to 0.67, for non-collapsed cases. In terms of collapses, both NDA methodologies predicted these to occur only for N4-S10-H3 structural typologies, where the PRA methodology identified numbers of 3, 3 and 3 collapses for the LL, LS and LC cases respectively, while the refined NDA predicted 1, 3 and 4 collapses for the same cases. Indeed, for the LL case and according to the more refined NDA, two of the frames predicted to collapse by the PRA actually survived, albeit displaying large rotational demands of 30.3 and 47.7 mrad. For the LS case, the same 3 collapses predicted by the PRA methodology were verified using the refined NDA. For the LC case, the same three out of the four collapses predicted in the PRA were also reported in the refined NDA. According to the refined NDA, the fourth case predicted to fail in the PRA survived, although having required a high rotational demand of 42.5 mrad to arrest the progressive collapse. In general both methodologies are consistent with each other in predicting collapse, with differences being ascribable to plasticity modelling assumptions (lumped plasticity for the PRA and distributed plasticity for the refined NDA), to the contribution of the “gravity” frame connections and to differences in the ultimate rotation capacity of MRF beam-to-column joints (bolted for PRA – see Figure 4.6, and welded for the refined NDA).

These results for the 4-storey bare steel frames highlight that the explicit modelling of the secondary frame connection response can significantly reduce the maximum rotational demand for corner column loss scenarios. Instead, for façade column losses, the much higher stiffness of the MRF members and connections when compared to the “gravity” frame contribution yielded very similar results according to both methodologies.

The effect of claddings on the reduction of the maximum dynamic rotational demand can be evaluated by comparing results from Figure 7.53 and Figure 7.54. For what concerns 6m span frames, claddings are shown to reduce rotation demand in

nearly all cases, although being largely more effective for the case of wind+seismically designed structures (DE), since these structures have MRF beams with smaller depth when compared to the wind designed frames (DW), owing to capacity design principles and resistance hierarchy. Indeed, for DW frames, the effect of claddings on façade column removals (cases LL and LS) is small, with rotation reductions lower than 19%, whereas for corner removals (LC) reductions go up to 38%. For DE frames, the efficacy of claddings is significantly higher, with average rotation reductions of 56% for façade removals cases and of 82% for corner removals. For the 10m span frames, the comparison between results from Figure 7.53b) and Figure 7.54b) shows that for non collapsed cases, the effect on seismically designed frames is more effective as well, with average rotation demand reductions of 38% and 65% for façade and corner column losses, respectively. For DW designed frames, numerical results did not show significant improvement regarding demand.

#### 7.3.1.6.2 *Eight storey frames*

The results for 8 storey frames are presented in Figure 7.55 and Figure 7.56 for bare steel frames (CN) and for frames with façade claddings (CM or CC), respectively.

For bare steel frames, results show that 6m span frames can effectively arrest progressive collapse for all removal scenarios while displaying rotation demands below 4 mrad, whereas 10m frames display larger rotations which go up to 18mrad.

The results from 6m span bare frames in Figure 7.55a) can be compared to previous results from the preliminary robustness assessment shown in Figure 4.23a), showing that rotational demand is similar for most cases, albeit smaller for the refined NDA, in particular for corner column loss cases, in which the “gravity” frame connections contribution is effective at reducing maximum rotation.

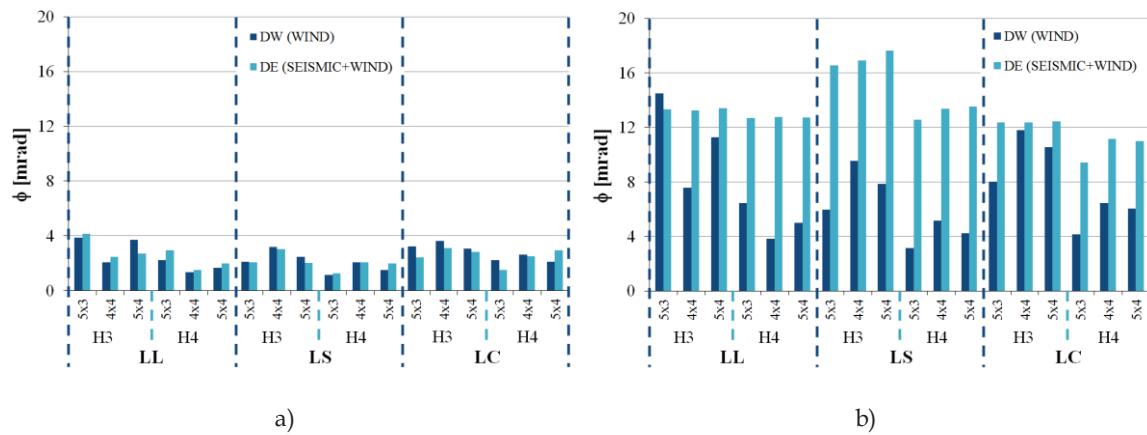


Figure 7.55: Maximum dynamic total chord rotation demand for 8 storey (N4) bare steel (CN) structures: a) 6m span frames; b) 10m span frames

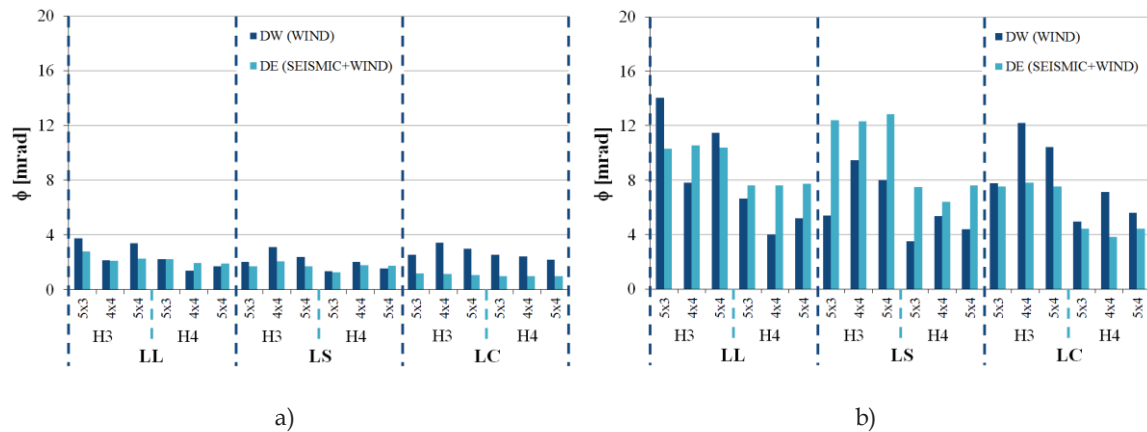


Figure 7.56: Maximum dynamic total chord rotation demand for 8 storey (N8) structures with façade claddings (CM/CC): a) 6m span frames; b) 10m span frames

Indeed, for façade removals (LL and LS cases) rotation reductions range between 4% and 37% with an average value of 20%, whereas for corner removals, reductions range between 40% and 63%, with an average value of 48%.

Regarding the 10m span frames, a comparison between results in Figure 7.55b) and Figure 4.23a) shows that the refined NDA led to slightly smaller rotations for the façade removals, with average differences in the order of 1.1 mrad. For corner removals, the maximum rotation difference is equal to 5.8 mrad, to which corresponds a reduction of 32% in comparison to PRA results.

For the bare steel 8-storey structures, the reported differences in maximum rotation demand between the PRA and the refined NDA indicate that for façade removals, the “gravity” frame contribution is small, since high load redistribution capacity is available to other the MRF members of the DAZ, which are responsible for

the larger part of the collapse resistance. Instead for corner removals, the contribution of the secondary frame can provide for significant reductions of the rotational demand, for which reason it should be explicitly considered when assessing robustness. Indeed, disregarding it would lead to unrealistic and severely unfavourable rotational demand verifications for connections.

The effect of claddings on 6m span frames can be perceived by comparing results from Figure 7.55a) to Figure 7.56a), where as seen for the 4-storey case, claddings are shown to be more effective for the wind+seismically designed (DE) frames, reducing demand on average by 13% for façade loss cases and by 57% for corner removals, while generally leading to negligible improvements for the case of wind designed frames (DW). For 10m span structures, the comparison between Figure 7.55b) to Figure 7.56b) indicates that claddings are not effective in reducing rotational demand for wind designed (DW) frames, since reductions are lower than 7% in all cases, whereas for wind+seismically designed frames the claddings consisting in cold formed steel “X” bracings were found to reduce rotational demand by 33% on average for façade column loss cases and by 49% for the corner column losses.

#### 7.3.1.7 Reserve displacement ductility ( $RDD_{equil}$ )

This indicator quantifies the robustness reserve, measured as the ratio between the ultimate displacement capacity of the directly affected zone  $u_{u,damaged}$  and the displacement in equilibrium of the damaged structures  $u_{dyn,equl,damaged}$  (see Eq.(7.2)). This measure of robustness is similar to the Degree of Plasticity  $DOP_{DAZ}$  (see Eq.(7.1)), in the sense that it measures the reserve displacement capacity further to the  $u_{dyn,equl,damaged}$  position. However, while the  $DOP_{DAZ}$  measures the reserve with regard to the maximum dynamic displacement at the zero kinetic energy condition, the  $RDD_{equil}$  measures the reserve robustness up to the first member/connection failure, which is deemed the limit state after which the structure collapses.

The  $RDD_{equil}$  presents the advantage that it provides a realistic measure of the reserve robustness. Its computation however requires precise data regarding the ultimate capacity of all members/connections of the DAZ, which is also dependent on the location of the removed column (see Figure 7.46).

7.3.1.7.1 Four storey frames

The results for the 4-storey frames are presented in Figure 7.57 and Figure 7.58 for bare steel frames (CN) and for frames with façade claddings (CM or CC), where zero values of  $RDD_{equil}$  are indicative of collapsed frames.

The results for the medium span (S6) bare steel (CN) frames in Figure 7.57a) show that these structural systems are characterised by a high displacement reserve up to failure, with a minimum  $RDD_{equil}$  value of 6.3 and average values of 10.7, 12.6 and 9.8 for the LL, LS and LC column removal scenarios, respectively. These values point to the fact that these structural systems are adequately detailed to sustain façade and corner column losses (interior column loss is not discussed in this study), since they display a large displacement reserve up to failure.

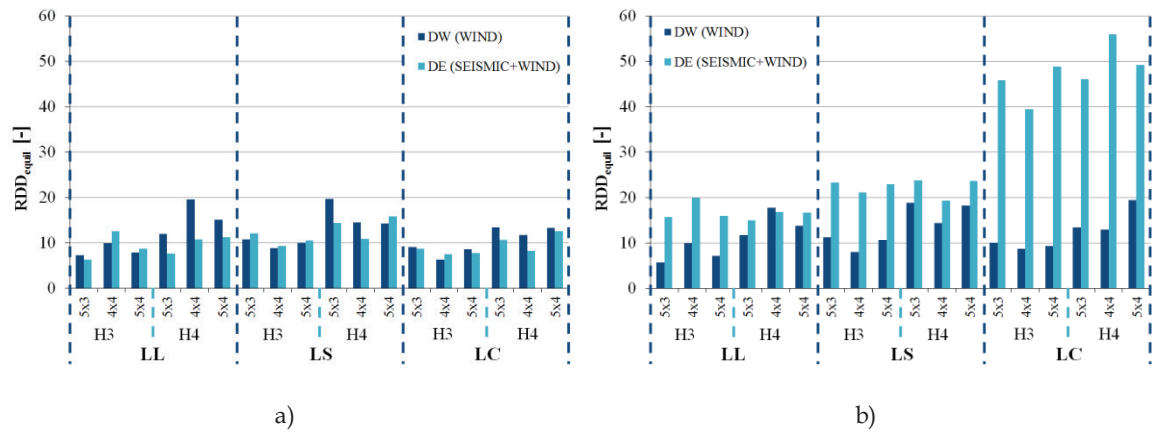


Figure 7.57: Reserve displacement ductility for 4 storey (N4) medium span (S6) structures: a) bare steel frames (CN); b) frames with façade claddings (CM/CC)

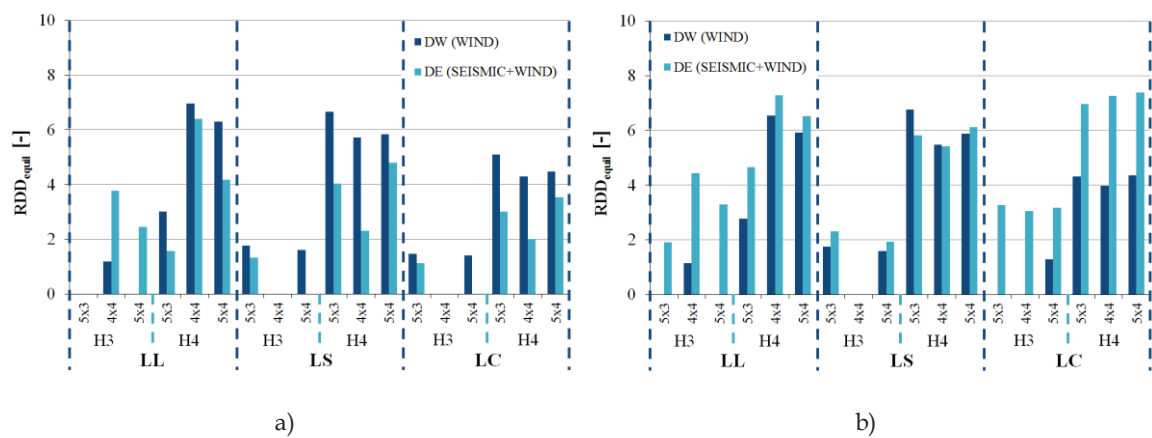


Figure 7.58: Reserve displacement ductility for 4 storey (N4) long span (S10) structures: a) bare steel frames (CN); b) frames with façade claddings (CM/CC)

By comparing Figure 7.57a) to Figure 7.57b), the effect of façade claddings in relation to bare frames can be observed. In this case, for wind+seismically designed (DE) frames, the  $RDD_{equil}$  which measures how close the damaged structure is to collapse in terms of displacements, is increased by 85% on average for façade removals and by 432% on average for corner column losses. For wind designed (DW) frames, no improvement is reported for façade removals, while for corner removals, the  $RDD_{equil}$  is increased on average by 19%. These results highlight the importance of façade claddings in increasing structural robustness for medium span frames, namely for cases of seismically designed frames under corner column loss.

For the long span (S10) bare steel (CN) frames, results in Figure 7.58a) highlight not only that this typology is prone to progressive collapse, but also that structures that do not collapse tend to display a lower displacement reserve when compared to corresponding 6m span structures. Indeed, for non collapsed cases,  $RDD_{equil}$  average values of 3.98, 3.78 and 2.93 and minimum values of 1.18, 1.32 and 1.12 are reported for the LL, LS and LC column removal scenarios, respectively. The effect of claddings is shown by comparing Figure 7.58a) to Figure 7.58b), where, as seen previously for the 6m span frames, the beneficial effect of claddings is higher for seismically designed (DE) frames, with  $RDD_{equil}$  average increases of 67% and 173% for façade and corner column losses, respectively, which compare to wind designed (DW) frames, which do not display reserve ductility improvements with the addition of claddings.

#### 7.3.1.7.2 Eight storey frames

The reserve displacement ductility values for 8 storey frames are shown in Figure 7.59 and Figure 7.60 for bare steel frames (CN) and for frames with façade claddings (CM or CC).

As seen in Figure 7.59a), bare steel frames display high reserve ductility values, which are indicative of high robustness and internal redistribution capacity, with corner removal (LC) cases showing smaller reserve when compared to façade removals (LL and LS). In terms of  $RDD_{equil}$  values, minimum values of 13.8, 14.6 and 11.2 and average values of 19.7, 21.5 and 15.0 are reported for the LL, LS and LC column removal scenarios, respectively. These values are indicative that this structural typology (i.e. N8-S6 frames) displays high structural robustness and is capable of arresting progressive collapse, if designed according to the Eurocodes and to actions

and methodologies defined in Chapter 3. For what concerns the effect of claddings, the comparison between Figure 7.59a) and Figure 7.59b) shows (as seen previously for the case of the 4-storey frames) that reserve ductility is augmented for wind+seismically designed (DE) frames, with average increases of 4% and 129% for façade and corner losses. Instead for wind designed (DW) frames, average increases in  $RDD_{equil}$  of 2% and 5% are reported for façade and corner removals, respectively.

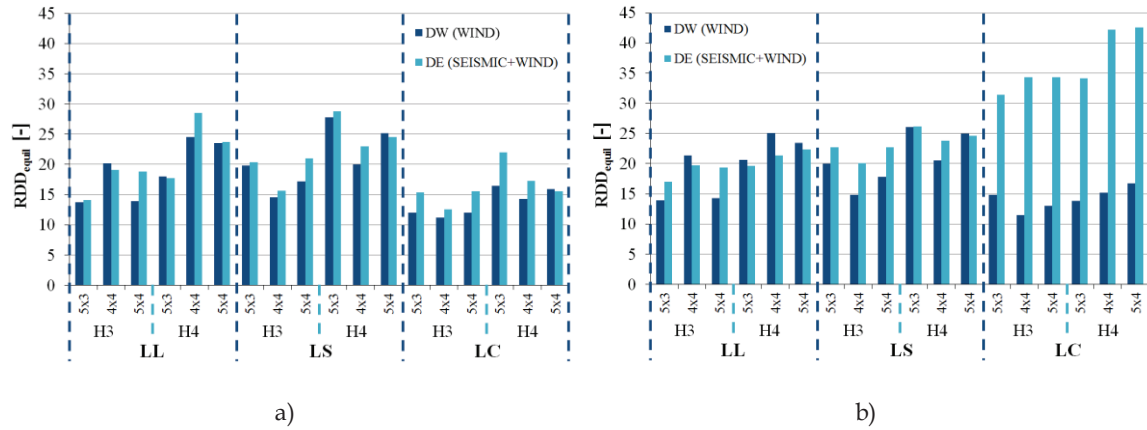


Figure 7.59: Reserve displacement ductility for 8 storey (N8) medium span (S6) structures: a) bare steel frames (CN); b) frames with façade claddings (CM/CC)

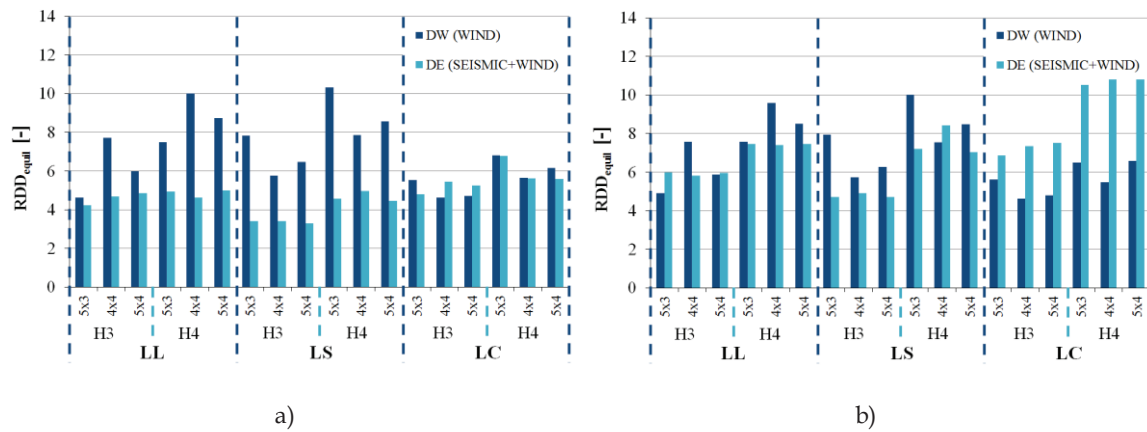


Figure 7.60: Reserve displacement ductility for 8 storey (N8) long span (S10) structures: a) bare steel frames (CN); b) frames with façade claddings (CM/CC)

For long span systems, results in Figure 7.60 show that  $RDD_{equil}$  values are smaller than those obtained for the medium span frames. Nevertheless, for bare frames (see Figure 7.60a)) the ratio values between the ultimate and the equilibrium displacements are higher than 4.2, 3.3 and 4.6 for the LL, LS and LC scenarios, respectively. This shows that despite the large span, medium rise structures display high redistribution capacity throughout the DAZ members and connections. Also in



this case, the effect of claddings on DW designed frames is negligible, whereas for DE frames, average increases of  $RDD_{equil}$  of 47% and 64% are reported for façade and corner losses.

#### 7.3.1.8 Demand to Capacity Ratios ( $DCR_{ductility,ij}$ )

The evaluation of the reserve displacement of different members/connections presented in this section was performed for the maximum dynamic displacement ( $u=u_{dyn,max,damaged}$ ). The chord rotations corresponding to  $u_{dyn,max,damaged}$  were computed for the different members/connections and compared to their predicted ultimate rotation capacities.

For the moment resisting frame welded beams-to-column joints, which are full strength rigid connections, the ultimate rotation capacity was evaluated according to the nonlinear modelling criteria for fully restrained moment connections provided in the UFC 2013 (United States of America Department of Defense, 2013). These modelling parameters were adopted in the present study, since they were derived from an extensive experimental programme and are deemed suitable for progressive collapse analysis according to the UFC 2013 (United States of America Department of Defense, 2013). The considered connection typology was the Welded Unreinforced Flange (WUF), which constitutes a rotation capacity lower bound for typical European welded beam-to-column joint detailing.

The ultimate rotation capacity, according to the UFC 2013 (United States of America Department of Defense, 2013) methodology, is computed as the sum of the yield rotation  $\theta_y$  and the plastic rotation  $\theta_p$  (see Figure 7.61a)), where  $\theta_y$  is computed according to Eq.(7.34) and the values for the plastic rotation parameters  $a$  and  $b$  defined in Figure 7.61b) can be determined according to the rules in Figure 7.62. The residual strength was disregarded and therefore  $c = 0$  was assumed (see Figure 7.62).

$$\theta_y = \frac{ZF_y e l_b}{6EI_b} \quad (7.34)$$

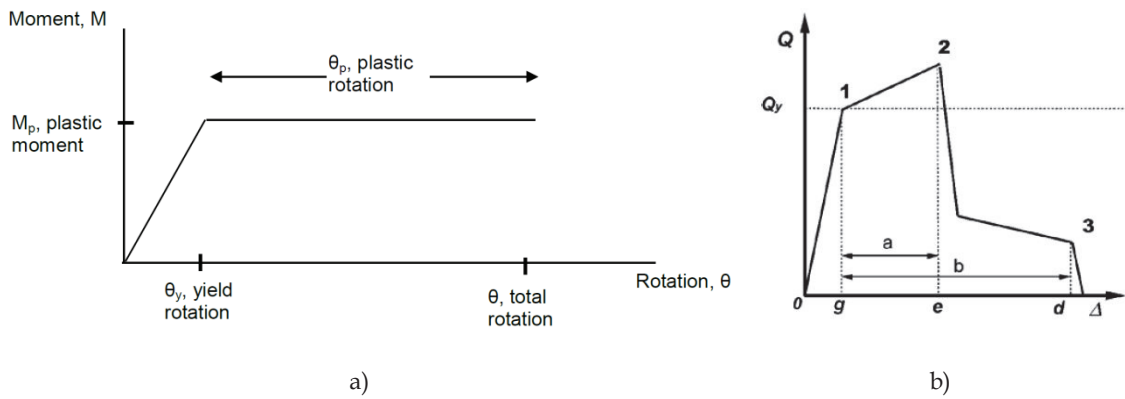


Figure 7.61: Rotation capacity of MRF beam-to-column joints: a) definition of yield, plastic and total rotation; b) deformation controlled response curve and modelling parameter definition (United States of America Department of Defense, 2013)

Connection Type	Nonlinear Modeling Parameters <sup>(1)</sup>			Nonlinear Acceptance Criteria	
	Plastic Rotation Angle, radians		Residual Strength Ratio	Plastic Rotation Angle, radians	
	a	b		Primary <sup>(2)</sup>	Secondary <sup>(2)</sup>
<b>Fully Restrained Moment Connections</b>					
Improved WUF with Bolted Web	0.021 - 0.0003d	0.050 - 0.0006d	0.2	0.021 - 0.0003d	0.050 - 0.0006d
Reduced Beam Section (RBS)	0.050 - 0.0003d	0.070 - 0.0003d	0.2	0.050 - 0.0003d	0.070 - 0.0003d
WUF	0.0284 - 0.0004d	0.043 - 0.0006d	0.2	0.0284 - 0.0004d	0.043 - 0.0006d
SidePlate <sup>®</sup>	0.089 - 0.0005d <sup>(3)</sup>	0.169 - 0.0001d	0.6	0.089 - 0.0005d	0.169 - 0.0001d

Figure 7.62: Nonlinear modelling parameters for steel frame beam-to-column joints (United States of America Department of Defense, 2013)

The ultimate displacement capacity of the web cleat beam-to-beam joints (see Section 7.2.6.4) was computed directly from the moment - chord rotation experimental response curve in Figure 7.19b) and the ultimate displacement of the secondary frame beam-to-column joints was computed from the FEP joint chord rotation capacities which were determined according to the methodology described in Section 7.2.6.5.

Considering that the different column loss scenarios (LL, LS and LC) mobilise different members of the DAZ (see Figure 7.46), the Demand-to-Capacity ratios  $DCR_{ductility,ij}$  defined in Eq.(7.3) were computed for each removal scenario.

For the XZ façade removal (LL case), MRF beams and Internal Secondary Beam (ISB) web cleat connections are activated (the ISB member itself remains elastic),

whereas for the YZ façade removal (LS case), MRF beams, Internal Secondary Beams (beam-to-beam web cleat joints) and Internal Primary Beams (beam-to-column flush end-plate joints) are mobilised. For the corner column loss (LC case), MRF beams, Internal Secondary Beams (beam-to-beam web cleat joints) and Perimeter Primary Beams (beam-to-column flush end-plate joints) are activated.

The results for the LL, LS and LC cases for 4-storey and 8-storey frames are presented in Figure 7.63, Figure 7.64 and Figure 7.65, where *DCR* ratios of 1.0 are indicative of member/connection failure and where MRF, ISB, IPB and PPB stand for Moment Resisting Frame, Internal Secondary Beam, Internal Primary Beam and Peripheral Primary Beam, respectively.

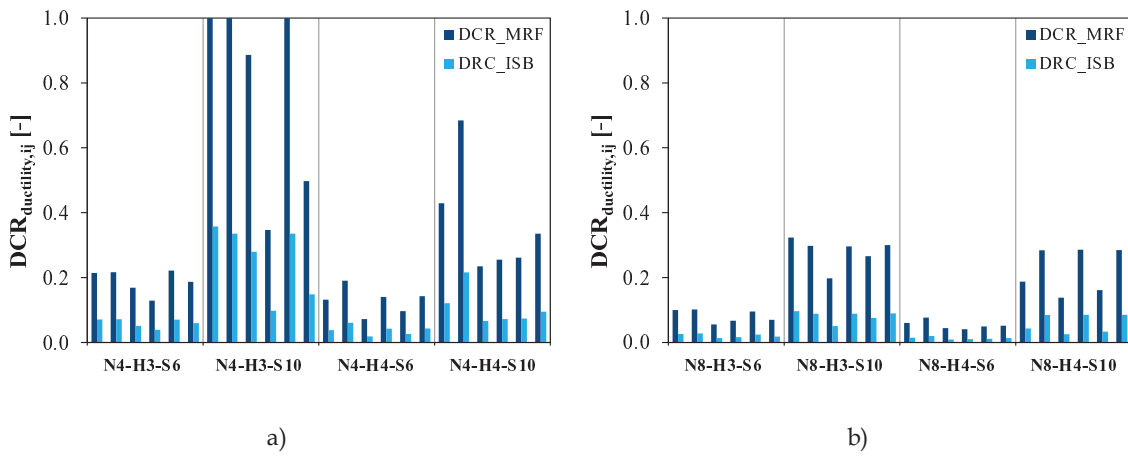


Figure 7.63: Ductility Demand-to-Capacity ratios for the XZ façade column removal (LL): a) 4-storey frames; b) 8-storey frames

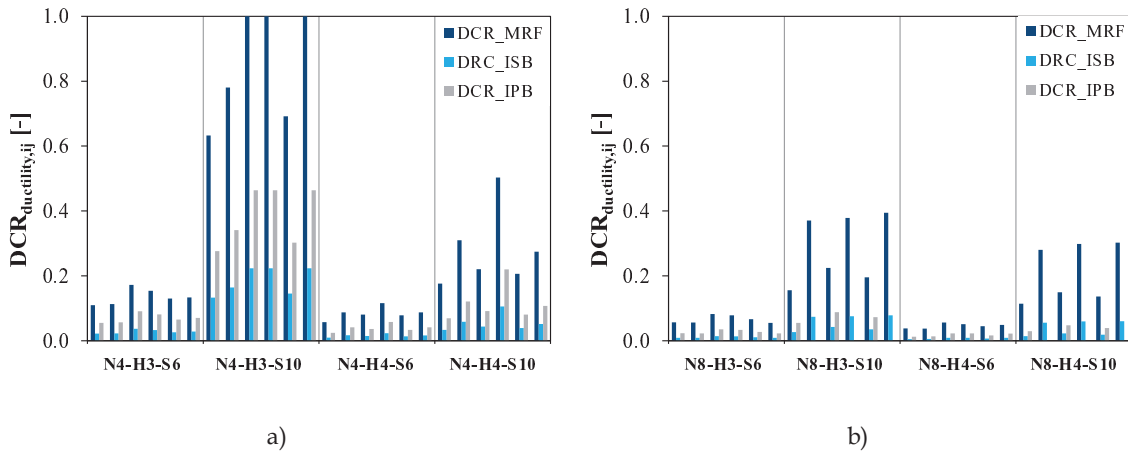


Figure 7.64: Ductility Demand-to-Capacity ratios for the YZ façade column removal (LS): a) 4-storey frames; b) 8-storey frames

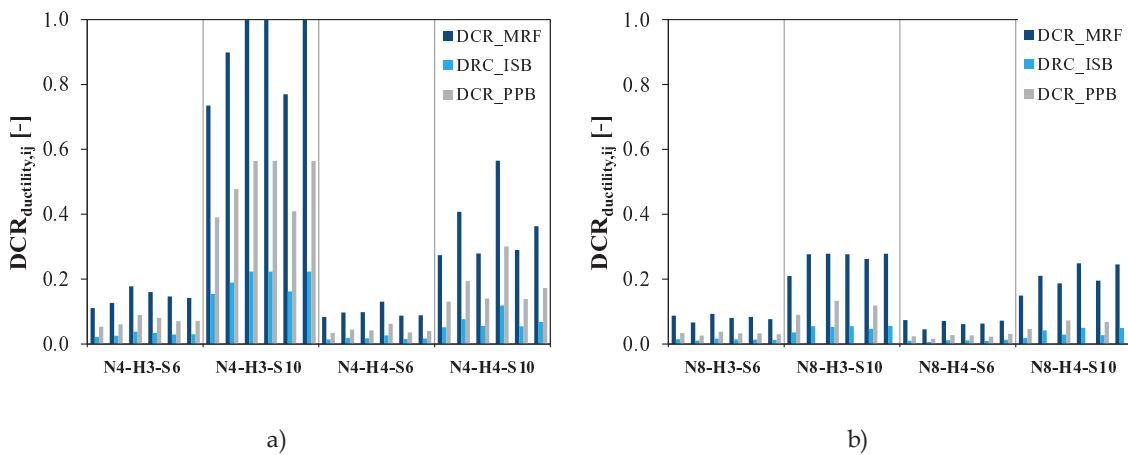


Figure 7.65: Ductility Demand-to-Capacity ratios for the corner column removal (LC): a) 4-storey frames; b) 8-storey frames

These results are summarised in Table 7.19 in terms of maximum  $DCR_{ductility,ij}$  values and broken down by joint type, in order to determine which joint types and structural typologies require improved detailing.

The summarised results show that for all analysed structural typologies, the MRF beam joints display the highest  $DCR$  values, while gravity frame joints tend to present very low values, owing to their high flexibility which can accommodate very large rotations without failure. Indeed, for N4-S6 frames, MRF beams display a maximum  $DCR_{ductility}$  of 0.22 while “gravity” frame joints display ratio values smaller than 0.09, i.e. approximately half. This is also seen for the cases of N8-S6 and N8-S10 typologies, with displayed maximum MRF ratio values of 0.10 and 0.39, which compare to maximum ratio values of the secondary frame joints of 0.04 and 0.13. It should be noted that it is for the LC removal scenario that secondary joints display the highest  $DCR_{ductility}$  values.

Table 7.19: Maximum ductility Demand-to-Capacity ratios by member/connection type and column loss scenario

N	S	H	MRF beams (welded joints)			ISB (web cleat joints)			IPB	PPB
			LL	LS	LC	LL	LS	LC	(FEP joints) LS	LC
[-]	[m]	[m]								
4	6	3	0.22	0.17	0.18	0.07	0.04	0.04	0.09	0.09
		4	0.19	0.12	0.13	0.06	0.02	0.03	0.06	0.06
	10	3	1.00	1.00	1.00	0.36	0.22	0.22	0.46	0.56
		4	0.68	0.50	0.57	0.22	0.11	0.12	0.22	0.30
8	6	3	0.10	0.08	0.09	0.03	0.01	0.02	0.04	0.04
		4	0.08	0.06	0.07	0.02	0.01	0.01	0.02	0.03
	10	3	0.32	0.39	0.28	0.10	0.08	0.06	0.09	0.13
		4	0.29	0.30	0.25	0.09	0.06	0.05	0.05	0.07

For these structural typologies that did not collapse under column loss, the reduced ratio values indicate that further reinforcement is not required since there is a large margin of safety between the maximum dynamic displacement and the ultimate displacement causing structural collapse, even if a safety factor was to be adopted.

This is not however the case for the N4-S10 frames, which displayed several cases of collapse, as highlighted in Table 7.19. At collapse situation ( $u=u_{u,damaged}$ ), the MRF beams’  $DCR_{ductility}$  ratios are equal to 1, indicating these to be the first members to

fail, whereas maximum ratio values of 0.36 for the ISB's beam-to-beam web cleat joints, 0.46 for the IPB's beam-to-column FEP joints and 0.56 for the PPB's beam-to-column FEP joints are reported. This points to the fact that at  $u=u_{u,damaged}$  these gravity frame elements still present a large displacement reserve before failing, suggesting that improving the detailing in these joints should not lead to significant gains in terms of robustness up to the first component failure. It is worth noting that  $DCR_{ductility}$  values for N4-S10 frames are lower for H4 cases in comparison to H3 cases, implying that for H4, gravity joint detailing improvements are also not likely to affect robustness.

#### 7.3.1.9 Effect of claddings

The favourable effect of claddings on robustness can be measured by the reduction of rotational demand, which can be computed as the ratio between the maximum rotational demand of frames with façade claddings  $\phi_{CM/C}$  and the maximum rotational demand for the corresponding bare steel frame  $\phi_{CN}$ . The ratio  $\phi_{CM/C}/\phi_{CN}$  is equal to 1 in cases in which claddings do not reduce the rotational demand and is taken as 0 to represent cases of failure of bare frames (CN), for which the ratio cannot be computed. It should be noted that in cases of low rotational demand values, as is typically the case for medium span frames (S6), small variations in absolute demand values can lead to large variations in  $\phi_{CM/C}/\phi_{CN}$  ratios.

The results for 4 storey frames are presented in Figure 7.66 and show that for 6m span frames (see Figure 7.66a), the masonry claddings adopted for the wind designed frames (DW) do not significantly reduce maximum rotational for the façade column loss cases (LL and LS), while for corner loss (LC) average reductions of 18% are reported. Instead, for wind+seismically designed frames (DE) the cold formed steel "X" bracing claddings are shown to lead to large rotational demand reductions, with average  $\phi_{CM/C}/\phi_{CN}$  ratio values of 0.43, 0.45 and 0.18 for the LL, LS and LC scenarios, respectively.

These differences in the effectiveness of claddings to reduce demand are ascribable to the relative differences in terms of the MRF beam stiffness and strength. Indeed, DW frames have deeper and therefore stiffer beams, which are subjected to smaller rotational demand and therefore do not mobilise the resistance of the masonry panel. Concurrently, according to the adopted masonry material properties (see Table 7.7), the fact that the masonry claddings display a much lower initial Young's modulus

in comparison to steel ( $E_{i,masonry} \approx 0.01 E_{steel}$ ) lead these elements to lose efficacy in façade column loss scenarios, while having a more preponderant role in corner removal scenarios, where the stiffness of the damaged bare steel frame (CN) is smaller. For the DE designed frames, the reduced bare frame stiffness, coupled with the cladding being composed of resisting elements with equal Young's modulus (cold formed steel) implies that these elements are more efficiently mobilised to arrest collapse, resulting in a higher rotational demand reduction.

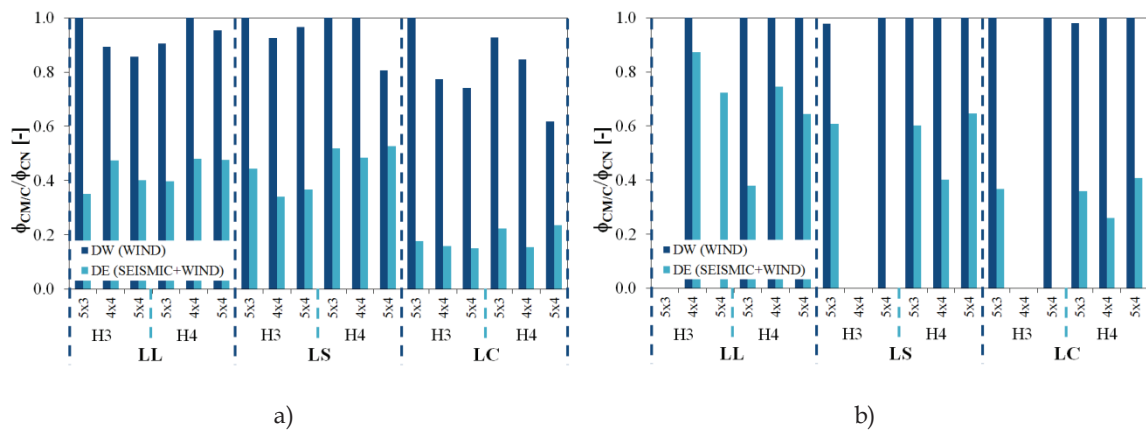


Figure 7.66: Effect of claddings on rotational demand for 4 storey (N4) frames with: a) 6m span; b) 10m span

The results for the 10m span frames presented in Figure 7.66b) show that, as for the 6m span frames, no reductions in rotational demand are reported for the DW frames with masonry claddings, whereas for the DE case, average  $\phi_{CM/C}/\phi_{CN}$  ratio values of 0.67, 0.56 and 0.35 for the LL, LS and LC scenarios are reported, respectively. The  $\phi_{CM/C}/\phi_{CN} = 1$  values obtained for DW frames point to the fact that masonry panels may be somewhat ineffective when the cladding's  $b/h$  aspect ratio increases, since the compressive strut angle is reduced. As seen for the N4-S6 frames, the stiffness of the DAZ members appears to influence the efficacy of the façade claddings, since higher reductions in rotational demand were obtained for the corner column loss case, in which the damaged structure is more flexible.

The results in Figure 7.66b) highlight the potential importance of non structural elements, namely façade panels, to reduce the maximum demand on structures that are prone to progressive collapse, such as low-rise long-span frames (N4-S10).

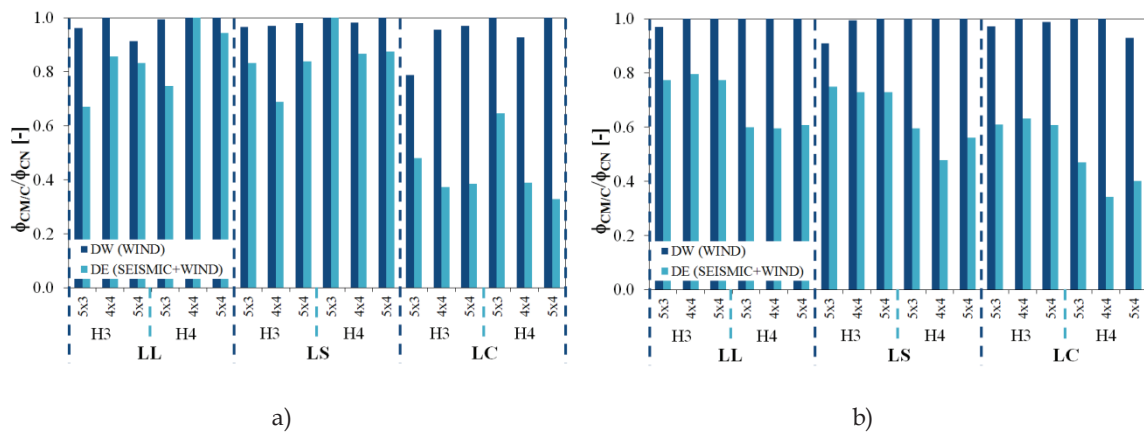


Figure 7.67: Effect of claddings on rotational demand for 8 storey (N8) frames with: a) 6m span; b) 10m span

The results for the 8-storey frames are presented in Figure 7.67a) and Figure 7.67b) for the 6m and 10m span cases respectively, where the wind designed frames with masonry claddings (CM-DW) are shown to not be able to significantly reduce the rotational demand in comparison to bare steel frames. Instead, for the DE designed frames, results show claddings to reduce the average rotational demand by 16%, 15% and 57% for 6m span frames and by 31%, 36% and 49% for 10m span frames, for the LL, LS and LC scenarios, respectively.

As seen for the 4-storey frames, the lower the span  $S$ , the lower the claddings'  $b/h$  aspect ratio and consequently the lower the  $\phi_{CM/C}/\phi_{CN}$  ratio value. The fact that the interstorey height variable  $H$  changes the panel's aspect ratio should, *ceteris paribus*, lead to lower  $\phi_{CM/C}/\phi_{CN}$  ratios for  $H=4\text{m}$  frames. However, the fact that  $H4$  structures are taller also requires stiffer structures to comply with the lateral sway verifications, which compensates the higher inclination of the compressive struts of the claddings.

The obtained results are summarised in Table 7.20, where lower  $\phi_{CM/C}/\phi_{CN}$  ratio values are seen for the wind+seismically designed (DE) frames, indicating that this cladding typology may be suitable to reduce rotational demand, especially for corner loss scenarios (LC) for which lower ratio values are consistently reported.



Table 7.20: Effect of claddings on the maximum rotational demand by number of storeys, span, lateral load design scenario and column loss scenario – average, standard deviation and coefficient of variation

N	S	D	L	$\phi_{CM/C}/\phi_{CN}$			
				AVG	SD	CoV	
[-]	[m]	[-]	[-]	[-]	[-]	[-]	
4	6	W	L/S	0.94	0.06	0.06	
			C	0.82	0.12	0.15	
		E	L/S	0.44	0.04	0.09	
			C	0.18	0.02	0.12	
		10	W	L/S	1.00	0.00	0.00
				C	1.00	0.00	0.00
	E	L/S	0.64	0.08	0.14		
		C	0.35	0.03	0.09		
	8	6	W	L/S	0.98	0.01	0.01
				C	0.94	0.06	0.06
			E	L/S	0.85	0.08	0.09
				C	0.43	0.09	0.21
10			W	L/S	0.99	0.01	0.01
				C	0.98	0.02	0.02
E		L/S	0.67	0.02	0.03		
		C	0.51	0.03	0.07		

The fact that the presence of façade claddings contributes to reduce rotational demand and consequently the expected damage on members in some cases constitutes a relevant finding. However, under column loss, some level of damage is expected and acceptable, for which reason the question becomes whether progressive collapse can be averted by considering the contribution of claddings. Since  $\phi_{CM/C}/\phi_{CN}$  ratios can only be computed for cases in which the bare steel frame did not collapse, the results in Table 7.20 alone do not allow to evaluate whether the inclusion of claddings as resisting elements is sufficient to avert progressive collapse.

For this reason, the number of collapse occurrences for bare steel frames and for the corresponding frames with façade claddings was compared, in order to determine for which cases was the adoption of claddings effective in averting collapse. It should be noted that for the analysed frames, collapses were verified only for the N4-S10 configuration. The comparison is presented in Table 7.21, showing that collapses were effectively averted due to the presence of claddings for H3-DE configurations in all column loss scenarios.

Table 7.21: Effectiveness of claddings for averting progressive collapse

N	S	L	H	D	CN collapses	CM/C collapses	Collapses averted	Claddings effective?	
[-]	[m]	[-]	[m]	[-]	[-]	[-]	[-]		
4	10	L	3	W	2	2	0	N	
				E	1	0	1	Y	
			4	W	0	0	0	-	
				E	0	0	0	-	
			S	3	W	1	1	0	N
					E	2	1	1	Y
		4		W	0	0	0	-	
				E	0	0	0	-	
		C		3	W	1	1	0	N
					E	2	0	2	Y
		4	W	0	0	0	-		
			E	0	0	0	-		

The fact that for wind designed frames with masonry claddings (CM-DW) no collapses were reported points to the importance of the stiffness of the steel frames surrounding the claddings panels. This factor was investigated by Farazman *et al.* (2012) which assessed the net contribution of masonry panels considering two steel frames with different stiffnesses, where the first is described in Vlassis *et al.* (2008) and the second frame displays double the stiffness of the first. It was shown by Farazman *et al.* (2012) that the overall response was clearly different for the two infilled frames, while the panel net contribution was found to be unaffected. The fact that the original structure in Vlassis *et al.* (2008) is characterised by a bracing system consisting of two braced cores and by façade beams with flexible partial depth end-plate beam-to-column joints is indicative that the stiffness of the frames surrounding the masonry panel is low. Instead, for the present study, lateral resistance is provided by the MRF members with full-strength rigid beam-to-column joints, resulting in deeper beams and much stiffer frames in comparison to the ones used in Farazman *et al.* (2012).

In this sense, the surrounding frame stiffnesses of the present study and that of the Farazman *et al.* (2012) study are not directly comparable. However, the fact that the obtained numerical results indicate that claddings add negligible improvements for DW frames suggests that if the frame stiffness is sufficiently high, the differences in the displacement levels required to mobilise steel and masonry resistance render the cladding element ineffective.

The influence of steel frame stiffness on the capacity of claddings to reduce maximum rotational demand is shown in Figure 7.68 and Figure 7.69 for the 4- and 8-storey frames, respectively.

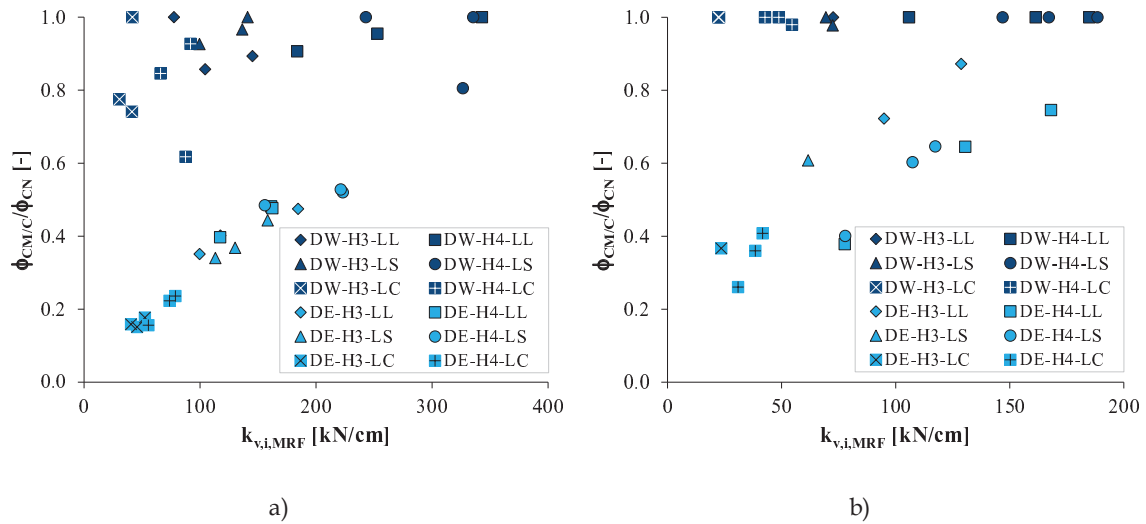


Figure 7.68: Effect of claddings in the reduction of the maximum rotational demand of 4 storey frames as a function of the initial vertical stiffness: a) 6m span frames; b) 10m span frames

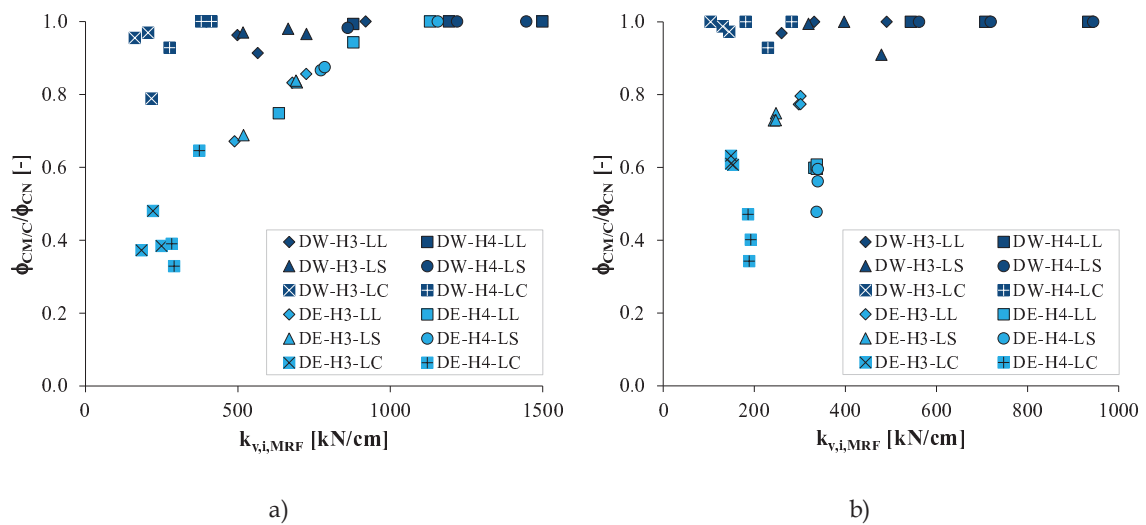


Figure 7.69: Effect of claddings in the reduction of the maximum rotational demand of 8 storey frames as a function of the initial vertical stiffness: a) 6m span frames; b) 10m span frames

The results show the difference in the efficacy of claddings between DW frames (with masonry claddings) and DE frames (with CFS claddings). Generally it can be recognised that the demand reduction in DW frames is typically below 20% (i.e.  $\phi_{CM/C}/\phi_{CN} > 0.8$ ), independently of the frame initial vertical stiffness  $k_{v,i,MRF}$ . Instead, for

DE frames, which are characterised by lower stiffness,  $\phi_{CM/C}/\phi_{CN}$  ratios tend to increase for increasing  $k_{v,i,MRF}$  stiffness.

The behaviour of the DW frames can be explained by the response of masonry infilled frames seen in Markulak *et al.* (2008) and presented in Figure 7.29a), which shows that the resistance of the “masonry+frame” system tends towards that of the bare steel frame, as displacement increases. In this sense, the masonry can absorb part of the kinetic energy during the initial stages of the progressive collapse, after which its resistance tends to zero for increasing displacements. By comparing  $\phi_{CM/C}/\phi_{CN}$  ratios for DW frames for 6m and 10m span frame, it is possible to verify that ratio values are lower for the 6m span frames, since the vertical displacement of the DAZ is smaller, rendering the masonry element more efficient. In addition, the masonry panel’s aspect ratio for 6m span frames is characterised by a compressive strut inclination angle which renders energy absorption more efficient. For 10m span frames, which require higher vertical displacements to arrest the collapse and for which the inclination of the compressive strut is small,  $\phi_{CM/C}/\phi_{CN}$  ratio values are close to 1.

The effect of CFS claddings on DE frames is seen in Figure 7.68 and Figure 7.69 to vary with the frame initial vertical stiffness  $k_{v,i,MRF}$ , although this is more noticeable for 4-storey frames. Indeed, results show that lower  $\phi_{CM/C}/\phi_{CN}$  ratio values are obtained for frames with lower stiffness  $k_{v,i,MRF}$ , indicating that rotational demand reduction is higher in more flexible frames. This trend, which can also be perceived to a smaller degree for the DW frames in Figure 7.68a) and Figure 7.69a), is in agreement with results by Farazman *et al.* (2012), which concluded that for the studied flexible steel frame, the claddings could play a major role in arresting collapse. The fact that the resistance of the cladding is provided by a steel “X” bracing with ductile behaviour (see Figure 7.36b)), enables these elements to absorb kinetic energy throughout the full duration of the collapse arrest, since MRF and cladding materials are characterised by equal Young’s moduli. The fact that  $\phi_{CM/C}/\phi_{CN}$  ratio values between 0.2 and 0.8 were obtained even for 10m span frames indicates that the introduction of CFS “X” bracing claddings may constitute an effective collapse prevention measure, even for long span systems. Furthermore, considering that current design trends favour the use of dry assembled systems for façade walls in order to minimise life cycle and construction costs, the use of CFS steel elements appears to be a more suitable solution for achieving robust steel structures, in comparison to the masonry cladding solution.

The numerical data presented in this section therefore points to the conclusion that the contribution of these non-structural elements is not negligible and may in fact be decisive in averting collapse. This is the case for structures with lower MRF beam capacity, namely seismically designed frames with reduced interstorey height (H3-DE). Further research is however necessary to better determine how variables such as span, cladding aspect ratio, frame stiffness, CFS bracing strength and CFS bracing stiffness influence robustness, so as to determine the most efficient cladding typologies for arresting progressive collapse.

#### 7.3.1.10 Comparison to EN 1991-1-7 tying requirements

In this section the EN 1991-1-7 (CEN, 2006) design tying requirements are compared to the maximum catenary forces in joints from the numerical simulations.

A discussion regarding the advantages and disadvantages of the tie force method is presented in Section 2.3.2 of this thesis, along with the expressions for computing the design tie forces according to recent design codes (see Table 2.4).

The EN 1991-1-7 (CEN, 2006) states that horizontal ties may consist of a combination of rolled steel sections, steel mesh reinforcements or profiled steel sheeting (if directly connected to the steel beams with shear connectors). The following expressions are used for the computation of the horizontal design tensile loads for internal ties ( $T_i$ ) and for perimeter ties ( $T_p$ ).

#### EN 1991-1-7 tying requirements:

$$\text{for internal ties: } T_i = \max \{ 0.8(g_k + \psi q_k)sL ; 75kN \} \quad (7.35)$$

$$\text{for perimeter ties: } T_p = \max \{ 0.4(g_k + \psi q_k)sL ; 75kN \} \quad (7.36)$$

where  $g_k$  is the characteristic permanent load,  $q_k$  is the characteristic variable load,  $\psi$  is the relevant combination factor for the accidental situation ( $\psi=0.3$ ),  $s$  is the spacing of ties and  $L$  is the span of the tie.

In terms of disposition, the EN 1991-1-7 (CEN, 2006) states that ties should be arranged as closely as practicable to the edges of the floors and lines of columns and walls, with at least 30% of ties being located in the vicinity of the grid lines defined by columns. Since no further constraints to the disposition of the ties are introduced,

different tie arrangements may be adopted to comply with tying requirements. In this sense, two limit scenarios are possible, namely: i) the structure comprises a steel-concrete composite floor system which is connected to beams by shear connectors and in which only 30% of the tying force is provided by the steel beams, while the remaining 70% is provided by the profiled steel sheeting and/or by the reinforcement mesh; ii) the structure is all-steel, the floor system cannot resist tie forces and 100% of the tie forces are resisted by the steel beams and respective end connections. Since the floor system membrane effect falls outside the scope of the present study, only the second scenario is analysed. The perimeter and internal tie force values for the second scenario are presented in Table 7.22.

In order to provide further context to the tying requirements comparison to results from numerical simulations, the tie forces were also computed according to the UFC 2009 (United States of America Department of Defense, 2009). This code states that, unless demonstrated that structural members (i.e. beams) and respective connections are capable of withstanding the loads induced by column loss while undergoing rotations of 200 mrad, the tie forces are to be carried only by the floor systems. Considering that for the analysed frames, the maximum rotation capacity of the connections is typically not compatible with the 200 mrad requirement, then tie forces must be 100% transmitted by the floor system. While this does not allow for a direct comparison to the numerical results, a comparison is however provided in Table 7.23 between the design tie forces from UFC 2009 (computed according to the expressions from Table 2.4 which are reproduced below) and the design tie forces from EN 1991-1-7 for the analysed frame typologies.

UFC 2009 tying requirements:

$$\text{for internal ties: } T_i = 3pL \quad (7.37)$$

$$\text{for perimeter ties: } T_p = 6pL \quad (7.38)$$

$$p = 1.2DL + 0.5LL \quad (7.39)$$

where  $T_i$  is the required internal tie strength in the longitudinal or transverse direction in kN/m,  $T_p$  is the required peripheral tie strength in the longitudinal or transverse direction in kN/m,  $p$  is the floor load in kN/m<sup>2</sup>,  $L$  is the greater of the distances in m between the centers of the columns supporting any two adjacent floor spaces in the

direction under consideration,  $DL$  is the dead load in  $\text{kN/m}^2$  and  $LL$  is the live load in  $\text{kN/m}^2$ .

Table 7.22: EN 1991-1-7 (CEN, 2006) design tie forces for the elevated storey elements

N	S	$g_k$	$q_k$	$\psi$	s	L	$T_{p,100\%}$	$T_{i,100\%}$
[-]	[m]	[ $\text{kN/m}^2$ ]	[ $\text{kN/m}^2$ ]	[-]	[m]	[m]	[kN]	[kN]
4	6	3.1	3.0	0.3	6	6	75	115
	10				10	160	320	
8	6	3.1	3.0	0.3	6	6	75	115
	10				10	160	320	

Table 7.23: Comparison between UFC 2009 (United States of America Department of Defense, 2009) and EN 1991-1-7 (CEN, 2006) design tie forces for the elevated storey elements

N	S	$g_k$	$q_k$	p	L	$T_{p,UFC}$	$T_{i,UFC}$	$T_{p,EC1-1-7}$	$T_{i,EC1-1-7}$
[-]	[m]	[ $\text{kN/m}^2$ ]	[ $\text{kN/m}^2$ ]	[ $\text{kN/m}^2$ ]	[m]	[kN/m]	[kN/m]	[kN/m]	[kN/m]
4	6	3.1	3.0	5.2	6	188	94	10	20
	10				10	313	157	16	32
8	6	3.1	3.0	5.2	6	188	94	10	20
	10				10	313	157	16	32

The large discrepancy between UFC and EN 1991-1-7 tie forces is attributable to the fact that the UFC tying requirements are aimed at preventing progressive collapse, while the EN 1991-1-7 are based on prescriptions initially introduced in The Building Regulations 1970 (see Table 2.1) and aimed at preventing disproportionate collapse, rather than progressive collapse.

It should therefore be noted that the adoption of the EN 1991-1-7 tying prescriptions as a single measure is likely to be insufficient for collapse arresting purposes. Indeed, the fact that buildings not exceeding 4 storeys are in a lower consequence class (CC2a) than buildings with more than 4 and less than 15 storeys (CC2b) is indicative that the actual proneness of buildings to progressive collapse is not effectively taken into account in the EN 1991-1-7.

Considering that, for some of the analysed frames, the areas at risk of collapse exceed the EN 1991-1-7 limit value (see Table 2.5), then the elements in these zones are required to be designed as “key elements” and hence rendered capable of sustaining an accidental action  $A_d=34 \text{ kN/m}^2$ , which introduces an additional level of robustness to the structures. The areas at risk ( $A_{risk}$ ), the tolerable areas at risk of collapse ( $A_{tolerable}$ ),

the classification of columns as “key elements” and the design forces applied at the joints ( $T_{key}$ ) are presented in Table 7.24 for the full set of analysed frames.

Table 7.24: EN 1991-1-7 (CEN, 2006) key element design requirements

N	H	S	T	EN 1991-1-7 key element design requirements							
				$A_{risk,p}$	$A_{risk,i}$	$A_{tolerable}$	Perimeter col. key?	Internal col. key?	$T_{key,per}$	$T_{key,int}$	
[-]	[m]	[-]	[-]	[m <sup>2</sup> ]	[m <sup>2</sup> ]	[m <sup>2</sup> ]	[-]	[-]	[kN]	[kN]	
4	3	6	5×3	72	144	81	N	Y	0	357	
			4×4								
		10	5×4	200	400	100	Y	Y	298	595	
			5×3								
		4	6	5×4	72	144	81	N	Y	0	459
				4×4							
	10		5×3	200	400	100	Y	Y	383	765	
			5×4								
	8	3	6	5×3	72	144	81	N	Y	0	357
				4×4							
			10	5×4	200	400	100	Y	Y	298	595
				5×3							
4			6	5×4	72	144	81	N	Y	0	459
				4×4							
		10	5×3	200	400	100	Y	Y	383	765	
			5×4								

It should be noted that for the computation of the design horizontal accidental force, the most unfavourable internal cladding configuration was considered, since it is not possible to predict all possible changes made to the internal divisions during a building’s life span.

Since all joints are required to be designed to withstand tying forces (see Table 7.22) and horizontal loads induced by the accidental action when applicable (see Table 7.36), the maximum tensile forces in the perimeter elements from NDA simulations ( $N_{max}$ ) can be compared to the greater of the two EN 1991-1-7 design requirements ( $\max\{T_{p,100\%}; T_{key,per}\}$ ), as shown in Figure 7.70.



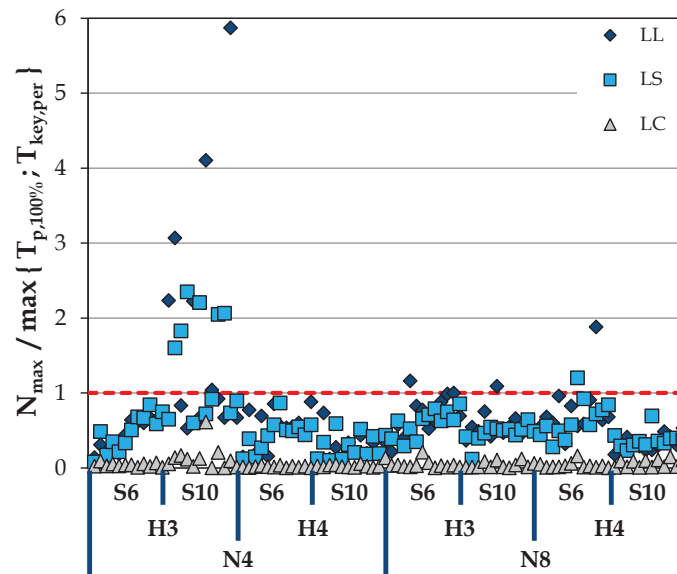


Figure 7.70: Comparison between maximum tensile force in MRF elements from NDA and maximum tensile design force from EN 1991-1-7 (CEN, 2006) considering tying and key element design requirements, by column loss scenario

The comparison presented in Figure 7.70 for the perimeter elements shows that for most cases, the maximum tensile force following column loss is lower than the maximum design tensile force (i.e.  $N_{max}/\max\{T_{p,100\%}; T_{key,per}\} < 1$ ).

A large difference can be observed when comparing façade loss scenarios (LL and LS cases) to corner loss scenarios (LC cases). Indeed, contrarily to façade loss cases, low tensile forces are reported in MRF elements for corner loss, which is ascribable to the differences in collapse resisting mechanisms. This aspect is further illustrated in Figure 7.71, where it can be seen that for LL and LS cases, both Vierendeel and catenary actions induce tensile forces in the MRF beams directly above the removed column; instead, for LC cases, Vierendeel action introduces compression in the MRF beam directly above the removed column, while catenary action introduces a tensile force.

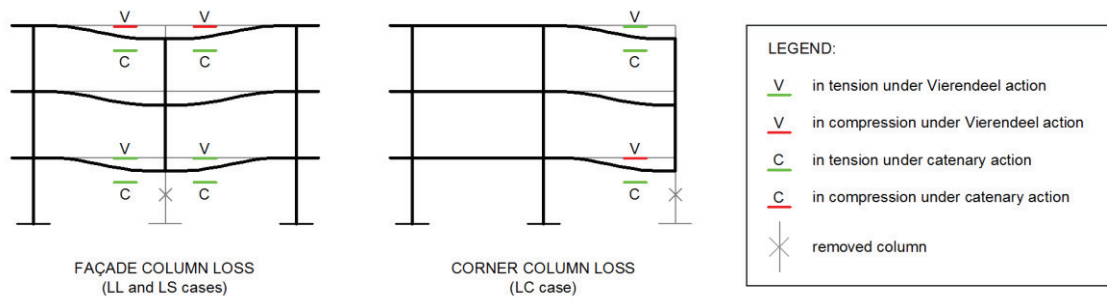


Figure 7.71: Axial force contributions to MRF beams from different mechanisms

Since the mechanism mobilised upon corner removal is comparatively flexible and considering that the load to be redistributed for LC cases is approximately half that of LL/LS cases, the Vierendeel action is found to play an important role in reducing tensile forces in MRF beams for LC cases.

The results in Figure 7.70 show that for most frames with smaller bays ( $S=6\text{m}$ ), which are required only to comply with tying requirements, the tensile forces developed following column loss are lower than the design tie forces. In the case of the frames with the larger bays ( $S=10\text{m}$ ), for which areas at risk for façade column losses ( $A_{risk,p}$ ) exceed the tolerable limit ( $A_{tolerable}$ ), the additional tensile forces for which members and connections must be designed in order to comply with the “key element” design were found to constitute a reasonable upper limit of the tensile forces induced by column loss.

This is not however the case for N4-H3-S10 frames, for which the  $N_{max}/\max\{T_{p,100\%};T_{key,per}\}$  ratio was found to considerably exceed 1 in thirteen different cases, reaching up to a value of 6. This indicates that the tensile forces required to arrest progressive collapse are significantly higher than those prescribed in EN 1991-1-7 (CEN, 2006) as minimum tying requirements or for “key element” design. In this sense, it is made clear that in order to prevent progressive collapse for this particular structural typology, additional measures are required, in addition to those prescribed in the current version of the EC1-1-7.

These considerations were taken into consideration for the new progressive collapse methodology proposal described in Section 7.4.2, since this structural typology is classified as Class PPC3, thus requiring Alternative Loadpath Analysis to be conducted, hence effectively quantifying tensile forces in members and connections

and enabling to perform connection design based on the actual internal force distribution under column loss. For both the N8-H3-S6 and N8-H3-S10 frame typologies, only in one case did the  $N_{max}/\max\{T_{p,100\%}; T_{key,per}\}$  ratio exceed 1 (i.e. in 2.6% of cases); the maximum reported ratio values for these typologies are 1.16 and 1.09, respectively. Finally, for the N8-H4-S6 typology, only in 2 cases did the ratio exceed 1 (i.e. in 5.6% of cases), with values of 1.20 and 1.88.

Considering these outcomes, a possible prescriptive design criterion for MRF structures consists of designing the members and joints in the façade zones for a design tensile force equal to the maximum between the EN 1991-1-7 tie forces and the forces induced by the accidental action ( $A_d=34\text{kPa}$ ), assuming the most unfavourable internal cladding distribution, no venting panels and that the internal claddings are sufficiently resistant so as to fully transmit loads to the main structural elements. By increasing this value by a factor  $\gamma_{PC,N}=1.2$ , the accuracy of  $N_{PC}$  with regard to the obtained results improves to 99.6% (if excluding N4-H3-S10 frames for which quantitative ALP design is required, according to the proposed method). The connections and members should therefore be verified for the maximum catenary force  $N_{PC}$  at the situation of progressive collapse arrest, which for the analysed set of structures may be estimated according to the following expression:

$$N_{PC} = \max\{T_{p,100\%}; T_{key,per}\} \times \gamma_{PC,N} \quad (7.40)$$

$$N_{PC} = \max\{ [\max\{0.4(g_k + \psi q_k)sL; 75\text{kN}\}]; [A_d \times (h/2) \times (L_{per}/2)] \} \times \gamma_{PC,N} \quad (7.41)$$

where,

- $A_d$  is the accidental design action for “key elements” defined in EC1-1-7;
- $h$  is the interstorey height;
- $L_{per}$  is the distance between the façade column and the adjacent internal column, measured in the direction perpendicular to the façade plane;
- $\gamma_{PC,N}$  is the adjustment factor for the maximum catenary force in progressive collapse (equal to 1.2);

The fact that the UFC 2009 (United States of America Department of Defense, 2009) indicates that tie forces to be carried only by the floor systems (unless members/connections can withstand column loss loads while undergoing rotations of

200 mrad) prevents a direct comparison to EN 1991-1-7 (CEN, 2006), since no such hypothesis is assumed in EC1-1-7. Nonetheless, a comparison between the maximum tensile force from NDA and the UFC tie forces is presented, in order to evaluate how UFC requirements compare with results from conducted simulations. To this end, the influence width for the computation of the tie forces was taken equal to  $L/2$  (where  $L$  is the span in the direction perpendicular to the MRF plane). The comparison is presented in Figure 7.72.

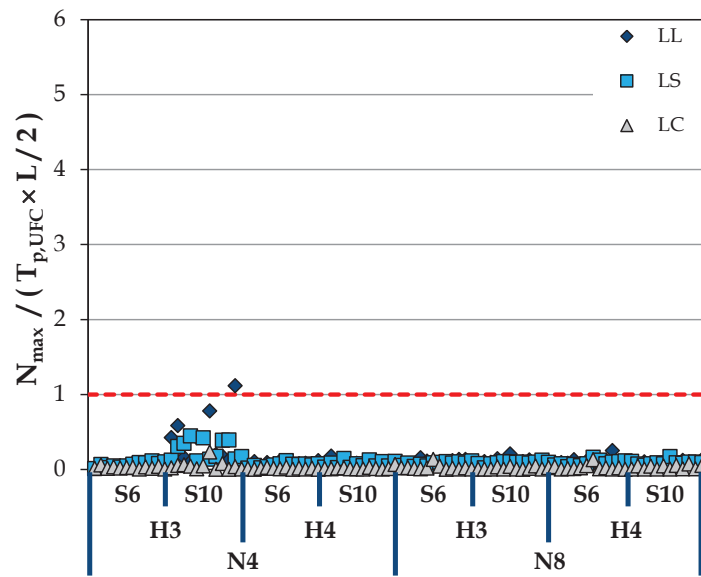


Figure 7.72: Comparison between maximum tensile force in MRF elements from NDA and maximum tie force according to UFC 2009 (United States of America Department of Defense, 2009), by column loss scenario

The UFC 2009 requirements are seen to provide an upper bound for practically all analysed cases, including even for the N4-H3-S10 frames which are very prone to progressive collapse. However the current EC1-1-7 tie force prescriptions, considering tie and key element design as previously indicated, are seen in Figure 7.70 to be better adjusted to the tensile force levels verified for the different analysed structural typologies.

For several structural typologies, the maximum rotational demand can be quite small and well below the 200 mrad value required by UFC 2009 to assume beam members and connections can carry the tie forces. As seen by the numerical simulations, in most analysed cases, the beams are capable of carrying tie forces and of

arresting progressive collapse. This indicates that this UFC constraint may be over conservative.

### 7.3.2 Post seismic robustness

In this section the seismic action effects on the MRF structures are evaluated in terms of natural vibration periods, lateral displacements and interstorey drift ratios. Comparisons to results from literature on MRF structures with similar characteristics are also presented and discussed, so as to provide context and to validate the obtained numerical outcomes.

Subsequently, the response under column loss for the post-seismic scenario is compared to results from the baseline robustness assessment (for which structures are initially undamaged) from Section 7.3.1, hence enabling to determine if the seismic action induced damage can influence the structural robustness.

#### 7.3.2.1 Natural vibration periods

In order to examine the effect of seismic actions of the MRF structures, the natural vibration periods were initially determined via Eigen Analysis. The MRF typology is typically characterised by its low stiffness, in comparison to braced frames, leading to higher natural periods of vibration. For the assumed base hypotheses (see also Section 3.3.3.5), namely  $a_{gR}=0.25g$ , soil type C and ductility class DCH, the set of structures analysed in the present study were found to be characterised by natural periods of vibration for the translational modes in the  $x$  and  $y$  direction that correspond to the constant velocity zone and start of the constant displacement zones of the group average response spectrum for Type 1 seismic action (see Figure 7.7).

The obtained values for the natural vibration periods were compared to values from a study by Liu (1997) on the seismic performance of MRF structures, which reported a 1<sup>st</sup> mode period value of approximately 1.37s for a comparable building in terms of number of storeys and occupancy distribution, namely a 5-storey office building. The values from Liu (1997) were found to agree with previous studies from literature by Osman *et al.* (1995), Redwood *et al.* (1990) or Naman and Goodno (1986), cited in Liu (1997)). Another study by Gupta and Krawinkler (1999) reported 1<sup>st</sup> mode period values around 1.4s for 3-storey office buildings with comparable MRF structure

layouts. The values from these studies therefore contribute to better define the expected values period values for the present study.

The values for the natural periods of vibration, obtained from the conducted Eigen Analysis on the seismically designed frames, are presented in Table 7.25, for the first 3 natural vibration modes. The obtained values show that, for structures without façade claddings (CN), the period of the first mode varies approximately between 1.1s and 1.9s, depending on bay layout configuration and interstorey height. Instead, for the structures with façade claddings (CC) the periods of vibration were found to be significantly lower due to the increased global lateral stiffness provided by the cold formed steel "X" bracings. In particular, for 6m and 10m span frames, the ratios between the periods of corresponding CC and CN frames are equal to 0.47 and 0.61 on average, respectively. It should however be noted that these values translate initial system stiffness, which may vary due to cladding stiffness degradation during the seismic action. This effect is explicitly accounted for, since the NDA was conducted using the tangent stiffness formulation, which updates the system stiffness matrix at each calculation step. The lower natural vibration periods for the CC frames are closer to the constant acceleration zone of the group average response spectrum, implying that these structures are initially subjected to higher accelerations, which may however decrease in case of cladding stiffness degradation.

Table 7.25: Natural periods of vibration of the first three modes for the set of seismically designed frames for the post seismic robustness assessment

<b>N</b>	<b>H</b>	<b>S</b>	<b>C</b>	<b>T</b>	<b>D</b>	<b>T<sub>M1</sub></b>	<b>Type</b>	<b>T<sub>M2</sub></b>	<b>Type</b>	<b>T<sub>M3</sub></b>	<b>Type</b>
<b>[-]</b>	<b>[m]</b>	<b>[m]</b>	<b>[-]</b>	<b>[-]</b>	<b>[-]</b>	<b>[s]</b>	<b>[-]</b>	<b>[s]</b>	<b>[-]</b>	<b>[s]</b>	<b>[-]</b>
4	3	6	N	5x3	E	1.406	Uy	1.143	Ux	0.899	Rz
				4x4		1.551	Uy	1.120	Ux	0.952	Rz
				5x4		1.623	Uy	1.156	Ux	1.013	Rz
		10	C	5x3	E	0.763	Uy	0.583	Ux	0.431	Rz
				4x4		0.700	Uy	0.644	Ux	0.413	Rz
				5x4		0.786	Uy	0.657	Ux	0.406	Uy
	6	N	5x3	E	1.462	Uy	1.247	Ux	0.949	Rz	
			4x4		1.524	Uy	1.182	Ux	0.980	Rz	
			5x4		1.648	Uy	1.183	Ux	1.034	Rz	
		4	C	5x3	E	1.029	Uy	0.809	Ux	0.559	Uy
				4x4		0.962	Uy	0.860	Ux	0.483	Uy
				5x4		1.082	Uy	0.866	Ux	0.549	Uy
4	6	N	5x3	E	1.657	Uy	1.499	Ux	1.062	Rz	
			4x4		1.881	Uy	1.466	Ux	1.171	Rz	
			5x4		1.751	Uy	1.498	Ux	1.115	Rz	
	10	C	5x3	E	0.827	Uy	0.650	Ux	0.438	Uy	
			4x4		0.762	Uy	0.729	Ux	0.378	Uy	
			5x4		0.831	Uy	0.736	Ux	0.428	Uy	
4	6	N	5x3	E	1.832	Uy	1.612	Ux	1.175	Rz	
			4x4		1.809	Uy	1.564	Ux	1.179	Rz	
			5x4		1.847	Uy	1.571	Ux	1.187	Rz	
	10	C	5x3	E	1.055	Uy	0.827	Ux	0.599	Uy	
			4x4		0.953	Uy	0.916	Ux	0.501	Uy	
			5x4		1.058	Uy	0.924	Ux	0.582	Uy	

U – translational vibration mode  
R – rotational vibration mode

The data presented in Table 7.25 is also shown in a condensed format in Table 7.26, in terms of intervals defined by the maximum and minimum periods for the 1<sup>st</sup> and 2<sup>nd</sup> natural vibration modes. In Figure 7.73, the intervals for CN and CC frames are overlapped with the target response spectrum for the group CN and CC frames, in order to illustrate how the introduction of façade elements influences the input seismic action.

Table 7.26: Minimum, maximum and average natural periods of vibration of the first two modes for the set of seismically designed frames for the post seismic robustness assessment

N	S	C	H	T <sub>1,MIN</sub>	T <sub>1,AVG</sub>	T <sub>1,MAX</sub>	T <sub>2,MIN</sub>	T <sub>2,AVG</sub>	T <sub>2,MAX</sub>
[-]	[m]	[-]	[m]	[s]	[s]	[s]	[s]	[s]	[s]
4	6	N	3	1.41	1.53	1.62	1.12	1.14	1.16
			4	1.66	1.76	1.88	1.47	1.49	1.50
		C	3	0.70	0.75	0.79	0.58	0.63	0.66
			4	0.76	0.81	0.83	0.65	0.71	0.74
	10	N	3	1.46	1.54	1.65	1.18	1.20	1.25
			4	1.81	1.83	1.85	1.56	1.58	1.61
C	3	0.96	1.02	1.08	0.81	0.85	0.87		
	4	0.95	1.02	1.06	0.83	0.89	0.92		

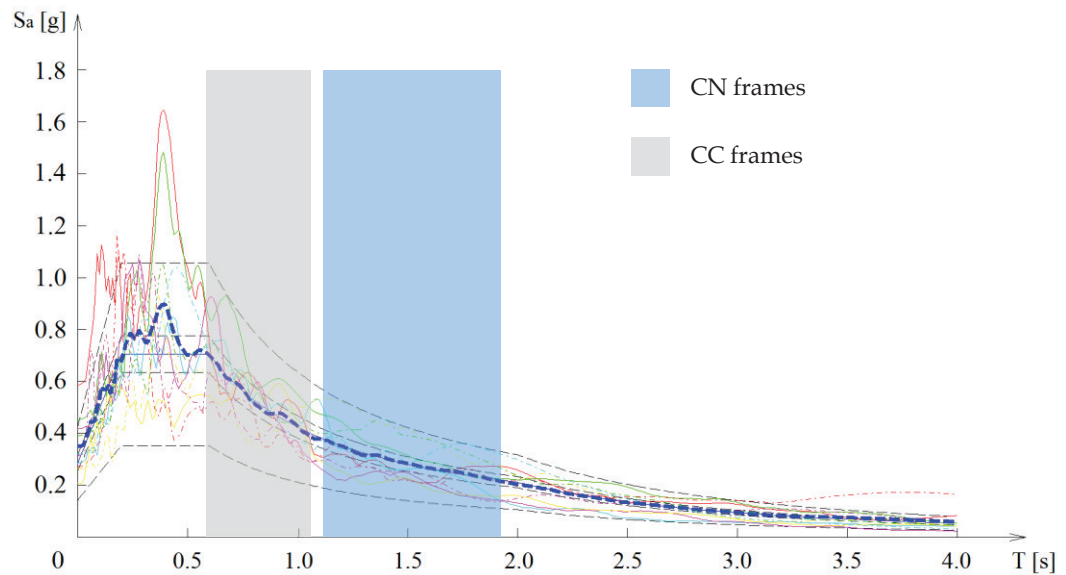


Figure 7.73: Minimum and maximum natural vibration periods intervals for the 1<sup>st</sup> and 2<sup>nd</sup> modes for CN and CC frames vs. target response spectrum for Type 1 action.

### 7.3.2.2 Lateral displacements

#### 7.3.2.2.1 Bare steel frames

The effect of the seismic action on the MRF structures was evaluated via the time-history functions for the horizontal displacements of the moment resisting frames at storey level. The horizontal displacements correspond in all cases to the displacements along the direction that maximises the damage to the relevant moment frame to which belongs the column to be removed. The direction of the displacements is indicated in all cases in the captions of the charts, for the sake of clarity. As an example, for the moment resisting frames aligned with the XZ plane, the horizontal



displacements shown correspond to displacements along the  $x$  direction (i.e. the  $x$  component of the displacement), which maximise the seismic damage to that moment frame; for moment frames aligned with the  $YZ$  plane, horizontal displacements correspond to displacements along the  $y$  direction (i.e. the  $y$  component of the displacement), which maximise the damage to the  $YZ$  oriented moment frame.

The effect of the seismic action on the MRF structures is illustrated in Figure 7.74 for the case of the N4-H3-S10-CN-T4×4-DE frame, subjected to the T1-1, T1-4 and T1-6 accelerogram signals (see Figure 7.6), where the instant of instantaneous notional column removal is represented by a dashed line. It should be noted that the horizontal displacements at the instant  $t=0$ s are not zero, due to the frame's initial geometrical sway imperfections, which are modelled using systems of equivalent horizontal forces, as prescribed in section 5.3.2 of the EN 1993-1-1 (CEN, 2005) and as previously described in Chapter 4.

The peak relative horizontal displacements at the different storey levels can be seen in the case shown in Figure 7.74 to yield similar horizontal displacement values for the different accelerograms signals. It can be observed that at the end of the seismic action, the structures tend towards the initial undamaged position, which indicates that the damage level sustained by the structure is low and that the majority of structural members/components remain elastic (see also Section 7.3.2.4). This implies that the structure retains its restitution capacity and is capable of returning to its original position. This is also seen in the displacement time history series from Liu (1997) for the Newhall and Santa Monica records of the 1994 Northridge earthquake, which are characterized by similar spectral acceleration values in the 1s to 2 s period range (see Figure 7.84). This trend indicates that MRF structures designed for moderate seismic actions in accordance with the EN 1998-1 (CEN, 2004) and in high ductility class DCH tend to remain elastic or to sustain limited damage. This is due to a combination of factors, namely the low horizontal stiffness of MRF structures inducing low seismic energy input, associated with stringent lateral drift limitation requirements and the Capacity Design component resistance hierarchy, which provides for a stable mechanism capable of avoiding drift instability.

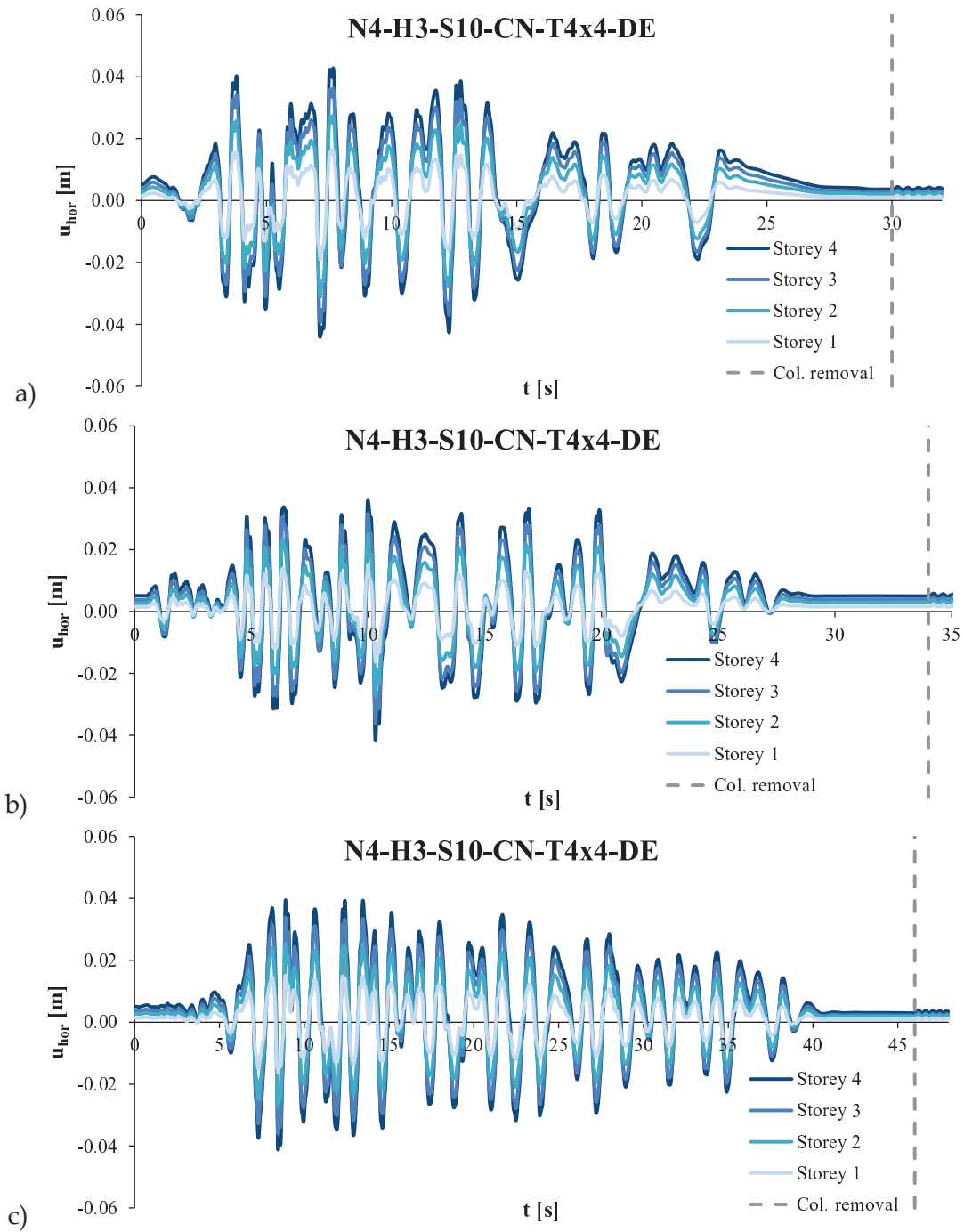


Figure 7.74: Horizontal displacements along the x direction of the XZ moment resisting frame at different storey levels for different accelerograms signals: a) T1-1; b) T1-4; c) T1-6

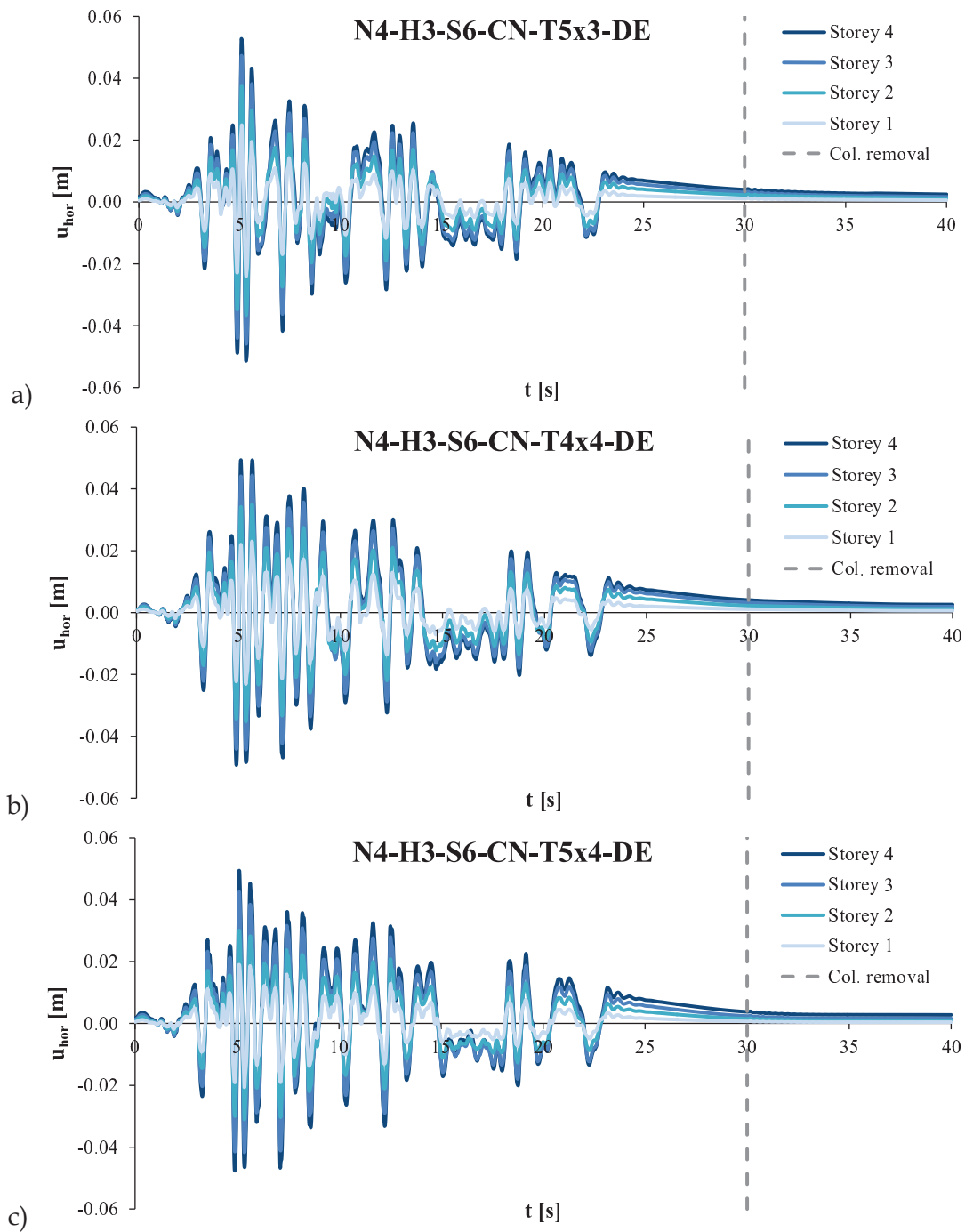


Figure 7.75: Horizontal displacements along the x direction of the XZ moment resisting frame at different storey levels for different bay configurations: a) T5x3; b) T4x4; c) T5x4

The effect of the bay layout configuration on the peak horizontal displacements was also examined. In Figure 7.75 a comparison is presented for the N4-H3-S6-CN-DE frame for the 3 examined bay layout configurations, namely T5x3, T4x4 and T5x4, so as to illustrate the effect of bay layout. As it can be recognised, this variable does not significantly influence the peak displacements, since structures which differ only in

terms of bay layout configuration are generally characterised by similar natural periods of vibration (see Table 7.25), implying that seismic action input is similar. The effects of bay layout and of the different accelerogram signals (T1-1, T1-4 and T1-6) are presented in more detail in Figure 7.76 and Figure 7.77 for bare steel frames under seismic actions oriented along the  $x$  and along the  $y$  directions, respectively.

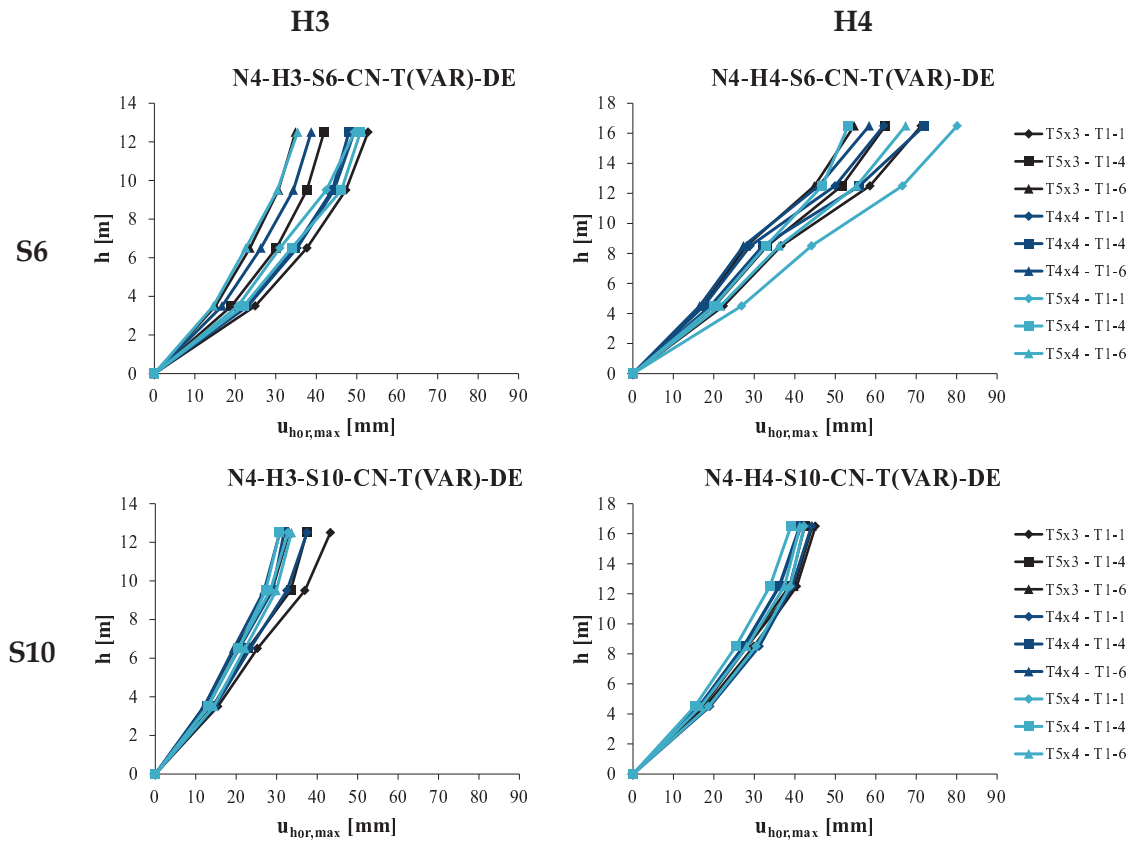


Figure 7.76: Maximum horizontal displacements along the  $x$  direction at storey level for bare steel frames (CN) in function of span and interstorey height

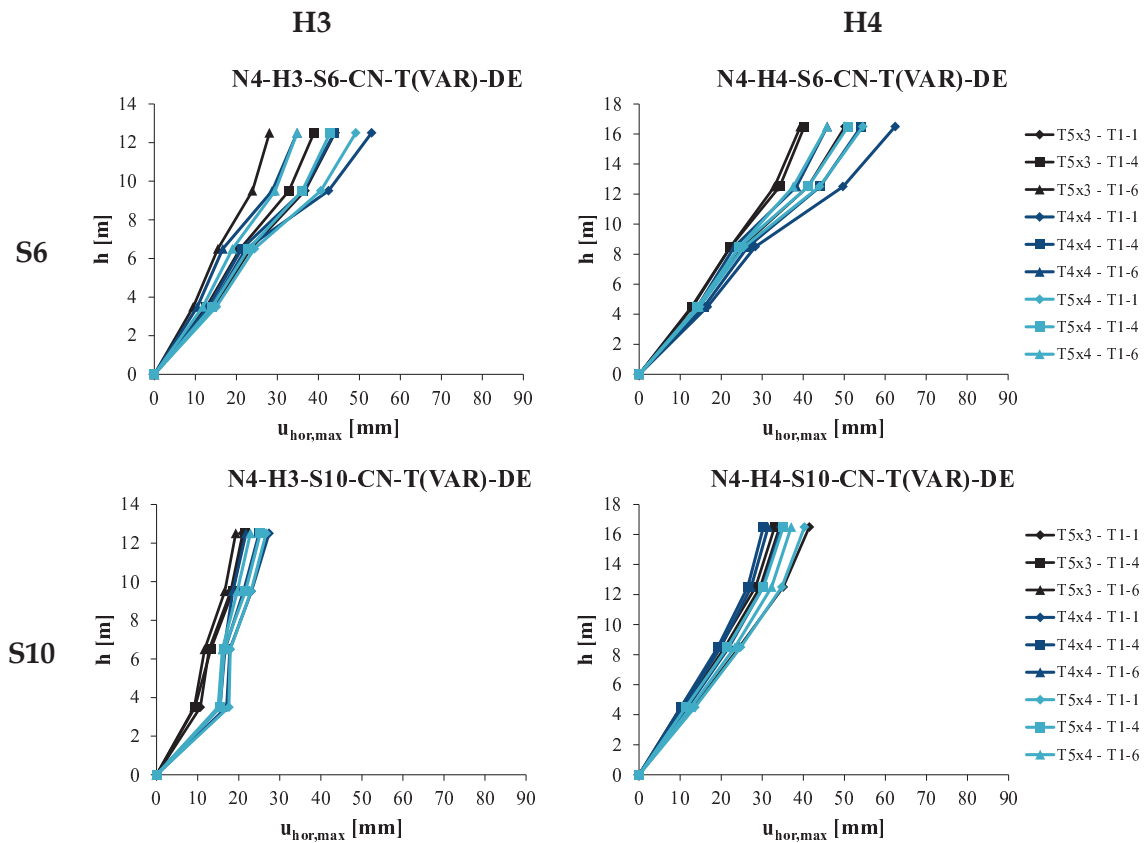


Figure 7.77: Maximum horizontal displacements along the y direction at storey level for bare steel frames (CN) in function of span and interstorey height

These outcomes were compared to results from a study by Liu (1997), which included the analysis of seismic action effects on a 5-storey office building with a MRF structure characterized by 5m and 10m spans in the N-S and E-W directions, respectively, with a 4m interstorey height. The lateral displacement time-history resulting from the Newhall and Santa Monica records of the 1994 Northridge earthquake were used as benchmark for the results obtained in the present study, since these records provide comparable spectral accelerations in the 1s-2s period range. It should however be noted that the 5-storey structure from Liu (1997) presents some differences in regard to those from the present study, namely the presence of a mechanical floor in the 4<sup>th</sup> storey and three beam and column cross section variations along the 5-storeys (for the present study only 2 variations are made for the 4-storey frames). Results by Liu (1997) showed maximum horizontal roof displacements of 0.095m and 0.125m, and 3<sup>rd</sup> floor displacements of 0.065m and 0.085m, for the Newhall and Santa Monica records respectively, which compare to a horizontal displacement of 0.080m for the 4<sup>th</sup> storey of the N4-H4-S6 frame, showing that despite the differences in

structural design, the values obtained in the present study are in line with expected horizontal displacements for this structural typology.

The results in Figure 7.76 and Figure 7.77 show larger dispersion in displacement values for 6m span frames (S6) than for 10m span ones (S10) as well as higher displacement values for frames with higher interstorey height. In general the bay layout variable is seen to not have a very significant influence on the storey displacements. Indeed, for the case of the main seismic action in the  $x$  direction, the maximum roof horizontal displacement values given by the envelope of the three signals for the N4-H3-S6-CN-DE frames were of 52.8mm, 49.3mm and 49.4mm for the 5×3, 4×4 and 5×4 bay layout configurations, respectively. Instead for the N4-H3-S6-CN-DE frames, higher value dispersion is verified, with reported values of 71.3mm, 72.0mm and 80.2mm for the 5×3, 4×4 and 5×4 bay layout configurations, respectively.

The discontinuity in lateral stiffness is clearly visible for example for the S6-H4 frames in Figure 7.76 and S6 frames in Figure 7.77 is due to the change in MRF beam cross section. As previously stated, only two types of beam sections were adopted along the height of the frame, with MRF beams in storeys 0, 1 and 2 having one type of beam cross section and MRF beams in storeys 3 and 4 having another. While this does not correspond to the structural solution that maximises interstorey drifts, according to the Author's professional experience, it corresponds to typical design practice and is more representative of real structures. Indeed, by limiting the number of profiles and joint detailing configurations, fabrication cost and time can be optimised (Santos and da Silva, 2011), for which reason this practice is typically adopted by structural designers. This is also in line with Liu (1997), in which beam and column sizes are changed over the frame height with the variation occurring every two storeys.

The results presented in Figure 7.76 and Figure 7.77 also show that the long span frames (S10) displayed smaller horizontal displacements than medium span ones (S6). For the case with the main seismic action along the  $x$  direction, maximum roof storey displacements of 43.3mm, 37.5mm and 33.6mm are reported for the 5×3, 4×4 and 5×4 bay layout configurations respectively, for the N4-H3-S10-CN-DE frames; instead for the N4-H3-S6-CN-DE frames, the corresponding values are equal to 52.8mm, 49.3mm and 50.9mm for the 5×3, 4×4 and 5×4 bay layout configurations, respectively. This is attributable to the higher natural vibration periods of S10 frames (see Table 7.25), which lead to lower seismic energy input.

The fact that the set of DCH steel frames sustained small or negligible levels of damage when subjected to the seismic action is consistent with results from Liu (1997), which showed that the Newhall and Santa Monica records of the 1994 Northridge earthquake induced very limited damage in the steel MRF structures, due to the low seismic energy contained in the fundamental period range around 1.4s. In particular, for the Newhall record, only one plastic hinge was formed in a single 1<sup>st</sup> storey MRF beam, whereas for the Santa Monica record, plastic hinges were formed at the ends of all 1<sup>st</sup> storey MRF beams. Furthermore, the fact that material overstrength randomness was modelled in the present assessment by factoring yield strength by the overstrength factor  $\gamma_{ov}=1.25$  recommended in EN 1998-1 (CEN, 2004), leads the frames to be even less prone to develop plasticity, in comparison to the frames analysed by Liu (1997) which did not account for this effect.

#### 7.3.2.2.2 Frames with façade claddings

The effect of claddings on the maximum storey displacements was evaluated through comparison with the results from bare steel (CN) frames. In Figure 7.78, four examples of the horizontal displacement time-history series for the roof storey (i.e. the top storey) are presented for both bare steel frames (CN) and frames with façade claddings (CC), when subjected to the most unfavourable accelerogram signal. The time series in Figure 7.78a) show that for this case, the façade claddings have a positive effect in reducing the maximum displacements. However, for the other cases presented Figure 7.78, the maximum displacement for the CC frames is higher than for CN frames, which is ascribable to the higher seismic energy input, resulting from the lower natural period of vibration of the CC frames.

The fact that the selected examples shown in Figure 7.78 correspond to the most unfavourable cases in terms of maximum displacement for CC frames does not however fully depict the system behaviour for different signals and bay layout configurations. The maximum horizontal displacements at storey level for the CC frames are presented in Figure 7.79 and Figure 7.80, along with the displacement ratios  $u_{CC}/u_{CN}$  between corresponding frames with (CC) and without (CN) façade claddings.

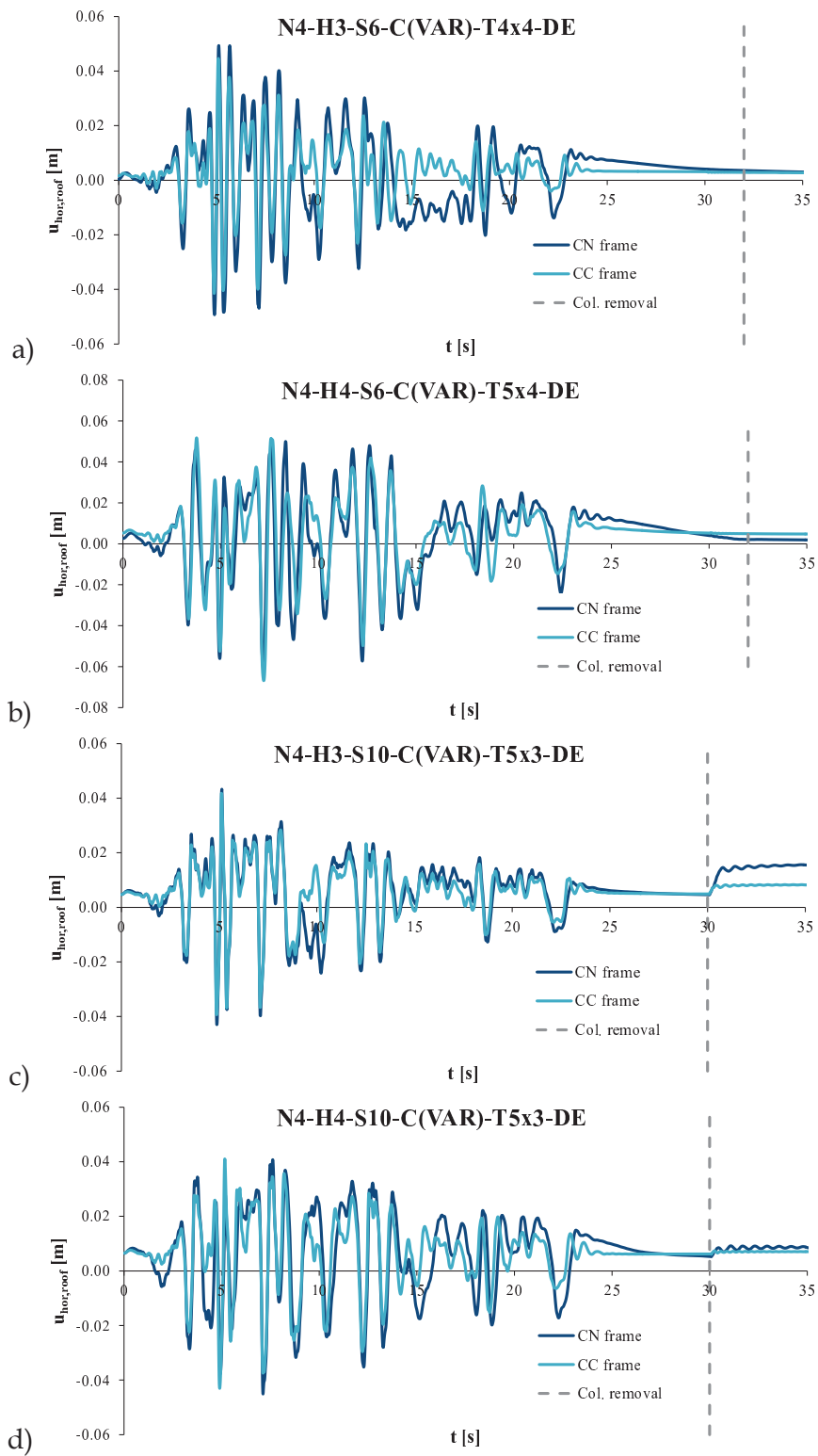


Figure 7.78: Roof storey horizontal x direction displacement time history comparison between bare steel frames (CN) and frames with façade claddings (CC) for signal T1-1: a) N4-H3-S6-T4x4-DE frame; b) N4-H4-S6-T5x4-DE frame; c) N4-H3-S10-T5x3-DE frame; d) N4-H4-S10-T5x4-DE frame



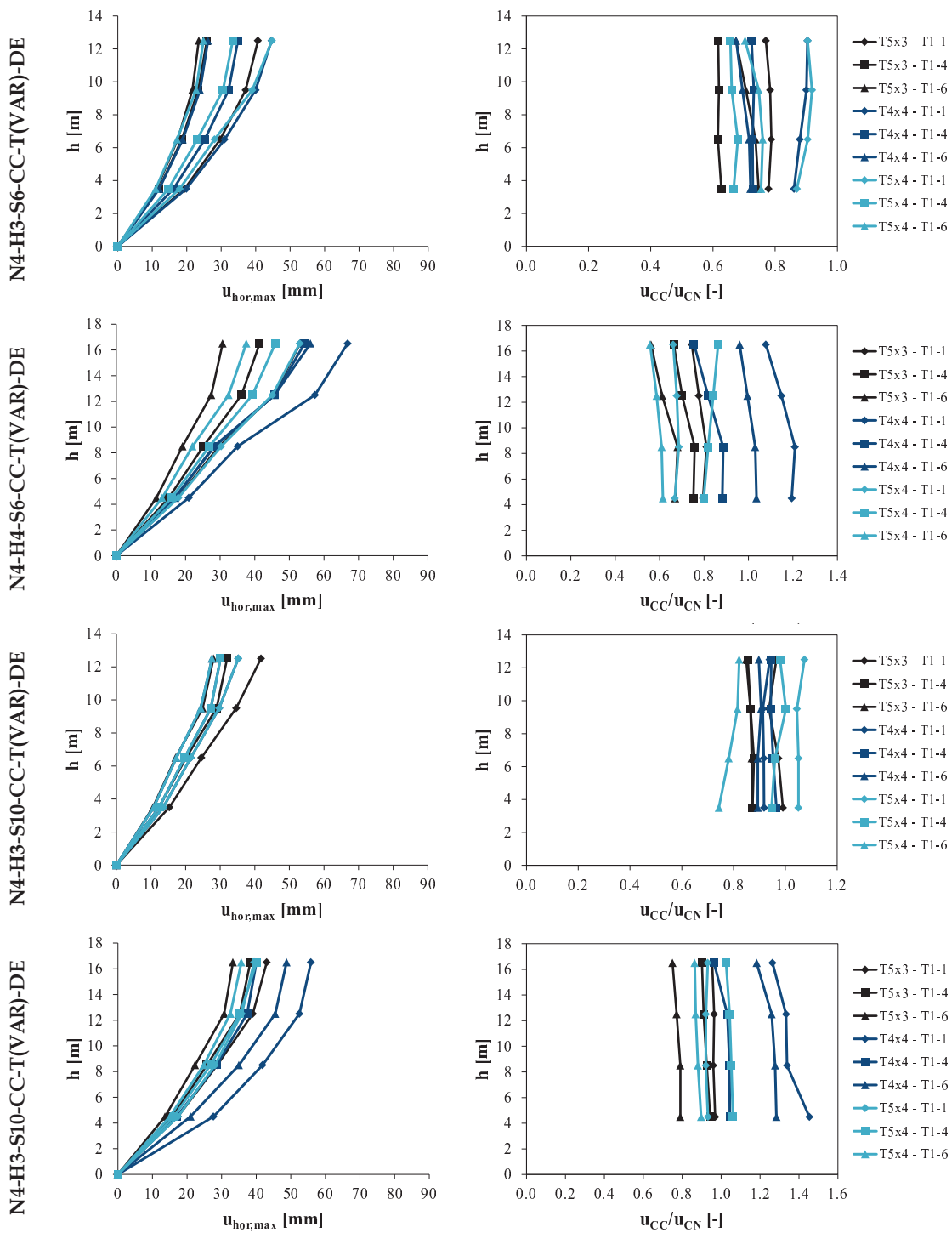


Figure 7.79: Maximum horizontal displacements at storey level for frames with façade claddings (CC) under seismic action in the x direction in function of span and interstorey height and displacement ratio values between CC and CN frames

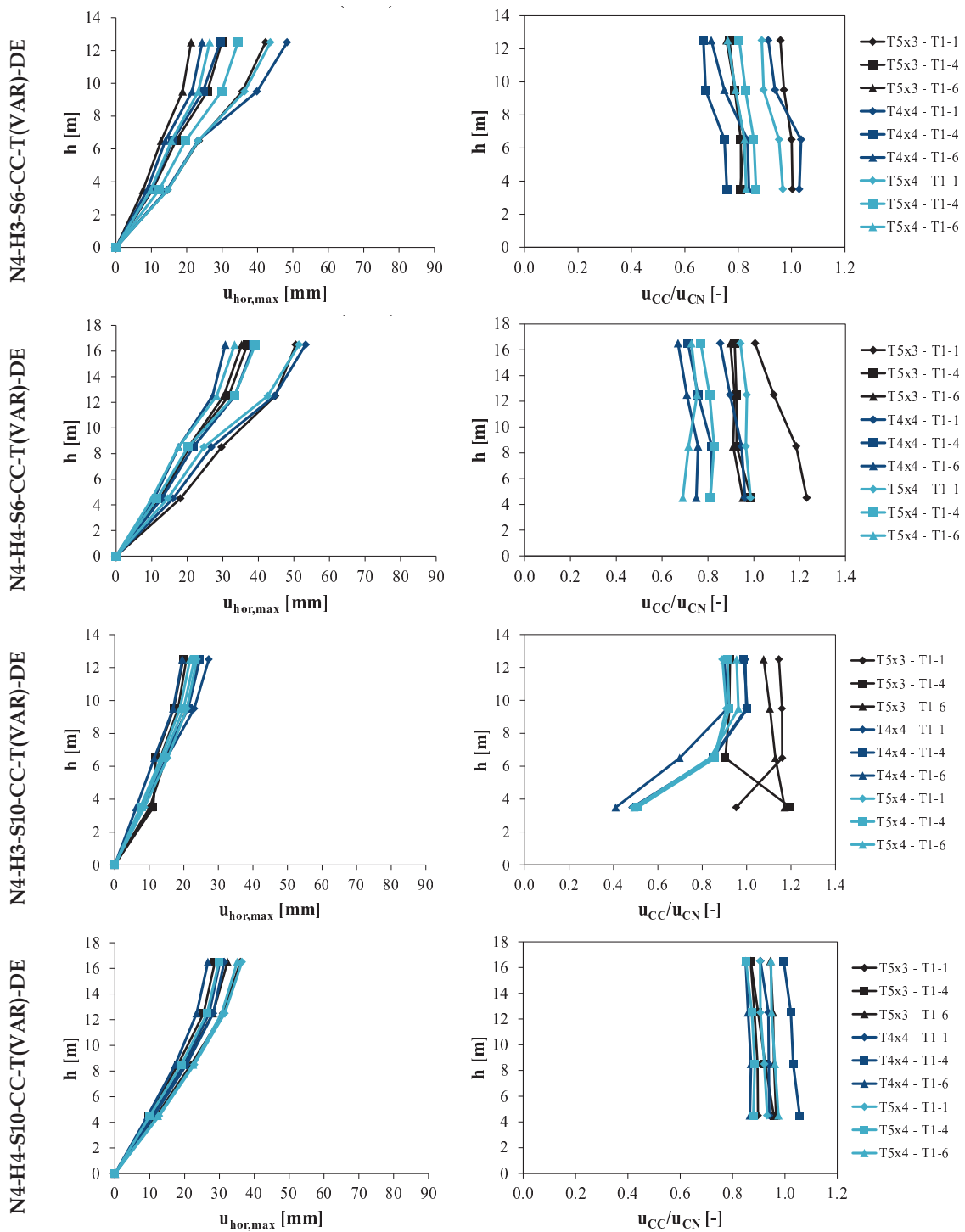


Figure 7.80: Maximum horizontal displacements at storey level for frames with façade claddings (CC) under seismic action in the y direction in function of span and interstorey height and displacement ratio values between CC and CN frames

As shown in Figure 7.79 and Figure 7.80, the  $u_{CC}/u_{CN}$  ratios indicate that for most cases characterised by different bay layout configurations and accelerograms signals, the effect of the adopted façade claddings is in general positive in reducing

maximum horizontal displacement demand (i.e.  $u_{CC}/u_{CN} < 1$ ). In the case of the N4-H3-S10-CC- DE frames, ratio values as low as 0.4 are reported for some bay configurations and accelerograms signals, translating cases in which the CN frame column yielded at ground floor level while the CC frame claddings were effective at limiting that displacement. However, as previously stated, claddings can also have a negative effect by amplifying displacement demand, namely when the higher structural stiffness it induces also a higher seismic energy input.

The results for the seismic action oriented along the  $x$  direction presented in Figure 7.79 show that the claddings were most effective for the H3-S6 frames, for which  $u_{CC}/u_{CN}$  roof displacement reductions of 0.77, 0.90 and 0.90 are reported for the most unfavourable signal (T1-1 in this case) for the T5×3, T4×4 and T5×4 bay layouts, respectively. Indeed, for this frame configuration all  $u_{CC}/u_{CN}$  ratio values are below 1. For the  $U_y+0.3U_x+0.3U_z$  case shown in Figure 7.80, the introduction of claddings also corresponded in general to improved behaviour, with only the T4×4 case under the T1-1 signal showing  $u_{CC}/u_{CN}$  ratio values higher than 1, namely equal to 1.03 and 1.04 for the 1<sup>st</sup> and 2<sup>nd</sup> storey, respectively. In this sense, the H3-S6 frames are shown to display improved seismic performance by adopting the façade claddings.

The displacement demand reduction (as measured by the  $u_{CC}/u_{CN}$  ratios) is seen to be characterised by some dispersion, which is larger for the sets of 6m span frames. Indeed, since the claddings appear to be less effective for the case of the 10m span frames, the  $u_{CC}/u_{CN}$  ratio values for S10 frames are in general closer to 1, hence leading to lower value dispersion.

The H3-S6 frames displayed average  $u_{CC}/u_{CN}$  ratio values of 0.69, 0.77 and 0.75, associated to coefficients of variation (CoV) of 0.09, 0.13 and 0.14 for the top storey in frames with T5×3, T4×4 and T5×4 layouts, respectively, for the case of the seismic action along the  $x$  direction. Instead for the case of the seismic action along the  $y$  direction, average top storey  $u_{CC}/u_{CN}$  values of 0.83, 0.76 and 0.82, associated to coefficients of variation (CoV) of 0.11, 0.14 and 0.06 for the same cases. These values indicate that the demand reduction may vary significantly for this structural typology, due to the complex interaction between claddings and MRF structural elements. It was also noted that for the H3-S6 frames, the  $u_{CC}/u_{CN}$  ratios tend to display similar values for the different storeys.

The H4-S6 frames displayed higher dispersion in terms of  $u_{CC}/u_{CN}$  ratios, with average values of 0.66, 0.93 and 0.69, associated to coefficients of variation of 0.11, 0.14 and 0.18 for the top storey in frames with T5×3, T4×4 and T5×4 bay layout cases, respectively for the seismic action along the  $x$  direction; for the seismic action along the  $y$  direction, average ratio values of 0.94, 0.75 and 0.81, associated to coefficients of variation of 0.05, 0.11 and 0.11 for the top storey are reported for the same bay layout cases.

The results for the H3-S10 and H4-S10 frames show lower  $u_{CC}/u_{CN}$  ratio dispersion, as previously stated, with values generally close to 1, which indicate the cladding system to be less effective for long span configurations. This is likely due to the higher storey masses (approximately 2.8 times higher) in comparison to corresponding S6 frames. For the H3-S10 frames under seismic along the  $x$  direction, average  $u_{CC}/u_{CN}$  ratio values of 0.89, 0.93 and 0.96, associated to coefficients of variation of 0.06, 0.02 and 0.12 are reported for the top storey in frames with T5×3, T4×4 and T5×4 bay layout cases, respectively; instead, for the seismic action along the  $y$  direction, average  $u_{CC}/u_{CN}$  ratio values of 1.05, 0.96 and 0.90, associated to coefficients of variation of 0.09, 0.04 and 0.01 are reported for the same cases.

Also for the case of the H4-S10 frames low dispersion is observed, resulting from the limited effectiveness of claddings in reducing displacement demand.

The obtained results hence indicate that the adopted façade claddings are more effective for medium span (S6) than for long span (S10) systems. This outcome results from the combination of several factors that influence seismic response. In particular, the natural periods of vibration of bare steel S6 and S10 frames are similar, whereas the natural periods of vibration of S6 frames with claddings are lower than corresponding S10 frames, indicating that the stiffening effect caused by the introduction of claddings is more pronounced for the S6 frames. This implies that the ratio between the stiffnesses of the claddings and that of the base steel frame is higher for the S6 cases, due to smaller storey masses being approximately 2.8 times smaller in comparison to S10 frames, while panel resistance is only about 1.7 times smaller. In this case, despite the higher seismic energy input to the S6 frames due to higher structural stiffness, the increase in lateral stiffness provided by the adopted cladding system is shown to compensate this effect.

The use of façade claddings as a design strategy for reducing the lateral displacement demand induced by seismic action should be carefully pondered, since the increased stiffness may lead to an increase of seismic input energy, ultimately resulting in higher displacement demands than those of the bare steel frame. While the reduced number simulations does not enable to draw more definitive conclusions, it nonetheless shows that the effect of the claddings on displacement demand reduction is characterised by high dispersion.

### 7.3.2.3 Storey drifts

#### 7.3.2.3.1 Bare steel frames

The results regarding the maximum interstorey drifts for the different analysed frames are presented in Figure 7.81 and Figure 7.82.

The obtained results show that the interstorey drift values are lower than 1% in all cases. The higher values of interstorey drift ratio  $d_i/h$  were obtained for the case of the N4-H4-S6 frames at the point of stiffness discontinuity, where the variation of MRF beam and column sections occurs, i.e. at the 2<sup>nd</sup> storey level. In this particular case, the stiffness variation coupled with the low structural stiffness resulted in the maximum drift ratio being verified between storeys 2 and 3. In all other cases, namely N4-H3-S6, N4-H3-S10 and N4-H4-S10, the general trend shows that the largest interstorey drift is verified between the ground and 1<sup>st</sup> storeys, with typical values around 0.5%, which tend in general to be lower for the upper storeys. These low values are attributed to the low lateral stiffness that characterises MRF structures, leading to natural periods of vibration for the bare frames in the range between 1.1s and 1.9s (see Table 7.26), to which correspond low spectral accelerations, as can be recognised in Figure 7.73.

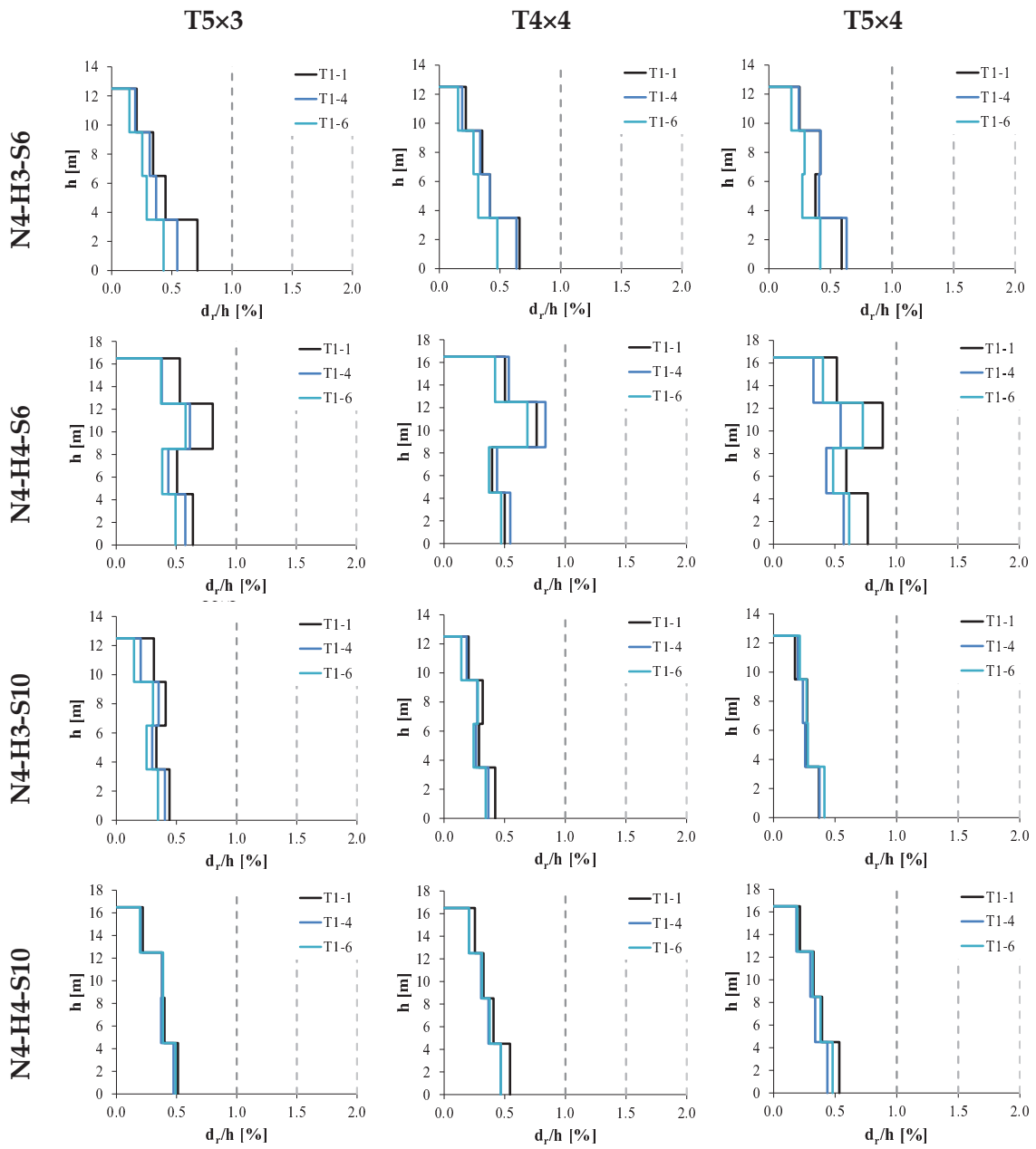


Figure 7.81: Maximum interstorey drifts for bare steel frames (CN) under seismic action in the x direction in function of span, interstorey height and bay layout configuration

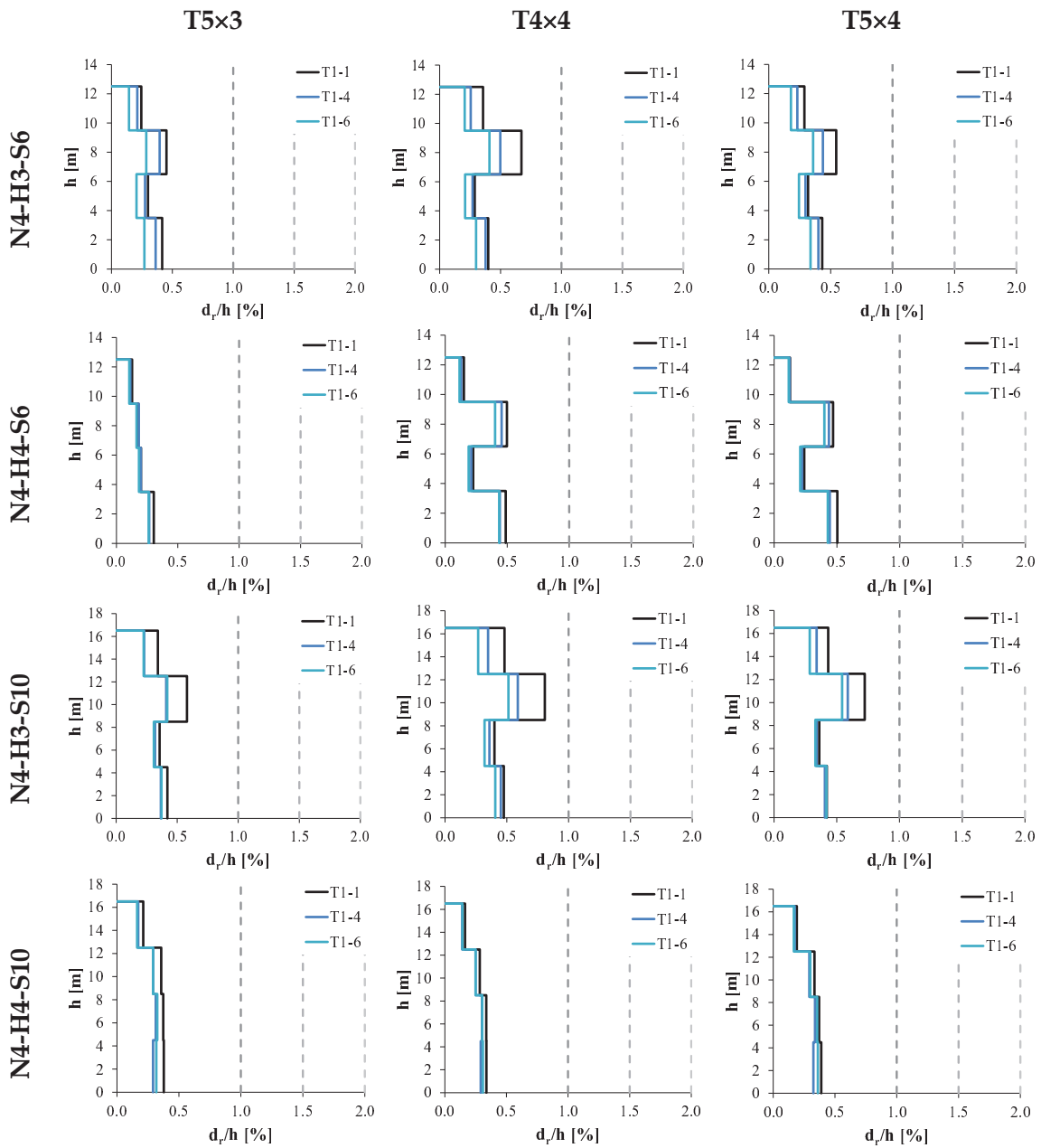


Figure 7.82: Maximum interstorey drifts for bare steel frames (CN) under seismic action in the y direction in function of span, interstorey height and bay layout configuration

To provide context for the numerical outcomes, a comparison was performed with results from Liu (1997), for a comparable 5-storey MRF structure subjected to the Newhall and Santa Monica station records of the 1994 Northridge earthquake. The recorded acceleration time-history data for these stations was retrieved from the Strong Motion Virtual Data Center (University of California Santa Barbara, 2016) and is presented in Figure 7.83.

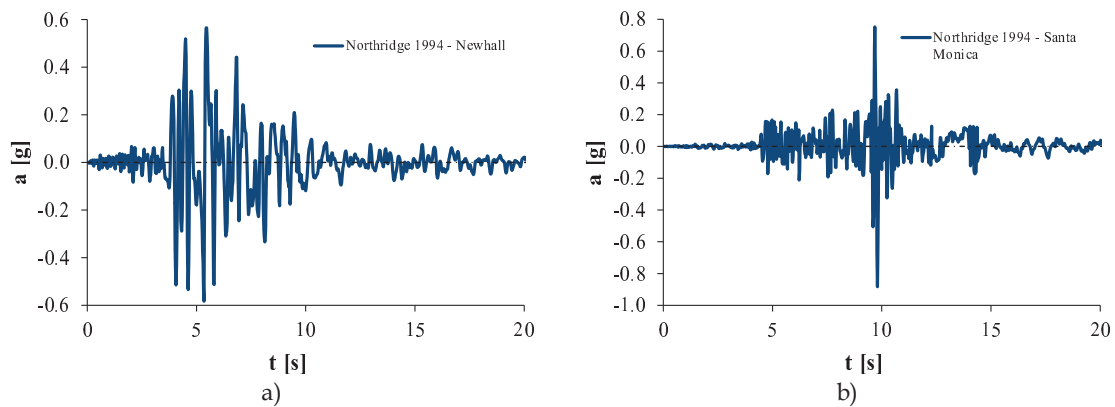


Figure 7.83: Recorded acceleration time-history for the 1994 Northridge earthquake from Liu (1997): a) Newhall station record; b) Santa Monica station record

These records were selected for the comparison given that they are characterised by values of spectral acceleration similar to those of the target spectrum in the period range corresponding to the first two modes, i.e. approximately between 1.1s and 1.9s. In Figure 7.84a) the acceleration response spectra for the T1-1, T1-4 and T1-6 signals used in the post seismic robustness assessment is shown, along with the average spectrum and standard deviation. In Figure 7.84b) the comparison between the average spectrum and the Newhall and Santa Monica spectra shown in (Liu J. , 1997) is presented.

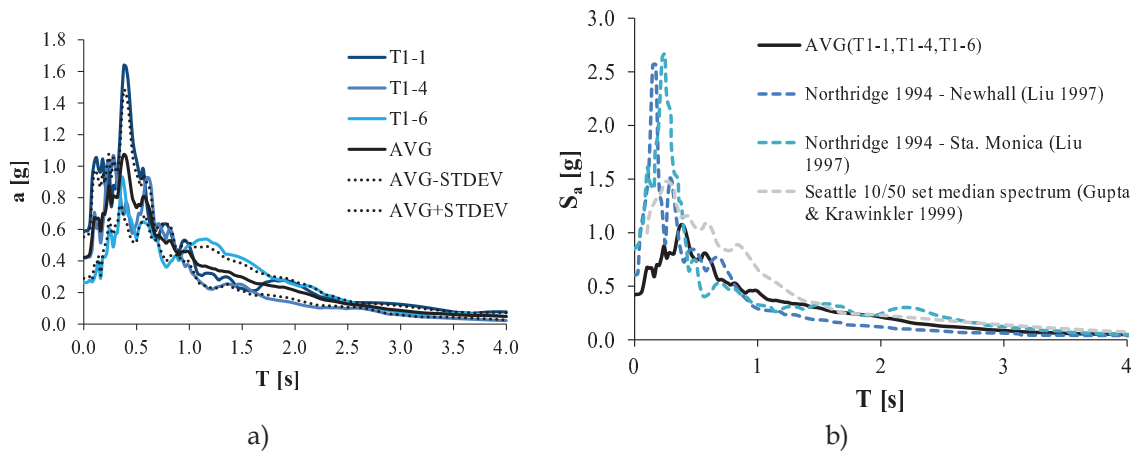


Figure 7.84: a) acceleration response spectra and average spectrum for the T1-1, T1-4 and T1-6 signals; b) response spectrum comparison between the average spectrum and the Newhall and Santa Monica records of the 1994 Northridge earthquake from Liu (1997)

Considering that the dynamic response of structural systems subjected to earthquakes is significantly affected by the frequency content of the ground motion (Rathje *et al.*, 2004), the Santa Monica and the Newhall signals were characterised in terms of frequency content, in order to verify if significant differences in frequency



content existed between these signals and those used in the post seismic robustness assessment.

According to Rathje *et al.* (2004), the acceleration response spectrum and the Fourier Amplitude spectrum provide for the most complete characterisation of the frequency content of strong ground motions. In that sense, the Fourier Amplitude spectra were computed using SeismoSignal (Seismosoft, 2016) to show how the amplitude of the ground motion is distributed with respect to frequency. The Fourier Amplitude spectra are plotted in Figure 7.85 for the 0.1Hz to 50Hz range and for the 0.1Hz to 1Hz range, to provide both an assessment for a broad range of frequency values and also for the frequency range of the frames' natural vibration modes.

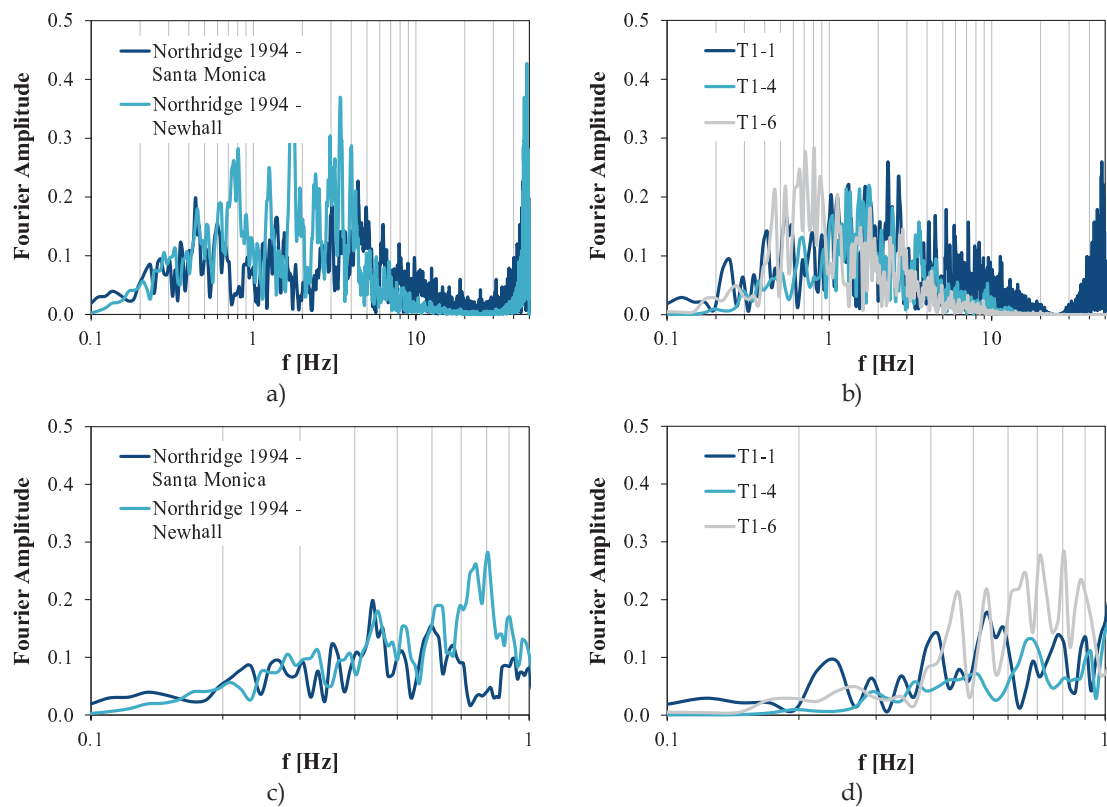


Figure 7.85: Fourier Amplitude spectra in the 0.1Hz-50Hz range: a) Northridge 1994 Newhall and Sta. Monica records; b) Signals T1-1, T1-4 and T1-6; Fourier Amplitude spectra in the 0.1Hz-1Hz range: c) Northridge 1994 Newhall and Sta. Monica records; d) Signals T1-1, T1-4 and T1-6

The spectra show that for the range of frequencies corresponding to the fundamental vibration modes of the bare steel frames (i.e. between 0.53Hz and 0.71Hz), the Fourier Amplitude values for the Newhall and Sta. Monica signals display comparable amplitude values to those of the T1-1, T1-4 and T1-6 signals.

The frequency content of the signals was also characterised using single scalar parameters, which allows for different ground motions to be compared quickly and easily. Furthermore, the scalar parameters can be directly compared to the natural period of a structural system, in order to evaluate for resonance conditions or for dynamic response enhancement. Various scalar parameters may be used to characterise the frequency content. In this study the mean period  $T_m$  (which is based on the Fourier Amplitude Spectrum) was selected, since, according to Rathje *et al.* (2004), it better characterises the frequency content of the ground motion, namely in comparison to the frequently used predominant period  $T_p$  (which is based on acceleration response spectrum). To provide further context, both  $T_m$  and  $T_p$  values were computed using SeismoSignal (Seismosoft, 2016) and are presented in Table 7.27.

Table 7.27: Predominant spectral period  $T_p$  and mean period  $T_m$  for the ground motion signals T1-1, T1-4, T1-6 and for the Newhall and Sta. Monica records of the Northridge 1994 earthquake

SIGNAL [-]	$T_p$ [s]	$T_m$ [s]
T1-1	0.38	0.46
T1-4	0.28	0.56
T1-6	0.36	0.96
Newhall	0.20	0.37
Sta. Monica	0.32	0.53

The computed  $T_p$  values for the Newhall and Sta. Monica signals are quite similar, namely with the latter being inside the  $T_p$  range for the T1-1 through T1-6. However, the fact that the predominant period  $T_p$  is simply defined as the period of the maximum spectral acceleration implies it cannot adequately describe the frequency content, as stated by Rathje *et al.* (2004). In this sense, the mean period  $T_m$  is more appropriate to compare frequency contents and results in Table 7.27 show all signals to have similar values of  $T_m$ , namely with the Sta. Monica signal ( $T_m=0.53$ s) being inside the  $T_m$  range of values defined by the T1-1 ( $T_m=0.46$ s) and the T1-6 ( $T_m=0.96$ s) signals. These results indicate that the frequency content of the selected records of the 1994 Northridge earthquake have a similar frequency content to the signals selected for the post seismic robustness analysis, hence validating the result comparison to the MRF structures analysed by Liu (1997).

Given that the structures analysed in Liu (1997) are 5 storeys high, while the ones studied in this work are 4 storeys high, the drift ratio results comparison is performed for the first and top storeys, where drift is measured relative to the ground, i.e. drift is computed as the storey displacement divided by the corresponding storey height relative to the ground level. Only frames with 4m interstorey height were considered for the comparison since all structures in Liu (1997) are also characterised by an interstorey height of 4m.

The results from another study on the seismic demands for steel MRF structures (Gupta and Krawinkler, 1999) were also used in the comparison, to provide further context to the obtained results. A 3-storey office building structure in Seattle, designed in the context of the SAC steel project, with perimeter moment resisting frames, 4m interstorey height and 9.15m spans was selected for the comparison. The natural vibration period of the 1<sup>st</sup> mode is equal to 1.36s, as previously stated, which is similar to the analysed structures. In terms of seismic action, the set of 20 records for Seattle described in Gupta and Krawinkler (1999) was selected, which represents a probability of exceedance of 10% in 50 years (475 year return period). This record set is henceforth designated as the 10/50 set. The median response spectrum for the Seattle 10/50 set from Gupta and Krawinkler (1999) is represented in Figure 7.84, where it can be recognised that the spectral accelerations are significantly higher than the target spectrum for the present study in the 1.1s to 1.9s period range, namely 1.5 and 1.1 times larger for period values of 1.1s and 1.9s, respectively. In this sense, a direct comparison with results from Gupta and Krawinkler (1999) is not possible, although it serves to show how interstorey drift varies with spectral acceleration levels.

The comparison between results from the present study and results from Liu (1997) and Gupta and Krawinkler (1999) is presented in Table 7.28 (N.B.: results from Gupta and Krawinkler (1999) are provided for context only, since seismic action is higher, therefore enabling to assess drift sensitivity to spectral acceleration levels).

Table 7.28: Comparison of maximum storey drifts relative to ground between N4-H4 frames and 5-storey frames from Liu (1997) and 3-storey frames from Gupta and Krawinkler (1999)

Storey	NDA results	$u_{hor,max}/h_{storey}$		
		Newhall (Liu 1997)	Sta. Monica (Liu 1997)	Seattle 10/50 median (Gupta and Krawinkler 1999)
[-]	[%]	[%]	[%]	[%]
1 <sup>st</sup>	0.60	0.48	0.56	-
Roof	0.49	0.44	0.60	1.55

As seen in Table 7.28, the obtained results in terms of drift are in line with values obtained by Liu (1997) at both 1<sup>st</sup> storey and roof levels. The drift value obtained by Gupta and Krawinkler (1999) serves to demonstrate the sensitivity of global drift to spectral acceleration. It should also be noted that in the study by Gupta and Krawinkler (1999), MRF beams were optimised for each storey level, hence contributing to achieve higher global drift values.

The obtained results show that for the conditions analysed in the present study, namely moderate seismicity conditions for soil type C and moment resisting frame structures designed according to EN 1998-1 (CEN, 2004) in DCH class, the seismic energy input is quite low, given the high natural vibration periods of the structures, resulting in overall low drift demand and low levels of damage.

#### 7.3.2.3.2 Frames with façade claddings

The introduction of the non-structural façade claddings increases the lateral system stiffness, which contributes to reduce lateral drift. However, the higher lateral system stiffness also leads to the reduction of the natural vibration periods of the structural system, which introduces a higher amount of seismic energy, potentially resulting in higher horizontal displacements. These aspects are assessed in this section, by comparing the drift results from bare steel frames (CN frames) seen previously in section 7.3.2.3.1 to the results obtained for frames with façade claddings (CC frames). The maximum interstorey drifts for CC frames are presented in Figure 7.86 and Figure 7.87.

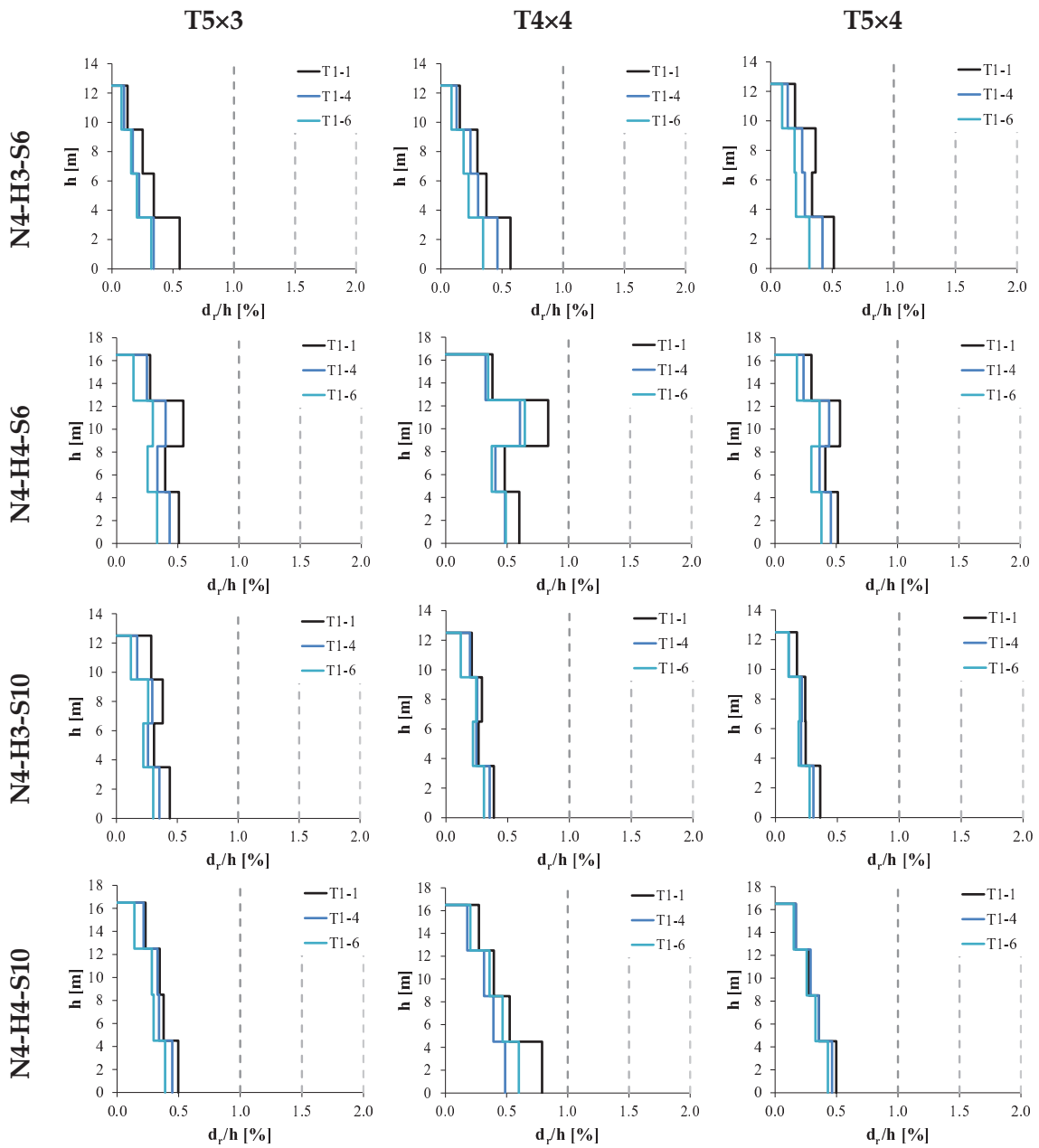


Figure 7.86: Maximum interstorey drifts for steel frames with claddings (CC) under seismic action in the x direction in function of span, interstorey height and bay layout configuration

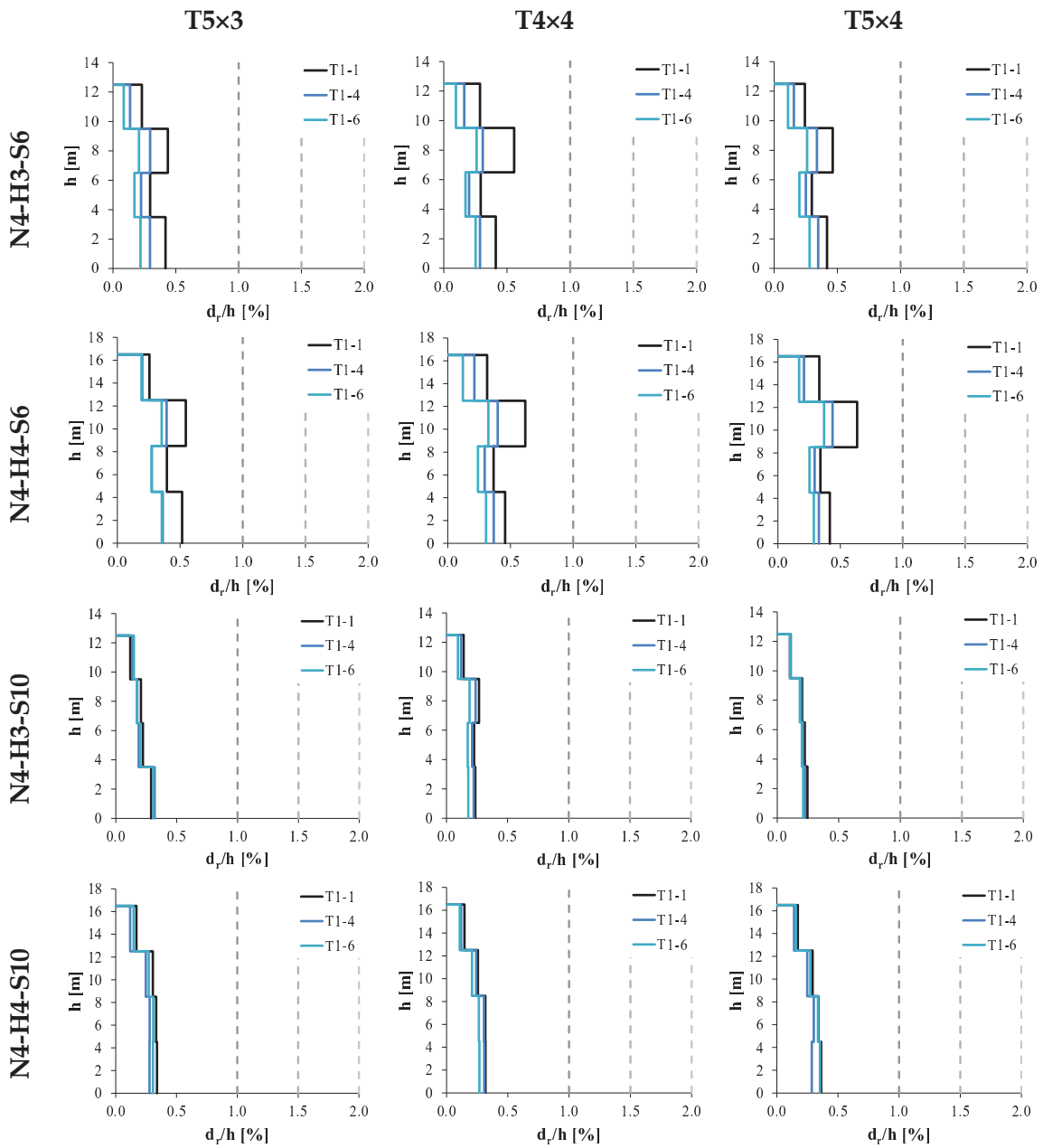


Figure 7.87: Maximum interstorey drifts for steel frames with claddings (CC) under seismic action in the y direction in function of span, interstorey height and bay layout configuration

The results in Figure 7.86 and Figure 7.87 show that the interstorey drift ratios for the CC frames are in all cases lower than 1%, similarly to the bare steel frames. The maximum value of 0.83% was obtained for the interstorey drift between the 2<sup>nd</sup> and 3<sup>rd</sup> floors of the N4-H4-S6-CC-T4x4-DE frame when subjected to the T1-1 accelerogram signal in the y direction. The large discontinuity in lateral stiffness occurring at the second storey is observed in many cases, namely for S6 frames, since the stiffness and

resistance of the cladding system is limited (being non-structural elements) and not sufficient to prevent the discontinuity.

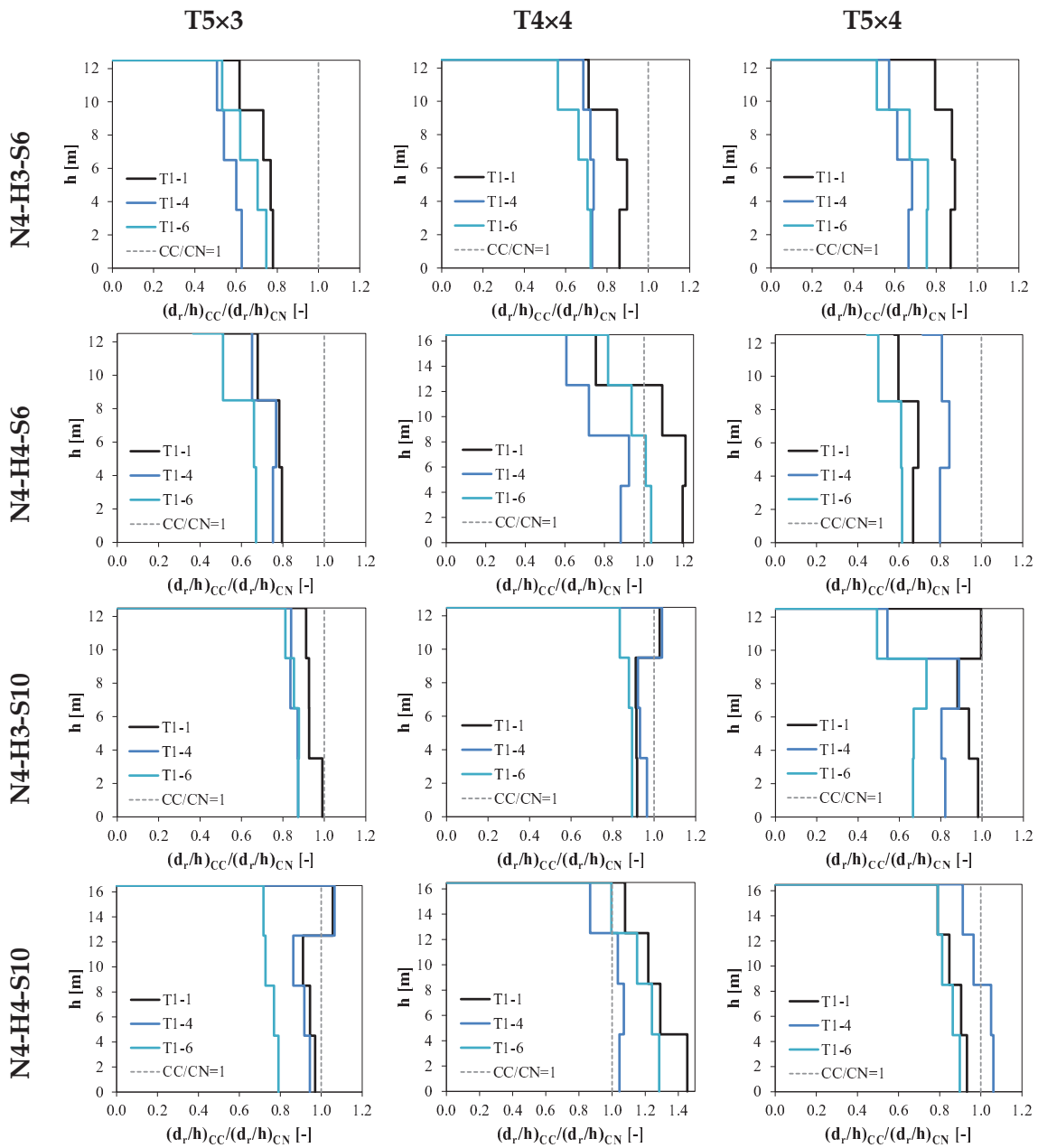


Figure 7.88: Ratios between maximum interstorey drifts of frames with claddings (CC) and bare steel frames (CN) under seismic action in the x direction in function of span, interstorey height and bay layout configuration

In order to evaluate the effectiveness of the adopted cladding system in reducing lateral drifts for the cases shown in Figure 7.86 and Figure 7.87, the ratios  $(d_r/h)_{CC} / (d_r/h)_{CN}$  between the maximum interstorey drifts for the CC and CN frames were computed. These ratios which can measure the effectiveness of the claddings are

presented in Figure 7.88 and Figure 7.89, where the threshold of no improvement in lateral drift (i.e.  $(d_r/h)_{CC}=(d_r/h)_{CN}$ ) is also highlighted with a dashed line.

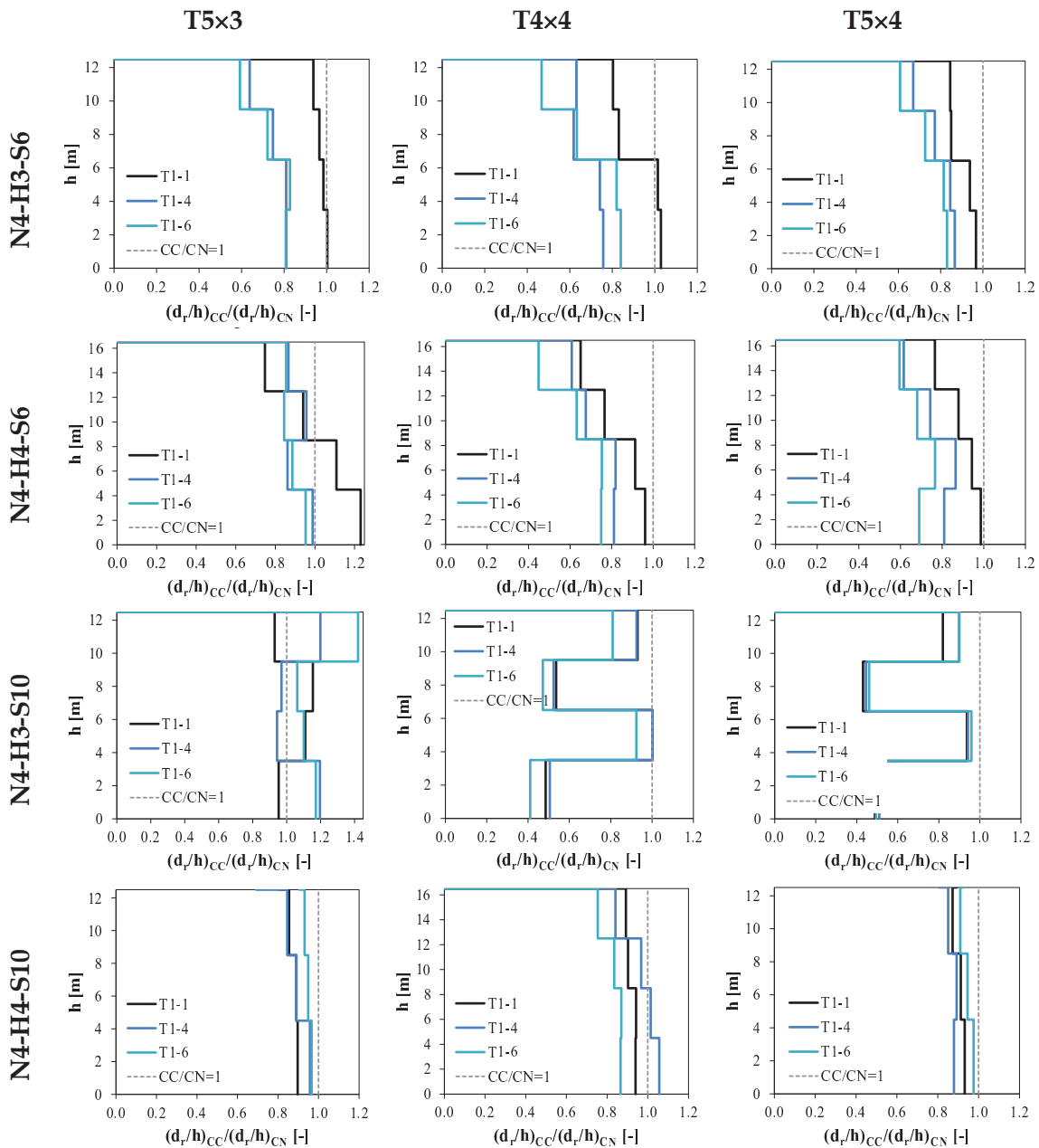


Figure 7.89: Ratios between maximum interstorey drifts of frames with claddings (CC) and bare steel frames (CN) under seismic action in the y direction in function of span, interstorey height and bay layout configuration

The results shown in Figure 7.86 and Figure 7.87 indicate that the adopted façade cladding system is capable in most cases of significantly reducing lateral drifts under seismic action. However, several cases of  $(d_r/h)_{CC} / (d_r/h)_{CN}$  ratio values above 1 are also reported, indicating that claddings may in some cases have an unfavourable effect on seismic performance.



The average and maximum  $(d_r/h)_{CC}/(d_r/h)_{CN}$  ratio values are summarised in Table 7.29, enabling to evaluate the influence of different structural features on this parameter.

Table 7.29: Average and maximum  $(d_r/h)_{CC}/(d_r/h)_{CN}$  ratio values

Storey	$(d_r/h)_{CC}/(d_r/h)_{CN}$ [-]															
	XZ MRF (Seismic action : X direction)								YZ MRF (Seismic action : Y direction)							
	N4-H3-S6		N4-H4-S6		N4-H3-S10		N4-H4-S10		N4-H3-S6		N4-H4-S6		N4-H3-S10		N4-H4-S10	
	Avg.	Max.	Avg.	Max.	Avg.	Max.	Avg.	Max.	Avg.	Max.	Avg.	Max.	Avg.	Max.	Avg.	Max.
1	0.75	0.87	0.82	1.19	0.89	0.99	1.04	1.45	0.88	1.03	0.91	1.23	0.69	1.20	0.94	1.06
2	0.75	0.90	0.83	1.21	0.87	0.94	1.01	1.29	0.87	1.01	0.88	1.11	0.99	1.11	0.92	1.01
3	0.70	0.88	0.72	1.09	0.87	0.93	0.95	1.22	0.76	0.97	0.79	0.96	0.67	1.15	0.89	0.97
4	0.61	0.80	0.61	0.82	0.83	1.04	0.92	1.08	0.69	0.94	0.68	0.87	0.98	1.42	0.83	0.93

The values shown in Table 7.29 show a general trend regarding the influence of the span variable. Indeed, for the 6m span frames, the average  $(d_r/h)_{CC}/(d_r/h)_{CN}$  ratio values range between 0.61 and 0.83 for seismic action along the  $x$  direction and between 0.68 and 0.91 for seismic action along the  $y$  direction, while for the 10m span frames average ratio values range between 0.83 and 1.04 for seismic action along the  $x$  direction and between 0.69 and 0.99 for seismic action along the  $y$  direction, indicating that the cladding system is more effective for the medium span structures.

Given the large differences in mass and stiffness between S6 and S10 structures, the natural vibration periods are used here to compare dynamic responses for these sets of frames. To this end, the ratios between the average natural vibration periods of the CC and CN frames for the 1<sup>st</sup> and 2<sup>nd</sup> modes are presented in Table 7.30, where lower ratio values are reported for the 6m span frames which indicate the stiffening effect to be more effective for 6m span frames.

Table 7.30: Ratio between average natural vibration periods of CC and CN frames for the 1<sup>st</sup> and 2<sup>nd</sup> modes

S	H	$T_{1,Avg,CC}/T_{1,Avg,CN}$	$T_{2,Avg,CC}/T_{2,Avg,CN}$
[m]	[m]	[-]	[-]
6	3	0.49	0.55
	4	0.46	0.47
10	3	0.66	0.70
	4	0.56	0.56

For the 10m span frames, the gain in stiffness due to the claddings does not compensate for the increase in mass, when comparing to 6m span frames (mass of S10 frames is approximately 2.8 times that of S6 frames). This leads the claddings in S10 frames to be less effective in reducing drift, as shown by the higher values of the  $((d_r/h)_{CC}/(d_r/h)_{CC})$  ratio seen in Table 7.29.

Results in Table 7.29 also show the effectiveness of claddings to be reduced for frames with larger interstorey height. For example, for the seismic action along the  $x$  direction, the obtained results show the 1<sup>st</sup> storey drift to be 10% and 17% higher on average for the H4-S6 and H4-S10 frames respectively, in comparison to corresponding H3 frames. This is due to lower stiffness contribution of the cladding system in relation to the overall system stiffness for the H4 frames, resulting from the higher stiffness of the bare steel H4 frames needed for verifying code drift limitation requirements.

As previously mentioned in this section, several cases of  $(d_r/h)_{CC}/(d_r/h)_{CC}$  ratio values above 1 are reported, implying the claddings can in some cases contribute to increase drifts, which is unfavourable for structural performance. Therefore, in order to determine how the stiffening effect of the cladding introduction influences the capacity to reduce interstorey drifts, the ratio between the 1<sup>st</sup> translational mode periods of CC and CN frames along the  $x$  and  $y$  directions, designated as  $T_{M1,CC}/T_{M1,CN}$  and  $T_{M2,CC}/T_{M2,CN}$ , respectively, were computed and compared to the most unfavourable interstorey drift reduction ratio, henceforth designated as  $\max[(d_r/h)_{CC}/(d_r/h)_{CC}]$ , as shown in Table 7.31.

Table 7.31: Comparison between 1<sup>st</sup> mode periods for CC and CN frames and maximum values of the interstorey drift ratio reduction due to cladding effect

MODEL				X DIRECTION				Y DIRECTION			
N	H	S	T	$T_{M1,CC}$	$T_{M1,CN}$	$T_{M1,CC}/T_{M1,CN}$	$\max[(d_r/h)_{CC}/(d_r/h)_{CN}]$	$T_{M2,CC}$	$T_{M2,CN}$	$T_{M2,CC}/T_{M2,CN}$	$\max[(d_r/h)_{CC}/(d_r/h)_{CN}]$
[-]	[m]	[m]	[-]	[s]	[s]	[-]	[-]	[s]	[s]	[-]	[-]
4	3	6	5x3	0.76	1.41	0.54	0.78	0.58	0.90	0.65	1.00
		6	4x4	0.70	1.55	0.45	0.90	0.64	0.95	0.68	1.03
		6	5x4	0.79	1.62	0.48	0.89	0.66	1.01	0.65	0.97
4	4	6	5x3	0.83	1.66	0.50	0.80	0.65	1.06	0.61	1.23
		6	4x4	0.76	1.88	0.41	1.21	0.73	1.17	0.62	0.96
		6	5x4	0.83	1.75	0.47	0.84	0.74	1.12	0.66	0.99
4	3	10	5x3	1.03	1.46	0.70	0.99	0.81	0.95	0.85	1.42
		10	4x4	0.96	1.52	0.63	1.04	0.86	0.98	0.88	1.00
		10	5x4	1.08	1.65	0.66	0.99	0.87	1.03	0.84	0.96
4	4	10	5x3	1.06	1.83	0.58	1.07	0.83	1.18	0.70	0.97
		10	4x4	0.95	1.81	0.53	1.45	0.92	1.18	0.78	1.06
		10	5x4	1.06	1.85	0.57	1.06	0.92	1.19	0.78	0.98

The values in Table 7.31 show that to lower values of the  $T_{Mn,CC}/T_{Mn,CN}$  ratio (where  $n$  is the vibration mode) generally correspond higher values of  $\max[(d_r/h)_{CC}/(d_r/h)_{CN}]$ , suggesting that if the stiffening effect of the claddings surpasses a given threshold, the higher seismic input energy results in larger drifts than those obtained for the bare steel frame (CN), implying claddings in such conditions have a negative effect on seismic performance.

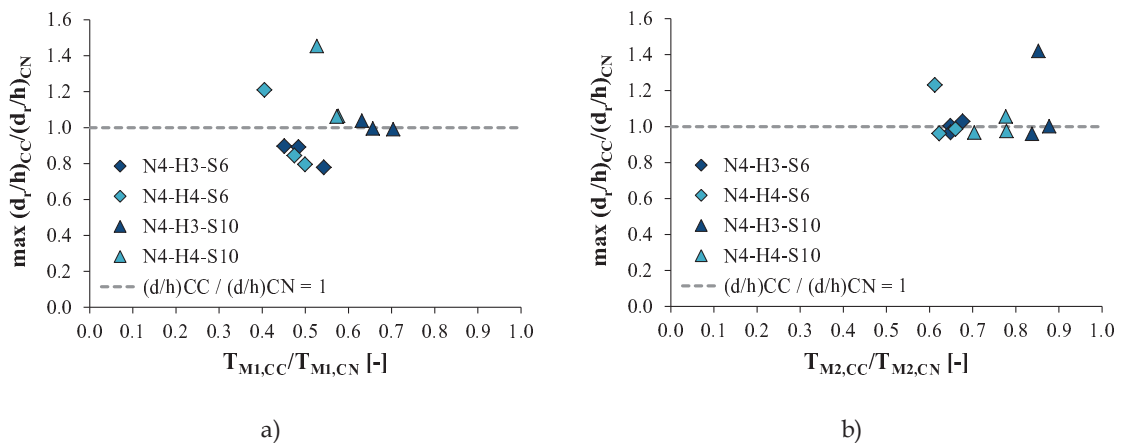


Figure 7.90: Comparison between 1<sup>st</sup> mode periods for CC and CN frames and maximum values of the interstorey drift ratio reduction due to cladding effect: a) in the x direction; b) in the y direction

This effect is graphically represented in Figure 7.90, where the results for seismic action along  $x$  are shown in Figure 7.90a) indicate that S6 frames with 1<sup>st</sup>

translational mode period reductions of over approximately 57% (i.e.  $T_{M1,CC}/T_{M1,CN} \approx 0.43$ ) have the maximum interstorey drift increased. Instead, for the S10 frames this threshold value is approximately equal to 33% (i.e.  $T_{M1,CC}/T_{M1,CN} \approx 0.67$ ).

This trend is also recognisable for the N4-H3-S6 and N4-H4-S6 frames in Figure 7.90b), where frames with translational mode period reductions of above 39% (i.e.  $T_{M2,CC}/T_{M2,CN} \approx 0.61$ ) sustain a significant interstorey drift increase. For the case of the S10 frames, this trend was not observed as clearly. Indeed a value of  $\max[(d_i/h)_{CC}/(d_i/h)_{CN}] = 1.42$  for  $T_{M2,CC}/T_{M2,CN} = 0.85$  was obtained for a N4-H3-S10 frame, which does not comply with the trend. It was subsequently verified that this value corresponds to a drift increase in the top storey, which is never the case for all other analysed cases, in which the most unfavourable ratio is obtained either for the segment between ground and 1<sup>st</sup> storey, or between the 2<sup>nd</sup> and 3<sup>rd</sup> storeys. This value therefore represents a singular case which does not necessarily invalidate the identified trend. Furthermore, considering that for the S10 frames in Figure 7.90b) the lowest value of  $T_{M2,CC}/T_{M2,CN}$  is 0.70, which is higher than the threshold identified for the S10 frames in Figure 7.90a) which is equal to  $T_{M1,CC}/T_{M1,CN} \approx 0.67$ , then it is possible that the range of  $T_{M2,CC}/T_{M2,CN}$  values does not reach sufficiently low values for the threshold to be recognised.

In this sense, further simulations using a cladding system with higher capacity that could lead to lower  $T_{Mn,CC}/T_{Mn,CN}$  ratio values would be required to test this hypothesis. While such tests fall outside the scope of the present thesis, they may be the subject of future studies devoted to investigating the role of non-structural façade elements on the lateral drift performance under seismic actions.

#### 7.3.2.4 Member forces

In this section the internal force distributions under seismic action in different structural members are evaluated, in order to determine the distribution of damage induced by the seismic action and its severity, hence enabling to determine whether design for post seismic column loss action requires local strengthening. The assessment is made by confronting internal forces and stresses from NDA with limit states that are computed considering average material properties, namely considering random material overstrength.

#### 7.3.2.4.1 Moment resisting frame beams

For the MRF beams, the maximum internal forces were evaluated, namely considering the bending moment - vertical shear interaction. Results were computed for each structural typology and for each accelerogram signal.

For what concerns shear forces, the NDA results showed the acting vertical shear forces in the MRF beams to be quite low, namely below  $0.5V_{pl,beam} \times \gamma_{ov}$  (i.e. half the plastic shear resistance of the beam cross section, accounting for material overstrength taken as 1.25) in all cases, implying the effect of shear on the moment resistance can be disregarded, as stated in EN 1993-1-1 (CEN, 2005).

The maximum bending moments in the MRF beams were computed for the beams of the different storeys and compared to the average yielding moment  $M_{y,m,beam}$ , which is computed on the basis of the nominal material yielding stress  $f_{y,nom}$  times the overstrength factor  $\gamma_{ov}=1.25$  prescribed in EN 1998-1 (CEN, 2004), in order to determine if the beam sections develop plasticity.

This comparison is presented in Figure 7.91a), showing  $M_{max}/M_{y,m,beam}$  ratio values lower than 1 for all cases, which are indicative that the MRF beam members remain elastic.

The maximum bending moment values were also compared to the column web panel yielding moment, accounting for material overstrength, as shown in Figure 7.91b). As it can be verified, also in this case the  $M_{max}/M_{y,m,cwp}$  ratio values are lower than 1, which imply that the column web panel remains elastic during the considered seismic action.

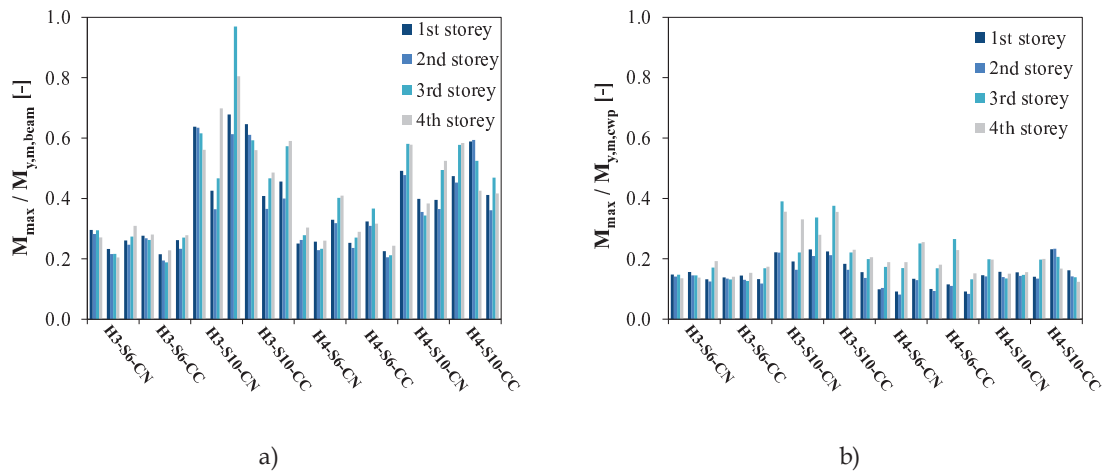


Figure 7.91: Comparison between maximum bending moments from NDA results and: a) beam section average yielding moment (accounting for material overstrength); b) column web panel yielding moment (accounting for material overstrength)

The fact that the MRF beams and column web panel remain elastic throughout the considered seismic action explains the zero residual drifts after the seismic action, as previously seen in Figure 7.74 and Figure 7.75.

The data presented in Figure 7.91 highlights the importance of considering aspects such as material overstrength or the contribution of the secondary structure to the seismic response of MRF structures in the sense that these factors contribute for the structures to remain in the elastic range.

#### 7.3.2.4.2 Moment resisting frame columns

The assessment of the columns of the MRFs was conducted through strength demand to capacity (*DCR*) ratios which account for the N-M-V internal force interaction. The capacity ( $DCR=1$ ) is defined here as the section reaching the yield stress in the first fiber.

It should be noted that while optimal design should lead to *DCR* ratios just below unity, in practice this is uncommon since frames are typically designed considering strong column blocks, each of several storeys, leading to the oversizing of profiles in the upper storeys of each block. Furthermore, drift criteria and capacity design rules lead to significant overstrength of the members, which are reflected on the strength *DCR*.

The strength ratios are presented in the format adopted by Naqash *et al.* (2012) in Figure 7.92 and Figure 7.93 for the 6m and 10m span frames, respectively, for both

the bare steel frames (CN case) and for the frames with façade claddings (CC frames). The *DCR* values correspond to the highest value for the envelope of the 3 accelerogram signals analysed in the simulations. Ratio values equal to 1 are indicative that the column section reached the yield stress (accounting for material overstrength) in at least one fiber.

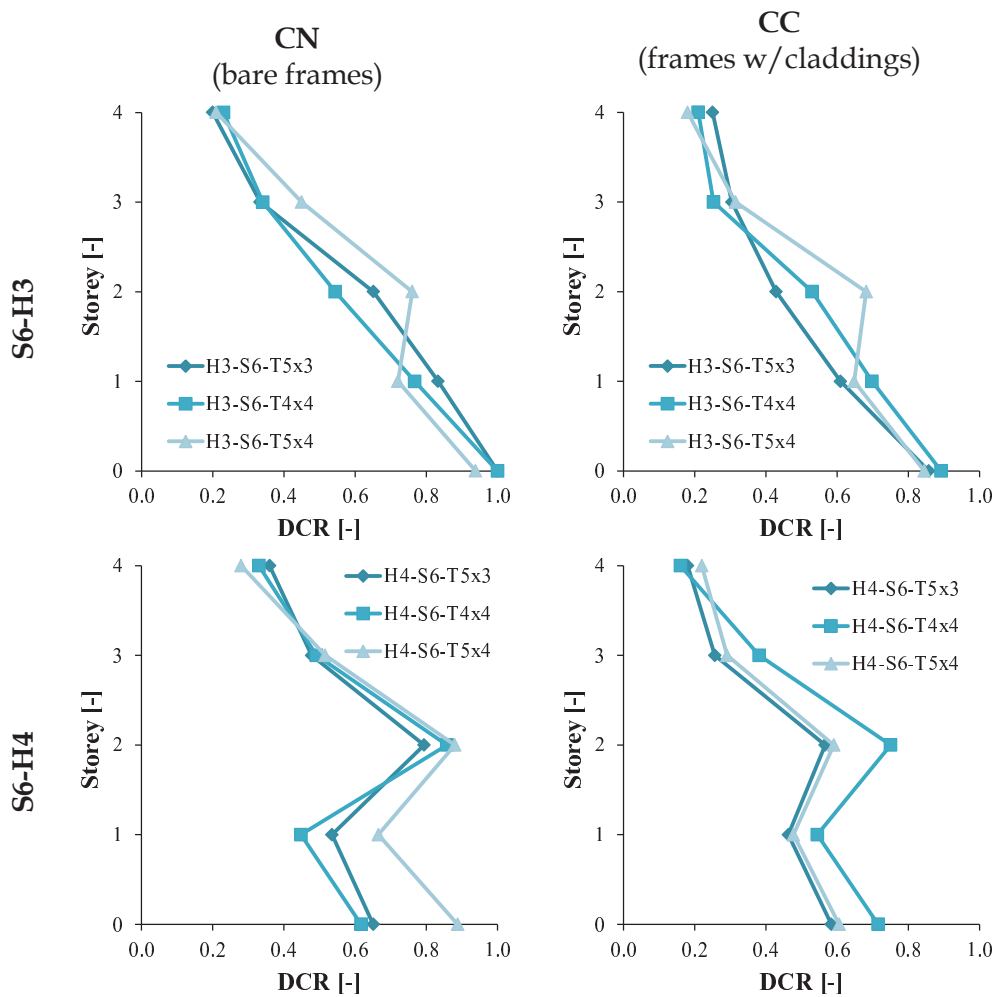


Figure 7.92: Moment resisting frame column maximum strength DCR for N4-S6 frames – variation with façade claddings and interstorey height

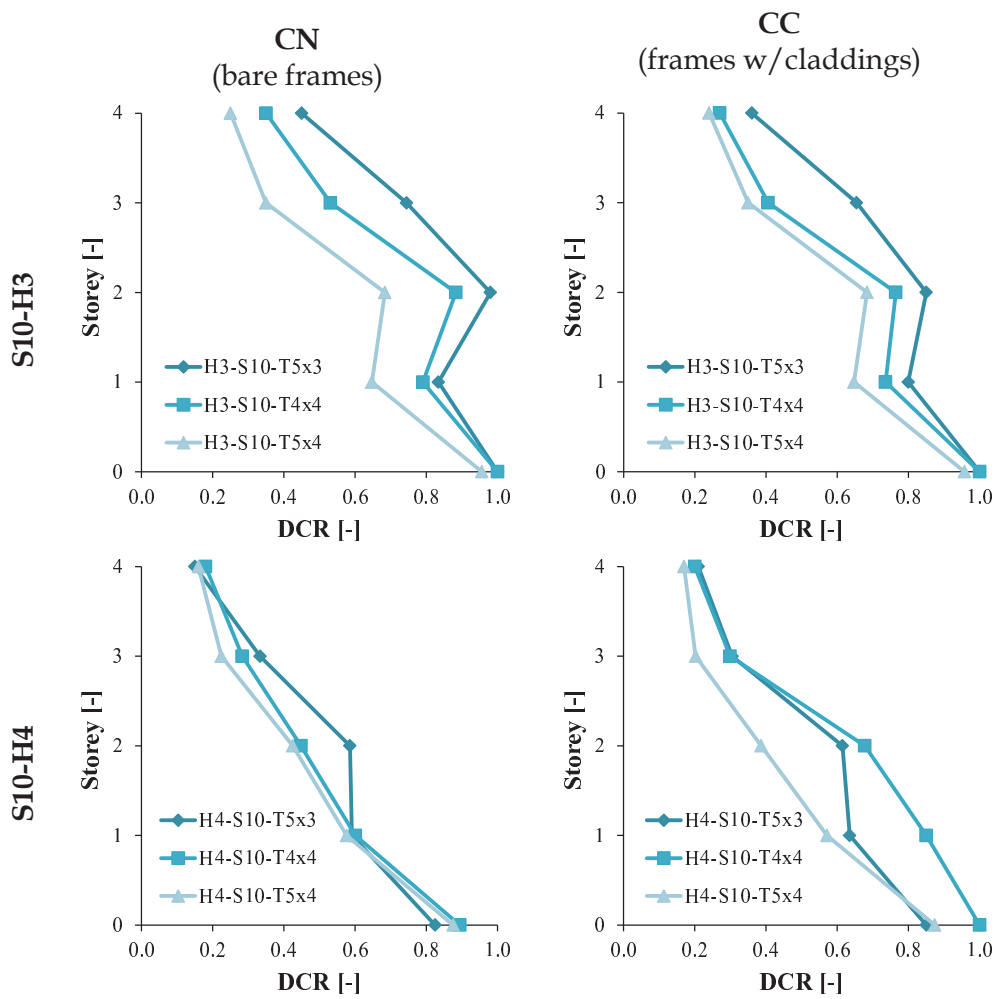


Figure 7.93: Moment resisting frame column maximum strength DCR for N4-S10 frames – variation with façade claddings and interstorey height

The results show *DCR* values to display significant variation along the height of the column, namely ranging approximately between 1 for the lower storey and 0.2 for the top storey. The column strong blocks can be identified by the increase in *DCR* values seen in many cases between the 2<sup>nd</sup> and the 3<sup>rd</sup> storeys, which translates the discontinuity in the lateral frame stiffness.

The comparison between CN and CC frames shows that the hardening effect induced by the introduction of the claddings can contribute to significantly increase the column strength *DCR* ratios. This effect is especially noticeable for the S6-H4 and S10-H4 frames with T4×4 bay layouts, for which the introduction of the façade claddings led to large shifts in the natural vibration periods, as evidenced by the lower  $T_{M1,CC}/T_{M1,CN}$  values shown in Table 7.31.



The obtained outcomes were confronted with results from a study on the seismic performance of steel MRF building structures conducted by Naqash *et al.* (2012). In this study, the behaviour of 3, 6 and 12 storey buildings, designed in accordance with EN 1998-1 (CEN, 2004) in ductility class DCH, assuming type C soil, importance class II and a type 1 design response spectrum characterised by 0.25g peak ground acceleration, is analysed. These seismic design assumptions are exactly the same as those considered for the present thesis (see section 3.3.3.5), thus rendering this result comparison significant. Despite the fact that no 4-storey structure was analysed by Naqash *et al.* (2012), the outcomes from the 6- and 3-storey frames provide a range of column *DCR* values with which to confront results from the present study. In terms of fundamental vibration period, modal analysis results showed values of 1.92s and 0.99s for the 6-storey and 3-storey frames, respectively, which compare to values averaging 1.5s for comparable 4-storey frames (see Table 7.25). The column strength *DCR* results from Naqash *et al.* (2012) are presented in Figure 7.94.

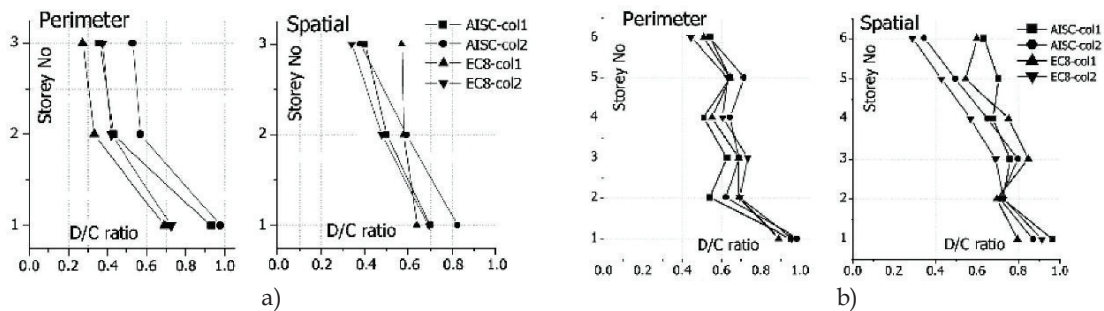


Figure 7.94: Moment resisting frame column strength *DCR* ratios from Naqash *et al.* (2012) for: a) 3-storey frames; b) 6-storey frames

The values obtained in the present study (see Figure 7.92 and Figure 7.93) are similar to those from the Naqash *et al.* (2012) study in Figure 7.94, displaying ratio values close to 1 at the ground storey level, which tend to decrease along the column height up to *DCR* values of approximately 0.3.

While this shows that for the analysed cases the MRF columns of DCH class moment frames remain elastic under the considered seismic action (i.e.  $DCR < 1$ ), it also indicates that in several cases these members develop plasticity at the ground level due to the high bending moments, which is admissible according to the expected plastic hinge distribution. The high levels of internal forces in the columns are also a consequence of the absence of damage in the beams, owing to factors explicitly

considered in this thesis such as material overstrength or the secondary “gravity” frame elements contribution. The occurrence of damage would in fact lead to an increase in the structure’s fundamental period, reducing the seismic input energy and internal forces.

### 7.3.2.4.3 Claddings

In this section, the maximum strength demand in the claddings is evaluated during the seismic action and during the subsequent column loss. To this end, the cladding member force time-histories were used to determine the maximum strength demand. In Figure 7.95, two examples of force time-histories responses are presented, highlighting the differences in cladding response.

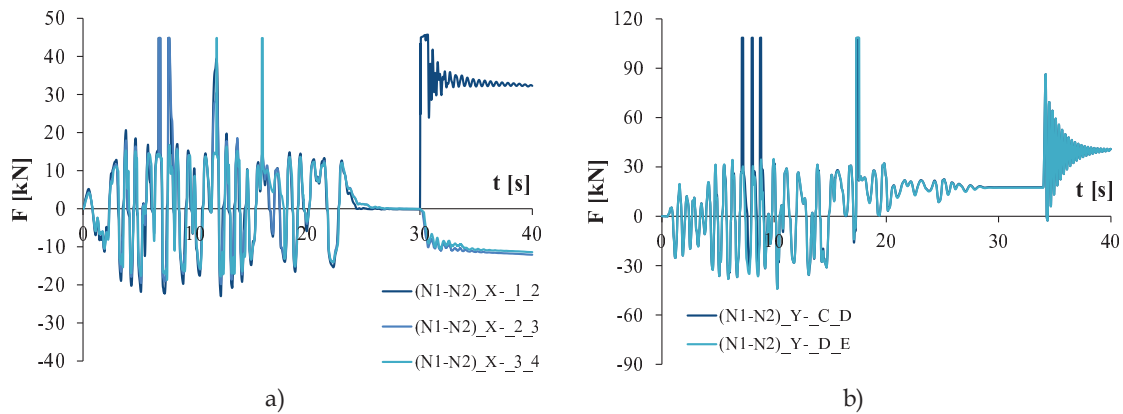


Figure 7.95: Cladding force time history for panels between storeys 1 and 2: a) N4-H3-S10-CC-T5×3-DE-LC case under T1-1 seismic action along y; b) N4-H4-S10-CC-T5×4-DE-LL case under T1-4 seismic action along x

In Figure 7.95a), the cladding force time-history of the N4-H3-S10-CC-T5×3-DE frame is presented, for the T1-1 seismic action followed by a corner column loss. The results show that during the seismic action, the claddings yield for very small time intervals, typically lower than 0.15s, due to the nature of the seismic action which is characterised by rapid displacement reversals. Instead, during the column loss stage, the corner cladding panel (represented in Figure 7.95a) by the  $(N1\_N2)\_X\_-1\_2$  curve) is seen to reach the yielding force and to sustain it for a larger time interval, namely of approximately 1s, dissipating the DAZ kinetic energy and contributing to limit the maximum dynamic displacement  $u_{dyn,max,damaged}$ . Indeed, for this particular case, the adoption of claddings was effective in reducing the rotational demand, as shown previously in Figure 7.66b), where results showed a  $\phi_{CM/C}/\phi_{CN}$  ratio value of 0.37.

Instead, when comparing the initially undamaged (I.U.) to the post-seismic (P.S.) response to column loss, the seismic action induced damage is seen to slightly increase  $u_{dyn,max,damaged}$  by approximately 3%, as seen by the  $\phi_{maxPS}/\phi_{IU}$  value in Table 7.33. This is ascribable to the irreversible small elongation of the diagonal members sustained during the seismic action, which reduces the vertical stiffness of the DAZ and contributes to increase the vertical momentum.

In Figure 7.95b), a different example is presented, namely the N4-H4-S10-CC-T5×4-DE-LL case under T1-4 seismic action along  $x$ , followed by an XZ façade column loss. Also in this case, the force time-history series shows panel yielding being reached for time intervals shorter than 0.3s, resulting in a slight increase of  $u_{dyn,max,damaged}$  by approximately 2%, as seen by the  $\phi_{maxPS}/\phi_{IU}$  value in Table 7.32. Under column loss (i.e. for  $t \geq 34s$ ), the force-time response is seen to equal for both the DAZ panels (i.e. for the  $(N1\_N2)\_Y\_C\_D$  and  $(N1\_N2)\_Y\_D\_E$  curves) and characterised by a significant degree of elastic recovery. Indeed, for this case, the force at the final equilibrium condition is approximately half the maximum force reported after the column removal.

In order to evaluate the distribution of plasticity throughout the cladding elements during the seismic and column loss actions, the ratios between the maximum force in the equivalent diagonal bracing member of the cladding and the corresponding yielding force factored by the overstrength factor  $\gamma_{ov}$  are computed.

Three different situations are analysed, namely: i) the highest strength demand in any cladding under seismic action [ $F_{max,seismic}/(F_y\gamma_{ov})$ ]; ii) the highest strength demand in a Directly Affected Zone cladding under seismic action [ $F_{max,DAZ,seismic}/(F_y\gamma_{ov})$ ]; iii) the highest strength demand in a Directly Affected Zone cladding under the post-seismic column loss [ $F_{max,DAZ,col.loss}/(F_y\gamma_{ov})$ ]. The results regarding the seismic action demand, the DAZ seismic action demand and the DAZ column loss demand are presented in Figure 7.96, Figure 7.97 and Figure 7.98, respectively, for seismic actions along both the  $x$  and  $y$  directions.

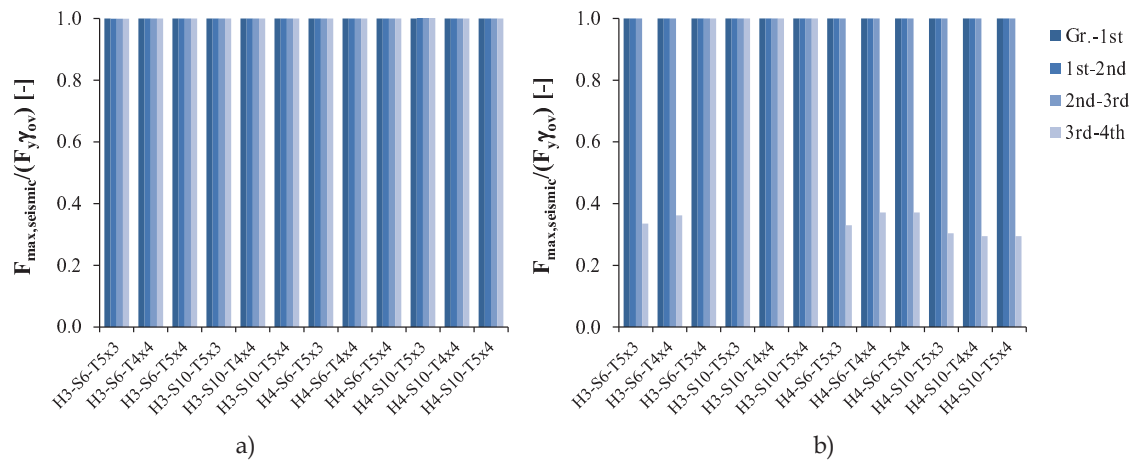


Figure 7.96: Maximum force demand in the cladding ties under seismic action, normalised to the cladding yield force accounting for overstrength: a) seismic action along x; a) seismic action along y

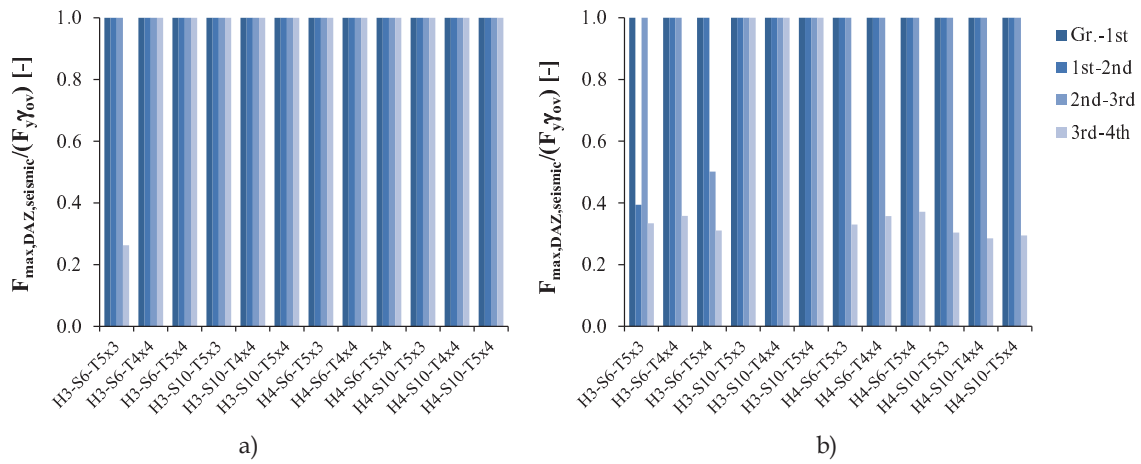


Figure 7.97: Maximum force demand in the DAZ cladding ties under seismic action, normalised to the cladding yield force accounting for overstrength: a) seismic action along x; a) seismic action along y

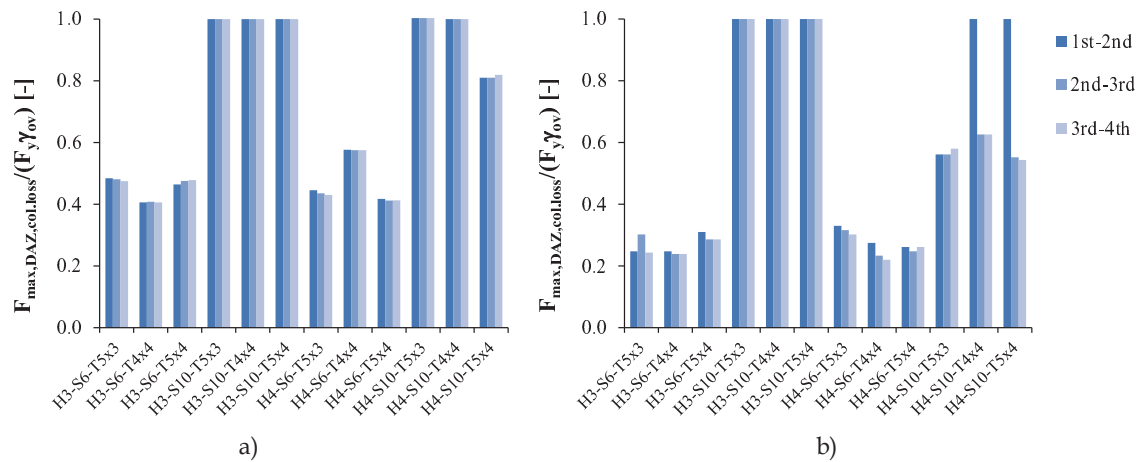


Figure 7.98: Maximum force demand in the DAZ cladding ties under post seismic column loss, normalised to the cladding yield force accounting for overstrength: a) seismic action along x; a) seismic action along y

The results in Figure 7.96 show that for the most unfavourable of the considered accelerograms, the façade claddings generally reach the yielding capacity, albeit for small time intervals, resulting in small plastic elongations of the bracing members, as seen above. For the seismic action along the  $x$  direction, the cladding panels for all the analysed structures and for all storeys are seen to reach the yielding force; for the case of the seismic action along the  $y$  direction, the same occurs for all storeys for the panels between the 3<sup>rd</sup> and 4<sup>th</sup> storeys, which is due to the slight difference in terms of the margins of safety (see Section 4.3.2) between the XZ and the YZ moment resisting frames.

While the façade claddings are seen to yield in general, it is also important to analyse the strength demand in the panels appertaining to the DAZ in particular. This is because it is those panels that will influence the most the post seismic column loss response. The results for the DAZ seismic action demand presented in Figure 7.97 are seen to be in line with the results in Figure 7.96, namely indicating that DAZ panel elements generally yield under seismic action. This is because the storeys display diaphragm behaviour and hence the interstorey drift produces the same effect on all façade panels.

Finally, the DAZ claddings post seismic column loss response is shown in Figure 7.98 to reach the yielding force for the 10m span frames, whereas for structures with 6m span, the maximum force in the tie elements is typically below 50% of the panel yielding force. This implies that medium span frames, for which the MRF members tend to remain elastic, cannot take advantage of the kinetic energy dissipation capacity of the claddings via yielding. Instead, the long span systems are seen to be capable of activating the cladding bracings in tension. However, as shown for the case in Figure 7.95a), the small bracing elongations sustained during the seismic action limit the efficacy of these elements in reducing the maximum dynamic displacement, as seen in more detail in the next Section.

#### 7.3.2.5 Post seismic robustness variation

The amount of damage induced by the seismic action to the analysed frames was also evaluated by comparing the differences in terms of vertical displacement time-history (TH) responses between initially undamaged (IU) and post seismic (PS)

column loss cases. This comparison was performed for all 4-storey frames (N4 cases) for the façade (LL) and corner column loss (LC) cases.

The obtained results indicate in general that the seismic action does not introduce significant variations to the maximum dynamic vertical displacements under the subsequent column loss action, as a consequence of the small damage levels introduced by the seismic action, as reported in Section 7.3.2.4. Two examples of this are presented in Figure 7.99, where the frame in Figure 7.99a) is characterised by a predominantly elastic response to column loss ( $DOP_{DAZ} \approx 0.5$ ), while the frame in Figure 7.99b) is characterised by a predominantly plastic response to column loss ( $DOP_{DAZ} \approx 1.0$ )

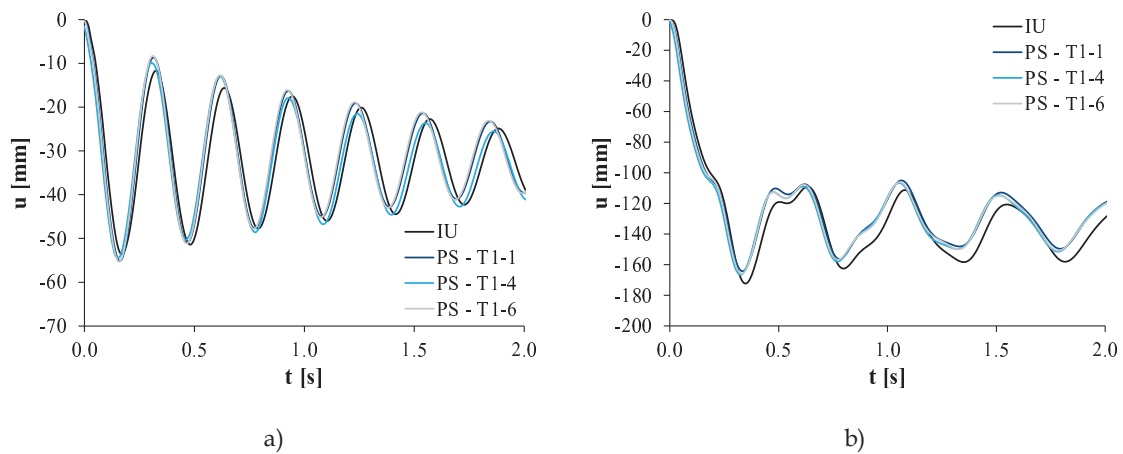


Figure 7.99: Vertical displacement time history comparison between initially undamaged (IU) and post seismic (PS) column loss: a) façade column loss for the N4-H3-S6-CN-T5x4-DE frame; b) corner column loss for the N4-H4-S10-CN-T5x3-DE frame

As seen in Figure 7.99 for both façade and corner removals, there is no significant difference between the column loss response for the initially undamaged frame (IU) and for the post seismic (PS) cases. Small differences can be attributed to fluctuations in the initial vertical position of the control node at the time of the column removal (i.e. after the cyclic action) and to very small residual velocities at the instant of column removal.

A summary of the differences between the IU and PS column loss responses is presented in Table 7.32 and Table 7.33 for the façade (LL) and corner (LC) column loss cases, respectively.

Table 7.32: Maximum chord rotations under façade column loss (LL case) – comparison between initially undamaged (IU) and post seismic (PS) scenarios

MODEL LIST						LL COLUMN LOSS - MAX. CHORD ROTATION						
N	H	S	C	T	D	IU	PS <sub>T1-1</sub>	PS <sub>T1-4</sub>	PS <sub>T1-6</sub>	max{PS}	max{PS} - IU	max{PS} / IU
[-]	[m]	[m]	[-]	[-]	[-]	$\phi_{dyn,max,IU}$ [mrad]	$\phi_{dyn,max}$ [mrad]	$\phi_{dyn,max}$ [mrad]	$\phi_{dyn,max}$ [mrad]	$\phi_{dyn,max,PS}$ [mrad]	$\phi_{maxPS}-\phi_{IU}$ [mrad]	$\phi_{maxPS}/\phi_{IU}$ [-]
3	6	N	4x4	E	5x3	10.7	11.1	11.1	11.0	11.1	0.40	1.04
					4x4	5.9	6.0	6.3	6.0	6.3	0.46	1.08
					5x4	8.9	9.2	9.0	9.2	9.2	0.28	1.03
	C	5x3	3.8	3.8	4.2	4.5	4.5	0.72	1.19			
		4x4	2.8	3.6	3.3	3.6	3.6	0.77	1.28			
		5x4	3.6	4.5	3.8	4.3	4.5	0.90	1.25			
4	10	N	4x4	E	5x3	FAIL	FAIL	FAIL	FAIL	N.A.	N.A.	N.A.
					4x4	14.7	14.9	14.7	14.8	14.9	0.21	1.01
					5x4	22.2	22.2	22.7	23.1	23.1	0.87	1.04
	C	5x3	28.9	29.2	28.0	28.0	29.2	0.27	1.01			
		4x4	12.8	12.6	12.9	12.7	12.9	0.11	1.01			
		5x4	16.1	15.6	15.5	16.5	16.5	0.45	1.03			
4	6	N	4x4	E	5x3	9.1	6.6	9.4	9.2	9.4	0.27	1.03
					4x4	6.4	6.5	6.7	6.7	6.7	0.35	1.06
					5x4	6.5	10.5	10.6	10.6	10.6	4.07	1.63
	C	5x3	3.6	3.7	3.6	3.5	3.7	0.14	1.04			
		4x4	3.1	3.8	3.6	3.8	3.8	0.73	1.24			
		5x4	3.1	3.1	3.4	3.3	3.4	0.33	1.11			
10	N	4x4	E	5x3	32.4	32.1	32.2	32.2	32.2	-0.13	1.00	
				4x4	10.8	10.9	10.8	10.9	10.9	0.12	1.01	
				5x4	14.2	14.2	14.2	14.2	14.2	0.05	1.00	
	C	5x3	12.2	11.9	11.8	11.7	11.9	-0.35	0.97			
		4x4	8.1	12.5	12.4	12.4	12.5	4.49	1.56			
		5x4	9.2	9.1	9.3	9.1	9.3	0.14	1.02			

Table 7.33: Maximum chord rotations under corner column loss (LC case) – comparison between initially undamaged (IU) and post seismic (PS) scenarios

MODEL LIST						LC COLUMN LOSS - MAX. CHORD ROTATION						
N	H	S	C	T	D	IU	PS <sub>T1-1</sub>	PS <sub>T1-4</sub>	PS <sub>T1-6</sub>	max{PS}	max{PS} - IU	max{PS} / IU
						$\phi_{dyn,max,IU}$ [mrad]	$\phi_{dyn,max}$ [mrad]	$\phi_{dyn,max}$ [mrad]	$\phi_{dyn,max}$ [mrad]	$\phi_{dyn,max,PS}$ [mrad]	$\phi_{maxPS}-\phi_{IU}$ [mrad]	$\phi_{maxPS}/\phi_{IU}$ [-]
3	6	N	4x4	E	5x3	5.8	5.8	5.0	5.4	5.4	0.04	1.01
						7.6	7.1	7.1	7.5	7.5	-0.16	0.98
						6.8	6.2	6.7	6.5	6.5	-0.10	0.99
	C	4x4	E	5x3	1.0	1.2	1.1	1.2	1.2	0.21	1.21	
					1.2	1.1	1.1	1.0	1.1	-0.10	0.92	
					1.0	1.0	1.0	1.2	1.2	0.20	1.20	
4	10	N	4x4	E	5x3	42.5	41.2	41.4	41.3	41.4	-1.06	0.98
						FAIL	FAIL	FAIL	FAIL	N.A.	N.A.	N.A.
						50.2	54.1	53.6	54.2	54.2	4.03	1.08
	C	4x4	E	5x3	15.6	16.1	15.7	15.9	16.1	0.52	1.03	
					17.6	16.9	17.0	16.9	17.0	-0.56	0.97	
					17.2	16.6	16.8	16.7	16.8	-0.41	0.98	
4	6	N	4x4	E	5x3	4.2	4.3	3.9	3.9	4.3	0.10	1.02
						5.9	5.2	5.4	5.7	5.7	-0.26	0.96
						3.8	3.5	3.7	3.9	3.9	0.11	1.03
	C	4x4	E	5x3	2.0	2.1	2.1	2.2	2.2	0.21	1.10	
					0.9	0.7	0.8	1.0	1.0	0.02	1.03	
					0.9	0.9	0.7	1.1	1.1	0.23	1.26	
10	N	4x4	E	5x3	17.2	17.3	16.7	16.6	17.3	0.07	1.00	
					26.7	27.0	25.7	25.6	27.0	0.28	1.01	
					15.4	14.5	14.7	14.6	14.7	-0.66	0.96	
	C	4x4	E	5x3	6.2	5.5	9.9	5.8	9.9	3.73	1.60	
					7.0	7.1	6.6	7.0	7.1	0.14	1.02	
					6.3	6.4	6.3	6.5	6.5	0.24	1.04	

The results for the façade column loss presented in Table 7.32 and Table 7.33 highlight that the differences in terms of maximum chord rotation of the DAZ are small for the majority of cases, as indicated by the  $(\phi_{maxPS}-\phi_{IU})$  values, which are lower than 1mrad ( $\approx 0.06^\circ$ ) in 19 out of the 23 analysed LL cases and in 20 out of the 23 analysed LC cases, considering non collapsed cases only (the N4-H3-S10-CN-T5x3-DE-LL and N4-H3-S10-CN-T4x4-DE-LC cases collapsed following column loss both for IU and PS scenarios).

The results for the façade column loss show that CC frames with 6m spans tend to display higher values of  $(\phi_{maxPS}/\phi_{IU})$  in comparison to CN frames. For example, for the case of the N4-H3-S6 frames, the CC frames displayed an average  $(\phi_{maxPS}/\phi_{IU})$  ratio value of 1.24 (owing to column yielding at ground level), while the corresponding CN frames displayed an value of 1.05 for the LL scenario. This can also be recognised for the corner column loss cases and it is attributable to the introduction of damage to the façade claddings' CFS steel bracings during the seismic action, which yield and for



which very small plastic elongations in the DAZ zone result in a subsequent higher rotation demand for collapse arrest following the column loss.

It should be noted that the axial force time histories of the cladding elements showed that in most cases the CFS bracings yielding occurs in very small time intervals ( $\Delta t \leq 0.02s$ ), which implies that residual plastic deformation is very limited and which explains why despite the fact that CFS yielding occurs in most cases, the post seismic rotation demand is generally not higher than that for the initially undamaged structural configuration.

In the N4-H4-S6-CN-T5×4-DE-LL case, the  $(\phi_{\max PS} - \phi_{IU})$  value of 4.07mrad, corresponding to a high  $(\phi_{\max PS} / \phi_{IU})$  ratio value of 1.63 is also related to the yielding of the CFS elements in the façades (see Section 7.3.2.4.3). In this way residual plastic deformation in the CFS elements led to higher post seismic rotation demand, which however did not translate to global structural residual drifts, since all column segments remained elastic, retaining therefore their elastic restitution force which pushes the structure back to its original position.

In the N4-H4-S10-CC-T4×4-DE-LL case, a difference between the IU and the maximum PS rotation demand of  $(\phi_{\max PS} - \phi_{IU}) = 4.49\text{mrad}$  ( $\approx 0.26^\circ$ ) is reported. This larger difference too is attributable, as stated above, to the damage sustained by the façade claddings in the DAZ during the seismic action, which is sufficiently low to not result in a residual drift of the building at the end of the seismic action.

A larger difference in terms of  $(\phi_{\max PS} / \phi_{IU})$  ratio was also verified for the N4-H4-S10-CC-T5×3-DE-LC case. In this case also, the difference in post seismic rotation demand is due to damage sustained by the CFS bracings of the façade elements of the DAZ during the seismic action, which resulted in a ratio value of  $\phi_{\max PS} / \phi_{IU} = 1.60$ , which nonetheless corresponds to a small difference in rotation demand of 3.73mrad ( $\approx 0.21^\circ$ ) which does not affect the overall system robustness.

The rotation demand ratios  $(\phi_{\max PS} / \phi_{IU})$  are also presented in a chart format in Figure 7.100.

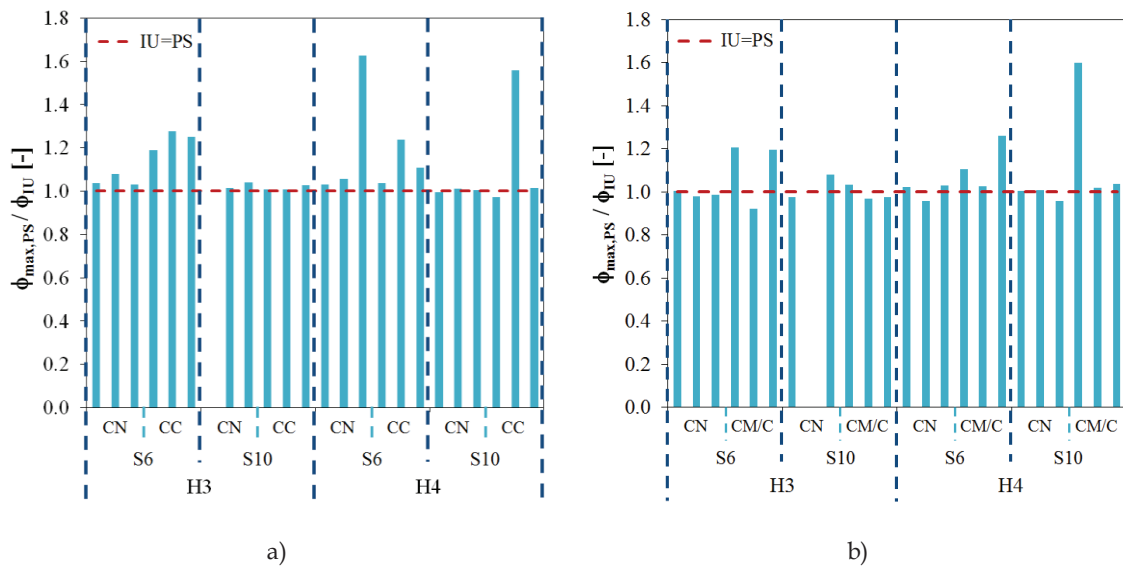


Figure 7.100: Chord rotational demand ratios between initially undamaged (IU) and post seismic (PS) scenarios: a) façade column loss (LL); b) corner column loss (LC)

As recognisable in Figure 7.100, the reported differences in terms of rotation demand between the IU and the PS scenarios are very low, with ratio values being close to 1 for nearly all cases. Furthermore, all IU structures that arrested the progressive collapse also arrested the collapse in the PS scenarios, while structures that collapsed for the IU case (N4-H3-S10-CN-T5×3-DE-LL and N4-H3-S10-CN-T4×4-DE-LC) also collapsed also for all PS scenarios, as expected.

Given the low damage levels or absence of damage introduced by the seismic action, the numerical results point to the fact that for the analysed frames, the post seismic robustness is therefore virtually the same as the robustness for the initially undamaged structure.

This further implies that evaluation and design for progressive collapse resistance in post seismic scenarios can be made considering the initially undamaged structure properties. To that aim, a discussion of the design methodology currently provided in EN 1991-1-7 (CEN, 2006) is presented in Section 7.4.1 and a new methodology for addressing progressive collapse based on the structural system’s proneness to progressive collapse is presented in Section 7.4.2.

## 7.4 Consequences for design

### 7.4.1 Current design methodology

The EN 1991-1-7 (CEN, 2006) states that structures must be designed for relevant accidental situations. The strategies proposed to address this issue are based on the type of accidental action, where a distinction is made between identified and unidentified accidental actions.

In the case of actions that cannot be foreseen or characterised, the EN 1991-1-7 proposes strategies based on limiting the extent of the localised failure (see Figure 7.101) which “*may provide adequate robustness against accidental actions ... or any other action resulting from an unspecified cause*”.

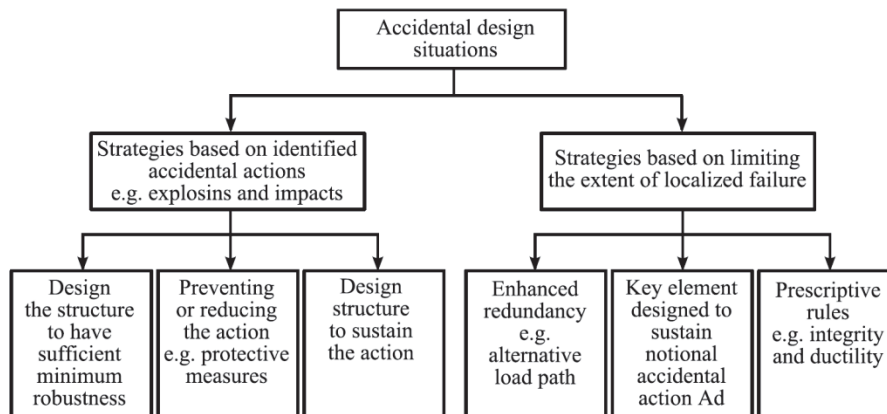


Figure 7.101: EN 1991-1-7 strategies for accidental design situations (CEN, 2006)

In order to limit the extent of the localised failure, one or more of the proposed strategies may be adopted and the EN 1991-1-7 states that “*the National Annex may state which of the approaches...are to be considered for various structures*”. However, the National Annexes to the EN 1991-1-7 are not currently available and the EN 1991-1-7 currently provides no guidance regarding how to apply the aforementioned strategies based on structural typologies.

In alternative, the EN 1991-1-7 states in Section 3.4 that “*strategies for accidental design situations may be based on ... consequence classes*” which reflect consequences in terms of loss of human life and of economic, social and environmental losses. In Annex A of the EN 1991-1-7, recommended strategies to address disproportionate collapse are provided, based on the building’s consequence class, which in turn depends on occupancy type, number of storeys and area.

## ***7.4.2 New performance based progressive collapse methodology proposal***

### *7.4.2.1 Comparison to current methodology*

The EN 1991-1-7 guidelines are intended to provide structures with sufficient robustness in order to avoid disproportionate collapse, hence limiting loss of human life based on expected occupancy.

However these guidelines do not provide a methodology aimed at preventing progressive collapse, i.e. aimed at limiting the spread of structural collapse from the initial failure of one or few localised elements. The limitation of the spread of the initial damage, typically verified using a scenario independent approach consisting of an instantaneous notional column removal, effectively ensures that structures are capable of redistributing load through alternative loadpaths, bridging over the removed element without sustaining further damage and therefore limiting further loss of human life other than that potentially caused by the initiating event.

It is the opinion of the Author and the current trend of recent robustness codes that designing structures for avoiding progressive collapse is preferable, first and foremost, since loss of human life is limited. This also allows for structures to retain structural integrity and a residual load bearing capacity after the accidental action, enabling users to safely evacuate the damaged structure, in consonance with the EN 1998-1 (CEN, 2004) fundamental performance requirements for structures in seismic areas.

The current methodology provided in the EN 1991-1-7, by not requiring that structures be checked for stability following notional column removal for buildings in Consequence Class 2a (CC2a) for example, cannot therefore ensure that progressive collapse will not occur. Indeed, for CC2a class structures, the code requires horizontal tying only, which should enhance robustness, although no quantification of its effect on robustness is provided. These tying requirements derive from regulations dating back to the 1970's and given that no extensive experimental campaign was since conducted to improve them, the present requirements may not be sufficient for arresting progressive collapse. By not requiring an alternative loadpath analysis for CC2a structures, the EN 1991-1-7 cannot therefore ensure that progressive collapse is averted and therefore loss of human life remains implicitly possible.

Considering now that the examples for Consequence Class 2a buildings provided in Table A.1 of the EN 1991-1-7 typically consist of residential and office buildings not exceeding 4 storeys, these structural typologies are therefore only designed with horizontal tying requirements. However, as shown in this Chapter, low rise frames are susceptible to progressive collapse since the number of resisting elements in the DAZ is lower, especially for the case of long span frames with small interstorey height.

This example serves to illustrate that the EN 1991-1-7 disproportionate collapse based methodology, which factors occupancy, area and expected loss of human life, requires less strict and non-quantitative detailing requirements for low rise buildings, classifying them in the lower risk group Consequence Class 2a, which is actually shown in this study for the MRF typology to be more susceptible to progressive collapse, namely for long span systems. Conversely, taller buildings up to 15 storeys are classified according to the EN 1991-1-7 in the upper risk group Consequence Class 2b, since a disproportionate collapse could involve more storeys, leading to greater loss of life. Instead, results from the present study show taller buildings to be less prone to progressive collapse owing to the higher number of resisting members in the DAZ.

#### *7.4.2.2 Description of the methodology*

The new proposed methodology proposed is based not on disproportionate collapse but on avoiding progressive collapse, which implicitly averts disproportionate collapse as well. The methodology is centred on the proneness of certain structural typologies to progressive collapse, as evaluated by the ductility Demand-to-Capacity Ratios  $DRC_{ductility,ij}$  of the different structural elements obtained from numerical simulations presented in this study.

The methodology is presented in the form of a proposal for the revision of the EN 1991-1-7 in Appendix C, which is not by any means intended to be exhaustive, but simply to provide a draft for a possible alternative methodology for minimising the possibility of occurrence of a progressive collapse for MRF structures. A rationalisation for the design rules is presented in Appendix D.

The flow chart for the application of the proposed methodology is presented in Figure 7.102.

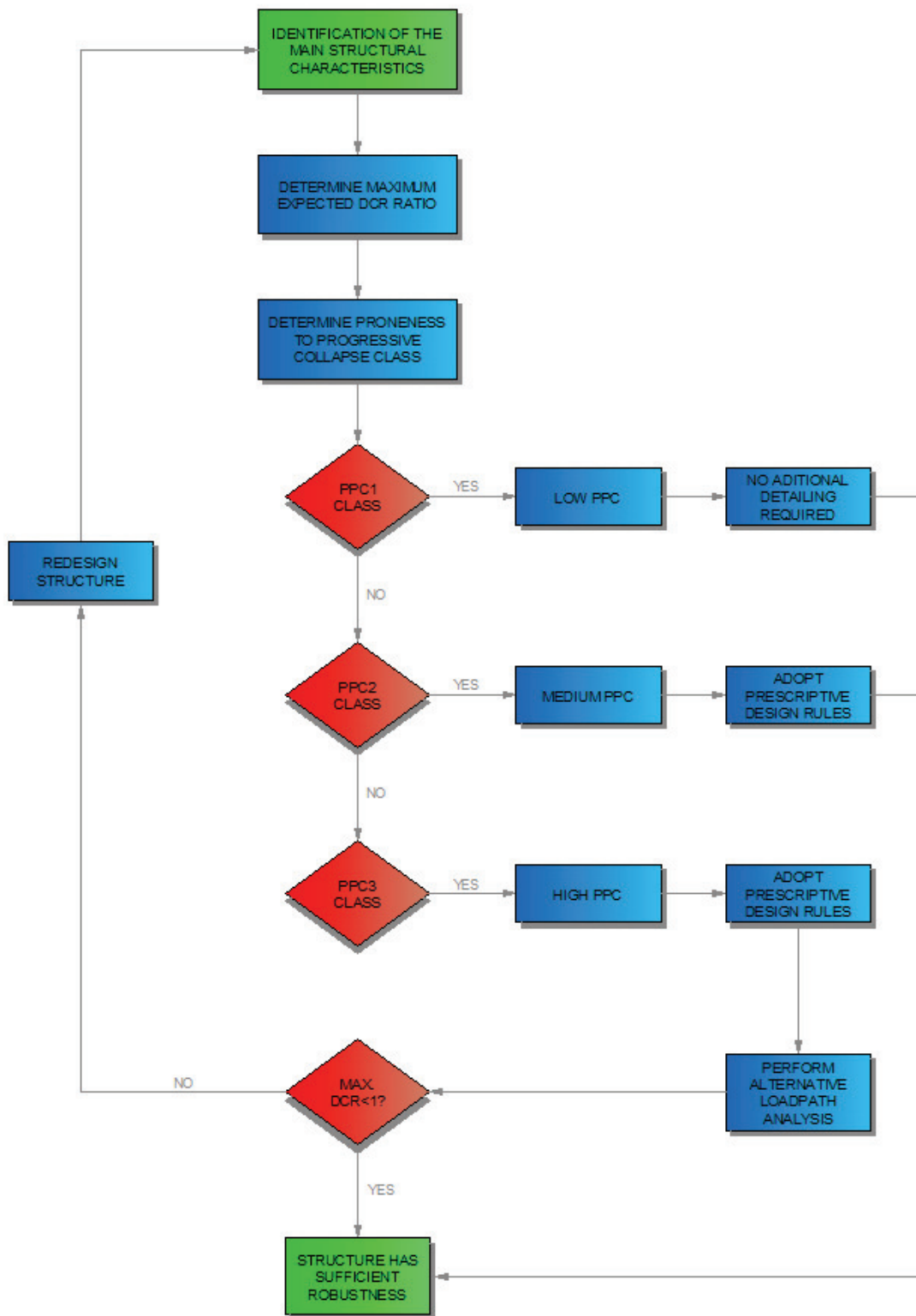


Figure 7.102: Proposed methodology flow chart

#### 7.4.2.2.1 Maximum Demand-to-Capacity Ratio

The first step of the proposed method consists on determining the maximum expected  $DCR_{ductility,ij}$  ratio based on the frame's main characteristics. This can be done using Table 7.34, in which the maximum DCR values correspond to those presented in Table 7.19.

Table 7.34: Maximum expected ductility Demand-to-Capacity ratios and chord rotation demands by structural typology

Bracing system	Number of storeys	Span	Interstorey Height	Maximum expected $DCR_{ductility,ij}$	Maximum expected chord rotation	Typology #
[-]	[-]	[m]	[m]	[-]	[mrad]	[-]
Moment Frame - full strength rigid joints (equal $x$ and $y$ spans)	4	6	3	0.22	11	T1
			4	0.19	9	T2
		10	3	1.00	$\infty$ (collapse)	T3
			4	0.68	64	T4
	8	6	3	0.10	7	T5
			4	0.08	5	T6
		10	3	0.39	18	T7
			4	0.30	11	T8

Since the present study is devoted only to MRF structures, limited data is available for the application of this methodology and engineering judgment should be used when extrapolating to structural configurations with different characteristics. Alternatively, it is possible to continue to design for disproportionate collapse according to the methodology described in the current version of the EN 1991-1-7.

Further research on structural response under column loss can easily be incorporated using this methodology by adjusting the expected DCR values as more tests are performed and as the degree of certainty regarding values increases, but also to progressively introduce information regarding structures with different bracing systems and structural configurations.

#### 7.4.2.2.2 Proneness to Progressive Collapse (PPC) classification

Upon determining the maximum expected DRC value, structures are classified into one of three classes, namely PPC1, PPC2 and PPC3, corresponding to structures

with low, medium and high proneness to progressive collapse, respectively, according to the classification system presented in Table 7.35.

Table 7.35: Proposed methodology – classification of the proneness of structures to progressive collapse

Maximum ductility DCR ratio $DCR_{ductility,ij,max}$ [-]	Proneness to Progressive Collapse (PPC)	PPC Class
0.0 - 0.3	Low	PPC1
0.3 - 0.7	Medium	PPC2
0.7 - 1.0	High	PPC3

The adopted proneness classification system while simple, enables to take into account the reserve ductility of structures with regard to progressive collapse. The proposed interval values for  $DCR_{ductility,ij,max}$  were selected according to the obtained results for MRF type structures.

In this sense, medium span (S6) structures were found to present  $DCR_{ductility,ij,max}$  ratios not exceeding 0.22 (see Table 7.34), implying that the proposed upper  $DCR_{ductility,ij,max}$  limit for Class PPC1 frames (i.e.  $DCR=0.3$ ) would translate the low proneness to progressive collapse displayed by these structures.

The numerical results also show the N4-S10-H3 typology (low number of storeys coupled with long span and low interstorey height) to be exceptionally prone to progressive collapse, with several cases of collapse having been reported in the simulations. The proposed  $DCR_{ductility,ij,max}$  limits were also designed to take this factor into account. Indeed, since no collapses were reported for the N4-S10-H4 frames, which displayed a maximum  $DCR_{ductility,ij,max}$  ratio of 0.68 (see Table 7.34), a minimum  $DCR_{ductility,ij,max}$  value of 0.7 was proposed for the PPC3 class, in order to translate the fact that N4-S10-H4 frames are not highly prone to collapse, contrarily to the N4-S10-H3 frames.

Finally, the proposed  $DCR_{ductility,ij,max}$  value range for class PPC2 is intended to encompass structures that are not highly prone to progressive collapse but which display intermediate  $DCR$  ratio values in some structural elements and for which the global structural system stands to benefit significantly in terms of robustness by adopting simple detailing rules.



The fact that structural typologies characterised by  $DCR_{ductility,ij,max}$  ratio values equal to 0.7 (i.e. with a 30% ductility margin to progressive collapse) can be classified as highly prone to collapse is due to the fact that the results for the computation of the DCR ratios do not take into account factors such as design/construction errors, loss of member capacity due to corrosion or insufficient maintenance, more severe damage scenarios and other factors that might contribute to reduce robustness.

#### 7.4.2.2.3 Recommended strategies for arresting progressive collapse

Similarly to the EN 1991-1-7 Consequence Class based methodology, the strategies to avoid progressive collapse are recommended on the basis of the PPC class, as presented in Table 7.36. In cases of structural typologies with low low proneness to collapse ( $DCR_{ductility,ij,max} < 0.3$ ), no additional detailing is considered to be necessary since the structure is considered to have sufficient ductility reserve under column loss. For structural typologies with medium proneness to collapse, the adoption of prescriptive detailing rules is recommended in order to improve robustness. Finally, for structural typologies that are highly prone to progressive collapse, the adoption of the detailing rules for PPC2 class is recommended in order to compensate for the low robustness of the structural typology in question. Furthermore, for PPC3 class building structures and in line with the recommended strategies for buildings in Consequence Class 2b (Upper Risk Group), Alternative Loadpath Analysis is required to ensure that progressive collapse is arrested, minimizing human and economical costs.

The recommended strategies are summarised in Table 7.36.

Table 7.36: Proposed methodology – recommended strategies for preventing progressive collapse

PPC Class	Recommended strategies
PPC1	Adopt recommended strategies for disproportionate collapse in Annex A of the EN 1991-1-7; No additional robustness detailing required.
PPC2	In addition to recommended strategies for class PPC1, adopt prescriptive robustness detailing rules.
PPC3	In addition to recommended strategies for class PPC2, perform Alternative Loadpath Analysis.

#### 7.4.2.2.4 Prescriptive robustness detailing rules

Prescriptive robustness detailing rules are provided independently for each type of structural typology, based on the maximum expected DCR ratios for the different structural elements. In this sense, detailing rules are recommended only for structural elements characterised by medium/high DCR ratios.

The fact that these measures are prescriptive, i.e. that no quantification of the robustness enhancement is provided, is deemed suitable since these detailing rules apply to structural typologies that are not highly prone to progressive collapse. In cases of structures that are highly prone to collapse, a deterministic method for robustness assessment is applied, namely using alternative loadpath analysis.

It is the opinion of the Author, based on personal experience in structural design, that the implementation of these detailing rules has negligible impacts in terms of construction cost and fabrication time and can easily be implemented at the design stage, contributing to significantly increase global structural robustness.

The sets of improved detailing rules to be adopted for each structural typology are presented in Table 7.37.

As seen in Table 7.37, the sets of detailing rules to be adopted differ according to the typology, where more sets of detailing rules are required for typologies with structural elements with higher DCR ratio values.

Each set of detailing rules is aimed at improving the robustness of one type of structural elements. It should be noted that the proposed sets of prescriptive detailing rules for improved robustness regard only façade column loss scenarios.

As previously stated, a more complete justification for each of the proposed detailing rules is presented in Appendix D.

Table 7.37: Prescriptive detailing rules for improved robustness by structural typology

Typology #	Sets of prescriptive detailing rules for improved robustness
T1	-
T2	-
T3	DR1, DR2, DR3
T4	DR1, DR2, DR3
T5	-
T6	-
T7	DR1
T8	DR1

### **Detailing Rules DR1 – Rules for steel moment resisting frame elements in facades**

#### DR 1.1 - Bolted beam-to-column joints:

- DR 1.1.1 An additional internal bolt row aligned with the beam section centroid should be introduced (see Figure 7.103).
- DR 1.1.2 The bolts for the additional bolt row should be of the same steel grade or higher than that adopted in other bolt rows of the same joint.
- DR 1.1.3 The nominal diameter of additional row bolts shall not be lower than the maximum diameter of the other bolts in the same joint, and if possible, should be larger in order to achieve higher resistance to column loss action.
- DR 1.1.4 The bolt assembly type to be used in the additional bolt row should have a failure mode characterised by bolt shank necking (e.g. SB bolts, HR bolts) in order to retain strength while arresting the progressive collapse. Bolt assemblies characterised by thread stripping failure (e.g. HV bolts)

should be avoided, unless proven to remain elastic for the maximum rotational joint demand under the most unfavourable column loss scenario.

DR 1.1.5 The welds between the beam flange and the end-plate and between the beam web and the end-plate should be full penetration welds (see Figure 7.104), executed in shop for quality assurance purposes.

DR 1.1.6 The adoption of joint configurations with stiffened extended end-plate or with beam haunches is considered to improve joint behaviour in bending. For structural typologies in which the moment resisting frame members are prone to remain elastic under column loss, these joint configurations may lead to improved joint response. For structural typologies that require large joint rotations to arrest collapse, there is not sufficient evidence that these joint configurations improve joint response.

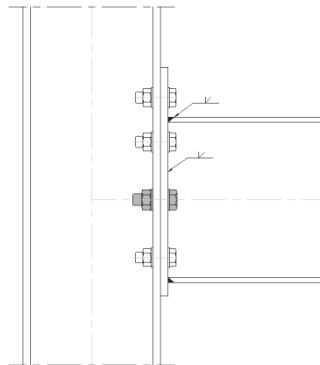


Figure 7.103: Bolted beam-to-column joints detailing rules – additional bolt row and beam-endplate weldings

DR 1.2 - Welded beam-to-column joints:

DR 1.2.1 The welds between the beam flange and the column and between the beam web and the column should be full penetration welds, executed in shop for quality assurance purposes.

DR 1.2.2 The adoption of joint configurations with stiffeners or haunches is considered to improve joint behaviour in bending. For structural

typologies in which the moment resisting frame members are prone to remain elastic under column loss, these joint configurations may lead to improved joint response. For structural typologies that require large joint rotations to arrest collapse, there is not sufficient evidence that these joint configurations improve joint response.

### Detailing Rules DR2 – Rules for secondary steel frame elements

The rules for the secondary frame elements apply to members and connections located on the DAZ for all possible façade column loss scenarios. These zones are shown in Figure 7.104 for 3 examples of plan layouts of MRF structures.

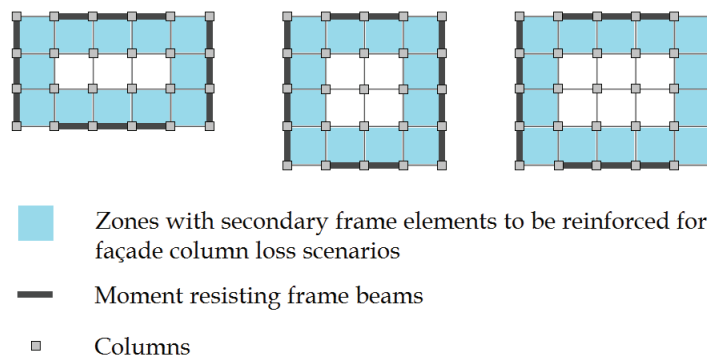


Figure 7.104: Plan view examples of zones to which to apply DR2 rules for secondary elements

#### DR 2.1 – General rules for beam-to-column and beam-to-beam joints:

- DR 2.1.1 Beam-to-column and beam-to beam joints should be designed to be semi-rigid, according to the stiffness classification provided in Section 5.5.2 of the EN 1993-1-8, in order to reduce the maximum rotational demand under column loss.
- DR 2.1.2 The selected joint typology should be capable of sustaining chord rotations under column loss action in excess of the predicted maximum demand for the structural typology in question. An estimation of the maximum predicted rotations is presented in Table 7.34.

DR 2.1.3 The selected joint typology should be able to accommodate the maximum rotation imposed by the moment resisting frame elements. In seismic zones, joints should be capable of sustaining cyclic bending actions of up to 40 mrad chord rotation.

DR 2.2 – Specific rules for flush end-plate joints:

DR 2.2.1 The welds between the beam flange and the end-plate and between the beam web and the end-plate should be full penetration welds, executed in shop for quality assurance purposes.

DR 2.2.2 When using flush end-plate joints, end-plate thickness should be selected so as to maximise joint robustness. This can be achieved by adopting the end-plate thickness range which induces failure mode 2, according to the design criteria expressed in Eq.(6.11) and Eq.(6.13). This criteria is also suitable for structures in seismic zones, in which joints are subjected to cyclic bending, since it contributes to avoid premature weld fracture.

DR 2.2.3 The adoption of thick endplates, namely leading to T-stub failure mode 3 (see EN 1993-1-8) should be avoided, since it leads to reduced joint ductility.

DR 2.2.4 An additional internal bolt row aligned with the beam section centroid should be introduced to improve the transmission of tensile axial force in the joint. Alternatively two additional internal bolt rows may be introduced, the centroid of which should be aligned with the beam section centroid.

DR 2.2.5 The bolts for the additional row(s) should be of the same steel grade or higher than that adopted in other bolt rows of the same joint.

DR 2.2.6 The nominal diameter of additional row bolts shall not be lower than the maximum diameter of the other bolts in the same joint, and if possible should be larger, in order to achieve higher resistance to column loss action.

- DR 2.2.7 Joints should preferably be designed using bolt assemblies with nominal diameters greater than 16mm, in order to maximise joint capacity at higher rotational demand.
- DR 2.2.8 The bolt assembly type to be used in the additional row bolts should have a failure mode characterised by bolt shank necking (e.g. SB bolts, HR bolts) in order to retain strength while arresting the progressive collapse. Bolt assemblies characterised by thread stripping failure (e.g. HV bolts) should be avoided, unless it can be demonstrated that the moment resisting frame elements alone are sufficient to arrest the progressive collapse for all column loss scenarios.

### **Detailing Rules DR3 – Rules for façade claddings**

The use of cladding elements in façades may contribute to reduce vertical displacements in the directly affected zone following a column loss, hence reducing the probability of occurrence of a progressive collapse.

#### *DR 3.1 – General rules for façade claddings:*

- DR 3.1.1 The adoption of cladding panels for robustness enhancement purposes is subjected to architectural constraints and requires authorisation from the Architectural designer, for which reason it is not mandatory.
- DR 3.1.2 The introduction of discontinuities or the partial adoption of cladding panels in a building façade (see Figure 7.105) should be avoided since it may lead to lateral force imbalance under some column loss scenarios, unless demonstrated otherwise.

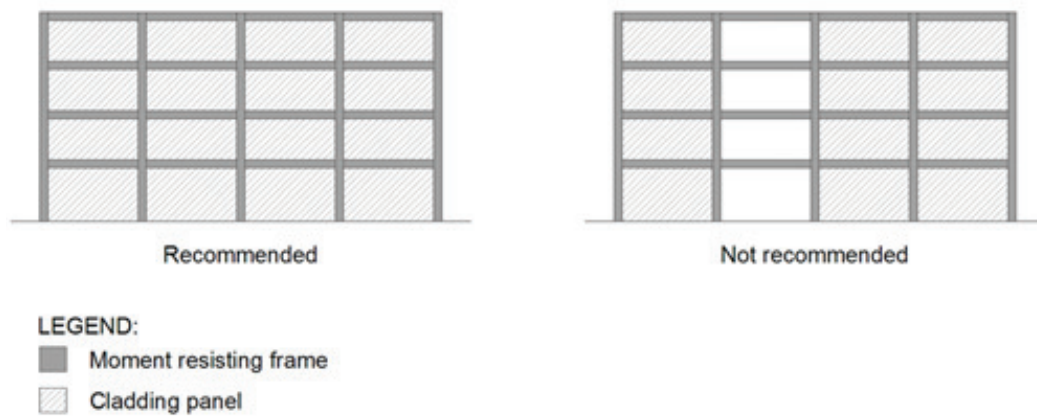


Figure 7.105: Cladding panel disposition in a façade

- DR 3.1.3 The adopted cladding panel solution should be able to transfer loads across corners through a truss system composed of single or multiple struts and/or ties.
- DR 3.1.4 For cladding panels composed of linear resisting elements (e.g. claddings with steel bracings), load redistribution following column loss should be achieved via a cladding truss mechanism that is symmetric about the removed column in the directly affected zone, in accordance with the recommendations shown in Figure 7.106.



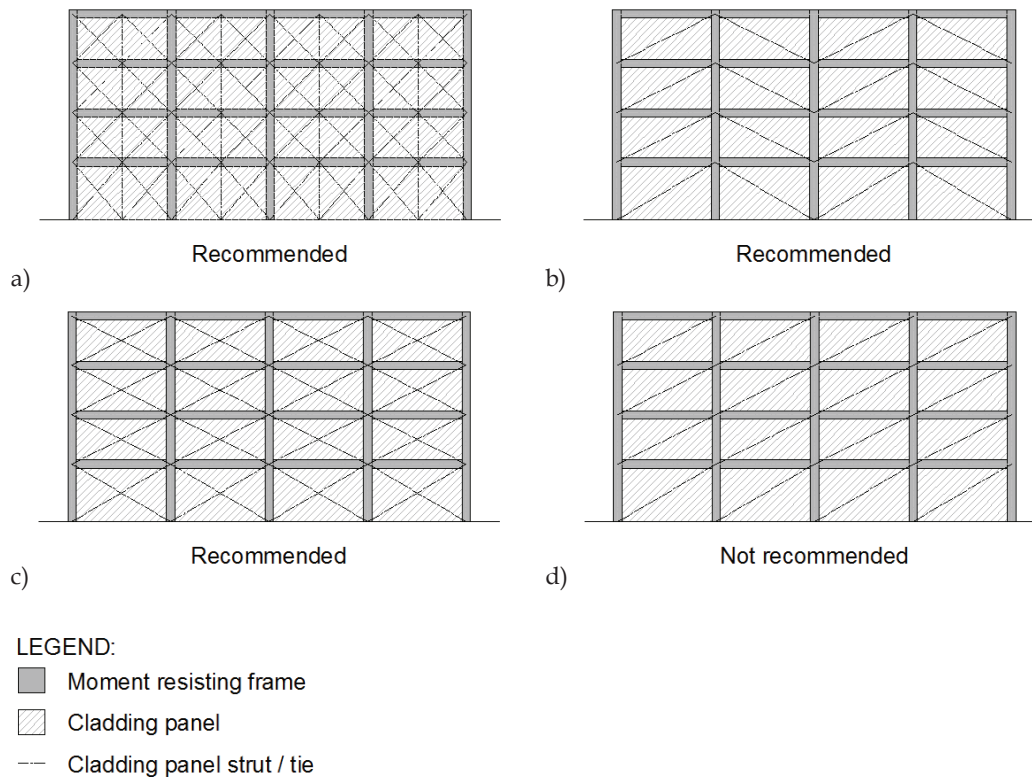


Figure 7.106: Cladding panel strut/tie system

- DR 3.1.5 For infilled panels (e.g. masonry panels), the load transfer may be achieved via the compressive struts that are mobilised upon column loss. The presence of openings may reduce the stiffness of the panel and alter the load redistribution following column loss. Panels with openings are therefore not recommended to be adopted for progressive collapse prevention, unless demonstrated to be effective.
- DR 3.1.6 In cases of infilled panels with openings, a physical gap between the infill element and the surrounding steel frame may be adopted, enabling to disconnect the cladding from the frame as shown in Figure 7.107. The dimension of the gap should be designed to accommodate the allowable interstorey drift.

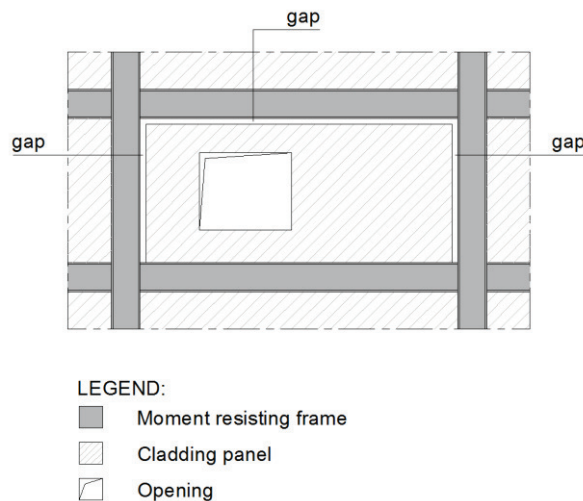


Figure 7.107: Gap between frame and infilled panel with opening

DR 3.2 – Rules for façade claddings in non seismic zones:

- DR 3.2.1 In non seismic zones, both infilled and strut/tie truss claddings systems may be adopted. Although this measure is not mandatory, its adoption is likely to enhance structural robustness and in some cases help prevent progressive collapse following column loss.
- DR 3.2.2 Strut/tie truss claddings systems, namely consisting of “X” bracings of the same material of the frame, are more likely to provide a higher reduction of displacements following column loss and are therefore considered preferable in general.
- DR 3.2.3 Infilled masonry claddings panels tend to be moderately effective for low rise and for short/medium span structural typologies and may therefore be adopted for such building typologies. For medium-rise long-span systems, masonry claddings have reduced effect on robustness and non-infilled solutions are preferable.
- DR 3.2.4 For buildings with infilled façade walls (e.g. masonry), no gaps are allowed between adjacent cladding panels nor between the cladding panels and the surrounding steel elements of the moment resisting frame.
- DR 3.2.5 Buildings with dry assembled façade wall systems can incorporate bracing systems (e.g. steel bracings) into the façade claddings that make

up a strut/tie truss system according to the recommended typologies (see Figure 7.106), hence creating alternative loadpaths and improving structural redundancy and load re-distribution capacity.

- DR 3.2.6 The members that make up the cladding strut/tie truss should, whenever possible, be designed for the additional accidental loads, accounting for dynamic effects, which can be conservatively accounted for using by a Dynamic Load Factor (DLF) equal to 2.0. Smaller DLF values may be adopted whenever properly justified.
- DR 3.2.7 The connections of the members that make up the cladding strut/tie truss should be designed to have sufficient overstrength so that potential yielding is limited to the members. This may be achieved by designing connections according to the design rule for non-dissipative connections indicated in Section 6.5.5(3) of EN 1998-1.
- DR 3.2.8 The members and connections of the strut/tie truss system should be designed to remain elastic (i.e. to sustain no permanent damage) for all characteristic load combinations. Damage is acceptable under the accidental load combinations (i.e. under column loss action).

DR 3.3 – Rules for façade claddings in seismic zones:

- DR 3.3.1 In seismic zones, the adoption of claddings systems, when not explicitly taken into account for structural design, may introduce changes both in terms of strength and energy dissipation to the resisting structure under seismic actions. For this reason, these elements must be classified and consequently designed as primary or as secondary seismic elements, in accordance with EN 1998-1.
- DR 3.3.2 Cladding systems with infilled panels should be designed according to the rules provided in EN 1998-1.
- DR 3.3.3 Cladding systems with strut/tie trusses (e.g. steel bracings) may be designed either as primary or as secondary seismic elements, in accordance with EN 1998-1. If the total contribution to the lateral stiffness of all secondary seismic members including claddings does not exceed 15% of that of all primary seismic members (see Section 4.2.2(4))

of the EN 1998-1), then claddings can be designed as secondary seismic elements. Otherwise claddings should be designed as primary seismic members.

DR 3.3.4 Cladding systems with strut/tie trusses classified as secondary seismic members are not required to be explicitly modelled for seismic design. Under seismic action, these elements are expected to sustain some level of damage, which may reduce compression strut capacity. It is therefore recommended to adopt cladding panels with “X” bracing configurations (see Figure 7.106a,c) that can mobilise ties under post-seismic column loss scenarios.

DR 3.3.5 Cladding systems with strut/tie trusses classified as primary seismic members are required to be explicitly modelled in the structural analysis and detailed for earthquake resistance in accordance with the rules provided in EN 1998-1.

DR 3.3.6 The members that make up the cladding strut/tie truss should, whenever possible, be designed for the additional accidental loads, accounting for dynamic effects, which can be conservatively accounted for using by a Dynamic Load Factor (DLF) equal to 2.0. Smaller DLF values may be adopted whenever properly justified.

DR 3.3.7 The connections of the members that make up the cladding strut/tie truss should be designed to have sufficient overstrength so that potential yielding is limited the members. This may be achieved by designing connections according to the design rule for non-dissipative connections indicated in Section 6.5.5(3) of EN 1998-1.

DR 3.3.8 The members and connections of the strut/tie truss system should be designed to remain elastic (i.e. to sustain no permanent damage) for all characteristic load combinations. Damage is acceptable under the accidental load combinations (i.e. under seismic and column loss actions).

The above indicated sets of prescriptive detailing rules are to be adopted for buildings structures in classes PPC2 and PPC3, as indicated in Table 7.36. However, due to their higher proneness to progressive collapse (PPC), buildings in PPC3 class are required in a first step to adopt the proposed design rules so as to enhance robustness, while in a second step the structure is analysed by means of Alternative Loadpath Analysis (ALA), to justify that the structure can arrest progressive collapse.

#### 7.4.2.2.5 Alternative Loadpath Analysis

The analysis of alternative loadpaths in a structure may be conducted according to different analysis procedures, namely via LSP, NSP or NDP, which subsequently require component classification, definition of component strength and deformation capacities, modelling, analysis and confrontation with acceptance criteria. Such a complete procedure is available in the US, namely the UFC 2009 (United States of America Department of Defense, 2013), which provides component modelling criteria, load increase factors (for LSP), dynamic increase factors (for NSP) and acceptance criteria.

Instead, in Europe, no similar procedure is currently available and the EN 1991-1-7 (CEN, 2006) only mentions ALA in the following sentence “*the building should be checked to ensure that upon the notional removal of each supporting column and each beam supporting a column, or any nominal section of load-bearing wall as defined in A.7 (one at a time in each storey of the building) the building remains stable and that any local damage does not exceed a certain limit.*”. The preparation of guidance on methods for conducting ALA is specifically mentioned as one of main priorities for the revision of robustness provisions in the Eurocodes (Centre for the Protection of National Infrastructure, 2011).

The creation of a complete ALA procedure for the European space would require a large experimental campaign to establish component modelling and acceptance criteria under column loss actions, accounting for construction components and construction technologies used in Europe and which are known to differ from US ones. Some data from the present study, namely semi-rigid flush end-plate joint response under column loss, may provide a modest contribution to the establishment of component modelling and acceptance criteria.

Due to these reasons, no complete set of indications on how to conduct ALA can currently be provided to designers. It therefore clearly falls outside the scope of the

present thesis to provide such a set of indications. Some comments resulting from the analysis conducted in this these can however be made, regarding the complexity, result accuracy and practical aspects of conducting Alternative Loadpath Analysis in structural design offices.

The different types of different analysis methods have been presented by different authors (National Institute of Standards and Technology, 2007; Centre for the Protection of National Infrastructure, 2011), which describe also their advantages, complexity and requirements. The adoption of a nonlinear static procedure combined with the Energy Balance method (Izzudin *et al.*, 2008) to assess the maximum dynamic response under column loss is considered to strike a fair balance between result accuracy and analysis requirements.

In Chapter 4, such a procedure was adopted and a comparison with nonlinear dynamic analysis results (see Section 4.4.2.4) for a set of 144 cases showed that for the analysed cases, the combined procedure provided a safe-side estimation of the maximum dynamic displacements, overestimating displacements by 21% on average, while identifying all cases of structural collapse reported by nonlinear dynamic analysis.

The combined pushdown + energy balance procedure therefore presents the following advantages:

- Its allows the ALA to be conducted using static analysis, which is well known to structural engineers;
- It does not require the estimation of a Dynamic Increase Factor (DIF) to account for dynamic effects;
- It does not rely on an the accuracy of an estimated Load Increase Factor (LIF), as is the case when using linear elastic analysis;
- The Energy Balance method can be implemented in a spreadsheet using simple and intuitive concepts;
- It is more computationally efficient that nonlinear dynamic procedures;
- It can be conducted on any finite element software capable of performing nonlinear static analysis, which available in most design offices;

- It does not require structural engineers with a higher level of expertise to perform complex and time consuming nonlinear dynamic analysis;
- Results are easier to interpret and verify.

For the abovementioned reasons, it is therefore possible say that the combined methodology constitutes a simple but effective means of conducting ALA. The validity of the application of the combined method should however be further investigated, namely for different structural typologies.

The following clauses are not intended to provide an exhaustive methodology regarding how to conduct ALA. Other deterministic or quantitative methodologies are available and may potentially provide more accurate results. These recommendations are intended to provide a simple methodology, which is believed to strike a fair balance between result accuracy and required computational time and expertise. The proposed methodology can easily be implemented by designers, allowing them to account for dynamic amplification effects and geometrical and material nonlinearity.

### **Alternative Loadpath Analysis**

#### Generalities:

In this section, a set of guidelines is provided for conducting Alternative Loadpath Analysis (ALA) in order to verify if a building structure is capable of arresting progressive collapse originating from an unspecified cause.

The indicated procedure is based on a Nonlinear Static Procedure combined with the Energy Balance method. It should be noted that ALA may be conducted using alternative analysis procedures, based on solid engineering mechanical and dynamic principles. The results of these alternative procedures shall be reviewed by an independent third-party engineer.

#### Component classification:

All structural elements and components are required to be classified by the designer either primary or secondary. All elements and components that contribute to the

structure's capacity to resist a progressive collapse induced by column loss should be classified as primary. All other elements and components should be classified as secondary.

Component capacity:

The verification of individual component strength and deformation capacities shall be conducted based on expected material performance and shall comply with material property definitions in EN 1990.

In general, lower bound material strength properties should be adopted and divided by a partial safety factor for progressive collapse  $\gamma_{PC}$ . The lower bound material property for the calculation of component capacities under progressive collapse is given by:

$$R_{PC} = R_k / \gamma_{PC} \quad (7.42)$$

where  $R_{PC}$  is the component capacity for progressive collapse,  $R_k$  is the characteristic component strength and  $\gamma_{PC}$  is the progressive collapse partial safety factor equal to 1. Material overstrength should not be accounted for (i.e.  $\gamma_{ov}=1.00$ ), since its consideration leads to unconservative results.

Modelling:

The modelling, analysis and evaluation of the resistance to progressive collapse shall be made using three-dimensional model. Two-dimensional models are not allowed. The model should account for geometrical and material nonlinearity. Lateral stability of members (i.e. lateral torsional buckling) must be considered.

The inclusion of secondary elements in the model is not mandatory. When not explicitly modelled, secondary elements must be checked to remain stable and to maintain load-carrying capacity under the displacements imposed by the primary elements. Connections classified as semi-rigid according to EN 1993-1-8 shall not be considered as secondary elements and must be explicitly modelled as primary



elements. Connections classified as nominally pinned in terms of stiffness according to EN 1993-1-8 may be considered as secondary elements.

Primary elements shall be modelled, accounting whenever possible for their initial stiffness, yielding, post-yield hardening, failure and residual strength. As a minimum initial stiffness, yielding and failure should be modelled. The definition of component material nonlinearity, namely its force-displacement or moment-rotation response curve should be determined according to the Components Method in EN 1993-1-8 whenever applicable or alternatively, according to available literature on joint performance. Plasticity distribution along members may be modelled using distributed inelasticity elements or by meshing members and adopting a lumped plasticity at the ends of each segment.

#### Loading procedure:

The combination of actions acting on the building structure prior to the column loss action is the accidental load combination given in expression (6.11b) of EN 1990.

The internal forces in each column to be removed shall be determined and the column to be removed shall be deleted from the model and replaced by the equivalent reaction forces. A loading procedure consisting of a downward displacement-controlled pushdown shall be implemented up to collapse or up to a displacement value deemed sufficiently high by the designer to enable to generate the vertical pushdown load-displacement curve. A minimum of 10 calculation steps shall be used to generate the pushdown curve.

#### Column removal locations:

Alternative Loadpath Analysis should be conducted considering, for each column removal scenario, that the full column segment defined between lateral restraints (i.e. between consecutive storeys) is removed.

In terms of location, as a minimum, the following column removal scenarios should be analysed: i) façade column near the middle of the long side; ii) façade column near the middle of the short side; iii) corner column. Additionally, engineering judgement should be used to identify discontinuity zones, characterised for example by changes in

bay size, re-entrant corners, change of member orientation, which require the consideration of additional removal scenarios.

For each plan location, as a minimum, column removals shall be considered for the following scenarios: i) column segment between ground floor and 1<sup>st</sup> storey; ii) column segment at building mid height; iii) column segment between penultimate storey and the roof.

For buildings with underground parking or with uncontrolled public areas, internal column removal scenarios must be considered, namely near the middle of the long side, near the middle of the short side and near the corner of the uncontrolled space. In these cases, the column segment to be removed is defined between the floor of the parking zone to the floor above it.

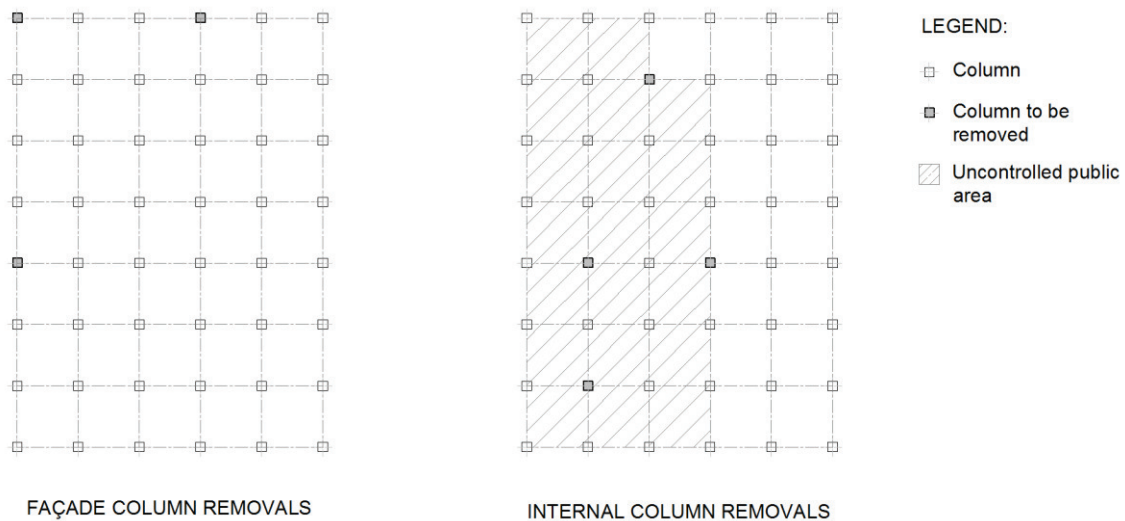


Figure 7.108: Façade and interior column removal scenarios

Energy Balance method:

The procedure is based on the balance between the work done by the application of the sudden gravity load and the internal strain energy of the system. When these quantities achieve equilibrium, the zero kinetic energy condition is reached, which corresponds to the maximum dynamic displacement under column loss. The method implicitly assumes that the directly affected zone of the structure responds as a Single Degree of Freedom (SDOF) system.

For the application of the Energy Balance method, the pushdown force-displacement curve must be plotted and the internal energy and work done must be computed for each vertical displacement step. The displacement value for which the difference between the work done and the internal strain energy is zero corresponds to the maximum dynamic displacement. For cases in which balance is not reached, the system is assumed to collapse.

#### Ductility assessment and acceptance criteria:

The maximum dynamic displacement ( $u_{dyn}$ ) must be compared to the ductility limit ( $u_f$ ), defined as the minimum value of  $u_{dyn}$  which exceeds the deformation capacity in any of the connections. The limit state corresponds to the failure of the first connection. Secondary elements must be checked to remain stable and to maintain load-carrying capacity under the displacements imposed by the primary elements.

In cases in which at least one component is found exceed the ductility limit, the building structure is found to not satisfy the progressive collapse requirements and must be re-designed.

#### *7.4.2.3 Advantages and disadvantages*

While the adoption of deterministic methodologies for the evaluation of the progressive collapse arrest capacity may provide more accurate results for robustness assessment, the implementation of such methodologies by structural designers is typically not feasible. Indeed, the high level of modelling expertise and experience, as well as the computational effort and the elevated number of man-hours required to validate the results of complex deterministic analysis render this option impractical. The first rules implemented in the UK for the design for disproportionate collapse (The Building (Fifth Amendment) Regulations 1970 (S.I. 1970/109), 1970) were conceived to provide designers with expedite verification methodologies that would provide structures with improved tying capacity which was believed to provide minimum levels of structures robustness.

In the same spirit, the proposed methodology provides a set of prescriptive measures based on the expected behaviour of structures that enables to improve the robustness/redundancy of structures with intermediate levels of robustness and which

determines in which cases an Alternative Loadpath Analysis (ALA) is actually required, since collapse is likely to occur following column loss, for which reason prescriptive measures alone may prove to be insufficient.

In cases in which ALA is required, no specific software is required to conduct the ALA and it can simply be executed using any FE software with Linear Elastic Analysis capability. Also, the Energy Balance Method can also be easily implemented using a simple spreadsheet and the physical principles behind the method are well known to all engineers allowing for easy result verification and validation.

The proposed prescriptive measures for improving robustness are simple and easy to implement and take into account the DCR of the different members and connections, taking into account which elements require more significant improvement.

The proposed methodology is hence believed to strike a fair balance between the need to prevent progressive collapse, the feasibility of the implementation of the methodology by structural design firms and the cost/difficulty of introducing the detailing requirements for enhancing robustness.

## **7.5 Conclusive remarks**

In this Chapter an assessment of the response of MRF structures to column loss accounting for the contributions of non-structural elements was conducted. In particular, the contributions of the secondary “gravity” frame structure and of the façade claddings were accounted for. The numerical modelling of beam-to-column joints of the “gravity” frame was based on results obtained in Chapter 6, while façade cladding response was calibrated to experimental results from literature. The response further to column loss was initially evaluated for both the frames in the undamaged condition (baseline robustness) and after sustaining seismic action (post seismic robustness), in order to evaluate whether earthquake-induced damage reduced structural robustness.

To this aim, a parametric study was conducted using NDA and the response to column loss was evaluated for a wide array of realistic MRF structures under different column loss location scenarios. In particular the robustness of initially undamaged MRFs was evaluated for 288 cases, with varying number of storeys, interstorey height, span, bay layout, façade claddings, lateral load design scenario and for 3 column

removal locations. The post seismic robustness of MRFs was evaluated for a total of 288 cases, although analysis was limited to 4 storey frames (which are prone to develop plasticity under seismic action and with lower internal force redistribution capacity further to column loss), two column removal location scenarios (XZ façade and corner) and 3 accelerogram signals, due to time/computational constraints. The following conclusive remarks are drawn on the basis of the obtained results.

The initial sensitivity tests to damping show that the maximum dynamic displacement ( $u_{dyn,max,damaged}$ ) under column loss is significantly affected by the damping ratio  $\zeta$ , namely for structures which are characterised by plastic response to column loss, i.e. which display high  $DOP_{DAZ}$  values, as is typically the case of long span systems, where differences of up to 10% in ( $u_{dyn,max,damaged}$ ) are reported between  $\zeta=1\%$  and  $\zeta=2\%$  cases.

Another initially conducted sensitivity test aimed at evaluating the sensitivity of column loss response to MRF beam material overstrength, for  $\gamma_{ov}$  ranging between 1.0 and 1.5. The numerical outcomes show the influence of  $\gamma_{ov}$  to be negligible for medium span (6m) frames but to have a great impact on ( $u_{dyn,max,damaged}$ ) for long span (10m) systems. Indeed, for the latter, results for the analysed case show a reduction of 25% in  $\gamma_{ov}$  to lead to a 40% increase in ( $u_{dyn,max,damaged}$ ), due to changes in the degree of plasticization of the DAZ, where members with higher strength remain in the elastic range, limiting irreversible plastic displacement under column loss. For the case with zero MRF beam overstrength ( $\gamma_{ov}=1.00$ ), collapse occurred following column loss, which further stresses the importance of this factor for long span systems.

In this sense, it should be noted that since the objective of this thesis is to perform an assessment of the average response of MRF structures, analyses were subsequently conducted considering the most representative material properties, namely with material overstrength taken with its average value ( $\gamma_{ov}=1.25$ ), in order to maximise the representativity of the results. However, to provide a broader picture of the robustness of MRFs, a complementary approach that is more focused on design is also required to be conducted in the future, namely considering the most unfavourable structural characteristics. This complementary approach can be achieved for example by taking  $\gamma_{ov}=1.00$  and disregarding all non-structural element contributions, hence establishing a lower robustness bound against which the average robustness can be compared. A better understanding of the distribution of material overstrength would

also enable to determine whether improved detailing for progressive collapse considering  $\gamma_{ov}=1.00$  is too conservative and/or cost inefficient. This evaluation however falls outside the scope of the present thesis and remains an open topic for future research.

The vertical displacement time-history results showed 10m span frames to develop high levels of plasticity in the DAZ ( $DOP_{DAZ}\approx 1$ ) and 6m span frames to instead retain a higher level of elasticity. The analysis of the different removal scenarios showed the importance of secondary frame joints in the DAZ that are mobilised following column loss, namely highlighting that in cases requiring equal load redistribution, differences in secondary frame joint capacities can lead to non-negligible differences in maximum dynamic displacements.

The more refined analyses described in the present Chapter reinforce several conclusions from the preliminary robustness assessment (see Chapter 4), namely for what concerns the importance of the number of storeys. Indeed, results show that the higher number of storeys (and hence the higher number of elements to which load can be redistributed) compensates for the increase in axial load in the column to be removed, leading to smaller maximum dynamic displacements ( $u_{dyn,max,damaged}$ ) and generally to higher robustness.

The evaluation of the degree of plasticity in the DAZ via the proposed  $DOP_{DAZ}$  ratio has enabled to characterise the response to column loss via a single scalar parameter. Results showed that significant plasticity is generally required to arrest progressive collapse in all cases. In contrast with the preliminary robustness assessment in Chapter 4,  $DOP_{DAZ}$  values higher than 0.5 are reported for all cases, reflecting the development of plasticity in the secondary frame joints. The span was found to influence  $DOP_{DAZ}$  ratios, namely for 4 storey frames, which have inherently lower structural robustness and which for 10m span frames display an average  $DOP_{DAZ}$  increase of 11% compared to 6m span frames.

The obtained  $DOP_{DAZ}$  results served also as the basis for the development of a methodology that provides a decision making process to Civil Protection Services regarding the need for temporary propping of structures in column loss scenarios for safe rescue party interventions.

The motion of the DAZ under column loss was characterised in terms of peak velocity  $v_{DAZ}$  and peak acceleration  $a_{DAZ}$ , showing these to vary according to key

structural features. Results show that low rise and/or long span structures (characterised by lower robustness) tend to develop higher peak velocities and accelerations and that claddings are most effective in reducing motion for structures with lower robustness.

The chord rotation demand in joints for the 4-storey bare steel frames is seen to be lower than 11 mrad and 42 mrad for 6m and 10m span frames, respectively, while for 8-storey structures, demand is lower than 4 mrad and 18 mrad for the 6m and 10m span frames, respectively. A comparison with the preliminary robustness assessment showed demand results to be very similar for façade removals, while differences by factors of up to 0.42 are reported for corner removals, showing that accounting for secondary frame joints can lead to significantly lower rotational demand.

The reserve robustness was evaluated via the Reserve Displacement Ductility ( $RDD_{equil}$ ) ratios and results for 4-storey frames show minimum  $RDD_{equil}$  values of 6.3 and 1.1 for the 6m and 10m span frames, respectively, while for 8-storey frames, minimum  $RDD_{equil}$  values of 11.2 and 1.1 are reported for the 6m and 10m span frames, respectively, highlighting the low robustness of long span systems.

The reserve capacity was also evaluated via Demand-to-Capacity ratios (DCR) for the different members/connections, showing that MRF joints display the highest DCR and can therefore benefit from improved progressive collapse detailing. Instead, the high flexibility of secondary frame joints led to very low DCR, indicating that these elements did not cause progressive collapse and that improved detailing in this case would not significantly improve overall structural robustness.

The effect of claddings showed the adopted CFS “X” bracing claddings adopted for the wind+seismically designed frames to be more effective in reducing rotational demand than the masonry claddings adopted for the wind designed structures. Results show the introduction of CFS type façade claddings to avert progressive collapse in some cases of low rise – long span structures. Furthermore, the numerical outcomes indicate that rotational demand reduction is higher in more flexible frames.

The comparison between the maximum catenary force under column loss and European and US code tying requirements show the former to provide the better upper boundary to the NDA derived catenary forces, at the exception of the low rise – long span structures, while US code provisions led to over conservatism which is however well suited to low rise – long span cases.

The post seismic robustness assessment showed that the damage sustained by DCH designed MRF structures under seismic action is not sufficient to significantly affect structural robustness. Results show that the introduction of façade claddings generally has a positive effect on reducing lateral drift, being more effective for medium span frames. In some cases however, results appear to indicate that when the stiffening effect of introducing claddings surpasses a given threshold, the resulting higher seismic energy input leads to larger drifts than those obtained for the bare steel frames.

The CFS cladding members were found to yield for nearly all cases and at all storey levels. Analysis of the force time-histories showed yielding to generally occur for very small time intervals, hence not resulting in large plastic deformations.

The simulation results show that the low seismically-induced damage sustained by MRF members (frame elastic restitution capacity is generally preserved), coupled with the low plastic deformations in the claddings led to negligible changes in joint rotation demand under column loss between the initially undamaged (IU) and the post seismic (PS) scenarios.

The numerical outcomes indicate that the structural robustness of DCH designed MRF structures following column removal in the IU and PS conditions is not significantly altered. This further implies that, for the analysed structural typology, evaluation and design for progressive collapse resistance in PS scenarios can be made considering the IU structure properties. In this sense, a new design methodology for preventing the progressive collapse of MRF structures is proposed on the basis of the results obtained in the present thesis.



## Chapter 8 General conclusions and perspectives

### 8.1 Conclusions

The present thesis reflects the author's work, which was developed at both the University of Coimbra and the University of Naples "Federico II". In this thesis, an assessment of the post seismic robustness of steel moment resisting frames under column loss was investigated, accounting also for the contribution of the secondary frames, the corresponding connections and the non-structural façade claddings. The main objective was to evaluate whether the damage induced by seismic actions could affect the structural robustness.

A parametric numerical study was devised and the parametric variables defining the building geometry and the design loads were selected to provide a representative array of realistic building structures, namely low and medium rise frames with medium and long spans. The building structures were designed in accordance with the Eurocodes and the all-steel beams were designed for the bays of the moment resisting frames (MRF), hence without considering the advantage of the composite slab. In terms of lateral load design, the frames were either designed for wind loads only ( $v_{b,0}=30\text{m/s}$ ; terrain category III) according to a strong beam - weak column hierarchy, or for wind and seismic loads ( $a_{gR}=0.25g$ ; soil type C, DCH class) according to the strong column- weak beam principle outlined in EN 1998-1 (CEN, 2004). The contribution for arresting progressive collapse given by non-structural elements such as the secondary "gravity" frame joints and the façade claddings (which are typically disregarded) was also considered.

The robustness was evaluated with a scenario-independent approach, consisting of the notional removal of a column. The behaviour of the set of elements

which lose support following the column removal and which are designated as the Directly Affected Zone (DAZ) was monitored.

A preliminary robustness assessment was initially conducted, so as to provide an early “rough picture” of the behaviour of the building structures under different column loss scenarios, as described in Chapter 4. Simplified plasticity modelling assumptions were adopted for the MRF and secondary joints and 3D FE models were used to conduct both Pushdown Analysis combined with the Energy Balance Method (Izzudin *et al.*, 2008) as well as Nonlinear Dynamic Analysis (NDA). The conducted analyses showed that the better performance under column loss is provided by the strong beam - weak column structures (i.e., for non-seismically designed frames), highlighting the key importance of the DAZ beams’ capacity for collapse arrest. Comparatively, structures designed in accordance with EN 1998-1 (CEN, 2004) displayed lower values of Residual Strength Ratio (*RSR*) although characterised by a ductile failure mode in all cases. Low-rise long-span frames were shown to be especially prone to collapse, with multiple collapses reported and generally displaying very low *RSR* values. The evaluation of the Dynamic Load Factors showed medium span frames to remain elastic following column loss. Displacement evaluation using NDA led to smaller maximum dynamic displacements, highlighting the importance of the explicit modelling of damping and dynamic effects.

These preliminary outcomes provided the basis for the selection of analysis cases for the more refined FE analysis described in Chapter 7. However, since the refined analysis required the effective simulation of the behaviour of the secondary frame members and connections, it was deemed necessary to investigate joint response in bending and under simultaneous bending and tensile force (as induced by column loss). The failure mode of joints under column loss action is typically characterised by bolt failure, for which reason the bolt assembly response may influence joint behaviour under column loss (Kwasniewski, 2010). Therefore, in order to fully account for the ultimate tensile capacity of bolt assemblies, an experimental campaign was carried out, as described in Chapter 5, to investigate bolt assembly tensile behaviour under monotonic and both constant (low-cycle fatigue) and variable amplitude cyclic actions.

The conducted experimental tests enabled to fully characterise the Force-Displacement (F-d) response of the bolt assemblies, as well as the ultimate displacements, which are not currently predicted by the EN 1993-1-8 (CEN, 2005) and which determine the ultimate joint rotation capacity in T-Stub modes 2 and 3. Furthermore, the outcomes from the cyclic tests also enabled to evaluate the response of bolts under solicitations as those potentially induced by seismic actions. In particular SB, HR and HV bolt assemblies were tested and failure modes were identified, showing shank necking failure for SB and HR types and thread stripping failure for HV assemblies. The latter type was seen to display a very different F-d response in comparison to SB or HR types, namely characterised by a resistance drop to about 30% - 40% of peak strength after yielding, followed by a residual strength plateau and a progressive drop to zero strength upon full nut removal. The test results showed that the F-d response is not affected by the imposed variable cyclic loading. The fatigue tests enabled to determine  $\varepsilon$ - $N$  curves for the HR and SB types, while HV assemblies were seen to cycle indefinitely without failure due to the thread crest flattening. The obtained experimental results enabled to develop and calibrate 3D solid finite element models, accounting for all sources of assembly deformability, namely the threaded zone contribution. The assembly stiffness was found to be lower than the EN 1993-1-8 (CEN, 2005) estimation, which does not account directly for thread stiffness. An equivalent shank model and a ductile damage model were calibrated for both HR and SB assemblies, where the latter model accounts for damage initiation and progression. Instead, for HV assemblies, given that the thread stripping failure cannot be simulated via equivalent plastic failure (unless thread geometry is modelled, resulting in very heavy and time consuming models), a new modelling strategy was proposed, combining 1D and 3D finite elements, which was shown to be effective. The differences in F-d response between HR and HV assemblies were put into evidence via an example with analytical T-Stub models in failure modes 2 and 3. The example showed that computing the T-stub failure mode based on bolt assembly nominal properties, as prescribed in EN 1993-1-8 (CEN, 2005), can be contrary to safety when using HV assemblies. It was therefore concluded that the design of bolted joints should take into account the bolt assembly type and the required rotation demand, to ensure that joint performance is consistent with the specific requirements.

The results from both experimental tests and finite element simulations for bolt assemblies discussed in Chapter 5 were adopted for the investigation of the behaviour of secondary frame bolted beam-to-column joints presented in Chapter 6.

Considering that the bolted Flush End-Plate (FEP) joint typology is one of the most widely adopted types in the European steel construction, it was selected for the beam-to-column joints in the secondary “gravity” frames. However, since limited data is available on FEP joint response under cyclic bending and under column loss action, in Chapter 6, a numerical parametric study devoted to investigating the response of FEP joints is presented and discussed. The following variables were examined: bolt diameter, end-plate thickness, number of bolt rows, beam section and the column axis orientation. Results from monotonic analyses of initially undamaged (I.U.) joints under column loss action show two different resisting mechanisms, namely compressive arching mode and catenary action mode. The thickness of end-plate is the key parameter which significantly influences the joint response. Hence, design criteria are proposed for both the optimal end-plate thickness range and for the welding details, in order to maximise FEP joint capacity under simultaneous bending and tensile force. The proposed criterion for the optimal thickness range is based on the principle of inducing a T-Stub failure mode 2, thus activating the deformation capacity of both the end-plate and the bolts. This enabled to achieve a higher ultimate rotation capacity, as shown by confronting the proposed criterion with the obtained results. Further detailing recommendations to enhance joint capacity are proposed, namely the adoption of a higher number of inner bolt rows, preferably with large nominal diameters, which can increase the efficiency of the catenary forces transmission in the connection, enhancing joint strength and rotation capacity. In light of the obtained results, FEP joints designed with the proposed criteria display ultimate rotation capacities larger than 100 mrad.

The FEP beam-column joint behaviour under cyclic action followed by column loss action was also investigated. Thin end-plates in T-Stub modes 1 and 2 led to joint moment-rotation ( $M-\theta$ ) response characterized by large hysteretic loops. Instead, thicker end-plates in mode 3 led to concentrated plasticization in the bolts with low dissipation capacity. Fracture in the beam flange - endplate weld in cyclic loading is reported for joints with thin endplates and compact beam section coupled with large bolt horizontal pitch. In these cases, the use of full penetration welds and/or thicker

plates may limit premature weld failure. At high rotational demand, severe softening of small diameter bolt assemblies led to strength capacities lower than predicted by EN 1993-1-8 (CEN, 2005). This results highlights that disregarding the bolt softening at the design stage may not be conservative. Increasing the number of bolt rows was found to be beneficial in terms of both strength and rotation capacity under cyclic actions.

For column loss action after cyclic bending, results show that FEP joints sustain shank elongation during the cyclic bending action leading to zero initial stiffness in the Post Cyclic (P.C.) column loss stage. For this reason, their contribution to arrest progressive collapse at low rotations should be disregarded. Instead, at higher rotational demand, reduced strength in comparison to the I.U. scenario is reported capacity for the P.C. stage, although ultimate joint rotation capacities are seen to be consistent with values for the I.U. joint response.

The numerical outcomes of the parametric study of FEP joints presented in Chapter 6 were subsequently used to simulate the response of the secondary frame joints in the more refined robustness assessment of the MRF structures presented in Chapter 7.

The robustness assessment of the MRF structures presented and discussed in Chapter 7 is aimed at evaluating the response to column loss and post-seismic column loss by means of refined modelling approach. To achieve this goal, full 3D finite element models were developed. The contribution of the secondary frame beam-to-column FEP joints was accounted for by adopting nonlinear springs calibrated to the  $M-\theta$  and  $N-\theta$  curves determined in Chapter 6. The web cleat typology was selected for the beam-to-beam joints, which were modelled via nonlinear springs calibrated to experimental results. The non-structural façade claddings were modelled using nonlinear infill panel formulations calibrated with experimental results. Nonlinear Dynamic Analyses (NDA) were carried out to investigate the performance of a set of building structures, which were selected in accordance with results from the preliminary robustness assessment presented in Chapter 4.

The comparison of the response further to a column loss was evaluated for the initially undamaged condition and for the post seismic condition, enabling to assess whether the earthquake-induced damage reduces structural robustness. The initial sensitivity tests show maximum dynamic displacements to be sensitive to the damping

ratio  $\zeta$  and to the beam yield stress, namely for long span (10m) structures. The results show that long span systems display high levels of plasticity, as seen by the Degree-Of-Plasticity ( $DOP_{DAZ}$ ) ratios close to 1, while medium span (6m) frames retain a much higher degree of elasticity. Differences in the capacity of secondary frame joints mobilised by column loss were found to lead to non-negligible differences in maximum dynamic displacements. The numerical outcomes are in agreement with results from Chapter 4 for what concerns the importance of the number of storeys, i.e., of the number of elements in the Directly Affected Zone (DAZ) to which load can be redistributed. Indeed, the higher number of storeys, which implies a higher redistribution capacity, is found to compensate for the increase in axial load, resulting in smaller peak dynamic displacements.

On the basis of the  $DOP_{DAZ}$  results, a flow chart is proposed to provide the Civil Protection Services/Emergency Management Agencies with a decision making tool regarding the need for temporary propping of structures in column loss scenarios. The motion of the DAZ was characterised in terms of peak acceleration and velocity and vertical displacement time-histories were monitored. Results showed maximum chord rotation demands for 4-storey bare steel frames to be lower than 11 mrad and 42 mrad for 6m and 10m span frames, respectively, while for 8-storey structures, demand is lower than 4 mrad and 18 mrad for the 6m and 10m span frames, respectively. The reserve of robustness was evaluated via the Reserve Displacement Ductility ( $RDD_{equil}$ ) ratios. Four storey frames show minimum  $RDD_{equil}$  values of 6.3 and 1.1 for the 6m and 10m span frames, respectively, while 8-storey frames have minimum  $RDD_{equil}$  values ranging from 11.2 to 1.1 for 6m and 10m span frames, respectively, thus highlighting the low robustness of long span systems. The Demand-to-Capacity Ratios ( $DCR$ ) were computed for the different structural members/connections, showing that MRF joints display the highest values and can benefit the most from improved progressive collapse detailing. Instead, secondary frame joints display lower  $DCR$  values and improved detailing for these elements may not significantly improve overall structural robustness. The Cold Formed Steel (CFS) cladding typology adopted for the seismically designed frames was found to be more effective in reducing rotational demand than the masonry claddings adopted for the wind designed frames. Furthermore, in some cases of low-rise long-span frames, the introduction of CFS

claddings was found to prevent the progressive collapse. The comparison between the maximum catenary force and state-of-the-art European and US tying requirements showed the former to provide a suitable upper boundary for catenary forces, at the exception of the low-rise long-span frames, while the latter tends to be over conservative. It was also concluded, on the basis of the obtained results, that while claddings generally have a positive effect on reducing lateral drifts, in some cases, if the stiffening effect due to the introduction of claddings surpasses a given threshold, the resulting increase in seismic energy input leads to larger drifts than those for the bare steel frames.

The post-seismic assessment showed that the damage sustained by DCH class designed MRF structures under seismic action does not appreciably affect the structural robustness. This implies that for the analysed structural typology, the design for progressive collapse in post-seismic scenarios can be made analogously to the initially undamaged structure scenario. A new proposal for progressive collapse design based on the maximum DCR ratios and on the proneness of structural typologies to collapse is proposed, as well as prescriptive robustness detailing rules.

## **8.2 Implications for design and contribution to the future revision of EN 1991-1-7**

The work developed in this thesis is aimed at assessing the response of a large set of steel moment resisting frames in a damaged situation. This evaluation enabled to determine which building structures are most prone to progressive collapse and in particular, which structural elements require improved detailing, in order to improve global structural robustness.

It is possible however, that structures with the same MRF typology exhibit poorer progressive collapse performance, owing to the variability in factors such as random material properties, geometric imperfections and construction or design mistakes. In this sense, the present results could in the future, be complemented with an evaluation of the statistical distribution of the above stated variables and their influence on the structural system robustness.

The application of the proposed progressive collapse design methodology, being based on average material properties, therefore prioritises the adoption of

improved detailing for the majority of the structures displaying a high proneness to collapse. In this sense, the proposed methodology takes into account that a column loss event has a very low probability of occurrence and that the simultaneous adoption of over conservative hypotheses for progressive collapse design could lead to using up resources without a meaningful benefit in risk reduction. It is the opinion of the author that this question should be analysed via a cost-benefit analysis, to confront the cost of reinforcing for progressive collapse against the benefit in terms of the reduction of the probability of collapse, loss of human life and economic costs. Such an analysis falls however outside the scope of the present thesis.

Presently the EN 1991-1-7 (CEN, 2006) provides guidance for designing structures to disproportionate collapse through strategies aimed at limiting the extent of localised failure. However, the prescriptive design methodologies prescribed in this regulation (e.g. Tie Force Method or Key Element design) are intended to avoid disproportionate collapse, implying that a progressive collapse situation is possible, as long as it is not disproportionate. Furthermore, the EN 1991-1-7 (CEN, 2006) requires performing Alternative Loadpath Analysis for structures in higher Consequence Classes, although it provides no guidance on how to conduct it.

Nonetheless, the EN 1991-1-7 (CEN, 2006) provides a set of simple design rules, which, in general, can easily be applied by structural designers to provide structures with minimum levels of robustness which should be compatible with preventing disproportionate collapses.

In this spirit, a design methodology for moment resisting frame structures was proposed in this thesis, aiming at providing structures with adequate levels of structural robustness, so as to arrest a progressive collapse following a column loss scenario. The proposed methodology follows the same structure as that currently provided in EN 1991-1-7 (CEN, 2006) and is intended to complement it via additional design rules for progressive collapse. In particular, building structures are required to be classified in terms of Proneness to Progressive Collapse (PPC) on the basis of their key geometrical features and subsequently, recommended reinforcement strategies are proposed for the PPC Class. For the higher PPC class, Alternative Loadpath Analysis is a requirement and guidelines to conduct the analysis are provided. The proposed methodology hence provides a simple set of design rules for MRF structures, which can easily be implemented by structural designers.



In the opinion of the Author, different approaches are possible for the future revision of the EN 1991-1-7 (CEN, 2006).

One possibility is to maintain the current prescriptions for disproportionate collapse and to indicate which building structures are required to be design for progressive collapse. The EN 1991-1-7 (CEN, 2006) could in that case state that design for progressive collapse is required to be made in compliance with a new design code. Such a design code however, does not yet exist in Europe and would require to conduct an extensive experimental programme to prequalify joints, provide Load Increase Factors and Dynamic Increase Factors for different building materials, structural typologies and joint types and to define component modelling and acceptance criteria. The fact that such design codes have been available in the U.S. for more than a decade (e.g. GSA 2003 (U.S. General Services Administration, 2003), UFC 2005 (United States of America Department of Defense, 2005)) provides a better picture of how a European progressive collapse design code could look like and the amount of investment to be made to achieve this goal.

Another possibility for the future revision of the EN 1991-1-7 (CEN, 2006) is to introduce a methodology like the one proposed in this thesis, which specifies detailing rules to provide structures with the required levels of robustness to avoid a progressive collapse. The list of structural typologies and corresponding maximum chord rotations and Demand-to-Capacity Ratios, as well as the proposed detailing rules can be easily and progressively be complemented by results from further robustness studies. In this way, guidance for progressive collapse design can be made available sooner to designers, by using a methodology that is both simple and also already familiar to them. This possibility can hence be regarded as a transition phase, providing the necessary time for a complete European progressive collapse design code to be prepared, while simultaneously improving the currently available design provisions. In the opinion of the Author, this latter possibility for the future revision of the EN 1991-1-7 (CEN, 2006) is the one that appears to be more feasible, taking into account the required coordination between CEN members and time to complete such a new code.

As a final note, it should be clear that a complete European progressive collapse design code, which can take into account the specificities of European construction

materials, design rules, fabrication systems and construction methods, is becoming increasingly necessary.

### 8.3 Personal contributions

The main personal contributions to the research work presented in this thesis were the following:

- i) Performing structural design for a total of 48 different moment resisting frame building structures in accordance with the Eurocodes;
- ii) Conducting preliminary analyses using nonlinear static pushdown analysis combined with the Energy Balance Method and nonlinear dynamic analysis to evaluate the Residual Strength Ratios, the Residual Ductility Ratios and the Dynamic Load Factors under façade and corner column loss scenarios;
- iii) Designing and preparing the experimental test set up for conducting monotonic and cyclic tensile tests on bolt assemblies: evaluating normative regulations on bolt assemblies, analysing the experimental set up strength and deformation capacities via hand calculations and detailed 3D solid FE models, developing drawings for the set up fabrication, measuring individual assembly component geometry, defining the instrumentation, control and measurements and deriving *ad hoc* inelastic cyclic loading protocols on the basis of the monotonic tensile test results;
- iv) Conducting 84 experimental tests on preloadable (HR and HV type) and non-preloadable (SB type) bolt assemblies: monitoring of the failure modes, computing assembly ductility, deriving the linearised force-displacement and true stress-strain curves and computing the inelastic low cycle fatigue  $\epsilon$ - $N$  curves;
- v) Developing, calibrating and validating 3D solid FE models using an equivalent shank model for HR and SB type bolt assemblies: evaluating assembly and threaded zone deformability and developing a constitutive law for the equivalent shank true stress-strain response in function of the bolt nominal diameter;

- vi) Developing, calibrating and validating 3D solid FE models using a ductile damage formulation for HR and SB type bolt assemblies: calibrating the damage evolution law for a material undamaged constitutive law and equivalent plastic strain vs. triaxiality stress state;
- vii) Developing, calibrating and validating a new modelling strategy for simulating the highly nonlinear response of HV bolt assemblies combining 1D and 3D finite elements: defining model boundary conditions and proposing constitutive laws for the 1D and 3D finite elements in function of the bolt nominal diameter;
- viii) Demonstrating the applicability of the linearised bolt assembly response curves in predicting T-Stub response accounting for all stages of the response including hardening and softening and up to failure: applying response curves to 2D analytical and 3D solid FE T-Stub models in failure modes 2 and 3, showing that joint design based on bolt nominal properties may be contrary to safety, namely for HV type assemblies;
- ix) Modelling 192 bolted flush end-plate beam-to-column joints using 3D FE models as part of a parametric study on joint response under monotonic column loss and under post-cyclic bending column loss, examining the effect of the number of bolt rows, bolt diameter, end-plate thickness, beam cross section and column orientation;
- x) Developing a new end-plate range thickness criterion for maximising joint strength and rotational capacity to column loss action, based on inducing a T-Stub failure mode 2 that activates the deformation contributions of both end-plate and bolts;
- xi) Computing the Dynamic Increase Factors for the analysed flush end-plate joint configurations: using the Energy Balance Method by likening the connections to a Single-Degree-Of-Freedom system and evaluating the influence of the parametric variables on the dynamic increase effect;
- xii) Evaluating the influence of different geometric variables on flush end-plate joint response to post cyclic bending followed by column loss action: comparing to initially undamaged joint response, evaluating the hysteretic dissipative capacity and the applicability of the endplate

- thickness design criterion, comparing the performance to EN 1993-1-8 (CEN, 2005) predictions and proposing welding detailing;
- xiii) Conducting an assessment of the response further to façade and corner column loss scenarios for a large set of low/medium rise steel moment resisting frame structures using nonlinear dynamic analysis: creating 96 FE models of the building structures using Seismostruct and calibrating nonlinear spring models to simulate secondary frame connections, column web panel distortion deformability and both cold formed steel and masonry cladding panel response under column loss.
  - xiv) Evaluating damping and MRF beam yield strength sensitivity, quantifying the degree of plasticity in the Directly Affected Zone (DAZ), characterising the DAZ motion in terms of displacement, velocity and acceleration, quantifying peak joint chord rotational demand, reserve ductility, Demand-to-Capacity Ratios (DCR) and the effect of claddings and comparing maximum catenary tensile forces to EN 1991-1-7 (CEN, 2006) disproportionate collapse design requirements;
  - xv) Comparing initially undamaged to post-seismic structural response to column loss to evaluate the impact of the seismic action induced damage on robustness;
  - xvi) Proposing a progressive collapse design methodology for MRF structures based on the concept of Proneness to Progressive Collapse (PPC): establishing PPC classes based on maximum expected DCR, prescribing strategies for preventing progressive collapse based on the PPC class and sets of prescriptive detailing rules for enhancing robustness and providing guidelines for structural designers to conduct Alternative Loadpath Analysis using a nonlinear static procedure combined with the Energy Balance method;
  - xvii) Developing a flow chart for assisting Civil Protection Services/Emergency Management Agencies with decision making regarding the need for installing temporary propping in structures that sustained column loss.

## 8.4 Open questions and further research

The work presented in this thesis concerns the response further to column loss at the local level in joints and at the global level in moment resisting frames. In the course of the conducted research, several topics were identified to require further examination, namely:

- i) Given the geometry of frames analysed in this thesis, the rotational demand on MRF joints was equal to the demand on the secondary frame joints, since spans were equal in both the x and y direction. However, this is not always the case and demands on secondary frame joints may be significantly higher than in MRF joints. In such cases, the adoption of HV type assemblies for secondary frame joints may prove to be more suitable, considering their higher deformation capacity at failure which derives from the thread stripping failure mode. In this sense, experimental and numerical studies should be conducted to compare the response of joints using HR and HV joints so as to provide more definitive conclusions on this topic;
- ii) Regarding the experimental tests on bolt assemblies, the obtained results indicate that the deformability of the threads is significant and therefore that FE modelling of bolt assemblies should explicitly take into account this source of deformability. The differences in terms of initial stiffness between the experimental results and the EN 1993-1-8 (CEN, 2005) prediction may partially explain the fact that the EN 1993-1-8 is consistently found to overestimate joint initial stiffness for flush end-plate joints for example, as seen in several past studies (Broderick and Thomson, 2002; Aribert et al., 2004; Girão Coelho and Bijlaard, 2007). This topic is believed to deserve further investigation since it could enable to improve to the accuracy of the Components Method. To achieve this goal, further experimental tests on bolt assemblies would be required to improve the accuracy of the initial stiffness model. Subsequently, experimental joint response curves could be compared to both the analytical curve using the Components Method with the new stiffness formulation and also with numerical FE models of the joints incorporating the new stiffness formulation, in order to evaluate on the accuracy of the stiffness formulation;

- iii) The numerical simulations on flush end-plate (FEP) joints both under column loss action and under cyclic bending action showed that fillet weld failure can impair joint response, as seen also in past experimental tests (Boorse, 1999; Aribert *et al.*, 2004; Yu *et al.*, 2011). Consequently, in order to guarantee the proper activation of the endplate, joint detailing recommendations for FEP joints are made in the sense of adopting full penetration welds in the beam-endplate interface. The effectiveness of this recommendation should however be tested, namely via experimental tests. It should be noted that these recommendations also apply to the case of steel columns to concrete foundation connections with FEP typology, which is a commonly adopted configuration by designers when no moment resistance at the column base is considered in the design.
- iv) The proposed end-plate thickness criterion for maximising resistance to progressive collapse is applicable to FEP beam-to-column joints. However, for the case of double angle web cleat connections or for FEP beam-to-beam splice connections, the criterion's applicability, effectiveness and limitations have not yet been demonstrated.
- v) Additional investigation is required to define modelling and acceptance criteria for plastic hinge response curves under column loss type action for European steel profiles and standard joint detailing and welding procedures. While this would require a large experimental programme to be conducted, it would in turn provide extremely valuable data to establish the joint rotation capacity;
- vi) Considering that MRF column loss response is sensitive to beam yield stress, a study on the structural robustness for varying levels of material overstrength (typically quantified via the  $\gamma_{ov}$  factor) accounting also for the statistical distribution of material overstrength (as provided by data from EU project OPUS for example) could be conducted. This would allow to determine the balance between the appropriate levels of robustness and the costs associated to the design options required to achieve such levels, as is the objective of correct design for robustness (Baker *et al.*, 2008);
- vii) The fact that structural design is performed by engineers that have different sensitivities regarding a structure's levels of safety in relation to Ultimate Limit States (ULS) and Serviceability Limit States (SLS), ranging for example between 0% and 20%, can ultimately lead to substantial differences in terms of maximum

dynamic displacements. For example, while a structure designed with 0% margin of safety in relation to a given ULS may display a highly plastic response to column loss, instead, a structure with a higher margin of safety may tend to remain elastic and to display smaller dynamic displacements. Future robustness studies should therefore clearly indicate the margins of safety of the structures to both Serviceability and Ultimate Limit States. Furthermore, studies devoted to quantifying how designing structures with higher margins of safety can indirectly provide structures with sufficient robustness to avoid progressive collapse following column loss could be conducted;

- viii) The structural robustness is typically evaluated via the alternative loadpath method for an instantaneous column removal, through which initial damage is introduced to the structural system. However, this scenario is in fact unrealistic, since in the case of an extreme event, the complete failure of a single structural element while all others sustain zero damage is highly unlikely. A recent study (Gerasimidis and Sideri, 2016) showed that partial damage distribution scenarios can alter the collapse modes and that the standard column removal scenario may in fact not be conservative. Future studies could therefore include more realistic damage scenarios such as those represented by partial damage distribution scenarios;
- ix) While moderate seismic action is seen in this thesis to not introduce sufficiently high damage to the DCH class designed structural systems so as to reduce robustness, it is still possible that this might be the case for MRF structures designed for strong seismic action. While only low rise MRFs appear to be feasible in zones characterised by high seismicity, this hypothesis is considered to still merit investigation;
- x) Considering that the MRF full strength rigid beam-to-column joints displayed the highest Demand-to-Capacity ratios under column loss action, it is believed that the development of improved detailing for these joints can lead to reducing or eliminating cases of collapse for low-rise long-span systems. In this sense numerical simulations considering different joint responses could be conducted so as to evaluate on the effectiveness of adopting improved joint detailing for averting progressive collapse.





## REFERENCES

- Abel, M. S. (1993). "Four-Bolt Extended Unstiffened Moment End-Plate Connections". MSc Thesis, Virginia Polytechnic Institute and State University, Blacksburg, Virginia, USA.
- Abolmaali, A., Matthys, J., Farooqi, M., & Choi, Y. (2005). "Development of moment-rotation model equations for flush end-plate connections". *Journal of Constructional Steel Research*, 61, 1595-1612.
- AISC. (2005). "Seismic provisions for structural steel buildings (AISC 341-05)". Chicago.
- Alashker, Y., & El-Tawil, S. (2011). "A design-oriented model for the collapse resistance of composite floors subjected to column loss". *Journal of Constructional Steel Research*, 67, 84-92.
- Alashker, Y., Honghao, L., & El-Tawil, S. (2011). "Approximations in progressive collapse modelling". *Journal of Structural Engineering*, 137, 914-924.
- American Society of Civil Engineers (ASCE). (1998). "Evaluation of earthquake damaged concrete and masonry wall buildings - FEMA 306 - ATC-43 project". Washington.
- American Society of Civil Engineers (ASCE). (2000). "Prestandard and commentary for the seismic rehabilitation of buildings - FEMA 356". Washington D.C.: Federal Emergency Management Agency.
- Aribert, J., Braham, M., & Lachal, A. (2004). "Testing of simple joints and their characterization for structural analysis". *Journal of Constructional Steel Research*, 60, 659-681.
- ASCE. (2006). "Seismic rehabilitation of existing buildings ASCE/SEI 41-06". Reston: ASCE.
- Augusto, H., Silva, L. S., Rebelo, C., & Castro, J. M. (2016). "Characterization of web panel components in double-extended bolted end-plate steel joints". *Journal of Constructional Steel Research*, 116.
- Augusto, H., Silva, L. S., Rebelo, C., & Castro, J. M. (2016). "Cyclic behaviour characterisation of web panel components in bolted end-plate steel joints". *Journal of Constructional Steel Research*, (submitted for publication).

## REFERENCES

- Baker, J. W., Schubert, M., & Faber, M. H. (2008). "On the assessment of robustness", 30, 253-267.
- Bickford, J. H., & Nassar, S. (1998). "Handbook of Bolts and Bolted Joints". New York: Marcel Dekker.
- Boorse, M. (1999). "Evaluation of the inelastic rotation capability of flush end-plate moment connections". MSc. Thesis. Virginia, USA: Virginia Polytechnic Institute and State University.
- Botez, M., Bredean, L., & Ioani, L. (2014). "Improving the accuracy of progressive collapse risk assessment: efficiency and contribution of supplementary progressive collapse resisting mechanisms". Proceedings of the 12th International Conference on Computational Structures Technology. Naples, Italy.
- Braham, M., & Jaspart, J. (2004). "Is it safe to design a building structure with simple joints, when they are known to exhibit a semi-rigid behaviour?". Journal of Constructional Steel Research, 60, 713-723.
- British Standards Institution. (2000). "BS 5950: Structural use of steelwork in building. Part 1: Code of practice for design in simple and continuous construction: hot-rolled sections". London: British Standards Institution.
- Broderick, B. M., & Thomson, A. W. (2002). "The response of flush end-plate joints under earthquake loading". Journal of Constructional Steel Research, 58, 1161-1175.
- Brown, K., Morrow, C., Durbin, S., & Baca, A. (2008). "Guideline for bolted joint design and analysis: version 1.0 (Report No. SAND2008-0371)". Albuquerque: Sandia National Laboratories.
- Canisius, T. D., Sorensen, J. D., & Baker, J. W. (2007). "Robustness of structural systems - a new focus for the Joint Committee on Structural Safety (JCSS)". In T. & Kanda (Ed.), Applications of Statistics and Probability in Civil Engineering. London: Taylor & Francis Group.
- Cassiano, D., D'Aniello, M., Rebelo, C., Landolfo, R., & da Silva, L. S. (2016). "Influence of seismic design rules on the robustness of steel moment resisting frames. Steel and Composite Structures", 21(3), 479-500.
- Cassiano, D., D'Aniello, M., Rebelo, C., Landolfo, R., & da Silva, L. S. (2016). "Parametric numerical analysis of flush endplate beam-column joints under

- column loss action". *Journal of Constructional Steel Research* (submitted for publication).
- Cassiano, D., D'Aniello, M., Rebelo, C., Landolfo, R., & Silva, L. S. (2016). "Robustness assessment of steel moment frames". *Open civil engineering journal*, 10.
- CEN. (1999). "EN ISO 898-1 - Mechanical properties of fasteners made of carbon steel and alloy steel - Part 1: Bolts, screws and studs".
- CEN. (2002). "EN 1991-1-1 - Eurocode 1 - Actions on structures - Part 1-1: General actions - Densities, self-weight, imposed loads for buildings".
- CEN. (2004). "EN 1992-1-1 - Eurocode 2 - Design of concrete structures - Part 1-1: General rules and rules for buildings".
- CEN. (2004). "EN 1994-1-1 - Eurocode 4 - Design of composite steel and concrete structures - Part 1-1: General rules and rules for buildings".
- CEN. (2004). "EN 1998-1 - Eurocode 8 - Design of structures for earthquake resistance - Part 1: General rules, seismic actions and rules for buildings".
- CEN. (2004). "EN 1998-1 - Eurocode 8: Design of structures for earthquake resistance - Part 1: General rules, seismic actions and rules for buildings".
- CEN. (2005). "EN 14399-1 - High-strength structural bolting assemblies for preloading - Part 1: General requirements".
- CEN. (2005). "EN 14399-3 - High strength structural bolting for preloading - Part 3: System HR - Hexagon bolt and nut assemblies".
- CEN. (2005). "EN 14399-4 - High strength structural bolting for preloading - Part 3: System HV - Hexagon bolt and nut assemblies".
- CEN. (2005). "EN 1990 - Eurocode - Basis of structural design".
- CEN. (2005). "EN 1991-1-4 - Eurocode 1 - Actions on structures - Part 1-4: General actions - Wind actions".
- CEN. (2005). "EN 1993-1-1 - Eurocode 3 - Design of steel structures - Part 1-1: General rules and rules for buildings".
- CEN. (2005). "EN 1993-1-8 - Eurocode 3 - Design of steel structures - Part 1-8: Design of joints".
- CEN. (2005). "EN 1993-1-8 - Eurocode 3 - Design of steel structures - Part 1-8: Design of joints".
- CEN. (2005). "EN 1996-1-1 - Eurocode 6 - Design of masonry structures - Part 1-1: general rules for reinforced and unreinforced masonry structures".

## REFERENCES

- CEN. (2006). « EN 1991-1-7 - Eurocode 1 - Actions on structures - Part 1-7: General actions - Accidental actions ».
- CEN. (2007). “EN 15048-1 - Non-preloaded structural bolt assemblies - Part 1: General requirements”.
- CEN. (2007). “EN 15048-2 - Non-preloaded structural bolt assemblies - Part 2: Suitability test”.
- CEN. (2008). “EN 1090-1 - Execution of steel structures and aluminium structures - Part 1: Requirements for conformity assessment of structural components”.
- CEN. (2008). “EN 1090-2 - Execution of steel structures and aluminium structures - Part 2: Technical requirements for steel structures”.
- Centre for the Protection of National Infrastructure. (2011). “Review of international research on structural robustness and disproportionate collapse”. London: Department for Communities and Local Government.
- Čermelj, B., Može, P., & Sinur, F. (2015). “On the prediction of low-cycle fatigue in steel welded beam-to-column joints”. *Journal of Constructional Steel Research*, 117, 49-63.
- Chi, W. M., Kanvinde, A. M., & Deierlein, G. G. (2006). “Prediction of Ductile Fracture in Steel Connections Using SMCS Criterion”. *Journal of Structural Engineering*, 132(2), 171-181.
- Chopra, A. (1995). “Dynamics of structures”. New Jersey: Prentice Hall.
- Ciutina, A. L., & Dubina, D. (2008). “Column web stiffening of steel beam-to-column joints subjected to seismic actions”. *Journal of structural engineering*, 134(3), 505-510.
- Comeliau, L., Demonceau, J. F., & Jaspard, J. P. (2010). “Robustness of steel and composite buildings under impact loading”. SDSS'Rio 2010 Stability and ductility of steel structures. Rio de Janeiro, Brazil.
- COST. (2011). “Robustness of Structures : Final Report of COST Action TU0601”. Prague: Czech Technical University in Prague.
- CSI. (2009). “CSI Analysis Reference Manual - For SAP 2000, ETABS and SAFE”. Berkeley: CSI.
- da Silva, L. S., & Santiago, A. (2003). “Manual de Ligações Metálicas”. Coimbra: CMM - Associação Portuguesa de Construção Metálica e Mista.

- da Silva, L. S., Lima, L., Vellasco, P., & Andrade, S. (2004). "Behaviour of flush end-plate beam to column joints under bending and axial force". *Journal of Steel Composite Structures*, 4(2), 77-94.
- D'Aniello, M., Cassiano, D., & Landolfo, R. (2016). "Monotonic and cyclic inelastic tensile response of european preloadable gr10.9 bolt assemblies". *Journal of Constructional Steel Research*, 124, 77-90.
- D'Aniello, M., Tartaglia, R., Costanzo, S., & Landolfo, R. (2017). "Seismic design of extended stiffened end-plate joints in the framework of Eurocodes". *Journal of Constructional Steel Research*, 128, 512-527.
- Dassault. (2010). "Abaqus 6.10 - Abaqus Analysis User's Manual". Dassault Systèmes Simulia Corp.
- Dassault. (2013). "Abaqus 6.13 - Abaqus Analysis User's Manual". Dassault Systèmes Simulia Corp.
- Dias, J., Castro, J. M., Romão, X., Gonçalves, M., & Lopes, J. C. (2010). "SeIEQ: a web-based application for the selection of earthquake ground motions for structural analysis". 14th European Conference on Earthquake Engineering. Ohrid, Macedonia.
- Dinu, F., Dubina, D., & Marginean, I. (2015). "Improving the structural robustness of multi-storey steel-frame buildings". *Structure and Infrastructure Engineering: Maintenance, Management, Life-Cycle Design and Performance*, 11(8), 1028-1041.
- Dubina, D., Ciutina, A., & Stratan, A. (2001). "Cyclic tests on double sided beam-to-column joints". *Journal of Structural Engineering*, 127(2), 129-136.
- ECCS. (1986). "Recommended testing procedure for assessing the behaviour of structural steel elements under cyclic loads". 1st Ed., Vol. 45. Brussels: ECCS.
- Elghazouli, A. Y. (2009). "Seismic Design of Buildings to Eurocode 8". Oxon: Spon Press.
- Ellingwood, B. (2006). "Mitigating risk from abnormal loads and progressive collapse". *Journal of Performance of Constructed Facilities*, 20, 315-323.
- El-Tawil, S., Li, H., & Kunnath, S. (2014). "Computational Simulation of Gravity-Induced Progressive Collapse of Steel-Frame Buildings: Current Trends and Future Research Needs". 140 (Special Issue: Computational Simulation in Structural Engineering, A2513001).

## REFERENCES

- El-Tawil, S., Vidarsson, E., Mikesell, T., & Kunnath, S. K. (1999). "Inelastic behaviour and design of steel panel zones". *J. Struct. Eng.*, 125(2), 183-193.
- Faella, C., Piluso, V., & Rizzano, G. (2000). "Structural steel semi-rigid connections - Theory design and software". Boca Raton: CRC Publishers.
- Farazman, S., Izzudin, B., & Cormie, D. (2012). "Influence of unreinforced masonry infill panels on the robustness of multi-story buildings". *Journal of Performance of Constructed Facilities*, 10(1061/(ASCE)CF.1943-5509).
- Federal Emergency Management Agency (FEMA). (2007). "FEMA 461 - Interim testing protocols for determining the seismic performance characteristics of structural and nonstructural components". Washington, DC.
- Ferraioli, M., Avossa, A., & Mandara, A. (2014). "Assessment of progressive collapse capacity of earthquake-resistant steel moment frames using pushdown analysis". *Open Construction and Building Technology Journal*, 8, 324-336.
- Formisano, A., Landolfo, R., & Mazzolani, F. M. (2015). "Robustness assessment approaches for steel framed structures under catastrophic events". *Computers and Structures*, 147, 216-228.
- Forni, D., Chiaia, B., & Cadoni, E. (2016). "Strain rate behaviour in tension of S355 steel: Base for progressive collapse analysis". *Engineering Structures*, 119, 164-173.
- Fu, F. (2010). "3-D nonlinear dynamic progressive collapse analysis of multi-storey steel composite frame buildings - Parametric study". *Engineering Structures*, 32, 3974-3980.
- Gerasimidis, S. (2014). "Analytical assessment of steel frames progressive collapse vulnerability to a corner loss". *Journal of Constructional Steel Research*, 95, 1-9.
- Gerasimidis, S., & Sideri, J. (2016). "A new partial-distributed damage method for progressive collapse analysis of steel frames". *Journal of Constructional Steel Research*, 119, 233-245.
- Girão Coelho, A. M., & Bijlaard, F. (2007). "Experimental behaviour of high strength steel end-plate connections". *Journal of Constructional Steel Research*, 63, 1228-1240.
- Goudarzi, A., Ghassemieh, M., & Baei, M. (2012). "The effect of axial force on the behaviour of flush end-plate moment connections". *Proceedings from the 15th World Conference on Earthquake Engineering*. Lisbon, Portugal.

- Guo, B., Gu, Q., & Liu, F. (2006). "Experimental Behavior of Stiffened and Unstiffened End-Plate Connections under Cyclic Loading". *Journal of Structural Engineering*, 132(9).
- Guo, L., Gao, S., & Fu, F. (2015). "Structural performance of semi-rigid composite frame under column loss". *Engineering structures*, 95, 112-126.
- Gupta, A., & Krawinkler, H. (1999). "Seismic demands for performance evaluation of steel moment resisting frame structures - Report N° 132". The John A. Blume Earthquake Engineering Center, Dept. of Civil and environmental engineering, Stanford University.
- Hai, L. (2009). "Structural Response of steel and composite building frames further to an impact leading to the loss of a column". PhD Thesis, University of Liège, Liège.
- Hancock, J. W., & Mackenzie, A. C. (1976). "On the mechanics of ductile failure in high-strength steel subjected to multi-axial stress-states". *Journal of the Mechanics and Physics of Solids*, 24(3), 147-160.
- Hanus, F., Zilli, G., & Franssen, J. M. (2011). "Experimental tests and analytical models for welds and grade 8.8 bolts under heating and subsequent cooling". *Journal of Structural Fire Engineering*, 2(3), 181-194.
- Hayes, J., Woodson, S., Pekelnicky, R., Poland, C., Corley, W., & Sozen, M. (2005). "Can strengthening for earthquake improve blast and progressive collapse resistance? ", 131(8), 1157-1177.
- Huvelle, C., Hoang, V., Jaspard, J., & Demonceau, J. (2015). "Complete analytical procedure to assess the response of a frame submitted to a column loss". *Engineering Structures*, 86, 33-42.
- Iannone, F., Latour, M., Piluso, V., & Rizzano, G. (2011). "Experimental analysis of bolted steel beam-to-column connections: component identification". *Journal of Earthquake Engineering*, 15, 214-244.
- ISO. (1993). "ISO 3800 - Threaded fasteners - Axial load fatigue testing - Test methods and evaluation of results".
- ISO. (2009). "EN ISO 2560 - Welding consumables. Covered electrodes for manual metal arc welding of non-alloy and fine grain steels. Classification".

## REFERENCES

- Iuorio, O., Macillo, V., Terracciano, M. T., Pali, T., Fiorino, L., & Landolfo, R. (2014). "Seismic response of Cfs strap-braced stud walls: Experimental investigation". *Thin-Walled Structures*, 85, 466-480.
- Izzudin, B. (2005). "A simplified model for axially restrained beams subject to extreme loading". *Steel Structures*, 5, 421-429.
- Izzudin, B., Vlassis, A., Elghazouli, A., & Nethercot, D. (2008). "Progressive collapse of multi-storey buildings due to sudden column loss - Part I: Simplified assessment framework". *Engineering Structures*, 30, 1308-1318.
- Jahromi, H. (2009). "Progressive collapse of building structures - influence of membrane action in floor slabs". MSc Thesis, Imperial College London, Department of Civil and Environmental Engineering.
- Jahromi, H., Izzudin, B., Nethercot, D., Donahue, S., Hadjioannou, M., Williamson, E., et al. (2012). "Robustness assessment of building structures under explosion". *Buildings*, 2, 497-518.
- Jaspart, J. P. (1991). "Etude de la semi-rigidité des noeuds poutre-colonne et son influence sur la résistance et la stabilité des ossatures en acier". Liège: Université de Liège.
- Jaspart, J., Braham, M., & Cerfontaine, F. (1999). "Strength of joints subject to combined action of bending moments and axial forces". In C. Prague (Ed.), *Proceedings of the Conference Eurosteel '99*, 2, 465-468. Prague.
- Johnson, G. R., & Cook, W. H. (1983). "A constitutive model and data for metals subjected to large strains, high strain rates and high temperatures". *Proceedings of the 7th international symposium on ballistics*, 541-547. The Hague.
- Johnson, L. (2014). "Microstructural characterisation of structural bolt assemblies in fire". Sheffield: University of Sheffield.
- Khandelwal, K., & El-Tawil, S. (2007). "Collapse behavior of steel special moment resisting frame connections", 133, 646-655.
- Khandelwal, K., & El-Tawil, S. (2011). "Pushdown resistance as a measure of robustness in progressive collapse analysis". *Engineering Structures*, 65, 2653-2661.
- Khandelwal, K., El-Tawil, S., Kunnath, S., & Lew, H. (2008). "Macromodel-Based Simulation of Progressive Collapse". *Steel Frame Structures*, 137(7), 1070-1078.



- Kim, J., & An, D. (2009). "Evaluation of progressive collapse potential of steel moment frames considering catenary action". *Tall and special buildings*, 18(4), 455-465.
- Kim, J., Park, J.-H., & Lee, T.-H. (2011). "Sensitivity analysis of steel buildings subjected to column loss". *Engineering Structures*, 33, 421-432.
- Kim, K., & Englehardt, M. D. (1995). "Development of analytical models for earthquake analysis of steel moment frames - Report N° PMFSEL 95-2". Dept. of Civil Eng. Austin: University of Texas.
- Kim, T., & Kim, J. (2009). "Collapse analysis of steel moment frames with various seismic connections". *Journal of Constructional Steel Research*, 65, 1316-1322.
- Krawinkler, H. (1978). "Shear design of steel frame joints". *Engineering Journal - AISC*, 15(3).
- Krawinkler, H. (2000). "System performance of steel moment resisting frame structures". 12th World Conference on Earthquake Engineering. Auckland: New Zealand Society for Earthquake Engineering.
- Krawinkler, H., Bertero, V. V., & Popov, E. P. (1971). "Inelastic behaviour of steel beam-to-column sub-assemblages - Report No. UCB/EERC-71/07". University of California at Berkeley. Berkeley: Earthquake Engineering Research Center (EERC).
- Kuhlmann, U., Rolle, L., Jaspert, J. P., Demonceau, J. F., Vassart, O., Weyland, K., et al. (2007). "Robust structures by joint ductility". Research Fund for Coal and Steel.
- Kwasniewski, L. (2010). "Nonlinear dynamic simulations of progressive collapse for a multistorey building". *Engineering Structures*, 32, 1223-1235.
- Lalani, M., & Shuttleworth, E. P. (1990). "The ultimate state of offshore platforms using reserve and residual strength principles". The 22nd offshore technology conference. Houston.
- Latour, M., Piluso, V., & Rizzano, G. (2011). "Cyclic modelling of bolted beam-to-column connections: component approach". *Journal of Earthquake Engineering*, 15, 537-563.
- Lee, C.-H., Kim, S., Han, K.-H., & Lee, K. (2009). "Simplified nonlinear progressive collapse analysis of welded steel moment frames". *Journal of Constructional Steel Research*, 65, 1130-1137.

## REFERENCES

- Lew, H., Main, J., Robert, S., Sadek, F., & Chiarito, V. (2013). "Performance of steel moment connections under a column removal scenario. I: Experiments". *Journal of Structural Engineering*, 139(1), 98-107.
- Li, H., & El-Tawil, S. (2013). "Three-Dimensional Effects and Collapse Resistance Mechanisms in Steel Frame Buildings". *Journal of Structural Engineering*, 10.
- Lima, L. (2003). "Comportamento de ligações com placa de extremidade em estruturas de aço submetidas a momento fletor e força axial". PhD Thesis, Pontifícia Universidade Católica do Rio de Janeiro, Rio de Janeiro.
- Liu, C., Tan, K. H., & Fung, T. C. (2013). "Dynamic behaviour of web cleat connections subjected to sudden column removal scenario". *Journal of Constructional Steel Research*, 86, 92-106.
- Liu, C., Tan, K. H., & Fung, T. C. (2015). "Component-based steel beam-column connections modelling for dynamic progressive collapse analysis". *Journal of constructional steel research*, 107, 24-36.
- Liu, J. (1997). "Earthquake analysis of steel moment resisting frame structures". MSc. Thesis, Carleton University, Department of Civil and Environmental Engineering, Ottawa.
- Liu, J., Main, J., & Sadek, F. (2012). "Modelling of double-angle shear connections for evaluation of structural robustness". 6th Congress on Forensic Engineering. San Francisco, USA.
- Liu, M. (2013). "A new dynamic increase factor for nonlinear static alternate path analysis of building frames against progressive collapse". *Engineering Structures*, 48, 666-673.
- Lu, D., Cui, S., Song, P., & Chen, Z. (2012). « Robustness assessment for progressive collapse of framed structures using pushdown analysis method". *International Journal of Reliability and Safety*, 6(1/2/3).
- Lu, L. W., Wang, S. J., & Lee, S. J. (1988). "Cyclic behaviour of steel and composite joints with panel zone deformation". Proceedings of the 9th world conference on earthquake engineering. Tokyo-Kyoto.
- Lulak, G., Fisher, J., & Struik, J. (1974). "Guide to design criteria for bolted and riveted joints". 2nd Ed., Chicago: American Institute of Steel Construction.

- Main, J. A., & Sadek, F. (2011). "Modeling of Bolted Connections for Collapse Analysis of Steel Structures". 14th International Symposium on Interaction of the Effects of Munitions with Structures. Seattle.
- Marchand, K. A., & Alfawakhiri, F. (2004). "Blast and progressive collapse". Facts for steel buildings, 2.
- Marchand, K., McKay, A., & Stevens, D. J. (2009). "Development and application of linear and nonlinear static approaches in UFC 4-023-03". Structures Congress. Austin.
- Markulak, D., Radic, I., & Sigmund, V. (2013). "Cyclic testing of single bay steel frames with various types of masonry infill". *Engineering Structures*, 51, 267-277.
- Markulak, D., Sigmund, V., & Radic, I. (2008). "Modeliranje celicnih okvira sa zidanim ispunom". *Gradevinar*, 60(4), 317-26.
- Mays, T. W. (2000). "Application of the Finite Element Method to the Seismic Design and Analysis of Large Moment End-Plate Connections". Ph.D. Dissertation, Virginia Polytechnic Institute and State University, Blacksburg, Virginia, USA.
- McConnell, J., Cotter, T., & Rollins, T. (2015). "Finite element analysis assessing partial catenary action in steel beams". *Journal of Constructional Steel Research*, 109, 1-12.
- Mohamadi-shooreh, M., & Mofid, M. (2013). "Prediction of the yielding moment of flush endplate splice connections using finite element modelling". *Scientia Iranica A*(20(2)), 270-277.
- Myers, A. T., Kanvinde, A. M., & Deierlein, G. G. (2010). "Calibration of the SMCS Criterion for Ductile Fracture in Steels: Specimen Size Dependence and Parameter Assessment". *Journal of Engineering Mechanics*, 136(11), 1401-1410.
- Naqash, M. T., De Matteis, G., & De Luca, A. (2012). "Seismic design of steel moment resisting frames - European versus American practice". *NED University Journal of Research*.
- National Institute of Standards and Technology. (2007). "Best Practices for Reducing the Potential for Progressive Collapse in Buildings". US Department of Commerce.
- New York City Department of Buildings. (2003). "Rules and Regulations of the Building Code of the City of New York". New York: New York City Department of Buildings.

- Ngo, T., Mendis, P., Gupta, A., & Ramsey, J. (2007). "Blast loading and blast effects on structures - an overview". *Electronic Journal of Structural Engineering, Special Issue: Loading on Structures*.
- Oosterhof, S. A., & Driver, R. G. (2014). "Behavior of Steel Shear Connections under Column-Removal Demands". *Journal of Structural Engineering*.
- Parisi, F., & Augenti, N. (2012). "Influence of seismic design criteria on blast resistance of RC framed buildings: a case study". *Engineering Structures, 44*, 78-93.
- Pavlovic, M., Heistermann, C., Veljkovic, M., Pak, D., Feldmann, M., Rebelo, C., et al. (2015). "Connections in towers for wind converters, part I: Evaluation of down-scaled experiments". *Journal of Constructional Steel Research, 115*, 445-457.
- Pearson, C., & Delatte, N. (2005). "Ronan Point Apartment Tower Collapse and its Effect on Building Codes". *Journal of Performance of Constructed Facilities, 19*(2), 172-177.
- Pereira, M. (2012). "Robustness of multi-storey steel composite buildings under column loss: rate-sensitivity and probabilistic framework". Ph.D. Thesis, Imperial College London, London.
- Prinz, G., Nussbaumer, A., Borges, L., & Khadka, S. (2014). "Experimental testing and simulation of bolted beam-column connections having thick extended endplates and multiple bolts per row". *Engineering Structures, 59*, 434-447.
- Rathje, E. M., Faraj, F., Russel, S., & Bray, J. D. (2004). "Empirical relationships for frequency content parameters of earthquake ground motions". *Earthquake spectra, 20*(1), 119-144.
- Rex, C., & Easterling, W. (2003). "Behaviour and modelling of a bolt bearing on a single plate". *Journal of structural engineering, 129*(6), 792-801.
- Ribeiro, J., Santiago, A., Rigueiro, C., Barata, P., & Veljkovic, M. (2016). "Numerical assessment of T-stub component subjected to impact loading". *106*, 450-460.
- Ruth, P., Marchand, K., & Williamson, E. (2006). "Static equivalency in progressive collapse alternate path analysis: Reducing conservatism while retaining structural integrity". *20*(4), 349-364.
- Sadek, F., Main, J. A., Lew, H. S., & Bao, Y. (2011). "Testing and Analysis of Steel and Concrete Beam-Column Assemblies under a Column Removal Scenario". *Journal of Structural Engineering, 137*(9), 881-892.

- Sadek, F., Main, J., Lew, H., & El-Tawil, S. (2013). "Performance of steel moment connections under a column removal scenario. II: Analysis". *Journal of Structural Engineering*, 139, 108-119.
- Santos, F., & Silva, L. S. (2011). "Manual de execução de estruturas metálicas". Coimbra: CMM Press.
- Schneider, S., & Amidi, A. (1998). "Seismic behavior of steel frames with deformable panel zones". *Journal of structural engineering*, 1241, 35-43.
- Seismosoft. (2014). "SeismoStruct v7.0 - A computer program for static and dynamic nonlinear analysis of framed structures".
- Seismosoft. (2016). "SeismoSignal 2016 - A computer program for signal processing of strong-motion data".
- Shahani, A., & Shakeri, I. (2015). "Experimental evaluation of the effect of preload on the fatigue life of bolts". *International Journal of Steel Structures*, 15(3), 693-701.
- Shaker, F., & Elrahman, W. (2014). "Behaviour of flush and extended end-plate beam-to-column joints under bedding and axial force". *World applied sciences journal*, 30(6), 685-695.
- Sherbourne, A. N., & Bahaari, M. R. (1997). "Finite Element Prediction of End Plate Bolted Connection Behavior. I: Parametric Study". 123(2), 157-164.
- Shi, G., Shi, Y., & Wang, Y. (2007). "Behaviour of end-plate moment connections under earthquake loading". *Engineering Structures*, 29, 703-716.
- Silva, L. S., Lima, L., Vellasco, P., & Andrade, S. (2004). "Behaviour of flush end-plate beam to column joints under bending and axial force". *Journal of Steel Composite Structures*, 4(2), 77-94.
- Song, B., & Sezen, H. (2013). "Experimental and analytical progressive collapse assessment of a steel frame building". *Engineering Structures*, 56, 664-672.
- Sorensen, J. D., Rizzuto, E., & Faber, M. H. (2009). "Robustness - theoretical framework - Joint Workshop of COST Actions TU0601 and E55". Ljubljana.
- Starossek, U., & Haberland, M. (2008). "Approaches to measures of structural robustness". IABMAS'08, 4th International Conference on Bridge Maintenance, Safety and Management. Seoul, Korea.
- Stevens, D., Crowder, B., Hall, B., & Marchand, K. (2008). "Unified progressive collapse design requirements for DoD and GSA". *Structures Congress*. Vancouver.

## REFERENCES

- Stevens, D., Crowder, B., Sunshine, D., Marchand, K., Smilowitz, R., Williamson, E., et al. (2011). "DoD research and criteria for the design of buildings to resist progressive collapse". *Journal of Structural Engineering*, 137, 870-880.
- Structural Engineering Institute. (1998). "ASCE Standard ASCE/SEI 7-98 - Minimum Design Loads for Buildings and Other Structures". American Society of Civil Engineers.
- Swanson, J. A. (1999). "Characterization of the Strength, Stiffness, and Ductility Behavior of T-Stub Connections". Atlanta, Georgia, USA: Georgia Institute of Technology.
- Swanson, J., & Leon, R. (2001). "Stiffness modelling of bolted T-Stub connection components". *Journal of Structural Engineering*, 127(5), 498-505.
- Swanson, J., & Leon, R. (2001). "Stiffness modelling of bolted T-Stub connection components". *Journal of Structural Engineering*, 127(5), 498-505.
- Taewan, K., & Jinkoo, K. (2009). "Collapse analysis of steel moment frames with various seismic connections". *Journal of Constructional Steel Research*, 65, 1316-1322.
- Tartaglia, R., D'Aniello, M., & Landolfo, R. (2016). "Nonlinear performance of extended stiffened end plate bolted beam-to-column joints subjected to column removal". *Open Civil Engineering Journal*, 10.
- The Building (Fifth Amendment) Regulations 1970 (S.I. 1970/109). (1970). London, UK: UK Government.
- The Building Regulations 1985 (S.I. 1985/1065). (1985). London, UK: UK Government.
- The Building Regulations 1991 (S.I. 1991/2580). (1991). London, UK: UK Government.
- The Building Regulations 2000 (S.I. 2000/2531). (2000). London, UK: UK Government.
- Tsai, M. (2012). "Assessment of analytical load and dynamic increase factors for progressive collapse analysis of building frames". *Advances in Structural Engineering*, 15, 41-54.
- Tsai, M. H. (2010). "An analytical methodology for the dynamic amplification factor in progressive collapse evaluation of building structures". *Mechanics Research Communications*, 37(1), 61-66.
- U.S. General Services Administration. (2003). "Progressive Collapse Analysis and Guidelines for New Federal Office Buildings and Major Modernization Projects".

- United States of America Department of Defense. (2005). "United Facilities Criteria (UFC) - Design of buildings to resist progressive collapse".
- United States of America Department of Defense. (2009). "United Facilities Criteria (UFC) - Design of buildings to resist progressive collapse".
- United States of America Department of Defense. (2009). "United Facilities Criteria (UFC) - Design of buildings to resist progressive collapse".
- United States of America Department of Defense. (2013). "United Facilities Criteria (UFC) - Design of buildings to resist progressive collapse".
- University of California Santa Barbara. (2016). Strong Motion Virtual Data Center (VDC). Retrieved 12 12, 2016, from <http://strongmotioncenter.org/vdc/scripts/search.plx>
- Vlassis, A., Izzudin, B., Elghazouli, A., & Nethercot, D. (2008). "Progressive collapse of multi-storey buildings due to sudden column loss - Part II: Application". *Engineering Structures*, 30, 1424-1438.
- Wade, P. M. (2006). "Characterization of high-strength bolt behavior in bolted moment connections". Raleigh, North Carolina, USA: North Carolina State University.
- Wang, W., Fang, C., Qin, X., Chen, Y., & Li, L. (2016). "Performance of practical beam-to-SHS column connections against progressive collapse". *Engineering Structures*, 106, 332-347.
- Wang, Y. C., Dai, X. H., & Bailey, C. G. (2011). "An experimental study of relative structural fire behaviour and robustness of different types of steel joint in restrained steel frames". *Journal of constructional steel research*, 67(7), 1149-1163.
- Wikipedia. (n.d.). "Ronan Point". Retrieved July 12, 2016, from [https://en.wikipedia.org/wiki/Ronan\\_Point](https://en.wikipedia.org/wiki/Ronan_Point)
- Xu, G., & Ellingwood, B. (2011). "Probabilistic assessment of pre-Northridge steel moment resisting frames". *Journal of Structural Engineering*, 137, 925-934.
- Yang, B., & Tan, K. (2012). "Numerical analyses of steel beam-column joints subjected to catenary action". *Journal of Constructional Steel Research*, 70, 1-11.
- Yang, B., & Tan, K. (2013). "Experimental tests of different types of bolted steel beam-column joints under a central-column removal scenario". *Engineering Structures*, 54, 112-130.

## REFERENCES

- Yang, B., & Tan, K. H. (2012). "Component-based model of bolted-angle connections subjected to catenary action". Proceedings of the 10th international conference on advances in steel concrete composite and hybrid structures, 654-661. Singapore.
- Yang, B., Tan, K., & Xiong, G. (2015). "Behaviour of composite beam-column joints under a middle column removal scenario: component based modelling". Journal of Constructional Steel Research, 104, 137-154.
- Yu, H. X., Burgess, I. W., Davison, J. B., & Plank, R. J. (2009). "Tying capacity of web cleat connections in fire, part 2: development of component-based model". Engineering structures, 31(3), 697-708.
- Yu, H., Burgess, I., Davison, J., & Planck, R. (2011). "Experimental and numerical investigations of the behaviour of flush end plate connections at elevated temperatures". Journal of Constructional Engineering, 137, 80-87.
- Zangouie, A. R., & Deylami, A. (2013). « Influence of beam flange thickness on seismic performance of flange plate connections". Sapporo, Japan: Proceedings of the 13th East Asia-Pacific Conference on Structural Engineering and Construction (EASEC-13).
- Zoetemeijer, P. (1983). "Summary of the research on bolted beam-to-column connections (period 1978-1983)". Delft: Stephen Laboratory.



## Appendix A Moment resisting frame member cross sections

In this section the frame model list reporting the main characteristics in terms of parametric variables (see for parametric variable definition), as well as the adopted cross section types for the different members of the frames designed in the scope of this thesis is presented.

### Model list and parametric variables

Model #	N	H	S	C	T	D
[-]	[-]	[m]	[m]	[-]	[-]	[-]
1	4	3	6	N	5x3	W
2	4	3	6	N	5x3	E
3	4	3	6	N	4x4	W
4	4	3	6	N	4x4	E
5	4	3	6	N	5x4	W
6	4	3	6	N	5x4	E
7	4	3	6	M	5x3	W
8	4	3	6	C	5x3	E
9	4	3	6	M	4x4	W
10	4	3	6	C	4x4	E
11	4	3	6	M	5x4	W
12	4	3	6	C	5x4	E
13	4	3	10	N	5x3	W
14	4	3	10	N	5x3	E
15	4	3	10	N	4x4	W
16	4	3	10	N	4x4	E
17	4	3	10	N	5x4	W
18	4	3	10	N	5x4	E
19	4	3	10	M	5x3	W
20	4	3	10	C	5x3	E
21	4	3	10	M	4x4	W
22	4	3	10	C	4x4	E
23	4	3	10	M	5x4	W
24	4	3	10	C	5x4	E
25	4	4	6	N	5x3	W
26	4	4	6	N	5x3	E
27	4	4	6	N	4x4	W
28	4	4	6	N	4x4	E
29	4	4	6	N	5x4	W
30	4	4	6	N	5x4	E
31	4	4	6	M	5x3	W
32	4	4	6	C	5x3	E
33	4	4	6	M	4x4	W
34	4	4	6	C	4x4	E
35	4	4	6	M	5x4	W
36	4	4	6	C	5x4	E
37	4	4	10	N	5x3	W
38	4	4	10	N	5x3	E
39	4	4	10	N	4x4	W

Model #	N	H	S	C	T	D
[-]	[-]	[m]	[m]	[-]	[-]	[-]
40	4	4	10	N	4x4	E
41	4	4	10	N	5x4	W
42	4	4	10	N	5x4	E
43	4	4	10	M	5x3	W
44	4	4	10	C	5x3	E
45	4	4	10	M	4x4	W
46	4	4	10	C	4x4	E
47	4	4	10	M	5x4	W
48	4	4	10	C	5x4	E
49	8	3	6	N	5x3	W
50	8	3	6	N	5x3	E
51	8	3	6	N	4x4	W
52	8	3	6	N	4x4	E
53	8	3	6	N	5x4	W
54	8	3	6	N	5x4	E
55	8	3	6	M	5x3	W
56	8	3	6	C	5x3	E
57	8	3	6	M	4x4	W
58	8	3	6	C	4x4	E
59	8	3	6	M	5x4	W
60	8	3	6	C	5x4	E
61	8	3	10	N	5x3	W
62	8	3	10	N	5x3	E
63	8	3	10	N	4x4	W
64	8	3	10	N	4x4	E
65	8	3	10	N	5x4	W
66	8	3	10	N	5x4	E
67	8	3	10	M	5x3	W
68	8	3	10	C	5x3	E
69	8	3	10	M	4x4	W
70	8	3	10	C	4x4	E
71	8	3	10	M	5x4	W
72	8	3	10	C	5x4	E
73	8	4	6	N	5x3	W
74	8	4	6	N	5x3	E
75	8	4	6	N	4x4	W
76	8	4	6	N	4x4	E
77	8	4	6	N	5x4	W
78	8	4	6	N	5x4	E
79	8	4	6	M	5x3	W
80	8	4	6	C	5x3	E
81	8	4	6	M	4x4	W
82	8	4	6	C	4x4	E
83	8	4	6	M	5x4	W
84	8	4	6	C	5x4	E
85	8	4	10	N	5x3	W
86	8	4	10	N	5x3	E
87	8	4	10	N	4x4	W
88	8	4	10	N	4x4	E
89	8	4	10	N	5x4	W
90	8	4	10	N	5x4	E
91	8	4	10	M	5x3	W
92	8	4	10	C	5x3	E
93	8	4	10	M	4x4	W
94	8	4	10	C	4x4	E
95	8	4	10	M	5x4	W
96	8	4	10	C	5x4	E

## Moment resisting frame beams - XZ façade

MODEL #	Gr.	Storey							
		1st	2nd	3rd	4th	5th	6th	7th	8th
1	IPE 330	IPE 330	IPE 330	IPE 300	IPE 300				
2	IPE 330	IPE 330	IPE 330	IPE 330	IPE 330				
3	IPE 400	IPE 400	IPE 400	IPE 360	IPE 360				
4	IPE 400	IPE 400	IPE 400	IPE 400	IPE 400				
5	IPE 360	IPE 360	IPE 360	IPE 330	IPE 330				
6	IPE 360	IPE 360	IPE 360	IPE 330	IPE 330				
7	IPE 330	IPE 330	IPE 330	IPE 300	IPE 300				
8	IPE 330	IPE 330	IPE 330	IPE 330	IPE 330				
9	IPE 400	IPE 400	IPE 400	IPE 360	IPE 360				
10	IPE 400	IPE 400	IPE 400	IPE 400	IPE 400				
11	IPE 360	IPE 360	IPE 360	IPE 330	IPE 330				
12	IPE 360	IPE 360	IPE 360	IPE 330	IPE 330				
13	IPE 400	IPE 400	IPE 400	IPE 400	IPE 400				
14	IPE 450	IPE 450	IPE 450	IPE 450	IPE 450				
15	IPE 500	IPE 500	IPE 500	IPE 450	IPE 450				
16	IPE 600	IPE 600	IPE 600	IPE 500	IPE 500				
17	IPE 450	IPE 450	IPE 450	IPE 400	IPE 400				
18	IPE 550	IPE 550	IPE 550	IPE 450	IPE 450				
19	IPE 400	IPE 400	IPE 400	IPE 400	IPE 400				
20	IPE 450	IPE 450	IPE 450	IPE 450	IPE 450				
21	IPE 500	IPE 500	IPE 500	IPE 450	IPE 450				
22	IPE 600	IPE 600	IPE 600	IPE 500	IPE 500				
23	IPE 450	IPE 450	IPE 450	IPE 400	IPE 400				
24	IPE 550	IPE 550	IPE 550	IPE 450	IPE 450				
25	IPE 450	IPE 450	IPE 450	IPE 400	IPE 400				
26	IPE 360	IPE 360	IPE 360	IPE 330	IPE 330				
27	IPE 550	IPE 550	IPE 550	IPE 500	IPE 500				
28	IPE 400	IPE 400	IPE 400	IPE 360	IPE 360				
29	IPE 500	IPE 500	IPE 500	IPE 450	IPE 450				
30	IPE 400	IPE 400	IPE 400	IPE 360	IPE 360				
31	IPE 450	IPE 450	IPE 450	IPE 400	IPE 400				
32	IPE 360	IPE 360	IPE 360	IPE 330	IPE 330				
33	IPE 550	IPE 550	IPE 550	IPE 500	IPE 500				
34	IPE 400	IPE 400	IPE 400	IPE 360	IPE 360				
35	IPE 500	IPE 500	IPE 500	IPE 450	IPE 450				
36	IPE 400	IPE 400	IPE 400	IPE 360	IPE 360				
37	IPE 600	IPE 600	IPE 600	IPE 500	IPE 500				
38	IPE 500	IPE 500	IPE 500	IPE 450	IPE 450				
39	HE 600 A	HE 600 A	HE 600 A	HE 550 A	HE 550 A				
40	IPE 600	IPE 600	IPE 600	IPE 600	IPE 600				
41	HE 600 A	HE 600 A	HE 600 A	HE 500 A	HE 500 A				
42	IPE 600	IPE 600	IPE 600	IPE 500	IPE 500				
43	IPE 600	IPE 600	IPE 600	IPE 500	IPE 500				
44	IPE 500	IPE 500	IPE 500	IPE 450	IPE 450				
45	HE 600 A	HE 600 A	HE 600 A	HE 550 A	HE 550 A				
46	IPE 600	IPE 600	IPE 600	IPE 600	IPE 600				
47	HE 600 A	HE 600 A	HE 600 A	HE 500 A	HE 500 A				
48	IPE 600	IPE 600	IPE 600	IPE 500	IPE 500				
49	IPE 550	IPE 550	IPE 550	IPE 500	IPE 500	IPE 500	IPE 450	IPE 450	IPE 450
50	IPE 500	IPE 500	IPE 500	IPE 450	IPE 450	IPE 450	IPE 400	IPE 400	IPE 400
51	HE 600 A	HE 600 A	HE 600 A	HE 550 A	HE 550 A	HE 550 A	HE 500 A	HE 500 A	HE 500 A
52	IPE 600	IPE 600	IPE 600	IPE 500	IPE 500	IPE 500	IPE 400	IPE 400	IPE 400
53	IPE 550	IPE 550	IPE 550	IPE 500	IPE 500	IPE 500	IPE 450	IPE 450	IPE 450
54	IPE 550	IPE 550	IPE 550	IPE 500	IPE 500	IPE 500	IPE 450	IPE 450	IPE 450
55	IPE 550	IPE 550	IPE 550	IPE 500	IPE 500	IPE 500	IPE 450	IPE 450	IPE 450
56	IPE 500	IPE 500	IPE 500	IPE 450	IPE 450	IPE 450	IPE 400	IPE 400	IPE 400
57	HE 600 A	HE 600 A	HE 600 A	HE 550 A	HE 550 A	HE 550 A	HE 500 A	HE 500 A	HE 500 A
58	IPE 600	IPE 600	IPE 600	IPE 500	IPE 500	IPE 500	IPE 400	IPE 400	IPE 400
59	IPE 550	IPE 550	IPE 550	IPE 500	IPE 500	IPE 500	IPE 450	IPE 450	IPE 450
60	IPE 550	IPE 550	IPE 550	IPE 500	IPE 500	IPE 500	IPE 450	IPE 450	IPE 450
61	HE 550 A	HE 550 A	HE 550 A	HE 500 A	HE 500 A	HE 500 A	HE 450 A	HE 450 A	HE 450 A
62	IPE 550	IPE 550	IPE 550	IPE 550	IPE 550	IPE 550	IPE 550	IPE 550	IPE 550
63	HE 700 A	HE 700 A	HE 700 A	HE 650 A	HE 650 A	HE 650 A	HE 600 A	HE 600 A	HE 600 A
64	IPE 550	IPE 550	IPE 550	IPE 550	IPE 550	IPE 550	IPE 550	IPE 550	IPE 550
65	HE 600 A	HE 600 A	HE 600 A	HE 550 A	HE 550 A	HE 550 A	HE 500 A	HE 500 A	HE 500 A
66	IPE 550	IPE 550	IPE 550	IPE 550	IPE 550	IPE 550	IPE 550	IPE 550	IPE 550
67	HE 550 A	HE 550 A	HE 550 A	HE 500 A	HE 500 A	HE 500 A	HE 450 A	HE 450 A	HE 450 A
68	IPE 550	IPE 550	IPE 550	IPE 550	IPE 550	IPE 550	IPE 550	IPE 550	IPE 550
69	HE 700 A	HE 700 A	HE 700 A	HE 650 A	HE 650 A	HE 650 A	HE 600 A	HE 600 A	HE 600 A
70	IPE 550	IPE 550	IPE 550	IPE 550	IPE 550	IPE 550	IPE 550	IPE 550	IPE 550

MODEL #	Gr.	Storey							
		1st	2nd	3rd	4th	5th	6th	7th	8th
71	HE 600 A	HE 600 A	HE 600 A	HE 550 A	HE 550 A	HE 550 A	HE 500 A	HE 500 A	HE 500 A
72	IPE 550	IPE 550	IPE 550	IPE 550	IPE 550	IPE 550	IPE 550	IPE 550	IPE 550
73	HE 600 A	HE 600 A	HE 600 A	HE 550 A	HE 550 A	HE 550 A	HE 500 A	HE 500 A	HE 500 A
74	IPE 550	IPE 550	IPE 550	IPE 500	IPE 500	IPE 500	IPE 400	IPE 400	IPE 400
75	HE 800 A	HE 800 A	HE 800 A	HE 700 A	HE 700 A	HE 700 A	HE 600 A	HE 600 A	HE 600 A
76	HE 600 A	HE 600 A	HE 600 A	HE 500 A	HE 500 A	HE 500 A	HE 400 A	HE 400 A	HE 400 A
77	HE 700 A	HE 700 A	HE 700 A	HE 650 A	HE 650 A	HE 650 A	HE 600 A	HE 600 A	HE 600 A
78	HE 550 A	HE 550 A	HE 550 A	HE 450 A	HE 450 A	HE 450 A	HE 360 A	HE 360 A	HE 360 A
79	HE 600 A	HE 600 A	HE 600 A	HE 550 A	HE 550 A	HE 550 A	HE 500 A	HE 500 A	HE 500 A
80	IPE 550	IPE 550	IPE 550	IPE 500	IPE 500	IPE 500	IPE 400	IPE 400	IPE 400
81	HE 800 A	HE 800 A	HE 800 A	HE 700 A	HE 700 A	HE 700 A	HE 600 A	HE 600 A	HE 600 A
82	HE 600 A	HE 600 A	HE 600 A	HE 500 A	HE 500 A	HE 500 A	HE 400 A	HE 400 A	HE 400 A
83	HE 700 A	HE 700 A	HE 700 A	HE 650 A	HE 650 A	HE 650 A	HE 600 A	HE 600 A	HE 600 A
84	HE 550 A	HE 550 A	HE 550 A	HE 450 A	HE 450 A	HE 450 A	HE 360 A	HE 360 A	HE 360 A
85	HE 800 A	HE 800 A	HE 800 A	HE 700 A	HE 700 A	HE 700 A	HE 650 A	HE 650 A	HE 650 A
86	IPE 550	IPE 550	IPE 550	IPE 550	IPE 550	IPE 550	IPE 550	IPE 550	IPE 550
87	HE 1000 A	HE 1000 A	HE 1000 A	HE 900 A	HE 900 A	HE 900 A	HE 800 A	HE 800 A	HE 800 A
88	IPE 550	IPE 550	IPE 550	IPE 550	IPE 550	IPE 550	IPE 550	IPE 550	IPE 550
89	HE 900 A	HE 900 A	HE 900 A	HE 800 A	HE 800 A	HE 800 A	HE 700 A	HE 700 A	HE 700 A
90	IPE 550	IPE 550	IPE 550	IPE 550	IPE 550	IPE 550	IPE 550	IPE 550	IPE 550
91	HE 800 A	HE 800 A	HE 800 A	HE 700 A	HE 700 A	HE 700 A	HE 650 A	HE 650 A	HE 650 A
92	IPE 550	IPE 550	IPE 550	IPE 550	IPE 550	IPE 550	IPE 550	IPE 550	IPE 550
93	HE 1000 A	HE 1000 A	HE 1000 A	HE 900 A	HE 900 A	HE 900 A	HE 800 A	HE 800 A	HE 800 A
94	IPE 550	IPE 550	IPE 550	IPE 550	IPE 550	IPE 550	IPE 550	IPE 550	IPE 550
95	HE 900 A	HE 900 A	HE 900 A	HE 800 A	HE 800 A	HE 800 A	HE 700 A	HE 700 A	HE 700 A
96	IPE 550	IPE 550	IPE 550	IPE 550	IPE 550	IPE 550	IPE 550	IPE 550	IPE 550

## Moment resisting frame beams - YZ façade

MODEL #	Gr.	Storey							
		1st	2nd	3rd	4th	5th	6th	7th	8th
1	IPE 400	IPE 400	IPE 400	IPE 360	IPE 360				
2	IPE 400	IPE 400	IPE 400	IPE 360	IPE 360				
3	IPE 360	IPE 360	IPE 360	IPE 330	IPE 330				
4	IPE 360	IPE 360	IPE 360	IPE 330	IPE 330				
5	IPE 400	IPE 400	IPE 400	IPE 360	IPE 360				
6	IPE 360	IPE 360	IPE 360	IPE 360	IPE 360				
7	IPE 400	IPE 400	IPE 400	IPE 360	IPE 360				
8	IPE 400	IPE 400	IPE 400	IPE 360	IPE 360				
9	IPE 360	IPE 360	IPE 360	IPE 330	IPE 330				
10	IPE 360	IPE 360	IPE 360	IPE 330	IPE 330				
11	IPE 400	IPE 400	IPE 400	IPE 360	IPE 360				
12	IPE 360	IPE 360	IPE 360	IPE 360	IPE 360				
13	IPE 500	IPE 500	IPE 500	IPE 450	IPE 450				
14	IPE 500	IPE 500	IPE 500	IPE 360	IPE 360				
15	IPE 450	IPE 450	IPE 450	IPE 400	IPE 400				
16	IPE 450	IPE 450	IPE 450	IPE 400	IPE 400				
17	IPE 500	IPE 500	IPE 500	IPE 450	IPE 450				
18	IPE 450	IPE 450	IPE 450	IPE 400	IPE 400				
19	IPE 500	IPE 500	IPE 500	IPE 450	IPE 450				
20	IPE 500	IPE 500	IPE 500	IPE 360	IPE 360				
21	IPE 450	IPE 450	IPE 450	IPE 400	IPE 400				
22	IPE 450	IPE 450	IPE 450	IPE 400	IPE 400				
23	IPE 500	IPE 500	IPE 500	IPE 450	IPE 450				
24	IPE 450	IPE 450	IPE 450	IPE 400	IPE 400				
25	IPE 550	IPE 550	IPE 550	IPE 500	IPE 500				
26	IPE 450	IPE 450	IPE 450	IPE 400	IPE 400				
27	IPE 500	IPE 500	IPE 500	IPE 450	IPE 450				
28	IPE 400	IPE 400	IPE 400	IPE 360	IPE 360				
29	IPE 550	IPE 550	IPE 550	IPE 500	IPE 500				
30	IPE 450	IPE 450	IPE 450	IPE 400	IPE 400				
31	IPE 550	IPE 550	IPE 550	IPE 500	IPE 500				
32	IPE 450	IPE 450	IPE 450	IPE 400	IPE 400				
33	IPE 500	IPE 500	IPE 500	IPE 450	IPE 450				
34	IPE 400	IPE 400	IPE 400	IPE 360	IPE 360				
35	IPE 550	IPE 550	IPE 550	IPE 500	IPE 500				
36	IPE 450	IPE 450	IPE 450	IPE 400	IPE 400				
37	HE 600 A	HE 600 A	HE 600 A	HE 550 A	HE 550 A				
38	IPE 600	IPE 600	IPE 600	IPE 400	IPE 400				
39	HE 550 A	HE 550 A	HE 550 A	HE 500 A	HE 500 A				





MODEL #	Gr.	Storey							
		1st	2nd	3rd	4th	5th	6th	7th	8th
71	HE 500 A	HE 500 A	HE 500 A	HE 500 A	HE 500 A	HE 500 A	HE 500 A	HE 500 A	HE 400 A
72	*	*	*	*	*	*	*	*	*
73	IPE 330	IPE 330	IPE 330	IPE 330	IPE 330	IPE 330	IPE 330	IPE 330	IPE 300
74	IPE 330	IPE 330	IPE 330	IPE 330	IPE 330	IPE 330	IPE 330	IPE 330	IPE 300
75	IPE 330	IPE 330	IPE 330	IPE 330	IPE 330	IPE 330	IPE 330	IPE 330	IPE 300
76	IPE 330	IPE 330	IPE 330	IPE 330	IPE 330	IPE 330	IPE 330	IPE 330	IPE 300
77	IPE 330	IPE 330	IPE 330	IPE 330	IPE 330	IPE 330	IPE 330	IPE 330	IPE 300
78	IPE 330	IPE 330	IPE 330	IPE 330	IPE 330	IPE 330	IPE 330	IPE 330	IPE 300
79	IPE 330	IPE 330	IPE 330	IPE 330	IPE 330	IPE 330	IPE 330	IPE 330	IPE 300
80	IPE 330	IPE 330	IPE 330	IPE 330	IPE 330	IPE 330	IPE 330	IPE 330	IPE 300
81	IPE 330	IPE 330	IPE 330	IPE 330	IPE 330	IPE 330	IPE 330	IPE 330	IPE 300
82	IPE 330	IPE 330	IPE 330	IPE 330	IPE 330	IPE 330	IPE 330	IPE 330	IPE 300
83	IPE 330	IPE 330	IPE 330	IPE 330	IPE 330	IPE 330	IPE 330	IPE 330	IPE 300
84	IPE 330	IPE 330	IPE 330	IPE 330	IPE 330	IPE 330	IPE 330	IPE 330	IPE 300
85	HE 500 A	HE 500 A	HE 500 A	HE 500 A	HE 500 A	HE 500 A	HE 500 A	HE 500 A	HE 400 A
86	*	*	*	*	*	*	*	*	*
87	HE 500 A	HE 500 A	HE 500 A	HE 500 A	HE 500 A	HE 500 A	HE 500 A	HE 500 A	HE 400 A
88	*	*	*	*	*	*	*	*	*
89	HE 500 A	HE 500 A	HE 500 A	HE 500 A	HE 500 A	HE 500 A	HE 500 A	HE 500 A	HE 400 A
90	*	*	*	*	*	*	*	*	*
91	HE 500 A	HE 500 A	HE 500 A	HE 500 A	HE 500 A	HE 500 A	HE 500 A	HE 500 A	HE 400 A
92	*	*	*	*	*	*	*	*	*
93	HE 500 A	HE 500 A	HE 500 A	HE 500 A	HE 500 A	HE 500 A	HE 500 A	HE 500 A	HE 400 A
94	*	*	*	*	*	*	*	*	*
95	HE 500 A	HE 500 A	HE 500 A	HE 500 A	HE 500 A	HE 500 A	HE 500 A	HE 500 A	HE 400 A
96	*	*	*	*	*	*	*	*	*

\* - internal primary beam cross section is the same as the moment resisting frame XZ façade beam cross section

## Peripheral primary beams

MODEL #	Gr.	Storey							
		1st	2nd	3rd	4th	5th	6th	7th	8th
1	IPE 270	IPE 270	IPE 270	IPE 270	IPE 240				
2	IPE 270	IPE 270	IPE 270	IPE 270	IPE 240				
3	IPE 270	IPE 270	IPE 270	IPE 270	IPE 240				
4	IPE 270	IPE 270	IPE 270	IPE 270	IPE 240				
5	IPE 270	IPE 270	IPE 270	IPE 270	IPE 240				
6	IPE 270	IPE 270	IPE 270	IPE 270	IPE 240				
7	IPE 270	IPE 270	IPE 270	IPE 270	IPE 240				
8	IPE 270	IPE 270	IPE 270	IPE 270	IPE 240				
9	IPE 270	IPE 270	IPE 270	IPE 270	IPE 240				
10	IPE 270	IPE 270	IPE 270	IPE 270	IPE 240				
11	IPE 270	IPE 270	IPE 270	IPE 270	IPE 240				
12	IPE 270	IPE 270	IPE 270	IPE 270	IPE 240				
13	HE 360 B	HE 360 B	HE 360 B	HE 360 B	HE 320 A				
14	HE 360 B	HE 360 B	HE 360 B	HE 360 B	HE 320 A				
15	HE 360 B	HE 360 B	HE 360 B	HE 360 B	HE 320 A				
16	HE 360 B	HE 360 B	HE 360 B	HE 360 B	HE 320 A				
17	HE 360 B	HE 360 B	HE 360 B	HE 360 B	HE 320 A				
18	HE 360 B	HE 360 B	HE 360 B	HE 360 B	HE 320 A				
19	HE 360 B	HE 360 B	HE 360 B	HE 360 B	HE 320 A				
20	HE 360 B	HE 360 B	HE 360 B	HE 360 B	HE 320 A				
21	HE 360 B	HE 360 B	HE 360 B	HE 360 B	HE 320 A				
22	HE 360 B	HE 360 B	HE 360 B	HE 360 B	HE 320 A				
23	HE 360 B	HE 360 B	HE 360 B	HE 360 B	HE 320 A				
24	HE 360 B	HE 360 B	HE 360 B	HE 360 B	HE 320 A				
25	IPE 270	IPE 270	IPE 270	IPE 270	IPE 240				
26	IPE 270	IPE 270	IPE 270	IPE 270	IPE 240				
27	IPE 270	IPE 270	IPE 270	IPE 270	IPE 240				
28	IPE 270	IPE 270	IPE 270	IPE 270	IPE 240				
29	IPE 270	IPE 270	IPE 270	IPE 270	IPE 240				
30	IPE 270	IPE 270	IPE 270	IPE 270	IPE 240				
31	IPE 270	IPE 270	IPE 270	IPE 270	IPE 240				
32	IPE 270	IPE 270	IPE 270	IPE 270	IPE 240				
33	IPE 270	IPE 270	IPE 270	IPE 270	IPE 240				
34	IPE 270	IPE 270	IPE 270	IPE 270	IPE 240				
35	IPE 270	IPE 270	IPE 270	IPE 270	IPE 240				
36	IPE 270	IPE 270	IPE 270	IPE 270	IPE 240				







MODEL #	Gr.	Storeys							
		1st	2nd	3rd	4th	5th	6th	7th	8th
71	IPE 360	IPE 360	IPE 360	IPE 360	IPE 360	IPE 360	IPE 360	IPE 360	IPE 360
72	IPE 360	IPE 360	IPE 360	IPE 360	IPE 360	IPE 360	IPE 360	IPE 360	IPE 360
73	IPE 220	IPE 220	IPE 220	IPE 220	IPE 220	IPE 220	IPE 220	IPE 220	IPE 220
74	IPE 220	IPE 220	IPE 220	IPE 220	IPE 220	IPE 220	IPE 220	IPE 220	IPE 220
75	IPE 220	IPE 220	IPE 220	IPE 220	IPE 220	IPE 220	IPE 220	IPE 220	IPE 220
76	IPE 220	IPE 220	IPE 220	IPE 220	IPE 220	IPE 220	IPE 220	IPE 220	IPE 220
77	IPE 220	IPE 220	IPE 220	IPE 220	IPE 220	IPE 220	IPE 220	IPE 220	IPE 220
78	IPE 220	IPE 220	IPE 220	IPE 220	IPE 220	IPE 220	IPE 220	IPE 220	IPE 220
79	IPE 220	IPE 220	IPE 220	IPE 220	IPE 220	IPE 220	IPE 220	IPE 220	IPE 220
80	IPE 220	IPE 220	IPE 220	IPE 220	IPE 220	IPE 220	IPE 220	IPE 220	IPE 220
81	IPE 220	IPE 220	IPE 220	IPE 220	IPE 220	IPE 220	IPE 220	IPE 220	IPE 220
82	IPE 220	IPE 220	IPE 220	IPE 220	IPE 220	IPE 220	IPE 220	IPE 220	IPE 220
83	IPE 220	IPE 220	IPE 220	IPE 220	IPE 220	IPE 220	IPE 220	IPE 220	IPE 220
84	IPE 220	IPE 220	IPE 220	IPE 220	IPE 220	IPE 220	IPE 220	IPE 220	IPE 220
85	IPE 360	IPE 360	IPE 360	IPE 360	IPE 360	IPE 360	IPE 360	IPE 360	IPE 360
86	IPE 360	IPE 360	IPE 360	IPE 360	IPE 360	IPE 360	IPE 360	IPE 360	IPE 360
87	IPE 360	IPE 360	IPE 360	IPE 360	IPE 360	IPE 360	IPE 360	IPE 360	IPE 360
88	IPE 360	IPE 360	IPE 360	IPE 360	IPE 360	IPE 360	IPE 360	IPE 360	IPE 360
89	IPE 360	IPE 360	IPE 360	IPE 360	IPE 360	IPE 360	IPE 360	IPE 360	IPE 360
90	IPE 360	IPE 360	IPE 360	IPE 360	IPE 360	IPE 360	IPE 360	IPE 360	IPE 360
91	IPE 360	IPE 360	IPE 360	IPE 360	IPE 360	IPE 360	IPE 360	IPE 360	IPE 360
92	IPE 360	IPE 360	IPE 360	IPE 360	IPE 360	IPE 360	IPE 360	IPE 360	IPE 360
93	IPE 360	IPE 360	IPE 360	IPE 360	IPE 360	IPE 360	IPE 360	IPE 360	IPE 360
94	IPE 360	IPE 360	IPE 360	IPE 360	IPE 360	IPE 360	IPE 360	IPE 360	IPE 360
95	IPE 360	IPE 360	IPE 360	IPE 360	IPE 360	IPE 360	IPE 360	IPE 360	IPE 360
96	IPE 360	IPE 360	IPE 360	IPE 360	IPE 360	IPE 360	IPE 360	IPE 360	IPE 360

## Moment resisting frame columns - XZ façade

MODEL #	Found-Gr.	Storeys							
		Gr.-1st	1st-2nd	2nd-3rd	3rd-4th	4th-5th	5th-6th	6th-7th	7th-8th
1	HE 280 A	HE 280 A	HE 280 A	HE 280 A	HE 280 A	HE 280 A	HE 280 A	HE 280 A	HE 280 A
2	HE 450 B	HE 450 B	HE 450 B	HE 450 B	HE 450 B	HE 450 B	HE 450 B	HE 450 B	HE 450 B
3	HE 340 A	HE 340 A	HE 340 A	HE 340 A	HE 320 A	HE 320 A	HE 320 A	HE 320 A	HE 320 A
4	HE 450 B	HE 450 B	HE 450 B	HE 450 B	HE 450 B	HE 450 B	HE 450 B	HE 450 B	HE 450 B
5	HE 300 A	HE 300 A	HE 300 A	HE 300 A	HE 280 A	HE 280 A	HE 280 A	HE 280 A	HE 280 A
6	HE 500 B	HE 500 B	HE 500 B	HE 500 B	HE 450 A	HE 450 A	HE 450 A	HE 450 A	HE 450 A
7	HE 280 A	HE 280 A	HE 280 A	HE 280 A	HE 280 A	HE 280 A	HE 280 A	HE 280 A	HE 280 A
8	HE 450 B	HE 450 B	HE 450 B	HE 450 B	HE 450 B	HE 450 B	HE 450 B	HE 450 B	HE 450 B
9	HE 340 A	HE 340 A	HE 340 A	HE 340 A	HE 320 A	HE 320 A	HE 320 A	HE 320 A	HE 320 A
10	HE 450 B	HE 450 B	HE 450 B	HE 450 B	HE 450 B	HE 450 B	HE 450 B	HE 450 B	HE 450 B
11	HE 300 A	HE 300 A	HE 300 A	HE 300 A	HE 280 A	HE 280 A	HE 280 A	HE 280 A	HE 280 A
12	HE 500 B	HE 500 B	HE 500 B	HE 500 B	HE 450 A	HE 450 A	HE 450 A	HE 450 A	HE 450 A
13	HE 360 B	HE 360 B	HE 360 B	HE 360 B	HE 360 A	HE 360 A	HE 360 A	HE 360 A	HE 360 A
14	HE 800 B	HE 800 B	HE 800 B	HE 800 B	HE 600 A	HE 600 A	HE 600 A	HE 600 A	HE 600 A
15	HE 450 B	HE 450 B	HE 450 B	HE 450 B	HE 450 A	HE 450 A	HE 450 A	HE 450 A	HE 450 A
16	HE 900 B	HE 900 B	HE 900 B	HE 900 B	HE 700 B	HE 700 B	HE 700 B	HE 700 B	HE 700 B
17	HE 360 B	HE 360 B	HE 360 B	HE 360 B	HE 360 A	HE 360 A	HE 360 A	HE 360 A	HE 360 A
18	HE 1000 B	HE 1000 B	HE 1000 B	HE 1000 B	HE 800 B	HE 800 B	HE 800 B	HE 800 B	HE 800 B
19	HE 360 B	HE 360 B	HE 360 B	HE 360 B	HE 360 A	HE 360 A	HE 360 A	HE 360 A	HE 360 A
20	HE 800 B	HE 800 B	HE 800 B	HE 800 B	HE 600 A	HE 600 A	HE 600 A	HE 600 A	HE 600 A
21	HE 450 B	HE 450 B	HE 450 B	HE 450 B	HE 450 B	HE 450 B	HE 450 B	HE 450 B	HE 450 B
22	HE 900 B	HE 900 B	HE 900 B	HE 900 B	HE 700 B	HE 700 B	HE 700 B	HE 700 B	HE 700 B
23	HE 360 B	HE 360 B	HE 360 B	HE 360 B	HE 360 A	HE 360 A	HE 360 A	HE 360 A	HE 360 A
24	HE 1000 B	HE 1000 B	HE 1000 B	HE 1000 B	HE 800 B	HE 800 B	HE 800 B	HE 800 B	HE 800 B
25	HE 300 B	HE 300 B	HE 300 B	HE 300 B	HE 280 A	HE 280 A	HE 280 A	HE 280 A	HE 280 A
26	HE 600 B	HE 600 B	HE 600 B	HE 600 B	HE 450 A	HE 450 A	HE 450 A	HE 450 A	HE 450 A
27	HE 400 A	HE 400 A	HE 400 A	HE 400 A	HE 360 A	HE 360 A	HE 360 A	HE 360 A	HE 360 A
28	HE 700 B	HE 700 B	HE 700 B	HE 700 B	HE 450 A	HE 450 A	HE 450 A	HE 450 A	HE 450 A
29	HE 320 B	HE 320 B	HE 320 B	HE 320 B	HE 300 A	HE 300 A	HE 300 A	HE 300 A	HE 300 A
30	HE 650 B	HE 650 B	HE 650 B	HE 650 B	HE 500 A	HE 500 A	HE 500 A	HE 500 A	HE 500 A
31	HE 300 B	HE 300 B	HE 300 B	HE 300 B	HE 280 A	HE 280 A	HE 280 A	HE 280 A	HE 280 A
32	HE 600 B	HE 600 B	HE 600 B	HE 600 B	HE 450 A	HE 450 A	HE 450 A	HE 450 A	HE 450 A
33	HE 400 A	HE 400 A	HE 400 A	HE 400 A	HE 360 A	HE 360 A	HE 360 A	HE 360 A	HE 360 A
34	HE 700 B	HE 700 B	HE 700 B	HE 700 B	HE 450 A	HE 450 A	HE 450 A	HE 450 A	HE 450 A
35	HE 320 B	HE 320 B	HE 320 B	HE 320 B	HE 300 A	HE 300 A	HE 300 A	HE 300 A	HE 300 A
36	HE 650 B	HE 650 B	HE 650 B	HE 650 B	HE 500 A	HE 500 A	HE 500 A	HE 500 A	HE 500 A
37	HE 360 B	HE 360 B	HE 360 B	HE 360 B	HE 340 A	HE 340 A	HE 340 A	HE 340 A	HE 340 A
38	HE 1000 B	HE 1000 B	HE 1000 B	HE 1000 B	HE 900 A	HE 900 A	HE 900 A	HE 900 A	HE 900 A

MODEL #	Found-Gr.	Gr.-1st	1st-2nd	2nd-3rd	Storeys				
					3rd-4th	4th-5th	5th-6th	6th-7th	7th-8th
39	HE 500 A	HE 500 A	HE 500 A	HE 450 A	HE 450 A				
40	HE 1000 B	HE 1000 B	HE 1000 B	HE 1000 B	HE 1000 B				
41	HE 360 B	HE 360 B	HE 360 B	HE 360 B	HE 360 B				
42	HE 1000 B	HE 1000 B	HE 1000 B	HE 1000 B	HE 1000 B				
43	HE 360 B	HE 360 B	HE 360 B	HE 340 A	HE 340 A				
44	HE 1000 B	HE 1000 B	HE 1000 B	HE 900 A	HE 900 A				
45	HE 500 A	HE 500 A	HE 500 A	HE 450 A	HE 450 A				
46	HE 1000 B	HE 1000 B	HE 1000 B	HE 1000 B	HE 1000 B				
47	HE 360 B	HE 360 B	HE 360 B	HE 360 B	HE 360 B				
48	HE 1000 B	HE 1000 B	HE 1000 B	HE 1000 B	HE 1000 B				
49	HE 320 A	HE 320 A	HE 320 A	HE 320 A	HE 320 A	HE 320 A	HE 300 A	HE 300 A	HE 300 A
50	HE 650 B	HE 650 B	HE 650 B	HE 550 A	HE 550 A	HE 550 A	HE 400 A	HE 400 A	HE 400 A
51	HE 400 A	HE 400 A	HE 400 A	HE 400 A	HE 400 A	HE 400 A	HE 360 A	HE 360 A	HE 360 A
52	HE 800 B	HE 800 B	HE 800 B	HE 700 A	HE 700 A	HE 700 A	HE 550 A	HE 550 A	HE 550 A
53	HE 400 A	HE 400 A	HE 400 A	HE 400 A	HE 400 A	HE 400 A	HE 360 A	HE 360 A	HE 360 A
54	HE 800 B	HE 800 B	HE 800 B	HE 650 A	HE 650 A	HE 650 A	HE 500 A	HE 500 A	HE 500 A
55	HE 320 A	HE 320 A	HE 320 A	HE 320 A	HE 320 A	HE 320 A	HE 300 A	HE 300 A	HE 300 A
56	HE 650 B	HE 650 B	HE 650 B	HE 550 A	HE 550 A	HE 550 A	HE 400 A	HE 400 A	HE 400 A
57	HE 400 A	HE 400 A	HE 400 A	HE 400 A	HE 400 A	HE 400 A	HE 360 A	HE 360 A	HE 360 A
58	HE 800 B	HE 800 B	HE 800 B	HE 700 A	HE 700 A	HE 700 A	HE 550 A	HE 550 A	HE 550 A
59	HE 400 A	HE 400 A	HE 400 A	HE 400 A	HE 400 A	HE 400 A	HE 360 A	HE 360 A	HE 360 A
60	HE 800 B	HE 800 B	HE 800 B	HE 650 A	HE 650 A	HE 650 A	HE 500 A	HE 500 A	HE 500 A
61	HE 500 A	HE 500 A	HE 500 A	HE 450 A	HE 450 A	HE 450 A	HE 400 A	HE 400 A	HE 400 A
62	X HE 800 B	X HE 800 B	X HE 800 B	X HE 550 B	X HE 550 B	X HE 550 B	X HE 550 B	X HE 550 B	X HE 550 B
63	HE 650 A	HE 650 A	HE 650 A	HE 600 A	HE 600 A	HE 600 A	HE 500 A	HE 500 A	HE 500 A
64	X HE 800 B	X HE 800 B	X HE 800 B	X HE 550 B	X HE 550 B	X HE 550 B	X HE 550 B	X HE 550 B	X HE 550 B
65	HE 550 A	HE 550 A	HE 550 A	HE 500 A	HE 500 A	HE 500 A	HE 450 A	HE 450 A	HE 450 A
66	X HE 800 B	X HE 800 B	X HE 800 B	X HE 550 B	X HE 550 B	X HE 550 B	X HE 550 B	X HE 550 B	X HE 550 B
67	HE 500 A	HE 500 A	HE 500 A	HE 450 A	HE 450 A	HE 450 A	HE 400 A	HE 400 A	HE 400 A
68	X HE 800 B	X HE 800 B	X HE 800 B	X HE 550 B	X HE 550 B	X HE 550 B	X HE 550 B	X HE 550 B	X HE 550 B
69	HE 650 A	HE 650 A	HE 650 A	HE 600 A	HE 600 A	HE 600 A	HE 500 A	HE 500 A	HE 500 A
70	X HE 800 B	X HE 800 B	X HE 800 B	X HE 550 B	X HE 550 B	X HE 550 B	X HE 550 B	X HE 550 B	X HE 550 B
71	HE 550 A	HE 550 A	HE 550 A	HE 500 A	HE 500 A	HE 500 A	HE 450 A	HE 450 A	HE 450 A
72	X HE 800 B	X HE 800 B	X HE 800 B	X HE 550 B	X HE 550 B	X HE 550 B	X HE 550 B	X HE 550 B	X HE 550 B
73	HE 450 A	HE 450 A	HE 450 A	HE 400 A	HE 400 A	HE 400 A	HE 360 A	HE 360 A	HE 360 A
74	HE 900 B	HE 900 B	HE 900 B	HE 700 B	HE 700 B	HE 700 B	HE 500 A	HE 500 A	HE 500 A
75	HE 600 A	HE 600 A	HE 600 A	HE 550 A	HE 550 A	HE 550 A	HE 500 A	HE 500 A	HE 500 A
76	HE 1000 B	HE 1000 B	HE 1000 B	HE 1000 B	HE 1000 B	HE 1000 B	HE 1000 B	HE 1000 B	HE 1000 B
77	HE 500 A	HE 500 A	HE 500 A	HE 450 A	HE 450 A	HE 450 A	HE 400 A	HE 400 A	HE 400 A
78	HE 1000 B	HE 1000 B	HE 1000 B	HE 800 A	HE 800 A	HE 800 A	HE 600 A	HE 600 A	HE 600 A
79	HE 450 A	HE 450 A	HE 450 A	HE 400 A	HE 400 A	HE 400 A	HE 360 A	HE 360 A	HE 360 A
80	HE 900 B	HE 900 B	HE 900 B	HE 700 B	HE 700 B	HE 700 B	HE 500 A	HE 500 A	HE 500 A
81	HE 600 A	HE 600 A	HE 600 A	HE 550 A	HE 550 A	HE 550 A	HE 500 A	HE 500 A	HE 500 A
82	HE 1000 B	HE 1000 B	HE 1000 B	HE 1000 B	HE 1000 B	HE 1000 B	HE 1000 B	HE 1000 B	HE 1000 B
83	HE 500 A	HE 500 A	HE 500 A	HE 450 A	HE 450 A	HE 450 A	HE 400 A	HE 400 A	HE 400 A
84	HE 1000 B	HE 1000 B	HE 1000 B	HE 800 A	HE 800 A	HE 800 A	HE 600 A	HE 600 A	HE 600 A
85	HE 550 A	HE 550 A	HE 550 A	HE 550 A	HE 550 A	HE 550 A	HE 500 A	HE 500 A	HE 500 A
86	X HE 1000 B	X HE 1000 B	X HE 1000 B	X HE 700 B	X HE 700 B	X HE 700 B	X HE 700 B	X HE 700 B	X HE 700 B
87	HE 800 A	HE 800 A	HE 800 A	HE 700 A	HE 700 A	HE 700 A	HE 650 A	HE 650 A	HE 650 A
88	X HE 1000 B	X HE 1000 B	X HE 1000 B	X HE 700 B	X HE 700 B	X HE 700 B	X HE 700 B	X HE 700 B	X HE 700 B
89	HE 650 A	HE 650 A	HE 650 A	HE 600 A	HE 600 A	HE 600 A	HE 550 A	HE 550 A	HE 550 A
90	X HE 1000 B	X HE 1000 B	X HE 1000 B	X HE 700 B	X HE 700 B	X HE 700 B	X HE 700 B	X HE 700 B	X HE 700 B
91	HE 550 A	HE 550 A	HE 550 A	HE 550 A	HE 550 A	HE 550 A	HE 500 A	HE 500 A	HE 500 A
92	X HE 1000 B	X HE 1000 B	X HE 1000 B	X HE 700 B	X HE 700 B	X HE 700 B	X HE 700 B	X HE 700 B	X HE 700 B
93	HE 800 A	HE 800 A	HE 800 A	HE 700 A	HE 700 A	HE 700 A	HE 650 A	HE 650 A	HE 650 A
94	X HE 1000 B	X HE 1000 B	X HE 1000 B	X HE 700 B	X HE 700 B	X HE 700 B	X HE 700 B	X HE 700 B	X HE 700 B
95	HE 650 A	HE 650 A	HE 650 A	HE 600 A	HE 600 A	HE 600 A	HE 550 A	HE 550 A	HE 550 A
96	X HE 1000 B	X HE 1000 B	X HE 1000 B	X HE 700 B	X HE 700 B	X HE 700 B	X HE 700 B	X HE 700 B	X HE 700 B

NOTE: The "X" marking before the column section indicates that the columns are cruciform and that all beam-column joints are moment resisting

# Moment resisting frame columns - YZ façade

MODEL #	Found-Gr.	Gr.-1st	1st-2nd	2nd-3rd	Storeys				
					3rd-4th	4th-5th	5th-6th	6th-7th	7th-8th
1	HE 300 A	HE 300 A	HE 300 A	HE 300 A	HE 300 A				
2	HE 500 B	HE 500 B	HE 500 B	HE 500 B	HE 340 B				
3	HE 260 A	HE 260 A	HE 260 A	HE 240 A	HE 240 A				
4	HE 450 B	HE 450 B	HE 450 B	HE 300 A	HE 300 A				
5	HE 280 A	HE 280 A	HE 280 A	HE 260 A	HE 260 A				
6	HE 450 B	HE 450 B	HE 450 B	HE 340 A	HE 340 A				
7	HE 300 A	HE 300 A	HE 300 A	HE 300 A	HE 300 A				
8	HE 500 B	HE 500 B	HE 500 B	HE 340 B	HE 340 B				
9	HE 260 A	HE 260 A	HE 260 A	HE 240 A	HE 240 A				
10	HE 450 B	HE 450 B	HE 450 B	HE 300 A	HE 300 A				
11	HE 280 A	HE 280 A	HE 280 A	HE 260 A	HE 260 A				
12	HE 450 B	HE 450 B	HE 450 B	HE 340 A	HE 340 A				
13	HE 450 A	HE 450 A	HE 450 A	HE 450 A	HE 450 A				
14	HE 1000 B	HE 1000 B	HE 1000 B	HE 800 B	HE 800 B				
15	HE 360 A	HE 360 A	HE 360 A	HE 360 A	HE 360 A				
16	HE 900 B	HE 900 B	HE 900 B	HE 900 B	HE 650 A				
17	HE 360 A	HE 360 A	HE 360 A	HE 360 A	HE 360 A				
18	HE 900 B	HE 900 B	HE 900 B	HE 700 B	HE 700 B				
19	HE 450 A	HE 450 A	HE 450 A	HE 450 A	HE 450 A				
20	HE 1000 B	HE 1000 B	HE 1000 B	HE 800 B	HE 800 B				
21	HE 360 A	HE 360 A	HE 360 A	HE 360 A	HE 360 A				
22	HE 900 B	HE 900 B	HE 900 B	HE 900 B	HE 650 A				
23	HE 360 A	HE 360 A	HE 360 A	HE 360 A	HE 360 A				
24	HE 900 B	HE 900 B	HE 900 B	HE 700 B	HE 700 B				
25	HE 360 A	HE 360 A	HE 360 A	HE 360 A	HE 340 A				
26	HE 600 B	HE 600 B	HE 600 B	HE 450 A	HE 450 A				
27	HE 300 A	HE 300 A	HE 300 A	HE 300 A	HE 280 A				
28	HE 500 B	HE 500 B	HE 500 B	HE 360 A	HE 360 A				
29	HE 320 A	HE 320 A	HE 320 A	HE 300 A	HE 300 A				
30	HE 600 B	HE 600 B	HE 600 B	HE 400 A	HE 400 A				
31	HE 360 A	HE 360 A	HE 360 A	HE 360 A	HE 340 A				
32	HE 600 B	HE 600 B	HE 600 B	HE 450 A	HE 450 A				
33	HE 300 A	HE 300 A	HE 300 A	HE 280 A	HE 280 A				
34	HE 500 B	HE 500 B	HE 500 B	HE 360 A	HE 360 A				
35	HE 320 A	HE 320 A	HE 320 A	HE 300 A	HE 300 A				
36	HE 600 B	HE 600 B	HE 600 B	HE 400 A	HE 400 A				
37	HE 450 B	HE 450 B	HE 450 B	HE 450 B	HE 450 A				
38	HE 1000 B	HE 1000 B	HE 1000 B	HE 1000 B	HE 900 A				
39	HE 360 B	HE 360 B	HE 360 B	HE 360 A	HE 360 A				
40	HE 1000 B	HE 1000 B	HE 1000 B	HE 900 B	HE 900 B				
41	HE 400 A	HE 400 A	HE 400 A	HE 400 A	HE 400 A				
42	HE 1000 B	HE 1000 B	HE 1000 B	HE 900 B	HE 900 B				
43	HE 450 B	HE 450 B	HE 450 B	HE 450 A	HE 450 A				
44	HE 1000 B	HE 1000 B	HE 1000 B	HE 900 A	HE 900 A				
45	HE 360 B	HE 360 B	HE 360 B	HE 360 A	HE 360 A				
46	HE 1000 B	HE 1000 B	HE 1000 B	HE 900 B	HE 900 B				
47	HE 400 A	HE 400 A	HE 400 A	HE 400 A	HE 400 A				
48	HE 1000 B	HE 1000 B	HE 1000 B	HE 900 B	HE 900 B				
49	HE 450 A	HE 450 A	HE 450 A	HE 400 A	HE 400 A	HE 400 A	HE 360 A	HE 360 A	HE 360 A
50	HE 650 B	HE 650 B	HE 650 B	HE 550 A	HE 550 A	HE 550 A	HE 450 A	HE 450 A	HE 450 A
51	HE 340 A	HE 340 A	HE 340 A	HE 320 A	HE 320 A	HE 320 A	HE 300 A	HE 300 A	HE 300 A
52	HE 600 B	HE 600 B	HE 600 B	HE 500 A	HE 500 A	HE 500 A	HE 400 A	HE 400 A	HE 400 A
53	HE 360 A	HE 360 A	HE 360 A	HE 340 A	HE 340 A	HE 340 A	HE 320 A	HE 320 A	HE 320 A
54	HE 800 B	HE 800 B	HE 800 B	HE 650 A	HE 650 A	HE 650 A	HE 450 A	HE 450 A	HE 450 A
55	HE 450 A	HE 450 A	HE 450 A	HE 400 A	HE 400 A	HE 400 A	HE 360 A	HE 360 A	HE 360 A
56	HE 650 B	HE 650 B	HE 650 B	HE 550 A	HE 550 A	HE 550 A	HE 450 A	HE 450 A	HE 450 A
57	HE 340 A	HE 340 A	HE 340 A	HE 320 A	HE 320 A	HE 320 A	HE 300 A	HE 300 A	HE 300 A
58	HE 600 B	HE 600 B	HE 600 B	HE 500 A	HE 500 A	HE 500 A	HE 400 A	HE 400 A	HE 400 A
59	HE 360 A	HE 360 A	HE 360 A	HE 340 A	HE 340 A	HE 340 A	HE 320 A	HE 320 A	HE 320 A
60	HE 800 B	HE 800 B	HE 800 B	HE 650 A	HE 650 A	HE 650 A	HE 450 A	HE 450 A	HE 450 A
61	HE 550 A	HE 550 A	HE 550 A	HE 550 A	HE 550 A	HE 550 A	HE 500 A	HE 500 A	HE 500 A
62	X HE 800 B	X HE 800 B	X HE 800 B	X HE 550 B	X HE 550 B	X HE 550 B	X HE 550 B	X HE 550 B	X HE 550 B
63	HE 450 A	HE 450 A	HE 450 A	HE 450 A	HE 450 A	HE 450 A	HE 400 A	HE 400 A	HE 400 A
64	X HE 800 B	X HE 800 B	X HE 800 B	X HE 550 B	X HE 550 B	X HE 550 B	X HE 550 B	X HE 550 B	X HE 550 B
65	HE 500 A	HE 500 A	HE 500 A	HE 500 A	HE 500 A	HE 500 A	HE 450 A	HE 450 A	HE 450 A
66	X HE 800 B	X HE 800 B	X HE 800 B	X HE 550 B	X HE 550 B	X HE 550 B	X HE 550 B	X HE 550 B	X HE 550 B
67	HE 550 A	HE 550 A	HE 550 A	HE 550 A	HE 550 A	HE 550 A	HE 500 A	HE 500 A	HE 500 A
68	X HE 800 B	X HE 800 B	X HE 800 B	X HE 550 B	X HE 550 B	X HE 550 B	X HE 550 B	X HE 550 B	X HE 550 B
69	HE 450 A	HE 450 A	HE 450 A	HE 450 A	HE 450 A	HE 450 A	HE 400 A	HE 400 A	HE 400 A
70	X HE 800 B	X HE 800 B	X HE 800 B	X HE 550 B	X HE 550 B	X HE 550 B	X HE 550 B	X HE 550 B	X HE 550 B

MODEL #	Found-Gr.	Gr.-1st	1st-2nd	2nd-3rd	Storeys				
					3rd-4th	4th-5th	5th-6th	6th-7th	7th-8th
71	HE 500 A	HE 500 A	HE 500 A	HE 500 A	HE 500 A	HE 500 A	HE 450 A	HE 450 A	HE 450 A
72	X HE 800 B	X HE 800 B	X HE 800 B	X HE 550 B	X HE 550 B	X HE 550 B	X HE 550 B	X HE 550 B	X HE 550 B
73	HE 550 A	HE 550 A	HE 550 A	HE 500 A	HE 500 A	HE 500 A	HE 450 A	HE 450 A	HE 450 A
74	HE 1000 B	HE 1000 B	HE 1000 B	HE 900 A	HE 900 A	HE 900 A	HE 800 A	HE 800 A	HE 800 A
75	HE 450 A	HE 450 A	HE 450 A	HE 450 A	HE 450 A	HE 450 A	HE 400 A	HE 400 A	HE 400 A
76	HE 800 B	HE 800 B	HE 800 B	HE 700 A	HE 700 A	HE 700 A	HE 500 A	HE 500 A	HE 500 A
77	HE 500 A	HE 500 A	HE 500 A	HE 450 A	HE 450 A	HE 450 A	HE 400 A	HE 400 A	HE 400 A
78	HE 900 B	HE 900 B	HE 900 B	HE 700 A	HE 700 A	HE 700 A	HE 550 A	HE 550 A	HE 550 A
79	HE 550 A	HE 550 A	HE 550 A	HE 500 A	HE 500 A	HE 500 A	HE 450 A	HE 450 A	HE 450 A
80	HE 1000 B	HE 1000 B	HE 1000 B	HE 900 A	HE 900 A	HE 900 A	HE 800 A	HE 800 A	HE 800 A
81	HE 450 A	HE 450 A	HE 450 A	HE 450 A	HE 450 A	HE 450 A	HE 400 A	HE 400 A	HE 400 A
82	HE 800 B	HE 800 B	HE 800 B	HE 700 A	HE 700 A	HE 700 A	HE 500 A	HE 500 A	HE 500 A
83	HE 500 A	HE 500 A	HE 500 A	HE 450 A	HE 450 A	HE 450 A	HE 400 A	HE 400 A	HE 400 A
84	HE 900 B	HE 900 B	HE 900 B	HE 700 A	HE 700 A	HE 700 A	HE 550 A	HE 550 A	HE 550 A
85	HE 800 A	HE 800 A	HE 800 A	HE 700 A	HE 700 A	HE 700 A	HE 650 A	HE 650 A	HE 650 A
86	X HE 1000 B	X HE 1000 B	X HE 1000 B	X HE 700 B	X HE 700 B	X HE 700 B	X HE 700 B	X HE 700 B	X HE 700 B
87	HE 600 A	HE 600 A	HE 600 A	HE 550 A	HE 550 A	HE 550 A	HE 500 A	HE 500 A	HE 500 A
88	X HE 1000 B	X HE 1000 B	X HE 1000 B	X HE 700 B	X HE 700 B	X HE 700 B	X HE 700 B	X HE 700 B	X HE 700 B
89	HE 650 A	HE 650 A	HE 650 A	HE 600 A	HE 600 A	HE 600 A	HE 550 A	HE 550 A	HE 550 A
90	X HE 1000 B	X HE 1000 B	X HE 1000 B	X HE 700 B	X HE 700 B	X HE 700 B	X HE 700 B	X HE 700 B	X HE 700 B
91	HE 800 A	HE 800 A	HE 800 A	HE 700 A	HE 700 A	HE 700 A	HE 650 A	HE 650 A	HE 650 A
92	X HE 1000 B	X HE 1000 B	X HE 1000 B	X HE 700 B	X HE 700 B	X HE 700 B	X HE 700 B	X HE 700 B	X HE 700 B
93	HE 600 A	HE 600 A	HE 600 A	HE 550 A	HE 550 A	HE 550 A	HE 500 A	HE 500 A	HE 500 A
94	X HE 1000 B	X HE 1000 B	X HE 1000 B	X HE 700 B	X HE 700 B	X HE 700 B	X HE 700 B	X HE 700 B	X HE 700 B
95	HE 650 A	HE 650 A	HE 650 A	HE 600 A	HE 600 A	HE 600 A	HE 550 A	HE 550 A	HE 550 A
96	X HE 1000 B	X HE 1000 B	X HE 1000 B	X HE 700 B	X HE 700 B	X HE 700 B	X HE 700 B	X HE 700 B	X HE 700 B

NOTE: The "X" marking before the column section indicates that the columns are cruciform and that all beam-column joints are moment resisting

## Internal columns

MODEL #	Found-Gr.	Gr.-1st	1st-2nd	2nd-3rd	Storeys				
					3rd-4th	4th-5th	5th-6th	6th-7th	7th-8th
1	HE 240 A	HE 240 A	HE 240 A	HE 220 A	HE 220 A				
2	HE 240 A	HE 240 A	HE 240 A	HE 220 A	HE 220 A				
3	HE 240 A	HE 240 A	HE 240 A	HE 220 A	HE 220 A				
4	HE 240 A	HE 240 A	HE 240 A	HE 220 A	HE 220 A				
5	HE 240 A	HE 240 A	HE 240 A	HE 220 A	HE 220 A				
6	HE 240 A	HE 240 A	HE 240 A	HE 220 A	HE 220 A				
7	HE 240 A	HE 240 A	HE 240 A	HE 220 A	HE 220 A				
8	HE 240 A	HE 240 A	HE 240 A	HE 220 A	HE 220 A				
9	HE 240 A	HE 240 A	HE 240 A	HE 220 A	HE 220 A				
10	HE 240 A	HE 240 A	HE 240 A	HE 220 A	HE 220 A				
11	HE 240 A	HE 240 A	HE 240 A	HE 220 A	HE 220 A				
12	HE 240 A	HE 240 A	HE 240 A	HE 220 A	HE 220 A				
13	HE 360 B	HE 360 B	HE 360 B	HE 340 A	HE 340 A				
14	HE 360 B	HE 360 B	HE 360 B	HE 340 A	HE 340 A				
15	HE 360 B	HE 360 B	HE 360 B	HE 340 A	HE 340 A				
16	HE 360 B	HE 360 B	HE 360 B	HE 340 A	HE 340 A				
17	HE 360 B	HE 360 B	HE 360 B	HE 340 A	HE 340 A				
18	HE 360 B	HE 360 B	HE 360 B	HE 340 A	HE 340 A				
19	HE 360 B	HE 360 B	HE 360 B	HE 340 A	HE 340 A				
20	HE 360 B	HE 360 B	HE 360 B	HE 340 A	HE 340 A				
21	HE 360 B	HE 360 B	HE 360 B	HE 340 A	HE 340 A				
22	HE 360 B	HE 360 B	HE 360 B	HE 340 A	HE 340 A				
23	HE 360 B	HE 360 B	HE 360 B	HE 340 A	HE 340 A				
24	HE 360 B	HE 360 B	HE 360 B	HE 340 A	HE 340 A				
25	HE 240 A	HE 240 A	HE 240 A	HE 220 A	HE 220 A				
26	HE 240 A	HE 240 A	HE 240 A	HE 220 A	HE 220 A				
27	HE 240 A	HE 240 A	HE 240 A	HE 220 A	HE 220 A				
28	HE 240 A	HE 240 A	HE 240 A	HE 220 A	HE 220 A				
29	HE 240 A	HE 240 A	HE 240 A	HE 220 A	HE 220 A				
30	HE 240 A	HE 240 A	HE 240 A	HE 220 A	HE 220 A				
31	HE 240 A	HE 240 A	HE 240 A	HE 220 A	HE 220 A				
32	HE 240 A	HE 240 A	HE 240 A	HE 220 A	HE 220 A				
33	HE 240 A	HE 240 A	HE 240 A	HE 220 A	HE 220 A				
34	HE 240 A	HE 240 A	HE 240 A	HE 220 A	HE 220 A				
35	HE 240 A	HE 240 A	HE 240 A	HE 220 A	HE 220 A				
36	HE 240 A	HE 240 A	HE 240 A	HE 220 A	HE 220 A				

MODEL #	Found-Gr.	Gr.-1st	1st-2nd	2nd-3rd	Storeys				
					3rd-4th	4th-5th	5th-6th	6th-7th	7th-8th
37	HE 360 B	HE 360 B	HE 360 B	HE 340 A	HE 340 A				
38	HE 360 B	HE 360 B	HE 360 B	HE 340 A	HE 340 A				
39	HE 360 B	HE 360 B	HE 360 B	HE 340 A	HE 340 A				
40	HE 360 B	HE 360 B	HE 360 B	HE 340 A	HE 340 A				
41	HE 360 B	HE 360 B	HE 360 B	HE 340 A	HE 340 A				
42	HE 360 B	HE 360 B	HE 360 B	HE 340 A	HE 340 A				
43	HE 360 B	HE 360 B	HE 360 B	HE 340 A	HE 340 A				
44	HE 360 B	HE 360 B	HE 360 B	HE 340 A	HE 340 A				
45	HE 360 B	HE 360 B	HE 360 B	HE 340 A	HE 340 A				
46	HE 360 B	HE 360 B	HE 360 B	HE 340 A	HE 340 A				
47	HE 360 B	HE 360 B	HE 360 B	HE 340 A	HE 340 A				
48	HE 360 B	HE 360 B	HE 360 B	HE 340 A	HE 340 A				
49	HE 300 A	HE 300 A	HE 300 A	HE 260 A	HE 260 A	HE 260 A	HE 220 A	HE 220 A	HE 220 A
50	HE 300 A	HE 300 A	HE 300 A	HE 260 A	HE 260 A	HE 260 A	HE 220 A	HE 220 A	HE 220 A
51	HE 300 A	HE 300 A	HE 300 A	HE 260 A	HE 260 A	HE 260 A	HE 220 A	HE 220 A	HE 220 A
52	HE 300 A	HE 300 A	HE 300 A	HE 260 A	HE 260 A	HE 260 A	HE 220 A	HE 220 A	HE 220 A
53	HE 300 A	HE 300 A	HE 300 A	HE 260 A	HE 260 A	HE 260 A	HE 220 A	HE 220 A	HE 220 A
54	HE 300 A	HE 300 A	HE 300 A	HE 260 A	HE 260 A	HE 260 A	HE 220 A	HE 220 A	HE 220 A
55	HE 300 A	HE 300 A	HE 300 A	HE 260 A	HE 260 A	HE 260 A	HE 220 A	HE 220 A	HE 220 A
56	HE 300 A	HE 300 A	HE 300 A	HE 260 A	HE 260 A	HE 260 A	HE 220 A	HE 220 A	HE 220 A
57	HE 300 A	HE 300 A	HE 300 A	HE 260 A	HE 260 A	HE 260 A	HE 220 A	HE 220 A	HE 220 A
58	HE 300 A	HE 300 A	HE 300 A	HE 260 A	HE 260 A	HE 260 A	HE 220 A	HE 220 A	HE 220 A
59	HE 300 A	HE 300 A	HE 300 A	HE 260 A	HE 260 A	HE 260 A	HE 220 A	HE 220 A	HE 220 A
60	HE 300 A	HE 300 A	HE 300 A	HE 260 A	HE 260 A	HE 260 A	HE 220 A	HE 220 A	HE 220 A
61	HE 650 B	HE 650 B	HE 650 B	HE 500 A	HE 500 A	HE 500 A	HE 300 A	HE 300 A	HE 300 A
62	*	*	*	*	*	*	*	*	*
63	HE 650 B	HE 650 B	HE 650 B	HE 500 A	HE 500 A	HE 500 A	HE 300 A	HE 300 A	HE 300 A
64	*	*	*	*	*	*	*	*	*
65	HE 650 B	HE 650 B	HE 650 B	HE 500 A	HE 500 A	HE 500 A	HE 300 A	HE 300 A	HE 300 A
66	*	*	*	*	*	*	*	*	*
67	HE 650 B	HE 650 B	HE 650 B	HE 500 A	HE 500 A	HE 500 A	HE 300 A	HE 300 A	HE 300 A
68	*	*	*	*	*	*	*	*	*
69	HE 650 B	HE 650 B	HE 650 B	HE 500 A	HE 500 A	HE 500 A	HE 300 A	HE 300 A	HE 300 A
70	*	*	*	*	*	*	*	*	*
71	HE 650 B	HE 650 B	HE 650 B	HE 500 A	HE 500 A	HE 500 A	HE 300 A	HE 300 A	HE 300 A
72	*	*	*	*	*	*	*	*	*
73	HE 300 B	HE 300 B	HE 300 B	HE 260 A	HE 260 A	HE 260 A	HE 220 A	HE 220 A	HE 220 A
74	HE 300 B	HE 300 B	HE 300 B	HE 260 A	HE 260 A	HE 260 A	HE 220 A	HE 220 A	HE 220 A
75	HE 300 B	HE 300 B	HE 300 B	HE 260 A	HE 260 A	HE 260 A	HE 220 A	HE 220 A	HE 220 A
76	HE 300 B	HE 300 B	HE 300 B	HE 260 A	HE 260 A	HE 260 A	HE 220 A	HE 220 A	HE 220 A
77	HE 300 B	HE 300 B	HE 300 B	HE 260 A	HE 260 A	HE 260 A	HE 220 A	HE 220 A	HE 220 A
78	HE 300 B	HE 300 B	HE 300 B	HE 260 A	HE 260 A	HE 260 A	HE 220 A	HE 220 A	HE 220 A
79	HE 300 B	HE 300 B	HE 300 B	HE 260 A	HE 260 A	HE 260 A	HE 220 A	HE 220 A	HE 220 A
80	HE 300 B	HE 300 B	HE 300 B	HE 260 A	HE 260 A	HE 260 A	HE 220 A	HE 220 A	HE 220 A
81	HE 300 B	HE 300 B	HE 300 B	HE 260 A	HE 260 A	HE 260 A	HE 220 A	HE 220 A	HE 220 A
82	HE 300 B	HE 300 B	HE 300 B	HE 260 A	HE 260 A	HE 260 A	HE 220 A	HE 220 A	HE 220 A
83	HE 300 B	HE 300 B	HE 300 B	HE 260 A	HE 260 A	HE 260 A	HE 220 A	HE 220 A	HE 220 A
84	HE 300 B	HE 300 B	HE 300 B	HE 260 A	HE 260 A	HE 260 A	HE 220 A	HE 220 A	HE 220 A
85	HE 800 B	HE 800 B	HE 800 B	HE 500 A	HE 500 A	HE 500 A	HE 300 A	HE 300 A	HE 300 A
86	*	*	*	*	*	*	*	*	*
87	HE 800 B	HE 800 B	HE 800 B	HE 500 A	HE 500 A	HE 500 A	HE 300 A	HE 300 A	HE 300 A
88	*	*	*	*	*	*	*	*	*
89	HE 800 B	HE 800 B	HE 800 B	HE 500 A	HE 500 A	HE 500 A	HE 300 A	HE 300 A	HE 300 A
90	*	*	*	*	*	*	*	*	*
91	HE 800 B	HE 800 B	HE 800 B	HE 500 A	HE 500 A	HE 500 A	HE 300 A	HE 300 A	HE 300 A
92	*	*	*	*	*	*	*	*	*
93	HE 800 B	HE 800 B	HE 800 B	HE 500 A	HE 500 A	HE 500 A	HE 300 A	HE 300 A	HE 300 A
94	*	*	*	*	*	*	*	*	*
95	HE 800 B	HE 800 B	HE 800 B	HE 500 A	HE 500 A	HE 500 A	HE 300 A	HE 300 A	HE 300 A
96	*	*	*	*	*	*	*	*	*

\* - internal column cross section is cruciform and is the same as the moment resisting frame column cross section

## **Appendix B Generation of the structures in Seismostruct**

## EXAMPLE

### Worksheet for the generation of the N4-H3-BM-S6-CN-T5x3-DG frame

## MODEL DEFINITION

MODEL #	1
N	4
H	3
B	M
S	6
C	N
T	5x3
D	G
TAG	N4-H3-BM-S6-CN-T5x3-DG

## MATERIALS INPUT

### MATERIALS INPUT

MATERIAL NAME	-	355
MATERIAL TYPE	-	stl_mp
MODULUS OF ELASTICITY E	kPa	200000000
YIELD STRENGTH	kPa	443750
STRAIN HARDENING PARAMETER	-	0.005
TRANSITION CURVE INITIAL SHAPE PARAM.	-	20
TRANSITION CURVE SHAPE CALIBRATING COEFF. A1	-	18.5
TRANSITION CURVE SHAPE CALIBRATING COEFF. A2	-	0.15
ISOTROPIC HARDENING CALIBRATING COEFF. A3	-	0
ISOTROPIC HARDENING CALIBRATING COEFF. A4	-	1
FRACTURE/BUCKLING STRAIN	-	0.1
SPECIFIC WEIGHT	kN/m3	78
GENERATING LINE		
	355 stl_mp	200000000 443750 0.005 20 18.5 0.15 0 1 0.1 78

MATERIAL NAME	-	S355_COL_MRF_X
MATERIAL TYPE	-	stl_mp
MODULUS OF ELASTICITY E	kPa	200000000
YIELD STRENGTH	kPa	443750
STRAIN HARDENING PARAMETER	-	0.005
TRANSITION CURVE INITIAL SHAPE PARAM.	-	20
TRANSITION CURVE SHAPE CALIBRATING COEFF. A1	-	18.5
TRANSITION CURVE SHAPE CALIBRATING COEFF. A2	-	0.15
ISOTROPIC HARDENING CALIBRATING COEFF. A3	-	0
ISOTROPIC HARDENING CALIBRATING COEFF. A4	-	1
FRACTURE/BUCKLING STRAIN	-	0.1
SPECIFIC WEIGHT	kN/m3	78
GENERATING LINE		
S355_COL_MRF_X	stl_mp	200000000 443750 0.005 20 18.5 0.15 0 1 0.1 78



<b>MATERIAL NAME</b>	-	<b>S355_COL_MRF_Y</b>
MATERIAL TYPE	-	stl_mp
MODULUS OF ELASTICITY E	kPa	200000000
YIELD STRENGTH	kPa	443750
STRAIN HARDENING PARAMETER	-	0.005
TRANSITION CURVE INITIAL SHAPE PARAM.	-	20
TRANSITION CURVE SHAPE CALIBRATING COEFF. A1	-	18.5
TRANSITION CURVE SHAPE CALIBRATING COEFF. A2	-	0.15
ISOTROPIC HARDENING CALIBRATING COEFF. A3	-	0
ISOTROPIC HARDENING CALIBRATING COEFF. A4	-	1
FRACTURE/BUCKLING STRAIN	-	0.1
SPECIFIC WEIGHT	kN/m3	78
GENERATING LINE		
S355_COL_MRF_Y	stl_mp	200000000 443750 0.005 20 18.5 0.15 0 1 0.1 78

<b>MATERIAL NAME</b>	-	<b>RIGID</b>
MATERIAL TYPE	-	el_mat
MODULUS OF ELASTICITY E	kPa	2E+16
SPECIFIC WEIGHT	kN/m3	0.0001
GENERATING LINE		
RIGID	el_mat	200000000000000000 0.0001

<b>MATERIAL NAME</b>	-	<b>C30/37_X_W_0</b>
MATERIAL TYPE	-	con_ma
MEAN COMPRESSIVE STRENGTH	kPa	38000
MEAN TENSILE STRENGTH	kPa	3263
MODULUS OF ELASTICITY E	kPa	2.897E+07
STRAIN AT PEAK STRESS	m/m	0.002
SPECIFIC WEIGHT	kN/m3	0.0001
GENERATING LINE		
C30/37_X_W_0	con_ma	38000 3263 28973000 0.002 0.0001

<b>MATERIAL NAME</b>	-	<b>C30/37_Y_W_0</b>
MATERIAL TYPE	-	con_ma
MEAN COMPRESSIVE STRENGTH	kPa	38000
MEAN TENSILE STRENGTH	kPa	3263
MODULUS OF ELASTICITY E	kPa	2.897E+07
STRAIN AT PEAK STRESS	m/m	0.002
SPECIFIC WEIGHT	kN/m3	0.0001
GENERATING LINE		
C30/37_Y_W_0	con_ma	38000 3263 28973000 0.002 0.0001

# SECTIONS INPUT

INTERNAL SECONDARY BEAMS																				
STOREY 0 STEEL PROFILE	-								IPE 220											
STOREY 1 STEEL PROFILE	-								IPE 220											
STOREY 2 STEEL PROFILE	-								IPE 220											
STOREY 3 STEEL PROFILE	-								IPE 220											
STOREY 4 STEEL PROFILE	-								IPE 220											
STOREY 5 STEEL PROFILE	-																			
STOREY 6 STEEL PROFILE	-																			
STOREY 7 STEEL PROFILE	-																			
STOREY 8 STEEL PROFILE	-																			
GENERATING LINE																				
ISB_NO	cp/s	355	C30/37_Y_W_D	0.11	0.0092	0.11	0.0092	0.2016	0.0059	1.5	1.49	0.041	0.03	auto135	(1.000	1.0	no	user	Vc_Vo[-]	0.780
ISB_N1	cp/s	355	C30/37_Y_W_D	0.11	0.0092	0.11	0.0092	0.2016	0.0059	1.5	1.49	0.041	0.03	auto135	(1.000	1.0	no	user	Vc_Vo[-]	0.780
ISB_N2	cp/s	355	C30/37_Y_W_D	0.11	0.0092	0.11	0.0092	0.2016	0.0059	1.5	1.49	0.041	0.03	auto135	(1.000	1.0	no	user	Vc_Vo[-]	0.780
ISB_N3	cp/s	355	C30/37_Y_W_D	0.11	0.0092	0.11	0.0092	0.2016	0.0059	1.5	1.49	0.041	0.03	auto135	(1.000	1.0	no	user	Vc_Vo[-]	0.780
ISB_N4	cp/s	355	C30/37_Y_W_D	0.11	0.0092	0.11	0.0092	0.2016	0.0059	1.5	1.49	0.041	0.03	auto135	(1.000	1.0	no	user	Vc_Vo[-]	0.592
MOMENT RESISTING FRAME BEAMS - X DIRECTION																				
STOREY 0 STEEL PROFILE	-																			IPE 330
STOREY 1 STEEL PROFILE	-																			IPE 330
STOREY 2 STEEL PROFILE	-																			IPE 330
STOREY 3 STEEL PROFILE	-																			IPE 300
STOREY 4 STEEL PROFILE	-																			IPE 300
STOREY 5 STEEL PROFILE	-																			
STOREY 6 STEEL PROFILE	-																			
STOREY 7 STEEL PROFILE	-																			
STOREY 8 STEEL PROFILE	-																			
GENERATING LINE																				
MRFBX_NO	slts	355		0.16	0.0115	0.16	0.0115	0.307	0.0075					not_pertinent	no	user	Vc_Vo[-]		0.179	
MRFBX_N1	slts	355		0.16	0.0115	0.16	0.0115	0.307	0.0075					not_pertinent	no	user	Vc_Vo[-]		0.153	
MRFBX_N2	slts	355		0.16	0.0115	0.16	0.0115	0.307	0.0075					not_pertinent	no	user	Vc_Vo[-]		0.153	
MRFBX_N3	slts	355		0.15	0.0107	0.15	0.0107	0.2786	0.0071					not_pertinent	no	user	Vc_Vo[-]		0.153	
MRFBX_N4	slts	355		0.15	0.0107	0.15	0.0107	0.2786	0.0071					not_pertinent	no	user	Vc_Vo[-]		0.000	
MOMENT RESISTING FRAME BEAMS - Y DIRECTION																				
STOREY 0 STEEL PROFILE	-																			IPE 400
STOREY 1 STEEL PROFILE	-																			IPE 400
STOREY 2 STEEL PROFILE	-																			IPE 400
STOREY 3 STEEL PROFILE	-																			IPE 360
STOREY 4 STEEL PROFILE	-																			IPE 360
STOREY 5 STEEL PROFILE	-																			
STOREY 6 STEEL PROFILE	-																			
STOREY 7 STEEL PROFILE	-																			
STOREY 8 STEEL PROFILE	-																			
GENERATING LINE																				
MRFBY_NO	slts	355		0.18	0.0135	0.18	0.0135	0.373	0.0086					not_pertinent	no	user	Vc_Vo[-]		0.719	
MRFBY_N1	slts	355		0.18	0.0135	0.18	0.0135	0.373	0.0086					not_pertinent	no	user	Vc_Vo[-]		0.543	
MRFBY_N2	slts	355		0.18	0.0135	0.18	0.0135	0.373	0.0086					not_pertinent	no	user	Vc_Vo[-]		0.543	
MRFBY_N3	slts	355		0.17	0.0127	0.17	0.0127	0.3346	0.008					not_pertinent	no	user	Vc_Vo[-]		0.543	
MRFBY_N4	slts	355		0.17	0.0127	0.17	0.0127	0.3346	0.008					not_pertinent	no	user	Vc_Vo[-]		0.296	

PERIMETER PRIMARY BEAMS																						
STOREY 0 STEEL PROFILE	-									IPE 270												
STOREY 1 STEEL PROFILE	-									IPE 270												
STOREY 2 STEEL PROFILE	-									IPE 270												
STOREY 3 STEEL PROFILE	-									IPE 270												
STOREY 4 STEEL PROFILE	-									IPE 240												
STOREY 5 STEEL PROFILE	-																					
STOREY 6 STEEL PROFILE	-																					
STOREY 7 STEEL PROFILE	-																					
STOREY 8 STEEL PROFILE	-																					
GENERATING LINE																						
PPB_N0	cp/s	355	C30/37_X_W_D	0.135	0.0102	0.135	0.0102	0.2496	0.0066	0.75	0.74	0.041	0.03	auto135	(1.000	1.0	no	user	Vc_Vp[-]		0.179	
PPB_N1	cp/s	355	C30/37_X_W_D	0.135	0.0102	0.135	0.0102	0.2496	0.0066	0.75	0.74	0.041	0.03	auto135	(1.000	1.0	no	user	Vc_Vp[-]		0.153	
PPB_N2	cp/s	355	C30/37_X_W_D	0.135	0.0102	0.135	0.0102	0.2496	0.0066	0.75	0.74	0.041	0.03	auto135	(1.000	1.0	no	user	Vc_Vp[-]		0.153	
PPB_N3	cp/s	355	C30/37_X_W_D	0.135	0.0102	0.135	0.0102	0.2496	0.0066	0.75	0.74	0.041	0.03	auto135	(1.000	1.0	no	user	Vc_Vp[-]		0.153	
PPB_N4	cp/s	355	C30/37_X_W_D	0.12	0.0098	0.12	0.0098	0.2204	0.0062	0.75	0.74	0.041	0.03	auto135	(1.000	1.0	no	user	Vc_Vp[-]		0.000	

INTERNAL PRIMARY BEAMS																						
STOREY 0 STEEL PROFILE	-									IPE 330												
STOREY 1 STEEL PROFILE	-									IPE 330												
STOREY 2 STEEL PROFILE	-									IPE 330												
STOREY 3 STEEL PROFILE	-									IPE 330												
STOREY 4 STEEL PROFILE	-									IPE 300												
STOREY 5 STEEL PROFILE	-																					
STOREY 6 STEEL PROFILE	-																					
STOREY 7 STEEL PROFILE	-																					
STOREY 8 STEEL PROFILE	-																					
GENERATING LINE																						
IPB_N0	cp/s	355	C30/37_X_W_D	0.16	0.0115	0.16	0.0115	0.307	0.0075	1.5	1.49	0.041	0.03	auto135	(1.000	1.0	no	user	Vc_Vp[-]		0	
IPB_N1	cp/s	355	C30/37_X_W_D	0.16	0.0115	0.16	0.0115	0.307	0.0075	1.5	1.49	0.041	0.03	auto135	(1.000	1.0	no	user	Vc_Vp[-]		0	
IPB_N2	cp/s	355	C30/37_X_W_D	0.16	0.0115	0.16	0.0115	0.307	0.0075	1.5	1.49	0.041	0.03	auto135	(1.000	1.0	no	user	Vc_Vp[-]		0	
IPB_N3	cp/s	355	C30/37_X_W_D	0.16	0.0115	0.16	0.0115	0.307	0.0075	1.5	1.49	0.041	0.03	auto135	(1.000	1.0	no	user	Vc_Vp[-]		0	
IPB_N4	cp/s	355	C30/37_X_W_D	0.15	0.0107	0.15	0.0107	0.2786	0.0071	1.5	1.49	0.041	0.03	auto135	(1.000	1.0	no	user	Vc_Vp[-]		0	

MOMENT RESISTING FRAME COLUMNS - X DIRECTION					
STOREYS - 1 TO 0 STEEL PROFILE	-	HE 280 A			
STOREYS 0 TO 1 STEEL PROFILE	-	HE 280 A			
STOREYS 1 TO 2 STEEL PROFILE	-	HE 280 A			
STOREYS 2 TO 3 STEEL PROFILE	-	HE 280 A			
STOREYS 3 TO 4 STEEL PROFILE	-	HE 280 A			
STOREYS 4 TO 5 STEEL PROFILE	-				
STOREYS 5 TO 6 STEEL PROFILE	-				
STOREYS 6 TO 7 STEEL PROFILE	-				
STOREYS 8 TO 8 STEEL PROFILE	-				
GENERATING LINE					
MRFCX_N-1_N0	sits	355 0.28 0.013 0.28 0.013 0.244 0.008	not_pertinent	no user Vc_Vol[-]	0
MRFCX_N0_N1	sits	355 0.28 0.013 0.28 0.013 0.244 0.008	not_pertinent	no user Vc_Vol[-]	0
MRFCX_N1_N2	sits	355 0.28 0.013 0.28 0.013 0.244 0.008	not_pertinent	no user Vc_Vol[-]	0
MRFCX_N2_N3	sits	355 0.28 0.013 0.28 0.013 0.244 0.008	not_pertinent	no user Vc_Vol[-]	0
MRFCX_N3_N4	sits	355 0.28 0.013 0.28 0.013 0.244 0.008	not_pertinent	no user Vc_Vol[-]	0

MOMENT RESISTING FRAME COLUMNS - Y DIRECTION					
STOREYS - 1 TO 0 STEEL PROFILE	-	HE 300 A			
STOREYS 0 TO 1 STEEL PROFILE	-	HE 300 A			
STOREYS 1 TO 2 STEEL PROFILE	-	HE 300 A			
STOREYS 2 TO 3 STEEL PROFILE	-	HE 300 A			
STOREYS 3 TO 4 STEEL PROFILE	-	HE 300 A			
STOREYS 4 TO 5 STEEL PROFILE	-				
STOREYS 5 TO 6 STEEL PROFILE	-				
STOREYS 6 TO 7 STEEL PROFILE	-				
STOREYS 8 TO 8 STEEL PROFILE	-				
GENERATING LINE					
MRFCY_N-1_N0	sits	355 0.3 0.014 0.3 0.014 0.262 0.0085	not_pertinent	no user Vc_Vol[-]	0
MRFCY_N0_N1	sits	355 0.3 0.014 0.3 0.014 0.262 0.0085	not_pertinent	no user Vc_Vol[-]	0
MRFCY_N1_N2	sits	355 0.3 0.014 0.3 0.014 0.262 0.0085	not_pertinent	no user Vc_Vol[-]	0
MRFCY_N2_N3	sits	355 0.3 0.014 0.3 0.014 0.262 0.0085	not_pertinent	no user Vc_Vol[-]	0
MRFCY_N3_N4	sits	355 0.3 0.014 0.3 0.014 0.262 0.0085	not_pertinent	no user Vc_Vol[-]	0

INTERNAL COLUMNS					
STOREYS - 1 TO 0 STEEL PROFILE	-	HE 240 A			
STOREYS 0 TO 1 STEEL PROFILE	-	HE 240 A			
STOREYS 1 TO 2 STEEL PROFILE	-	HE 240 A			
STOREYS 2 TO 3 STEEL PROFILE	-	HE 220 A			
STOREYS 3 TO 4 STEEL PROFILE	-	HE 220 A			
STOREYS 4 TO 5 STEEL PROFILE	-				
STOREYS 5 TO 6 STEEL PROFILE	-				
STOREYS 6 TO 7 STEEL PROFILE	-				
STOREYS 8 TO 8 STEEL PROFILE	-				
GENERATING LINE					
IC_N-1_N0	sits	355 0.24 0.012 0.24 0.012 0.206 0.0075	not_pertinent	no user Vc_Vol[-]	0
IC_N0_N1	sits	355 0.24 0.012 0.24 0.012 0.206 0.0075	not_pertinent	no user Vc_Vol[-]	0
IC_N1_N2	sits	355 0.24 0.012 0.24 0.012 0.206 0.0075	not_pertinent	no user Vc_Vol[-]	0
IC_N2_N3	sits	355 0.22 0.011 0.22 0.011 0.188 0.007	not_pertinent	no user Vc_Vol[-]	0
IC_N3_N4	sits	355 0.22 0.011 0.22 0.011 0.188 0.007	not_pertinent	no user Vc_Vol[-]	0

FICTITIOUS FRAME ELEMENT					
IN GENERAL	-	TANGJULAR SOLID SECTION			
GENERATING LINE					
F	rss	RIGID 0.1 0.1	not_pertinent	no user Vc_Vol[-]	0

# ELEMENT CLASSES INPUT

ELEMENT CLASSES INPUT			
<b>INELASTIC FORCE BASED ELEMENTS</b>			
<b>INTERNAL SECONDARY BEAMS</b>			
GENERATING LINES			
ELEMENT CLASS	SECTION NAME	INTEGRATION SECTIONS	SECTION FIBRES
InfrmFB_ISB_NO	ISB_NO	5	100
InfrmFB_ISB_N1	ISB_N1	5	100
InfrmFB_ISB_N2	ISB_N2	5	100
InfrmFB_ISB_N3	ISB_N3	5	100
InfrmFB_ISB_N4	ISB_N4	5	100
<b>MOMENT RESISTING FRAME BEAMS - X DIRECTION</b>			
GENERATING LINES			
ELEMENT CLASS	SECTION NAME	INTEGRATION SECTIONS	SECTION FIBRES
InfrmFB_MRFBX_NO	MRFBX_NO	5	100
InfrmFB_MRFBX_N1	MRFBX_N1	5	100
InfrmFB_MRFBX_N2	MRFBX_N2	5	100
InfrmFB_MRFBX_N3	MRFBX_N3	5	100
InfrmFB_MRFBX_N4	MRFBX_N4	5	100
<b>MOMENT RESISTING FRAME BEAMS - Y DIRECTION</b>			
GENERATING LINES			
ELEMENT CLASS	SECTION NAME	INTEGRATION SECTIONS	SECTION FIBRES
InfrmFB_MRFBY_NO	MRFBY_NO	5	100
InfrmFB_MRFBY_N1	MRFBY_N1	5	100
InfrmFB_MRFBY_N2	MRFBY_N2	5	100
InfrmFB_MRFBY_N3	MRFBY_N3	5	100
InfrmFB_MRFBY_N4	MRFBY_N4	5	100
<b>PERIMETER PRIMARY BEAMS</b>			
GENERATING LINES			
ELEMENT CLASS	SECTION NAME	INTEGRATION SECTIONS	SECTION FIBRES
InfrmFB_PPB_NO	PPB_NO	5	100
InfrmFB_PPB_N1	PPB_N1	5	100
InfrmFB_PPB_N2	PPB_N2	5	100
InfrmFB_PPB_N3	PPB_N3	5	100
InfrmFB_PPB_N4	PPB_N4	5	100
<b>INTERNAL PRIMARY BEAMS</b>			
GENERATING LINES			
ELEMENT CLASS	SECTION NAME	INTEGRATION SECTIONS	SECTION FIBRES
InfrmFB_IPB_NO	IPB_NO	5	100
InfrmFB_IPB_N1	IPB_N1	5	100
InfrmFB_IPB_N2	IPB_N2	5	100
InfrmFB_IPB_N3	IPB_N3	5	100
InfrmFB_IPB_N4	IPB_N4	5	100

MOMENT RESISTING FRAME COLUMNS - X DIRECTION			
GENERATING LINES			
ELEMENT CLASS	SECTION NAME	INTEGRATION SECTIONS	SECTION FIBRES
InfrmFB_MRFCX_N-1_NO	MRFCX_N-1_NO	5	52
InfrmFB_MRFCX_NO_N1	MRFCX_NO_N1	5	52
InfrmFB_MRFCX_N1_N2	MRFCX_N1_N2	5	52
InfrmFB_MRFCX_N2_N3	MRFCX_N2_N3	5	52
InfrmFB_MRFCX_N3_N4	MRFCX_N3_N4	5	52
MOMENT RESISTING FRAME COLUMNS - Y DIRECTION			
GENERATING LINES			
ELEMENT CLASS	SECTION NAME	INTEGRATION SECTIONS	SECTION FIBRES
InfrmFB_MRFCY_N-1_NO	MRFCY_N-1_NO	5	52
InfrmFB_MRFCY_NO_N1	MRFCY_NO_N1	5	52
InfrmFB_MRFCY_N1_N2	MRFCY_N1_N2	5	52
InfrmFB_MRFCY_N2_N3	MRFCY_N2_N3	5	52
InfrmFB_MRFCY_N3_N4	MRFCY_N3_N4	5	52
INTERNAL COLUMNS			
GENERATING LINES			
ELEMENT CLASS	SECTION NAME	INTEGRATION SECTIONS	SECTION FIBRES
InfrmFB_IC_N-1_NO	IC_N-1_NO	5	52
InfrmFB_IC_NO_N1	IC_NO_N1	5	52
InfrmFB_IC_N1_N2	IC_N1_N2	5	52
InfrmFB_IC_N2_N3	IC_N2_N3	5	52
InfrmFB_IC_N3_N4	IC_N3_N4	5	52

ELASTIC FORCE BASED ELEMENTS			
FICTITIOUS FRAME ELEMENT			
GENERATING LINES			
ELEMENT CLASS	SECTION	PARAMETERS	DAMPING
elfrm_F	F	6666666.667 16666666666.667	10833855614

ELASTIC ELEMENTS			
INTERNAL SECONDARY BEAMS			
GENERATING LINES			
ELEMENT CLASS	SECTION	PARAMETERS	DAMPING
elfrm_ISB_NO	ISB_NO	231033.86340677 265.15614739	1.1075
elfrm_ISB_N1	ISB_N1	231033.86340677 265.15614739	1.1075
elfrm_ISB_N2	ISB_N2	231033.86340677 265.15614739	1.1075
elfrm_ISB_N3	ISB_N3	231033.86340677 265.15614739	1.1075
elfrm_ISB_N4	ISB_N4	231033.86340677 265.15614739	1.1075

PERIMETER PRIMARY BEAMS			
GENERATING LINES			
ELEMENT CLASS	SECTION	PARAMETERS	DAMPING
elfrm_PPb_N0	PPB_N0	6829 0.18799584	
elfrm_PPb_N1	PPB_N1	6829 0.18799584	
elfrm_PPb_N2	PPB_N2	6829 0.18799584	
elfrm_PPb_N3	PPB_N3	6829 0.18799584	
elfrm_PPb_N4	PPB_N4	9258 0.02956621	
INTERNAL PRIMARY BEAMS			
GENERATING LINES			
ELEMENT CLASS	SECTION	PARAMETERS	DAMPING
elfrm_IPB_N0	IPB_N0	00096 0.04756791	
elfrm_IPB_N1	IPB_N1	00096 0.04756791	
elfrm_IPB_N2	IPB_N2	00096 0.04756791	
elfrm_IPB_N3	IPB_N3	00096 0.04756791	
elfrm_IPB_N4	IPB_N4	99149 0.04125126	

## SECTION ADDITIONAL MASS INPUT

BEAM STOREY LEVEL - GROUND					
BEAM TYPE	-	Internal Secondary Beam	Perimeter Primary Beam	MRF Beam X	MRF Beam Y
Beam influence length	m	2.00	0.00	0.00	1.00
Interstorey Height	m	3.00	3.00	3.00	3.00
Cladding influence height	m	0.00	3.50	3.50	3.50
CHARACTERISTIC LOADS					
DL - Composite floor	kN/m	3.40	0.00	0.00	1.70
NS DL - Floor finishing	kN/m	0.80	0.00	0.00	0.40
NS DL - Facade	kN/m	0.00	1.75	1.75	1.75
NS DL - Susp. Ceiling	kN/m	0.00	0.00	0.00	0.00
NS DL - Internal Walls	kN/m	1.60	0.00	0.00	0.80
LL	kN/m	8.00	0.00	0.00	4.00
ACCIDENTAL COMBINATION LOADS					
1.0 x DL	kN/m	3.40	0.00	0.00	1.70
1.0 x NS DL	kN/m	2.40	1.75	1.75	2.95
$\psi_c$ x LL	kN/m	4.80	0.00	0.00	2.40
ADDITIONAL MASS AND WEIGHT (ACC. COMBINATION)					
$M_{add,acc.comb.}$	ton/m	1.082	0.179	0.179	0.719
$W_{add,acc.comb.}$	kN/m	10.600	1.750	1.750	7.050

BEAM STOREY LEVEL - ELEVATED - 1st					
BEAM TYPE	-	Internal Secondary Beam	Perimeter Primary Beam	MRF Beam X	MRF Beam Y
Beam influence length	m	2.00	0.00	0.00	1.00
Interstorey Height	m	3.00	3.00	3.00	3.00
Cladding influence height	m	0.00	3.00	3.00	3.00
CHARACTERISTIC LOADS					
DL - Composite floor	kN/m	3.40	0.00	0.00	1.70
NS DL - Floor finishing	kN/m	0.80	0.00	0.00	0.40
NS DL - Facade	kN/m	0.00	1.50	1.50	1.50
NS DL - Susp. Ceiling	kN/m	0.40	0.00	0.00	0.20
NS DL - Internal Walls	kN/m	1.60	0.00	0.00	0.80
LL	kN/m	6.00	0.00	0.00	3.00
ACCIDENTAL COMBINATION LOADS					
1.0 x DL	kN/m	3.40	0.00	0.00	1.70
1.0 x NS DL	kN/m	2.80	1.50	1.50	2.90
$\psi_c$ x LL	kN/m	1.44	0.00	0.00	0.72
ADDITIONAL MASS AND WEIGHT (ACC. COMBINATION)					
$M_{add,acc.comb.}$	ton/m	0.780	0.153	0.153	0.543
$W_{add,acc.comb.}$	kN/m	7.640	1.500	1.500	5.320

BEAM STOREY LEVEL - ELEVATED - 2nd TO UPPER					
BEAM TYPE	-	Internal Secondary Beam	Perimeter Primary Beam	MRF Beam X	MRF Beam Y
Beam influence length	m	2.00	0.00	0.00	1.00
Interstorey Height	m	3.00	3.00	3.00	3.00
Cladding influence height	m	0.00	3.00	3.00	3.00
CHARACTERISTIC LOADS					
DL - Composite floor	kN/m	3.40	0.00	0.00	1.70
NS DL - Floor finishing	kN/m	0.80	0.00	0.00	0.40
NS DL - Facade	kN/m	0.00	1.50	1.50	1.50
NS DL - Susp. Ceiling	kN/m	0.40	0.00	0.00	0.20
NS DL - Internal Walls	kN/m	1.60	0.00	0.00	0.80
LL	kN/m	6.00	0.00	0.00	3.00
ACCIDENTAL COMBINATION LOADS					
1.0 x DL	kN/m	3.40	0.00	0.00	1.70
1.0 x NS DL	kN/m	2.80	1.50	1.50	2.90
$\psi_2$ x LL	kN/m	1.44	0.00	0.00	0.72
ADDITIONAL MASS AND WEIGHT (ACC. COMBINATION)					
M <sub>add,acc.comb.</sub>	ton/m	0.780	0.153	0.153	0.543
W <sub>add,acc.comb.</sub>	kN/m	7.640	1.500	1.500	5.320

BEAM STOREY LEVEL - ROOF					
BEAM TYPE	-	Internal Secondary Beam	Perimeter Primary Beam	MRF Beam X	MRF Beam Y
Beam influence length	m	2.00	0.00	0.00	1.00
Interstorey Height	m	3.00	3.00	3.00	3.00
Cladding influence height	m	0.00	0.00	0.00	0.00
CHARACTERISTIC LOADS					
DL - Composite floor	kN/m	3.40	0.00	0.00	1.70
NS DL - Floor finishing	kN/m	2.00	0.00	0.00	1.00
NS DL - Facade	kN/m	0.00	0.00	0.00	0.00
NS DL - Susp. Ceiling	kN/m	0.40	0.00	0.00	0.20
NS DL - Internal Walls	kN/m	0.00	0.00	0.00	0.00
LL	kN/m	0.80	0.00	0.00	0.40
ACCIDENTAL COMBINATION LOADS					
1.0 x DL	kN/m	3.40	0.00	0.00	1.70
1.0 x NS DL	kN/m	2.40	0.00	0.00	1.20
$\psi_2$ x LL	kN/m	0.00	0.00	0.00	0.00
ADDITIONAL MASS AND WEIGHT (ACC. COMBINATION)					
M <sub>add,acc.comb.</sub>	ton/m	0.592	0.000	0.000	0.296
W <sub>add,acc.comb.</sub>	kN/m	5.800	0.000	0.000	2.900

## CLADDING ELEMENT CLASS INPUT

### CLADDING ELEMENT CLASS INPUT

Element Class	Curve Types	Curve Parameters	Other Parameters	Damping
INFILL_MASONRY	inf_strut inf_shear	9 1. 1.5 3. 1.4 380 0.7 600. 1.5	5. 0.04 40. 23. 2.6 2.6 20 5.	
INFILL_CFS	multi_lin lin_sym	9000 19 84 0.032 0.21 0.001 -19.	0.004 100 0.00056 100 1 1 1	0.001 0.01



# ELEMENT CLASSES INPUT

## ELEMENT CLASSES INPUT

LINK			
PERFECTLY PINNED LINKS			
LINK TYPE	1 (ESSKO [kN/m or kNm/rad])		
PERFECTLY RIGID	1000000		
PERFECTLY PINNED	0.001		
GENERATING LINES			
ELEMENT CLASS	CURVE TYPES	CURVE PARAMETERS	DAMPING
Link PINNED M1	lin sym lin sym lin	1000000 1000000 1000000 0.001 1000000 1000000	
Link PINNED M2	lin sym lin sym lin	1000000 1000000 1000000 0.001 1000000	

MRF COLUMN WEB ROTATION LINK - XZ FRAME										
$f_{cylinder}$	MPa	444								
$E_{cylinder}$	GPa	210								
$M_{cylinder} / M_{cylinder}$	-	1.038								
$M_{cylinder} / M_{cylinder}$	-	1.038								
Ramberg-Osgood parameter	-	10.0								
Ramb-Osg. Converg. Limit	-	0.005								
SEGMENT	-	ST. -1 TO 0	ST. 0 TO 1	ST. 1 TO 2	ST. 2 TO 3	ST. 3 TO 4	ST. 4 TO 5	ST. 5 TO 6	ST. 6 TO 7	ST. 7 TO 8
BEAM SECTION	-	IPE 330	IPE 330	IPE 330	IPE 300	IPE 300	#N/A	#N/A	#N/A	#N/A
$d_{cylinder}$	mm	330	330	300	300	#N/A	#N/A	#N/A	#N/A	#N/A
COLUMN SECTION	-	HE 280 A	HE 280 A	HE 280 A	HE 280 A	HE 280 A	#N/A	#N/A	#N/A	#N/A
$E_{cylinder}$	MPa	444	444	444	444	444	444	444	444	444
$E_{cylinder}$	GPa	210	210	210	210	210	210	210	210	210
$G_{cylinder}$	GPa	81	81	81	81	81	81	81	81	81
$b_{cylinder}$	mm	280.0	280.0	280.0	280.0	#N/A	#N/A	#N/A	#N/A	#N/A
$t_{cylinder}$	mm	13.0	13.0	13.0	13.0	#N/A	#N/A	#N/A	#N/A	#N/A
$t_{cylinder}$	mm	8.0	8.0	8.0	8.0	#N/A	#N/A	#N/A	#N/A	#N/A
$t_{cylinder}$	mm	0.0	0.0	0.0	0.0	0.0	0.0	0.0	0.0	0.0
$t_{cylinder}$	mm	8.0	8.0	8.0	8.0	#N/A	#N/A	#N/A	#N/A	#N/A
$d_{cylinder}$	mm	270.0	270.0	270.0	270.0	#N/A	#N/A	#N/A	#N/A	#N/A
$V_c$	kN	526	526	526	526	#N/A	#N/A	#N/A	#N/A	#N/A
$\gamma_c$	-	0.0032	0.0032	0.0032	0.0032	0.0032	0.0032	0.0032	0.0032	0.0032
$K_c$	kN	165738	165738	165738	165738	#N/A	#N/A	#N/A	#N/A	#N/A
$V_c$	kN	632	632	643	643	#N/A	#N/A	#N/A	#N/A	#N/A
$\gamma_c$	-	0.0127	0.0127	0.0127	0.0127	0.0127	0.0127	0.0127	0.0127	0.0127
$K_c$	kN	11186	11186	12289	12289	#N/A	#N/A	#N/A	#N/A	#N/A
$\alpha$	%	0.7	0.7	0.7	0.7	0.7	0.7	0.7	0.7	0.7
$K_c$	kN	1160	1160	1160	1160	#N/A	#N/A	#N/A	#N/A	#N/A
$V_c$	kN	647	647	657	657	#N/A	#N/A	#N/A	#N/A	#N/A
$\gamma_c$	-	0.0254	0.0254	0.0254	0.0254	0.0254	0.0254	0.0254	0.0254	0.0254
$M_c$	kNm	173	173	158	158	#N/A	#N/A	#N/A	#N/A	#N/A
$M_c$	kNm	209	209	193	193	#N/A	#N/A	#N/A	#N/A	#N/A
$M_c$	kNm	213	213	197	197	#N/A	#N/A	#N/A	#N/A	#N/A
$\varphi_c$	rad	0.0032	0.0032	0.0032	0.0032	0.0032	0.0032	0.0032	0.0032	0.0032
$\varphi_c$	rad	0.0127	0.0127	0.0127	0.0127	0.0127	0.0127	0.0127	0.0127	0.0127
$\varphi_c$	rad	0.0254	0.0254	0.0254	0.0254	0.0254	0.0254	0.0254	0.0254	0.0254
GENERATING LINES										
ELEMENT CLASS	CURVE TYPES	CURVE PARAMETERS	DAMPING							
L_CW_MRF_X_N0	lin sym lin sym rfa	1000000 1000000 1000000 216 0.026 10 0.005 1000000								
L_CW_MRF_X_N1	lin sym lin sym rfa	1000000 1000000 1000000 216 0.026 10 0.005 1000000								
L_CW_MRF_X_N2	lin sym lin sym rfa	1000000 1000000 1000000 216 0.026 10 0.005 1000000								
L_CW_MRF_X_N3	lin sym lin sym rfa	1000000 1000000 1000000 200 0.026 10 0.005 1000000								
L_CW_MRF_X_N4	lin sym lin sym rfa	1000000 1000000 1000000 200 0.026 10 0.005 1000000								

MRF COLUMN WEB ROTATION LINK - YZ FRAME										
$f_{cylinder}$	MPa	444								
$E_{cylinder}$	GPa	210								
$M_{cylinder} / M_{cylinder}$	-	1.038								
$M_{cylinder} / M_{cylinder}$	-	1.038								
Ramberg-Osgood parameter	-	10.0								
Ramb-Osg. Converg. Limit	-	0.005								
SEGMENT	-	ST. -1 TO 0	ST. 0 TO 1	ST. 1 TO 2	ST. 2 TO 3	ST. 3 TO 4	ST. 4 TO 5	ST. 5 TO 6	ST. 6 TO 7	ST. 7 TO 8
BEAM SECTION	-	IPE 400	IPE 400	IPE 400	IPE 360	IPE 360	#N/A	#N/A	#N/A	#N/A
$d_{cylinder}$	mm	400	400	400	360	360	#N/A	#N/A	#N/A	#N/A
COLUMN SECTION	-	HE 300 A	HE 300 A	HE 300 A	HE 300 A	HE 300 A	#N/A	#N/A	#N/A	#N/A
$E_{cylinder}$	MPa	444	444	444	444	444	444	444	444	444
$E_{cylinder}$	GPa	210	210	210	210	210	210	210	210	210
$G_{cylinder}$	GPa	81	81	81	81	81	81	81	81	81
$b_{cylinder}$	mm	300.0	300.0	300.0	300.0	#N/A	#N/A	#N/A	#N/A	#N/A
$t_{cylinder}$	mm	14.0	14.0	14.0	14.0	#N/A	#N/A	#N/A	#N/A	#N/A
$t_{cylinder}$	mm	8.5	8.5	8.5	8.5	#N/A	#N/A	#N/A	#N/A	#N/A
$t_{cylinder}$	mm	0.0	0.0	0.0	0.0	0.0	0.0	0.0	0.0	0.0
$t_{cylinder}$	mm	17.0	8.5	8.5	8.5	#N/A	#N/A	#N/A	#N/A	#N/A
$d_{cylinder}$	mm	290.0	290.0	290.0	290.0	#N/A	#N/A	#N/A	#N/A	#N/A
$V_c$	kN	1200	600	600	600	#N/A	#N/A	#N/A	#N/A	#N/A
$\gamma_c$	-	0.0032	0.0032	0.0032	0.0032	0.0032	0.0032	0.0032	0.0032	0.0032
$K_c$	kN	378283	189141	189141	189141	189141	#N/A	#N/A	#N/A	#N/A
$V_c$	kN	1311	709	709	721	721	#N/A	#N/A	#N/A	#N/A
$\gamma_c$	-	0.0127	0.0127	0.0127	0.0127	0.0127	0.0127	0.0127	0.0127	0.0127
$K_c$	kN	11659	11485	11485	12742	12742	#N/A	#N/A	#N/A	#N/A
$\alpha$	%	0.7	0.7	0.7	0.7	0.7	0.7	0.7	0.7	0.7
$K_c$	kN	2648	1324	1324	1324	1324	#N/A	#N/A	#N/A	#N/A
$V_c$	kN	1344	726	726	738	738	#N/A	#N/A	#N/A	#N/A
$\gamma_c$	-	0.0254	0.0254	0.0254	0.0254	0.0254	0.0254	0.0254	0.0254	0.0254
$M_c$	kNm	480	240	240	216	216	#N/A	#N/A	#N/A	#N/A
$M_c$	kNm	524	284	284	260	260	#N/A	#N/A	#N/A	#N/A
$M_c$	kNm	538	290	290	266	266	#N/A	#N/A	#N/A	#N/A
$\varphi_c$	rad	0.0032	0.0032	0.0032	0.0032	0.0032	0.0032	0.0032	0.0032	0.0032
$\varphi_c$	rad	0.0127	0.0127	0.0127	0.0127	0.0127	0.0127	0.0127	0.0127	0.0127
$\varphi_c$	rad	0.0254	0.0254	0.0254	0.0254	0.0254	0.0254	0.0254	0.0254	0.0254
GENERATING LINES										
ELEMENT CLASS	CURVE TYPES	CURVE PARAMETERS	DAMPING							
L_CW_MRF_Y_N0	lin sym ram_osp lin	1000000 1000000 1000000 543 0.026 10 0.005 1000000 1000000								
L_CW_MRF_Y_N1	lin sym ram_osp lin	1000000 1000000 1000000 294 0.026 10 0.005 1000000 1000000								
L_CW_MRF_Y_N2	lin sym ram_osp lin	1000000 1000000 1000000 294 0.026 10 0.005 1000000 1000000								
L_CW_MRF_Y_N3	lin sym ram_osp lin	1000000 1000000 1000000 269 0.026 10 0.005 1000000 1000000								
L_CW_MRF_Y_N4	lin sym ram_osp lin	1000000 1000000 1000000 269 0.026 10 0.005 1000000 1000000								

ISB - IPB LINK						
SPAN	6					
GENERATING LINES FOR 6m AND 10m SPAN STRUCTURE LINKS						
S	ISB PROFILE	IPB PROFILE	ELEMENT CLASS	CURVE TYPES	RVE PARAMETE	DAMPING
6	IPE 220	IPE 330	L_ISB_IPB_Nx	bl_kin bl_kin I	124400 200 0.	None
10	IPE 360	HE 500 A	L_ISB_IPB_Nx	bl_kin bl_kin I	124400 200 0.	None
STOREY	ISB PROFILE	IPB PROFILE	ELEMENT CLASS	CURVE TYPES	RVE PARAMETE	DAMPING
0	IPE 220	IPE 330	L_ISB_IPB_N0	bl_kin bl_kin I	124400 200 0.	None
1	IPE 220	IPE 330	L_ISB_IPB_N1	bl_kin bl_kin I	124400 200 0.	None
2	IPE 220	IPE 330	L_ISB_IPB_N2	bl_kin bl_kin I	124400 200 0.	None
3	IPE 220	IPE 330	L_ISB_IPB_N3	bl_kin bl_kin I	124400 200 0.	None
4	IPE 220	IPE 300	L_ISB_IPB_N4	bl_kin bl_kin I	124400 200 0.	None
5						
6						
7						
8						

ISB - PPB LINK						
GENERATING LINES FOR 6m AND 10m SPAN STRUCTURE LINKS						
S	ISB PROFILE	PPB PROFILE	ELEMENT CLASS	CURVE TYPES	RVE PARAMETE	DAMPING
6	IPE 220	IPE 270	L_ISB_PPb_Nx	bl_kin bl_kin I	124400 200 0.	None
10	IPE 360	HE 360 B	L_ISB_PPb_Nx	bl_kin bl_kin I	124400 200 0.	None
STOREY	ISB PROFILE	PPB PROFILE	ELEMENT CLASS	CURVE TYPES	RVE PARAMETE	DAMPING
0	IPE 220	IPE 270	L_ISB_PPb_N0	bl_kin bl_kin I	124400 200 0.	None
1	IPE 220	IPE 270	L_ISB_PPb_N1	bl_kin bl_kin I	124400 200 0.	None
2	IPE 220	IPE 270	L_ISB_PPb_N2	bl_kin bl_kin I	124400 200 0.	None
3	IPE 220	IPE 270	L_ISB_PPb_N3	bl_kin bl_kin I	124400 200 0.	None
4	IPE 220	IPE 240	L_ISB_PPb_N4	bl_kin bl_kin I	124400 200 0.	None
5						
6						
7						
8						

ISB - MRFBX LINK						
GENERATING LINES FOR 6m AND 10m SPAN STRUCTURE LINKS						
S	ISB PROFILE	MRFBX PROFILE	ELEMENT CLASS	CURVE TYPES	RVE PARAMETE	DAMPING
6	IPE 220	VARIES	_ISB_MRFBX_N	bl_kin bl_kin I	124400 200 0.	None
10	IPE 360	VARIES	_ISB_MRFBX_N	bl_kin bl_kin I	124400 200 0.	None
STOREY	ISB PROFILE	MRFBX PROFILE	ELEMENT CLASS	CURVE TYPES	RVE PARAMETE	DAMPING
0	IPE 220	IPE 330	_ISB_MRFBX_N	bl_kin bl_kin I	124400 200 0.	None
1	IPE 220	IPE 330	_ISB_MRFBX_N	bl_kin bl_kin I	124400 200 0.	None
2	IPE 220	IPE 330	_ISB_MRFBX_N	bl_kin bl_kin I	124400 200 0.	None
3	IPE 220	IPE 300	_ISB_MRFBX_N	bl_kin bl_kin I	124400 200 0.	None
4	IPE 220	IPE 300	_ISB_MRFBX_N	bl_kin bl_kin I	124400 200 0.	None
5						
6						
7						
8						

ISB - MRFCX LINK						
GENERATING LINES FOR 6m AND 10m SPAN STRUCTURE LINKS						
S	ISB PROFILE	MRFCX PROFILE	ELEMENT CLASS	CURVE TYPES	RVE PARAMETE	DAMPING
6	IPE 220	VARIES	_ISB_MRFCX_N	n_sym bl_kin I	10000 3000 38	None
10	IPE 360	VARIES	_ISB_MRFCX_N	n_sym bl_kin I	10000 8000 90	None
STOREY	ISB PROFILE	MRFCX PROFILE	ELEMENT CLASS	CURVE TYPES	RVE PARAMETE	DAMPING
0	IPE 220	HE 280 A	_ISB_MRFCX_N	n_sym bl_kin I	10000 3000 38	None
1	IPE 220	HE 280 A	_ISB_MRFCX_N	n_sym bl_kin I	10000 3000 38	None
2	IPE 220	HE 280 A	_ISB_MRFCX_N	n_sym bl_kin I	10000 3000 38	None
3	IPE 220	HE 280 A	_ISB_MRFCX_N	n_sym bl_kin I	10000 3000 38	None
4	IPE 220	HE 280 A	_ISB_MRFCX_N	n_sym bl_kin I	10000 3000 38	None
5						
6						
7						
8						

PPB - MRF CY LINK							
GENERATING LINES FOR 6m AND 10m SPAN STRUCTURE LINKS							
S	PPB PROFILE	MRF CY PROFILE	ELEMENT CLASS	CURVE TYPES	RVE PARAMETE	DAMPING	
6	IPE 240	VARIES	PPB_MRF CX_N	lin_sym lin_sym	3000 100000	None	
6	IPE 270	VARIES	PPB_MRF CX_N	lin_sym lin_sym	4000 100000	None	
10	HE 320 A	VARIES	PPB_MRF CX_N	lin_sym lin_sym	13000 100000	None	
10	HE 360 B	VARIES	PPB_MRF CX_N	lin_sym lin_sym	8000 100000	None	
STOREY	PPB PROFILE	MRF CY PROFILE	ELEMENT CLASS	CURVE TYPES	RVE PARAMETE	DAMPING	
0	IPE 270	HE 300 A	PPB_MRF CY_N	lin_sym lin_sym	4000 100000	None	
1	IPE 270	HE 300 A	PPB_MRF CY_N	lin_sym lin_sym	4000 100000	None	
2	IPE 270	HE 300 A	PPB_MRF CY_N	lin_sym lin_sym	4000 100000	None	
3	IPE 270	HE 300 A	PPB_MRF CY_N	lin_sym lin_sym	4000 100000	None	
4	IPE 240	HE 300 A	PPB_MRF CY_N	lin_sym lin_sym	3000 100000	None	
5							
6							
7							
8							

IPB - MRF CY LINK							
GENERATING LINES FOR 6m AND 10m SPAN STRUCTURE LINKS							
S	IPB PROFILE	MRF CY PROFILE	ELEMENT CLASS	CURVE TYPES	RVE PARAMETE	DAMPING	
6	IPE 300	VARIES	IPB_MRF CY_N	lin_sym lin_sym	15000 100000	None	
6	IPE 330	VARIES	IPB_MRF CY_N	lin_sym lin_sym	15000 100000	None	
10	HE 400 A	VARIES	IPB_MRF CY_N	lin_sym lin_sym	20000 100000	None	
10	HE 500 A	VARIES	IPB_MRF CY_N	lin_sym lin_sym	5000 100000	None	
STOREY	IPB PROFILE	MRF CY PROFILE	ELEMENT CLASS	CURVE TYPES	RVE PARAMETE	DAMPING	
0	IPE 330	HE 300 A	IPB_MRF CY_N	lin_sym lin_sym	15000 100000	None	
1	IPE 330	HE 300 A	IPB_MRF CY_N	lin_sym lin_sym	15000 100000	None	
2	IPE 330	HE 300 A	IPB_MRF CY_N	lin_sym lin_sym	15000 100000	None	
3	IPE 330	HE 300 A	IPB_MRF CY_N	lin_sym lin_sym	15000 100000	None	
4	IPE 300	HE 300 A	IPB_MRF CY_N	lin_sym lin_sym	15000 100000	None	
5							
6							
7							
8							

ISB - IC LINK							
GENERATING LINES FOR 6m AND 10m SPAN STRUCTURE LINKS							
S	ISB PROFILE	IC PROFILE	ELEMENT CLASS	CURVE TYPES	RVE PARAMETE	DAMPING	
6	IPE 220	VARIES	L_ISB_IC_Nx	n_sym bl_kin	10000 3000 38	None	
10	IPE 360	VARIES	L_ISB_IC_Nx	lin_sym bl_kin	10000 8000 90	None	
STOREY	ISB PROFILE	IC PROFILE	ELEMENT CLASS	CURVE TYPES	RVE PARAMETE	DAMPING	
0	IPE 220	HE 240 A	L_ISB_IC_N0	n_sym bl_kin	10000 3000 38	None	
1	IPE 220	HE 240 A	L_ISB_IC_N1	n_sym bl_kin	10000 3000 38	None	
2	IPE 220	HE 240 A	L_ISB_IC_N2	n_sym bl_kin	10000 3000 38	None	
3	IPE 220	HE 220 A	L_ISB_IC_N3	n_sym bl_kin	10000 3000 38	None	
4	IPE 220	HE 220 A	L_ISB_IC_N4	n_sym bl_kin	10000 3000 38	None	
5							
6							
7							
8							

IPB - IC LINK							
GENERATING LINES FOR 6m AND 10m SPAN STRUCTURE LINKS							
S	IPB PROFILE	MRF CY PROFILE	ELEMENT CLASS	CURVE TYPES	RVE PARAMETE	DAMPING	
6	IPE 300	VARIES	L_IPB_IC_Nx	lin_sym lin_sym	15000 100000	None	
6	IPE 330	VARIES	L_IPB_IC_Nx	lin_sym lin_sym	15000 100000	None	
10	HE 400 A	VARIES	L_IPB_IC_Nx	lin_sym lin_sym	20000 100000	None	
10	HE 500 A	VARIES	L_IPB_IC_Nx	lin_sym lin_sym	5000 100000	None	
STOREY	IPB PROFILE	IC PROFILE	ELEMENT CLASS	CURVE TYPES	RVE PARAMETE	DAMPING	
0	IPE 330	HE 240 A	L_IPB_IC_N0	lin_sym lin_sym	15000 100000	None	
1	IPE 330	HE 240 A	L_IPB_IC_N1	lin_sym lin_sym	15000 100000	None	
2	IPE 330	HE 240 A	L_IPB_IC_N2	lin_sym lin_sym	15000 100000	None	
3	IPE 330	HE 220 A	L_IPB_IC_N3	lin_sym lin_sym	15000 100000	None	
4	IPE 300	HE 220 A	L_IPB_IC_N4	lin_sym lin_sym	15000 100000	None	
5							
6							
7							
8							

PPB - MRF CX LINK						
GENERATING LINES FOR 6m AND 10m SPAN STRUCTURE LINKS						
	PPB PROFILE	MRF CX PROFILE	ELEMENT CLASS	CURVE TYPES	RVE PARAMETE	DAMPING
5	IPE 240	VARIES	PPB_MRF CX_N	lin_sym lin_sym	3000 100000	None
6	IPE 270	VARIES	PPB_MRF CX_N	lin_sym lin_sym	12000 100000	None
10	HE 320 A	VARIES	PPB_MRF CX_N	lin_sym lin_sym	15000 100000	None
10	HE 360 B	VARIES	PPB_MRF CX_N	lin_sym lin_sym	15000 100000	None
STOREY	PPB PROFILE	MRF CX PROFILE	ELEMENT CLASS	CURVE TYPES	RVE PARAMETE	DAMPING
0	IPE 270	HE 280 A	PPB_MRF CX_N	lin_sym lin_sym	12000 100000	None
1	IPE 270	HE 280 A	PPB_MRF CX_N	lin_sym lin_sym	12000 100000	None
2	IPE 270	HE 280 A	PPB_MRF CX_N	lin_sym lin_sym	12000 100000	None
3	IPE 270	HE 280 A	PPB_MRF CX_N	lin_sym lin_sym	12000 100000	None
4	IPE 240	HE 280 A	PPB_MRF CX_N	lin_sym lin_sym	3000 100000	None
5						
6						
7						
8						

## MAIN NODE GENERATION

MAIN NODE GENERATION - Columns vs. Primary and MRF beams																	
STOREY -1									STOREY 0								
Nodes along axis 1									Nodes along axis 1								
#	Node Storey	Node Axis	Node Axis	Node Name	X Position	Y Position	Z Position	Type	#	Node Storey	Node Axis	Node Axis	Node Name	X Position	Y Position	Z Position	Type
0	-1	A	1	N-1_A_1	0.0	0.0	-1.0	structural	0	0	A	1	NO_A_1	0.0	0.0	0.0	structural
1	-1	B	1	N-1_B_1	6.0	0.0	-1.0	structural	1	0	B	1	NO_B_1	6.0	0.0	0.0	structural
2	-1	C	1	N-1_C_1	12.0	0.0	-1.0	structural	2	0	C	1	NO_C_1	12.0	0.0	0.0	structural
3	-1	D	1	N-1_D_1	18.0	0.0	-1.0	structural	3	0	D	1	NO_D_1	18.0	0.0	0.0	structural
4	-1	E	1	N-1_E_1	24.0	0.0	-1.0	structural	4	0	E	1	NO_E_1	24.0	0.0	0.0	structural
5	-1	F	1	N-1_F_1	30.0	0.0	-1.0	structural	5	0	F	1	NO_F_1	30.0	0.0	0.0	structural
Nodes along axis 2									Nodes along axis 2								
0	-1	A	2	N-1_A_2	0.0	6.0	-1.0	structural	0	0	A	2	NO_A_2	0.0	6.0	0.0	structural
1	-1	B	2	N-1_B_2	6.0	6.0	-1.0	structural	1	0	B	2	NO_B_2	6.0	6.0	0.0	structural
2	-1	C	2	N-1_C_2	12.0	6.0	-1.0	structural	2	0	C	2	NO_C_2	12.0	6.0	0.0	structural
3	-1	D	2	N-1_D_2	18.0	6.0	-1.0	structural	3	0	D	2	NO_D_2	18.0	6.0	0.0	structural
4	-1	E	2	N-1_E_2	24.0	6.0	-1.0	structural	4	0	E	2	NO_E_2	24.0	6.0	0.0	structural
5	-1	F	2	N-1_F_2	30.0	6.0	-1.0	structural	5	0	F	2	NO_F_2	30.0	6.0	0.0	structural
Nodes along axis 3									Nodes along axis 3								
0	-1	A	3	N-1_A_3	0.0	12.0	-1.0	structural	0	0	A	3	NO_A_3	0.0	12.0	0.0	structural
1	-1	B	3	N-1_B_3	6.0	12.0	-1.0	structural	1	0	B	3	NO_B_3	6.0	12.0	0.0	structural
2	-1	C	3	N-1_C_3	12.0	12.0	-1.0	structural	2	0	C	3	NO_C_3	12.0	12.0	0.0	structural
3	-1	D	3	N-1_D_3	18.0	12.0	-1.0	structural	3	0	D	3	NO_D_3	18.0	12.0	0.0	structural
4	-1	E	3	N-1_E_3	24.0	12.0	-1.0	structural	4	0	E	3	NO_E_3	24.0	12.0	0.0	structural
5	-1	F	3	N-1_F_3	30.0	12.0	-1.0	structural	5	0	F	3	NO_F_3	30.0	12.0	0.0	structural
Nodes along axis 4									Nodes along axis 4								
0	-1	A	4	N-1_A_4	0.0	18.0	-1.0	structural	0	0	A	4	NO_A_4	0.0	18.0	0.0	structural
1	-1	B	4	N-1_B_4	6.0	18.0	-1.0	structural	1	0	B	4	NO_B_4	6.0	18.0	0.0	structural
2	-1	C	4	N-1_C_4	12.0	18.0	-1.0	structural	2	0	C	4	NO_C_4	12.0	18.0	0.0	structural
3	-1	D	4	N-1_D_4	18.0	18.0	-1.0	structural	3	0	D	4	NO_D_4	18.0	18.0	0.0	structural
4	-1	E	4	N-1_E_4	24.0	18.0	-1.0	structural	4	0	E	4	NO_E_4	24.0	18.0	0.0	structural
5	-1	F	4	N-1_F_4	30.0	18.0	-1.0	structural	5	0	F	4	NO_F_4	30.0	18.0	0.0	structural
Nodes along axis 5									Nodes along axis 5								
0	-1	A							0	0	A						
1	-1	B							1	0	B						
2	-1	C							2	0	C						
3	-1	D							3	0	D						
4	-1	E							4	0	E						
5	-1	F							5	0	F						

# SECONDARY NODE GENERATION

SECONDARY NODE GENERATION - Ends of internal secondary beams

STOREY 0										STOREY 1												
Nodes along axis 1										Nodes along axis 1												
Bay #	Node Axis	Node Axis	Node Axis	Node Storey	Term. Beam	Node Name	X Position	Y Position	Z Position	Type	Bay #	Node Axis	Node Axis	Node Axis	Node Storey	Term. Beam	Node Name	X Position	Y Position	Z Position	Type	
-	-	-	-	-	-	-	-	-	-	-	-	-	-	-	-	-	-	-	-	-	-	-
1	A	B	1	0	1	A1_B1_IN	2	0.0	0	structural	1	A	B	1	1	1	A1_B1_IN	2	0.0	3.5	structural	
1	A	B	1	0	2	A1_B1_IN	4	0.0	0		1	A	B	1	2	2	A1_B1_IN	4	0.0	3.5	structural	
1	A	B	1	0							1	A	B	1	1							
2	B	C	1	0	1	B1_C1_IN	8	0.0	0	structural	2	B	C	1	1	1	B1_C1_IN	8	0.0	3.5	structural	
2	B	C	1	0	2	B1_C1_IN	10	0.0	0		2	B	C	1	2	2	B1_C1_IN	10	0.0	3.5	structural	
2	B	C	1	0							2	B	C	1	1							
2	B	C	1	0							2	B	C	1	1							
3	C	D	1	0	1	C1_D1_IN	14	0.0	0	structural	3	C	D	1	1	1	C1_D1_IN	14	0.0	3.5	structural	
3	C	D	1	0	2	C1_D1_IN	16	0.0	0		3	C	D	1	2	2	C1_D1_IN	16	0.0	3.5	structural	
3	C	D	1	0							3	C	D	1	1							
3	C	D	1	0							3	C	D	1	1							
4	D	E	1	0	1	D1_E1_IN	20	0.0	0	structural	4	D	E	1	1	1	D1_E1_IN	20	0.0	3.5	structural	
4	D	E	1	0	2	D1_E1_IN	22	0.0	0		4	D	E	1	2	2	D1_E1_IN	22	0.0	3.5	structural	
4	D	E	1	0							4	D	E	1	1							
4	D	E	1	0							4	D	E	1	1							
5	E	F	1	0	1	E1_F1_IN	26	0.0	0	structural	5	E	F	1	1	1	E1_F1_IN	26	0.0	3.5	structural	
5	E	F	1	0	2	E1_F1_IN	28	0.0	0		5	E	F	1	2	2	E1_F1_IN	28	0.0	3.5	structural	
5	E	F	1	0							5	E	F	1	1							
5	E	F	1	0							5	E	F	1	1							
Nodes along axis 2										Nodes along axis 2												
Bay #	Node Axis	Node Axis	Node Axis	Node Storey	Term. Beam	Node Name	X Position	Y Position	Z Position	Type	Bay #	Node Axis	Node Axis	Node Axis	Node Storey	Term. Beam	Node Name	X Position	Y Position	Z Position	Type	
-	-	-	-	-	-	-	-	-	-	-	-	-	-	-	-	-	-	-	-	-	-	-
1	A	B	2	0	1	A2_B2_IN	2	6.0	0	structural	1	A	B	2	1	1	A2_B2_IN	2	6.0	3.5	structural	
1	A	B	2	0	2	A2_B2_IN	4	6.0	0		1	A	B	2	2	2	A2_B2_IN	4	6.0	3.5	structural	
1	A	B	2	0							1	A	B	2	1							
1	A	B	2	0							1	A	B	2	1							
2	B	C	2	0	1	B2_C2_IN	8	6.0	0	structural	2	B	C	2	1	1	B2_C2_IN	8	6.0	3.5	structural	
2	B	C	2	0	2	B2_C2_IN	10	6.0	0		2	B	C	2	2	2	B2_C2_IN	10	6.0	3.5	structural	
2	B	C	2	0							2	B	C	2	1							
2	B	C	2	0							2	B	C	2	1							
3	C	D	2	0	1	C2_D2_IN	14	6.0	0	structural	3	C	D	2	1	1	C2_D2_IN	14	6.0	3.5	structural	
3	C	D	2	0	2	C2_D2_IN	16	6.0	0		3	C	D	2	2	2	C2_D2_IN	16	6.0	3.5	structural	
3	C	D	2	0							3	C	D	2	1							
3	C	D	2	0							3	C	D	2	1							
4	D	E	2	0	1	D2_E2_IN	20	6.0	0	structural	4	D	E	2	1	1	D2_E2_IN	20	6.0	3.5	structural	
4	D	E	2	0	2	D2_E2_IN	22	6.0	0		4	D	E	2	2	2	D2_E2_IN	22	6.0	3.5	structural	
4	D	E	2	0							4	D	E	2	1							
4	D	E	2	0							4	D	E	2	1							
5	E	F	2	0	1	E2_F2_IN	26	6.0	0	structural	5	E	F	2	1	1	E2_F2_IN	26	6.0	3.5	structural	
5	E	F	2	0	2	E2_F2_IN	28	6.0	0		5	E	F	2	2	2	E2_F2_IN	28	6.0	3.5	structural	
5	E	F	2	0							5	E	F	2	1							
5	E	F	2	0							5	E	F	2	1							

# MRF X COLUMN WEB PANEL NODE GENERATION

MRF X COLUMN WEB PANEL NODE GENERATION									
STOREY0									
Nodes along XZ plane Y=side					Nodes along XZ plane Y=side				
Node Name	-	NO_B_1	Aux Node #	Node Name	X Position	Y Position	Z Position	Node Type	
X Position	m	6.0	-	-	m	m	m	-	
Y Position	m	0.0	1	0_B_1CW1	5.865	0.000	0.165	structural	
Z Position	m	0.0	2	0_B_1CW2	6.000	0.000	0.165	structural	
Beam section	-	IPE 330	3	0_B_1CW3	6.135	0.000	0.165	structural	
Col. Section	-	HE 280 A	4	0_B_1CW4	5.865	0.000	0.165	structural	
d <sub>flange</sub>	m	0.330	5	0_B_1CW5	6.135	0.000	0.165	structural	
d <sub>web</sub>	m	0.270	6	0_B_1CW6	5.865	0.000	0.000	structural	
			7	0_B_1CW7	6.135	0.000	0.000	structural	
			8	0_B_1CW8	5.865	0.000	-0.165	structural	
			9	0_B_1CW9	6.135	0.000	-0.165	structural	
			10	0_B_1CW1	5.865	0.000	-0.165	structural	
			11	0_B_1CW1	6.000	0.000	-0.165	structural	
			12	0_B_1CW1	6.135	0.000	-0.165	structural	
			13	0_B_1CW1	6.000	0.000	0.165	structural	
			14	0_B_1CW1	6.000	0.000	-0.165	structural	
			15	0_B_1CW1	5.865	0.000	0.000	structural	
Node Name	-	NO_C_1	Aux Node #	Node Name	X Position	Y Position	Z Position	Node Type	
X Position	m	12.0	-	-	m	m	m	-	
Y Position	m	0.0	1	0_C_1CW1	11.865	0.000	0.165	structural	
Z Position	m	0.0	2	0_C_1CW2	12.000	0.000	0.165	structural	
Beam section	-	IPE 330	3	0_C_1CW3	12.135	0.000	0.165	structural	
Col. Section	-	HE 280 A	4	0_C_1CW4	11.865	0.000	0.165	structural	
d <sub>flange</sub>	m	0.330	5	0_C_1CW5	12.135	0.000	0.165	structural	
d <sub>web</sub>	m	0.270	6	0_C_1CW6	11.865	0.000	0.000	structural	
			7	0_C_1CW7	12.135	0.000	0.000	structural	
			8	0_C_1CW8	11.865	0.000	-0.165	structural	
			9	0_C_1CW9	12.135	0.000	-0.165	structural	
			10	0_C_1CW1	11.865	0.000	-0.165	structural	
			11	0_C_1CW1	12.000	0.000	-0.165	structural	
			12	0_C_1CW1	12.135	0.000	-0.165	structural	
			13	0_C_1CW1	12.000	0.000	0.165	structural	
			14	0_C_1CW1	12.000	0.000	-0.165	structural	
Node Name	-	NO_D_1	Aux Node #	Node Name	X Position	Y Position	Z Position	Node Type	
X Position	m	18.0	-	-	m	m	m	-	
Y Position	m	0.0	1	0_D_1CW1	17.865	0.000	0.165	structural	
Z Position	m	0.0	2	0_D_1CW2	18.000	0.000	0.165	structural	
Beam section	-	IPE 330	3	0_D_1CW3	18.135	0.000	0.165	structural	
Col. Section	-	HE 280 A	4	0_D_1CW4	17.865	0.000	0.165	structural	
d <sub>flange</sub>	m	0.330	5	0_D_1CW5	18.135	0.000	0.165	structural	
d <sub>web</sub>	m	0.270	6	0_D_1CW6	17.865	0.000	0.000	structural	
			7	0_D_1CW7	18.135	0.000	0.000	structural	
			8	0_D_1CW8	17.865	0.000	-0.165	structural	
			9	0_D_1CW9	18.135	0.000	-0.165	structural	
			10	0_D_1CW1	17.865	0.000	-0.165	structural	
			11	0_D_1CW1	18.000	0.000	-0.165	structural	
			12	0_D_1CW1	18.135	0.000	-0.165	structural	
			13	0_D_1CW1	18.000	0.000	0.165	structural	
			14	0_D_1CW1	18.000	0.000	-0.165	structural	
Node Name	-	NO_E_1	Aux Node #	Node Name	X Position	Y Position	Z Position	Node Type	
X Position	m	24.0	-	-	m	m	m	-	
Y Position	m	0.0	1	0_E_1CW1	23.865	0.000	0.165	structural	
Z Position	m	0.0	2	0_E_1CW2	24.000	0.000	0.165	structural	
Beam section	-	IPE 330	3	0_E_1CW3	24.135	0.000	0.165	structural	
Col. Section	-	HE 280 A	4	0_E_1CW4	23.865	0.000	0.165	structural	
d <sub>flange</sub>	m	0.330	5	0_E_1CW5	24.135	0.000	0.165	structural	
d <sub>web</sub>	m	0.270	6	0_E_1CW6	23.865	0.000	0.000	structural	
			7	0_E_1CW7	24.135	0.000	0.000	structural	
			8	0_E_1CW8	23.865	0.000	-0.165	structural	
			9	0_E_1CW9	24.135	0.000	-0.165	structural	
			10	0_E_1CW1	23.865	0.000	-0.165	structural	
			11	0_E_1CW1	24.000	0.000	-0.165	structural	
			12	0_E_1CW1	24.135	0.000	-0.165	structural	
			13	0_E_1CW1	24.000	0.000	0.165	structural	
			14	0_E_1CW1	24.000	0.000	-0.165	structural	
			15	0_E_1CW1	24.135	0.000	0.000	structural	
Node Name	-	NO_B_4	Aux Node #	Node Name	X Position	Y Position	Z Position	Node Type	
X Position	m	18.0	-	-	m	m	m	-	
Y Position	m	18.0	1	0_B_4CW1	5.865	18.000	0.165	structural	
Z Position	m	0.0	2	0_B_4CW2	6.000	18.000	0.165	structural	
Beam section	-	IPE 330	3	0_B_4CW3	6.135	18.000	0.165	structural	
Col. Section	-	HE 280 A	4	0_B_4CW4	5.865	18.000	0.165	structural	
d <sub>flange</sub>	m	0.330	5	0_B_4CW5	6.135	18.000	0.165	structural	
d <sub>web</sub>	m	0.270	6	0_B_4CW6	5.865	18.000	0.000	structural	
			7	0_B_4CW7	6.135	18.000	0.000	structural	
			8	0_B_4CW8	5.865	18.000	-0.165	structural	
			9	0_B_4CW9	6.135	18.000	-0.165	structural	
			10	0_B_4CW1	5.865	18.000	-0.165	structural	
			11	0_B_4CW1	6.000	18.000	-0.165	structural	
			12	0_B_4CW1	6.135	18.000	-0.165	structural	
			13	0_B_4CW1	6.000	18.000	0.165	structural	
			14	0_B_4CW1	6.000	18.000	-0.165	structural	
			15	0_B_4CW1	5.865	18.000	0.000	structural	
Node Name	-	NO_C_4	Aux Node #	Node Name	X Position	Y Position	Z Position	Node Type	
X Position	m	12.0	-	-	m	m	m	-	
Y Position	m	18.0	1	0_C_4CW1	11.865	18.000	0.165	structural	
Z Position	m	0.0	2	0_C_4CW2	12.000	18.000	0.165	structural	
Beam section	-	IPE 330	3	0_C_4CW3	12.135	18.000	0.165	structural	
Col. Section	-	HE 280 A	4	0_C_4CW4	11.865	18.000	0.165	structural	
d <sub>flange</sub>	m	0.330	5	0_C_4CW5	12.135	18.000	0.165	structural	
d <sub>web</sub>	m	0.270	6	0_C_4CW6	11.865	18.000	0.000	structural	
			7	0_C_4CW7	12.135	18.000	0.000	structural	
			8	0_C_4CW8	11.865	18.000	-0.165	structural	
			9	0_C_4CW9	12.135	18.000	-0.165	structural	
			10	0_C_4CW1	11.865	18.000	-0.165	structural	
			11	0_C_4CW1	12.000	18.000	-0.165	structural	
			12	0_C_4CW1	12.135	18.000	-0.165	structural	
			13	0_C_4CW1	12.000	18.000	0.165	structural	
			14	0_C_4CW1	12.000	18.000	-0.165	structural	
Node Name	-	NO_D_4	Aux Node #	Node Name	X Position	Y Position	Z Position	Node Type	
X Position	m	18.0	-	-	m	m	m	-	
Y Position	m	18.0	1	0_D_4CW1	17.865	18.000	0.165	structural	
Z Position	m	0.0	2	0_D_4CW2	18.000	18.000	0.165	structural	
Beam section	-	IPE 330	3	0_D_4CW3	18.135	18.000	0.165	structural	
Col. Section	-	HE 280 A	4	0_D_4CW4	17.865	18.000	0.165	structural	
d <sub>flange</sub>	m	0.330	5	0_D_4CW5	18.135	18.000	0.165	structural	
d <sub>web</sub>	m	0.270	6	0_D_4CW6	17.865	18.000	0.000	structural	
			7	0_D_4CW7	18.135	18.000	0.000	structural	
			8	0_D_4CW8	17.865	18.000	-0.165	structural	
			9	0_D_4CW9	18.135	18.000	-0.165	structural	
			10	0_D_4CW1	17.865	18.000	-0.165	structural	
			11	0_D_4CW1	18.000	18.000	-0.165	structural	
			12	0_D_4CW1	18.135	18.000	-0.165	structural	
			13	0_D_4CW1	18.000	18.000	0.165	structural	
			14	0_D_4CW1	18.000	18.000	-0.165	structural	
Node Name	-	NO_E_4	Aux Node #	Node Name	X Position	Y Position	Z Position	Node Type	
X Position	m	24.0	-	-	m	m	m	-	
Y Position	m	18.0	1	0_E_4CW1	23.865	18.000	0.165	structural	
Z Position	m	0.0	2	0_E_4CW2	24.000	18.000	0.165	structural	
Beam section	-	IPE 330	3	0_E_4CW3	24.135	18.000	0.165	structural	
Col. Section	-	HE 280 A	4	0_E_4CW4	23.865	18.000	0.165	structural	
d <sub>flange</sub>	m	0.330	5	0_E_4CW5	24.135	18.000	0.165	structural	
d <sub>web</sub>	m	0.270	6	0_E_4CW6	23.865	18.000	0.000	structural	
			7	0_E_4CW7	24.135	18.000	0.000	structural	
			8	0_E_4CW8	23.865	18.000	-0.165	structural	
			9	0_E_4CW9	24.135	18.000	-0.165	structural	
			10	0_E_4CW1	23.865	18.000	-0.165	structural	
			11	0_E_4CW1	24.000	18.000	-0.165	structural	
			12	0_E_4CW1	24.135	18.000	-0.165	structural	
			13	0_E_4CW1	24.000	18.000	0.165	structural	
			14	0_E_4CW1	24.000	18.000	-0.165	structural	
			15	0_E_4CW1	24.135	18.000	0.000	structural	

# MRF Y COLUMN WEB PANEL NODE GENERATION

MRF Y COLUMN WEB PANEL NODE GENERATION																	
STOREY0																	
Nodes along YZ plane X= side						Nodes along YZ plane X= side											
Node Name	-	NO_A_1	Aux Node #	Node Name	X Position	Y Position	Z Position	Node Type	Node Name	-	NO_F_1	Aux Node #	Node Name	X Position	Y Position	Z Position	Node Type
X Position	m	0.0	-	-	m	m	m	-	X Position	m	30.0	-	-	m	m	m	-
Y Position	m	0.0	1	0_A_1CW1	0.000	-0.145	0.200	structural	Y Position	m	0.0	1	0_F_1CW1	30.000	-0.145	0.200	structural
Z Position	m	0.0	2	0_A_1CW2	0.000	0.000	0.200	structural	Z Position	m	0.0	2	0_F_1CW2	30.000	0.000	0.200	structural
Beam section	-	IPE 400	3	0_A_1CW3	0.000	0.145	0.200	structural	Beam section	-	IPE 400	3	0_F_1CW3	30.000	0.145	0.200	structural
Col. Section	-	HE 300 A	4	0_A_1CW4	0.000	-0.145	0.200	structural	Col. Section	-	HE 300 A	4	0_F_1CW4	30.000	-0.145	0.200	structural
d <sub>col</sub>	m	0.400	5	0_A_1CW5	0.000	0.145	0.200	structural	d <sub>col</sub>	m	0.400	5	0_F_1CW5	30.000	0.145	0.200	structural
d <sub>col,web</sub>	m	0.290	6	0_A_1CW6	0.000	-0.145	0.000	structural	d <sub>col,web</sub>	m	0.290	6	0_F_1CW6	30.000	-0.145	0.000	structural
			7	0_A_1CW7	0.000	0.145	0.000	structural				7	0_F_1CW7	30.000	0.145	0.000	structural
			8	0_A_1CW8	0.000	-0.145	-0.200	structural				8	0_F_1CW8	30.000	-0.145	-0.200	structural
			9	0_A_1CW9	0.000	0.145	-0.200	structural				9	0_F_1CW9	30.000	0.145	-0.200	structural
			10	0_A_1CW10	0.000	-0.145	-0.200	structural				10	0_F_1CW10	30.000	-0.145	-0.200	structural
			11	0_A_1CW11	0.000	0.000	-0.200	structural				11	0_F_1CW11	30.000	0.000	-0.200	structural
			12	0_A_1CW12	0.000	0.145	-0.200	structural				12	0_F_1CW12	30.000	0.145	-0.200	structural
			13	0_A_1CW13	0.000	0.000	0.200	structural				13	0_F_1CW13	30.000	0.000	0.200	structural
			14	0_A_1CW14	0.000	0.000	-0.200	structural				14	0_F_1CW14	30.000	0.000	-0.200	structural
Node Name	-	NO_A_2	Aux Node #	Node Name	X Position	Y Position	Z Position	Node Type	Node Name	-	NO_F_2	Aux Node #	Node Name	X Position	Y Position	Z Position	Node Type
X Position	m	0.0	-	-	m	m	m	-	X Position	m	30.0	-	-	m	m	m	-
Y Position	m	6.0	1	0_A_2CW1	0.000	5.855	0.200	structural	Y Position	m	6.0	1	0_F_2CW1	30.000	5.855	0.200	structural
Z Position	m	0.0	2	0_A_2CW2	0.000	6.000	0.200	structural	Z Position	m	0.0	2	0_F_2CW2	30.000	6.000	0.200	structural
Beam section	-	IPE 400	3	0_A_2CW3	0.000	6.145	0.200	structural	Beam section	-	IPE 400	3	0_F_2CW3	30.000	6.145	0.200	structural
Col. Section	-	HE 300 A	4	0_A_2CW4	0.000	5.855	0.200	structural	Col. Section	-	HE 300 A	4	0_F_2CW4	30.000	5.855	0.200	structural
d <sub>col</sub>	m	0.400	5	0_A_2CW5	0.000	6.145	0.000	structural	d <sub>col</sub>	m	0.400	5	0_F_2CW5	30.000	6.145	0.000	structural
d <sub>col,web</sub>	m	0.290	6	0_A_2CW6	0.000	5.855	0.000	structural	d <sub>col,web</sub>	m	0.290	6	0_F_2CW6	30.000	5.855	0.000	structural
			7	0_A_2CW7	0.000	6.145	0.000	structural				7	0_F_2CW7	30.000	6.145	0.000	structural
			8	0_A_2CW8	0.000	5.855	-0.200	structural				8	0_F_2CW8	30.000	5.855	-0.200	structural
			9	0_A_2CW9	0.000	6.145	-0.200	structural				9	0_F_2CW9	30.000	6.145	-0.200	structural
			10	0_A_2CW10	0.000	5.855	-0.200	structural				10	0_F_2CW10	30.000	5.855	-0.200	structural
			11	0_A_2CW11	0.000	6.000	-0.200	structural				11	0_F_2CW11	30.000	6.000	-0.200	structural
			12	0_A_2CW12	0.000	6.145	-0.200	structural				12	0_F_2CW12	30.000	6.145	-0.200	structural
			13	0_A_2CW13	0.000	6.000	0.200	structural				13	0_F_2CW13	30.000	6.000	0.200	structural
			14	0_A_2CW14	0.000	6.000	-0.200	structural				14	0_F_2CW14	30.000	6.000	-0.200	structural
Node Name	-	NO_A_3	Aux Node #	Node Name	X Position	Y Position	Z Position	Node Type	Node Name	-	NO_F_3	Aux Node #	Node Name	X Position	Y Position	Z Position	Node Type
X Position	m	0.0	-	-	m	m	m	-	X Position	m	30.0	-	-	m	m	m	-
Y Position	m	12.0	1	0_A_3CW1	0.000	11.855	0.200	structural	Y Position	m	12.0	1	0_F_3CW1	30.000	11.855	0.200	structural
Z Position	m	0.0	2	0_A_3CW2	0.000	12.000	0.200	structural	Z Position	m	0.0	2	0_F_3CW2	30.000	12.000	0.200	structural
Beam section	-	IPE 400	3	0_A_3CW3	0.000	12.145	0.200	structural	Beam section	-	IPE 400	3	0_F_3CW3	30.000	12.145	0.200	structural
Col. Section	-	HE 300 A	4	0_A_3CW4	0.000	11.855	0.200	structural	Col. Section	-	HE 300 A	4	0_F_3CW4	30.000	11.855	0.200	structural
d <sub>col</sub>	m	0.400	5	0_A_3CW5	0.000	12.145	0.200	structural	d <sub>col</sub>	m	0.400	5	0_F_3CW5	30.000	12.145	0.200	structural
d <sub>col,web</sub>	m	0.290	6	0_A_3CW6	0.000	11.855	0.000	structural	d <sub>col,web</sub>	m	0.290	6	0_F_3CW6	30.000	11.855	0.000	structural
			7	0_A_3CW7	0.000	12.145	0.000	structural				7	0_F_3CW7	30.000	12.145	0.000	structural
			8	0_A_3CW8	0.000	11.855	-0.200	structural				8	0_F_3CW8	30.000	11.855	-0.200	structural
			9	0_A_3CW9	0.000	12.145	-0.200	structural				9	0_F_3CW9	30.000	12.145	-0.200	structural
			10	0_A_3CW10	0.000	11.855	-0.200	structural				10	0_F_3CW10	30.000	11.855	-0.200	structural
			11	0_A_3CW11	0.000	12.000	-0.200	structural				11	0_F_3CW11	30.000	12.000	-0.200	structural
			12	0_A_3CW12	0.000	12.145	-0.200	structural				12	0_F_3CW12	30.000	12.145	-0.200	structural
			13	0_A_3CW13	0.000	12.000	0.200	structural				13	0_F_3CW13	30.000	12.000	0.200	structural
			14	0_A_3CW14	0.000	12.000	-0.200	structural				14	0_F_3CW14	30.000	12.000	-0.200	structural
Node Name	-	NO_A_4	Aux Node #	Node Name	X Position	Y Position	Z Position	Node Type	Node Name	-	NO_F_4	Aux Node #	Node Name	X Position	Y Position	Z Position	Node Type
X Position	m	0.0	-	-	m	m	m	-	X Position	m	30.0	-	-	m	m	m	-
Y Position	m	18.0	1	0_A_4CW1	0.000	17.855	0.200	structural	Y Position	m	18.0	1	0_F_4CW1	30.000	17.855	0.200	structural
Z Position	m	0.0	2	0_A_4CW2	0.000	18.000	0.200	structural	Z Position	m	0.0	2	0_F_4CW2	30.000	18.000	0.200	structural
Beam section	-	IPE 400	3	0_A_4CW3	0.000	18.145	0.200	structural	Beam section	-	IPE 400	3	0_F_4CW3	30.000	18.145	0.200	structural
Col. Section	-	HE 300 A	4	0_A_4CW4	0.000	17.855	0.200	structural	Col. Section	-	HE 300 A	4	0_F_4CW4	30.000	17.855	0.200	structural
d <sub>col</sub>	m	0.400	5	0_A_4CW5	0.000	18.145	0.200	structural	d <sub>col</sub>	m	0.400	5	0_F_4CW5	30.000	18.145	0.200	structural
d <sub>col,web</sub>	m	0.290	6	0_A_4CW6	0.000	17.855	0.000	structural	d <sub>col,web</sub>	m	0.290	6	0_F_4CW6	30.000	17.855	0.000	structural
			7	0_A_4CW7	0.000	18.145	0.000	structural				7	0_F_4CW7	30.000	18.145	0.000	structural
			8	0_A_4CW8	0.000	17.855	-0.200	structural				8	0_F_4CW8	30.000	17.855	-0.200	structural
			9	0_A_4CW9	0.000	18.145	-0.200	structural				9	0_F_4CW9	30.000	18.145	-0.200	structural
			10	0_A_4CW10	0.000	17.855	-0.200	structural				10	0_F_4CW10	30.000	17.855	-0.200	structural
			11	0_A_4CW11	0.000	18.000	-0.200	structural				11	0_F_4CW11	30.000	18.000	-0.200	structural
			12	0_A_4CW12	0.000	18.145	-0.200	structural				12	0_F_4CW12	30.000	18.145	-0.200	structural
			13	0_A_4CW13	0.000	18.000	0.200	structural				13	0_F_4CW13	30.000	18.000	0.200	structural
			14	0_A_4CW14	0.000	18.000	-0.200	structural				14	0_F_4CW14	30.000	18.000	-0.200	structural
Node Name	-		Aux Node #	Node Name	X Position	Y Position	Z Position	Node Type	Node Name	-		Aux Node #	Node Name	X Position	Y Position	Z Position	Node Type
X Position	m		-	-	m	m	m	-	X Position	m	30.0	-	-	m	m	m	-
Y Position	m		1						Y Position	m		1					
Z Position	m		2						Z Position	m		2					
Beam section	-	IPE 400	3						Beam section	-	IPE 400	3					
Col. Section	-	HE 300 A	4						Col. Section	-	HE 300 A	4					
d <sub>col</sub>	m	0.400	5						d <sub>col</sub>	m	0.400	5					
d <sub>col,web</sub>	m	0.290	6						d <sub>col,web</sub>	m	0.290	6					
			7									7					
			8									8					
			9									9					
			10									10					
			11									11					
			12									12					
			13									13					

# JOINT NODE GENERATION - ISB vs MRFX Columns

JOINT NODE GENERATION - Internal Secondary Beams vs. MRFX Columns

STOREY 0					STOREY 1					STOREY 2				
Nodes along XZ plane Y+ side					Nodes along XZ plane Y- side					Nodes along XZ plane Y+ side				
Node Name	X Position	Y Position	Z Position	Node Type	Node Name	X Position	Y Position	Z Position	Node Type	Node Name	X Position	Y Position	Z Position	Node Type
-	m	m	m	-	-	m	m	m	-	-	m	m	m	-
NO_B_1_ISB_MRFXC	6.0	0.0	0.0	structural	N1_B_1_ISB_MRFXC	6.0	0.0	3.5	structural	N2_B_1_ISB_MRFXC	6.0	0.0	6.5	structural
NO_C_1_ISB_MRFXC	12.0	0.0	0.0	structural	N1_C_1_ISB_MRFXC	12.0	0.0	3.5	structural	N2_C_1_ISB_MRFXC	12.0	0.0	6.5	structural
NO_D_1_ISB_MRFXC	18.0	0.0	0.0	structural	N1_D_1_ISB_MRFXC	18.0	0.0	3.5	structural	N2_D_1_ISB_MRFXC	18.0	0.0	6.5	structural
NO_E_1_ISB_MRFXC	24.0	0.0	0.0	structural	N1_E_1_ISB_MRFXC	24.0	0.0	3.5	structural	N2_E_1_ISB_MRFXC	24.0	0.0	6.5	structural

Nodes along XZ plane Y+ side					Nodes along XZ plane Y+ side					Nodes along XZ plane Y+ side				
Node Name	X Position	Y Position	Z Position	Node Type	Node Name	X Position	Y Position	Z Position	Node Type	Node Name	X Position	Y Position	Z Position	Node Type
-	m	m	m	-	-	m	m	m	-	-	m	m	m	-
NO_B_4_ISB_MRFXC	6.0	18.0	0.0	structural	N1_B_4_ISB_MRFXC	6.0	18.0	3.5	structural	N2_B_4_ISB_MRFXC	6.0	18.0	6.5	structural
NO_C_4_ISB_MRFXC	12.0	18.0	0.0	structural	N1_C_4_ISB_MRFXC	12.0	18.0	3.5	structural	N2_C_4_ISB_MRFXC	12.0	18.0	6.5	structural
NO_D_4_ISB_MRFXC	18.0	18.0	0.0	structural	N1_D_4_ISB_MRFXC	18.0	18.0	3.5	structural	N2_D_4_ISB_MRFXC	18.0	18.0	6.5	structural
NO_E_4_ISB_MRFXC	24.0	18.0	0.0	structural	N1_E_4_ISB_MRFXC	24.0	18.0	3.5	structural	N2_E_4_ISB_MRFXC	24.0	18.0	6.5	structural

# JOINT NODE GENERATION - PPB vs MRFY Columns

JOINT NODE GENERATION - Perimeter Primary Beams vs. MRFY Columns

STOREY 0					STOREY 1					STOREY 2				
Nodes along YZ plane X- side					Nodes along YZ plane X- side					Nodes along YZ plane X- side				
Node Name	X Position	Y Position	Z Position	Node Type	Node Name	X Position	Y Position	Z Position	Node Type	Node Name	X Position	Y Position	Z Position	Node Type
-	m	m	m	-	-	m	m	m	-	-	m	m	m	-
NO_A_1_PPBMRFYC	0.0	0.0	0.0	structural	N1_A_1_PPBMRFYC	0.0	0.0	3.5	structural	N2_A_1_PPBMRFYC	0.0	0.0	6.5	structural
NO_A_4_PPBMRFYC	0.0	18.0	0.0	structural	N1_A_4_PPBMRFYC	0.0	18.0	3.5	structural	N2_A_4_PPBMRFYC	0.0	18.0	6.5	structural

Nodes along YZ plane X+ side					Nodes along YZ plane X+ side					Nodes along YZ plane X+ side				
Node Name	X Position	Y Position	Z Position	Node Type	Node Name	X Position	Y Position	Z Position	Node Type	Node Name	X Position	Y Position	Z Position	Node Type
-	m	m	m	-	-	m	m	m	-	-	m	m	m	-
NO_F_1_PPBMRFYC	30.0	0.0	0.0	structural	N1_F_1_PPBMRFYC	30.0	0.0	3.5	structural	N2_F_1_PPBMRFYC	30.0	0.0	6.5	structural
NO_F_4_PPBMRFYC	30.0	18.0	0.0	structural	N1_F_4_PPBMRFYC	30.0	18.0	3.5	structural	N2_F_4_PPBMRFYC	30.0	18.0	6.5	structural

# JOINT NODE GENERATION - IPB vs MRFY Columns

JOINT NODE GENERATION - Internal Primary Beams vs. MRFY Columns

STOREY 0					STOREY 1					STOREY 2				
Nodes along YZ plane X- side					Nodes along YZ plane X- side					Nodes along YZ plane X- side				
Node Name	X Position	Y Position	Z Position	Node Type	Node Name	X Position	Y Position	Z Position	Node Type	Node Name	X Position	Y Position	Z Position	Node Type
-	m	m	m	-	-	m	m	m	-	-	m	m	m	-
NO_A_2_IPBMRFYC	0.0	6.0	0.0	structural	N1_A_2_IPBMRFYC	0.0	6.0	3.5	structural	N2_A_2_IPBMRFYC	0.0	6.0	6.5	structural
NO_A_3_IPBMRFYC	0.0	12.0	0.0	structural	N1_A_3_IPBMRFYC	0.0	12.0	3.5	structural	N2_A_3_IPBMRFYC	0.0	12.0	6.5	structural

Nodes along YZ plane X+ side					Nodes along YZ plane X+ side					Nodes along YZ plane X+ side				
Node Name	X Position	Y Position	Z Position	Node Type	Node Name	X Position	Y Position	Z Position	Node Type	Node Name	X Position	Y Position	Z Position	Node Type
-	m	m	m	-	-	m	m	m	-	-	m	m	m	-
NO_F_2_IPBMRFYC	30.0	6.0	0.0	structural	N1_F_2_IPBMRFYC	30.0	6.0	3.5	structural	N2_F_2_IPBMRFYC	30.0	6.0	6.5	structural
NO_F_3_IPBMRFYC	30.0	12.0	0.0	structural	N1_F_3_IPBMRFYC	30.0	12.0	3.5	structural	N2_F_3_IPBMRFYC	30.0	12.0	6.5	structural







# JOINT NODE GENERATION - ISB vs MRFX Beams

JOINT NODE GENERATION - Internal Secondary Beams vs. MRFX Beams														
STOREY 0				STOREY 1				STOREY 2						
Nodes along XZ plane Y- side				Nodes along XZ plane Y- side				Nodes along XZ plane Y- side						
Node Name	X Position	Y Position	Z Position	Node Name	X Position	Y Position	Z Position	Node Name	X Position	Y Position	Z Position	Node Type		
m	m	m	m	m	m	m	m	m	m	m	m	m		
NO_B1_C1_INT1_ISB_MRFBX	8.0	0.0	0.0	structural	N1_B1_C1_INT1_ISB_MRFBX	8.0	0.0	3.5	structural	N2_B1_C1_INT1_ISB_MRFBX	8.0	0.0	6.5	structural
NO_B1_C1_INT2_ISB_MRFBX	10.0	0.0	0.0	structural	N1_B1_C1_INT2_ISB_MRFBX	10.0	0.0	3.5	structural	N2_B1_C1_INT2_ISB_MRFBX	10.0	0.0	6.5	structural
NO_C1_D1_INT1_ISB_MRFBX	14.0	0.0	0.0	structural	N1_C1_D1_INT1_ISB_MRFBX	14.0	0.0	3.5	structural	N2_C1_D1_INT1_ISB_MRFBX	14.0	0.0	6.5	structural
NO_C1_D1_INT2_ISB_MRFBX	16.0	0.0	0.0	structural	N1_C1_D1_INT2_ISB_MRFBX	16.0	0.0	3.5	structural	N2_C1_D1_INT2_ISB_MRFBX	16.0	0.0	6.5	structural
NO_D1_E1_INT1_ISB_MRFBX	20.0	0.0	0.0	structural	N1_D1_E1_INT1_ISB_MRFBX	20.0	0.0	3.5	structural	N2_D1_E1_INT1_ISB_MRFBX	20.0	0.0	6.5	structural
NO_D1_E1_INT2_ISB_MRFBX	22.0	0.0	0.0	structural	N1_D1_E1_INT2_ISB_MRFBX	22.0	0.0	3.5	structural	N2_D1_E1_INT2_ISB_MRFBX	22.0	0.0	6.5	structural
Nodes along XZ plane Y+ side				Nodes along XZ plane Y+ side				Nodes along XZ plane Y+ side						
Node Name	X Position	Y Position	Z Position	Node Name	X Position	Y Position	Z Position	Node Name	X Position	Y Position	Z Position	Node Type		
m	m	m	m	m	m	m	m	m	m	m	m	m		
NO_B4_C4_INT1_ISB_MRFBX	8.0	18.0	0.0	structural	N1_B4_C4_INT1_ISB_MRFBX	8.0	18.0	3.5	structural	N2_B4_C4_INT1_ISB_MRFBX	8.0	18.0	6.5	structural
NO_B4_C4_INT2_ISB_MRFBX	10.0	18.0	0.0	structural	N1_B4_C4_INT2_ISB_MRFBX	10.0	18.0	3.5	structural	N2_B4_C4_INT2_ISB_MRFBX	10.0	18.0	6.5	structural
NO_C4_D4_INT1_ISB_MRFBX	14.0	18.0	0.0	structural	N1_C4_D4_INT1_ISB_MRFBX	14.0	18.0	3.5	structural	N2_C4_D4_INT1_ISB_MRFBX	14.0	18.0	6.5	structural
NO_C4_D4_INT2_ISB_MRFBX	16.0	18.0	0.0	structural	N1_C4_D4_INT2_ISB_MRFBX	16.0	18.0	3.5	structural	N2_C4_D4_INT2_ISB_MRFBX	16.0	18.0	6.5	structural
NO_D4_E4_INT1_ISB_MRFBX	20.0	18.0	0.0	structural	N1_D4_E4_INT1_ISB_MRFBX	20.0	18.0	3.5	structural	N2_D4_E4_INT1_ISB_MRFBX	20.0	18.0	6.5	structural
NO_D4_E4_INT2_ISB_MRFBX	22.0	18.0	0.0	structural	N1_D4_E4_INT2_ISB_MRFBX	22.0	18.0	3.5	structural	N2_D4_E4_INT2_ISB_MRFBX	22.0	18.0	6.5	structural

# JOINT NODE GENERATION - ISB vs PPB

JOINT NODE GENERATION - Internal Secondary Beams vs. Perimeter Primary Beams														
STOREY 0				STOREY 1				STOREY 2						
Nodes along XZ plane Y- side				Nodes along XZ plane Y- side				Nodes along XZ plane Y- side						
Node Name	X Position	Y Position	Z Position	Node Name	X Position	Y Position	Z Position	Node Name	X Position	Y Position	Z Position	Node Type		
m	m	m	m	m	m	m	m	m	m	m	m	m		
NO_A1_B1_INT1_ISB_PPFB	2.0	0.0	0.0	structural	N1_A1_B1_INT1_ISB_PPFB	2.0	0.0	3.5	structural	N2_A1_B1_INT1_ISB_PPFB	2.0	0.0	6.5	structural
NO_A1_B1_INT2_ISB_PPFB	4.0	0.0	0.0	structural	N1_A1_B1_INT2_ISB_PPFB	4.0	0.0	3.5	structural	N2_A1_B1_INT2_ISB_PPFB	4.0	0.0	6.5	structural
NO_E1_F1_INT1_ISB_PPFB	26.0	0.0	0.0	structural	N1_E1_F1_INT1_ISB_PPFB	26.0	0.0	3.5	structural	N2_E1_F1_INT1_ISB_PPFB	26.0	0.0	6.5	structural
NO_E1_F1_INT2_ISB_PPFB	28.0	0.0	0.0	structural	N1_E1_F1_INT2_ISB_PPFB	28.0	0.0	3.5	structural	N2_E1_F1_INT2_ISB_PPFB	28.0	0.0	6.5	structural
Nodes along XZ plane Y+ side				Nodes along XZ plane Y+ side				Nodes along XZ plane Y+ side						
Node Name	X Position	Y Position	Z Position	Node Name	X Position	Y Position	Z Position	Node Name	X Position	Y Position	Z Position	Node Type		
m	m	m	m	m	m	m	m	m	m	m	m	m		
NO_A4_B4_INT1_ISB_PPFB	2.0	18.0	0.0	structural	N1_A4_B4_INT1_ISB_PPFB	2.0	18.0	3.5	structural	N2_A4_B4_INT1_ISB_PPFB	2.0	18.0	6.5	structural
NO_A4_B4_INT2_ISB_PPFB	4.0	18.0	0.0	structural	N1_A4_B4_INT2_ISB_PPFB	4.0	18.0	3.5	structural	N2_A4_B4_INT2_ISB_PPFB	4.0	18.0	6.5	structural
NO_E4_F4_INT1_ISB_PPFB	26.0	18.0	0.0	structural	N1_E4_F4_INT1_ISB_PPFB	26.0	18.0	3.5	structural	N2_E4_F4_INT1_ISB_PPFB	26.0	18.0	6.5	structural
NO_E4_F4_INT2_ISB_PPFB	28.0	18.0	0.0	structural	N1_E4_F4_INT2_ISB_PPFB	28.0	18.0	3.5	structural	N2_E4_F4_INT2_ISB_PPFB	28.0	18.0	6.5	structural

# CONNECTIVITY GENERATION - PPB

CONNECTIVITY GENERATION - PERIMETER PRIMARY BEAMS									
STOREY 0									
Side X	Side Y	Segment	Element name	Element class	Node name(s)	Rigid offsets	Force/Moment release	Activation Time/L.F.	
X-	Y-	1	PPB_NO_X-Y-1	elfrm_PPB_NO	NO_A_1_PPB_MRFXY NO_A1_B1_INT1 deg=0.00	), 0. 0. 0. 0. 0.		-1e20 1e20	
X-	Y-	2	PPB_NO_X-Y-2	elfrm_PPB_NO	NO_A1_B1_INT1 NO_A1_B1_INT2 deg=0.00	), 0. 0. 0. 0. 0.		-1e20 1e20	
X-	Y-	3	PPB_NO_X-Y-3	elfrm_PPB_NO	NO_A1_B1_INT2 NO_B_1(CW15) deg=0.00	), 0. 0. 0. 0. 0.		-1e20 1e20	
X+	Y-	1	PPB_NO_X+Y-1	elfrm_PPB_NO	NO_E_1(CW15) NO_E1_F1_INT1 deg=0.00	), 0. 0. 0. 0. 0.		-1e20 1e20	
X+	Y-	2	PPB_NO_X+Y-2	elfrm_PPB_NO	NO_E1_F1_INT1 NO_E1_F1_INT2 deg=0.00	), 0. 0. 0. 0. 0.		-1e20 1e20	
X+	Y-	3	PPB_NO_X+Y-3	elfrm_PPB_NO	NO_E1_F1_INT2 NO_F_1_PPB_MRFXY deg=0.00	), 0. 0. 0. 0. 0.		-1e20 1e20	
X-	Y+	1	PPB_NO_X-Y+1	elfrm_PPB_NO	NO_A_4_PPB_MRFXY NO_A4_B4_INT1 deg=0.00	), 0. 0. 0. 0. 0.		-1e20 1e20	
X-	Y+	2	PPB_NO_X-Y+2	elfrm_PPB_NO	NO_A4_B4_INT1 NO_A4_B4_INT2 deg=0.00	), 0. 0. 0. 0. 0.		-1e20 1e20	
X-	Y+	3	PPB_NO_X-Y+3	elfrm_PPB_NO	NO_A4_B4_INT2 NO_B_4(CW15) deg=0.00	), 0. 0. 0. 0. 0.		-1e20 1e20	
X+	Y+	1	PPB_NO_X+Y+1	elfrm_PPB_NO	NO_E_4(CW15) NO_E4_F4_INT1 deg=0.00	), 0. 0. 0. 0. 0.		-1e20 1e20	
X+	Y+	2	PPB_NO_X+Y+2	elfrm_PPB_NO	NO_E4_F4_INT1 NO_E4_F4_INT2 deg=0.00	), 0. 0. 0. 0. 0.		-1e20 1e20	
X+	Y+	3	PPB_NO_X+Y+3	elfrm_PPB_NO	NO_E4_F4_INT2 NO_F_4_PPB_MRFXY deg=0.00	), 0. 0. 0. 0. 0.		-1e20 1e20	

# CONNECTIVITY GENERATION - MRFX Beams

CONNECTIVITY GENERATION - MRFX BEAMS									
STOREY 0									
Side Y	Zone	Segment	Element name	Element class	No de name(s)	Rigid offsets	Force/Moment releases	Activation Time/L.F.	
Y-	B_C	1	MRFBX_NO_Y-_B_C_1	lrfmFB_MRFBX_NO	NO_B_1(CW7) NO_B1_C1_INT1 deg=0.00	0.0 0.0 0.0 0.0		-1e20 1e20	
Y-	B_C	2	MRFBX_NO_Y-_B_C_2	lrfmFB_MRFBX_NO	NO_B1_C1_INT1 NO_B1_C1_INT2 deg=0.00	0.0 0.0 0.0 0.0		-1e20 1e20	
Y-	B_C	3	MRFBX_NO_Y-_B_C_3	lrfmFB_MRFBX_NO	NO_B1_C1_INT2 NO_C_1(CW6) deg=0.00	0.0 0.0 0.0 0.0		-1e20 1e20	
Y-	B_C	4							
Y-	B_C	5							
Y-	C_D	1	MRFBX_NO_Y-_C_D_1	lrfmFB_MRFBX_NO	NO_C_1(CW7) NO_C1_D1_INT1 deg=0.00	0.0 0.0 0.0 0.0		-1e20 1e20	
Y-	C_D	2	MRFBX_NO_Y-_C_D_2	lrfmFB_MRFBX_NO	NO_C1_D1_INT1 NO_C1_D1_INT2 deg=0.00	0.0 0.0 0.0 0.0		-1e20 1e20	
Y-	C_D	3	MRFBX_NO_Y-_C_D_3	lrfmFB_MRFBX_NO	NO_C1_D1_INT2 NO_D_1(CW6) deg=0.00	0.0 0.0 0.0 0.0		-1e20 1e20	
Y-	C_D	4							
Y-	C_D	5							
Y-	D_E	1	MRFBX_NO_Y-_D_E_1	lrfmFB_MRFBX_NO	NO_D_1(CW7) NO_D1_E1_INT1 deg=0.00	0.0 0.0 0.0 0.0		-1e20 1e20	
Y-	D_E	2	MRFBX_NO_Y-_D_E_2	lrfmFB_MRFBX_NO	NO_D1_E1_INT1 NO_D1_E1_INT2 deg=0.00	0.0 0.0 0.0 0.0		-1e20 1e20	
Y-	D_E	3	MRFBX_NO_Y-_D_E_3	lrfmFB_MRFBX_NO	NO_D1_E1_INT2 NO_E_1(CW6) deg=0.00	0.0 0.0 0.0 0.0		-1e20 1e20	
Y-	D_E	4							
Y-	D_E	5							
Y+	B_C	1	MRFBX_NO_Y+_B_C_1	lrfmFB_MRFBX_NO	NO_B_4(CW7) NO_B4_C4_INT1 deg=0.00	0.0 0.0 0.0 0.0		-1e20 1e20	
Y+	B_C	2	MRFBX_NO_Y+_B_C_2	lrfmFB_MRFBX_NO	NO_B4_C4_INT1 NO_B4_C4_INT2 deg=0.00	0.0 0.0 0.0 0.0		-1e20 1e20	
Y+	B_C	3	MRFBX_NO_Y+_B_C_3	lrfmFB_MRFBX_NO	NO_B4_C4_INT2 NO_C_4(CW6) deg=0.00	0.0 0.0 0.0 0.0		-1e20 1e20	
Y+	B_C	4							
Y+	B_C	5							
Y+	C_D	1	MRFBX_NO_Y+_C_D_1	lrfmFB_MRFBX_NO	NO_C_4(CW7) NO_C4_D4_INT1 deg=0.00	0.0 0.0 0.0 0.0		-1e20 1e20	
Y+	C_D	2	MRFBX_NO_Y+_C_D_2	lrfmFB_MRFBX_NO	NO_C4_D4_INT1 NO_C4_D4_INT2 deg=0.00	0.0 0.0 0.0 0.0		-1e20 1e20	
Y+	C_D	3	MRFBX_NO_Y+_C_D_3	lrfmFB_MRFBX_NO	NO_C4_D4_INT2 NO_D_4(CW6) deg=0.00	0.0 0.0 0.0 0.0		-1e20 1e20	
Y+	C_D	4							
Y+	C_D	5							
Y+	D_E	1	MRFBX_NO_Y+_D_E_1	lrfmFB_MRFBX_NO	NO_D_4(CW7) NO_D4_E4_INT1 deg=0.00	0.0 0.0 0.0 0.0		-1e20 1e20	
Y+	D_E	2	MRFBX_NO_Y+_D_E_2	lrfmFB_MRFBX_NO	NO_D4_E4_INT1 NO_D4_E4_INT2 deg=0.00	0.0 0.0 0.0 0.0		-1e20 1e20	
Y+	D_E	3	MRFBX_NO_Y+_D_E_3	lrfmFB_MRFBX_NO	NO_D4_E4_INT2 NO_E_4(CW6) deg=0.00	0.0 0.0 0.0 0.0		-1e20 1e20	
Y+	D_E	4							
Y+	D_E	5							

# CONNECTIVITY GENERATION - MRFY Beams

CONNECTIVITY GENERATION - MRFY BEAMS									
STOREY 0									
Side X	Zone	Segment	Element name	Element class	No de name(s)	Rigid offsets	Force/Moment releases	Activation Time/L.F.	
X-	1_2		MRFY_NO_X-_1_2	lrfmFB_MRFY_NO	NO_A_1(CW7) NO_A_2(CW6) deg=0.00	0.0 0.0 0.0 0.0		-1e20 1e20	
X-	2_3		MRFY_NO_X-_2_3	lrfmFB_MRFY_NO	NO_A_2(CW7) NO_A_3(CW6) deg=0.00	0.0 0.0 0.0 0.0		-1e20 1e20	
X-	3_4		MRFY_NO_X-_3_4	lrfmFB_MRFY_NO	NO_A_3(CW7) NO_A_4(CW6) deg=0.00	0.0 0.0 0.0 0.0		-1e20 1e20	
X-	4_5								
X+	1_2		MRFY_NO_X+_1_2	lrfmFB_MRFY_NO	NO_F_1(CW7) NO_F_2(CW6) deg=0.00	0.0 0.0 0.0 0.0		-1e20 1e20	
X+	2_3		MRFY_NO_X+_2_3	lrfmFB_MRFY_NO	NO_F_2(CW7) NO_F_3(CW6) deg=0.00	0.0 0.0 0.0 0.0		-1e20 1e20	
X+	3_4		MRFY_NO_X+_3_4	lrfmFB_MRFY_NO	NO_F_3(CW7) NO_F_4(CW6) deg=0.00	0.0 0.0 0.0 0.0		-1e20 1e20	
X+	4_5								

# CONNECTIVITY GENERATION - IPB

CONNECTIVITY GENERATION - INTERNAL PRIMARY BEAMS									
STOREY 0									
Horizontal Axis	Vert. Axis Zone	Segment	Element name	Element class	Node name(s)	Rigid offsets	Force/Moment releases	Activation Time(L, F)	
2	A_B	1	IPB_NO_2_A_B_1	efrm.JPB_NO	NO_A_2.JPB_MRFYC NO_A2_B2.JNT1 deg=0.00	0.0 0.0 0.0 0.0		-1e20 1e20	
2	A_B	2	IPB_NO_2_A_B_2	efrm.JPB_NO	NO_A2_B2.JNT1 NO_A2_B2.JNT2 deg=0.00	0.0 0.0 0.0 0.0		-1e20 1e20	
2	A_B	3	IPB_NO_2_A_B_3	efrm.JPB_NO	NO_A2_B2.JNT2 NO_B_2.X-.JPB.JC deg=0.00	0.0 0.0 0.0 0.0		-1e20 1e20	
2	A_B	4							
2	A_B	5							
2	B_C	1	IPB_NO_2_B_C_1	efrm.JPB_NO	NO_B_2.X+.JPB.JC NO_B2_C2.JNT1 deg=0.00	0.0 0.0 0.0 0.0		-1e20 1e20	
2	B_C	2	IPB_NO_2_B_C_2	efrm.JPB_NO	NO_B2_C2.JNT1 NO_B2_C2.JNT2 deg=0.00	0.0 0.0 0.0 0.0		-1e20 1e20	
2	B_C	3	IPB_NO_2_B_C_3	efrm.JPB_NO	NO_B2_C2.JNT2 NO_C_2.X-.JPB.JC deg=0.00	0.0 0.0 0.0 0.0		-1e20 1e20	
2	B_C	4							
2	B_C	5							
2	C_D	1	IPB_NO_2_C_D_1	efrm.JPB_NO	NO_C_2.X+.JPB.JC NO_C2_D2.JNT1 deg=0.00	0.0 0.0 0.0 0.0		-1e20 1e20	
2	C_D	2	IPB_NO_2_C_D_2	efrm.JPB_NO	NO_C2_D2.JNT1 NO_C2_D2.JNT2 deg=0.00	0.0 0.0 0.0 0.0		-1e20 1e20	
2	C_D	3	IPB_NO_2_C_D_3	efrm.JPB_NO	NO_C2_D2.JNT2 NO_D_2.X-.JPB.JC deg=0.00	0.0 0.0 0.0 0.0		-1e20 1e20	
2	C_D	4							
2	C_D	5							
2	D_E	1	IPB_NO_2_D_E_1	efrm.JPB_NO	NO_D_2.X+.JPB.JC NO_D2_E2.JNT1 deg=0.00	0.0 0.0 0.0 0.0		-1e20 1e20	
2	D_E	2	IPB_NO_2_D_E_2	efrm.JPB_NO	NO_D2_E2.JNT1 NO_D2_E2.JNT2 deg=0.00	0.0 0.0 0.0 0.0		-1e20 1e20	
2	D_E	3	IPB_NO_2_D_E_3	efrm.JPB_NO	NO_D2_E2.JNT2 NO_E_2.X-.JPB.JC deg=0.00	0.0 0.0 0.0 0.0		-1e20 1e20	
2	D_E	4							
2	D_E	5							
2	E_F	1	IPB_NO_2_E_F_1	efrm.JPB_NO	NO_E_2.X+.JPB.JC NO_E2_F2.JNT1 deg=0.00	0.0 0.0 0.0 0.0		-1e20 1e20	
2	E_F	2	IPB_NO_2_E_F_2	efrm.JPB_NO	NO_E2_F2.JNT1 NO_E2_F2.JNT2 deg=0.00	0.0 0.0 0.0 0.0		-1e20 1e20	
2	E_F	3	IPB_NO_2_E_F_3	efrm.JPB_NO	NO_E2_F2.JNT2 NO_F_2.JPB_MRFYC deg=0.00	0.0 0.0 0.0 0.0		-1e20 1e20	
2	E_F	4							
2	E_F	5							
3	A_B	1	IPB_NO_3_A_B_1	efrm.JPB_NO	NO_A_3.JPB_MRFYC NO_A3_B3.JNT1 deg=0.00	0.0 0.0 0.0 0.0		-1e20 1e20	
3	A_B	2	IPB_NO_3_A_B_2	efrm.JPB_NO	NO_A3_B3.JNT1 NO_A3_B3.JNT2 deg=0.00	0.0 0.0 0.0 0.0		-1e20 1e20	
3	A_B	3	IPB_NO_3_A_B_3	efrm.JPB_NO	NO_A3_B3.JNT2 NO_B_3.X-.JPB.JC deg=0.00	0.0 0.0 0.0 0.0		-1e20 1e20	
3	A_B	4							
3	A_B	5							
3	B_C	1	IPB_NO_3_B_C_1	efrm.JPB_NO	NO_B_3.X+.JPB.JC NO_B3_C3.JNT1 deg=0.00	0.0 0.0 0.0 0.0		-1e20 1e20	
3	B_C	2	IPB_NO_3_B_C_2	efrm.JPB_NO	NO_B3_C3.JNT1 NO_B3_C3.JNT2 deg=0.00	0.0 0.0 0.0 0.0		-1e20 1e20	
3	B_C	3	IPB_NO_3_B_C_3	efrm.JPB_NO	NO_B3_C3.JNT2 NO_C_3.X-.JPB.JC deg=0.00	0.0 0.0 0.0 0.0		-1e20 1e20	
3	B_C	4							
3	B_C	5							
3	C_D	1	IPB_NO_3_C_D_1	efrm.JPB_NO	NO_C_3.X+.JPB.JC NO_C3_D3.JNT1 deg=0.00	0.0 0.0 0.0 0.0		-1e20 1e20	
3	C_D	2	IPB_NO_3_C_D_2	efrm.JPB_NO	NO_C3_D3.JNT1 NO_C3_D3.JNT2 deg=0.00	0.0 0.0 0.0 0.0		-1e20 1e20	
3	C_D	3	IPB_NO_3_C_D_3	efrm.JPB_NO	NO_C3_D3.JNT2 NO_D_3.X-.JPB.JC deg=0.00	0.0 0.0 0.0 0.0		-1e20 1e20	
3	C_D	4							
3	C_D	5							
3	D_E	1	IPB_NO_3_D_E_1	efrm.JPB_NO	NO_D_3.X+.JPB.JC NO_D3_E3.JNT1 deg=0.00	0.0 0.0 0.0 0.0		-1e20 1e20	
3	D_E	2	IPB_NO_3_D_E_2	efrm.JPB_NO	NO_D3_E3.JNT1 NO_D3_E3.JNT2 deg=0.00	0.0 0.0 0.0 0.0		-1e20 1e20	
3	D_E	3	IPB_NO_3_D_E_3	efrm.JPB_NO	NO_D3_E3.JNT2 NO_E_3.X-.JPB.JC deg=0.00	0.0 0.0 0.0 0.0		-1e20 1e20	
3	D_E	4							
3	D_E	5							
3	E_F	1	IPB_NO_3_E_F_1	efrm.JPB_NO	NO_E_3.X+.JPB.JC NO_E3_F3.JNT1 deg=0.00	0.0 0.0 0.0 0.0		-1e20 1e20	
3	E_F	2	IPB_NO_3_E_F_2	efrm.JPB_NO	NO_E3_F3.JNT1 NO_E3_F3.JNT2 deg=0.00	0.0 0.0 0.0 0.0		-1e20 1e20	
3	E_F	3	IPB_NO_3_E_F_3	efrm.JPB_NO	NO_E3_F3.JNT2 NO_F_3.JPB_MRFYC deg=0.00	0.0 0.0 0.0 0.0		-1e20 1e20	
3	E_F	4							
3	E_F	5							
4	A_B	1							
4	A_B	2							
4	A_B	3							
4	A_B	4							
4	A_B	5							
4	B_C	1							
4	B_C	2							
4	B_C	3							
4	B_C	4							
4	B_C	5							
4	C_D	1							
4	C_D	2							
4	C_D	3							
4	C_D	4							
4	C_D	5							
4	D_E	1							
4	D_E	2							
4	D_E	3							
4	D_E	4							
4	D_E	5							
4	E_F	1							
4	E_F	2							
4	E_F	3							
4	E_F	4							
4	E_F	5							

# CONNECTIVITY GENERATION - ISB

## CONNECTIVITY GENERATION - INTERNAL SECONDARY BEAMS

STOREY 0									
Horiz. Axis Zone	Vert. Axis Zone	Segment	Element name	Element class	Node name(s)	Rigid offsets	Force/Moment releases	Activation Time(L, F)	
1,2	A, B	1	ISB_NO_1_2_A_B_1	elfrm_ISB_NO	A1_B1_INT1_ISB_PPB NO_A2_B2_INT1_Y- ISB_IPB deg=0	0 0 0 0 0 0		-1e20 1e20	
1,2	A, B	2	ISB_NO_1_2_A_B_2	elfrm_ISB_NO	A1_B1_INT2_ISB_PPB NO_A2_B2_INT2_Y- ISB_IPB deg=0	0 0 0 0 0 0		-1e20 1e20	
1,2	A, B	3	ISB_NO_1_2_A_B_3	elfrm_ISB_NO	NO_B_1_ISB_MRFXC NO_B_2_Y- ISB_IC deg=0.00	0 0 0 0 0 0		-1e20 1e20	
1,2	A, B	4							
1,2	A, B	5							
1,2	B, C	1	ISB_NO_1_2_B_C_1	elfrm_ISB_NO	B1_C1_INT1_ISB_MRFBX NO_B2_C2_INT1_Y- ISB_IPB deg=	0 0 0 0 0 0		-1e20 1e20	
1,2	B, C	2	ISB_NO_1_2_B_C_2	elfrm_ISB_NO	B1_C1_INT2_ISB_MRFBX NO_B2_C2_INT2_Y- ISB_IPB deg=	0 0 0 0 0 0		-1e20 1e20	
1,2	B, C	3	ISB_NO_1_2_B_C_3	elfrm_ISB_NO	NO_C_1_ISB_MRFXC NO_C_2_Y- ISB_IC deg=0.00	0 0 0 0 0 0		-1e20 1e20	
1,2	B, C	4							
1,2	B, C	5							
1,2	C, D	1	ISB_NO_1_2_C_D_1	elfrm_ISB_NO	C1_D1_INT1_ISB_MRFBX NO_C2_D2_INT1_Y- ISB_IPB deg=	0 0 0 0 0 0		-1e20 1e20	
1,2	C, D	2	ISB_NO_1_2_C_D_2	elfrm_ISB_NO	C1_D1_INT2_ISB_MRFBX NO_C2_D2_INT2_Y- ISB_IPB deg=	0 0 0 0 0 0		-1e20 1e20	
1,2	C, D	3	ISB_NO_1_2_C_D_3	elfrm_ISB_NO	NO_D_1_ISB_MRFXC NO_D_2_Y- ISB_IC deg=0.00	0 0 0 0 0 0		-1e20 1e20	
1,2	C, D	4							
1,2	C, D	5							
1,2	D, E	1	ISB_NO_1_2_D_E_1	elfrm_ISB_NO	D1_E1_INT1_ISB_MRFBX NO_D2_E2_INT1_Y- ISB_IPB deg=	0 0 0 0 0 0		-1e20 1e20	
1,2	D, E	2	ISB_NO_1_2_D_E_2	elfrm_ISB_NO	D1_E1_INT2_ISB_MRFBX NO_D2_E2_INT2_Y- ISB_IPB deg=	0 0 0 0 0 0		-1e20 1e20	
1,2	D, E	3	ISB_NO_1_2_D_E_3	elfrm_ISB_NO	NO_E_1_ISB_MRFXC NO_E_2_Y- ISB_IC deg=0.00	0 0 0 0 0 0		-1e20 1e20	
1,2	D, E	4							
1,2	D, E	5							
1,2	E, F	1	ISB_NO_1_2_E_F_1	elfrm_ISB_NO	E1_F1_INT1_ISB_PPB NO_E2_F2_INT1_Y- ISB_IPB deg=0	0 0 0 0 0 0		-1e20 1e20	
1,2	E, F	2	ISB_NO_1_2_E_F_2	elfrm_ISB_NO	E1_F1_INT2_ISB_PPB NO_E2_F2_INT2_Y- ISB_IPB deg=0	0 0 0 0 0 0		-1e20 1e20	
1,2	E, F	3							
1,2	E, F	4							
2,3	A, B	1	ISB_NO_2_3_A_B_1	elfrm_ISB_NO	A2_B2_INT1_Y+ ISB_IPB NO_A3_B3_INT1_Y- ISB_IPB deg=	0 0 0 0 0 0		-1e20 1e20	
2,3	A, B	2	ISB_NO_2_3_A_B_2	elfrm_ISB_NO	A2_B2_INT2_Y+ ISB_IPB NO_A3_B3_INT2_Y- ISB_IPB deg=	0 0 0 0 0 0		-1e20 1e20	
2,3	A, B	3	ISB_NO_2_3_A_B_3	elfrm_ISB_NO	NO_B_2_Y+ ISB_IC NO_B_3_Y- ISB_IC deg=0.00	0 0 0 0 0 0		-1e20 1e20	
2,3	A, B	4							
2,3	A, B	5							
2,3	B, C	1	ISB_NO_2_3_B_C_1	elfrm_ISB_NO	B2_C2_INT1_Y+ ISB_IPB NO_B3_C3_INT1_Y- ISB_IPB deg=	0 0 0 0 0 0		-1e20 1e20	
2,3	B, C	2	ISB_NO_2_3_B_C_2	elfrm_ISB_NO	B2_C2_INT2_Y+ ISB_IPB NO_B3_C3_INT2_Y- ISB_IPB deg=	0 0 0 0 0 0		-1e20 1e20	
2,3	B, C	3	ISB_NO_2_3_B_C_3	elfrm_ISB_NO	NO_C_2_Y+ ISB_IC NO_C_3_Y- ISB_IC deg=0.00	0 0 0 0 0 0		-1e20 1e20	
2,3	B, C	4							
2,3	B, C	5							
2,3	C, D	1	ISB_NO_2_3_C_D_1	elfrm_ISB_NO	C2_D2_INT1_Y+ ISB_IPB NO_C3_D3_INT1_Y- ISB_IPB deg=	0 0 0 0 0 0		-1e20 1e20	
2,3	C, D	2	ISB_NO_2_3_C_D_2	elfrm_ISB_NO	C2_D2_INT2_Y+ ISB_IPB NO_C3_D3_INT2_Y- ISB_IPB deg=	0 0 0 0 0 0		-1e20 1e20	
2,3	C, D	3	ISB_NO_2_3_C_D_3	elfrm_ISB_NO	NO_D_2_Y+ ISB_IC NO_D_3_Y- ISB_IC deg=0.00	0 0 0 0 0 0		-1e20 1e20	
2,3	C, D	4							
2,3	C, D	5							
2,3	D, E	1	ISB_NO_2_3_D_E_1	elfrm_ISB_NO	D2_E2_INT1_Y+ ISB_IPB NO_D3_E3_INT1_Y- ISB_IPB deg=	0 0 0 0 0 0		-1e20 1e20	
2,3	D, E	2	ISB_NO_2_3_D_E_2	elfrm_ISB_NO	D2_E2_INT2_Y+ ISB_IPB NO_D3_E3_INT2_Y- ISB_IPB deg=	0 0 0 0 0 0		-1e20 1e20	
2,3	D, E	3	ISB_NO_2_3_D_E_3	elfrm_ISB_NO	NO_E_2_Y+ ISB_IC NO_E_3_Y- ISB_IC deg=0.00	0 0 0 0 0 0		-1e20 1e20	
2,3	D, E	4							
2,3	D, E	5							
2,3	E, F	1	ISB_NO_2_3_E_F_1	elfrm_ISB_NO	E2_F2_INT1_Y+ ISB_IPB NO_E3_F3_INT1_Y- ISB_IPB deg=0	0 0 0 0 0 0		-1e20 1e20	
2,3	E, F	2	ISB_NO_2_3_E_F_2	elfrm_ISB_NO	E2_F2_INT2_Y+ ISB_IPB NO_E3_F3_INT2_Y- ISB_IPB deg=0	0 0 0 0 0 0		-1e20 1e20	
2,3	E, F	3							
2,3	E, F	4							
3,4	A, B	1	ISB_NO_3_4_A_B_1	elfrm_ISB_NO	A3_B3_INT1_Y+ ISB_IPB NO_A4_B4_INT1_ISB_PPB deg=0	0 0 0 0 0 0		-1e20 1e20	
3,4	A, B	2	ISB_NO_3_4_A_B_2	elfrm_ISB_NO	A3_B3_INT2_Y+ ISB_IPB NO_A4_B4_INT2_ISB_PPB deg=0	0 0 0 0 0 0		-1e20 1e20	
3,4	A, B	3	ISB_NO_3_4_A_B_3	elfrm_ISB_NO	NO_B_3_Y+ ISB_IC NO_B_4_ISB_MRFXC deg=0.00	0 0 0 0 0 0		-1e20 1e20	
3,4	A, B	4							
3,4	A, B	5							
3,4	B, C	1	ISB_NO_3_4_B_C_1	elfrm_ISB_NO	B3_C3_INT1_Y+ ISB_IPB NO_B4_C4_INT1_ISB_MRFBX deg=	0 0 0 0 0 0		-1e20 1e20	
3,4	B, C	2	ISB_NO_3_4_B_C_2	elfrm_ISB_NO	B3_C3_INT2_Y+ ISB_IPB NO_B4_C4_INT2_ISB_MRFBX deg=	0 0 0 0 0 0		-1e20 1e20	
3,4	B, C	3	ISB_NO_3_4_B_C_3	elfrm_ISB_NO	NO_C_3_Y+ ISB_IC NO_C_4_ISB_MRFXC deg=0.00	0 0 0 0 0 0		-1e20 1e20	
3,4	B, C	4							
3,4	B, C	5							
3,4	C, D	1	ISB_NO_3_4_C_D_1	elfrm_ISB_NO	C3_D3_INT1_Y+ ISB_IPB NO_C4_D4_INT1_ISB_MRFBX deg=	0 0 0 0 0 0		-1e20 1e20	
3,4	C, D	2	ISB_NO_3_4_C_D_2	elfrm_ISB_NO	C3_D3_INT2_Y+ ISB_IPB NO_C4_D4_INT2_ISB_MRFBX deg=	0 0 0 0 0 0		-1e20 1e20	
3,4	C, D	3	ISB_NO_3_4_C_D_3	elfrm_ISB_NO	NO_D_3_Y+ ISB_IC NO_D_4_ISB_MRFXC deg=0.00	0 0 0 0 0 0		-1e20 1e20	
3,4	C, D	4							
3,4	C, D	5							
3,4	D, E	1	ISB_NO_3_4_D_E_1	elfrm_ISB_NO	D3_E3_INT1_Y+ ISB_IPB NO_D4_E4_INT1_ISB_MRFBX deg=	0 0 0 0 0 0		-1e20 1e20	
3,4	D, E	2	ISB_NO_3_4_D_E_2	elfrm_ISB_NO	D3_E3_INT2_Y+ ISB_IPB NO_D4_E4_INT2_ISB_MRFBX deg=	0 0 0 0 0 0		-1e20 1e20	
3,4	D, E	3	ISB_NO_3_4_D_E_3	elfrm_ISB_NO	NO_E_3_Y+ ISB_IC NO_E_4_ISB_MRFXC deg=0.00	0 0 0 0 0 0		-1e20 1e20	
3,4	D, E	4							
3,4	D, E	5							
3,4	E, F	1	ISB_NO_3_4_E_F_1	elfrm_ISB_NO	E3_F3_INT1_Y+ ISB_IPB NO_E4_F4_INT1_ISB_PPB deg=0	0 0 0 0 0 0		-1e20 1e20	
3,4	E, F	2	ISB_NO_3_4_E_F_2	elfrm_ISB_NO	E3_F3_INT2_Y+ ISB_IPB NO_E4_F4_INT2_ISB_PPB deg=0	0 0 0 0 0 0		-1e20 1e20	
3,4	E, F	3							
3,4	E, F	4							
4,5	A, B	1							
4,5	A, B	2							
4,5	A, B	3							
4,5	A, B	4							
4,5	A, B	5							
4,5	B, C	1							
4,5	B, C	2							
4,5	B, C	3							
4,5	B, C	4							
4,5	B, C	5							
4,5	C, D	1							
4,5	C, D	2							
4,5	C, D	3							
4,5	C, D	4							
4,5	C, D	5							
4,5	D, E	1							
4,5	D, E	2							
4,5	D, E	3							
4,5	D, E	4							
4,5	D, E	5							
4,5	E, F	1							
4,5	E, F	2							
4,5	E, F	3							
4,5	E, F	4							

## CONNECTIVITY GENERATION - MRFY Columns

CONNECTIVITY GENERATION - MRFY COLUMNS									
STOREY -1 TO 0									
Vert. Axis Zone	Horiz. Axis Zone	Segment	Element name	Element class	Node name(s)	Rigid offsets	Force/Moment releases	Activation Time/L.F.	
A	1	N-1_N0	MRFY_A_1_N-1_N0	InfrmFB_MRFY_N-1_N0	N-1_A_1 NO_A_1(CW11) deg=90.00	0.0 0.0 0.0 0.0		-1e20	1e20
A	2	N-1_N0	MRFY_A_2_N-1_N0	InfrmFB_MRFY_N-1_N0	N-1_A_2 NO_A_2(CW11) deg=90.00	0.0 0.0 0.0 0.0		-1e20	1e20
A	3	N-1_N0	MRFY_A_3_N-1_N0	InfrmFB_MRFY_N-1_N0	N-1_A_3 NO_A_3(CW11) deg=90.00	0.0 0.0 0.0 0.0		-1e20	1e20
A	4	N-1_N0	MRFY_A_4_N-1_N0	InfrmFB_MRFY_N-1_N0	N-1_A_4 NO_A_4(CW11) deg=90.00	0.0 0.0 0.0 0.0		-1e20	1e20
F	1	N-1_N0	MRFY_F_1_N-1_N0	InfrmFB_MRFY_N-1_N0	N-1_F_1 NO_F_1(CW11) deg=90.00	0.0 0.0 0.0 0.0		-1e20	1e20
F	2	N-1_N0	MRFY_F_2_N-1_N0	InfrmFB_MRFY_N-1_N0	N-1_F_2 NO_F_2(CW11) deg=90.00	0.0 0.0 0.0 0.0		-1e20	1e20
F	3	N-1_N0	MRFY_F_3_N-1_N0	InfrmFB_MRFY_N-1_N0	N-1_F_3 NO_F_3(CW11) deg=90.00	0.0 0.0 0.0 0.0		-1e20	1e20
F	4	N-1_N0	MRFY_F_4_N-1_N0	InfrmFB_MRFY_N-1_N0	N-1_F_4 NO_F_4(CW11) deg=90.00	0.0 0.0 0.0 0.0		-1e20	1e20
F									

## CONNECTIVITY GENERATION - MRFX Columns

CONNECTIVITY GENERATION - MRFX COLUMNS									
STOREY -1 TO 0									
Horiz. Axis Zone	Vert. Axis Zone	Segment	Element name	Element class	Node name(s)	Rigid offsets	Force/Moment releases	Activation Time/L.F.	
1	B	N-1_N0	MRFXC_1_B_N-1_N0	InfrmFB_MRFXC_N-1_N0	N-1_B_1 NO_B_1(CW11) deg=0.00	0.0 0.0 0.0 0.0		-1e20	1e20
1	C	N-1_N0	MRFXC_1_C_N-1_N0	InfrmFB_MRFXC_N-1_N0	N-1_C_1 NO_C_1(CW11) deg=0.00	0.0 0.0 0.0 0.0		-1e20	1e20
1	D	N-1_N0	MRFXC_1_D_N-1_N0	InfrmFB_MRFXC_N-1_N0	N-1_D_1 NO_D_1(CW11) deg=0.00	0.0 0.0 0.0 0.0		-1e20	1e20
1	E	N-1_N0	MRFXC_1_E_N-1_N0	InfrmFB_MRFXC_N-1_N0	N-1_E_1 NO_E_1(CW11) deg=0.00	0.0 0.0 0.0 0.0		-1e20	1e20
4	B	N-1_N0	MRFXC_4_B_N-1_N0	InfrmFB_MRFXC_N-1_N0	N-1_B_4 NO_B_4(CW11) deg=0.00	0.0 0.0 0.0 0.0		-1e20	1e20
4	C	N-1_N0	MRFXC_4_C_N-1_N0	InfrmFB_MRFXC_N-1_N0	N-1_C_4 NO_C_4(CW11) deg=0.00	0.0 0.0 0.0 0.0		-1e20	1e20
4	D	N-1_N0	MRFXC_4_D_N-1_N0	InfrmFB_MRFXC_N-1_N0	N-1_D_4 NO_D_4(CW11) deg=0.00	0.0 0.0 0.0 0.0		-1e20	1e20
4	E	N-1_N0	MRFXC_4_E_N-1_N0	InfrmFB_MRFXC_N-1_N0	N-1_E_4 NO_E_4(CW11) deg=0.00	0.0 0.0 0.0 0.0		-1e20	1e20

## CONNECTIVITY GENERATION - Internal Columns

CONNECTIVITY GENERATION - INTERNAL COLUMNS									
STOREY -1 TO 0									
Horiz. Axis Zone	Vert. Axis Zone	Segment	Element name	Element class	Node name(s)	Rigid offsets	Force/Moment releases	Activation Time/L.F.	
2	B	N-1_N0	IC_2_B_N-1_N0	InfrmFB_IC_N-1_N0	N-1_B_2 NO_B_2 deg=0.00	0.0 0.0 0.0 0.0		-1e20	1e20
2	C	N-1_N0	IC_2_C_N-1_N0	InfrmFB_IC_N-1_N0	N-1_C_2 NO_C_2 deg=0.00	0.0 0.0 0.0 0.0		-1e20	1e20
2	D	N-1_N0	IC_2_D_N-1_N0	InfrmFB_IC_N-1_N0	N-1_D_2 NO_D_2 deg=0.00	0.0 0.0 0.0 0.0		-1e20	1e20
2	E	N-1_N0	IC_2_E_N-1_N0	InfrmFB_IC_N-1_N0	N-1_E_2 NO_E_2 deg=0.00	0.0 0.0 0.0 0.0		-1e20	1e20
3	B	N-1_N0	IC_3_B_N-1_N0	InfrmFB_IC_N-1_N0	N-1_B_3 NO_B_3 deg=0.00	0.0 0.0 0.0 0.0		-1e20	1e20
3	C	N-1_N0	IC_3_C_N-1_N0	InfrmFB_IC_N-1_N0	N-1_C_3 NO_C_3 deg=0.00	0.0 0.0 0.0 0.0		-1e20	1e20
3	D	N-1_N0	IC_3_D_N-1_N0	InfrmFB_IC_N-1_N0	N-1_D_3 NO_D_3 deg=0.00	0.0 0.0 0.0 0.0		-1e20	1e20
3	E	N-1_N0	IC_3_E_N-1_N0	InfrmFB_IC_N-1_N0	N-1_E_3 NO_E_3 deg=0.00	0.0 0.0 0.0 0.0		-1e20	1e20
4	B								
4	C								
4	D								
4	E								







# LINK CONNECTIVITY GENERATION - CWP - PPB - MRFCX

LINK CONNECTIVITY GENERATION - COL. WEB PANEL - PPB - MRFCX

STOREY 0									
Side X	Side Y	Link #	Element name	Element class	Node name(s)	Rigid offsets	Force/Moment releases	Activation Time/L.F.	
X-	Y-	1	LNK_CWP_PPB_MRFCX_NO_X-Y-11	Link_PINNED_M2	NO_B_1(CW3) NO_B_1(CW4)	default default	-	-	-1e20 1e20
X-	Y-	2	LNK_CWP_PPB_MRFCX_NO_X-Y-12	Link_PINNED_M2	NO_B_1(CW2) NO_B_1(CW13)	default default	-	-	-1e20 1e20
X-	Y-	3	LNK_CWP_PPB_MRFCX_NO_X-Y-13	L_CW_MRFX_NO	NO_B_1(CW3) NO_B_1(CW5)	default default	-	-	-1e20 1e20
X-	Y-	4	LNK_CWP_PPB_MRFCX_NO_X-Y-14	L_PPB_MRFCX_NO	NO_B_1(CW6) NO_B_1(CW15)	default default	-	-	-1e20 1e20
X-	Y-	5	LNK_CWP_PPB_MRFCX_NO_X-Y-15	L_ISB_MRFCX_NO	NO_B_1 NO_B_1 ISB_MRFCX	default default	-	-	-1e20 1e20
X-	Y-	6	LNK_CWP_PPB_MRFCX_NO_X-Y-16	Link_PINNED_M2	NO_B_1(CW9) NO_B_1(CW10)	default default	-	-	-1e20 1e20
X-	Y-	7	LNK_CWP_PPB_MRFCX_NO_X-Y-17	Link_PINNED_M2	NO_B_1(CW11) NO_B_1(CW14)	default default	-	-	-1e20 1e20
X-	Y-	8	LNK_CWP_PPB_MRFCX_NO_X-Y-18	Link_PINNED_M2	NO_B_1(CW9) NO_B_1(CW12)	default default	-	-	-1e20 1e20
X+	Y-	1	LNK_CWP_PPB_MRFCX_NO_X+Y-11	Link_PINNED_M2	NO_E_1(CW1) NO_E_1(CW4)	default default	-	-	-1e20 1e20
X+	Y-	2	LNK_CWP_PPB_MRFCX_NO_X+Y-12	Link_PINNED_M2	NO_E_1(CW2) NO_E_1(CW13)	default default	-	-	-1e20 1e20
X+	Y-	3	LNK_CWP_PPB_MRFCX_NO_X+Y-13	L_CW_MRFX_NO	NO_E_1(CW3) NO_E_1(CW5)	default default	-	-	-1e20 1e20
X+	Y-	4	LNK_CWP_PPB_MRFCX_NO_X+Y-14	L_PPB_MRFCX_NO	NO_E_1(CW7) NO_E_1(CW15)	default default	-	-	-1e20 1e20
X+	Y-	5	LNK_CWP_PPB_MRFCX_NO_X+Y-15	L_ISB_MRFCX_NO	NO_E_1 NO_E_1 ISB_MRFCX	default default	-	-	-1e20 1e20
X+	Y-	6	LNK_CWP_PPB_MRFCX_NO_X+Y-16	Link_PINNED_M2	NO_E_1(CW8) NO_E_1(CW10)	default default	-	-	-1e20 1e20
X+	Y-	7	LNK_CWP_PPB_MRFCX_NO_X+Y-17	Link_PINNED_M2	NO_E_1(CW11) NO_E_1(CW14)	default default	-	-	-1e20 1e20
X+	Y-	8	LNK_CWP_PPB_MRFCX_NO_X+Y-18	Link_PINNED_M2	NO_E_1(CW9) NO_E_1(CW12)	default default	-	-	-1e20 1e20
X+	Y+	1	LNK_CWP_PPB_MRFCX_NO_X+Y+11	Link_PINNED_M2	NO_E_4(CW3) NO_E_4(CW4)	default default	-	-	-1e20 1e20
X+	Y+	2	LNK_CWP_PPB_MRFCX_NO_X+Y+12	Link_PINNED_M2	NO_E_4(CW2) NO_E_4(CW13)	default default	-	-	-1e20 1e20
X+	Y+	3	LNK_CWP_PPB_MRFCX_NO_X+Y+13	L_CW_MRFX_NO	NO_E_4(CW3) NO_E_4(CW5)	default default	-	-	-1e20 1e20
X+	Y+	4	LNK_CWP_PPB_MRFCX_NO_X+Y+14	L_PPB_MRFCX_NO	NO_E_4(CW7) NO_E_4(CW15)	default default	-	-	-1e20 1e20
X+	Y+	5	LNK_CWP_PPB_MRFCX_NO_X+Y+15	L_ISB_MRFCX_NO	NO_E_4 NO_E_4 ISB_MRFCX	default default	-	-	-1e20 1e20
X+	Y+	6	LNK_CWP_PPB_MRFCX_NO_X+Y+16	Link_PINNED_M2	NO_E_4(CW8) NO_E_4(CW10)	default default	-	-	-1e20 1e20
X+	Y+	7	LNK_CWP_PPB_MRFCX_NO_X+Y+17	Link_PINNED_M2	NO_E_4(CW11) NO_E_4(CW14)	default default	-	-	-1e20 1e20
X+	Y+	8	LNK_CWP_PPB_MRFCX_NO_X+Y+18	Link_PINNED_M2	NO_E_4(CW9) NO_E_4(CW12)	default default	-	-	-1e20 1e20

# LINK CONNECTIVITY GENERATION - CWP - MRFCX

LINK CONNECTIVITY GENERATION - COL. WEB PANEL - MRFCX

STOREY 0									
Axis Z	Axis Z	Link #	Element name	Element class	Node name(s)	Rigid offsets	Force/Moment releases	Activation Time/L.F.	
1	C	1	LNK_CWP_MRFCX_NO_1C_11	Link_PINNED_M2	NO_C_1(CW1) NO_C_1(CW4)	default default	-	-	-1e20 1e20
1	C	2	LNK_CWP_MRFCX_NO_1C_12	Link_PINNED_M2	NO_C_1(CW2) NO_C_1(CW13)	default default	-	-	-1e20 1e20
1	C	3	LNK_CWP_MRFCX_NO_1C_13	L_CW_MRFX_NO	NO_C_1(CW3) NO_C_1(CW5)	default default	-	-	-1e20 1e20
1	C	4	LNK_CWP_MRFCX_NO_1C_14	L_ISB_MRFCX_NO	NO_C_1 NO_C_1 ISB_MRFCX	default default	-	-	-1e20 1e20
1	C	5	LNK_CWP_MRFCX_NO_1C_15	Link_PINNED_M2	NO_C_1(CW9) NO_C_1(CW10)	default default	-	-	-1e20 1e20
1	C	6	LNK_CWP_MRFCX_NO_1C_16	Link_PINNED_M2	NO_C_1(CW11) NO_C_1(CW14)	default default	-	-	-1e20 1e20
1	C	7	LNK_CWP_MRFCX_NO_1C_17	Link_PINNED_M2	NO_C_1(CW9) NO_C_1(CW12)	default default	-	-	-1e20 1e20
1	D	1	LNK_CWP_MRFCX_NO_1D_11	Link_PINNED_M2	NO_D_1(CW1) NO_D_1(CW4)	default default	-	-	-1e20 1e20
1	D	2	LNK_CWP_MRFCX_NO_1D_12	Link_PINNED_M2	NO_D_1(CW2) NO_D_1(CW13)	default default	-	-	-1e20 1e20
1	D	3	LNK_CWP_MRFCX_NO_1D_13	L_CW_MRFX_NO	NO_D_1(CW3) NO_D_1(CW5)	default default	-	-	-1e20 1e20
1	D	4	LNK_CWP_MRFCX_NO_1D_14	L_ISB_MRFCX_NO	NO_D_1 NO_D_1 ISB_MRFCX	default default	-	-	-1e20 1e20
1	D	5	LNK_CWP_MRFCX_NO_1D_15	Link_PINNED_M2	NO_D_1(CW9) NO_D_1(CW10)	default default	-	-	-1e20 1e20
1	D	6	LNK_CWP_MRFCX_NO_1D_16	Link_PINNED_M2	NO_D_1(CW11) NO_D_1(CW14)	default default	-	-	-1e20 1e20
1	D	7	LNK_CWP_MRFCX_NO_1D_17	Link_PINNED_M2	NO_D_1(CW9) NO_D_1(CW12)	default default	-	-	-1e20 1e20
4	C	1	LNK_CWP_MRFCX_NO_4C_11	Link_PINNED_M2	NO_C_4(CW1) NO_C_4(CW4)	default default	-	-	-1e20 1e20
4	C	2	LNK_CWP_MRFCX_NO_4C_12	Link_PINNED_M2	NO_C_4(CW2) NO_C_4(CW13)	default default	-	-	-1e20 1e20
4	C	3	LNK_CWP_MRFCX_NO_4C_13	L_CW_MRFX_NO	NO_C_4(CW3) NO_C_4(CW5)	default default	-	-	-1e20 1e20
4	C	4	LNK_CWP_MRFCX_NO_4C_14	L_ISB_MRFCX_NO	NO_C_4 NO_C_4 ISB_MRFCX	default default	-	-	-1e20 1e20
4	C	5	LNK_CWP_MRFCX_NO_4C_15	Link_PINNED_M2	NO_C_4(CW8) NO_C_4(CW10)	default default	-	-	-1e20 1e20
4	C	6	LNK_CWP_MRFCX_NO_4C_16	Link_PINNED_M2	NO_C_4(CW11) NO_C_4(CW14)	default default	-	-	-1e20 1e20
4	C	7	LNK_CWP_MRFCX_NO_4C_17	Link_PINNED_M2	NO_C_4(CW9) NO_C_4(CW12)	default default	-	-	-1e20 1e20
4	D	1	LNK_CWP_MRFCX_NO_4D_11	Link_PINNED_M2	NO_D_4(CW1) NO_D_4(CW4)	default default	-	-	-1e20 1e20
4	D	2	LNK_CWP_MRFCX_NO_4D_12	Link_PINNED_M2	NO_D_4(CW2) NO_D_4(CW13)	default default	-	-	-1e20 1e20
4	D	3	LNK_CWP_MRFCX_NO_4D_13	L_CW_MRFX_NO	NO_D_4(CW3) NO_D_4(CW5)	default default	-	-	-1e20 1e20
4	D	4	LNK_CWP_MRFCX_NO_4D_14	L_ISB_MRFCX_NO	NO_D_4 NO_D_4 ISB_MRFCX	default default	-	-	-1e20 1e20
4	D	5	LNK_CWP_MRFCX_NO_4D_15	Link_PINNED_M2	NO_D_4(CW8) NO_D_4(CW10)	default default	-	-	-1e20 1e20
4	D	6	LNK_CWP_MRFCX_NO_4D_16	Link_PINNED_M2	NO_D_4(CW11) NO_D_4(CW14)	default default	-	-	-1e20 1e20
4	D	7	LNK_CWP_MRFCX_NO_4D_17	Link_PINNED_M2	NO_D_4(CW9) NO_D_4(CW12)	default default	-	-	-1e20 1e20

# LINK CONNECTIVITY GENERATION - CWP - MRFCY

LINK CONNECTIVITY GENERATION - COL WEB PANEL - MRFCY							
STOREY 0							
Horiz. Axis Zone/vert. Axis Zone	Segment	Element name	Element class	Node name(s)	Rigid offsets	Force/Moment releases	Activation Time/L.F.
1	A	1	LNK_CWP_MRFCY_NO_1A_L1	Link_PINNED_M1	NO_A_1(CW1) NO_A_1(CW4) default default	-	-1e20 1e20
1	A	2	LNK_CWP_MRFCY_NO_1A_L2	Link_PINNED_M1	NO_A_1(CW2) NO_A_1(CW13) default default	-	-1e20 1e20
1	A	3	LNK_CWP_MRFCY_NO_1A_L3	L_CW_MRFCY_NO	NO_A_1(CW3) NO_A_1(CW5) default default	-	-1e20 1e20
1	A	4	LNK_CWP_MRFCY_NO_1A_L4	L_PPB_MRFCY_NO	NO_A_1 NO_A_1_PPB_MRFCY default default	-	-1e20 1e20
1	A	5	LNK_CWP_MRFCY_NO_1A_L5	Link_PINNED_M1	NO_A_1(CW8) NO_A_1(CW10) default default	-	-1e20 1e20
1	A	6	LNK_CWP_MRFCY_NO_1A_L6	Link_PINNED_M1	NO_A_1(CW11) NO_A_1(CW14) default default	-	-1e20 1e20
1	A	7	LNK_CWP_MRFCY_NO_1A_L7	Link_PINNED_M1	NO_A_1(CW9) NO_A_1(CW12) default default	-	-1e20 1e20
2	A	1	LNK_CWP_MRFCY_NO_2A_L1	Link_PINNED_M1	NO_A_2(CW1) NO_A_2(CW4) default default	-	-1e20 1e20
2	A	2	LNK_CWP_MRFCY_NO_2A_L2	Link_PINNED_M1	NO_A_2(CW2) NO_A_2(CW13) default default	-	-1e20 1e20
2	A	3	LNK_CWP_MRFCY_NO_2A_L3	L_CW_MRFCY_NO	NO_A_2(CW3) NO_A_2(CW5) default default	-	-1e20 1e20
2	A	4	LNK_CWP_MRFCY_NO_2A_L4	L_PPB_MRFCY_NO	NO_A_2 NO_A_2_PPB_MRFCY default default	-	-1e20 1e20
2	A	5	LNK_CWP_MRFCY_NO_2A_L5	Link_PINNED_M1	NO_A_2(CW8) NO_A_2(CW10) default default	-	-1e20 1e20
2	A	6	LNK_CWP_MRFCY_NO_2A_L6	Link_PINNED_M1	NO_A_2(CW11) NO_A_2(CW14) default default	-	-1e20 1e20
2	A	7	LNK_CWP_MRFCY_NO_2A_L7	Link_PINNED_M1	NO_A_2(CW9) NO_A_2(CW12) default default	-	-1e20 1e20
3	A	1	LNK_CWP_MRFCY_NO_3A_L1	Link_PINNED_M1	NO_A_3(CW1) NO_A_3(CW4) default default	-	-1e20 1e20
3	A	2	LNK_CWP_MRFCY_NO_3A_L2	Link_PINNED_M1	NO_A_3(CW2) NO_A_3(CW13) default default	-	-1e20 1e20
3	A	3	LNK_CWP_MRFCY_NO_3A_L3	L_CW_MRFCY_NO	NO_A_3(CW3) NO_A_3(CW5) default default	-	-1e20 1e20
3	A	4	LNK_CWP_MRFCY_NO_3A_L4	L_PPB_MRFCY_NO	NO_A_3 NO_A_3_PPB_MRFCY default default	-	-1e20 1e20
3	A	5	LNK_CWP_MRFCY_NO_3A_L5	Link_PINNED_M1	NO_A_3(CW8) NO_A_3(CW10) default default	-	-1e20 1e20
3	A	6	LNK_CWP_MRFCY_NO_3A_L6	Link_PINNED_M1	NO_A_3(CW11) NO_A_3(CW14) default default	-	-1e20 1e20
3	A	7	LNK_CWP_MRFCY_NO_3A_L7	Link_PINNED_M1	NO_A_3(CW9) NO_A_3(CW12) default default	-	-1e20 1e20
4	A	1	LNK_CWP_MRFCY_NO_4A_L1	Link_PINNED_M1	NO_A_4(CW1) NO_A_4(CW4) default default	-	-1e20 1e20
4	A	2	LNK_CWP_MRFCY_NO_4A_L2	Link_PINNED_M1	NO_A_4(CW2) NO_A_4(CW13) default default	-	-1e20 1e20
4	A	3	LNK_CWP_MRFCY_NO_4A_L3	L_CW_MRFCY_NO	NO_A_4(CW3) NO_A_4(CW5) default default	-	-1e20 1e20
4	A	4	LNK_CWP_MRFCY_NO_4A_L4	L_PPB_MRFCY_NO	NO_A_4 NO_A_4_PPB_MRFCY default default	-	-1e20 1e20
4	A	5	LNK_CWP_MRFCY_NO_4A_L5	Link_PINNED_M1	NO_A_4(CW8) NO_A_4(CW10) default default	-	-1e20 1e20
4	A	6	LNK_CWP_MRFCY_NO_4A_L6	Link_PINNED_M1	NO_A_4(CW11) NO_A_4(CW14) default default	-	-1e20 1e20
4	A	7	LNK_CWP_MRFCY_NO_4A_L7	Link_PINNED_M1	NO_A_4(CW9) NO_A_4(CW12) default default	-	-1e20 1e20
5	A	1					
5	A	2					
5	A	3					
5	A	4					
5	A	5					
5	A	6					
5	A	7					
1	F	1	LNK_CWP_MRFCY_NO_1F_L1	Link_PINNED_M1	NO_F_1(CW1) NO_F_1(CW4) default default	-	-1e20 1e20
1	F	2	LNK_CWP_MRFCY_NO_1F_L2	Link_PINNED_M1	NO_F_1(CW2) NO_F_1(CW13) default default	-	-1e20 1e20
1	F	3	LNK_CWP_MRFCY_NO_1F_L3	L_CW_MRFCY_NO	NO_F_1(CW3) NO_F_1(CW5) default default	-	-1e20 1e20
1	F	4	LNK_CWP_MRFCY_NO_1F_L4	L_PPB_MRFCY_NO	NO_F_1 NO_F_1_PPB_MRFCY default default	-	-1e20 1e20
1	F	5	LNK_CWP_MRFCY_NO_1F_L5	Link_PINNED_M1	NO_F_1(CW8) NO_F_1(CW10) default default	-	-1e20 1e20
1	F	6	LNK_CWP_MRFCY_NO_1F_L6	Link_PINNED_M1	NO_F_1(CW11) NO_F_1(CW14) default default	-	-1e20 1e20
1	F	7	LNK_CWP_MRFCY_NO_1F_L7	Link_PINNED_M1	NO_F_1(CW9) NO_F_1(CW12) default default	-	-1e20 1e20
2	F	1	LNK_CWP_MRFCY_NO_2F_L1	Link_PINNED_M1	NO_F_2(CW1) NO_F_2(CW4) default default	-	-1e20 1e20
2	F	2	LNK_CWP_MRFCY_NO_2F_L2	Link_PINNED_M1	NO_F_2(CW2) NO_F_2(CW13) default default	-	-1e20 1e20
2	F	3	LNK_CWP_MRFCY_NO_2F_L3	L_CW_MRFCY_NO	NO_F_2(CW3) NO_F_2(CW5) default default	-	-1e20 1e20
2	F	4	LNK_CWP_MRFCY_NO_2F_L4	L_PPB_MRFCY_NO	NO_F_2 NO_F_2_PPB_MRFCY default default	-	-1e20 1e20
2	F	5	LNK_CWP_MRFCY_NO_2F_L5	Link_PINNED_M1	NO_F_2(CW8) NO_F_2(CW10) default default	-	-1e20 1e20
2	F	6	LNK_CWP_MRFCY_NO_2F_L6	Link_PINNED_M1	NO_F_2(CW11) NO_F_2(CW14) default default	-	-1e20 1e20
2	F	7	LNK_CWP_MRFCY_NO_2F_L7	Link_PINNED_M1	NO_F_2(CW9) NO_F_2(CW12) default default	-	-1e20 1e20
3	F	1	LNK_CWP_MRFCY_NO_3F_L1	Link_PINNED_M1	NO_F_3(CW1) NO_F_3(CW4) default default	-	-1e20 1e20
3	F	2	LNK_CWP_MRFCY_NO_3F_L2	Link_PINNED_M1	NO_F_3(CW2) NO_F_3(CW13) default default	-	-1e20 1e20
3	F	3	LNK_CWP_MRFCY_NO_3F_L3	L_CW_MRFCY_NO	NO_F_3(CW3) NO_F_3(CW5) default default	-	-1e20 1e20
3	F	4	LNK_CWP_MRFCY_NO_3F_L4	L_PPB_MRFCY_NO	NO_F_3 NO_F_3_PPB_MRFCY default default	-	-1e20 1e20
3	F	5	LNK_CWP_MRFCY_NO_3F_L5	Link_PINNED_M1	NO_F_3(CW8) NO_F_3(CW10) default default	-	-1e20 1e20
3	F	6	LNK_CWP_MRFCY_NO_3F_L6	Link_PINNED_M1	NO_F_3(CW11) NO_F_3(CW14) default default	-	-1e20 1e20
3	F	7	LNK_CWP_MRFCY_NO_3F_L7	Link_PINNED_M1	NO_F_3(CW9) NO_F_3(CW12) default default	-	-1e20 1e20
4	F	1	LNK_CWP_MRFCY_NO_4F_L1	Link_PINNED_M1	NO_F_4(CW1) NO_F_4(CW4) default default	-	-1e20 1e20
4	F	2	LNK_CWP_MRFCY_NO_4F_L2	Link_PINNED_M1	NO_F_4(CW2) NO_F_4(CW13) default default	-	-1e20 1e20
4	F	3	LNK_CWP_MRFCY_NO_4F_L3	L_CW_MRFCY_NO	NO_F_4(CW3) NO_F_4(CW5) default default	-	-1e20 1e20
4	F	4	LNK_CWP_MRFCY_NO_4F_L4	L_PPB_MRFCY_NO	NO_F_4 NO_F_4_PPB_MRFCY default default	-	-1e20 1e20
4	F	5	LNK_CWP_MRFCY_NO_4F_L5	Link_PINNED_M1	NO_F_4(CW8) NO_F_4(CW10) default default	-	-1e20 1e20
4	F	6	LNK_CWP_MRFCY_NO_4F_L6	Link_PINNED_M1	NO_F_4(CW11) NO_F_4(CW14) default default	-	-1e20 1e20
4	F	7	LNK_CWP_MRFCY_NO_4F_L7	Link_PINNED_M1	NO_F_4(CW9) NO_F_4(CW12) default default	-	-1e20 1e20
5	F	1					
5	F	2					
5	F	3					
5	F	4					
5	F	5					
5	F	6					
5	F	7					

# LINK CONNECTIVITY GENERATION - ISB - MRFBX

LINK CONNECTIVITY GENERATION - ISB TO MRFBX								
STOREY 0								
Horiz. Axis Zone	Vert. Axis Zone	Segment	Element name	Element class	Node name(s)	Rigid offsets	Force/Moment releases	Activation Time/L.F.
1	B,C	1	LNK_ISB_MRFBX_NO_1_B_C_L1	L_ISB_MRFBX_NO	NO_B1_C1 INT1 NO_B1_C1 INT1 ISB_MRFBX default default	-	-	-1e20 1e20
1	B,C	2	LNK_ISB_MRFBX_NO_1_B_C_L2	L_ISB_MRFBX_NO	NO_B1_C1 INT2 NO_B1_C1 INT2 ISB_MRFBX default default	-	-	-1e20 1e20
1	B,C	3						
1	B,C	4						
1	C,D	1	LNK_ISB_MRFBX_NO_1_C_D_L1	L_ISB_MRFBX_NO	NO_C1_D1 INT1 NO_C1_D1 INT1 ISB_MRFBX default default	-	-	-1e20 1e20
1	C,D	2	LNK_ISB_MRFBX_NO_1_C_D_L2	L_ISB_MRFBX_NO	NO_C1_D1 INT2 NO_C1_D1 INT2 ISB_MRFBX default default	-	-	-1e20 1e20
1	C,D	3						
1	C,D	4						
1	D,E	1	LNK_ISB_MRFBX_NO_1_D_E_L1	L_ISB_MRFBX_NO	NO_D1_E1 INT1 NO_D1_E1 INT1 ISB_MRFBX default default	-	-	-1e20 1e20
1	D,E	2	LNK_ISB_MRFBX_NO_1_D_E_L2	L_ISB_MRFBX_NO	NO_D1_E1 INT2 NO_D1_E1 INT2 ISB_MRFBX default default	-	-	-1e20 1e20
1	D,E	3						
1	D,E	4						
4	B,C	1	LNK_ISB_MRFBX_NO_4_B_C_L1	L_ISB_MRFBX_NO	NO_B4_C4 INT1 NO_B4_C4 INT1 ISB_MRFBX default default	-	-	-1e20 1e20
4	B,C	2	LNK_ISB_MRFBX_NO_4_B_C_L2	L_ISB_MRFBX_NO	NO_B4_C4 INT2 NO_B4_C4 INT2 ISB_MRFBX default default	-	-	-1e20 1e20
4	B,C	3						
4	B,C	4						
4	C,D	1	LNK_ISB_MRFBX_NO_4_C_D_L1	L_ISB_MRFBX_NO	NO_C4_D4 INT1 NO_C4_D4 INT1 ISB_MRFBX default default	-	-	-1e20 1e20
4	C,D	2	LNK_ISB_MRFBX_NO_4_C_D_L2	L_ISB_MRFBX_NO	NO_C4_D4 INT2 NO_C4_D4 INT2 ISB_MRFBX default default	-	-	-1e20 1e20
4	C,D	3						
4	C,D	4						
4	D,E	1	LNK_ISB_MRFBX_NO_4_D_E_L1	L_ISB_MRFBX_NO	NO_D4_E4 INT1 NO_D4_E4 INT1 ISB_MRFBX default default	-	-	-1e20 1e20
4	D,E	2	LNK_ISB_MRFBX_NO_4_D_E_L2	L_ISB_MRFBX_NO	NO_D4_E4 INT2 NO_D4_E4 INT2 ISB_MRFBX default default	-	-	-1e20 1e20
4	D,E	3						
4	D,E	4						

# LINK CONNECTIVITY GENERATION - IC - IPB/ISB

LINK CONNECTIVITY GENERATION - INTERNAL COLUMNS TO IPB AND ISB

STOREY 0										
Horiz. Axis Zone	Vert. Axis Zone	Zone	Storey	Element name	Element class	Node name(s)	Rigid offsets	Force/Moment releases	Activation Time/L.F.	
2	B	X+	0	LNK_IPB_IC_NO_B_2_X+	L_IPB_IC_NO	NO_B_2_NO_B_2_X+ IPB_IC default default	-	-	-1e20 1e20	
2	B	X-	0	LNK_IPB_IC_NO_B_2_X-	L_IPB_IC_NO	NO_B_2_NO_B_2_X- IPB_IC default default	-	-	-1e20 1e20	
2	B	Y+	0	LNK_ISB_IC_NO_B_2_Y+	L_ISB_IC_NO	NO_B_2_NO_B_2_Y+ ISB_IC default default	-	-	-1e20 1e20	
2	B	Y-	0	LNK_ISB_IC_NO_B_2_Y-	L_ISB_IC_NO	NO_B_2_NO_B_2_Y- ISB_IC default default	-	-	-1e20 1e20	
2	C	X+	0	LNK_IPB_IC_NO_C_2_X+	L_IPB_IC_NO	NO_C_2_NO_C_2_X+ IPB_IC default default	-	-	-1e20 1e20	
2	C	X-	0	LNK_IPB_IC_NO_C_2_X-	L_IPB_IC_NO	NO_C_2_NO_C_2_X- IPB_IC default default	-	-	-1e20 1e20	
2	C	Y+	0	LNK_ISB_IC_NO_C_2_Y+	L_ISB_IC_NO	NO_C_2_NO_C_2_Y+ ISB_IC default default	-	-	-1e20 1e20	
2	C	Y-	0	LNK_ISB_IC_NO_C_2_Y-	L_ISB_IC_NO	NO_C_2_NO_C_2_Y- ISB_IC default default	-	-	-1e20 1e20	
2	D	X+	0	LNK_IPB_IC_NO_D_2_X+	L_IPB_IC_NO	NO_D_2_NO_D_2_X+ IPB_IC default default	-	-	-1e20 1e20	
2	D	X-	0	LNK_IPB_IC_NO_D_2_X-	L_IPB_IC_NO	NO_D_2_NO_D_2_X- IPB_IC default default	-	-	-1e20 1e20	
2	D	Y+	0	LNK_ISB_IC_NO_D_2_Y+	L_ISB_IC_NO	NO_D_2_NO_D_2_Y+ ISB_IC default default	-	-	-1e20 1e20	
2	D	Y-	0	LNK_ISB_IC_NO_D_2_Y-	L_ISB_IC_NO	NO_D_2_NO_D_2_Y- ISB_IC default default	-	-	-1e20 1e20	
2	E	X+	0	LNK_IPB_IC_NO_E_2_X+	L_IPB_IC_NO	NO_E_2_NO_E_2_X+ IPB_IC default default	-	-	-1e20 1e20	
2	E	X-	0	LNK_IPB_IC_NO_E_2_X-	L_IPB_IC_NO	NO_E_2_NO_E_2_X- IPB_IC default default	-	-	-1e20 1e20	
2	E	Y+	0	LNK_ISB_IC_NO_E_2_Y+	L_ISB_IC_NO	NO_E_2_NO_E_2_Y+ ISB_IC default default	-	-	-1e20 1e20	
2	E	Y-	0	LNK_ISB_IC_NO_E_2_Y-	L_ISB_IC_NO	NO_E_2_NO_E_2_Y- ISB_IC default default	-	-	-1e20 1e20	
3	B	X+	0	LNK_IPB_IC_NO_B_3_X+	L_IPB_IC_NO	NO_B_3_NO_B_3_X+ IPB_IC default default	-	-	-1e20 1e20	
3	B	X-	0	LNK_IPB_IC_NO_B_3_X-	L_IPB_IC_NO	NO_B_3_NO_B_3_X- IPB_IC default default	-	-	-1e20 1e20	
3	B	Y+	0	LNK_ISB_IC_NO_B_3_Y+	L_ISB_IC_NO	NO_B_3_NO_B_3_Y+ ISB_IC default default	-	-	-1e20 1e20	
3	B	Y-	0	LNK_ISB_IC_NO_B_3_Y-	L_ISB_IC_NO	NO_B_3_NO_B_3_Y- ISB_IC default default	-	-	-1e20 1e20	
3	C	X+	0	LNK_IPB_IC_NO_C_3_X+	L_IPB_IC_NO	NO_C_3_NO_C_3_X+ IPB_IC default default	-	-	-1e20 1e20	
3	C	X-	0	LNK_IPB_IC_NO_C_3_X-	L_IPB_IC_NO	NO_C_3_NO_C_3_X- IPB_IC default default	-	-	-1e20 1e20	
3	C	Y+	0	LNK_ISB_IC_NO_C_3_Y+	L_ISB_IC_NO	NO_C_3_NO_C_3_Y+ ISB_IC default default	-	-	-1e20 1e20	
3	C	Y-	0	LNK_ISB_IC_NO_C_3_Y-	L_ISB_IC_NO	NO_C_3_NO_C_3_Y- ISB_IC default default	-	-	-1e20 1e20	
3	D	X+	0	LNK_IPB_IC_NO_D_3_X+	L_IPB_IC_NO	NO_D_3_NO_D_3_X+ IPB_IC default default	-	-	-1e20 1e20	
3	D	X-	0	LNK_IPB_IC_NO_D_3_X-	L_IPB_IC_NO	NO_D_3_NO_D_3_X- IPB_IC default default	-	-	-1e20 1e20	
3	D	Y+	0	LNK_ISB_IC_NO_D_3_Y+	L_ISB_IC_NO	NO_D_3_NO_D_3_Y+ ISB_IC default default	-	-	-1e20 1e20	
3	D	Y-	0	LNK_ISB_IC_NO_D_3_Y-	L_ISB_IC_NO	NO_D_3_NO_D_3_Y- ISB_IC default default	-	-	-1e20 1e20	
3	E	X+	0	LNK_IPB_IC_NO_E_3_X+	L_IPB_IC_NO	NO_E_3_NO_E_3_X+ IPB_IC default default	-	-	-1e20 1e20	
3	E	X-	0	LNK_IPB_IC_NO_E_3_X-	L_IPB_IC_NO	NO_E_3_NO_E_3_X- IPB_IC default default	-	-	-1e20 1e20	
3	E	Y+	0	LNK_ISB_IC_NO_E_3_Y+	L_ISB_IC_NO	NO_E_3_NO_E_3_Y+ ISB_IC default default	-	-	-1e20 1e20	
3	E	Y-	0	LNK_ISB_IC_NO_E_3_Y-	L_ISB_IC_NO	NO_E_3_NO_E_3_Y- ISB_IC default default	-	-	-1e20 1e20	
4		X+	0							
4		X-	0							
4		Y+	0							
4		Y-	0							
4		X+	0							
4		X-	0							
4		Y+	0							
4		Y-	0							
4		X+	0							
4		X-	0							
4		Y+	0							
4		Y-	0							
4		X+	0							
4		X-	0							
4		Y+	0							
4		Y-	0							

# LINK CONNECTIVITY GENERATION - ISB - PPB

LINK CONNECTIVITY GENERATION - ISB TO PPB

STOREY 0										
Side X	Side Y	Segment	Element name	Element class	Node name(s)	Rigid offsets	Force/Moment releases	Activation Time/L.F.		
X-	Y-	1	LNK_ISB_PPB_NO_X-Y-_L1	L_ISB_PPB_NO	NO_A1_B1_INT1 NO_A1_B1_INT1_ISB_PPB default default	-	-	-1e20 1e20		
X-	Y-	2	LNK_ISB_PPB_NO_X-Y-_L2	L_ISB_PPB_NO	NO_A1_B1_INT2 NO_A1_B1_INT2_ISB_PPB default default	-	-	-1e20 1e20		
X-	Y-	3								
X-	Y-	4								
X+	Y-	1	LNK_ISB_PPB_NO_X-Y-_L1	L_ISB_PPB_NO	NO_E1_F1_INT1 NO_E1_F1_INT1_ISB_PPB default default	-	-	-1e20 1e20		
X+	Y-	2	LNK_ISB_PPB_NO_X-Y-_L2	L_ISB_PPB_NO	NO_E1_F1_INT2 NO_E1_F1_INT2_ISB_PPB default default	-	-	-1e20 1e20		
X+	Y-	3								
X+	Y-	4								
X-	Y+	1	LNK_ISB_PPB_NO_X-Y+_L1	L_ISB_PPB_NO	NO_A4_B4_INT1 NO_A4_B4_INT1_ISB_PPB default default	-	-	-1e20 1e20		
X-	Y+	2	LNK_ISB_PPB_NO_X-Y+_L2	L_ISB_PPB_NO	NO_A4_B4_INT2 NO_A4_B4_INT2_ISB_PPB default default	-	-	-1e20 1e20		
X-	Y+	3								
X-	Y+	4								
X+	Y+	1	LNK_ISB_PPB_NO_X-Y+_L1	L_ISB_PPB_NO	NO_E4_F4_INT1 NO_E4_F4_INT1_ISB_PPB default default	-	-	-1e20 1e20		
X+	Y+	2	LNK_ISB_PPB_NO_X-Y+_L2	L_ISB_PPB_NO	NO_E4_F4_INT2 NO_E4_F4_INT2_ISB_PPB default default	-	-	-1e20 1e20		
X+	Y+	3								
X+	Y+	4								

# LINK CONNECTIVITY GENERATION - ISB - IPB

LINK CONNECTIVITY GENERATION - ISB TO IPB									
STOREY 0									
Horiz. Axis Zone	Vert. Axis Zone	Segment	Element name	Element class	Node name(s)	Rigid offsets	Force/Moment releases	Activation Time/L.F.	
2	A B	1 Y	LNK ISB IPB NO 2 A B L1 Y-	L ISB IPB NO	NO A2 B2 INT1 NO A2 B2 INT1 Y- ISB IPB default default	-	-	-1e20 1e20	
2	A B	1 Y	LNK ISB IPB NO 2 A B L1 Y+	L ISB IPB NO	NO A2 B2 INT1 NO A2 B2 INT1 Y+ ISB IPB default default	-	-	-1e20 1e20	
2	A B	2 Y	LNK ISB IPB NO 2 A B L2 Y-	L ISB IPB NO	NO A2 B2 INT2 NO A2 B2 INT2 Y- ISB IPB default default	-	-	-1e20 1e20	
2	A B	2 Y	LNK ISB IPB NO 2 A B L2 Y+	L ISB IPB NO	NO A2 B2 INT2 NO A2 B2 INT2 Y+ ISB IPB default default	-	-	-1e20 1e20	
2	A B	3 Y							
2	A B	3 Y							
2	A B	4 Y							
2	A B	4 Y							
2	B C	1 Y	LNK ISB IPB NO 2 B C L1 Y-	L ISB IPB NO	NO B2 C2 INT1 NO B2 C2 INT1 Y- ISB IPB default default	-	-	-1e20 1e20	
2	B C	1 Y	LNK ISB IPB NO 2 B C L1 Y+	L ISB IPB NO	NO B2 C2 INT1 NO B2 C2 INT1 Y+ ISB IPB default default	-	-	-1e20 1e20	
2	B C	2 Y	LNK ISB IPB NO 2 B C L2 Y-	L ISB IPB NO	NO B2 C2 INT2 NO B2 C2 INT2 Y- ISB IPB default default	-	-	-1e20 1e20	
2	B C	2 Y	LNK ISB IPB NO 2 B C L2 Y+	L ISB IPB NO	NO B2 C2 INT2 NO B2 C2 INT2 Y+ ISB IPB default default	-	-	-1e20 1e20	
2	B C	3 Y							
2	B C	3 Y							
2	B C	4 Y							
2	B C	4 Y							
2	C D	1 Y	LNK ISB IPB NO 2 C D L1 Y-	L ISB IPB NO	NO C2 D2 INT1 NO C2 D2 INT1 Y- ISB IPB default default	-	-	-1e20 1e20	
2	C D	1 Y	LNK ISB IPB NO 2 C D L1 Y+	L ISB IPB NO	NO C2 D2 INT1 NO C2 D2 INT1 Y+ ISB IPB default default	-	-	-1e20 1e20	
2	C D	2 Y	LNK ISB IPB NO 2 C D L2 Y-	L ISB IPB NO	NO C2 D2 INT2 NO C2 D2 INT2 Y- ISB IPB default default	-	-	-1e20 1e20	
2	C D	2 Y	LNK ISB IPB NO 2 C D L2 Y+	L ISB IPB NO	NO C2 D2 INT2 NO C2 D2 INT2 Y+ ISB IPB default default	-	-	-1e20 1e20	
2	C D	3 Y							
2	C D	3 Y							
2	C D	4 Y							
2	C D	4 Y							
2	D E	1 Y	LNK ISB IPB NO 2 D E L1 Y-	L ISB IPB NO	NO D2 E2 INT1 NO D2 E2 INT1 Y- ISB IPB default default	-	-	-1e20 1e20	
2	D E	1 Y	LNK ISB IPB NO 2 D E L1 Y+	L ISB IPB NO	NO D2 E2 INT1 NO D2 E2 INT1 Y+ ISB IPB default default	-	-	-1e20 1e20	
2	D E	2 Y	LNK ISB IPB NO 2 D E L2 Y-	L ISB IPB NO	NO D2 E2 INT2 NO D2 E2 INT2 Y- ISB IPB default default	-	-	-1e20 1e20	
2	D E	2 Y	LNK ISB IPB NO 2 D E L2 Y+	L ISB IPB NO	NO D2 E2 INT2 NO D2 E2 INT2 Y+ ISB IPB default default	-	-	-1e20 1e20	
2	D E	3 Y							
2	D E	3 Y							
2	D E	4 Y							
2	D E	4 Y							
2	E F	1 Y	LNK ISB IPB NO 2 E F L1 Y-	L ISB IPB NO	NO E2 F2 INT1 NO E2 F2 INT1 Y- ISB IPB default default	-	-	-1e20 1e20	
2	E F	1 Y	LNK ISB IPB NO 2 E F L1 Y+	L ISB IPB NO	NO E2 F2 INT1 NO E2 F2 INT1 Y+ ISB IPB default default	-	-	-1e20 1e20	
2	E F	2 Y	LNK ISB IPB NO 2 E F L2 Y-	L ISB IPB NO	NO E2 F2 INT2 NO E2 F2 INT2 Y- ISB IPB default default	-	-	-1e20 1e20	
2	E F	2 Y	LNK ISB IPB NO 2 E F L2 Y+	L ISB IPB NO	NO E2 F2 INT2 NO E2 F2 INT2 Y+ ISB IPB default default	-	-	-1e20 1e20	
2	E F	3 Y							
2	E F	3 Y							
2	E F	4 Y							
2	E F	4 Y							
3	A B	1 Y	LNK ISB IPB NO 3 A B L1 Y-	L ISB IPB NO	NO A3 B3 INT1 NO A3 B3 INT1 Y- ISB IPB default default	-	-	-1e20 1e20	
3	A B	1 Y	LNK ISB IPB NO 3 A B L1 Y+	L ISB IPB NO	NO A3 B3 INT1 NO A3 B3 INT1 Y+ ISB IPB default default	-	-	-1e20 1e20	
3	A B	2 Y	LNK ISB IPB NO 3 A B L2 Y-	L ISB IPB NO	NO A3 B3 INT2 NO A3 B3 INT2 Y- ISB IPB default default	-	-	-1e20 1e20	
3	A B	2 Y	LNK ISB IPB NO 3 A B L2 Y+	L ISB IPB NO	NO A3 B3 INT2 NO A3 B3 INT2 Y+ ISB IPB default default	-	-	-1e20 1e20	
3	A B	3 Y							
3	A B	3 Y							
3	A B	4 Y							
3	A B	4 Y							
3	B C	1 Y	LNK ISB IPB NO 3 B C L1 Y-	L ISB IPB NO	NO B3 C3 INT1 NO B3 C3 INT1 Y- ISB IPB default default	-	-	-1e20 1e20	
3	B C	1 Y	LNK ISB IPB NO 3 B C L1 Y+	L ISB IPB NO	NO B3 C3 INT1 NO B3 C3 INT1 Y+ ISB IPB default default	-	-	-1e20 1e20	
3	B C	2 Y	LNK ISB IPB NO 3 B C L2 Y-	L ISB IPB NO	NO B3 C3 INT2 NO B3 C3 INT2 Y- ISB IPB default default	-	-	-1e20 1e20	
3	B C	2 Y	LNK ISB IPB NO 3 B C L2 Y+	L ISB IPB NO	NO B3 C3 INT2 NO B3 C3 INT2 Y+ ISB IPB default default	-	-	-1e20 1e20	
3	B C	3 Y							
3	B C	3 Y							
3	B C	4 Y							
3	B C	4 Y							
3	C D	1 Y	LNK ISB IPB NO 3 C D L1 Y-	L ISB IPB NO	NO C3 D3 INT1 NO C3 D3 INT1 Y- ISB IPB default default	-	-	-1e20 1e20	
3	C D	1 Y	LNK ISB IPB NO 3 C D L1 Y+	L ISB IPB NO	NO C3 D3 INT1 NO C3 D3 INT1 Y+ ISB IPB default default	-	-	-1e20 1e20	
3	C D	2 Y	LNK ISB IPB NO 3 C D L2 Y-	L ISB IPB NO	NO C3 D3 INT2 NO C3 D3 INT2 Y- ISB IPB default default	-	-	-1e20 1e20	
3	C D	2 Y	LNK ISB IPB NO 3 C D L2 Y+	L ISB IPB NO	NO C3 D3 INT2 NO C3 D3 INT2 Y+ ISB IPB default default	-	-	-1e20 1e20	
3	C D	3 Y							
3	C D	3 Y							
3	C D	4 Y							
3	C D	4 Y							
3	D E	1 Y	LNK ISB IPB NO 3 D E L1 Y-	L ISB IPB NO	NO D3 E3 INT1 NO D3 E3 INT1 Y- ISB IPB default default	-	-	-1e20 1e20	
3	D E	1 Y	LNK ISB IPB NO 3 D E L1 Y+	L ISB IPB NO	NO D3 E3 INT1 NO D3 E3 INT1 Y+ ISB IPB default default	-	-	-1e20 1e20	
3	D E	2 Y	LNK ISB IPB NO 3 D E L2 Y-	L ISB IPB NO	NO D3 E3 INT2 NO D3 E3 INT2 Y- ISB IPB default default	-	-	-1e20 1e20	
3	D E	2 Y	LNK ISB IPB NO 3 D E L2 Y+	L ISB IPB NO	NO D3 E3 INT2 NO D3 E3 INT2 Y+ ISB IPB default default	-	-	-1e20 1e20	
3	D E	3 Y							
3	D E	3 Y							
3	D E	4 Y							
3	D E	4 Y							
3	E F	1 Y	LNK ISB IPB NO 3 E F L1 Y-	L ISB IPB NO	NO E3 F3 INT1 NO E3 F3 INT1 Y- ISB IPB default default	-	-	-1e20 1e20	
3	E F	1 Y	LNK ISB IPB NO 3 E F L1 Y+	L ISB IPB NO	NO E3 F3 INT1 NO E3 F3 INT1 Y+ ISB IPB default default	-	-	-1e20 1e20	
3	E F	2 Y	LNK ISB IPB NO 3 E F L2 Y-	L ISB IPB NO	NO E3 F3 INT2 NO E3 F3 INT2 Y- ISB IPB default default	-	-	-1e20 1e20	
3	E F	2 Y	LNK ISB IPB NO 3 E F L2 Y+	L ISB IPB NO	NO E3 F3 INT2 NO E3 F3 INT2 Y+ ISB IPB default default	-	-	-1e20 1e20	
3	E F	3 Y							
3	E F	3 Y							
3	E F	4 Y							
3	E F	4 Y							
4	A B	1 Y							
4	A B	1 Y							
4	A B	2 Y							
4	A B	2 Y							
4	A B	3 Y							
4	A B	3 Y							
4	A B	4 Y							
4	A B	4 Y							
4	B C	1 Y							
4	B C	1 Y							
4	B C	2 Y							
4	B C	2 Y							
4	B C	3 Y							
4	B C	3 Y							
4	B C	4 Y							
4	B C	4 Y							
4	C D	1 Y							
4	C D	1 Y							
4	C D	2 Y							
4	C D	2 Y							
4	C D	3 Y							
4	C D	3 Y							
4	C D	4 Y							
4	C D	4 Y							
4	D E	1 Y							
4	D E	1 Y							
4	D E	2 Y							
4	D E	2 Y							
4	D E	3 Y							
4	D E	3 Y							
4	D E	4 Y							
4	D E	4 Y							
4	E F	1 Y							
4	E F	1 Y							
4	E F	2 Y							
4	E F	2 Y							
4	E F	3 Y							
4	E F	3 Y							
4	E F	4 Y							
4	E F	4 Y							

## **Appendix C Proposal for a new EN 1991-1-7 Annex E**

## **Annex E (informative)**

### **Design of building structures to prevent progressive collapse**

#### **E.1 Scope**

(1) This Annex E provides rules and methods for designing building structures to limit the probability of occurrence of a progressive collapse originating from a column loss. The adoption of this methodology is likely to ensure that a building structure is sufficiently robust so as to limit the progression of the initial damage, effectively arresting the progressive collapse.

#### **E.2 Introduction**

(1) The design strategy is based on the concept of limiting the extent of the localised failure, defined in Section 3. It is intended to provide building structures with sufficient robustness to prevent the spread of the initial damage of unidentified origin into a progressive collapse.

(2) The recommended strategies are provided on the basis of the building structure's Proneness to Progressive Collapse (PPC) Class (see Table E.2), which accounts for the Demand-to-Capacity (DCR) ratios of the different structural elements under notional column removal scenarios.

(3) The prevention of the progressive collapse is likely to assure that the building survives for a minimum period of time compatible with the safe evacuation and rescue of personnel from the building and its surroundings. Longer periods of survival may be required for buildings used for handling hazardous materials, provision of essential services, or for national security reasons.

NOTE 1 The values of the maximum expected DCR ratios for the different structural typologies were determined based on façade and corner column loss scenarios. Internal column loss scenarios fall outside the scope of this Annex and should be evaluated separately. The design methodology does not therefore provide any guarantee regarding collapse arrest in cases of internal column loss.

(4) The design strategy methodology can be described by means of the flow chart shown in Figure E.1.

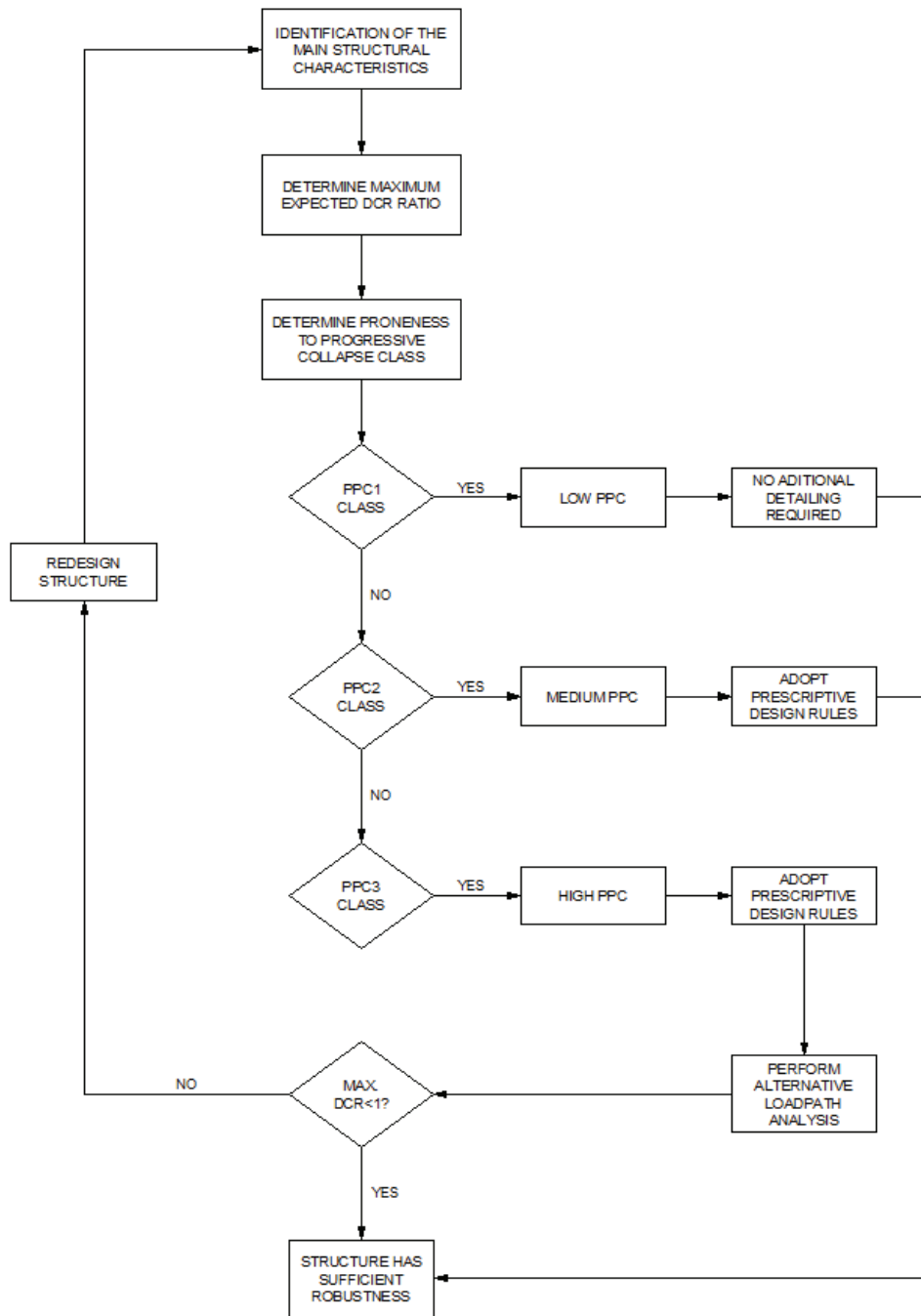


Figure E.1 – Design strategy methodology flow chart

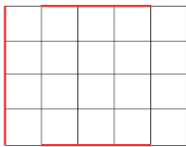


### E.3 Maximum expected DCR ratios for building structures

(1) Table E.1 provides the maximum expected DCR ratio values based on the building structure's main characteristics. Values for the the maximum expected chord rotation are also provided.

(2) Structural designers should be extremely cautious when extrapolating data to structural configurations not described in Table E.1, considering the complexity of structural response further to a column loss. In such cases, it is deemed advisable to resort to additional specialised literature on the structural typology in question. Alternatively, such structures can be designed for disproportionate collapse according to the methodology described in Annex A.

**Table E.1 – Maximum expected DCR by building structure typology**

Bracing system [-]	Number of storeys [-]	Span [m]	Interstorey Height [m]	Maximum expected DCR ratio [-]	Maximum expected chord rotation [mrad]	Typology # [-]
Moment Frame - full strength rigid joints (equal x and y spans) 	4	6	3	0.22	11	T1
			4	0.19	9	T2
		10	3	1.00	$\infty$ (collapse)	T3
			4	0.68	64	T4
	8	6	3	0.10	7	T5
			4	0.08	5	T6
		10	3	0.39	18	T7
			4	0.30	11	T8

NOTE 1 Table E.1 is not exhaustive and can be progressively adjusted and completed to incorporate data for other structural typologies.

### E.4 Proneness to Progressive Collapse (PPC) classes of buildings

(1) Table E.2 provides a categorisation of the proneness to progressive collapse (PPC), based on the maximum expected DCR ratio values determined in Table E.1.

**Table E.2 – Categorisation of proneness to progressive collapse**

Maximum DCR ratio [-]	Proneness to Progressive Collapse (PPC)	PPC Class
[0.0 ; 0.3[	Low	PPC1
[0.3 ; 0.7[	Medium	PPC2
[0.7 ; 1.0]	High	PPC3

NOTE 1 The fact that structural typologies with maximum DCR ratio equal to 0.7 (i.e. with a 30% safety margin to progressive collapse) are classified as highly prone to collapse is to account for factors such as design/construction errors, corrosion and insufficient maintenance, more severe damage scenarios and other unpredictable factors which were not explicitly accounted for.

### E.5 Recommended strategies

(1) Adoption of the following recommended strategies should provide a building with an acceptable level of robustness to sustain localised failure without resulting in a progressive collapse.

**Table E.3 – Recommended strategies for PPC classes**

PPC Class	Recommended strategies
PPC1	Adopt recommended strategies for disproportionate collapse in Annex A of the EN 1991-1-7; Provided that a building has been designed and constructed in accordance with the rules given in EN 1990 to EN 1999, no additional robustness detailing required.
PPC2	In addition to recommended strategies for class PPC1, adopt prescriptive robustness detailing rules.
PPC3	In addition to recommended strategies for class PPC2, perform Alternative Loadpath Analysis.

NOTE 1 The adoption of prescriptive detailing rules is recommended only for structural typologies presenting elements with by medium/high DCR ratios. The use of prescriptive

measures (i.e. that provide no quantification of the robustness enhancement) is acceptable since the detailing rules alone are directly and without further measures only for structural typologies with medium proneness to progressive collapse. For structures with high propensity to progressive collapse, while the adoption of the prescriptive measures is recommended, it is required to be complemented with the use of a deterministic method (e.g. Alternative Loadpath analysis) to effectively assess if the structure is capable of arresting progressive collapse.

## **E.6 Prescriptive detailing rules for improved structural robustness**

(1) Adoption of the following recommended strategies should provide a building with an acceptable level of robustness to sustain localised failure without resulting in a progressive collapse.

(2) The sets of detailing rules to be adopted differ according to the typology, where more sets of detailing rules are required for typologies with structural elements characterised by higher DCR ratio values. Each set of detailing rules is aimed at improving the robustness of a single type of structural elements.

(3) The implementation of the detailing rules is considered to have negligible impacts in terms of construction cost and fabrication time and can easily be implemented at the design stage, while significantly enhancing global structural robustness and resistance to progressive collapse.

(4) The correspondence between the structural typologies (see Table E.1) and the required prescriptive detailing rules for improved robustness is presented in Table E.4.

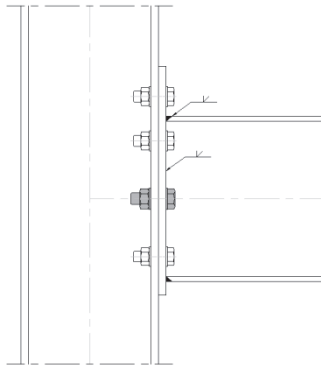
**Table E.4 – Prescriptive detailing rules by structural typology**

<b>Typology #</b>	<b>Sets of prescriptive detailing rules for improved robustness</b>
T1	-
T2	-
T3	DR1, DR2, DR3
T4	DR1, DR2, DR3
T5	-
T6	-
T7	DR1
T8	DR1

## **E.6.1 Detailing Rules DR1 – Rules for steel moment resisting frame elements in facades**

### DR 1.1 – Bolted beam-to-column joints

- DR 1.1.1 An additional internal bolt row aligned with the beam section centroid should be introduced (see Figure E.2).
- DR 1.1.2 The bolts for the additional bolt row should be of the same steel grade or higher than that adopted in other bolt rows of the same joint.
- DR 1.1.3 The nominal diameter of additional row bolts shall not be lower than the maximum diameter of the other bolts in the same joint, and if possible, should be larger in order to achieve higher resistance to column loss action.
- DR 1.1.4 The bolt assembly type to be used in the additional bolt row should have a failure mode characterised by bolt shank necking (e.g. SB bolts, HR bolts) in order to retain strength while arresting the progressive collapse. Bolt assemblies characterised by thread stripping failure (e.g. HV bolts) should be avoided, unless proven to remain elastic for the maximum rotational joint demand under the most unfavourable column loss scenario.
- DR 1.1.5 The welds between the beam flange and the end-plate and between the beam web and the end-plate should be full penetration welds (see Figure E.2), executed in shop for quality assurance purposes.
- DR 1.1.6 The adoption of joint configurations with stiffened extended end-plate or with beam haunches is considered to improve joint behaviour in bending. For structural typologies in which the moment resisting frame members are prone to remain elastic under column loss, these joint configurations may lead to improved joint response. For structural typologies that require large joint rotations to arrest collapse, there is not sufficient evidence that these joint configurations improve joint response.



**Figure E.2 – Bolted beam-to-column joints – additional bolt row and beam-endplate weldings**

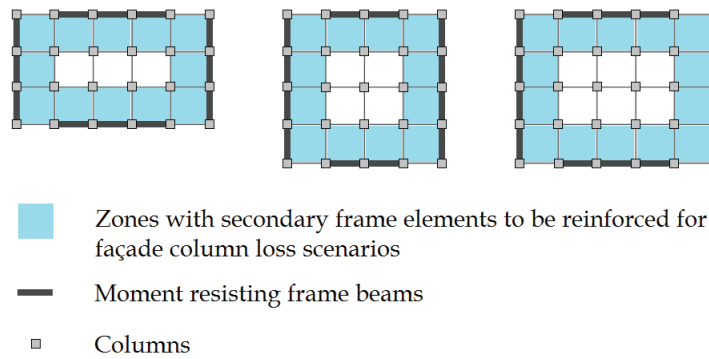
#### DR 1.2 – Welded beam-to-column joints

DR 1.2.1 The welds between the beam flange and the column and between the beam web and the column should be full penetration welds, executed in shop for quality assurance purposes.

DR 1.2.2 The adoption of joint configurations with stiffeners or haunches is considered to improve joint behaviour in bending. For structural typologies in which the moment resisting frame members are prone to remain elastic under column loss, these joint configurations may lead to improved joint response. For structural typologies that require large joint rotations to arrest collapse, there is not sufficient evidence that these joint configurations improve joint response.

#### **E.6.2 Detailing Rules DR2 – Rules for secondary steel frame elements**

The rules for the secondary steel frame elements apply to members and connections located on the directly affected zone for all possible façade column loss scenarios. Examples of these zones are shown in Figure E.3 for 3 cases of plan layouts of moment resisting frame type structures.



**Figure E.3 – Plan view examples of zones to which to apply DR2 rules for secondary elements**

#### DR 2.1 – General rules for beam-to-column and beam-to-beam joints

- DR 2.1.1 Beam-to-column and beam-to beam joints should be designed to be semi-rigid, according to the stiffness classification provided in Section 5.5.2 of the EN 1993-1-8, in order to reduce the maximum rotational demand under column loss.
- DR 2.1.2 The selected joint typology should be capable of sustaining chord rotations under column loss action in excess of the predicted maximum demand for the structural typology in question presented in Table E.1.
- DR 2.1.3 The selected joint typology should be able to accommodate the maximum rotation imposed by the moment resisting frame elements. In seismic zones, joints should be capable of sustaining cyclic bending actions of up to 40 mrad chord rotation.

#### DR 2.2 – Specific rules for flush end-plate joints

- DR 2.2.1 The welds between the beam flange and the end-plate and between the beam web and the end-plate should be full penetration welds, executed in shop for quality assurance purposes.
- DR 2.2.2 When using flush end-plate joints, end-plate thickness should be selected so as to maximise joint robustness. This can be achieved by adopting the end-plate thickness range which

induces failure mode 2, according to the design criterion expressed in (E.1).

$$0.9 \frac{1.35 \cdot d}{\sqrt{\gamma_{ov} \gamma_{sh}}} \cdot \sqrt{\frac{\gamma_{M0} \cdot f_{ub}}{\gamma_{M2} \cdot \alpha \cdot f_y}} \geq t_{end-plate} \geq \frac{0.40 \cdot d}{\sqrt{\gamma_{ov} \gamma_{sh}}} \cdot \sqrt{\frac{\gamma_{M0} \cdot f_{ub}}{\gamma_{M2} \cdot f_y}} \quad (E.1)$$

The criterion in (E.1) is also suitable for structures in seismic zones, in which joints are subjected to cyclic bending, since it contributes to avoid premature weld fracture.

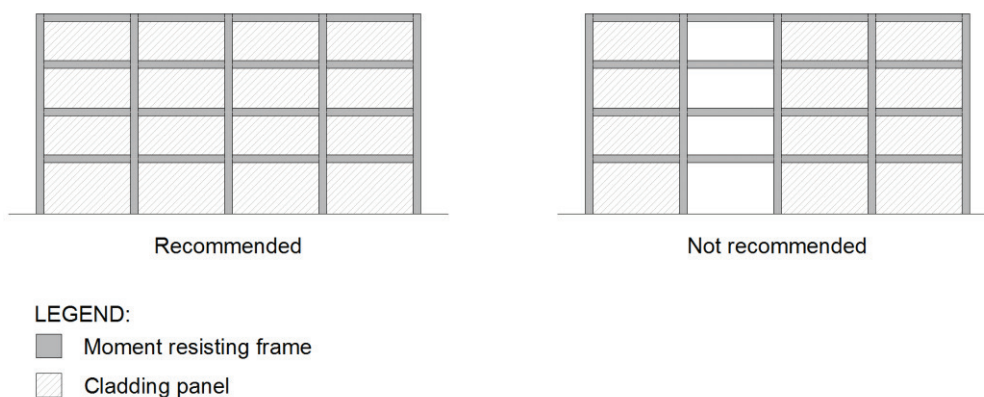
- DR 2.2.3 The adoption of thick endplates, namely leading to T-stub failure mode 3 (see EN 1993-1-8) should be avoided, since it leads to reduced joint ductility.
- DR 2.2.4 An additional internal bolt row aligned with the beam section centroid should be introduced to improve the transmission of tensile axial force in the joint. Alternatively two additional internal bolt rows may be introduced, the centroid of which should be aligned with the beam section centroid.
- DR 2.2.5 The bolts for the additional row(s) should be of the same steel grade or higher than that adopted in other bolt rows of the same joint.
- DR 2.2.6 The nominal diameter of additional row bolts shall not be lower than the maximum diameter of the other bolts in the same joint, and if possible should be larger, in order to achieve higher resistance to column loss action.
- DR 2.2.7 Joints should preferably be designed using bolt assemblies with nominal diameters greater than 16mm, in order to maximise joint capacity at higher rotational demand.
- DR 2.2.8 The bolt assembly type to be used in the additional row bolts should have a failure mode characterised by bolt shank necking (e.g. SB bolts, HR bolts) in order to retain strength while arresting the progressive collapse. Bolt assemblies characterised by thread stripping failure (e.g. HV bolts) should be avoided, unless it can be demonstrated that the moment resisting frame elements alone are sufficient to arrest the progressive collapse for all column loss scenarios.

### E.6.3 Detailing Rules DR3 – Rules for façade claddings

The use of cladding elements in façades may contribute to reduce vertical displacements in the directly affected zone following a column loss, hence reducing the probability of occurrence of a progressive collapse.

#### DR 3.1 – General rules for façade claddings

- DR 3.1.1 The adoption of cladding panels for robustness enhancement purposes is subjected to architectural constraints and requires authorisation from the Architectural designer, for which reason it is not mandatory.
- DR 3.1.2 The introduction of discontinuities or the partial adoption of cladding panels in a building façade (see Figure E.4) should be avoided since it may lead to lateral force imbalance under some column loss scenarios, unless demonstrated otherwise.

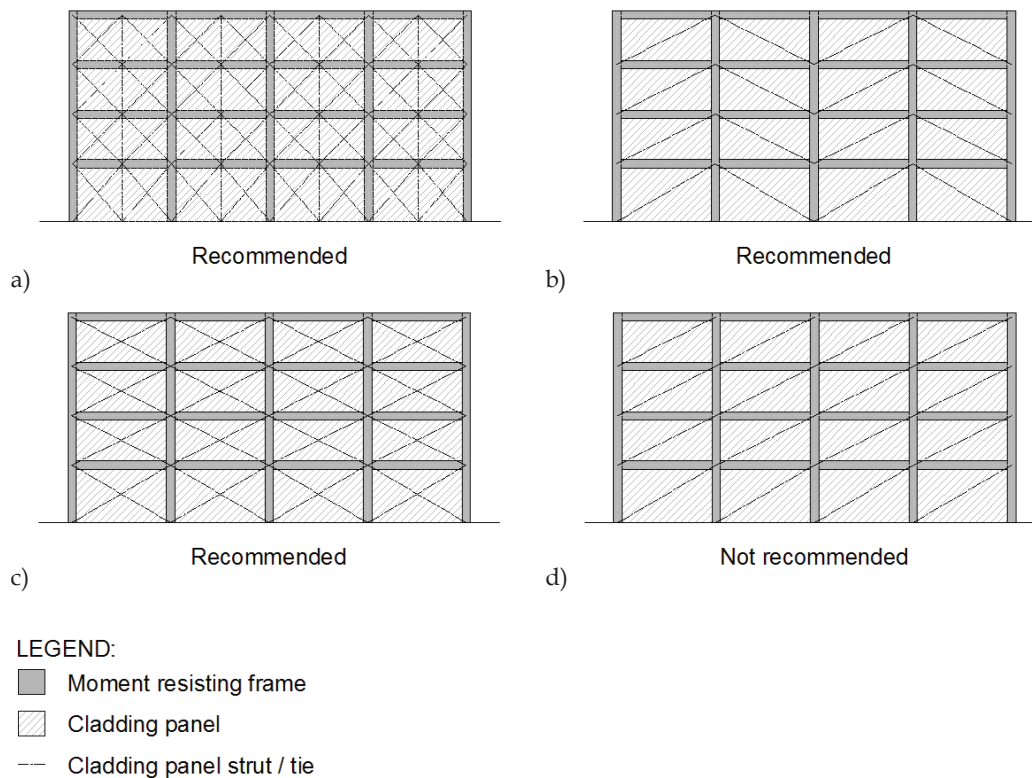


**Figure E.4 – Recommended cladding panel disposition in a façade**

- DR 3.1.3 The adopted cladding panel solution should be able to transfer loads across corners through a truss system composed of single or multiple struts and/or ties.
- DR 3.1.4 For cladding panels composed of linear resisting elements (e.g. claddings with steel bracings), load redistribution following



column loss should be achieved via a cladding truss mechanism that is symmetric about the removed column in the directly affected zone, in accordance with the recommendations shown in Figure E.5.

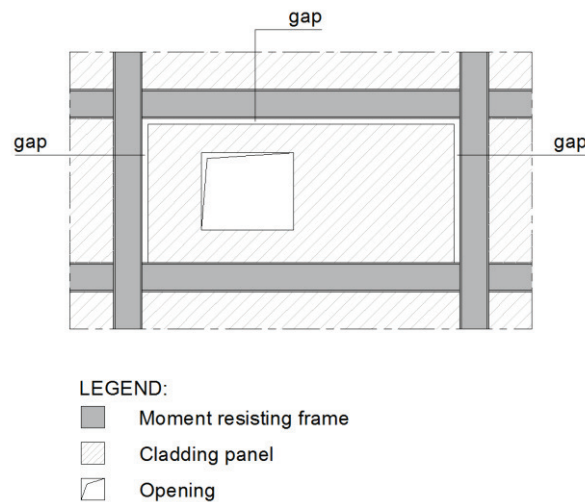


**Figure E.5 – Recommended cladding panel strut / tie system**

DR 3.1.5 For infilled panels (e.g. masonry panels), the load transfer may be achieved via the compressive struts that are mobilised upon column loss. The presence of openings may reduce the stiffness of the panel and alter the load redistribution following column loss. Panels with openings are therefore not recommended to be adopted for progressive collapse prevention, unless demonstrated to be effective.

DR 3.1.6 In cases of infilled panels with openings, a physical gap between the infill element and the surrounding steel frame may be adopted, enabling to disconnect the cladding from the frame as

shown in Figure E.6. The dimension of the gap should be designed to accommodate the allowable interstorey drift.



**Figure E.6 – Gap between frame and infilled panel with opening**

#### DR 3.2 – Rules for façade claddings in non seismic zones

- DR 3.2.1 In non seismic zones, both infilled and strut/tie truss claddings systems may be adopted. Although this measure is not mandatory, its adoption is likely to enhance structural robustness and in some cases help prevent progressive collapse following column loss.
- DR 3.2.2 Strut / tie truss claddings systems, namely consisting of “X” bracings of the same material of the frame, are more likely to provide a higher reduction of displacements following column loss and are therefore considered preferable in general.
- DR 3.2.3 Infilled masonry claddings panels tend to be moderately effective for low rise and for short/medium span structural typologies and may therefore be adopted for such building typologies. For medium-rise long-span systems, masonry claddings have reduced effect on robustness and non-infilled solutions are preferable.
- DR 3.2.4 For buildings with infilled façade walls (e.g. masonry), no gaps are allowed between adjacent cladding panels nor between the

cladding panels and the surrounding steel elements of the moment resisting frame.

- DR 3.2.5 Buildings with dry assembled façade wall systems can incorporate bracing systems (e.g. steel bracings) into the façade claddings that make up a strut/tie truss system according to the recommended typologies (see Figure E.5), hence creating alternative loadpaths and improving structural redundancy and load re-distribution capacity.
- DR 3.2.6 The members that make up the cladding strut / tie truss should, whenever possible, be designed for the additional accidental loads, accounting for dynamic effects, which can be conservatively accounted for using by a Dynamic Load Factor (DLF) equal to 2.0. Smaller DLF values may be adopted whenever properly justified.
- DR 3.2.7 The connections of the members that make up the cladding strut/tie truss should be designed to have sufficient overstrength so that potential yielding is limited to the members. This may be achieved by designing connections according to the design rule for non-dissipative connections indicated in Section 6.5.5(3) of EN 1998-1.
- DR 3.2.8 The members and connections of the strut/tie truss system should be designed to remain elastic (i.e. to sustain no permanent damage) for all characteristic load combinations. Damage is acceptable under the accidental load combinations (i.e. under column loss action).

### DR 3.3 – Rules for façade claddings in seismic zones

- DR 3.3.1 In seismic zones, the adoption of claddings systems, when not explicitly taken into account for structural design, may introduce changes both in terms of strength and energy dissipation to the resisting structure under seismic actions. For this reason, these elements must be classified and consequently designed as primary or as secondary seismic elements, in accordance with EN 1998-1.

- DR 3.3.2 Cladding systems with infilled panels should be designed according to the rules provided in EN 1998-1.
- DR 3.3.3 Cladding systems with strut / tie trusses (e.g. steel bracings) may be designed either as primary or as secondary seismic elements, in accordance with EN 1998-1. If the total contribution to the lateral stiffness of all secondary seismic members including claddings does not exceed 15% of that of all primary seismic members (see Section 4.2.2(4) of the EN 1998-1), then claddings can be designed as secondary seismic elements. Otherwise claddings should be designed as primary seismic members.
- DR 3.3.4 Cladding systems with strut / tie trusses classified as secondary seismic members are not required to be explicitly modelled for seismic design. Under seismic action, these elements are expected to sustain some level of damage, which may reduce compression strut capacity. It is therefore recommended to adopt cladding panels with “X” bracing configurations (see Figure E.5a,c)) that can mobilise ties under post-seismic column loss scenarios.
- DR 3.3.5 Cladding systems with strut/tie trusses classified as primary seismic members are required to be explicitly modelled in the structural analysis and detailed for earthquake resistance in accordance with the rules provided in EN 1998-1.
- DR 3.3.6 The members that make up the cladding strut / tie truss should, whenever possible, be designed for the additional accidental loads, accounting for dynamic effects, which can be conservatively accounted for using by a Dynamic Load Factor (DLF) equal to 2.0. Smaller DLF values may be adopted whenever properly justified.
- DR 3.3.7 The connections of the members that make up the cladding strut / tie truss should be designed to have sufficient overstrength so that potential yielding is limited the members. This may be achieved by designing connections according to the design rule for non-dissipative connections indicated in Section 6.5.5(3) of EN 1998-1.

- DR 3.3.8 The members and connections of the strut / tie truss system should be designed to remain elastic (i.e. to sustain no permanent damage) for all characteristic load combinations. Damage is acceptable under the accidental load combinations (i.e. under seismic and column loss actions).

## **E.7 Alternative Loadpath Analysis**

### **E.7.1 Generalities**

(1) In this section, a set of guidelines is provided for conducting Alternative Loadpath Analysis (ALA) in order to verify if a building structure is capable of arresting progressive collapse originating from an unspecified cause.

(2) The indicated procedure is based on a Nonlinear Static Procedure combined with the Energy Balance method. It should be noted that ALA may be conducted using alternative analysis procedures, based on solid engineering mechanical and dynamic principles. The results of these alternative procedures shall be reviewed by an independent third-party engineer.

### **E.7.2 Component classification**

(1) All structural elements and components are required to be classified by the designer either primary or secondary.

(2) All elements and components that contribute to the structure's capacity to resist a progressive collapse induced by column loss should be classified as primary.

(3) All other elements and components should be classified as secondary.

### **E.7.3 Component capacity**

(1) The verification of individual component strength and deformation capacities shall be conducted based on expected material performance and shall comply with material property definitions in EN 1990.

(2) In general, lower bound material strength properties should be adopted and divided by a partial safety factor for progressive collapse  $\gamma_{PC}$ . The lower bound material property for the calculation of component capacities under progressive collapse is

given in (E.2), where  $R_{PC}$  is the component capacity for progressive collapse,  $R_k$  is the characteristic component strength and  $\gamma_{PC}$  is the progressive collapse partial safety factor equal to 1.

$$R_{PC} = R_k / \gamma_{PC} \quad (\text{E.2})$$

#### **E.7.4 Modelling**

- (1) The modelling, analysis and evaluation of the resistance to progressive collapse shall be made using three-dimensional model. Two-dimensional models are not allowed.
- (2) The model should account for geometrical and material nonlinearity. Lateral stability of members (i.e. lateral torsional buckling) must be considered.
- (3) The inclusion of secondary elements in the model is not mandatory. When not explicitly modelled, secondary elements must be checked to remain stable and to maintain load-carrying capacity under the displacements imposed by the primary elements.
- (4) Connections classified as semi-rigid according to EN 1993-1-8 shall not be considered as secondary elements and must be explicitly modelled as primary elements. Connections classified as nominally pinned in terms of stiffness according to EN 1993-1-8 may be considered as secondary elements.
- (5) Primary elements shall be modelled, accounting whenever possible for their initial stiffness, yielding, post-yield hardening, failure and residual strength. As a minimum initial stiffness, yielding and failure should be modelled.
- (6) The definition of component material nonlinearity, namely its force-displacement or moment-rotation response curve should be determined according to the Components Method in EN 1993-1-8 whenever applicable or alternatively, according to available literature on joint performance.

(7) Plasticity distribution along members may be modelled using distributed inelasticity elements or by meshing members and adopting a lumped plasticity at the ends of each segment.

#### **E.7.5 Loading procedure**

(1) The combination of actions acting on the building structure prior to the column loss action is the accidental load combination given in expression (6.11b) of EN 1990.

(2) The internal forces in each column to be removed shall be determined and the column to be removed shall be deleted from the model and replaced by the equivalent reaction forces.

(3) A loading procedure consisting of a downward displacement-controlled pushdown shall be implemented up to collapse or up to a displacement value deemed sufficiently high by the designer to enable to generate the vertical pushdown load-displacement curve.

(4) A minimum of 10 calculation steps shall be used to generate the pushdown curve.

#### **E.7.6 Column removal locations**

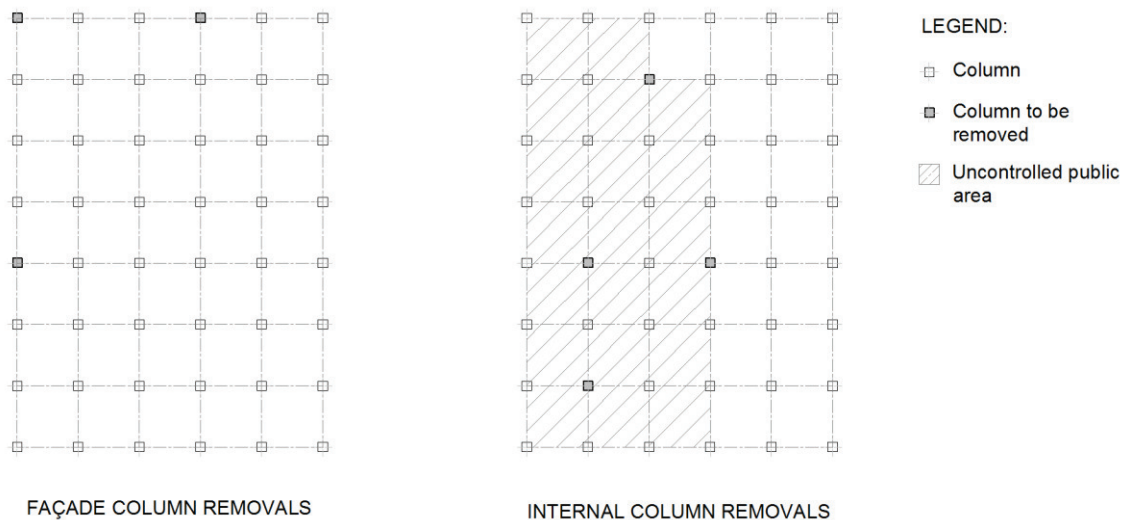
(1) Alternative Loadpath Analysis should be conducted considering, for each column removal scenario, that the full column segment defined between lateral restraints (i.e. between consecutive storeys) is removed.

(2) In terms of location, as a minimum, the following column removal scenarios should be analysed: i) façade column near the middle of the long side; ii) façade column near the middle of the short side; iii) corner column.

(3) Additionally, engineering judgement should be used to identify discontinuity zones, characterised for example by changes in bay size, re-entrant corners, change of member orientation, which require the consideration of additional removal scenarios.

(4) For each plan location, as a minimum, column removals shall be considered for the following scenarios: i) column segment between ground floor and 1st storey; ii) column segment at building mid height; iii) column segment between penultimate storey and the roof.

(5) For buildings with underground parking or with uncontrolled public areas, internal column removal scenarios must be considered, namely near the middle of the long side, near the middle of the short side and near the corner of the uncontrolled space. In these cases, the column segment to be removed is defined between the floor of the parking zone to the floor above it.

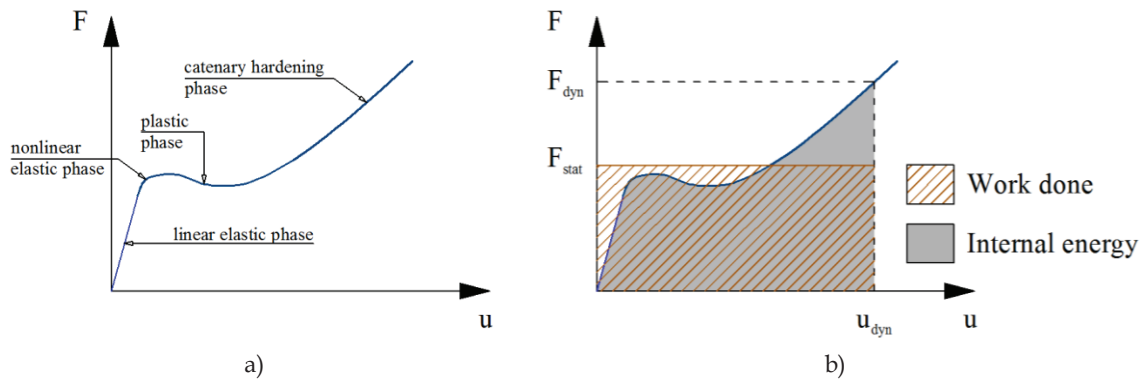


**Figure E.7 – Façade and interior column removal scenarios**

### E.7.7 Energy Balance method

(1) The procedure is based on the balance between the work done by the application of the sudden gravity load and the internal strain energy of the system (see Figure E.7). When these quantities achieve equilibrium, the zero kinetic energy condition is reached, which corresponds to the maximum dynamic displacement  $u_{dyn}$  under column loss.





**Figure E.7 – Energy Balance method: a) nonlinear static response; b) work done and internal strain energy**

(2) The method implicitly assumes that the directly affected zone of the structure responds as a Single Degree of Freedom (SDOF) system.

(3) For the application of the Energy Balance method, the pushdown force-displacement curve must be plotted and the internal energy and work done must be computed for each vertical displacement step  $i$  according to expressions (E.3) and (E.4), respectively,

$$W_{int} = \int_0^{u_i} F(u) du \quad (E.3)$$

$$W_{ext} = F_{stat} \times u_i \quad (E.4)$$

where  $W_{int}$  is the internal energy,  $W_{ext}$  is the external work done,  $\int F(u) du$  is the area below the pushdown curve up to the displacement at step  $i$ ,  $F_{stat}$  is the axial force in the column before the column removal and  $u_i$  is the displacement at step  $i$ .

(4) The displacement value  $u_i$  for which the difference between the work done  $W_{ext}$  and the internal strain energy  $W_{int}$  is zero (see expression (E.5)) corresponds to the maximum dynamic displacement  $u_{dyn}$ .

$$F_{stat} \times u_i - \int_0^{u_i} F(u) du = 0 \quad (E.5)$$

(5) For cases in which balance is not reached, the system is assumed to collapse.

### **E.7.8 Ductility assessment and acceptance criteria**

- (1) The maximum dynamic displacement ( $u_{dyn}$ ) must be compared to the ductility limit ( $u_l$ ), defined as the minimum value of  $u_{dyn}$  which exceeds the deformation capacity in any of the connections. The limit state corresponds to the failure of the first connection.
- (2) Secondary elements must be checked to remain stable and to maintain load-carrying capacity under the displacements imposed by the primary elements.
- (3) In cases in which at least one component is found exceed the ductility limit, the building structure is found to not satisfy the progressive collapse requirements and must be re-designed.

## Appendix D Detailing rules justification

In this section, the considerations at the base of the proposed recommendations and detailing rules described in Section 7.4.2.2 are presented. Reference is made to the relevant data and results obtained in the present thesis, as well or to other sources from literature. This section is divided by sets of detailing rules, within which the text for each individual numbered rule is reproduced and justified.

### D.1 Detailing rules DR1

#### DR 1.1 - Bolted beam-to-column joints:

##### **DR 1.1.1:**

*An additional internal bolt row aligned with the beam section centroid should be introduced.*

##### **Justification:**

Bolted beam-to-column joints are typically designed for combined and shear. However, under column loss action, joints are subjected also to very strong tensile forces, justifying the introduction of a new resisting element designed to improve the axial force transmission in the joint.

The adoption of a joint configuration with an additional bolt row has been shown to be very effective in improving the transmission of axial force in the joint (see Figure 4.6) and can be considered a viable solution to improve joint performance (Tartaglia, D'Aniello, & Landolfo, 2016). Considering that the additional bolt row is aligned with the beam section centroid, it does not influence joint response under seismic action. Instead, under column loss action and at large rotations, the catenary action becomes the main resistance mechanism in the collapse arrest, mobilising the resistance of the additional bolt row, which also serves the purpose of introducing redundancy in case of premature failure of other components such as external bolt rows or flange welds

##### **DR 1.1.2:**

*The bolts for the additional bolt row should be of the same steel grade or higher than that adopted in other bolt rows of the same joint.*

**Justification:**

Under column loss action, the catenary action causes beam-to-column joints and in particular the additional row bolts to be subjected to high tensile forces. These elements should therefore be designed to have sufficient resistance. In order to achieve this objective, these bolts should be designed with a steel grade equal to or greater than the bolts in the other rows.

**DR 1.1.3:**

*The nominal diameter of additional row bolts shall not be lower than the maximum diameter of the other bolts in the same joint, and if possible, should be larger in order to achieve higher resistance to column loss action.*

**Justification:**

This recommendation is justified in order to avoid the additional bolt row from becoming a “weak link” in the joint, which upon failure would cause the tensile forces to be redistributed to other bolt rows, which were not designed to that end and which are less effective in transferring axial loads. In cases in which the joint configuration allows it, adopting higher nominal diameter for the additional row bolts contributes to keep these elements in the elastic range, hence increasing the joint robustness.

**DR 1.1.4:**

*The bolt assembly type to be used in the additional bolt row should have a failure mode characterised by bolt shank necking (e.g. SB bolts, HR bolts) in order to retain strength while arresting the progressive collapse. Bolt assemblies characterised by thread stripping failure (e.g. HV bolts) should be avoided, unless proven to remain elastic for the maximum rotational joint demand under the most unfavourable column loss scenario.*

**Justification:**

The preference for bolt assembly types characterised by shank necking failure is justified by the fact that the tensile forces in the additional row bolts remain high during and after the progressive collapse arrest, requiring bolt assemblies to be capable of retaining integrity and high strength levels until stabilised. This can be better accomplished by bolts with shank failure than by bolts with thread-stripping failure, considering that the latter are characterised by a sudden drop in strength at low displacements (see Figure 5.10), which would lead to tensile force redistribution to

other components, defeating the purpose of the introduction of the additional bolt row. Their use is only admitted in case it can be shown that these bolts remain elastic (i.e. that no drop in bolt resistance occurs) for maximum rotational demand under the most unfavourable column loss scenario.

**DR 1.1.5:**

*The welds between the beam flange and the end-plate and between the beam web and the end-plate should be full penetration welds, executed in shop for quality assurance purposes.*

**Justification:**

The adoption of full penetration welds in these interfaces is aimed at minimising the risk of fragile weld fracture which may lead to unanticipated internal force redistribution, potentially impairing joint response. The added cost of the full penetration welds is deemed justifiable when considering the possible consequences arising from premature fragile weld failure. Indeed, weld failure leading to reduced joint performance under column loss may ultimately limit the building structure's capacity to arrest progressive collapse, implying loss of human life and severe economic losses.

**DR 1.1.6:**

*The adoption of joint configurations with stiffened extended end-plate or with beam haunches is considered to improve joint behaviour in bending. For structural typologies in which the moment resisting frame members are prone to remain elastic under column loss, these joint configurations may lead to improved joint response. For structural typologies that require large joint rotations to arrest collapse, there is not sufficient evidence that these joint configurations improve joint response.*

**Justification:**

The adoption of stiffeners or haunches has been shown in recent studies to play an important role in joint performance in bending (Guo, Gu, & Liu, 2006), (Shi, Shi, & Wang, 2007), (D'Aniello, Tartaglia, Costanzo, & Landolfo, 2017). However, few studies are available on the column loss response of different seismic connections (Kim & Kim, 2009). Since many structural typologies are prone to remain elastic under column loss, the adoption of stiffeners or haunches should contribute to increase joint capacity in arresting progressive collapse. Instead, for typologies that typically require very large

rotations to arrest collapse, the role of these stiffening elements on joint strength and rotation capacity cannot be predicted, owing to the unavailability of data. It is not therefore presently clear whether the increased stiffness leads external bolt rows to premature failure or whether the increase in lever arm provided by the stiffeners can contribute to increase joint capacity.

#### DR 1.2 – Welded beam-to-column joints:

##### **DR 1.2.1:**

*The welds between the beam flange and the column and between the beam web and the column should be full penetration welds, executed in shop for quality assurance purposes.*

##### **Justification:**

(See DR 1.1.5)

##### **DR 1.2.2:**

*The adoption of joint configurations with stiffeners or haunches is considered to improve joint behaviour in bending. For structural typologies in which the moment resisting frame members are prone to remain elastic under column loss, these joint configurations may lead to improved joint response. For structural typologies that require large joint rotations to arrest collapse, there is not sufficient evidence that these joint configurations improve joint response.*

##### **Justification:**

(See DR 1.1.6)

## **D.2 Detailing rules DR2**

#### DR 2.1 – General rules for beam-to-column and beam-to-beam joints:

##### **DR 2.1.1:**

*Beam-to-column and beam-to beam joints should be designed to be semi-rigid, according to the stiffness classification provided in Section 5.5.2 of the EN 1993-1-8, in order to reduce the maximum rotational demand under column loss.*

##### **Justification:**

The recommendation to design the joints in the zones identified in Figure 7.104 as semi-rigid is motivated by the fact that the adoption of stiffer secondary frame joints can contribute to reduce the momentum of the DAZ, hence reducing the maximum vertical displacement. The results presented in Section 7.3.1.6 indicate that the differences in the stiffness of the secondary frame joints highlighted in Figure 7.46 contribute to reduce rotational demands. Indeed, the maximum chord rotational demands for the LL column removal scenario shown in Figure 7.53, Figure 7.54, Figure 7.55 and Figure 7.56 are consistently smaller than the corresponding demands under the LS removal scenario.

**DR 2.1.2:**

*The selected joint typology should be capable of sustaining chord rotations under column loss action in excess of the predicted maximum demand for the structural typology in question. An estimation of the maximum predicted rotations is presented in Table 7.34.*

**Justification:**

As a minimum, the selected semi-rigid joints should be capable of resisting the maximum expected rotations under column loss action. The values for the expected rotations were derived from the conducted numerical tests. Further tests on different configurations may contribute to expand the data presented in Table 7.34 and to improve the statistical backing of the maximum expected rotation demands.

**DR 2.1.3:**

*The selected joint typology should furthermore be able to accommodate the maximum rotation imposed by the moment resisting frame elements. In seismic zones, joints should be capable of sustaining cyclic bending actions of up to 40 mrad chord rotation.*

**Justification:**

Secondary frame members are generally required to be able to maintain integrity and load carrying capacity while subjected to the end displacements induced by the primary resisting elements. In this case, the secondary frame joints should therefore be designed for maximum rotations imposed by the primary resisting elements.

For structures in seismic zones, the EN 1998-1 (CEN, 2004) states that for dissipative semi-rigid and/or partial strength joints, the rotation capacity of the plastic hinge should not be less than 35 mrad for DCH class structures. On the other hand, the AISC

341-05 (AISC, 2005) allows the use of connections in special moment frame beam-to-column joints subjected to seismic actions that are capable of accommodating an interstorey drift angle of 40 mrad.

Considering the small difference in terms of required rotational capacity for primary elements stated in these two codes, it is therefore considered that secondary joints should be required to be capable of sustaining cyclic bending actions up to 40 mrad chord rotation.

#### DR 2.2 – Specific rules for flush end-plate joints:

##### **DR 2.2.1:**

*The welds between the beam flange and the end-plate and between the beam web and the end-plate should be full penetration welds, executed in shop for quality assurance purposes.*

##### **Justification:**

(See DR 1.1.5)

##### **DR 2.2.2:**

*When using flush end-plate joints, end-plate thickness should be selected so as to maximise joint robustness. This can be achieved by adopting the minimum plate thickness which induces failure mode 2, according to the design criterion expressed in Eq.(**Error! Reference source not found.**). This criterion is also suitable for structures in seismic zones, in which joints are subjected to cyclic bending, since it contributes to avoid premature weld fracture.*

##### **Justification:**

The design of the flush end-plate joints should be conducted so as to maximise joint capacity to resist the simultaneous bending and tensile axial force induced by the column loss action. The end-plate thickness should therefore be carefully selected so as to be thin enough to provide sufficient rotational capacity, while also being sufficiently thick in order to have sufficient resistance under a column loss event. Results presented in Sections 6.3.1 and 6.3.2 indicate that joints compliant with the proposed design criterion are capable of developing significantly larger rotational capacities. Furthermore, results presented in Section 6.3.3 indicate that design in compliance with the proposed minimum thickness criterion leads to increased joint capacity to



withstand cyclic loading up to 4% chord rotations without the initiation of weld fractures that may impair joint performance.

**DR 2.2.3:**

*The adoption of thick endplates, namely leading to T-stub failure mode 3 (see EN 1993-1-8) should be avoided, since it leads to reduced joint ductility.*

**Justification:**

The adoption of thick end-plates leading to T-stub failure mode 3, characterised by the development of plasticity in the bolts alone, was shown in a past experimental study (Broderick & Thomson, 2002) to lead to reduced joint bending ductility.

Adiotionally, the numerical results described in Section 6.3.1.3 point to the fact that under column loss action, the adoption of thick endplates inducing failure mode 3, namely if combined with large diameter bolts, tends to lead to reductions in joint rotation capacity when compared to joints in failure mode 2.

The selection of end-plate thickness values failure yielding mode 3 is therefore deemed inadvisable.

**DR 2.2.4:**

*An additional internal bolt row aligned with the beam section centroid should be introduced to improve the transmission of tensile axial force in the joint. Alternatively two additional internal bolt rows may be introduced, the centroid of which should be aligned with the beam section centroid.*

**Justification:**

The effect of increasing the number of internal bolt rows aligned with the centroid of the beam section was investigated in 0. The results presented in Section 6.3.1.4 point to important enhancements in joint strength and ductility when the number of bolt rows is increased. This is due to the improved redundancy and internal force re-distribution capacity to the remaining bolt rows.

**DR 2.2.5:**

*The bolts for the additional bolt row(s) should be of the same steel grade or higher than that adopted in other bolt rows of the same joint.*

**Justification:**

This is intended to prevent the introduction of bolt steel grades lower than those adopted for the other bolt rows, which could potentially constitute a weak link for the joint and which could potentially present differences in strain at failure, leading to unanticipated behaviour under column loss. Furthermore, considering that the numerical tests described in 0 were conducted assuming equal bolt steel grade for all bolt rows, the validity of the conclusions regarding FEP joint response stated in Section 6.4 is limited to this case.

**DR 2.2.6:**

*The nominal diameter of additional row bolts shall not be lower than the maximum diameter of the other bolts in the same joint, and if possible should be larger, in order to achieve higher resistance to column loss action.*

**Justification:**

The effect of bolt nominal diameter on the behaviour of FEP joints under column loss action is presented and discussed in Section 6.3.1.4. The obtained results point towards substantial enhancements in both strength and ductility of the FEP joints. In particular, joints with the largest analysed diameter case (i.e. M24) were found to maximise joint robustness. Considering that the additional row bolts constitute the joint components which should account for most of the transmission of the tensile forces in the joint, then these elements should be designed to withstand levels of axial forces, which can easily be achieved by adopting large diameter bolt assemblies.

**DR 2.2.7:**

*Joints should preferably be designed using bolt assemblies with nominal diameters greater than 16mm, in order to maximise joint capacity at higher rotational demand.*

**Justification:**

This recommendation is based on the comparatively lower performance of joints with small diameter bolt assemblies (i.e. M16), as shown in Section 6.3.1.4. The fact that in most cases the ultimate rotation capacity of joints with M16 bolts is nonetheless compatible with the predicted rotational demands indicated in Table 7.34 led to considering a non-mandatory recommendation regarding the use of small diameter bolts in this case. However, considering that robustness maximisation is the primary

goal of these design recommendations, it is therefore deemed advisable to adopt larger bolt diameters.

**DR 2.2.8:**

*The bolt assembly type to be used in the additional row bolts should have a failure mode characterised by bolt shank necking (e.g. SB bolts, HR bolts) in order to retain strength while arresting the progressive collapse. Bolt assemblies characterised by thread stripping failure (e.g. HV bolts) should be avoided, unless it can be demonstrated that the moment resisting frame elements alone are capable of arresting the progressive collapse for all column loss scenarios.*

**Justification:**

The preference for bolt assembly types characterised by shank necking failure is justified by the fact that the tensile forces in the additional row bolts remain high during and after the progressive collapse arrest, requiring bolt assemblies to be capable of retaining integrity and high strength levels until stabilised. This can be better accomplished by bolts with shank failure than by bolts with thread-stripping failure, considering that the latter are characterised by a sudden drop in strength at low displacements (see Figure 5.10), which would lead to tensile force redistribution to other components, defeating the purpose of the introduction of the additional bolt row. In case it is demonstrated that the moment resisting frame alone is capable of arresting the progressive collapse and that contribution of the secondary frame joints is not required, then the use of bolt assemblies characterised by thread stripping failure (e.g. HV bolts) is allowed.

## D.3 Detailing rules DR3

### DR 3.1 – General rules for façade claddings:

#### **DR 3.1.1:**

*The adoption of cladding panels for robustness enhancement purposes is subjected to architectural constraints and requires authorisation from the Architectural designer, for which reason it is not mandatory.*

#### **Justification:**

The use of façade cladding elements may introduce changes to the façade which render it incompatible with the Architectural design of the building. For this reason its adoption is not mandatory and is subjected to the approval of the responsible for the Architectural design.

#### **DR 3.1.2:**

*The introduction of discontinuities or the partial adoption of cladding panels in a building façade (see Figure 7.105) should be avoided since it may lead to lateral force imbalance under some column loss scenarios, unless demonstrated otherwise.*

#### **Justification:**

The existence of cladding panel discontinuities in a façade may lead to differences in terms of lateral stiffness of the elements adjacent to the removed column. For cases in which one side of the structure adjacent to the removed column has cladding panels whereas the other side consists of the bare steel frame, the column loss action, which is presumed to occur instantaneously introduces a pulse action. The local horizontal stiffness imbalance in the DAZ may contribute to introduce a horizontal pulse action for which the structure was not designed nor verified against.

Considering that this effect has not yet been quantified, a safe-side approach appears suitable and therefore the partial adoption of cladding panels in a building façade is non recommended.

**DR 3.1.3:**

*The adopted cladding panel solution should be able to transfer loads across corners through a truss system composed of single or multiple struts and/or ties.*

**Justification:**

This provision is intended to establish how the load transfer between panel corners may occur and also be analysed. The strut and tie truss model is considered suitable to describe not only the behaviour of one-dimensional truss systems, but also that of two-dimensional infilled panels. For the latter, suitable strut and tie models should be carefully selected, in order to ensure that the stress field in the panel element is described with sufficient accuracy.

**DR 3.1.4:**

*For cladding panels composed of linear resisting elements (e.g. claddings with steel bracings), load redistribution following column loss should be achieved via a cladding truss mechanism that is symmetric about the removed column in the directly affected zone, in accordance with the recommendations shown in Figure 7.106.*

**Justification:**

The recommendation for the selection of cladding resisting element configurations that are symmetric about the removed column in the DAZ is intended to avoid that differences in the stiffness of the members adjacent to the removed column result in the introduction of a horizontal force pulse, for which the structure was not designed. Since no research was found on this topic and as a safe-side approach, it was considered to be better to avoid asymmetric truss mechanisms.

**DR 3.1.5:**

*For infilled panels (e.g. masonry panels), the load transfer may be achieved via the compressive struts that are mobilised upon column loss. The presence of openings may reduce the stiffness of the panel and alter the load redistribution following column loss. Panels with openings are therefore not recommended to be adopted for progressive collapse prevention, unless demonstrated to be effective.*

**Justification:**

The recommendation to consider panels with openings as non effective for progressive collapse prevention is motivated by the fact that there is not sufficient research

conducted on this topic. In this sense, it is presently not clear how opening location, dimensions or aspect ratio influence the stiffness and capacity of the cladding panel to resist the distortions induced by the column loss action. For this motive, a conservative approach consisting of disregarding the contribution of these panels was assumed.

**DR 3.1.6:**

*In cases of infilled panels with openings, a physical gap between the infill element and the surrounding steel frame may be adopted, enabling to disconnect the cladding from the frame as shown in Figure 7.107. The dimension of the gap should be designed to accommodate the allowable interstorey drift.*

**Justification:**

Since the contribution of panels with openings is to be disregarded, then these panels should physically be disconnected from the frame. This can easily be achieved by introducing a gap between the infill panel(s) and the steel frame, which can be filled with compressible material. Considering however that the structure may be subjected to lateral loads due to wind loads, seismic action or other actions, the gap should allow the frame to deform without making contact with the infill panel(s). The gap width can therefore easily be computed from the maximum allowable interstorey drift.

By imposing that panels with openings be disconnected from the frame in DR 3.1.5 and by stating in DR 3.1.2 that discontinuities in façade claddings are to be avoided, these measures indirectly imply that all panels of a given façade in which at least one infill panel with opening(s) exists be disconnected from the frame. While this is likely overly conservative, it is intended to avoid the introduction of a horizontal pulse action into the structure until sufficient research has been conducted on this topic.

## DR 3.2 – Rules for façade claddings in non seismic zones:

### **DR 3.2.1:**

*In non seismic zones, both infilled and strut/tie truss claddings systems may be adopted. Although this measure is not mandatory, its adoption is likely to enhance structural robustness and in some cases help prevent progressive collapse following column loss.*

#### **Justification:**

In non seismic zones, the adoption of façade claddings introduces alternative loadpaths, hence enhancing structural redundancy. For this reason, both cladding systems are allowed.

### **DR 3.2.2:**

*Strut/tie truss claddings systems, namely consisting of “X” bracings of the same material of the frame, are more likely to provide a higher reduction of displacements following column loss and are therefore considered preferable in general.*

#### **Justification:**

This statement is based on the numerical results presented in Section 7.3.1.9 which indicate that the “X” bracing system is more effective at arresting progressive collapse, in part due to the fact that the strut/tie truss elements have the same Young’s modulus as the frame. Instead, the effectiveness of the masonry infilled cladding system was found to be quite low, especially for the cases of long span and/or medium rise frames. Since structures with CFS “X” bracing claddings were found to contribute to considerably reduce the maximum rotational demand under column loss action for all analysed structural typologies, this system was deemed preferable.

### **DR 3.2.3:**

*Infilled masonry claddings panels tend to be moderately effective for low rise and for short/medium span structural typologies and may therefore be adopted for such building typologies. For medium-rise long-span systems, masonry claddings have reduced effect on robustness and non-infilled solutions are preferable.*

#### **Justification:**

(See DR 3.2.2)

**DR 3.2.4:**

*For buildings with infilled façade walls (e.g. masonry), no gaps are allowed between adjacent cladding panels nor between the cladding panels and the surrounding steel elements of the moment resisting frame.*

**Justification:**

In order for the panel to be able to redistribute loads by transferring loads across panel corners in an optimised manner, the infilled panel should be in contact with the surrounding frame along all of its perimeter. While this enables to maximise the stiffness of the panel and to decrease the stresses in the equivalent compressive struts, it also contributes to avoid the introduction of load eccentricities at the frame joints zones, which may reduce the capacity of the frame to arrest the progressive collapse.

**DR 3.2.5:**

*Buildings with dry assembled façade wall systems can incorporate bracing systems (e.g. steel bracings) into the façade claddings that make up a strut/tie truss system according to the recommended typologies (see Figure 7.106), hence creating alternative loadpaths and improving structural redundancy and load re-distribution capacity.*

**Justification:**

The dry assembled wall systems are increasingly being adopted in building construction and easily allow for the incorporation of bracing members that make up a truss system. The bracing element disposition should be in accordance with the recommended dispositions shown in Figure 7.106, namely being symmetric about the removed column. Given that in non seismic zones, the bracing elements are undamaged when the progressive collapse initiates, dispositions in which only compression struts are mobilised are allowed.

**DR 3.2.6:**

*The members that make up the cladding strut/tie truss should, whenever possible, be designed for the additional accidental loads, accounting for dynamic effects, which can be conservatively accounted for using by a Dynamic Load Factor (DLF) equal to 2.0. Smaller DLF values may be adopted whenever properly justified.*



**Justification:**

In cases in which the façade cladding panels correspond to commercial solutions, the resistance of the bracing elements in the panel is likely pre-defined and cannot be directly designed. However, despite the fact that these elements may not be able to withstand the additional forces introduced by the column loss action, they can nonetheless contribute to dissipate energy, reducing the maximum rotational demand and contributing to prevent the spread of the initial damage and to arrest the progressive collapse.

Instead, when it is possible to directly design the bracing elements in the cladding panel, these can simply be designed for the internal force distribution obtained from a linear elastic analysis, considering the damaged structure (i.e. the structure with a removed column); the column to be removed should initially be replaced by the equivalent reactions after which a vertical downward force equal to the vertical column reaction multiplied by a DLF should be applied. The adoption of a DLF of 2.0 is known to be a conservative estimation and lower values can be obtained, namely for long span frames, as seen previously in Chapter 4. However this allows for a quick and safe-side estimation of the internal force distribution in the cladding truss members. In cases in which the design of the cladding truss elements leads to member sizes that are incompatible with the wall system, the largest possible member size should be adopted, since it leads to greater energy absorption and smaller maximum rotational demands.

**DR 3.2.7:**

*The connections of the members that make up the cladding strut/tie truss should be designed to have sufficient overstrength so that potential yielding is limited to the members. This may be achieved by designing connections according to the design rule for non-dissipative connections indicated in Section 6.5.5(3) of EN 1998-1.*

**Justification:**

By designing the cladding truss member connections with sufficient overstrength, a failure hierarchy is established in which strut/tie section axial ductile yielding precedes connection failure. The design rule for non-dissipative connections from EN 1998-1 was considered suitable since it accounts for random material overstrength.

**DR 3.2.8:**

*The members and connections of the strut/tie truss system should be designed to remain elastic (i.e. to sustain no permanent damage) for all characteristic load combinations. Damage is acceptable under the accidental load combinations (i.e. under column loss action).*

**Justification:**

The characteristic load combination defined in EN 1990 is normally used for irreversible limit states. In this sense, this disposition is intended to make sure that the strut/tie truss components do not sustain damage that irreversibly impairs the performance of these elements for progressive collapse. If this condition is verified, the truss elements are in the undamaged state when mobilised to arrest the progressive collapse.

**DR 3.3 – Rules for façade claddings in seismic zones:****DR 3.3.1:**

*In seismic zones, the adoption of claddings systems, when not explicitly taken into account for structural design, may introduce changes both in terms of strength and energy dissipation to the resisting structure under seismic actions. For this reason, these elements must be classified and consequently designed as primary or as secondary seismic elements, in accordance with EN 1998-1.*

**Justification:**

The introduction of structural elements that increase the lateral stiffness and strength of the building structure must be carefully analysed, since this may lead to changes in the structure's fundamental vibration periods, potentially leading to increased seismic demand. It should therefore be verified if the claddings are primary or secondary elements, since the modelling and detailing requirements depend on this classification.

**DR 3.3.2:**

*Cladding systems with infilled panels should be designed according to the rules provided in EN 1998-1.*

**Justification:**

The design methodology for structures with infilled panels is already described in the EN 1998-1. No additional dispositions were found to be required.

**DR 3.3.3:**

*Cladding systems with strut/tie trusses (e.g. steel bracings) may be designed either as primary or as secondary seismic elements, in accordance with EN 1998-1. If the total contribution to the lateral stiffness of all secondary seismic members including claddings does not exceed 15% of that of all primary seismic members (see Section 4.2.2(4) of the EN 1998-1), then claddings can be designed as secondary seismic elements. Otherwise claddings should be designed as primary seismic members.*

**Justification:**

This disposition corresponds to the classification methodology for primary and secondary seismic elements described in EN 1998-1.

**DR 3.3.4:**

*Cladding systems with strut/tie trusses classified as secondary seismic members are not required to be explicitly modelled for seismic design. Under seismic action, these elements are expected to sustain some level of damage, which may reduce compression strut capacity. It is therefore recommended to adopt cladding panels with "X" bracing configurations (see Figure 7.106a,c) that can mobilise ties under post-seismic column loss scenarios.*

**Justification:**

According to the EN 1998-1, elements classified as secondary seismic members are not required to be explicitly modelled.

Considering that the cladding panel is subjected to cyclic load reversal during seismic action, the compressive struts are likely to suffer damage due to buckling which may reduce the compression struts' capacity. For this reason and given that it is difficult to quantify the strut damage *a priori*, it is deemed preferable to adopt a system that relies

on elements in tension, i.e. on ties. For this reason, claddings panels with “X” bracings were found to be more suitable for buildings in seismic zones.

**DR 3.3.5:**

*Cladding systems with strut/tie trusses classified as primary seismic members are required to be explicitly modelled in the structural analysis and detailed for earthquake resistance in accordance with the rules provided in EN 1998-1.*

**Justification:**

For elements classified as primary seismic members, a design methodology is already provided in EN 1998-1.

**DR 3.3.6:**

*The members that make up the cladding strut/tie truss should, whenever possible, be designed for the additional accidental loads, accounting for dynamic effects, which can be conservatively accounted for using by a Dynamic Load Factor (DLF) equal to 2.0. Smaller DLF values may be adopted whenever properly justified.*

**Justification:**

(See DR 3.2.6)

**DR 3.3.7:**

*The connections of the members that make up the cladding strut/tie truss should be designed to have sufficient overstrength so that potential yielding is limited the members. This may be achieved by designing connections according to the design rule for non-dissipative connections indicated in Section 6.5.5(3) of EN 1998-1.*

**Justification:**

(See DR 3.2.8)

**DR 3.3.8:**

*The members and connections of the strut/tie truss system should be designed to remain elastic (i.e. to sustain no permanent damage) for all characteristic load combinations. Damage is acceptable under the accidental load combinations (i.e. under seismic and column loss actions).*

**Justification:**

(See DR 3.2.7)